#6714 - RADIATION EFFECTS IN SEMICONDUCTORS

June 5-9, 1967

Chairman: Professor Chihiro Kikuchi
Classroom: 325 West Engineering Building

FIRST WEEK

	Monday June 5	Tuesday June 6	Wednesday June 7	Thursday June 8	Friday June 9
8:30 - 10:00*	Kikuchi	Kikuchi	King	King	Kikuchi
10:00 - 10:15	←	—	B R E A K	—	→
10:15 - 11:45	Vincent	Vincent	Vincent	Hanson	Hanson
11:45 - 1:15	←	—	L U N C H	—	→
1:15 - 2:30	Oswald	Oswald	Oswald	Oswald	Oswald
2:30 - 2:45	←	—	B R E A K	—	→
2:45 - 4:00	Kikuchi	Kikuchi	Vincent	Vincent	Vincent

SECOND WEEK

	Monday June 12	Tuesday June 13	Wednesday June 14	Thursday June 15	Friday June 16
8:30 - 10:00	Kikuchi	Crawford	Crawford	Crawford	Crawford
10:00 - 10:15	←	—	B R E A K	—	→
10:15 - 11:45	Loferski	Loferski	Loferski	Loferski	Gregory
11:45 - 1:15	←	—	L U N C H	—	→
1:15 - 2:30	Messenger	Messenger	Messenger	Messenger	
2:30 - 2:45	←	—	B R E A K	—	→
2:45 - 4:00	Oswald	Vincent	Kikuchi	Gregory	

STAFF

Dr. James Crawford, Solid State Physics Division, Oakridge National Laboratory

B. L. Gregory, Sandia Corporation

Gordon Hanson, Missile Information and Systems Division, Boeing Company

Professor Chihiro Kikuchi, Department of Nuclear Engineering, The University of Michigan

Professor John S. King, Department of Nuclear Engineering, The University of Michigan

J. J. Loferski, Division of Engineering, Brown University

Dr. George Messenger, Neutronics Division, Northrup Corporation

Robert B. Oswald, Nuclear Vulnerability Division, Harry Diamond Laboratories

Dr. Dietrich H. Vincent, Department of Nuclear Engineering, The University of Michigan

*Class begins at 9:00 on Monday, June 5

ENGINEERING SUMMER CONFERENCES

VISITORS GUIDE

Contents:

ENGINEERING SUMMER CONFERENCES

Library Information

Engineering Library
Room 312 (3rd floor) Undergraduate Library Building (located on South University adjacent to Clements Library, door facing away from the street). Hours are: week days 8:00 a.m. to 12:00 midnight, Saturday 8:00 a.m. to 10:00 p.m., and Sunday 1:00 p.m. to 12:00 midnight.

General Library
Center of Campus between Haven Hall and Economics Building. Hours are: week days 8:00 a.m. to 12:00 midnight, Saturday 8:00 a.m. to 6:00 p.m., and Sunday 12:00 noon to 12:00 midnight.

Business Administration Library
Second floor of Business Administration Building located on the corner of Tappan Avenue and Monroe Street. Hours are: Monday through Thursday 8:00 a.m. to 11:00 p.m., Friday 8:00 a.m. to 6:00 p.m., Saturday 8:00 a.m. to 5:00 p.m., and Sunday 5:00 p.m. to 9:00 p.m.

Mathematics Library
Room 3027 Angell Hall (located on State Street across from the Administration Building). Hours are: Monday through Thursday 8:00 a.m. to 10:00 p.m., Friday 8:00 a.m. to 5:00 p.m., and Saturday 9:00 a.m. to 12:00 noon. Closed Sundays.

Physics-Astronomy Library
290 Physics & Astronomy Building (located on East University adjacent to East Engineering Building). Hours are: Monday through Thursday 8:00 a.m. to 10:00 p.m., Friday 8:00 a.m. to 5:00 p.m., and Saturday 9:00 a.m. to 12:00 noon. Closed Sundays.

Phoenix Library
Room 2054 Phoenix Memorial Laboratory (located on North Campus Blvd. adjacent to Cooley Memorial Laboratory). Hours are: week days 9:00 a.m. to 5:00 p.m. Possibly some Saturday hours; closed Sundays.

Clements Library
South University Avenue. Exhibits of rare books and historic documents of early America (1492 to 1830). Open 9:00 a.m. to 12:00 noon and 1:00 p.m. to 5:00 p.m. Monday through Friday. Closed weekends and holidays.

Places of Interest on Campus

GENERAL

Current activities are listed in the University of Michigan Weekly Calendar posted on classroom bulletin boards. For information on group tours, inquire at the desk in the main lobby of the Administration Building.

Buses to North Campus leave every 7 or 8 minutes starting at 7:15 a.m. from the bus stop at the intersection of North University and East University Streets. Copies of the bus schedule can be obtained at the Engineering Summer Conferences Office.

Burton Memorial Tower
(Across from Michigan League) View of campus and city from bell chamber (10 stories high) which houses carillon of 55 tuned bells. Open by appointment. For information call 764-7268.

Law Quadrangle
(South State Street and South University Avenue) Beautiful collegiate gothic structures and grounds providing residence, dining hall, classroom building and library for law students.

Michigan Stadium
(South Main Street and Stadium Blvd.) Largest college-owned stadium in the country. Seats 101,001 spectators. Open daily: enter through South-east Gate on Stadium Blvd. (Parking is available.)

Phoenix Memorial Laboratory
(North Campus Blvd.) The Ford Nuclear Reactor and laboratories are devoted to peaceful uses of atomic energy. Guided tours available 1:30 to 4:00 p.m. Monday through Friday.

Radio Telescope
(10280 North Territorial Road near Dexter, Michigan, about 15 miles from campus) Metal dish 85 feet in diameter is main instrument of the Radio Astronomy Observatory. Open to visitors: Third Sunday of May, June, July, August, and September from 2:00 to 4:30 p.m. For information phone: 426-8441.

MUSEUMS

Exhibit (Natural History) Museum
(North University and Washtenaw Avenue) Extension exhibits and colorful reproductions of plants and animals and early man; Michigan birds and wildlife; American Indian life and other cultures. Open 9:00 a.m. to 5:00 p.m. Monday through Saturday. Sunday 1:30 p.m. to 5:30 p.m. Closed holidays. Planetarium showings at 2:00, 3:00, and 4:00 p.m. Saturday and Sunday.

Museum of Art
(South State Street and South University Avenue) Exhibits of painting, sculpture and other art forms. Open 9:00 a.m. to 5:00 p.m. Monday through Saturday; 2:00 to 5:00 p.m. Sunday.

Kelsey Museum of Archeology
(South State Street next to the Administration Building) Exhibits from ancient Egypt and Graeco-Roman antiquities. Open 1:00 to 4:00 p.m. Monday through Friday; 3:00 to 5:00 p.m. Sunday. Closed Saturdays, holidays, and University vacation periods.

Stearns Collection of Musical Instruments
(Second floor of Hill Auditorium, enter building through East door) Extensive exhibits of old and rare musical instruments. Open 3:00 to 4:00 p.m. Tuesday and Friday. For information call: 764-7628.

Pathology Museum
(Off Main Lobby of Medical Science Building, University Medical Center) Exhibits of human pathology. Displays periodically changed. Open 8:00 a.m. to 5:00 p.m. Monday through Friday.

Other interesting and educational displays may be found in the corridors of the Natural Science Building, including the Mineralogy Collection (Room 2071). The Undergraduate Library and the General Library have interesting exhibits in their lobbies. The Michigan Historical Collections (160 Rackham Building) have items of historical interest on display. These buildings are open 8:00 a.m. to 5:00 p.m. Monday through Saturday. Closed holidays.

BOTANICAL GARDENS

Nichols Arboretum
(Pedestrian entrance from Geddes Avenue or Washington Heights) A 125 acre area, wooded and gently rolling, with a varied collection of shrubs and trees. Open daily until sundown.

Botanical Gardens
(1800 Dixboro Road, take Plymouth Road east to Dixboro Road, turn right (south), about 5 miles from campus) A beautiful 200 acre site with varied natural growing conditions. Greenhouses open daily (except holidays) 8:00 a.m. to 5:00 p.m. Monday through Friday.

Fair Lane Estate
(On the U-M Dearborn Campus, Dearborn, Michigan, enter from Ford Road and Evergreen). The home and gardens of the Henry Ford Estate now serve as a conference center. There are more than 3,000 rose bushes in the gardens. Open the first Sunday of each month; during summer months every Sunday from 1:00 to 4:00 p.m. Guided tours are conducted at a charge of $1.00 per person. Proceeds are used for scholarships.

Recreation Facilities in Ann Arbor

PARKS HAVING PICNIC FACILITIES

West Park
Bounded by Miller, Chapin, W. Huron and N. Seventh St. Complete playground equipment; horseshoes, ping-pong; wading pool; stove and picnic tables; tennis courts; lighted skating pond; orchestra shell; toilet facilities; shelter.

Arboretum
Off Geddes Ave. at Nichols Drive; wooded area and drives; sledding and skiing on some hills; picnicking, but no fires.

Island Park
Along Huron River east of Wall St.; playground equipment; picnic area with stove; toilet facilities.

Riverside Park
Along North side of Huron River between Wall Street and Fuller Street bridge; playground equipment; stoves and picnic tables.

Allmendinger
Pauline & Hutchins; playground equipment; stoves and picnic tables; lighted skating pond; toilet facilities.

Fritz Park
North side of Pauline 1/2 mile from S. Main; two fireplaces under shelter; two picnic stoves; tables and benches.

Burns Park
Wells & Baldwin; complete playground equipment; horseshoes; suffleboard; wading pool; picnic tables; tennis courts; lighted skating pond; toilet facilities; shelter.

Community Park
Platt and Edgewood; playground equipment; skating, baseball; picnic tables; fireplaces; shelter.

For recreation facilities outside the Ann Arbor area see the Metropark Guide available at the Engineering Summer Conference office, Room 126 West Engineering Building.

GOLF COURSES AND DRIVING RANGES

University Golf Courses
500 E. Stadium Blvd., 663-5005; open weekdays 8:00 a.m. until dark and from 7:00 a.m. until dark Saturday and Sunday. Green fee with student receipt is $2.00. Reservations are not needed, but can be made 7 days in advance.

Ann Arbor Municipal Golf Course
1519 Fuller Road, 668-9230; open weekdays; green fee $1.25 for 9 holes and $2.00 for 18 holes. Reservations are needed on Saturday, Sunday & Holidays; green fee $2.00 for 9 holes, $2.50 for 18 holes; club rental $1.00.

Huron Municipal Golf Course
3465 E. Huron River Drive, 668-9437; open weekdays, green fee $2.00 and $1.25 after 5:00 p.m. Reservations are needed on Saturday and Sunday; green fee $2.50 and $2.00 after 4:00 p.m.; club rental $1.50.

Pat's Par 3 Golf Course and Driving Range
3113 Carpenter Road, 668-9514; Golf course green fee $1.25; club rental 30¢.

Tee and Ski Inc., Driving Range
2455 South State Street, 662-7307. Hours are 10:00 a.m. to 8:00 p.m.

BOWLING LANES

Colonial Lanes
1950 S. Industrial Highway, 662-2655.

Huron Lanes
320 E. Huron, 663-2510.

Washtenaw Lanes
3400 Washtenaw Road, 662-2422.

Ypsi-Arbor Lanes
295 Washtenaw Road, Ypsilanti, 482-0166.

YM-YWCA
350 S. Fifth Avenue, 663-0536, open to all adults, $1.00 fee for non-members plus 50¢ for equipment. Hours are 9:00 a.m. to 10:00 p.m. Monday through Saturday.

THEATERS & PLAYS (see local newspaper for current offerings)

Campus Theater
1214 S. University, 668-6416.

Michigan Theater
603 E. Liberty, 668-8480.

State Theater
231 South State Street, 662-5296.

Scio Drive-In Theater
6588 Jackson Road, 668-7083.

Ypsi-Ann Drive-In Theater
4675 Washtenaw Road, 761-0100

University Drive-In Theater
4100 Carpenter Road, 483-4680.

Ann Arbor Civic Theater
803 W. Washington, 668-9739.

Trueblood Auditorium
2005 Frieze Building, 764-5387.

Lydia Mendelssohn Theater
227 S. Ingalls, 668-6300.

Vth Forum Theater
210 South Fifth Avenue, 761-9700.

NOTES

for

RADIATION EFFECTS IN SEMICONDUCTORS

D. H. Vincent

CHAPTER I.

DESCRIPTION OF THE INTERACTION OF TWO PARTICLES

For a better understanding of the first three chapters of these notes it will be helpful to first read the appendix on "Relative coordinates and the central force problem".

1. The Problem

We wish to describe the interaction of two particles 1 and 2 with Mass M_1, initial velocity $\underline{v}_1$ in the laboratory system and Mass M_2, initial velocity $\underline{v}_2$ in the laboratory system respectively. $\underline{v}_2$ is usually assumed to be zero, since we let particle 2 be the target particle, which is usually assumed to be at rest before the interaction. In particular we are interested in particles of kind 2, which are bound in a solid (crystal lattice).

2. Differential Cross Section

Definition:

$$d\sigma = \frac{\text{Number of incident particles undergoing a particular interaction per scattering center per unit time.}}{\text{Incident intensity}}$$

Intensity = Number of incident particles per unit area per unit time.

The differential cross section can be interpreted as an infinitesimal target area associated with one scattering center:

From the total number of particles incident on a unit area we select a number, which will undergo a particular interaction. Associated with this number is a certain fraction of unit area, which is the "target area" subtended by our scattering center for this particular interaction.

Most specific cross section for our problem:

$$d\sigma = K(\underline{v}_1, \underline{v}_1', \underline{v}_2')\, d\underline{v}_1'\, d\underline{v}_2' \qquad (1.1)$$

$d\sigma \equiv$ number of incident particles of velocity $\underline{v}_1$ which produce interactions leading to velocities in the interval $(\underline{v}_1', \underline{v}_1' + d\underline{v}_1')$ for particle 1 and to velocities in the interval $(\underline{v}_2', \underline{v}_2' + d\underline{v}_2')$ for particle 2

per scattering center (per target particle)

per unit time

per unit incident intensity.

Let: N_1 = density of incident particles

N_2 = density of target particles

$N_1 v_1 = \varphi_{v_1}$ = incident intensity

Then, from the above definition of $d\sigma$:

a) $N_1 v_1\, d\sigma\, dt$ = number of incident particles of velocity $\underline{v}_1$ which produce interactions leading to velocities in the intervals $(\underline{v}_1', \underline{v}_1' + d\underline{v}_1')$ and $(\underline{v}_2', \underline{v}_2' + d\underline{v}_2')$ during the time interval dt <u>per target particle</u>.

b) $v_1\, d\sigma\, dt\, N_2$ = number of interactions leading to velocities in the intervals $(\underline{v}_1', \underline{v}_1' + d\underline{v}_1')$ and $(\underline{v}_2', \underline{v}_2' + d\underline{v}_2')$ during time dt <u>per incident particle.</u>

c) $N_1 v_1 \, d\sigma \, dt \, N_2$ = number of incident particles of velocity which produce interactions leading to velocities in the intervals $(\underline{v}_1', \underline{v}_1' + d\underline{v}_1')$ and $(\underline{v}_2', \underline{v}_2' + d\underline{v}_2')$ per unit volume of target material.

The three expressions a), b) and c) may be considered as probabilities as long as their magnitude is small compared to 1.

The knowledge of the function

$$K(\underline{v}_1, \underline{v}_1', \underline{v}_2')$$

for all $\underline{v}_1$, $\underline{v}_1'$, $\underline{v}_2'$

and all kinds of incident particles as well as all kinds of target material would furnish us with a complete description of all possible interaction processes. In reality we usually have to be content with much less information.

3. Alternate Notation

In the treatment of radiation effects in solids, the parameters of the incident particle (called 1 above) are often not marked with indices, whereas the parameters of the target particle get the subscript "p". This stands for "primary", indicating that this particle may receive sufficient energy from the interaction to act itself as a projectile and cause secondary, tertiary etc. collisions.

Our cross section, defined in (1.1), would read

$$d\sigma = K(\underline{v}, \underline{v}', \underline{v}_p) \, d\underline{v}' \, d\underline{v}_p$$

4. Less Specific Cross Sections

A differential cross section which can be determined with less difficulty than the one defined in equation (1.1) is the cross section that specifies only the energy received by the target particle, Ep:

$$d\sigma = K(E, E_p)\, dE_p \tag{1.2}$$

The connection between $K(\underline{v}, \underline{v}', \underline{v}_p)$ and $K(E, E_p)$, which are of course two completely different functions, is:

$$K(E,E_p)\, dE_p = \left[\iint \delta\left(\frac{M_p}{2} v_p^2 - E_p\right) K(\underline{v}, \underline{v}', \underline{v}_p)\, d\underline{v}'\, d\underline{v}_p \right] dE_p \tag{1.3}$$

K(E,Ep) will be the differential cross section which we will usually look for. This indicates that our interest is not so much in the fate of the incident particle but in that of the primary knock-on.

Notation: The kinetic energy of a lattice atom is often designated by the letter T, which is applied regardless of whether the lattice atom is a primary knock-on, or receives its energy from secondary or tertiary collisions. T will therefore often be used instead of Ep.

5. Relation between Differential Cross Sections Depending on Different Parameters.

Given, for example, the differential cross section as a function of the scattering angle θ in relative coordinates, $K(\theta)\, d\theta$, we can obtain the cross section as a function of primary energy Ep by the relation:

$$K(E_p)\,|dE_p| = K(\theta)\,|d\theta| \tag{1.4}$$

or

$$K(E_p) = K(\theta(E_p))\left|\frac{d\theta}{dE_p}\right|$$

One very useful relation is that which establishes connection with the impact parameter b. Because of the isotropy around the direction of incidence for a central potential we have:

$$d\sigma = 2\pi b\,db = \pi\,db^2 \tag{1.5}$$

from which e.g.

$$K(\cos\theta) = \pi\left|\frac{db^2}{d(\cos\theta)}\right| \tag{1.6}$$

i.e. to obtain K(cos θ), we must know the relation between b and cos θ . Such relations will be derived for two kinds of interaction potentials in Chapter 2.

6. Total Cross Section

$$\sigma = \int_0^{E_{pmax}} K(E, E_p)\,dE_p \tag{1.7}$$

E_{pmax} is the maximum possible energy which a primary can receive in an interaction with a particular incident radiation. An expression for E_{pmax} is derived in the Appendix, in section 6.

7. Displacement Cross Section

A displacement is the removal of an atom from its regular lattice position. The minimum energy necessary to produce a displacement depends in general on the direction of $\underline{v}$ of the incident particle with respect to the lattice coordinates. In the simplified

treatment of radiation effects, however, one assumes that the introduction of <u>one</u> specific threshold energy for each material is sufficient.

E_d = displacement threshold

σ_d = displacement cross section

$$\sigma_d = \int_{E_d}^{E_{pmax}} K(E,E_p)\, dE_p \qquad (1.8)$$

8. <u>Energy Distribution of the Primaries.</u>

It is customary and practical to split the differential cross section, equation (1.2) into a product of a cross section, depending only on the energy of the incident particle and a normalized distribution function for the primary energies:

$$K(E,E_p)\, dE_p = \sigma(E)\, k(E,E_p)\, dE_p \qquad (1.9)$$

$$\text{with} \quad \int_0^{E_{pmax}} k(E,E_p)\, dE_p = 1$$

$k(E,E_p)\, dE_p$ = probability, that the energy of the lattice atom after the collision is in the interval $(E_p, E_p + dE_p)$

Notation: Frequently the dependence of k and K on the incident energy is not expressed explicitely, and $k(E_p)$ or $k(T)$ is written instead of $k(E,E_p)$.

We may now apply this to our expression c) on page 3:

Let

$N(E_p)dE_p$ = number of events per unit volume producing primary recoils of energy in the interval (E_p, dE_p) during an irradiation of length t in a time-independent, monoenergetic flux φ_E.

Then by comparison with the expression on page 3 we have:

$$N(E_p)dE_p = N_1 v_1 t \; K(E,E_p) N_2 \, dE_p$$

or

$$N(E_p)dE_p = \underbrace{\varphi_E t N_A \sigma(E)}_{\text{number of primary events per unit volume in time t}} \cdot \underbrace{k(E_p)dE_p}_{\text{normalized energy distribution of the primary recoils}} \qquad (1.10)$$

Here we replaced in the second equation

N_2 by the more commonly used N_A

$N_1 v_1$ by φ_E

$K(E,E_p)$ by $\sigma(E)k(E_p)$

It is obvious, that $N(E_p)dE$ is a useful distribution function for the discussion of radiation effects. However, of the number of particles having a certain energy E_p, we are really interested only in those which will be able to leave their lattice site. This number can be accounted for in a general way by the introduction of a probability.

$W_d(T)$ = probability that a lattice atom with energy T will leave its lattice position.

With this we obtain

$$N_d(T) = N(T)\, W_d(T) \tag{1.11}$$

$$K_d(T) = K(T)\, W_d(T) \tag{1.12}$$

$$\sigma_d(E) = \int_0^{T_{max}} K_d(E,T)\, dT \tag{1.13}$$

For an infinitely steep threshold (step function), i.e.

$$W_d(T) = \begin{cases} 0 & \text{for } T \leq E_d \\ 1 & \text{for } T \geq E_d \end{cases}$$

equation (1.8) is identical with equation (1.13) above.

9. Mean Values

Mean energy transfer in a collision

$$\bar{T} = \int_0^{T_{max}} T\, k(E,T)\, dT \tag{1.14}$$

Mean free path of the incident particle between collisions.

From equation (1.10) one can see that $N_A \sigma(E)$ is the number of collisions, which one incident particle makes while traversing 1 cm. The mean free path is the reciprocal of this number

$$\lambda = \frac{1}{N_A \sigma(E)} \tag{1.15.a}$$

and in particular for displacement collisions

$$\lambda_d = \frac{1}{N_A \sigma_d(E)} \tag{1.15.b}$$

This expression is to be used with some care, because the incident particle will lose energy with each collision. Since $\sigma(E)$ depends on this energy in general, the mean free path will not be constant. One tries to use samples, which are small (in one dimension) compared to λ_d . Except for fission fragments, λ_d always large compared to the range of the primary.

10. Incident Particles With Energy Distribution

If the incident flux is not monoenergetic at energy E, indicated so far by φ_E , but has an energy distribution $\varphi(E)$ (not necessarily normalized), then the number $N(E_p)dE_p$, equation (1.10) becomes

$$N(E_p)dE_p = \left[\int \varphi(E)\, t\, N_A \sigma(E) k(E,E_p)\, dE \right] dE_p \qquad (1.16)$$

This can be expressed in a form like equation (1.10) by the introduction of appropriate mean values:

$$\bar{k}(E_p) = \frac{1}{\varphi \bar{\sigma}} \int \varphi(E)\sigma(E) k(E,E_p)\, dE \qquad (1.17)$$

$$\bar{\sigma} = \frac{1}{\varphi} \int \varphi(E)\sigma(E)\, dE \qquad (1.18)$$

$$\varphi = \int \varphi(E)\, dE \qquad (1.19)$$

$$N(E_p)dE_p = \varphi t\, N_A \bar{\sigma}\, \bar{k}(E_p)\, dE_p \qquad (1.10a)$$

CHAPTER II.

CLASSICAL COLLISION THEORY

1. The Equation of Motion and its General Solution

The equation of motion in relative coordinates is (see App. equ.(A.10)

$$\boxed{\mu \ddot{\underline{r}} = -\frac{\partial}{\partial \underline{r}} V(\underline{r})} \tag{2.1}$$

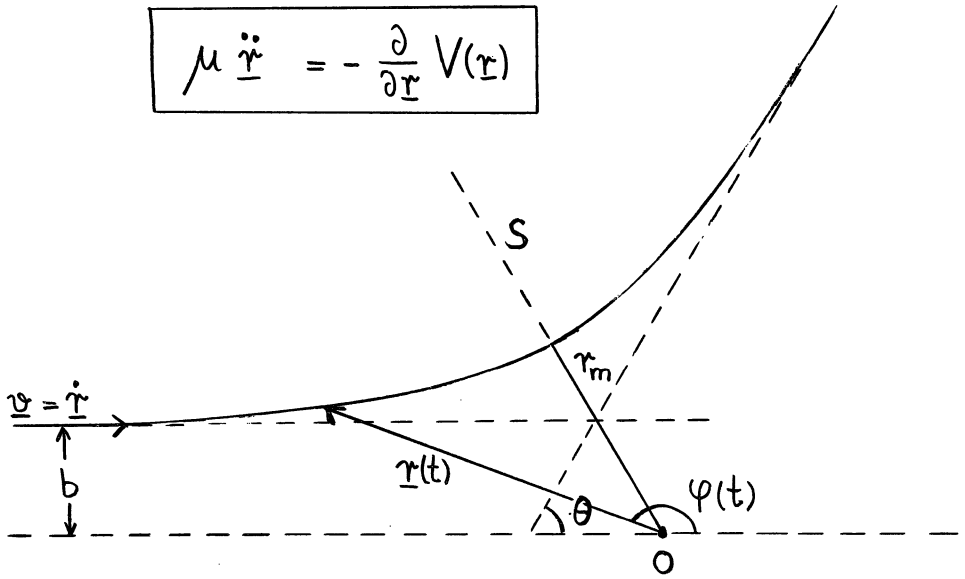

FIG. 1.

REPRESENTATION OF A SCATTERING EVENT

If we have a central potential $V(r)$, the motion will be confined to a plane due to the conservation of angular momentum.
The motion can then be described by writing down energy and angular momentum conservation in the x,y - plane

$$E_r = \frac{\mu}{2}(\dot{x}^2 + \dot{y}^2) + V(r) \tag{2.2}$$

$$L = L_z = (\underline{r} \times \underline{p})_z = m(x\dot{y} - y\dot{x}) \tag{2.3}$$

Because V depends on r only, it is useful to convert these equations to polar coordinates:

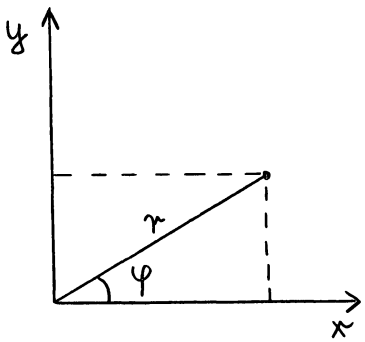

FIG. 2

$$x = r\cos\varphi$$
$$y = r\sin\varphi$$
$$\dot{x} = \dot{r}\cos\varphi - r\dot{\varphi}\sin\varphi$$
$$\dot{y} = \dot{r}\sin\varphi + r\dot{\varphi}\cos\varphi \qquad (2.4)$$

$$E_r = \frac{\mu}{2}(\dot{r}^2 + r^2\dot{\varphi}^2) + V(r) \qquad (2.2.a)$$

$$L = \mu r^2\dot{\varphi} = \mu v b \qquad (2.3.a)$$

The relation $L = \mu v b$, where v is the speed of the particle at infinite distance from the scattering center, becomes obvious upon inspection of FIG. 1, where it can be seen, that $\mu v b$ is just the magnitude of $(\underline{r} \times \underline{p})$ for this particular case.

We can eliminate $\dot{\varphi}$ from equations (2.2.a) and (2.3.a) by substituting one into the other. The result can be solved for $\dot{r}$:

$$\dot{r} = \pm v\sqrt{1 - \frac{V(r)}{E_r} - \frac{b^2}{r^2}} \qquad (2.5)$$

The path of the particle is symmetric.

The negative sign holds before the symmetry axis S (see FIG. 1.), the positive sign holds thereafter.

The condition $\dot{r} = 0$ defines the minimum distance $r_m(b)$ as a function of the impact parameter b.

From (2.3a) we have: $\dot{\varphi} = \frac{v b}{r^2}$

With this and equation (2.5), we obtain

$$\frac{d\varphi}{dr} = \frac{\dot{\varphi}}{\dot{r}} = \pm \frac{b/r^2}{\sqrt{1 - \frac{V(r)}{E_r} - \frac{b^2}{r^2}}} \qquad (2.6)$$

+ sign before symmetry axis.

- sign after symmetry axis.

Equation (2.6) serves to compute the angle of deflection θ in the relative coordinate system.

$$\varphi(t = +\infty) - \varphi(t = -\infty) = \theta - \pi \qquad \text{(see Fig. 1)}$$

$$\theta = \pi + 2\int_{r_m}^{+\infty} \frac{d\varphi}{dr}\, dr = \pi - \int_{r_m}^{\infty} \frac{2b\, dr}{r^2\sqrt{1 - V(r)/E_r - b^2/r^2}}$$

or with $u = 1/r$ and $u_m = 1/r_m$

$$\theta = \pi - \int_0^{u_m} \frac{2b\, du}{\sqrt{1 - V/E_r - b^2u^2}} \qquad (2.7)$$

2. <u>Special Solutions of the Classical Collision Theory</u>.

Integrals of equation (2.7) can be found in elementary form only for very specific potentials V.

We shall discuss:

a. <u>Hard Sphere Potential</u>

$$V(r) = 0 \quad \text{for} \quad r > R$$
$$V(r) = \infty \quad \text{for} \quad r < R \qquad (2.8)$$

b. Coulomb Potential

$$V(r) = \frac{C}{r} \qquad C = Z_1 Z_2 e^2 \tag{2.9}$$

a.) Hard Sphere Potential

Application of equation (2.7) to this potential yields

$$\theta = \pi - 2b\int_0^{1/R} \frac{du}{\sqrt{1 - b^2u^2}}$$

$$\theta = \pi - 2 \arcsin \frac{b}{R}$$

$$\frac{b}{R} = \sin\left(\frac{\pi}{2} - \frac{\theta}{2}\right) = \cos\frac{\theta}{2}$$

$$\boxed{b = R\cos\frac{\theta}{2}} \tag{2.10}$$

With equation (1.6), we may now obtain

$$K(\cos\theta) = \pi \left|\frac{d\,b^2}{d(\cos\theta)}\right|$$

$$b^2 = R^2\cos^2\frac{\theta}{2} = \frac{R^2}{2}(1 + \cos\theta)$$

$$\boxed{K(\cos\theta) = \frac{\pi R^2}{2}} \tag{2.11}$$

Making use of equ. (A.21) with $E_2' = E_p$

$$E_p = E_{pmax}\frac{(1-\cos\theta)}{2}$$

$$K(E_p) = K(\cos\theta)\left|\frac{d(\cos\theta)}{d\,E_p}\right| = K(\cos\theta)\frac{2}{E_{pmax}}$$

$$\boxed{K(E_p) = \frac{\pi R^2}{E_{pmax}}} \tag{2.12}$$

$$K(E, E_p) = \sigma(E) \times k(E, E_p) = \pi R^2 \cdot \frac{1}{E_{pmax}}$$

Result: Equ. (2.11) shows that scattering is isotropic in the relative coordinate system and from equ. (2.12) we see that $K(E_p)$ is independent of the primary energy (see FIG. 3).

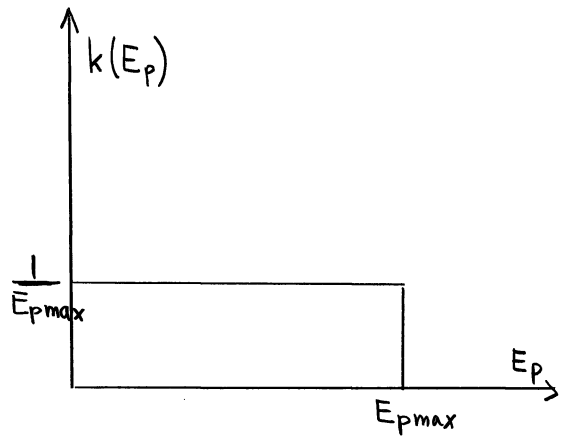

FIG. 3

Finally the total cross section according to equation (1.7)

$$\sigma = \int_0^{E_{pmax}} K(E_p)\, dE_p = \pi R^2 \qquad (2.13)$$

which is the result one would expect for classical hard-sphere scattering.

b.) Coulomb Potential

With the potential $V(r) = \frac{C}{r}$ and the substitution $\frac{C}{E_r} = R$ equation (2.7) becomes

$$\theta = \pi - \int_0^{u_m} \frac{2b\,du}{\sqrt{1 - Ru - b^2u^2}}$$

u_m is determined by applying the condition $\dot{r} = 0$ at $r = r_m$ to equ. (2.5) for $V(r) = C/r$. This yields

$$u_m = -\frac{R}{2b^2} + \frac{1}{b^2}\sqrt{(R^2/4) + b^2} \qquad (2.14)$$

With this as the upper limit the integral yields

$$\boxed{b = \frac{R}{2} \cot \frac{\theta}{2}} \tag{2.15}$$

In the same manner as demonstrated for the Hard Sphere potential, we obtain now

$$K(\cos\theta) = \frac{\pi R^2}{2(\cos\theta - 1)^2} \tag{2.16}$$

With the help of the trigonometric relation

$$1 - \cos 2x = 2 \sin^2 x$$

equation (2.16) can be converted to the form in which the cross section for Rutherford Scattering is usually presented

$$K(\cos\theta)\,|d(\cos\theta)| = K(\theta)\,|\sin\theta\, d\theta|$$

$$d\sigma = \frac{\pi R^2}{8 \sin^4 \frac{\theta}{2}} \sin\theta\, d\theta$$

$$d\sigma = \frac{R^2}{16 \sin^4 \frac{\theta}{2}}\, d\Omega \tag{2.17}$$

By using equation (1.6) on K(cos θ) we obtain

$$\boxed{K(E_p) = \frac{\pi R^2}{4} E_{pmax} \frac{1}{E_p^2}} \tag{2.18}$$

CHAPTER III.

PRIMARY INTERACTION OF VARIOUS RADIATIONS

In this chapter we shall discuss the interactions of various incident radiations that may produce lattice defects.
We shall be interested in the interaction cross section σ (E) of these radiations, in the energy distribution function of the primaries, $k(E, E_p)$ and in functions that can be derived from these two basic parameters like the mean free path of the incident particles, their range and the mean energy of the primary knock ons.
Our efforts will be confined to neutrons and heavy charged particles with a brief reference to electron interactions.

1. Neutron Interactions in General

The quantum-mechanical treatment of the scattering of neutrons furnishes the result, that for slow neutrons for which the de-Broglie wave length is large compared to the nuclear radius, the interaction cross section is independent of the neutron energy and may be expressed by

$$\sigma = 4\pi R_A^2 \tag{3.1}$$

where R_A represents the nuclear radius given by

$$R_A = A^{1/3} \times 1.5 \times 10^{-13} \text{ cm} \tag{3.2}$$

The scattering is isotropic in the relative coordinate system and σ may be compared with the total cross section for hard-sphere scattering, equation (2.13) from which it differs only by a factor of four.

For higher neutron energies for which the condition $\lambda\!\!\!^{-} \gg R_A$ no longer holds, deviations from the isotropy of scattering occur. By taking into account terms linear in $\cos\theta$ in the series expansion of the quantum mechanical scattering amplitude one can make an estimate of the inaccuracy introduced by assuming isotropy even at higher neutron energies. One obtains for the energy E_s at which 20% deviation from isotropy occur:

$$E_s \cong A^{-2/3} \times 2 \text{ Mev}$$

A plot of this function (FIG. 4) shows, that E_s is roughly .1 Mev for $A > 50$.

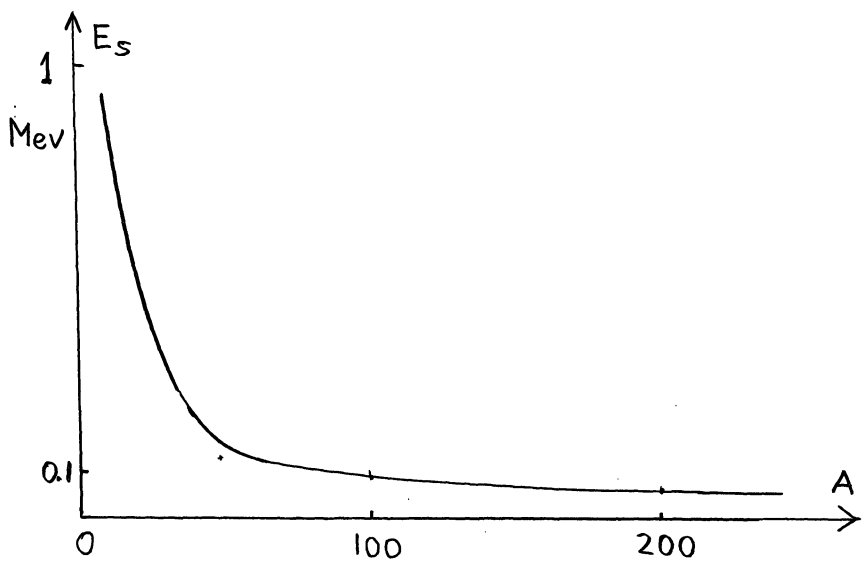

FIG. 4

LIMITING ENERGY E_s FOR ISOTROPIC SCATTERING AS A FUNCTION OF MASS NUMBER A

For larger neutron energies (in the order of kev to Mev) we will also have to take account of the energy dependence of σ , which may be a smoothly decreasing function or which may show resonance peaks.

Mean free path.

This was already introduced in general in Chapter 1, Section 9. We shall first show, that for isotropic scattering the difference between

$$\lambda = \frac{1}{N_A \sigma} \qquad \text{and} \qquad \lambda_d = \frac{1}{N_A \sigma_d}$$

is negligible.

$$\sigma_d = \sigma\left(1 - \frac{E_d}{T_{max}}\right) = \sigma\left(1 - \frac{E_d}{\alpha E}\right) = \sigma\left(1 - \frac{AE_d}{4E}\right) \qquad (3.3)$$

Assumming $E_d = 25\,ev$ we see that $\frac{A}{4} E_d$ can be at most $60\, E_d = 1500\,ev$. For neutron energies large compared to that number the second term in bracketts may be neglected.

Example for Cu:

$$\sigma = 5 \text{ barn} = 5 \times 10^{-24} cm^2 \quad \text{for } E = .3 \text{ Mev}$$

$$\frac{AE_d}{4E} \cong .001 \qquad N_A(Cu) \cong 8.5 \times 10^{22}\ cm^{-3}$$

$$\lambda(Cu) = \frac{1}{.05 \times 8.5} cm = 2.4\ cm$$

This means, there is a large distance between collisions for energetic neutrons.

If the cross section and thereby the mean free path do not change much with energy, one may obtain the total range $\mathcal{S}(E)$ of the neutron by

$$\mathcal{S}(E) \cong \frac{E}{\bar{T}(E)}\,\lambda(E) \tag{3.4}$$

For isotropic scattering:

$$\bar{T}(E) = \frac{T_{max}}{2} = \frac{\alpha E}{2} \cong \frac{2E}{A} \qquad (M_1 \ll M_2)$$

$$\mathcal{S}(E) = \frac{A}{2}\,\lambda(E)$$

For copper $\frac{A}{2} \cong 30$

Neutron Spectra

Neutrons which are used for radiation effects experiments are most often not monoenergetic. Since the nuclear reactor is a neutron source with a particularly high yield, spectral distributions for neutrons as they occur in the reactor are usually used for primary interaction calculations. We shall look at two such distributions: the fission spectrum and moderated neutrons. We shall obtain the case of monoenergetic neutrons as a convenient though rough approximation for the fission spectrum.

2. Fission Spectrum Neutrons

This spectrum may be described by the empirical formula

$$P(E) = \frac{2}{E_f}\sqrt{\frac{E}{\pi E_f}}\; e^{-E/E_f} \tag{3.5}$$

With

$$E_f \cong 1.4 \text{ Mev} \qquad \text{and} \qquad \int_0^\infty P(E)\,dE = 1$$

(Ref. Beckurts and Wirtz, Neutron Physics, Springer, 1965)

$P(E)\,dE$ is the fraction of neutrons with energies in the interval $(E,\ E+dE)$.

Average energy: $\bar{E} = 3E_f/2 \cong 2 \text{ Mev}$

Most probable energy: $E_f/2 \cong .7 \text{ Mev}$

According to equation (1.17) we can now try to obtain

$$\bar{k}(T) = \frac{\int P(E)\sigma(E)k(E,T)\,dE}{\int P(E)\sigma(E)\,dE}$$

and

$$\bar{\sigma} = \int P(E)\sigma(E)\,dE$$

We shall use

$$k(E,T) = \frac{1}{T_{max}} = \frac{1}{\alpha E} \tag{3.6}$$

which holds for isotropic scattering, and

$$\sigma(E) = \sigma_0\, e^{-E/E_\sigma} \tag{3.7}$$

which describes quite well the actual behavior of most scattering cross sections. For copper the measured total cross section can be seen in FIG. 5.

The parameters needed to fit these data are

$$\sigma_0 \cong 8 \text{ barn}$$

$$E_\sigma \cong 1 \text{ Mev}$$

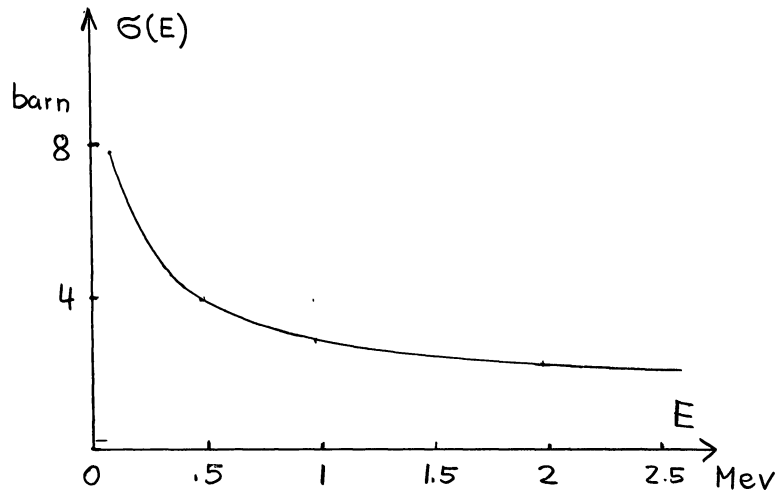

FIG. 5.

TOTAL SCATTERING CROSS SECTION FOR NEUTRONS IN Cu.

(Ann. of Physics, 12, 135, 1961)

The results of the integrations are:

$$\bar{\sigma} = \frac{\sigma_0}{(1 + E_f / E_\sigma)^{3/2}} \tag{3.8}$$

$$\bar{k}(T) = \frac{2}{\alpha}\left(\frac{1}{E_f} + \frac{1}{E_\sigma}\right)\left[1 - \text{erf}\left(\sqrt{\frac{T}{\alpha}\left(\frac{1}{E_f} + \frac{1}{E_\sigma}\right)}\right)\right] \tag{3.9}$$

Specializations:

a.) $E_\sigma \to \infty$ or $\sigma(E) = \text{constant}$

$$\bar{\sigma} = \sigma_0 \tag{3.10}$$

$$\bar{k}(T) = \frac{2}{\alpha E_f}\left[1 - \text{erf}\left(\sqrt{\frac{T}{\alpha E_f}}\right)\right] \tag{3.11}$$

b.) Replace fission spectrum $P(E)$ by monoenergetic neutrons of energy E_f'

$$\bar{\sigma} = \sigma(E_f') \quad \text{and} \quad \bar{k} = \frac{1}{\alpha E_f'} \qquad (3.12 \text{ and } 13)$$

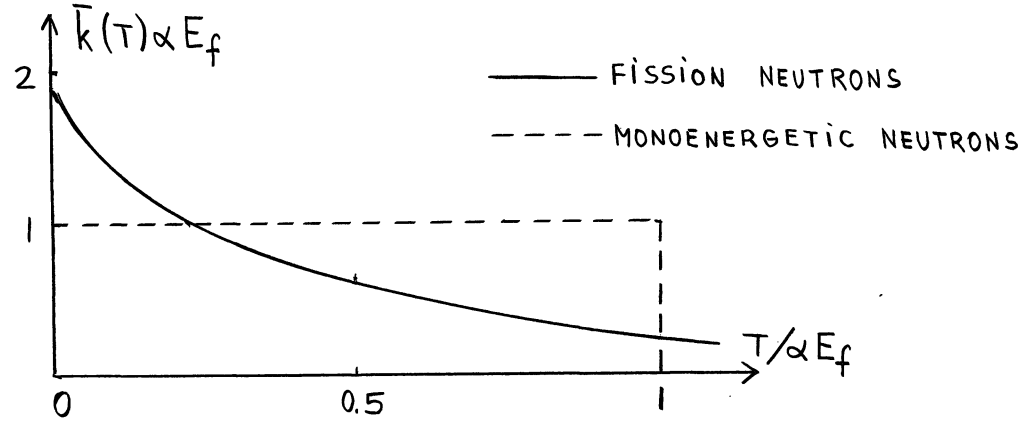

FIG. 6.

COMPARISON OF $\bar{k}$ FOR FISSION SPECTRUM NEUTRONS AND MONOENERGETIC NEUTRONS

A comparison of equation (3.11) and equation (3.13) for the case of $E_f' = E_f$ is made in FIG. 6. Wether it is permissible to use monoenergetic neutrons instead of the fission spectrum for rough estimates of radiation effects produced by neutrons depends on the effect one is looking for. If the radiation effect of interest depends only on the total amount of energy deposited one can answer the question by comparing the average primary energy produced per interaction.

$$\bar{T} = \int \bar{k}(T)\, T\, dT \qquad (3.14)$$

a.) Fission spectrum, energy independent isotropic scattering

$$\bar{T} = \int P(E) \int_0^{T_{max}} k(E,T)\, T\, dT\, dE = \int P(E) \frac{\alpha E}{2}\, dE = \frac{\alpha}{2} \bar{E} \qquad (3.15)$$

b.) Monoenergetic neutrons of energy E_f , energy independent isotropic scattering

$$\bar{T} = \frac{\alpha E_f'}{2} \qquad (3.16)$$

One may, therefore replace the fission spectrum by monoenergetic neutrons of energy $E_f' = \bar{E} = \frac{3}{2} E_f$.

We will in the future refer to monoenergetic neutrons of an appropriate energy E_f' as "fission neutrons".

3. Reactor Neutrons

Here we are mainly interested in that part of the neutron spectrum in a nuclear reactor which has an energy distribution proportional to $\frac{1}{E}$.

$$\varphi(E) = \frac{\text{const.}}{E} \qquad (3.17)$$

The value of the proportionality constant is of no consequence since it drops out in the averages which we have to perform.

Usually the neutron spectrum in a moderator in a reactor contains also a fission spectrum part. It can be shown, however, that this is small for a graphite moderator. We shall therefore accept $\varphi(E)$ of equation (3.17) as representative for moderated neutrons.

Applying again equation (1.17) under the assumption of isotropic energy independent scattering, we obtain

$$\bar{k}(T) = \frac{\int_{T/\alpha}^{E_f} \varphi(E)\, k(E,T)\, dE}{\int_{E_{th}}^{E_f} \varphi(E)\, dE} = \frac{1}{\alpha} \cdot \frac{\int_{T/\alpha}^{E_f} \frac{dE}{E^2}}{\int_{E_{th}}^{E_f} \frac{dE}{E}}$$

The lower limit of the integral in the numerator must correspond to the lowest energy E which can produce primaries of energy T, i.e. $E_{min} = T/\alpha$ as long as $T \geq E_{th}$. For $T \leq \alpha E_{th}$ one must take E_{th} as the lower limit.

The result of the integration is

$$\bar{k}(T) = \frac{1}{\ln (E_f/E_{th})} \left(\frac{1}{T} - \frac{1}{T_{max}} \right) \quad \text{for } \alpha E_{th} \leq T \leq T_{max} \tag{3.18}$$

Whereas for fission neutrons $T_{max} \gg E_d$, so that the displacement cross sections are approximately the same as the total cross sections, this is no longer true for reactor neutrons. For isotropic scattering and energy independent σ, we have

$$\sigma_d = \sigma_0 \left(1 - \frac{E_d}{\alpha E} \right) \tag{3.19}$$

This means that σ_d is a function of E. With that we obtain for $\bar{\sigma}_d$

$$\bar{\sigma}_d = \frac{\int_{E_d/\alpha}^{E_f} \sigma_d(E)\frac{1}{E}\,dE}{\int_{E_d/\alpha}^{E_f} \frac{1}{E}\,dE} = \sigma_0 \frac{\ln(\alpha E_f/E_d) - 1 + E_d/\alpha E_f}{\ln(\alpha E_f/E_d)}$$

and with $1 = \ln e$

$$\bar{\sigma}_d = \sigma_0 \frac{\ln(\alpha E_f/e E_d) + E_d/\alpha E_f}{\ln(\alpha E_f/E_d)} \tag{3.20}$$

In a similar manner we obtain

$$\bar{k}_d(T) = \frac{\frac{1}{T} - \frac{1}{T_{max}}}{\ln(T_{max}/e E_d) + E_d/T_{max}} \tag{3.21}$$

Comparing this with $\bar{k}(T)$ for fission neutrons we notice, that there the final energies T were approximately uniformly distributed, whereas here the distribution behaves roughly like $1/T$, i.e. the low primary energies are dominating the distribution. This becomes also apparent, when we compute the average primary energy

$$\bar{T}_d = \int_{E_d}^{T_{max}} \bar{k}_d(T)\, T\, dT = \frac{T_{max}}{\ln(T_{max}/E_d)} \tag{3.22}$$

For $E_f \approx 1.5$ Mev, $E_d = 25$ ev and $A = 60$ (copper) we get $\ln(T_{max}/E_d) \approx 8$, that is $\bar{T}_d$ is approximately four times smaller for reactor neutrons than for fission neutrons.

In the following sections we shall discuss various aspects of the interaction of charged particles.

4. The Differential Cross Section for Free Charged Particles

From equation (2.17) we get

$$K(T) = \frac{\pi R^2}{4} T_{max} \frac{1}{T^2} \tag{2.17}$$

with

$$R = \frac{Z_1 Z_2 e^2}{E_{rel}} \qquad \text{and} \qquad T_{max} = \alpha E_{lab}$$

This expression may also be written

$$K(T) = \frac{2\pi Z_1^2 Z_2^2 e^4}{M_2 v_1^2} \cdot \frac{1}{T^2} \tag{3.23}$$

The relativistic generalization of it is $(\text{for } T \ll T_{max})$

$$K(T) = \frac{2\pi Z_1^2 Z_2^2 e^4 (E + M_1 c^2)}{M_2 c^2 E (E + 2 M_1 c^2)} \cdot \frac{1}{T^2} \tag{3.24}$$

For the scattering of energetic electrons from nuclei, $(M_1 = M_{el} \ll M_2 \,;\, T_{max} \ll E)$ one must include some correction factors in the above equation. If we let $\tau = T/T_{max}$ we obtain the following expression for the differential cross section:

$$K(\tau) = \pi \left\{ \frac{Z_2 e^2 (E + M_{el} c^2)}{E(E + 2 M_{el} c^2)} \right\} \frac{1}{\tau^2} \left\{ 1 - \frac{v_{el}^2}{c^2} \tau - \pi Z_2 \frac{e^2}{\hbar c} \frac{v_{el}}{c} (\sqrt{\tau} - \tau) \right\} \tag{3.25}$$

5. Primary Distributions of Atomic Nuclei for Incident Heavy Charged Particles

For transferred energies T which are greater than E_d, the interaction may be regarded as one between free particles. We may therefore directly use equation (2.17) for the differential interaction cross section.

$$K(T) = \frac{\pi R^2}{4} \cdot \frac{T_{max}}{T^2}$$

From this the displacement cross section may be obtained by

$$\sigma_d = \int_{E_d}^{T_{max}} K(E,T)\, dT = \frac{\pi R^2}{4}\left(\frac{T_{max}}{E_d} - 1\right) \tag{3.26}$$

For $T_{max} \gg E_d$, this becomes

$$\sigma_d \cong \frac{\pi R^2}{4} \cdot \frac{T_{max}}{E_d} \tag{3.27}$$

We assume here and in the following a monoenergetic incident radiation and also samples which are thin enough, so that intensity and energy of the incident radiation do not change appreciably over the thickness of the sample.

Example for Cu

For 10 Mev deuterons as incident radiation one obtains

$$\sigma_d = .7 \times 10^{-20}\ cm^2$$

$$\lambda_d = \frac{1}{N_A \sigma_d} = 1.7 \times 10^{-3}\ cm$$

The displacement cross section is much larger than that for neutrons, whereas the mean free path is quite small but still about five orders of magnitude larger than the lattice constants.

The average energy transfer is obtained from

$$\overline{T}_d = \frac{1}{\sigma_d} \int_{E_d}^{T_{max}} K(E,T)\, T\, dT = E_d \ln \frac{T_{max}}{E_d} \tag{3.28}$$

This is much smaller than for neutrons. There $\overline{T}_d$ was of the order of T_{max}, whereas here it is of the order of E_d.

The energy distribution of the primaries is obtained by

$$\overline{k}(T) = \frac{K(T)}{\sigma_d} = \frac{T_{max}\, E_d}{T_{max} - E_d} \cdot \frac{1}{T^2} \cong \frac{E_d}{T^2} \tag{3.29}$$

(The approximation holds for $T_{max} \gg E_d$.)

6. Comparison of the Primary Distributions for Heavy Particles

Most instructive for the graphical comparison of the primary distributions for fission neutrons, reactor neutrons, and heavy charged particles is a plot of

$f(T) \equiv$ fraction of primaries with energies less than T.

Obviously,

$$f(T) = \int_{E_d}^{T} k_d(T')\, dT' \tag{3.30}$$

This function is plotted for the three heavy particle radiations discussed in Figure 7.

The computation of these curves was done for 1.5 Mev protons, 1.5 Mev fission neutrons, and reactor neutrons with $E_f = 1.5$ Mev. The target material is copper and E_d was assumed to be 25 ev.

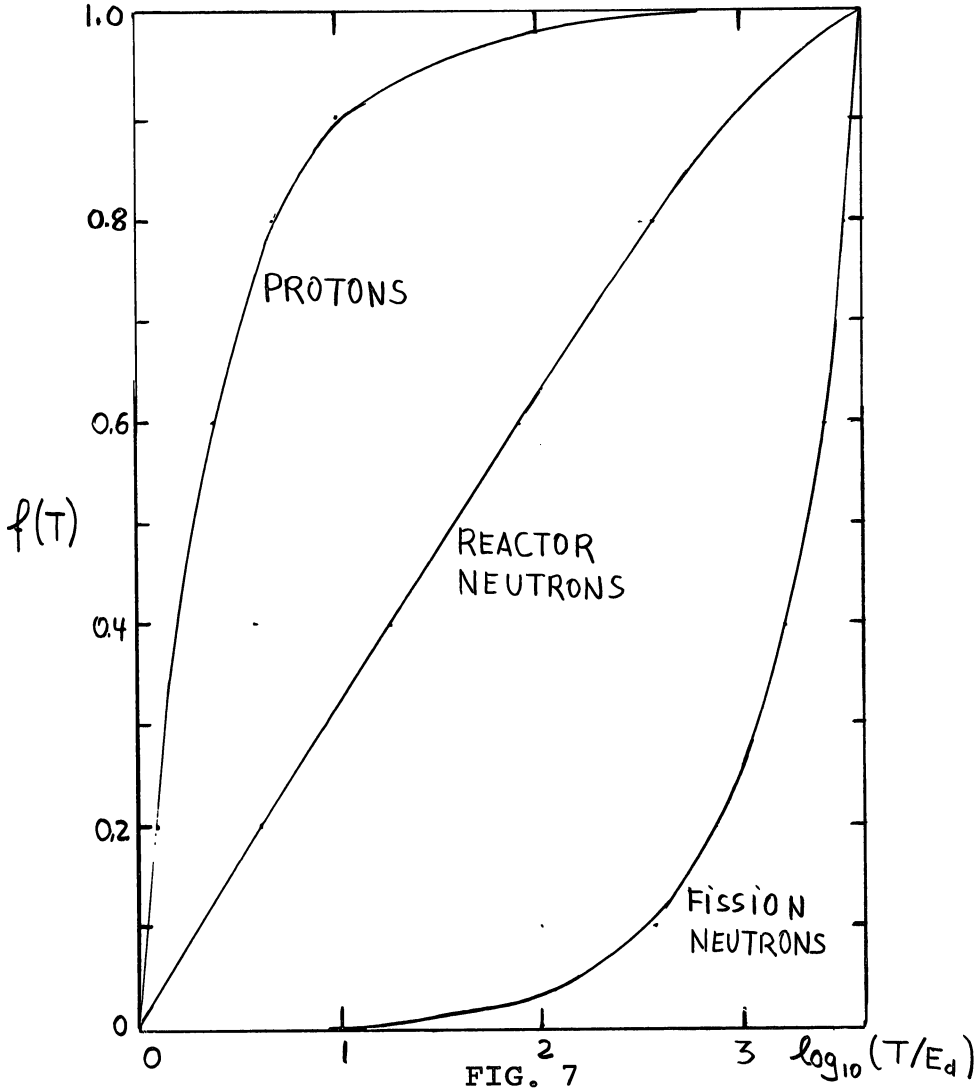

FIG. 7

COMPARISON OF THE FRACTION OF PRIMARIES WITH ENERGY LESS THAN T FOR HEAVY PARTICLE RADIATIONS OF COMPARABLE ENERGY.

The interesting parameters of the different heavy particle radiations, $\overline{k_d}(T)$, $\overline{T}$ and f(T) have been compiled in Table 1.

TABLE I

RADIATION	$k_d(T)$	$\bar{T} = \int_{E_d}^{T_{max}} T\, k_d(T)\, dT$	$f(T) = \int_{E_d}^{T} k_d(T')\, dT'$
CHARGED PARTICLES	$\frac{T_{max}}{T_{max} - E_d}\frac{E_d}{T^2}, \frac{1}{T^2} \cong \frac{E_d}{T^2}$	$\cong E_d \ln \frac{T_{max}}{E_d}$	$\cong 1 - \frac{E_d}{T}$
REACTOR NEUTRONS	$\frac{\frac{1}{T} - \frac{1}{T_{max}}}{\ln \frac{T_{max}}{eE_d} + \frac{E_d}{T_{max}}} \cong \frac{\frac{1}{T} - \frac{1}{T_{max}}}{\ln \frac{T_{max}}{eE_d}}$	$\cong \frac{1}{2}\frac{T_{max}}{\ln \frac{T_{max}}{eE_d}}$	$\ln \frac{T}{E_d} - \frac{T - E_d}{T_{max}} \cong \frac{}{\ln \frac{T_{max}}{eE_d}}$
FISSION NEUTRONS	$\frac{1}{T_{max} - E_d} \cong \frac{1}{T_{max}}$	$\cong \frac{T_{max}}{2}$	$\cong \frac{T - E_d}{T_{max}}$

7. Primary Distributions of Atomic Nuclei for Incident Electrons

Electrons as incident radiation are of particular interest for the following reason. The energy distributions of the primaries in radiation effects experiments are usually rather wide, so that it is difficult to produce primaries with a well defined energy. This is feasible only for transferred energies for which $T_{max} \gtrapprox E_d$. To achieve T_{max} of this magnitude ($\gtrapprox$ 25ev), the initial energies of heavy particles would have to be in the order of 1000 ev. Neutrons of this energy are quite difficult to separate in sufficient quantity; heavy charged particles have total ranges which make them useless for radiation effects experiments. Electrons, on the other hand, have energies of a few Mev and ranges in the order of mm in dense material. They are, therefore, quite useful for the determination of threshold energies. Figure 8 shows T_{max} as a function of electron energy for a number of materials.

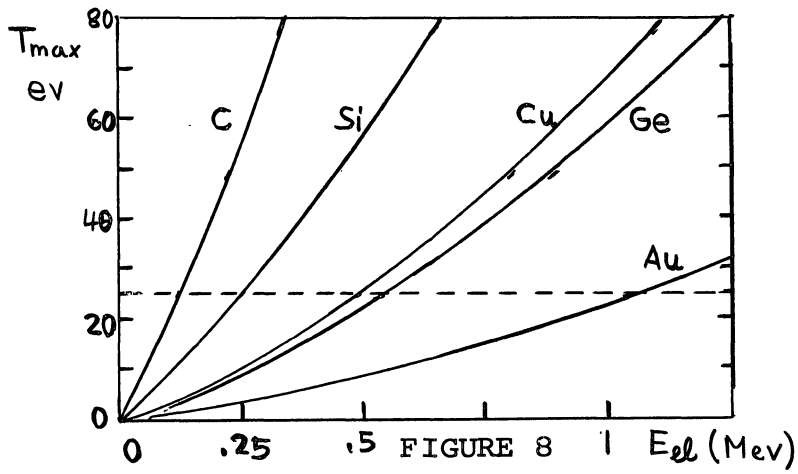

FIGURE 8

T_{max} AS A FUNCTION OF E_{el} FOR VARIOUS SOLIDS

The distribution of primaries for energetic electrons can be taken directly from Equation (3.25). For the displacement cross section one obtains

$$\sigma_d(E) = \pi \left\{ \frac{Z_2 e^2 (E + M_{el}c^2)^2}{E^2(E + 2M_{el}c^2)} \right\} \left\{ \frac{T_{max}}{E_d} - 1 - \frac{v_{el}^2}{c^2} \ln \frac{T_{max}}{E_d} + \right.$$

$$\left. + \pi Z_2 \frac{e^2}{\hbar c} \frac{v_{el}}{c} \left[2\sqrt{\frac{T_{max}}{E_d}} - 2 - \ln \frac{T_{max}}{E_d} \right] \right\} \quad (3.31)$$

For $M_{el}c^2 \ll E \ll \frac{1}{\alpha} M_{el}c^2 \cong \frac{M_2 c^2}{4}$ this reduces to

$$\sigma_d \cong 2\pi \frac{Z_2^2 e^4}{M_2 c^2 E_d} \quad (3.32)$$

The behavior of σ_d as a function of electron energy is shown for C, Ge, and Cu in Figure 9. The curve for C shows particularly well the flat portion corresponding to Equation (3.32).

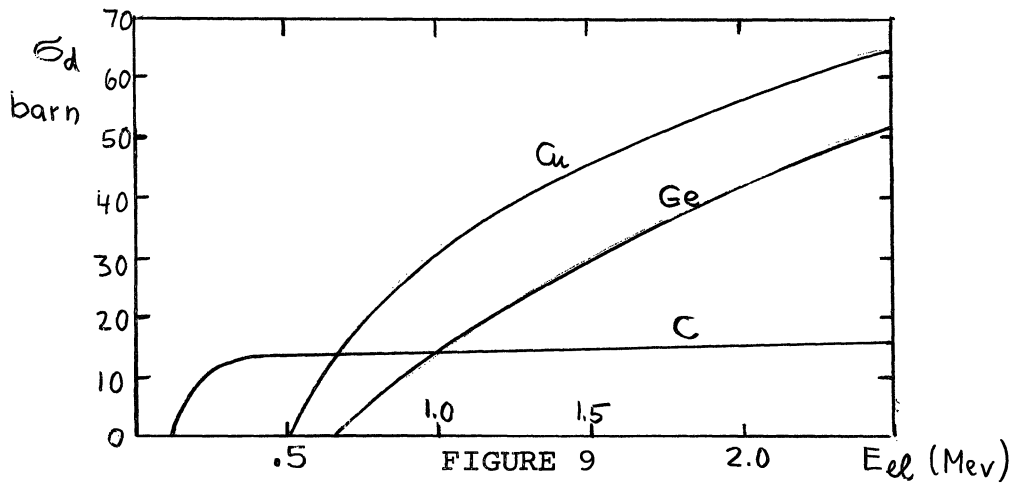

FIGURE 9

σ_d AS A FUNCTION OF E_{el} FOR VARIOUS SOLIDS

For Cu the energy independent σ_d value leads to $\lambda_d \cong 3$ mm. The results of some E_d determinations are shown in Table II.

TABLE II

EXPERIMENTAL VALUES FOR E_d FOR VARIOUS SOLIDS

Solid	Displacement Energy (ev)
Graphite	25
Silicon (minority carrier lifetime)	13
Germanium (resistivity)	31
Germanium (minority carrier lifetime)	13
Copper	25

8. Primary Distributions of Electrons for Incident Charged Particles; Ionization

Incident charged particles as well as energetic primaries may lose energy by ionization or excitation of electrons in the solid through which they move. The accurate description of these events is quite involved. We shall confine ourselves to the discussion of some rough estimates, which will not do more than point to the orders of magnitude of the interesting parameters.

We will represent the process for an incident heavy charged particle (or a partly ionized primary) by the collision of a moving charge $Z_1'e$ (where Z_1' represents the effective charge) and a bound electron with binding energy = ionization energy I. Let T_{max} be the maximum energy transferrable to the electron and let $T_{max} \gg I$. Then we can treat the collision as one between free particles, so that we may apply Equation (3.26) with E_d replaced by I to obtain the cross section for ionization.

$$\sigma_I = \frac{\pi R^2}{4}\left(\frac{T_{max}}{I} - 1\right) \cong \frac{\pi R^2 T_{max}}{4 I} \qquad (3.33)$$

Example for Cu

If we again consider 10 Mev deuterons incident on copper, we obtain $\sigma_I = 10^{-17}cm^2$, i.e. a cross section which is 10^3 times greater than the displacement cross section for the same case (see page 27). We have assumed I = 2 ev for the calculation. The corresponding mean free path would be $\lambda_I = 10^{-6}cm$ by assuming $N_I = N_A$, i.e. only one ionizable electron per atom.

We conclude that the energy loss and the range of charged particles in a solid is determined by ionization and electron excitation, as long as the particle energies are sufficiently large. To obtain more accurate results on the cross section for ionization, one has to consider that as the velocity of the moving particle increases both the effective charge on the moving particle and the number of ionizable electrons increases. The maximum ionization energy would be of the order $I_{max} = Z_2^2 I_H$ where I_H is the ionization energy of hydrogen. For the lower limit of I, one has to consider both ionization and excitation. For solid insulators, I_{min} is the distance between the valence band and the conduction band. For metals, the Fermi energy may be taken. For coarse approximations, one uses

$$I_{min} = 2 \text{ ev}.$$

One may now define a lower limit for ionization by saying: Only

particles which can transfer more than 2 ev onto an electron will lose energy by ionization. Below this limit, the energy loss will be exclusively by elastic collisions.

Using $T_{max} = \alpha E$, we find

$$E_{min} = \frac{I_{min}}{\alpha} = \frac{I_{min}}{\frac{4 M_{el} M_A}{(M_{el} + M_A)^2}} \cong \frac{I_{min} M_A}{4 M_{el}} \cong 500 A I_{min} \qquad (3.34)$$

and with $I_{min} = 2$ ev

$$E_{min} = A \text{ kev} \qquad (3.35)$$

where A is the mass number of the moving particle. For electrons as incident particles, one obtains with the same cross section as used in Equation (3.33) $\sigma_I \cong 10^{-21}$ cm^2 and $\lambda_I = 10^{-2}$ cm for $E_{el} = 1$ Mev and copper as the target material.

CHAPTER IV.

THE PRODUCTION OF FRENKEL PAIRS

The Frenkel pair, consisting of an interstitial atom and the vacant site from which the interstitial was removed, is the most elementary defect that is used in radiation effect theory. After their creation, the interstitial and the vacancy may each move on independently. In the first two sections we discuss the structure of these two defects.

1. The Structure of a Vacancy

The structure of a vacancy is quite simple. The lattice atoms around the vacancy relax somewhat, but only to the extent of a few percent of the lattice constants.

2. The Structure of Interstitials

It is much more difficult to find the correct structure of an interstitial. In the following, the problem will be discussed for the face centered cubic (fcc) lattice only.

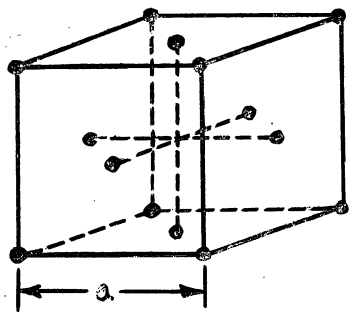

FIGURE 10

THE ELEMENTARY CELL OF THE FCC LATTICE

Figure 10 shows the elementary cell for the fcc lattice. Figure 11 shows three possible symmetric positions of an interstitial in that cell and gives their coordinates in terms of the lattice constant a.

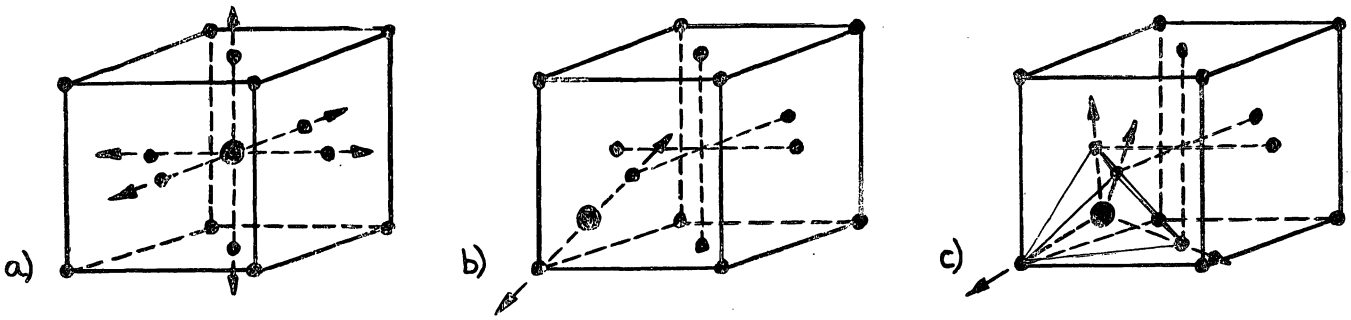

Center of Cube
½ (111)

Face Diagonal
½ (101)

Body Diagonal
¼ (111)

FIGURE 11

POSSIBLE SYMMETRIC POSITIONS OF THE INTERSTITIAL IN AN FCC LATTICE

Naively, one would assume that the position in the center of the cube (Figure 11.a) is the most likely one for an interstitial. It is symmetric and, therefore, free of forces. However, whether it is a stable or unstable position depends on whether the potential energy is a minimum or a maximum. The other two positions are also symmetric, but to a lesser degree.

In all these positions an interstitial has a fairly large space to occupy. One may express the space available by the distance D_n to the nearest neighbor in units of the lattice constant a.

a.) $D_n = \frac{a}{2}$

b.) $D_n = .815\ \frac{a}{2}$

c.) $D_n = .708\ \frac{a}{2}$.

Space may also be made available by putting two lattice atoms into one particular lattice position and letting them relax symmetrically. This is shown in Figure 12 for the face centered position at the interface of two basic lattice cells. The three configurations described in Figure 12 are often referred to as dumbbell positions.

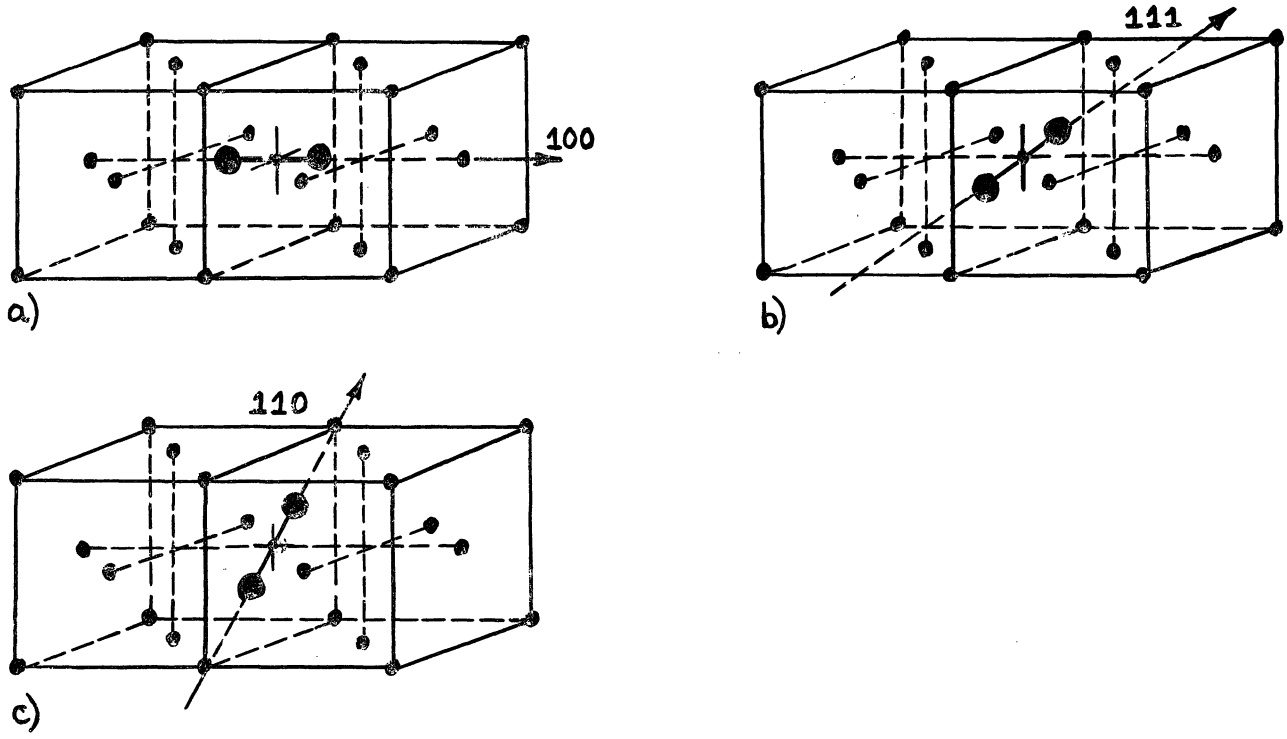

FIGURE 12

INTERSTITIALS IN DUMBBELL POSITIONS IN A FCC LATTICE

The actual configuration of an interstitial will depend on which one of the possibilities outlined above will have the lowest potential energy. The most thorough theoretical studies have been done on copper, for which the energies are given below:

$$D_{100} = 2.8 \text{ ev}$$
$$S_a \approx S_b = 3.4 \text{ ev}$$
$$D_{110} = 3.5 \text{ ev}$$
$$S_c = 3.6 \text{ ev}$$
$$D_{111} = 3.8 \text{ ev} \quad .$$

The symbols used here correspond to those used in Figures 11 and 12. The energy values represent the energy difference between an atom at the surface of the crystal and in one of the interstitial positions. According to this, only the D_{100} configuration is stable.

One way to differentiate between the S and D configurations may be the way they move through the lattice. One would expect:

Symmetric position - the interstitial itself diffuses;

Dumbbell position - the interstitial character is handed on from atom to atom, but these do not move much from their original position.

Conditions are different and more complicated for close Frenkel pairs. We will not go into this in detail.

3. The Displacement Energy E_d

In general, the amount of energy necessary to remove an atom from its regular lattice position and into an interstitial position will depend on the direction $\underline{e}$ in which the momentum is transferred onto the atom.

The threshold energy is dependent on direction:

$$E_d = E_d\ (\underline{e})$$

and when we can assume isotropic energy transfer, we will have

$$W_d(T) = \int_{T \geq E_d(\underline{e})} \frac{d\Omega}{4\pi} \tag{4.1}$$

where the integral is taken over all directions $\underline{e}$ for which $T \geq E_d(\underline{e})$. (In Section 8 of Chapter I, we have already defined $W_d(T)$ as the probability that a lattice atom with energy T will leave its lattice position.)

In principle, one should be able to measure $E_d(\underline{e})$ by using electron irradiation of a single crystal. But since the primary interaction is a Coulomb interaction, the differential cross section for momentum transfer perpendicular to the incident direction ($\theta_s = 90^\circ$) is much greater than that for momentum transfer in the beam direction ($\theta = 180^\circ$). Since the production of defects at $T_m = E_d$ will be quite small, we will have to make the incident energy somewhat larger. But then we may already have a considerable amount of energy transfer outside of the beam direction. The conditions are further complicated by the fact that the incident electrons will change their energy and direction through interaction in the interior of the sample.

For an isotropic distribution of the primary directions, we have according to Equation (1.11)

$$N_d(T) = N(T) W_d(T) \tag{1.11}$$

The number of Frenkel pairs produced is then

$$N_{FP} = \int N_d(T)\, dT \tag{4.2}$$

and in particular for a monoenergetic electron flux

$$N_{FP} = \int W_d(T) K(E,T)\, dT \cdot \varphi_E N_A t \tag{4.3}$$

If we can determine N_{Fp} experimentally, then it is also possible to find $W_d(T)$ by solving Equation (4.3) for this variable. In reality, this seems much too complicated and one proceeds by assuming a particular function $W_d(T)$ with free parameters which are then adjusted to fit the experimental values. The two simplest and, therefore, favorite functions are the following:

a. The Step Function

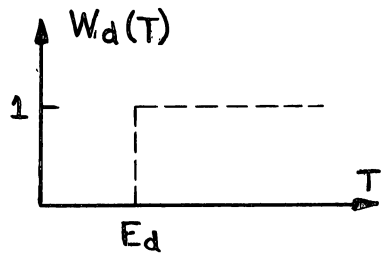

$$W_d(T) = \begin{cases} 0 & \text{for } T < E_d \\ 1 & \text{for } T \geq E_d \end{cases} \tag{4.4}$$

FIGURE 13

W_d AS A STEP FUNCTION

b. The Linear Threshold Function

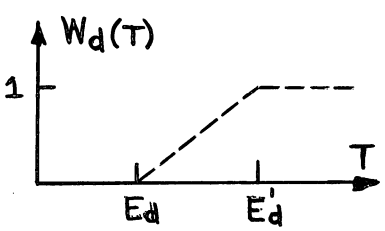

$$W_d(T) = \begin{cases} 0 & \text{for } T \leq E_d \\ \dfrac{T-E_d}{E_d'-E_d} & \text{for } E_d \leq T \leq E_d' \\ 1 & \text{for } E_d' \leq T \end{cases} \tag{4.5}$$

FIGURE 14

W_d AS A LINEAR THRESHOLD

Vineyard and coworkers have computed E_d values for various directions in the copper lattice. These are shown in Figure 15. This behavior could be described by a function according to Equation (4.5) with

$$E_d \cong 25 \text{ ev}$$

and

$$E_d' \cong 85 \text{ ev}.$$

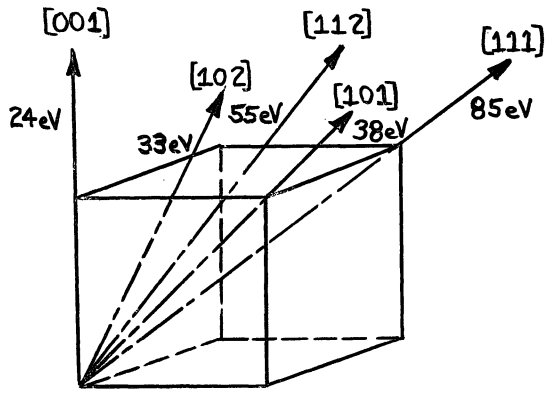

FIGURE 15

VALUES FOR E_d COMPUTED BY VINEYARD ET AL.

Phys. Rev. 120, 1229 (1960)

4. Models for the Displacement Process

We shall introduce models for the description of the collision process, in which a primary knock-on collides with another lattice atom. These models will help us to compute the number of Frenkel pairs produced by a primary of energy E. (NOTE: In the following, the kinetic energy of the incident primary will be represented by E, whereas the symbol T will be used for the energy transferred to a secondary, tertiary, etc. knock-on.)

Common to both models which are to be discussed is the assumption that between collisions the primary moves in a constant average lattice potential V_{ad}. A lattice atom may be bound to its lattice position by a spherically symmetric potential well of radius ℓ and depth E_{ad} (see Figure 16.a). The fact that a close Frenkel pair may be stable is taken care of by the introduction of an additive potential V_d, which has the form of a vertical wall of thickness $\delta\ell$. The height of this wall may be different in different directions. The two models are: the Kinchin and Pease model--this does not use a well, but just the potential wall which, by the way, does not act on the incident particle before collision; and the Seitz and Harrison model--this makes use only of the potential well without the walls. In the following discussion we assume complete symmetry and isotropy.

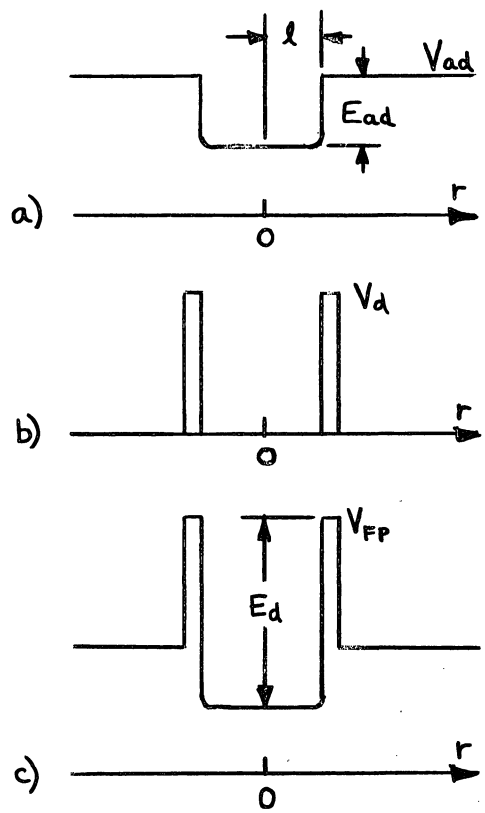

FIGURE 16

POTENTIALS FOR FRENKEL PAIR PRODUCTION

a. The Kinchin and Pease Model (KPM)

Conditions as assumed by this model are indicated in Figure 17.

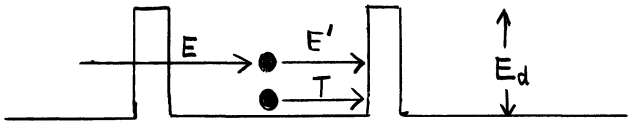

FIGURE 17

POTENTIAL OF THE KPM

The energy of the incident particle (E) is divided into two parts: that which remains with the incident particle after collision (E'), and that which is transferred to the seconary particle T. Depending on whether E' or T or both or none are greater than E_d, one can distinguish four different cases, which can also be read off the diagram in Figure 18 for a step function (Equation (4.4)) for $W_d(T)$.

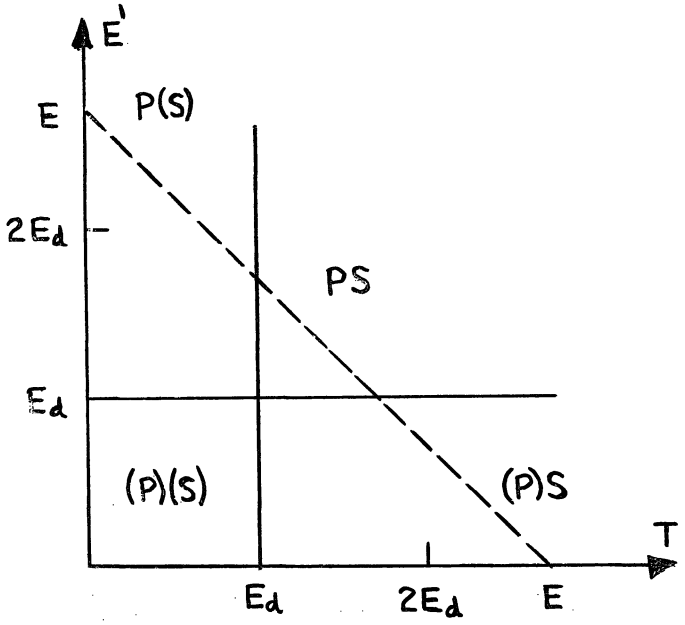

FIGURE 18

E', T-DIAGRAM FOR THE KPM

$$E',\ T \geq E_d$$

Both primary particle P and secondary particle S escape. A new Frenkel pair is created.

$$E' \geq E_d \geq T$$

P escapes, S remains. No new Frenkel pair is formed. Energy of P is reduced.

$$T \geq E_d \geq E'$$

Replacement collision, usually connected with a net loss in kinetic energy.

$$E',\ T \leq E_d$$

Both P and S remain in the same position. The line $E = E' + T$ is drawn in the diagram. Conservation of kinetic energy requires that E' and T must both lie on this line. It is obvious then that if $E \leq 2E_d$ no new Frenkel pairs may be created.

b. The Harrison-Seitz Model (HSM)

Figure 19 shows that in this model the incident particle makes the energy $E + E_d$ available for distribution among P and S.

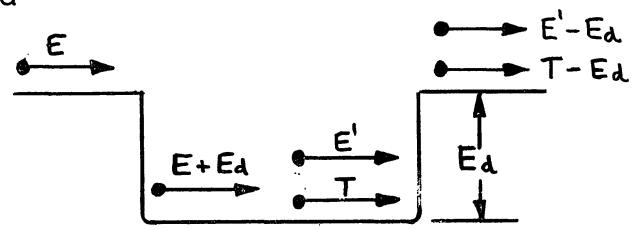

FIGURE 19

POTENTIAL OF THE HSM

However, both P and S need at least energy E_d to escape from the well. In contrast to the KPM, an incident particle with energy less than 2 E_d (but $E \geq E_d$) may create a new Frenkel pair. This may be seen from the fact that the line $E + E_d$ for $E \cong 1.4\ E_d$ drawn in Figure 20 runs through the area labelled PS.

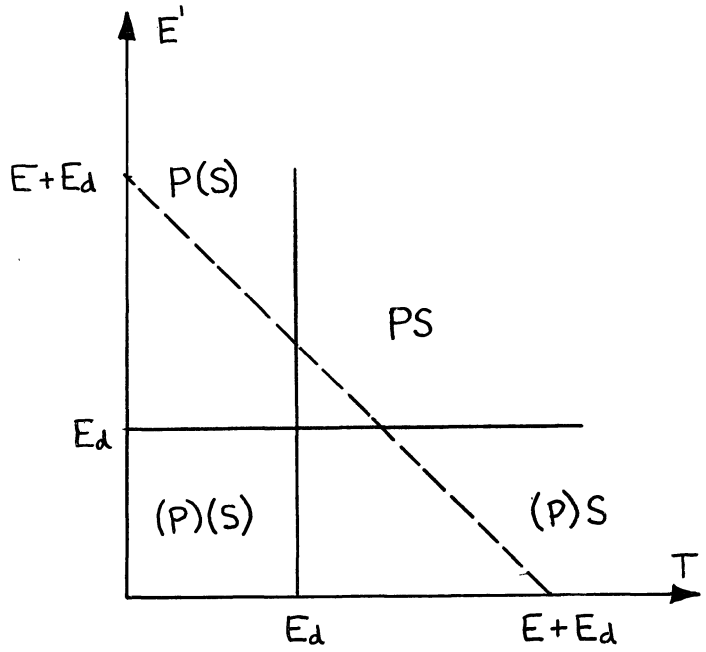

FIGURE 20

E', T-DIAGRAM FOR THE HSM

It will be shown below that the choice of the model for the displacement process does not have too great an influence on the results of computations of cascades of Frenkel pairs.

5. The Number of Frenkel Pairs in a Cascade

We introduce:

ν = number of Frenkel pairs in a cascade, which was started by a primary of energy E and which includes the primary.

$W_\nu(E)$ = probability that a cascade contains exactly ν Frenkel pairs.

ν is obviously a statistical number, and we shall have to try and determine its average or expectation value. For $E \gg E_d$ we can recognize the following limits for ν :

Upper limit: $\nu_{max} = E/E_d$

The primary particle transfers just the amount E_d in every collision. No energy is lost.

Lower limit: $\nu_{min} = 1$

The primary particle (which counts as one Frenkel pair) transfers energy in every collision which is just below the threshold energy. The lattice is heated but no additional displacements are produced.

We may further expect that the larger $\frac{E}{E_d}$, the narrower will be the distribution.

The expectation value for ν is

$$\bar{\nu}(E) = \sum_{\nu} \nu W_{\nu}(E) \tag{4.6}$$

We shall not derive a general expression for $\bar{\nu}(E)$, but we shall concentrate on one particular case--the Kinchin and Pease model with a step function for $W_d(E)$ and hard sphere scattering as the interaction process.

We start out with a primary of energy E. After its first collision, its energy is divided as

$$E = E' + T$$

according to the KPM. For hard sphere scattering interaction, the probability of the occurrence of particular energies E' or T is

$\frac{1}{E}$ for both. The average number of Frenkel pairs produced by the primary P is

$$\bar{\nu}_p(E) = \int_{E_d}^{E} \frac{1}{E} \bar{\nu}(E')\, dE' \tag{4.7}$$

The corresponding average for the secondary knock-on is

$$\bar{\nu}_s(E) = \int_{E_d}^{E} \frac{1}{E} \bar{\nu}(T)\, dT \tag{4.8}$$

Addition of these two equations results in an integral equation for $\bar{\nu}(E)$ (E' and T under the integral are just dummy variables and may now both be called E", for instance)

$$\bar{\nu}_p(E) + \bar{\nu}_s(E) = \bar{\nu}(E) = \frac{2}{E} \int_{E_d}^{E} \bar{\nu}(E'')\, dE'' \tag{4.9}$$

Solution:

Multiply with E and differentiate with respect to E:

$$\frac{d}{dE}\left(\bar{\nu}(E) \cdot E\right) = 2 \frac{d}{dE} \int_{E_d}^{E} \bar{\nu}(E'')\, dE''$$

$$\frac{d\bar{\nu}}{dE} \cdot E + \bar{\nu}(E) \frac{dE}{dE} = 2\bar{\nu}(E)$$

$$\frac{d\bar{\nu}}{\bar{\nu}} = \frac{dE}{E}$$

$$\ln \bar{\nu} = \ln E + C'$$

$$\bar{\nu} = C'' E \tag{4.10}$$

We obtain a linear relation. C" must be determined by the expected behavior at low values for E. For the KPM with a step function we have:

$$W_\nu(E) = \delta_{\nu 0} \quad \text{for } E \leq E_d$$
$$W_\nu(E) = \delta_{\nu 1} \quad \text{for } E_d \leq E \leq 2E_d$$

since only <u>one</u> Frenkel pair can be produced for $E_d \leq E \leq 2E_d$. Therefore,

$$\bar{\nu} = 0 \text{ for } E \leq E_d \qquad \text{(a)}$$

$$\bar{\nu} = 1 \text{ for } E_d \leq E \leq 2E_d \qquad \text{(b)} \qquad (4.11)$$

Applying this to equation (4.10), we obtain $C" = \frac{1}{2E_d}$ so that

$$\bar{\nu} = \frac{E}{2E_d} \quad \text{for } E \geq 2E_d \qquad \text{(c)} \qquad (4.11)$$

6. <u>Influence of Various Models on the Number $\bar{\nu}$.</u>

We repeat, that the result for $\bar{\nu}(E)$ given in equation (4.11. a,b and c) was obtained by a combination of three different models:

a) The hard sphere approximation for the interaction process

b) A step function for $W_d(E)$

c) The Kinchin and Pease model for the displacement process

We shall now replace these models separately by different models to observe the influence that such modifications may have. Before we

do this, we will introduce the reduced value for $\bar{\nu}(E)$. This reduced value is $\tilde{\nu}(E)$. It has the property, that $\bar{\nu}(E)$ can be obtained from $\tilde{\nu}(E)$ by multiplication with $W_d(E)$:

$$\bar{\nu}(E) = W_d(E)\,\tilde{\nu}(E) \tag{4.12}$$

$\tilde{\nu}(E)$ then has the advantage of better allowing a comparison between different models for $W_d(E)$ and for the displacement process without interference from the actual value of $W_d(E)$ at low energies.

a) Deviation from the Hard Sphere Approximation

Fig. 21 shows the result of a machine calculation by Brown and Goedecke [J.Appl.Phys. 31, 932, (1960)].

They used a Yukawa-potential instead of the hard sphere potential

$$V(r) = \frac{Z_1 Z_2 e^2}{r}\, e^{-r/a} \tag{4.13}$$

$$a = a_H \Big/ \sqrt{Z_1^{2/3} + Z_2^{2/3}} \tag{4.14}$$

a_H = radius of the hydrogen atom

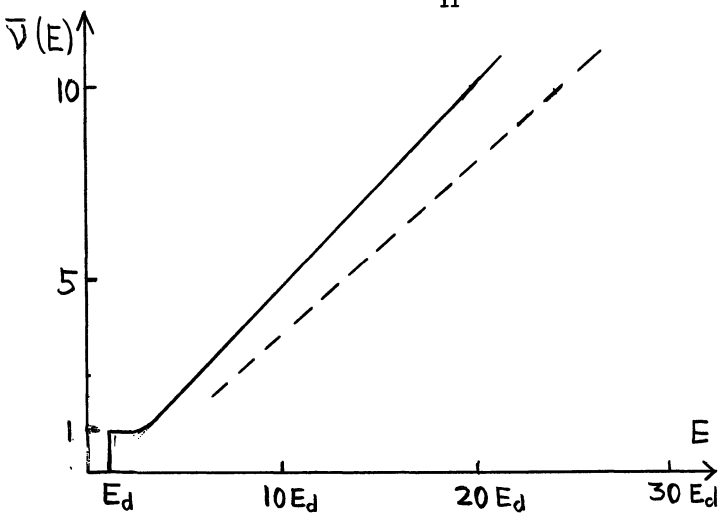

FIG. 21 COMPARISON OF $\bar{\nu}(E)$ FOR Cu FOR TWO DIFFERENT POTENTIALS WITH $W_d(E)$ A STEPFUNCTION AND USING THE KPM.

b) Deviation from the Step Function

Fig. 22 shows the result on $\tilde{\nu}(E)$ of replacing the step function for $W_d(E)$ by a linear function between E_d and E_d'.

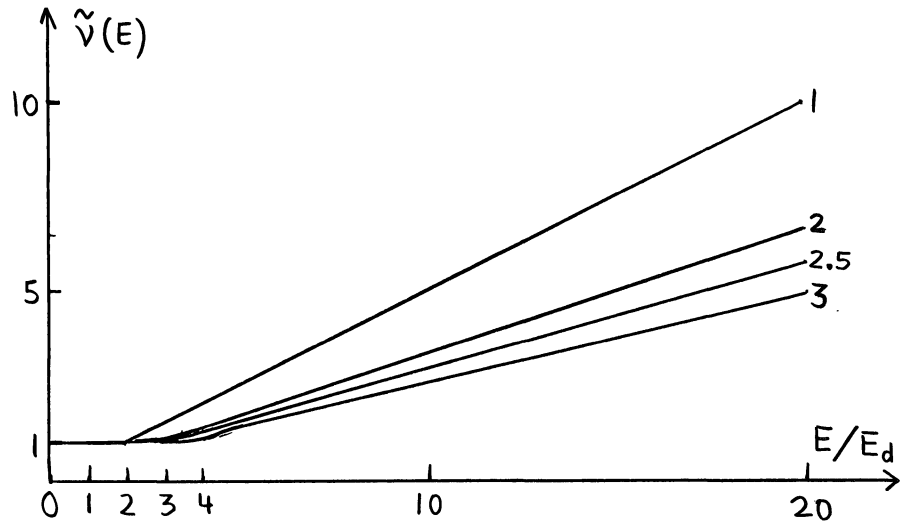

Fig. 22 $\tilde{\nu}(E)$ FOR A LINEAR INCREASE OF $W_d(E)$ BETWEEN E_d AND E_d' FOR VARIOUS VALUES OF E_d'/E_d.

It is obvious, that $\tilde{\nu}(E)$ decreases as E_d increases. For higher energies ($E \geq 2\ E_d'$) one can express $\tilde{\nu}(E)$ as

$$\tilde{\nu}(E) = \bar{\nu}(E) = C\,\frac{E}{2E_d} \qquad (4.15)$$

where C decreases as E_d' increases. One can look at E_d/C as an effective threshold energy and compare the effect of a step function at E_d/C with that of a linear increase between E_d and E_d'. This has been done in Fig. 23, where a third possibility, a double step function has also been included. Again, the influence of the various $W_d(E)$ is seen to be very small.

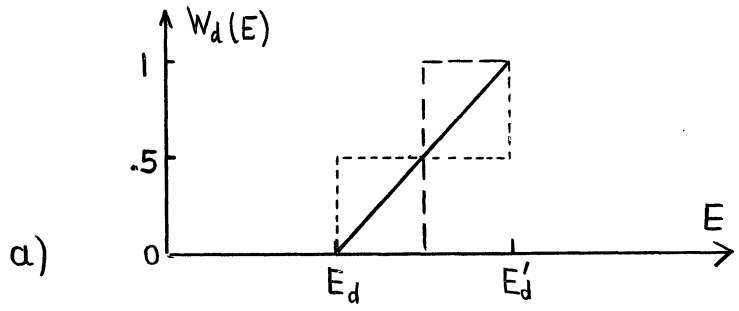

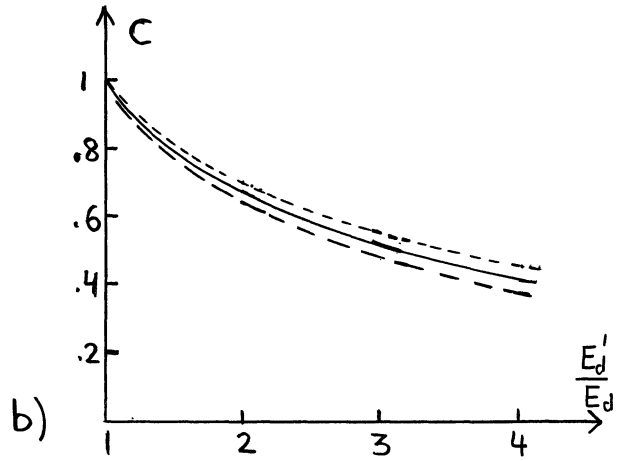

FIG. 23 a) VARIOUS POSSIBILITIES FOR $W_d(E)$

b) THE CORRESPONDING VALUES OF THE CONSTANT C.

c.) Deviation from the Kinchin and Pease Model

Here we compare $\tilde{\nu}(E)$ according to the KPM with that obtained by using the Harrison/Seitz Model:

KPM
$$\tilde{\nu}(E) = \begin{cases} 1 & E \leq 2\ E_d \\ E/2\ E_d & 2\ E_d \quad E \end{cases} \tag{4.16}$$

HSM
$$\tilde{\nu}(E) = \begin{cases} 1 & E \leq E_d \\ \frac{1}{2} + \frac{E}{2E_d} & E_d \leq E \end{cases} \tag{4.17}$$

The two different functions $\tilde{\nu}$ are shown in Fig. 24

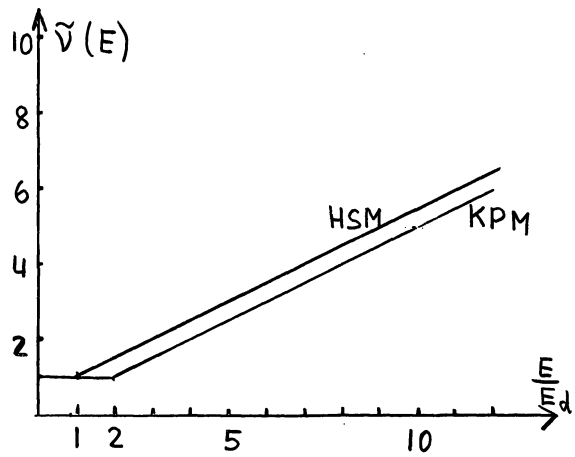

Fig. 24 $\tilde{\nu}(E)$ FOR THE KPM AND THE HSM.

Though the functions $\tilde{\nu}(E)$ differ somewhat for the two models, the results for $\bar{\nu}(E)$ are identically the same. This comes from the fact, that to obtain $\bar{\nu}(E)$ for the HSM, we must use $\tilde{\nu}(E-E_d)$, due to the fact, that a particle in that model loses energy to the amount of E_d to get out of the potential well.

$$\bar{\nu}(E) = W_d(E)\,\tilde{\nu}(E-E_d) \tag{4.18}$$

is therefore the same as $\bar{\nu}(E)$ for the KPM.

7. The Influence of Ionization

In Ch.III, equation (3.35), we introduced $E_1 \approx A$ keV as a very rough limit of energies below which energy transfer from a moving atom is mainly by elastic collision with other atoms, whereas above the limit the energy loss of the atom is due almost entirely by ionization. If we adopt this limit as valid, we can take account of ionization losses very simply by stating in place of (4.11.c)

for instance:

$$\bar{\nu}(E) = \begin{cases} \dfrac{E}{2E_d} & E \leq E_I \\ \dfrac{E_I}{2E_d} & E_I \leq E \end{cases} \tag{4.19}$$

Under the assumption that the mass of the incident radiation is 1 amu and that it is small compared to the mass number A of the target material, we can represent T_{max} by $4E/A$ where E is the energy of the incident radiation. By plotting this along with $E_I \cong A(kev)$, we can see at which mass numbers for the target material ionization as energy loss becomes important. Figure 25 shows this for E = 1.5 Mev. We see that it is only for fairly low mass numbers that ionization occurs at these incident energies.

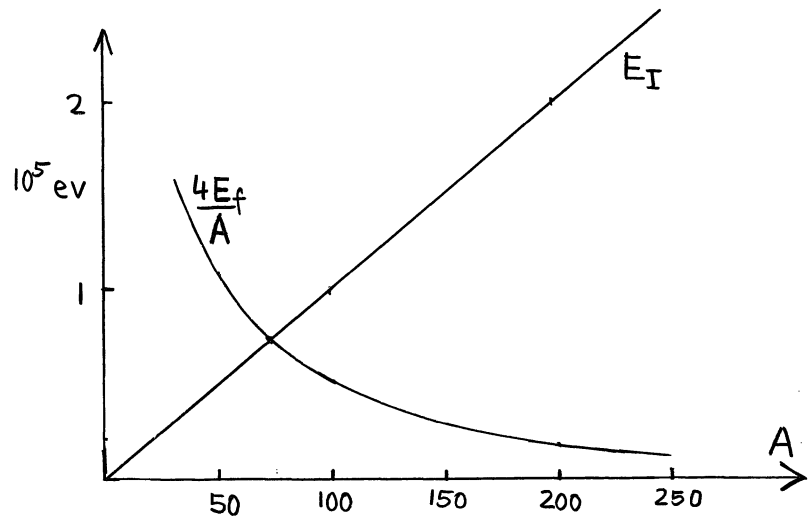

FIGURE 25

E_I = A kev AND T_{max} FOR INCIDENT PARTICLES OF MASS NUMBER 1 AND ENERGY E (=1.5 Mev)

Since for incident charged particles the average primary energy is far below T_{max}, we do not have to worry too much about ionization there, whereas for neutrons ionization becomes more important.

Topics which had to be left out because of the lack of time were: 1) $\bar{\nu}(E)$ for small energies, where the assumed linearity of $\bar{\nu}$ is no longer true; 2) replacement collisions; and 3) displacements in polyatomic solids.

CHAPTER V.

INTERACTION AND RANGE OF THE PRIMARIES

1. The Interaction Potential

The determination of the proper interaction potential to describe the collision of two atoms is a difficult problem. At the relative energies with which we are concerned here, one usually assumes that the electrons all move with the nucleus, i.e. that there is no ionization. This is referred to as the "adiabatic approximation." The collision takes place, therefore, between two nuclei, the charges of which are screened by the surrounding electrons.

N. Bohr proposed the use of the "Yukawa potential" for the description of such interactions (see Equations (4.13) and (4.14)):

$$V(r) = \frac{Z_1 Z_2 e^2}{r} e^{-r/a} \tag{5.1}$$

with

$$a = \frac{a_H}{Z_2^{1/3}} \qquad \text{for the collision of a point charge } Z_1 e \text{ with a neutral atom of atomic number } Z_2 \tag{5.2}$$

$$a = \frac{a_H}{\sqrt{Z_1^{2/3} + Z_2^{2/3}}} \qquad \text{for the collision of two neutral atoms of atomic number } Z_1 \text{ and } Z_2 \tag{5.3}$$

Obviously, the a-value of Equation (5.3) is appropriate for us and since $Z_1 = Z_2$ we obtain $a = \frac{a_H}{\sqrt{2}\, Z^{1/3}}$. The range of validity of

the Bohr potential (Equation (5.1)) seems to be confined to small distances, $r \leq a$.

For larger distances, where the screening of the nuclear charge by the electrons is even more complete, Born and Mayer proposed a purely exponential potential:

$$V(r) = A\, e^{-r/a} \tag{5.4}$$

The a-value here is usually a different one than that used in the Bohr potential. We give here values of the parameters for both potentials, which have been adjusted to fit experimental data for Cu.

Bohr: $a_B = \frac{D}{21}$ $\quad D = 2.55$ Å

Born-Mayer: $a_{BM} = \frac{D}{13}$ $\quad A_{BM} = 2.2 \times 10^4$ ev

The Born-Mayer potential is thought to be valid up to the equilibrium distance between lattice atoms.

There is a large variety of approaches to the problem of determining the range of primary knock-ons and, thereby, of determining the spatial extent of the damage produced by one primary. In this chapter we shall confine ourselves to: 1) the description of an experiment to determine the ranges of primaries in various materials, and 2) the brief sketching of a theoretical calculation of these ranges.

2. An Experimental Determination of Primary Ranges
(R. A. Schmitt and R. A. Sharp, Phys. Rev. Letters, 1, 445 (1958).)

In this experiment foils of various interesting materials were sandwiched between aluminum catcher foils and then irradiated with 24 Mev Bremsstrahlung from a betatron. The high energy photons produce (γ,n) reactions. Upon emission of the neutron, the residual nucleus receives recoil momentum (and energy). The kinetic energy of the emitted neutrons was determined for Cu and Pb to be 1.5 Mev with a distribution of 2 Mev full width at half maximum. It was assumed that the neutrons emitted from the other substances would have the same energy.

The recoiling residual nuclei are radioactive due to the loss of one neutron. They can, therefore, be detected at the end of their range by measuring the radioactivity of the sample foil and the catcher foils. The range of the recoils is determined from the ratio of these activities. Figure 26 indicates how we shall describe the problem for the following analysis.

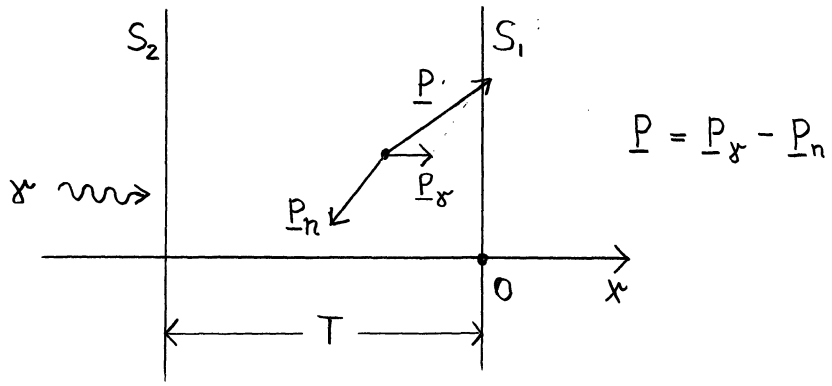

FIGURE 26

SCHEMATIC OF THE EXPERIMENT FOR THE DETERMINATION OF PRIMARY RANGES

We introduce:

$W_e^{(1)}(x)$	probability that a particle originating at x will escape through the surface S_1.
$W_e^{(2)}(x)$	correspondingly for surface S_2.
$N_e^{(1)}$	number of particles escaping through S_1 if $n_\gamma dx$ is the number of (γ,n) processes in the layer dx of the foil.
$N_e^{(2)}$	correspondingly for S_2.

We then have:

$$N_e^{(1)} = \int_{-T}^{0} W_e^{(1)}(x)\, n_\gamma\, dx \cong \int_{-\infty}^{0} W_e^{(1)}(x)\, n_\gamma\, dx \tag{5.5}$$

The second integral assumes that T is so large that $W_e^{(1)}(-T)$ is negligibly small.

Similarly,

$$N_e^{(2)} = \int_{-T}^{0} W_e^{(2)}(x)\, n_\gamma\, dx \cong \int_{-T}^{\infty} W_e^{(2)}(x)\, n_\gamma\, dx \tag{5.6}$$

Define

$N \equiv$ total number of primaries created

$$N = \int_{0}^{T} n_\gamma\, dx = n_\gamma T \tag{5.7}$$

The ratio of activities in the catcher foils over the total activity is then

$$\frac{N_e}{N} = \frac{-\int_{-\infty}^{0} W_e^{(1)}(x) n_\gamma dx + \int_{-T}^{\infty} W_e^{(2)}(x) n_\gamma dx}{n_\gamma T} = \frac{-\int_{-\infty}^{0} W_e^{(1)}(x)\, dx + \int_{-T}^{\infty} W_e^{(2)}(x) dx}{T} \qquad (5.8)$$

Evidently we assumed that the production of radioactive nuclei is uniform across the thickness T of the foil

The problem is now reduced to the determination of the $W_e(X)$. We make here a very rough approximation: The primary particle travels along a straight line path ϱ before coming to rest. The distances ϱ are distributed according to $g(\varrho,E)d\varrho$ where E is the initial particle energy. The initial direction of the particle is described by the unit vector $\underline{e}$. The distribution of initial directions and energies shall be $f(\underline{e},E)d\Omega dE$. With the help of the distribution functions just introduced and with some reference to Figure 27, we can now write down expressions for the $W_e(x)$.

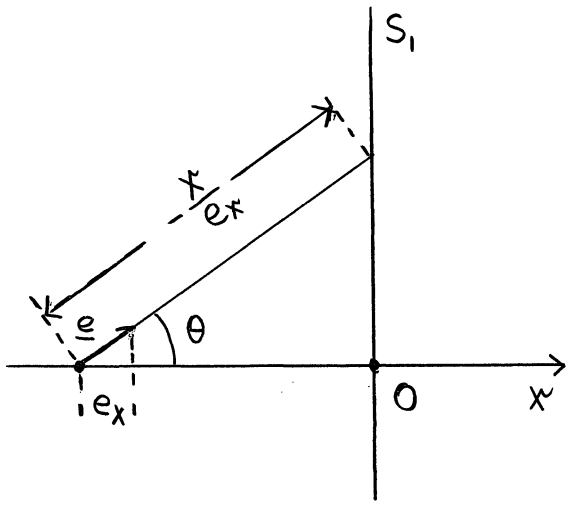

FIGURE 27

$$W_e^{(1)}(x) = \int_{e_x \geq 0} dE\, d\Omega\, f(E,\underline{e}) \left\{ \int_{-x/e_x}^{-\infty} g(\varrho,E)\, d\varrho \right\}$$

$$\int_{-\infty}^{0} W_e^{(1)}(x)\, dx = \int_{e_x \geq 0} dE\, d\Omega\, f(E,\underline{e}) \left\{ \int_0^{\infty} dx \int_{x/e_x}^{\infty} g(\varrho,E)\, d\varrho \right\} \tag{5.9}$$

Evaluation of the integral over x results in

$$\int_0^{\infty} dx \int_{x/e_x}^{\infty} g(\varrho,E)\, d\varrho = e_x \int_0^{\infty} \varrho\, g(\varrho,E)\, d\varrho \tag{5.10}$$

We introduce here

$$\text{Range} \qquad \bar{\varrho}(E) = \int_0^{\infty} \varrho\, g(\varrho,E)\, d\varrho \tag{5.11}$$

$$\int_{-\infty}^{0} W_e^{(1)}(x)\, dx = \int_{e_x \geq 0} dE\, d\Omega\, f(E,\underline{e})\, e_x\, \bar{\varrho}(E)$$

$$\int_{-T}^{\infty} W_e^{(2)}(x)\, dx = -\int_{e_x \geq 0} dE\, d\Omega\, f(E,\underline{e})\, e_x\, \bar{\varrho}(E)$$

Two further assumptions are now made concerning $f(E,\underline{e})$:

a) a well defined initial energy E,

b) isotropy.

Therefore,

$$f(E', \underline{e}) = \frac{\delta(E' - E)}{4\pi} \tag{5.12}$$

$$\int_{-\infty}^{0} W_e^{(1)}(x)\,dx = \bar{\varsigma}(E) \int_{e_x \geq 0} d\Omega \frac{e_x}{4\pi} = \bar{\varsigma}(E) \int_0^1 \frac{\cos\theta\, d(\cos\theta)}{2} = \frac{\bar{\varsigma}(E)}{4} \tag{5.13}$$

With this result, we go into Equation (5.8) to obtain

$$\frac{N_e}{N} = \frac{\frac{1}{2}\,\bar{\varsigma}(E)}{T} = \frac{\bar{\varsigma}(E)}{2T} \tag{5.14}$$

N_f = number of radioactive nuclei remaining in the irradiated foil.

$$N = N_e + N_f$$

$$\boxed{\bar{\varsigma}(E) = 2\,\frac{N_e}{N_f}\,T} \tag{5.15}$$

Some results are listed in Table III.

TABLE III

RESULTS OF PRIMARY RANGE MEASUREMENT BY SCHMITT AND SHARP

Recoiling Atom	Most Probable Recoil Energy	Observed Range $\bar{\varsigma}(E)$ in Å
C^{11}	130 kev	11,000
Fe^{53}	30 kev	560
Cu^{64}	25 ± 16 kev	157
Ag^{106}	14 kev	71
An^{196}	9 kev	28

3. Theory of Primary Ranges
(D. K. Holmes and G. Leibfried, J. Appl. Phys., 31, 1046 (1960).)

The authors of this theoretical calculation of ranges consider the path of a primary in a solid as composed of undisturbed straight line parts of length ℓ_i as shown in Figure 28.

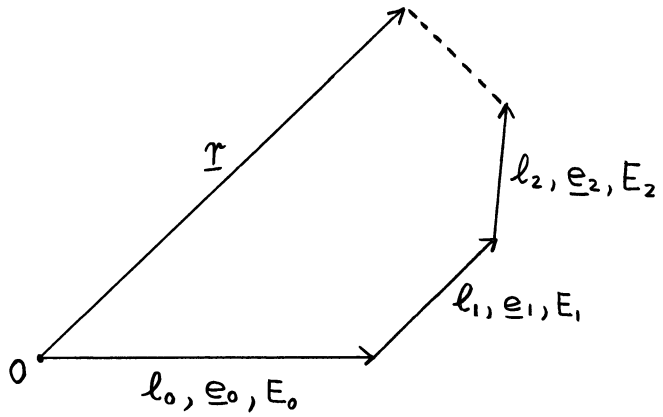

FIGURE 28

SCHEMATIC DIAGRAM OF THE PATH OF A PRIMARY ACCORDING TO THE HARD SPHERE APPROXIMATION

Such a behavior is in agreement with the hard sphere approximation of interactions.

Distribution Functions

By introduction of a number of distribution functions one may obtain the interesting parameters for the total path of the particle as moments of these distribution functions. We introduce:

$W_\ell d\ell$ probability of finding the path length between collisions in the range $(\ell, \ell + d\ell)$, when the mean free path is λ.

$$W_\ell \, d\ell = e^{-\ell/\lambda} \frac{d\ell}{\lambda} \tag{5.16}$$

$f(E_o, \underline{e}_o) dE_o d\Omega_o$ probability that the initial energy of the primary is in (E_o, E_o+dE_o) and that its initial direction is in $d\Omega_o$ about $\underline{e}_o$.

$G(E_i, \underline{e}_i; E_{i+1}, \underline{e}_{i+1})$ distribution of energy E_{i+1} and direction $\underline{e}_{i+1}$ after collision for a primary with energy E_i and direction $\underline{e}_i$ before collision.

From this we obtain the total distribution function for any number ν of collisions:

$$W_\nu (E_o, e_o, \ell_o; E_1, \underline{e}_1, \ell_1; \ldots; E_\nu, \underline{e}_\nu, \ell_\nu) =$$

$$= f(E_o, \underline{e}_o) \frac{1}{\lambda(E_o)} e^{-\ell_o/\lambda(E_o)} G(E_o, \underline{e}_o; E_1, \underline{e}_1) \cdot \frac{1}{\lambda(E_1)} \cdots\cdots d\tau \tag{5.17}$$

$$d\tau = dE_o \, d\Omega_o \, d\ell_o \text{ ------- } dE_\nu \, d\Omega_\nu \, d\ell_\nu .$$

The corresponding distribution function for $\nu \to \infty$ will be called W.

Mean Values

The parameters of interest to us are:

a) Total path length $$L = \sum_{\nu=0}^{\infty} \ell_\nu \tag{5.18}$$

b) Vectorial distance $$\underline{r} = \sum_{\nu=0}^{\infty} \ell_\nu \underline{e}_\nu \tag{5.19}$$

With the help of the total distribution function introduced in

Equation (5.17), we can now write the following expressions:

$$\bar{L} = \sum_{\nu} \bar{\ell}_{\nu} = \sum_{\nu=0}^{\infty} \int \ell_{\nu} W \, d\tau \tag{5.20}$$

where W is the total distribution function for $\nu \to \infty$,

$$\langle L^2 \rangle_{av} = \sum_{\mu,\nu=0}^{\infty} \langle \ell_{\mu} \ell_{\nu} \rangle_{av} \tag{5.21}$$

$$\bar{\underline{r}} = \sum_{\nu=0}^{\infty} \int \ell_{\nu} \underline{e}_{\nu} W \, d\tau \tag{5.22}$$

$$\langle \underline{r}^2 \rangle_{av} = \sum_{\mu,\nu} \langle \ell_{\mu} \ell_{\nu} \underline{e}_{\mu} \cdot \underline{e}_{\nu} \rangle_{av} \tag{5.23}$$

The calculations leading to the final forms for the above averages will not be demonstrated here. The main physical assumption that goes into the solution is that of hard sphere interaction between the atoms.

We obtain (for monoenergetic radiation of fixed direction $(E, \underline{e})$):

$$\bar{L} = \lambda(E) + \int_0^E \lambda(\varepsilon) \frac{d\varepsilon}{\varepsilon} \tag{5.24}$$

$$\langle L^2 \rangle_{av} = \bar{L}^2 + \lambda^2(E) + 2\int_0^E \lambda^2(\varepsilon)\frac{d\varepsilon}{\varepsilon} \qquad (\mu > \nu \geq 1) \tag{5.25}$$

$$\bar{r} = \left[\lambda(E) + \frac{1}{\sqrt{E}}\int_0^E \lambda(\varepsilon)\frac{d\varepsilon}{\sqrt{\varepsilon}}\right]\underline{e} \tag{5.26}$$

$$\langle r^2 \rangle_{av} = 2\left[\lambda^2(E) + \int_0^E \lambda^2(\varepsilon)\frac{d\varepsilon}{\varepsilon} + \frac{\lambda(E)}{\sqrt{E}}\int_0^E \lambda(\varepsilon)\frac{d\varepsilon}{\sqrt{\varepsilon}} + \int_0^E \lambda(\varepsilon)\frac{d\varepsilon}{\varepsilon^{3/2}}\int_0^\varepsilon \lambda(\varepsilon')\frac{d\varepsilon'}{\sqrt{\varepsilon'}}\right] \tag{5.27}$$

Interaction Potential

In all our averages above the parameter that depends on the interaction potential is $\lambda(E)$, the mean free path between collisions. To make a comparison with experimental results, we must replace $\lambda(E)$ by an expression derived from a scattering potential. Holmes and Leibfried have chosen the Bohr potential (Equation (5.1)), which we rewrite in the following manner:

$$V(r) = \frac{Z^2e^2}{r}\, e^{-r/a} = \frac{E_B}{2}\cdot\frac{a_B}{r}\cdot e^{-r/a_B} \tag{5.28}$$

$$E_B = \frac{2Z^2e^2}{a_B} \cdot \qquad a_B = \alpha\frac{a_H}{Z^{1/3}}$$

where according to Bohr $1/\sqrt{2}$ should be taken for α . The scattering by such a potential can be treated with sufficient accuracy as scattering from a hard sphere if only the distance of closest approach R(E) defined by

$$E = E_B \frac{a_B}{R(E)} e^{-R(E)/a_B} \tag{5.29}$$

is larger than the screening radius a_B. (For a central collision, the total energy of a particle in relative coordinates is equal to V(R) at closest distance. This must also be equal to E_r, the initial kinetic energy (at infinite distance) of the particle. For equal masses of the two participating particles, $E_{lab} = 2\ E_r$.)

Since the total cross section is simply $R^2(E)$, we obtain for $\lambda(E)$

$$\lambda(E) = \frac{1}{N \pi R^2(E)} \tag{5.30}$$

This expression may now be substituted into our averages, Equations (5.24) through (5.27),

$$\bar{L} = \frac{1}{N \pi R^2} \left[\frac{3}{2} + \frac{R}{a_B} \right] \tag{5.31}$$

$$\langle L^2 \rangle_{av} = \frac{1}{(N \pi R^2)^2} \left[\frac{3}{2} + \frac{2}{3} \frac{R}{a_B} \right] + \bar{L}^2 \tag{5.32}$$

and similarly for the $\langle r^2 \rangle$ average. For the latter, one must make the assumption $R \gg a$ to obtain an easily soluble integral, but this agrees surprisingly well with the accurate solution. The asymptotic expression is

$$\langle r^2 \rangle_{av} \cong \frac{1}{(N\pi R^2)^2}\left[\frac{7}{2} + \frac{2R}{a_B}\right] \tag{5.33}$$

Figure 29 shows the variation of some of the parameters above as a function of E/E_B.

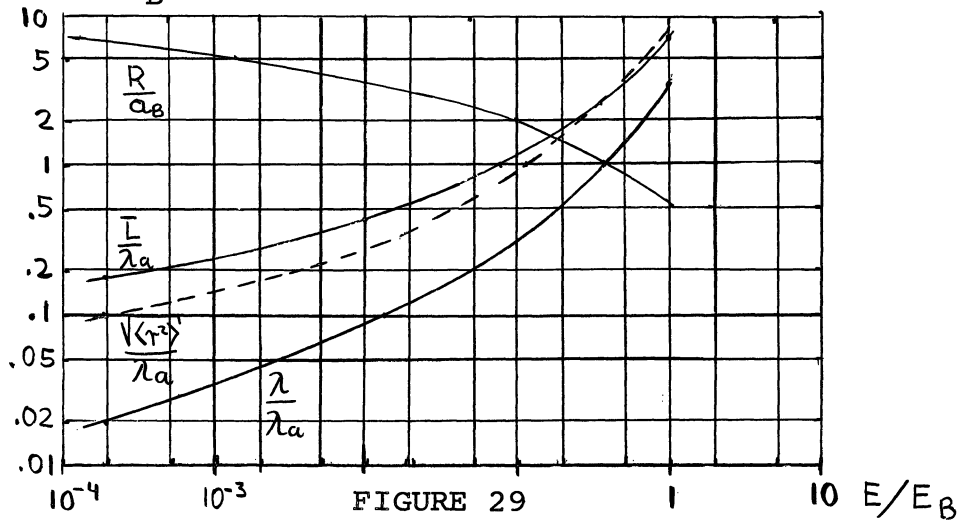

FIGURE 29

DEPENDENCE OF CHARACTERISTIC AVERAGES ON ENERGY FOR A BOHR POTENTIAL

(λ_a is λ for $R = a_B$)

Range

How is the range of a particle connected with any of the averages we quoted? There seems to be a certain ambiguity in the selection of what one wants to call the range of a primary. Holmes and Leibfried chose

$$\bar{\varrho} = \int_0^\infty \varrho\, f(\varrho, E)\, d\varrho \tag{5.34}$$

where ρ is the farthest distance that the primary gets away from the origin. This is sketched in Figure 30.

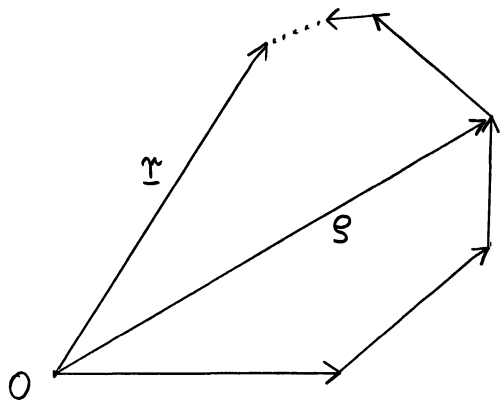

FIGURE 30

RELATION BETWEEN THE ACTUAL PATH
OF A PRIMARY AND ITS RANGE S

None of the averages computed so far corresponds exactly to S.

Upper limit: $\bar{L}$, this is always larger than $\bar{\rho}$.

Lower limit: $\bar{r}$, this will always be smaller than $\bar{\rho}$.

Essential differences between r and ρ come from scattering events which involve large scattering angles. But if the scattering angle is large, then the energy loss to the primary is also large, so that the remainder of the path can be neglected. Therefore, $\bar{r}$ seems to be quite a good approximation to $\bar{\rho}$. However, $\bar{r}$ is not among the averages which we computed. We do have $\langle r^2 \rangle_{av}$ which is always greater than $\bar{r}^2$ since $\langle r^2 \rangle_{av} - \bar{r}^2$ is the variance of $\bar{r}$ which is always positive. Since $\bar{\rho}$ is also always greater than $\bar{r}$, it turns out that

$$\bar{\rho} \cong \sqrt{\langle r^2 \rangle_{av}} \tag{5.35}$$

is a good approximation.

Table IV shows a comparison of the data by Schmitt and Sharp and theoretically computed ranges according to Equation (5.35). The ranges have been computed for three different values of α (see Equation (5.28)) where $\alpha = \frac{1}{\sqrt{2}}$ is the original Bohr proposal. For copper $\alpha = 2$ seems to fit the data best. For Fe, Zn, and Au there is strong disagreement between the measured range and any of the calculated ones. This may be due to the fact that the recoil spectrum for these materials disagreed with that for copper, which was the only one that was measured in detail

TABLE IV

COMPARISON OF EXPERIMENTAL RANGES WITH THEORY

Element	$\bar{E}$ (E_B 10 kev)		R/a	ρ_{theo} 10^{-6} cm	ρ_{obs} cm	L	α
Ti	5.28	10.4	0.85	10.4	3.1	10.6	1
		7.38	0.70	7.4		7.3	$\sqrt{2}$
		5.28	0.55	5.51		5.5	2
Fe	4.8	15.5	1.1	4.8	5.6	5.2	1
		10.9	.91	3.3		3.4	$\sqrt{2}$
		7.74	.75	2.3		2.3	2
Cu	4.0	20.0	1.3	3.5	1.6	4.1	1
		14.3	.1	2.3		2.6	$\sqrt{2}$
		10.0	.95	1.6		1.65	2
Zn	4.0	21.1	1.35	4.5	1.37	5.2	1
		15.4	1.15	2.9		3.35	$\sqrt{2}$
		10.8	1.0	2.1		2.1	2
Ag	2.24	60.5	2.45	2.5	.71	3.3	1
		43.1	2.2	1.5		1.9	$\sqrt{2}$
		30.7	1.95	.9		1.15	2
Au	1.44	205.7	3.65	1.8	.28	2.7	1
		144.0	3.4	1.0		1.5	$\sqrt{2}$
		103.0	3.1	.58		.84	2

In conclusion, we might say that considering the uncertainties in both the experimental ranges as well as the theoretical ones the agreement between the two is really quite good. A completely different approach to the problem of range determinations for primaries is that of machine calculations of the actual paths of particles in a regular lattice. This has the advantage of being somewhat closer to the real problem since in all the above calculations we have assumed a statistical distribution of the lattice atoms. On the other hand, the capacity of presently available computers limits one to motions within one lattice plane and to fairly small lattice fragments. The method is applicable only to small primary energies.

These are some phenomena which occur when one discusses interactions in real lattices and which we have no time to discuss here. The two most important ones are the focussing collisions and the reduced interaction (channeling) of particles moving in lattice directions with low Miller indices.

APPENDIX

RELATIVE COORDINATES AND THE CENTRAL FORCE PROBLEM

1. Introduction of Relative Coordinates.

A central force between two bodies is a force which is directed along the straight line connecting the two bodies.

For such a force the two body problem can be reduced to a one-body problem by the introduction of relative coordinates. This is done as follows (see also Fig. A.1):

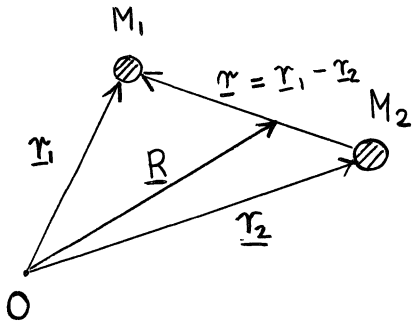

FIG. A.1.

VECTORS DESCRIBING THE LOCATION OF TWO MASSES M_1 AND M_2 IN SPACE. $\underline{R}$ = VECTOR TO THE CENTER OF MASS.

For an attractive force between the bodies we have:

Force on mass M_1:

$$\underline{F}_1 = F(|\underline{r}_1 - \underline{r}_2|)\,\frac{\underline{r}_2 - \underline{r}_1}{|\underline{r}_1 - \underline{r}_2|} \qquad \text{(A.1.a)}$$

Force on mass M_2:

$$\underline{F}_2 = F(|\underline{r}_1 - \underline{r}_2|)\,\frac{\underline{r}_1 - \underline{r}_2}{|\underline{r}_1 - \underline{r}_2|} \qquad \text{(A.1.b)}$$

Introduce $\underline{r} = \underline{r}_1 - \underline{r}_2$, $r = |\underline{r}_1 - \underline{r}_2|$

Equations of motion for the two masses:

$$M_1 \ddot{\underline{r}}_1 = -F(r)\frac{\underline{r}}{r} \quad (a) \qquad M_2 \ddot{\underline{r}}_2 = F(r)\frac{\underline{r}}{r} \qquad \text{(A.2)}$$

We obtain two different equations of motion by adding and subtracting these two equations:

ADDITION

$$M_1 \ddot{\underline{r}}_1 + M_2 \ddot{\underline{r}}_2 = 0 \qquad \text{(A.3)}$$

The radius vector to the center of mass, $\underline{R}$, is defined as:

$$\underline{R} = \frac{M_1 \underline{r}_1 + M_2 \underline{r}_2}{M_1 + M_2} \qquad \text{(A.4)}$$

By differentiating this twice we obtain

$$\ddot{\underline{R}} = \frac{M_1 \ddot{\underline{r}}_1 + M_2 \ddot{\underline{r}}_2}{M_1 + M_2} \qquad \text{(A.5)}$$

With this, our above equation can be read as:

$$\boxed{\ddot{\underline{R}} = 0} \qquad \text{(A.6)}$$

In words:

If the only force on a system of two bodies is a central force between these bodies, then the motion of the center mass does not change with time.

SUBTRACTION

Before taking the difference between the two equations (A.2.a,b) we divide by the appropriate mass:

$$\ddot{\underline{r}}_1 - \ddot{\underline{r}}_2 = -\left(\frac{1}{M_1} + \frac{1}{M_2}\right) F(r) \frac{\underline{r}}{r} \qquad \text{(A.7)}$$

$$\ddot{\underline{r}} = -\frac{1}{\mu} F(r) \frac{\underline{r}}{r} \qquad \text{(A.8)}$$

where we used:

$$\frac{1}{\mu} = \frac{1}{M_1} + \frac{1}{M_2} \qquad \text{(A.9)}$$

μ is called the reduced mass. Finally

$$\boxed{\mu \ddot{\underline{r}} = -F(r) \frac{\underline{r}}{r}} \qquad \text{(A.10)}$$

In words:

For a central force, the motion of two bodies may be described as the motion of one body of reduced mass with respect to an origin located in the other body.

Coordinates describing the position of one body with respect to the other are called relative coordinates.

2. Description of the Collision Problem

a) In the laboratory system

$\underline{v}_1$, $\underline{v}_2$ initial velocities of particles 1 and 2

$\underline{v}_1'$, $\underline{v}_2'$ final velocities of particles 1 and 2

b impact parameter

θ_1 , θ_2 scattering angles

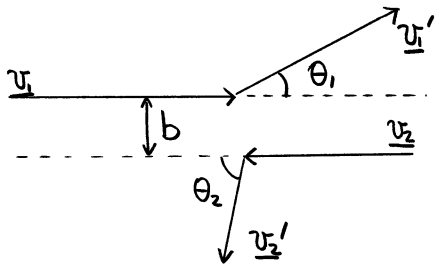

FIG. A.2

SCHEMATIC OF A COLLISION OF TWO PARTICLES IN THE LABORATORY SYSTEM.

It is customary to consider particle 1 as the incident particle and particle 2 as the target particle which may usually be considered as being at rest, i.e. $\underline{v}_2 = 0$.

b) In relative coordinates

$\underline{v}$ initial relative velocity

$\underline{v}'$ final relative velocity

θ scattering angle

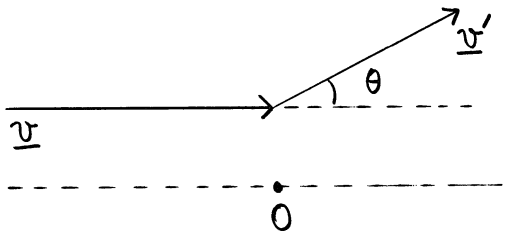

FIG. A.3

SCHEMATIC OF A COLLISION IN RELATIVE COORDINATES

We want to establish relations between the velocitics in the two systems:

From a simple differentation of equation (A.4) we obtain

$$(M_1 + M_2)\,\underline{V} = M_1\,\underline{v}_1 + M_2\,\underline{v}_2 \qquad \text{(A.11)}$$

where $\underline{V} = \dot{\underline{R}}$ is the velocity of the center of mass. The relative velocity is $\underline{v} = \underline{v}_1 - \underline{v}_2$. Solving this for $\underline{v}_2$ and substituting in equation (A.11) we obtain:

$$(M_1 + M_2)\,\underline{V} = (M_1 + M_2)\,\underline{v}_1 - M_2\,\underline{v} \qquad \text{or}$$

$$\underline{v}_1 = \underline{V} + \frac{M_2}{M_1 + M_2}\,\underline{v} \qquad \text{(a)}$$

Similarly (A.12)

$$\underline{v}_2 = \underline{V} - \frac{M_1}{M_1 + M_2}\,\underline{v} \qquad \text{(b)}$$

Since <u>linear momentum is conserved</u> during the collision, we have:

$$M_1\,\underline{v}_1 + M_2\,\underline{v}_2 = M_1\,\underline{v}_1' + M_2\,\underline{v}_2' \qquad \text{(A.13)}$$

and therefore

$$(M_1 + M_2)\,\underline{V} = M_1\,\underline{v}_1' + M_2\,\underline{v}_2'$$

from which we get equations analogous to equations (A.12.a.b.)

The complete result is then:

<u>Transformation equations</u>

$$\underline{v}_1 = \underline{V} + \frac{M_2}{M_1+M_2}\,\underline{v} \qquad \text{(a)} \qquad\qquad \underline{v}_1' = \underline{V} + \frac{M_2}{M_1+M_2}\,\underline{v}' \qquad \text{(c)}$$

$$\underline{v}_2 = \underline{V} - \frac{M_1}{M_1+M_2}\,\underline{v} \qquad \text{(b)} \qquad\qquad \underline{v}_2' = \underline{V} - \frac{M_1}{M_1+M_2}\,\underline{v}' \qquad \text{(d)}$$

(A.12)

3. Kinetic Energy Relations for Elastic Scattering

$$E_1 = \frac{M_1}{2}\underline{v}_1^2 = \frac{M_1}{2}V^2 + \mu\,\underline{v}\cdot\underline{V} + \frac{1}{2}\frac{M_2}{M_1+M_2}\mu v^2$$

$$E_2 = \frac{M_2}{2}\underline{v}_2^2 = \frac{M_2}{2}V^2 - \mu\,\underline{v}\cdot\underline{V} + \frac{1}{2}\frac{M_1}{M_1+M_2}\mu v^2$$

} add

$$E_1 + E_2 = \underbrace{\frac{M_1+M_2}{2}V^2}_{\substack{\text{Kinetic energy}\\ \text{of the CM-motion}}} + \underbrace{\frac{\mu}{2}v^2}_{\substack{\text{Kinetic energy}\\ \text{of the relative}\\ \text{motion}}} \equiv E_R + E_r \qquad \text{(A.13)}$$

Conservation of kinetic energy in an elastic collision requires that:

$$E_1 + E_2 = E_1' + E_2' = \frac{M_1+M_2}{2}V^2 + \frac{\mu}{2}v'^2$$

Consequently

$$\boxed{v^2 = v'^2} \qquad \text{(A.14)}$$

In words:

Kinetic energy is conserved in the relative coordinate system. The interaction process will change the direction of the particle but not its kinetic energy.

4. Scattering Angle

The scattering angle in relative coordinates, θ, is the angle between the initial and the final direction of the scattered particle. Its cosine is obtained from:

$$\cos\theta = \frac{\underline{v}\cdot\underline{v}'}{v^2} \qquad \text{(A.15)}$$

Collision theory will most easily yield the angle θ as a function of the imput parameters to a particular problem. For the discussion of radiation effects, on the other hand, we are mainly interested in the energy of particle 2 in the laboratory system after the collision, i.e. we want to know E_2'. Therefore we will now derive a relation between these two variables.

5. Relation between θ and E_2'

$$E_2' = \frac{M_2}{2}(\underline{v}_2')^2 = \frac{M_2}{2}\left(\underline{V} - \frac{M_1}{M_1+M_2}\underline{v}'\right)^2$$ Use equation (A.12.d)!

We now make the usually justified assumption that $\underline{v}_2^2 = 0$, i.e. that the target particle is at rest before the collision. With that, we obtain from equation (A.12.b)

$$\underline{V} = \frac{M_1}{M_1+M_2}\underline{v} \tag{A.16}$$

Substituting this above we obtain:

$$E_2' = \frac{M_2}{2}\left(\frac{M_1}{M_1+M_2}\underline{v} - \frac{M_1}{M_1+M_2}\underline{v}'\right)^2$$

$$= \frac{M_1^2 M_2}{2(M_1+M_2)^2}\left(v^2 - 2\,\underline{v}\cdot\underline{v}' + v'^2\right)$$

Using relations (A.14) and (A.15) we further obtain

$$E_2' = \frac{M_1^2 M_2}{2(M_1+M_2)^2}\left(2v^2 - 2v^2\cos\theta\right)$$

$$\boxed{E_2' = \frac{M_1^2 M_2}{(M_1+M_2)^2}v^2(1-\cos\theta)} \tag{A.17}$$

This is the desired relation between E_2' and θ.

6. Maximum Transferrable Energy

From equation (A.17) we can determine the maximum transferrable energy in an elastic collision, E'_{2max}.

E'_2 has its largest value, when $\cos\theta = -1$, i.e. when the scattering angle is 180°.

In that case:

$$E'_{2\,max} = \frac{2 M_1^2 M_2}{(M_1 + M_2)^2} v^2 \qquad (A.18)$$

We will now express this as a function of the incident energy of the particle 1 in the laboratory system, E_1. The assumption of $\underline{v}_2 = 0$ allows the following transformation of equation (A.12.a).

$$\underline{v}_1 = \underline{V} + \frac{M_2}{M_1 + M_2} \underline{v} \qquad (A.12.a)$$

$$\underline{V} = \frac{M_1}{M_1 + M_2} \underline{v} \qquad (A.16)$$

from which

$$\boxed{\underline{v}_1 = \underline{v} \quad \text{if} \quad \underline{v}_2 = 0} \qquad (A.19)$$

and therefore

$$\boxed{E'_{2\,max} = \frac{4 M_1 M_2}{(M_1 + M_2)^2} E_1 = \alpha E_1} \qquad (A.20)$$

Relation A.17 may now be rewritten as

$$\boxed{E'_2 = E'_{2\,max} \frac{1 - \cos\theta}{2}} \qquad (A.21)$$

A BRIEF REVIEW OF POINT DEFECTS IN SEMI-CONDUCTORS

John S. King

A BRIEF REVIEW OF

POINT DEFECTS IN SEMI-CONDUCTORS

By
John S. King

I. Point Defects in Crystal Lattices

Introduction

The bulk of the study of the solid state of materials is concerned with polycrystals or single crystals, since true amorphous solids, such as the glasses, are relatively rare. Furthermore, most physical properties of the crystalline state are controlled more by the imperfections in the lattice than by the lattice itself. Hence a study of lattice defects really encompasses most of the solid state world. It is obvious that our review here must, therefore, be confined to a rather brief and elementary description of those lattice defects that will be encountered in the irradiation of semi-conductor crystals. Even so, it will become evident that the effects on these crystals causes a very broad spectrum of physical changes and provides, therefore, many experimental methods of observation.

It will be our purposes here to (a) describe the possible lattice defects that can be produced by irradiation, to briefly examine the energetics of their formation and subsequent movement, and (b) to review the experimental techniques that have been developed for observing their effects on semi-conductors. The notes are based on material presented in References , , , and of the attached bibliography.

Types of Defects

The ideal or perfect crystal is an infinite three-dimensional array of point masses fixed in a lattice, every point of which can be reached by successive translations along the primitive lattice vectors. Real crystals deviate from this exact geometrical arrangement because of thermal excitation (phonon generation, electron-hole pairs), impurities (either substitutional or interstitial), and the formation and diffusion of vacancy sites and/or interstitial atoms.

The vacancy and interstitial sites may be randomly distributed or associated in clusters. If many vacancies or interstitials are arranged in an extended array, they are called "dislocations," whereas if randomly distributed they are called "point defects." Dislocations are "accidents" of crystal growth and include combinations of edge and screw dislocations. The surfaces, grain boundaries, twinning, stacking faults, and slip lines are evidences of dislocation. These defects are frozen into the crystal or generated by mechanical work; they are not in thermodynamic equilibrium. By contrast, a finite number of point defects must exist in a crystal in thermodynamic equilibrium at a fixed (non-zero) temperature.

Our discussion will not be concerned with dislocations. Their principal role in radiation damage is in the pinning of dislocations by radiation induced point defects, leading to embrittlement in metals.

The possible types of point defects are:

1. Simple vacancies, called Schottky defects. This is the complete removal of an atom from its lattice site to a point outside the crystal volume, i.e. on the crystal surface. This is shown

schematically in Figure 1 by a square around the vacated site. (This figure represents an ionic crystal for purposes of illustration only.) The introduction of Schottky defects lowers the crystal density, since the same mass is distributed over a larger crystal volume.

FIGURE 1

DEFECTS IN AN IONIC CRYSTAL

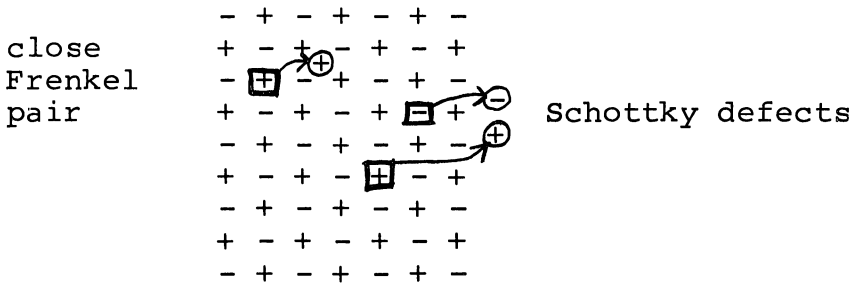

2. Separated pairs of Schottky defects. This is particularly appropriate to ionic crystals where a positive and negative ion can be simultaneously removed without disturbing charge neutrality.

3. Frenkel defects. This is the displacement of an atom from its normal site to an interstitial site internal to the crystal. In this case the density is not changed. If the interstitial position is only one or two lattice points removed from the vacancy site, the defects are called a "close Frenkel pair." In this case some degree of correlation between the two exists, and an enhanced probability of subsequent annihilation exists. If the interstitial is displaced many lattice distances away, a "separated Frenkel pair" is produced. Figure 1 shows a close

Frenkel pair. Essentially all radiation induced displacements to be encountered in semi-conductors are Frenkel pairs.

4. Clustered defects, the divacancy. There is ample evidence that defects form stable clusters. It will be shown below that the formation energy of a divacancy, for example, is lower than the formation energy of two separated vacancies. Figure 2 shows a divacancy and a single Frenkel pair.

FIGURE 2

SINGLE VACANCY AND DIVACANCY FORMATION

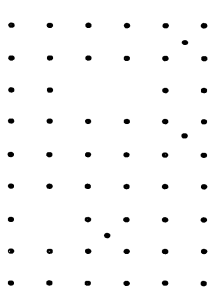

5. Impurity substitution. A substituted atom occupies a normal site of the host crystal. If its valence is the same as that of the host atom, its presence will create only a local perturbation in the electronic wave functions. If the valence is different, it (a) may create an electron or hole in a semiconductor, or (b) may induce a nearby ion vacancy in an ionic crystal in order to preserve charge neutrality.

Thermodynamic Equilibrium of Defects

It is instructive at this point to exhibit some simple thermodynamic arguments to show the equilibrium number of vacancies and interstitials that exist at temperature T. The arguments will be

useful also in the discussion of diffusion and of equilibrium hole-electron concentration in semi-conductors.

Positive work on the crystal is necessary to create a vacancy. At the same time the disturbance to the surrounding lattice by virtue of removing an atom changes both the thermal (lattice vibrational) and configurational entropy of the lattice. The change in the free energy of the crystal is, therefore, determined by the difference in formation energy and entropy increase. At thermodynamic equilibrium, the change in free energy with defect concentration must be zero, i.e. a balance exists between formation energy and lattice entropy. From the second law of thermodynamics, the Gibbs free energy, G, or Helmholtz free energy, F, can be defined. Since the volume changes are relatively small, we may use the simpler Helmholtz function. If n is the number of defects per unit volume at temperature T, the total differential free energy is

$$dF(n,T) = d(n\phi - TS) \leq 0 \qquad (1)$$

$$T, V = \text{constant}$$

where ϕ is the formation energy and S is both configurational entropy, S_c, and thermal entropy, S_{th}; at equilibrium dF=0. Graphically, the function F(n,t) versus n can be depicted by Figure 3.

FIGURE 3

HELMHOLTZ FUNCTION VERSUS n

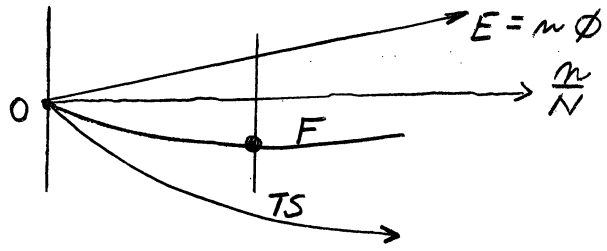

If F_o was the free energy of the undisturbed lattice, then after the introduction of n defects

$$F(n,T) = F_o + n\phi - nT(\Delta S_{th}) - TS_c$$

$$\left(\frac{\partial F}{\partial n}\right)_T = 0 = \phi - T\Delta S_{th} - T\frac{\partial S_c}{\partial n} \qquad (2)$$

at equilibrium.

The entropy is calculable from the Boltzmann formula for the entropy of an ensemble

$$S_c = k \ln W_c$$
$$S_{th} = k \ln W_{th} \qquad (3)$$

W is a probability function, although not the usual one, since $W >> 1$. W_c is the sum of different ways in which n defects can be arranged on N original lattice sites, and the greater this large number, the greater is the new entropy. This can be easily written down for a given type of defect. W_{th} is less available and requires some model of the lattice vibrational states. It is common in the literature to regard ΔS_{th} either as an unspecified parameter or to consider it negligible relative to the change in configurational entropy.

The free energy for <u>simple vacancies</u> introduced into the lattice can be written down. It can be easily established that the configurational probability W_c is

$$W_c = \frac{(N+n)!}{N!\,n!} \tag{4}$$

where N=total number of crystal atoms, (N+n)=number of sites, and n=the number of vacancies. Then at equilibrium, and applying Sterling's formula $(\ln A! \approx A \ln A - A)$. Equation (2) gives

$$\left(\frac{\partial F}{\partial n}\right)_T = \phi - T\Delta S_{th} - kT \frac{\partial}{\partial n} \ln \frac{(N+n)!}{N!\,n!}$$

$$= \phi - T\Delta S_{th} - kT \frac{\partial}{\partial n} \{(N+n)\ln(N+n) - (N+n) - N\ln N + N - n\ln n + n\}$$

or

$$\left(\frac{\partial F}{\partial n}\right)_T \simeq \phi - T\Delta S_{th} - kT \ln \frac{N}{n} = 0$$

since $N \gg n$. Solving for n

$$\frac{n}{N} = e^{\frac{\Delta S_{th}}{k}} e^{-\phi/kT} \tag{5}$$

If ΔS_{th} is assumed small, Equation (5) gives the fractional number of vacancies at thermal equilibrium as a simple exponential. A typical value of ϕ is about 1.0 ev. Hence, at, say, room temperature

$$\frac{n}{N} \simeq e^{-\frac{1}{.025}} \simeq 4 \cdot 10^{-18}$$

This is a small but naturally occurring fraction. It can become much greater at elevated temperatures and is, of course, very sensitive to the actual value of ϕ.

For simple vacancies, ΔS_{th} may not be negligible. An estimate of the magnitude can be had by invoking the crude model of the lattice as a 3N set of Einstein oscillators, all vibrating with the same frequency ν. This can be envisioned as the generation of n phonon quanta, with no restriction on the number of quanta belonging to any one oscillator. In this case W_{th} in Equation (3) is the number of ways n phonons can be distributed among the 3N Einstein oscillators. It can be shown that W_{th} is given by

$$W_{th} = \frac{(3N+n)!}{(3N)!\,n!} \tag{6}$$

if no a priori restriction is placed on the occupation numbers. The total energy of vibration is

$$E_{th} = n h\nu = 3NkT \tag{7}$$

and hence

$$n = \frac{3NkT}{h\nu}$$

Again using Sterling's formula, and recalling that the total ΔS_{th} in Equation (2) was written $n\Delta S_{th}$,

$$(S_{th})_{TOTAL} = n S_{th} = k\left[3N \ln\left(\frac{3N+n}{3N}\right) + n \ln\left(\frac{3N+n}{n}\right)\right]$$

In many cases $h\nu \gg kT$, corresponding to a $T \gg \Theta_{Debye}$. For these cases, $n \gg 3N$ from Equation 7. Then, roughly,

$$n S_{th} \approx 3Nk\left(1 + \ln \frac{kT}{h\nu}\right)$$

Now, for every vacancy introduced, the frequency of the oscillators corresponding to the nearest neighbor lattice atom is lowered due to the missing atom. If there are n vacancies and m nearest neighbors (coordination number is m), the perturbed S_{th} is

$$n S_{th} = 3mn\, k \left(1 + \ln\left(\frac{kT}{h\nu'}\right)\right) + 3(N - mn)k\left(1 + \ln\frac{kT}{h\nu}\right)$$

and subtracting the unperturbed entropy

$$\Delta S_{th} \approx 3mn\, k \ln\left(\frac{\nu}{\nu'}\right) = k \ln\left(\frac{\nu}{\nu'}\right)^{3mn}$$

Hence, Equation (5) becomes

$$\frac{n}{N} \approx \left(\frac{\nu}{\nu'}\right)^{3m} e^{-\Phi/kT} \tag{8}$$

Since m is of the order of 8, even a small shift in frequency introduced a significant increase in entropy and hence in $\frac{n}{N}$. The determination of the frequency shift is, of course, difficult to obtain. Incidentally, the ratio of entropy changes is from this expression

$$\frac{\Delta S_{th}}{\Delta S_c} = \frac{\ln\left(\frac{\nu}{\nu'}\right)^{3m}}{\ln\left(\frac{N}{n}\right)}$$

and is presumably less than unity.

The free energy for Frenkel pairs proceeds in the same fashion. In this case, the disorder probability is a product probability

$$W_c = W_v \cdot W_i$$
$$= \frac{N!}{(N-n)!\,n!} \cdot \frac{N_i!}{(N_i-n)!\,n!}$$

where N=number of atoms, n=number of Frenkel pairs, and Ni=number of possible interstitial sites, where Ni is commensurate with N. The equilibrium number of pairs existing in any lattice at T is

$$n = \sqrt{NN_i}\, e^{-\phi_f/kT} \cdot e^{\Delta S_{th}/k} \qquad (9)$$

where ϕ_f is the total positive work to remove an atom from a normal site and deposit it in a "stable" interstitial site. We must assume $\phi_f > \phi_v$.

The free energy of a simple cluster such as a <u>divacancy</u> can be determined in the same manner. It must be that the total number of possible adjacent pair positions is $\frac{mN}{2}$. Then the configurational probability is

$$W_c = \frac{\left(\frac{mN}{2}\right)!}{\left(\frac{mN}{2} - n_{II}\right)!\, n_{II}!}$$

where n_{II} is the number of divacancies existing. The energy of formation of a divacancy, ϕ_{II}, is

$$\phi_{II} = 2\phi - B$$

where ϕ is the single vacancy formation and B is the binding energy of the divacancy. We assume B is positive. The calculated equilibrium number of divacancies is then

$$\frac{n_{II}}{N} = \frac{1}{2} n w \, e^{-\phi_{II}/kT} \cdot e^{\frac{\Delta S_{th_{II}}}{k}} \tag{10}$$

If one assumes $\Delta S_{th_{II}} \simeq 2 \Delta S_{th}$, then use of Equation (10) gives

$$\frac{n_{II}}{N} = \frac{nw}{2}\left(\frac{n}{N}\right)^2 e^{B/kT} \tag{11}$$

and the ratio of divacancies to single vacancies is

$$\frac{n_{II}}{n} \simeq \frac{n}{N} \cdot \frac{w}{2} \, e^{B/kT}$$

and this can exceed unity even for binding energies small relative to ϕ_{II}.

Energy of Formation of Defects

The theoretical calculation of the magnitude of the formation energy is a complicated task, because of the difficulty in calculating the rearrangement energy attributed to the lattice atoms adjacent to the defect created. A first attempt at determining the vacancy formation energy, ϕ_v, can be obtained from the sublimation energy. The cohesive energy of the lattice is, per atom of lattice,

$$E_s = -\frac{1}{2} \sum_i V(R_i)$$

where $V(R_i)$ is the interaction potential of any atom with another at distance R_i (factor of $\frac{1}{2}$ prevents counting pairwise interactions twice). The cohesive energy is equal to the energy per atom required to remove atoms from the surface. The energy required to completely remove an interior atom to infinity is

$$E_\infty = -\sum_i V(R_i)$$

Hence, the difference $E_\infty - E_S$ must be the energy to form a vacancy by moving an atom to the surface:

$$\phi_v = E_\infty - E_S = 2E_S - E_S = E_S \tag{12}$$

On an energy scale with 0 at ∞, the formation energy can be pictured as in Figure 4.

FIGURE 4

ENERGY TO REMOVE LATTICE ATOM TO ∞

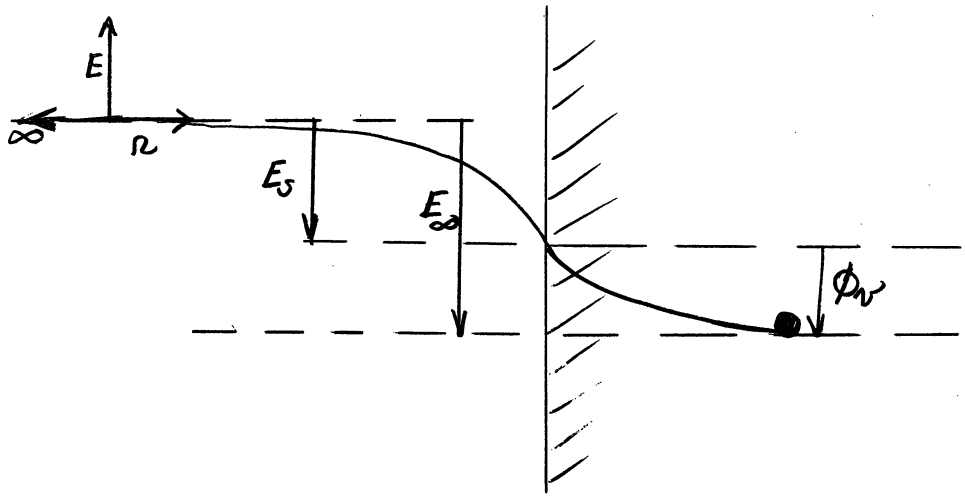

The problem can also be stated as the net number of interatomic bonds that must be broken to put an interior atom on the surface. For a fcc crystal, the average number of bonds at the surface is 6, and in the interior is 12. The average surface bond strength is $6E=E_s$, hence $E=\frac{E_s}{6}$, and the net bond breaking energy is

$$\phi_v = \frac{E_s}{6}(12-6) = E_s$$

This simple energy diagram can also be applied to the formation of an isolated Frenkel pair. The formation energy $\phi_f = \phi_i + \phi_v$ can be pictured as the net energy required to remove an atom to ∞ and then bring it back to an interstitial point.

FIGURE 5

ENERGY TO FORM FRENKEL PAIR

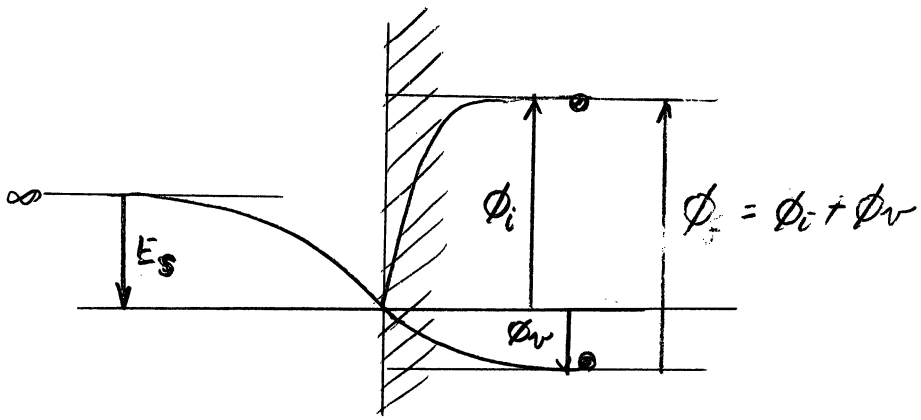

The interstitial formation energy is considerably greater than the vacancy formation energy and depends on the model assumed for the equilibrium interstitial arrangement. There is evidence, for example in the fcc system, that the "split" configuration is most stable, i.e. the interstitial "shares" a face lattice point with its normal occupant.

This picture is not a good approximation to the thermodynamically reversible process of forming a defect pair, because the rearrangement energy of the electronic, atomic configuration near a defect has been ignored. In a "fully relaxed" lattice, this energy is considerable and it reduces, for example, the formation energy in Cu by a large factor

$$\phi_v = E_s - W_r$$

For copper, Es=3.52 ev, but the best calculation of ϕ_v is about 1.3 ev, indicating Wr=2.2 ev. The best calculation for the interstitial formation energy, ϕ_i, is about 5.0 ev, giving a reversible Frenkel pair energy of $\approx$ 6.3 ev.

It must be assumed, therefore, that the irreversible energy required to form a Frenkel pair is considerably larger than the equilibrium ϕ_f. The formation produced by irradiation displacements must be irreversible in nature, and hence the energy required larger than the reversible value. In addition to this fact, there is a finite probability that a close Frenkel pair will be unstable and recombine. Furthermore, the jump diffusion barrier, i.e. the local barrier between interstitial points, must be overcome in a displacement, and this can be a function of direction of the displacement. Hence, it is not surprising to find that the minimum irradiation displacement energy, E_d, is two to four times larger than the calculated reversible ϕ_f. For Cu, for example, the best E_d is between 25 and 30 ev, and not the calculated reversible formation energy ϕ_f=6.3 ev.

To the author's knowledge, no similar calculations have been performed for the semi-conductor elements such as Si and Ge, but extensive experimental determinations of E_d have been reported.[1] These indicate that the threshold value of E_d may be as low as 6.2 ev for In Sb, and 13 ev in Si or Ge, but the most probable value is nearer 25 to 30 ev for the latter. The probability for displacement versus threshold energy for Ge, therefore, looks qualitatively as follows in Figure 6.

FIGURE 6

DISPLACEMENT ENERGY PROBABILITY CURVE

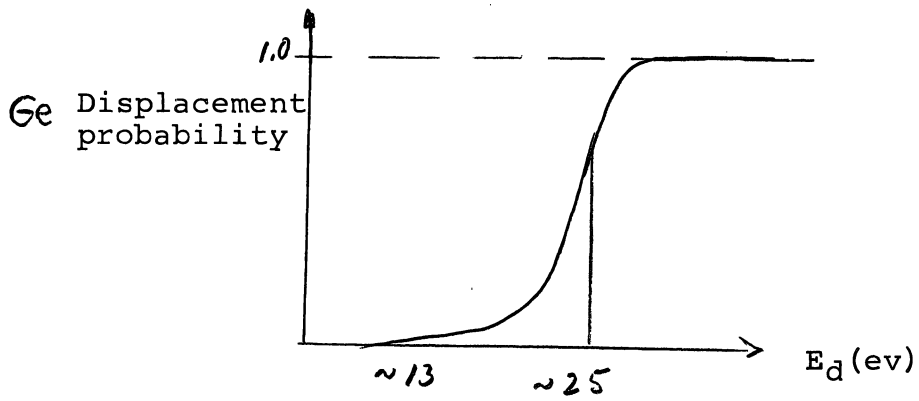

Energy for Motion of Defects

Defects exist within a local potential well produced by the lattice environment. In order to move through this crystal lattice, the defect must surmount the local potential barrier. Depending on the barrier height, the probability of overcoming the barrier depends strongly on the ambient temperature. Hence, motion effects, including diffusion of isolated defects and recombination of Frenkel defects (annealing) should also be strongly temperature dependent.

A qualitative picture of the relation between formation energies, ϕ_v and ϕ_i, and barrier heights, E_{bv} and E_{bi}, are shown below for isolated defects relative to a crystal surface.

FIGURE 7

QUALITATIVE COMPARISON OF E_{bv}, E_{bi}, ϕ_v, ϕ_i

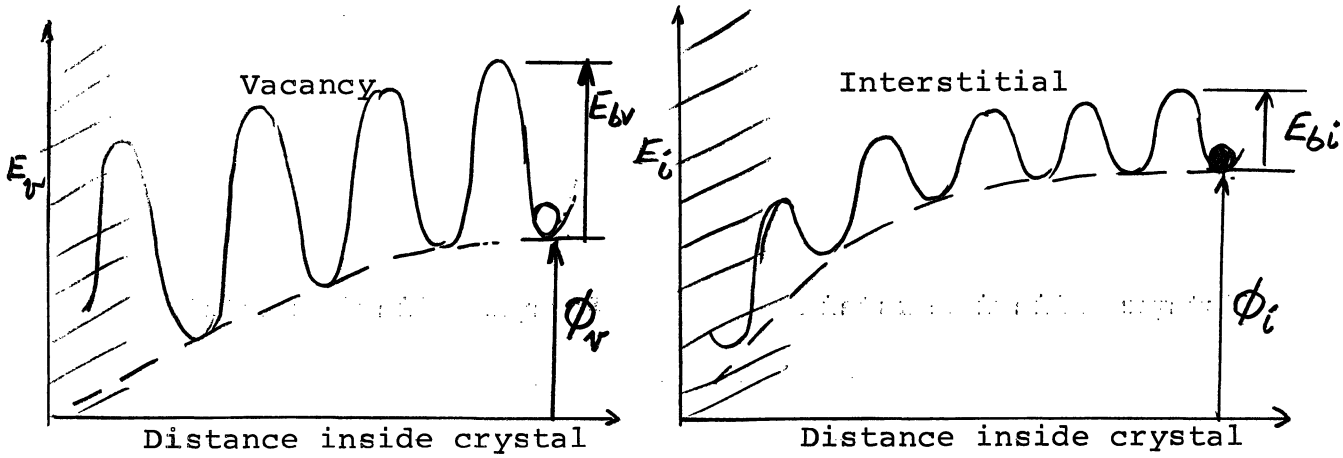

The total energy is a superposition of the formation energy and a barrier potential energy which has the periodicity of the lattice. We note the general features that:

1. the barrier energies against internal motion are smaller than the formation energies;
2. the asymptotic values of ϕ are reached within about three lattice distances from the surface (as noted above, $\phi_v < \phi_i$);
3. the potential barrier height for interstitials is much less than for vacancies. For Cu, for example, E_{bi}=.05-.10 ev while E_{bv}=0.6-1.3 ev.

If No. 3 is generally true, then we can expect the picture for a close Frenkel pair to look as in Figure 8, and the barrier height against recombination of the pair is crudely E_{bi}.

FIGURE 8

QUALITATIVE BARRIER FOR CLOSE FRENKEL PAIR

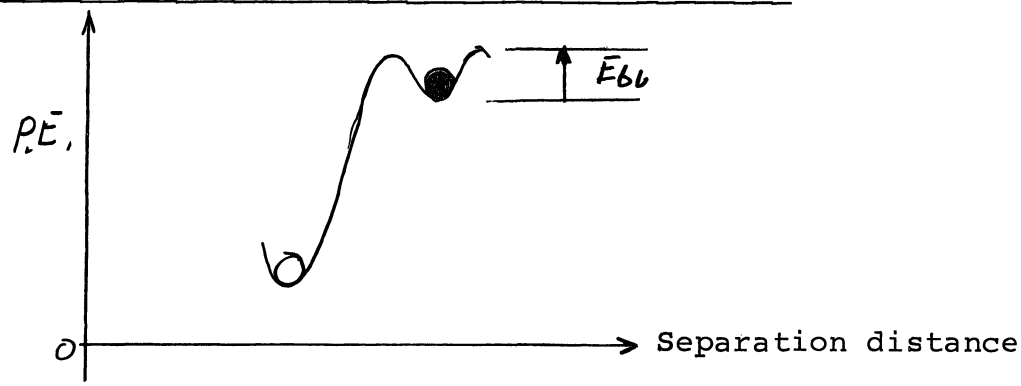

The probability per unit time that a defect will surmount the potential barrier can be estimated. Each defect is vibrating within its well with some frequency ν, which is determined by all the neighboring lattice motions and which may be different for different jump directions. For the sake of illustration, let us take the Einstein crystal model so that there is one oscillator frequency ν. The probability that the oscillator energy $E_\nu \geq E_b$ is the integral of the Boltzmann factor,

$$\frac{1}{kT}\int_{E_b}^{\infty} e^{-E/kT}\,dE = e^{-E_b/kT}$$

Therefore, the probability per unit time that the barrier is surmounted is

$$p \simeq \nu e^{-E_b/kT}$$

In actual crystals, the probability is modified to take account of all directions and because there is an entropy change for the crystal

when the defect passes to a point midway between potential wells. This can be roughly represented by an effective average vibration rate $\bar{\nu}$, entropy change ΔS_M, and barrier height E_{bM} and

$$p \simeq \bar{\nu} e^{\Delta S_M/k} e^{-E_{bM}/kT} \tag{13}$$

Clearly the jump probability is greater at low E_b and strongly depends on T.

The process of <u>diffusion</u> of defects is dependent on this jump probability, and indeed this is the ordinary diffusion of impurities in a host lattice. In fact, it is possible to derive an ordinary diffusion equation

$$\frac{\partial n}{\partial t} - D\nabla^2 n = 0$$

where the diffusion coefficient D is proportional to the jump probability

$$D = \frac{a^2 p}{\gamma} = \frac{a^2}{\gamma} \sum_j \nu_j e^{\Delta S_j/k} e^{-E_{bj}/kT} \tag{14}$$

and a is the lattice constant and γ is a geometric constant giving the number of equivalent directions for a given crystal. (As an example, consider the diffusion of carbon impurities in α-iron. The motion is interstitial in a bcc host. A good experimental value of $D=D_o e^{-E/kt}$ with $D_o=0.02$ cm^2/sec and E=0.874 ev. Using Equation (13) in Equation (14) with a=½ x unit cell dimension and γ=6 for bcc,

$D_o = \frac{a^2}{6}\bar{\nu}\, e^{\Delta S_M/k}$. From the Debye temperature $\Theta = 420^oK$, $\bar{\nu}$ is estimated as $\bar{\nu} \simeq \frac{k\Theta}{h} \simeq 10^{13}/cm$. From these numbers $e^{\Delta S_M/k}$ is inferred to be about 7.)

Of particular importance in radiation damage is the annealing of the defects produced, and this is also dependent on the jump probability. At least three annealing mechanisms should be noted. First, simple vacancies may migrate to crystal surfaces or to internal boundaries, such as dislocations, which act as infinite sinks. In bulk material, the dislocation boundaries are perhaps the most important sinks. This is the classical diffusion problem noted above. The long time response is a simple exponential (transient response has died), which is equivalent to a first order rate process.

$$\frac{dn}{dt} = -Kn$$

$$n(t) = n(0)\, e^{-Kt}$$

and K is related to the diffusion coefficient D through the spatial diffusion equation,

$$D\nabla^2 n + Kn = 0$$

It can be shown[2] that the migration to dislocation lines can be approximated in bulk media by solving the diffusion equation between infinite concentric cylinders. This gives

$$K \simeq N_o D \qquad (15)$$

where N_o is the dislocation density in lines per unit area.

Second, pairs of close Frenkel defects can annihilate by recombining. Since the pairs are coupled, they recombine independently of other pairs, and hence the annealing rate is a simple first order rate process in which the time dependence does not depend on the defect concentration. The rate constant is just the jump probability (Equation (13)). If n is the number of correlated pairs,

$$\frac{dn}{dt} = -K_0 n$$
$$n(t) = n(0)\, e^{-K_0 t} \qquad (16)$$
$$K_0 = p$$

wherein the activation energy is the interstitial barrier E_{bi}.

If the Frenkel defects are randomly distributed and not correlated, a second order rate process occurs. Since the activation energy for interstitials is much less than for vacancies, then at normal temperatures the interstitials are migrating relatively freely through a system of fixed vacancies. If the only effect of spatial diffusion is to redistribute the interstitials in a random way in the close vicinity of a vacancy, then for all time the probability, p_i , that an interstitial lies within the volume v associated with each lattice point is $p_i = vn_i$, where n_i is the interstitial concentration. If the lattice volume element contains z possible interstitial sites, then the vacancy concentration n_v changes according to

$$\frac{dn_v}{dt} = -K_1 z v n_i \cdot n_v$$

If this is the only important loss mechanism, then at any time

$$n_i(0) - n_i = n_v(0) - n_v$$

and so $$\frac{dn_i}{dt} = -K_1 z \nu \left(n_v(0) - n_i(0) + n_i\right) n_i$$

For $n_i(0) \approx n_v(0)$

$$\frac{dn_i}{dt} = -K_1 z \nu n_i^2 = K_1' n_i^2$$

$$n_i(t) = \frac{n_i(0)}{1 + n_i(0) K_1' t} \tag{17}$$

K_1 will be of the same order as K_0 if only interstitials move.

The loss rate by this process is much smaller than for coupled Frenkel pairs, for a given temperature, as can be verified for typical lattices. This means that close Frenkel pairs will disappear first when the temperature is raised. In either case, the temperature dependence of the annealing rate is in the jump probability, and over the available experimental irradiation temperatures this probability has a large variation.

It must be added that the above description of annealing is much oversimplified. Close and separated Frenkel defects are only the limits of the degree of correlation. Other processes also occur, including recombination at an impurity site, cluster migration, and vacancy migration.

II. Defect States in Semi-Conductors

Introduction

Before reviewing experimental methods, it is well to recall a few fundamental and well-known facts about the physics of defect states in semi-conductors. In the band picture, a lattice defect, whether it be a chemical substitution or a radiation induced vacancy, etc., produces a local perturbation in the electronic states and can be represented by an allowed energy level (or levels) introduced into the forbidden gap between the top of the valence band (let this energy=0) and the bottom of the conduction band (at E=Eg). The introduction of radiation induced states has two important consequences: a) the free carrier concentration is changed (usually but not always it is decreased) due to trapping at the local state, and b) the increase in local states increases the total atomic scattering cross section for carriers, thereby reducing the carrier mobility. Both events obviously have a strong influence on the electrical properties of the semi-conductor and these become the dominant radiation effects. Structural changes belong to a much higher concentration regime.

Carrier Concentration and Defect States

The free carrier concentrations are determined by the position of the Fermi level in the forbidden gap, according to the well-known integrals

$$n_e = \int_{E_g}^{\infty} Z_e(E) f_e(E) dE = 2 C_e(T) e^{-E_g - E_f/kT}$$

$$n_h = \int_{-\infty}^{0} Z_h(E) f_h(E) dE = 2 C_h(T) e^{-E_f/kT} \qquad (18)$$

for electrons and holes, where $Z_e(E)$ is the density of states for conduction electrons at energy E,

$$Z_e(E) = \frac{1}{4\pi^2}\left(\frac{2m_e}{\hbar^2}\right)^{3/2} E^{1/2}$$

and $f_e(E)$ is the Fermi occupation probability

$$f_e(E) = \frac{1}{1 + e^{(E-E_F)/kT}}$$

m_e is the effective electron mass and

$$C_e(T) = \left(\frac{2\pi m_e kT}{h^2}\right)^{3/2}$$

Similar definitions apply to the conduction holes with $f_h = 1 - f_e$.

For <u>intrinsic</u> crystals with no impurities, charge conservation requires $n_e = n_h$, which requires from Equation (18)

$$C_e(T)\, e^{-(E_g - E_F)/kT} = C_h(T)\, e^{-E_F/kT}$$

This defines the Fermi energy for intrinsic crystals

$$E_F = \frac{E_g}{2} + \frac{3}{4} kT \ln\left(\frac{m_h}{m_e}\right) \qquad (19)$$

which is weakly temperature dependent and half-way up the forbidden gap at absolute zero. The temperature dependence of the carrier concentration is then explicitly given by

$$n_e \simeq \left(\frac{2\pi m_e kT}{h^2}\right)^{3/2} e^{-E_g/2kT} \qquad (20)$$

The introduction of chemical substitutions, as for example by doping group IV crystals (Si, Ge) with groups III or V impurities, introduces donor (group V giving n-type Si) or acceptor (group III giving p-type Si) energy states near the conduction or valence limits respectively.

FIGURE 9

ENERGY STATES FROM CHEMICAL SUBSTITUTIONS

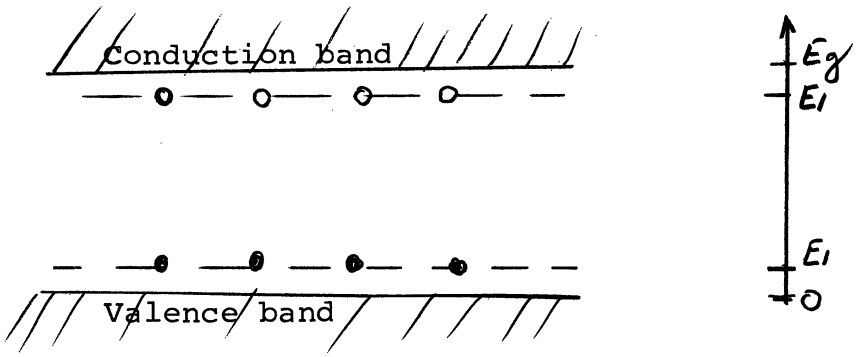

For illustration, we may look at a p-type Si, wherein donor impurities (P) have been added. The effect on carrier concentration can be dramatic if the donor concentration N_d is large relative to the intrinsic number n_e in Equation (20). The result is a shift of the Fermi level toward the conduction band, as can be seen from the

following arguments. If N_d is the donor density introduced, and N_d^o and N_d^+ the neutral and ionized states respectively, then if the unionized states lies at E_1, near E_g

$$N_d^o = \frac{N_d}{\gamma e^{E_i - E_f/kT} + 1}$$
$$N_d^+ = N_d - N_d^o \qquad (21)$$
$$N_d^+ = \frac{N_d}{1 + \frac{1}{\gamma} e^{-E_i - E_f/kT}}$$

γ is a statistical factor arising from the partition functions for the neutral and ionized donor states; it has the value of ½ if the neutral donor has an unpaired s electron, and 2 if not.[3] The number of free electron carriers is now determined by the chemical equilibrium, as revealed by the zero gradient of the free energy, just as developed from Equation (4). This is, however, equivalent to simultaneous statements of: a) the law of mass action applied to allowed transitions, and b) conservation of all charge carriers. The law of mass action can be written for both the impurity donor states and the intrinsic hole states:

$$n_e + N_d^+ \rightleftharpoons N_d^o = N_d - N_d^+; \quad \frac{n_e N_d^+}{N_d^o} = K_1$$
$$n_e + n_h \rightleftharpoons 1 \qquad n_e n_h = K_0 \qquad (22)$$

where K_1 and K_0 are equilibrium constants. The conservation of carriers requires

$$n_e = N_d^+ + n_h \qquad (23)$$

which becomes, using Equation (22),

$$n_e = \frac{K_1 N_d}{n_e + K_1} + \frac{K_0}{n_e} \tag{24}$$

The system of Equations (18), (21), (23), and (24) can be solved for all unknowns; most particularly we are interested in values for n_e and E_f in terms of the known parameters N_d, T, and E_1. For significant levels of doping, the second term in Equation (24) can be ignored as very small. Then it is quickly found that

$$\begin{aligned} K_1 &= 2\gamma_1 C(T)\, e^{-E_g - E_1/kT} \\ E_f &= \frac{E_1 + E_g}{2} + \frac{kT}{2} \ln\left[\frac{N_d}{2\gamma_1 C(T)}\right] \\ \frac{n_e^2}{N_d - n_e} &= 2\gamma_1 C(T)\, e^{-E_g - E_1/kT} \end{aligned} \tag{25}$$

For $N_d \gg n_e$

$$n_e \approx N_d^{\frac{1}{2}} (2\gamma_1)^{\frac{1}{2}} \left(\frac{2\pi m_e kT}{h^2}\right)^{3/4} e^{-E_g - E_1/kT \cdot 2}$$

The new Fermi level is midway between Eg and E_1 at absolute zero, but drops toward $\frac{Eg}{2}$ as $T \to \infty$, or $N_d \to 0$. The shift is indicated crudely below for donor introduction:

FIGURE 10

DEPENDENCE OF FERMI LEVEL ON T, N_d

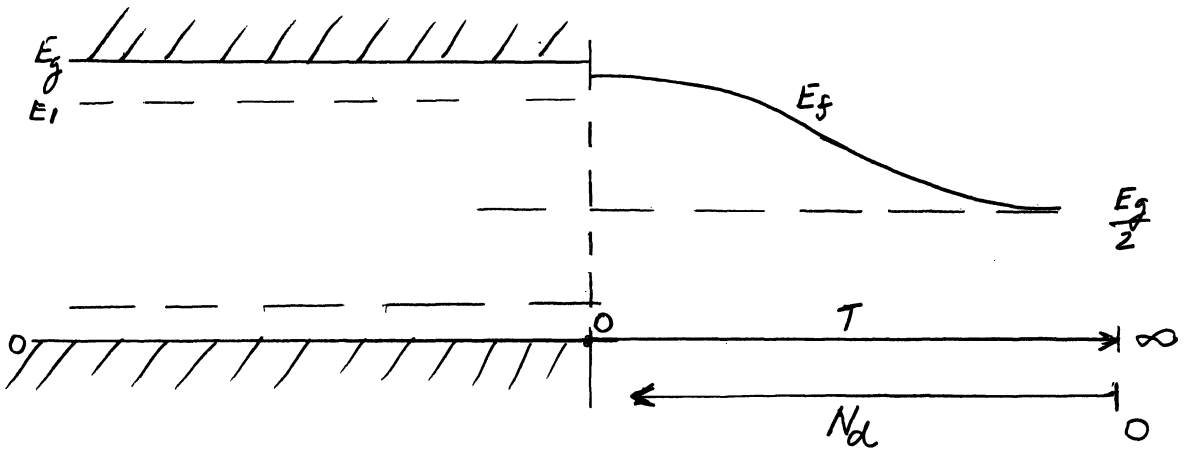

Let us now examine this same extrinsic semi-conductor when a second defect state is introduced at some energy below the conduction band:

FIGURE 11

TWO DEFECT SYSTEM

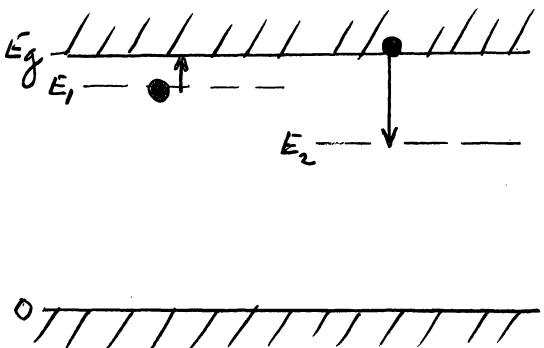

Let us furthermore require that this second state is born with an electron deficiency, i.e. as an acceptor, and that it lies deep in the forbidden gap relative to E_1. Such requirements have been ascribed in the literature to a possible state of the vacancy defect from a radiation induced separated Frenkel pair.[4] If we assume the hole carrier concentration is negligible, then the expressions

of ionization state, mass action, and charge concentration require

$$N_2^0 = \frac{N_2}{\gamma_2 e^{E_2-E_f/kT}+1} \quad ; \quad N_2^+ = N_2 - N_2^0 = \frac{N_2}{1+\frac{1}{\gamma_2} e^{E_f-E_2/kT}}$$

$$N_1^+ = \frac{N_1}{1+\frac{1}{\gamma_1} e^{-(E_1-E_f)/kT}} \qquad (26)$$

$$\frac{n_e N_2^+}{N_2^0} = K_2 \; ; \; \frac{n_e N_1^+}{N_1^0} = K_1$$

$$n_e + N_2^0 = N_1^+$$

In particular note that the charge conservation is an inventory of the location of conduction electrons on the assumption that E_2 is indeed a trap (if it had been a deep donor we would write $n_e=N_2^++N_1^+$). If $N_2 < N_1$, E_f will lie high enough such that at all reasonable temperatures $E_f-E_2/kT \gg 1$. This means that the trapping level is essentially filled and K_2, $N_2^+ \simeq 0$ and $N_2^0 \simeq N_2$. Under these conditions, and using Equation (18),

$$n_e + N_2 = \frac{N_1}{1+\frac{1}{\gamma_1} e^{-E_1/kT} \cdot \frac{n_e}{2C e^{-E_g/kT}}}$$

or

$$n_e + N_2 = \frac{N_1}{1+\frac{n_e}{2\gamma_1 C e^{-(E_g-E_1)/kT}}}$$

This can be rewritten in the more familiar form

$$\frac{n_e(n_e+N_2)}{N_1-N_2-n_e} = 2\gamma_1 C(T) e^{-(E_g-E_1)/kT} \qquad (27)$$

This is to be compared with the carrier concentration in Equation (25); the concentration is lowered by the presence of N_2.

Precisely this situation was demonstrated by Charles Barnes, of this department, after the thermal neutron irradiation of n-type Cd Te.[5] N_1 corresponded to a chemical impurity at approximately 0.01 ev below Eg, and N_2 to a cadmium vacancy. The loss rate of electron carriers at the early stages of the total irradiation dose showed a removal rate of nearly one free electron per cadmium vacancy created.

It is important to point out that while this simple model apparently works well in this example no knowledge is given about the charge state or the level energy--the model only requires an acceptor state lying deep, but near the conduction band. The situation can become much less clear when more than one level is required to fit experimental data. The work of Cleland, Crawford, and Pigg on Ge is an example of the fit to a multi-level model for Ge by James and Lark-Horovitz.[6]

REFERENCES

1. See for example the resumé of Billington and Crawford, "Radiation Damage in Solids," page 319.

2. A. C. Damask and G. J. Dienes, Point Defects in Metals, Gordon and Breach, 1963, p. 80.

3. J. H. Crawford, Jr., and D. K. Holmes, Proc. Phys. Soc. (London), A67, 294 (1954).

4. H. M. James and K. Lark-Horowitz, Z. Physik, Chime., 198, 107 (1951).

5. C. E. Barnes and C. Kikuchi, "Thermal-Neutron-Induced Defects in Cadmium Telluride and Cadmium Sulfide," University of Michigan Technical Report 04381-10-T, March 1967.

6. J. W. Cleland, J. H. Crawford, Jr., and J. C. Pigg, "Fast Neutron Bombardment of p-Type Germanium," Phys. Rev., 99, 1170 (1955).

7. J. W. Corbett, "Electron Radiation Damage in Semiconductors and Metals," in Solid State Physics, Supplement 7, Academic Press, 1966.

8. A. J. Dekker, Solid State Physics, Prentice-Hall, 1957.

IONIZATION EFFECTS IN SEMICONDUCTORS

R. B. Oswald, Jr.

Harry Diamond Laboratories
Washington, D. C. 20438

Ionization Effects in Semiconductors

I. Introduction:

The two most important effects resulting from the interaction of radiation with a semiconductor are permanent damage and ionization effects. Permanent damage results from atomic displacement produced primarily by the scattering of energetic neutrons or charged particles. Ionization effects are created by the generation of free carriers within the bulk material and by the "replacement currents" generated by secondary electron emission. The most sensitive manifestation of the ionization effects in a semiconductor is the generation of excess electron hole pairs.

It is the object of this discussion to provide the reader with a fundamental knowledge of the ionization effects which result in a semiconductor materials. Toward this end we have devided the discussion into three basic areas, a) the electronic band structure of solids b) ionization and the generation of free carriers and c) the response of a semiconductor to ionization. The text presented here follows three basic sources 1) A.J. Dekker, Solid State Physics, Prentice Hall, Inc. Englewood Cliffs, N.J., 1957, 2) V.S. Vavilov, Effects of Radiation on Semiconductors, Consultants Bureau, New York, New York, 1965 and 3) S.M. Ryvkin, Photoelectric Effects in Semiconductors, Consultants Bureau, New York, New York, 1964.

II. Electronic Band Structure in Solids

A. Crystal Structure:

Before we can adequately describe the effects of energetic radiation on a semiconductor it is necessary to describe the properties which control the electronic processes in the material. Most of these properties are a direct result of the atomic order and bonding of the atoms in the solid. In general, the solids which occur in nature are in the crystalline state, in either single or polycrystalline form. It is the crystalline solid-state which we shall be concerned with in this discussion. Solids which are not characterizied by the crystalline state are called amorphous.

The crystalline state of solids in characterizied by the regular periodic arrangement of the constituent atoms in the solid.

The fact that the atoms in a solid are ordered is best illustrated by comparing the atomic order in a liquid with the order in a solid, as illustrated in figure 1.

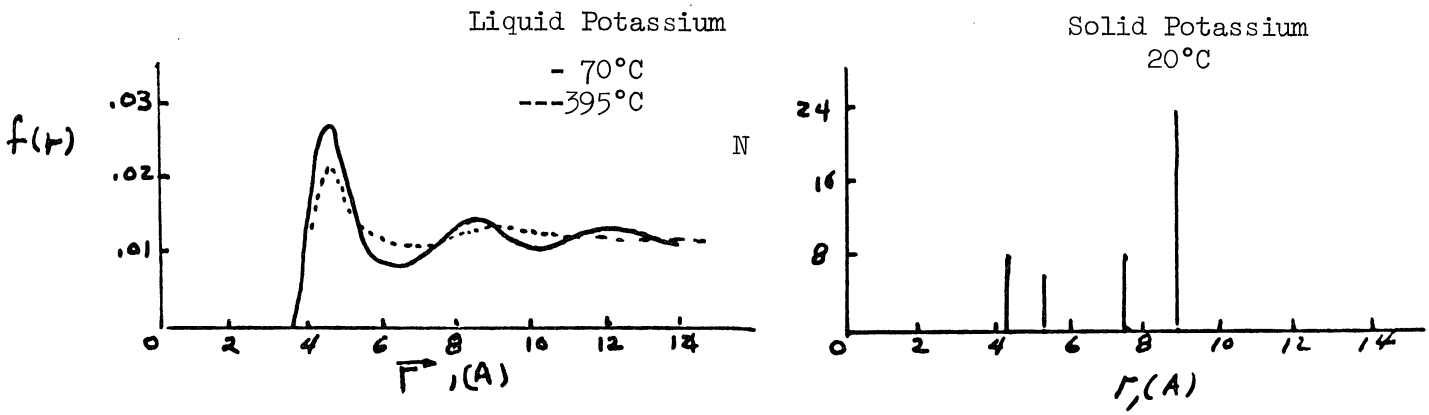

Figure 1. Number of atoms in potassium as a function of distance from a given K atom for the Liquid and Solid state.

The atoms of the solid are stacked in a regular manner, forming a three-diminsional pattern, which can be constructed by a three-dimensional translation of a characteristic unit cell. If the periodicaity of the pattern continues uniterrupted throughout the solid then it is called a single crystal. When the pattern is not continuously reproduced, but is interrupted at grain boundrys then it is called polycrystalline.

Typical crystal structures which occur in nature are shown in the following samples.

a) Cesium Chloride
Structure: Body Center Cubic

C_s = O
Cl = ●

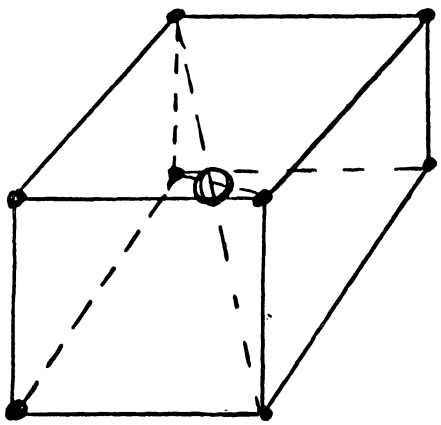

b) Germanium and Silicon
Structure: Diamond (Described as a face centered cubic point lattice in which each point corresponds to two atoms, one at (0,0,0) the other at (1/4, 1/4, 1/4).

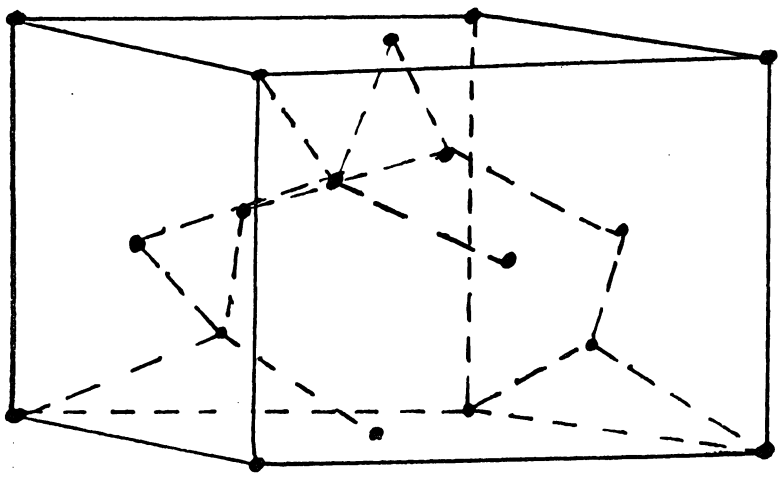

Figure 2.

B. Description of a Solid

2. Atomic Bonding and the Classification of Solids:

From the very existance of solids and their general characteristics two conclusions can be made about the forces which act between atoms in a solid, 1) large attractive forces act between the atoms to hold them together, as illustrated by the existance of the solid and there tensil strength, 2) there must also be large repulsive forces acting between the atoms in a solid since we know that extremely large forces are required to produce compression of a solid and obviously a repulsive force is needed to prevent complete collapse of the system due to the attrictive forces. Neglecting for the moment the exact origin of the forces which bond the atoms, the potential energy of atom A in a compound AB can be represented by

$$E(r) = -\alpha/r^n + \beta/r^m$$

where r is the distance between the two nuclei of the two atoms, α, β, n and m are constants characteristic for the AB molecule. The zero energy is choosen such that @ $r = \infty$, $E = 0$ The first term then corresponds to the energy associated with the attractive forces while the second term is associated with the repulsive forces. For this model the energy is schematically represented as a function of the atomic seperation r by

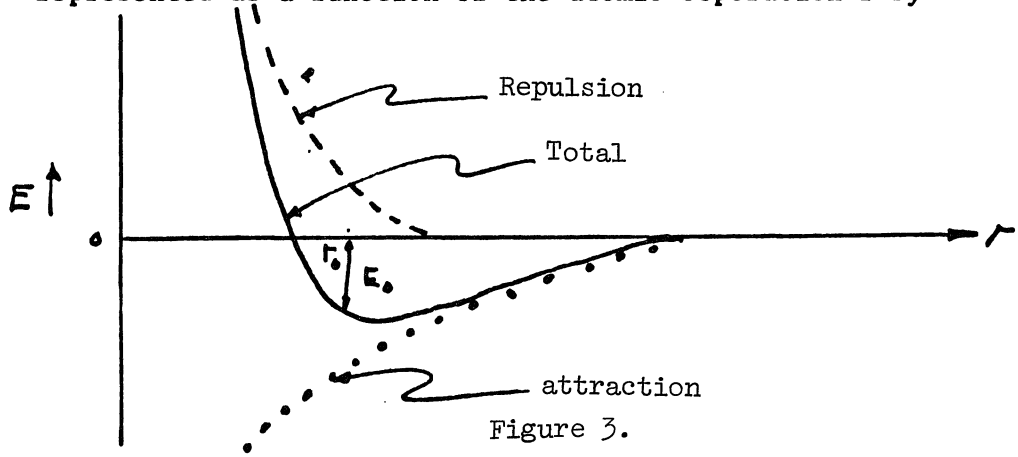

Figure 3.

In real solids this is in general the manner with which interatomic force acts to produce a stable lattice. The actual nature of the bonding varies from one solid to another. There is a calssification system which has resulted based upon the extreme types of bonding. These are 1) Ionic Bonding, 2) Covalent Bonding, 3) Metalic Bonding and 4) van der Waals Bonding.

The ionic crystal is characterizied by the ionization of one of the constituent by the other, forming positive and negative ions. The attraction force results from coloumb interaction of the ions and the repulsive force results from the overlap of the charge bonds and the Paulic exclusion principle. An example of this type of solid is the alkali halides, (NaCl, KCl, etc).

The covalent crystal results from sharing of valence electrons by neighboring atoms to complete their outer electron shell. The sharing is done by pairing of electrons with opposite spin. Examples of this are elements of group IX of the periodic table (C, Si, Ge, Sn, Pb).

The metallic bond is different than either the ionic or covalent bond. As we all know the properties of metals originate from the high degree of mobility of the electrons. The metalic bond also arises from the coulomb interaction of the electron sea and the positive metallic ions. Example of this type of bonding would be Li, Na, K etc.

van der Waals bonding results in materials with completed outer electronic shells. The cohessive force results from dipole-dipole interaction. Examples would be argon, krypton, etc.

3. Electronic Band Structure in Solids:

Many of the physical properties of solids are determined

directly from the electronic energy levels of the crystal. Although the discussion which follows is limited in its approach to the real crystal, it will point out the salient features of the electronic properties of solids. We shall consider the behavior of electrons in a periodic one-dimensional potential. Essentially each of the potential energy wells may be considered to represent the potential an electron sees in the vicinity of an atom in a linear chain. This is called the "Kronig-Penney" model or the one electron model. We first make the assumption that

1. The potential energy of an electron in a one-dimensional crystal has the form of a periodic array of square wells.
2. The energy E of electrons is less the potential V_o.

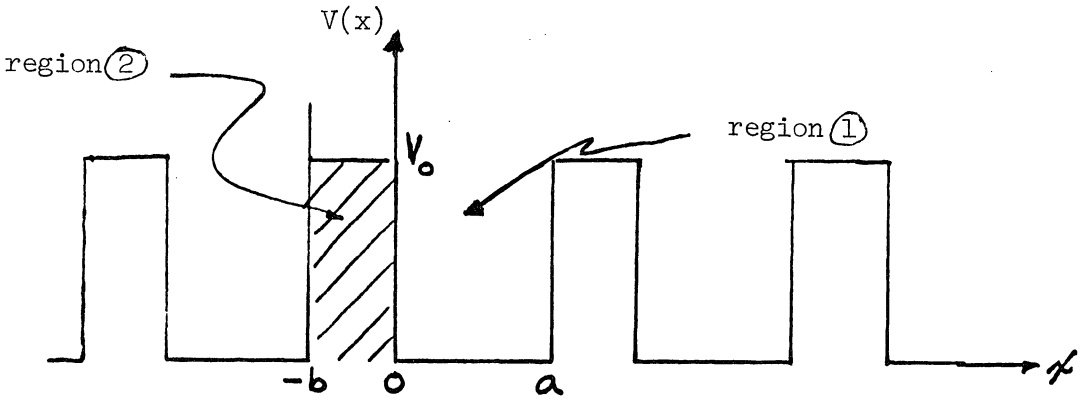

Figure 4.

The Schrodinger equation for an electron in each of these two regions is

$$\textcircled{1} \quad \frac{d^2\psi}{dx^2} + \left(\frac{2m}{\hbar^2}\right) E\psi = 0 \quad , \text{ for } \quad 0 < x < a$$

$$\textcircled{2} \quad \frac{d^2\psi}{dx^2} + \left(\frac{2m}{\hbar^2}\right)(E - V_o)\psi = 0 \quad , \text{ for } \quad -b < x < 0$$

Now define two real quantities α and β by

$$\alpha^2 = \left(\frac{2m}{\hbar^2}\right) E$$

$$\beta^2 = \left(\frac{2m}{\hbar^2}\right)(V_0 - E) \qquad , E < V_0$$

then we get after substitution

$$(1) \quad \frac{d^2\psi}{dx^2} + \alpha^2\psi = 0$$

$$(2) \quad \frac{d^2\psi}{dx^2} - \beta^2\psi = 0$$

Using the Bloch theorem for a periodic potential we know

$$(3) \quad \psi(x) = e^{ikx} u_k(x)$$

substituting into (1) and (2) we get

$$-k^2 e^{ikx} u_k(x) + 2ik e^{ikx} \frac{d}{dx} u_k(x) + e^{ikx} \frac{d^2}{dx^2} u_k(x) + \alpha^2 e^{ikx} u_k(x) = 0$$

and

$$-k^2 e^{ikx} u_k(x) + 2ik e^{ikx} \frac{d}{dx} u_k(x) + e^{ikx} \frac{d^2}{dx^2} u_k(x) - \beta^2 e^{ikx} u_k(x) = 0$$

thus

$$(4) \quad \frac{d^2}{dx^2} u_k(x) + 2ik \frac{d}{dx} u_k(x) + (\alpha^2 - k^2) u_k(x) = 0 \qquad (4)$$

for $0 < x < a$

and

$$\frac{d^2}{dx^2} u_k(x) + 2ik \frac{d}{dx} u_k(x) - (\beta^2 + k^2) u_k(x) = 0 \qquad (5)$$

for $-b < x < 0$.

The solutions are:

$$u_1(x) = A e^{i(\alpha-k)x} + B e^{-i(\alpha+k)x} \qquad (6)$$

$$u_2(x) = C e^{(\beta-ik)x} + D e^{-(\beta+ik)x} \qquad (7)$$

with the Boundry Conditions:

$u_1(0) = u_2(0)$, continuity @ $x=0$

$u_1(a) = u_2(-b)$, periodicity

$$\left(\frac{du_1}{dx}\right)_{x=0} = \left(\frac{du_2}{dx}\right)_{x=0}$$

$$\left(\frac{du_2}{dx}\right)_{x=-b} = \left(\frac{du_1}{dx}\right)_{x=a}$$

It can be shown that this leads to the following condition:

$$\frac{\beta^2-\alpha^2}{2\alpha\beta}\sinh\beta b \sin\alpha a + \cosh\beta b \cos\alpha a = \cos k(a+b) \qquad (8a)$$

To obtain a simpler relation we let the potential barriers become a delta function i.e.

$$V_0 \longrightarrow \infty$$

$$b \longrightarrow 0$$

and $\quad b \cdot V_0 = \text{constant}$

After rearranging (8) we get

$$\frac{\beta}{2\alpha}\sinh\beta b \sin\alpha a + \cosh\beta b \cos\alpha a - \frac{\alpha}{2\beta}\sinh\beta b \sin\alpha a = \cos k(a+b) \qquad (8b)$$

now take the limit as $\beta^2 \to \infty$ and $b \to 0$

$$\lim_{\substack{\beta^2\to\infty \\ b\to 0}} \beta^2 \cdot b = \lim_{\substack{V\to\infty \\ b\to 0}} \left[\frac{2m(V_0-E)}{\hbar^2}\right] \cdot b = \frac{2mV_0 b}{\hbar^2}$$

and

$$\lim_{\substack{\beta^2\to\infty \\ b\to 0}} \cos k(a+b) \longrightarrow \cos ka$$

$$\lim_{\substack{\beta^2\to\infty \\ b\to 0}} \cosh\beta b \cos\alpha a \longrightarrow \cosh 0 \cos\alpha a \longrightarrow \cos\alpha a$$

$$\lim_{\substack{\beta^2\to\infty \\ b\to 0}} \frac{-\alpha}{2\beta} \sinh\beta b \sin\alpha a = 0$$

while

$$\lim_{\substack{\beta^2\to\infty \\ b\to 0}} \frac{\beta}{2\alpha} \sinh\beta b \sin\alpha a \longrightarrow \frac{\beta^2 b}{2\alpha} \frac{\sinh\beta b}{\beta b} \sin\alpha a$$

$$\longrightarrow \frac{\beta^2 b}{2\alpha} \sin\alpha a \longrightarrow \frac{m V_0 b}{\alpha\hbar^2} \sin\alpha a$$

Therefore (8b) becomes in the limit

$$\frac{m V_0 b}{\alpha\hbar^2} \sin\alpha a + \cos\alpha a = \cos ka \qquad (9)$$

Now define

$$P \equiv \frac{m V_0 b a}{\hbar^2}$$

then we have

$$\boxed{\frac{P}{\alpha a} \sin\alpha a + \cos\alpha a = \cos ka} \qquad (10)$$

The solution to the wave equation for an electron in periodic delta function potential exist only if (10) is satisfied.

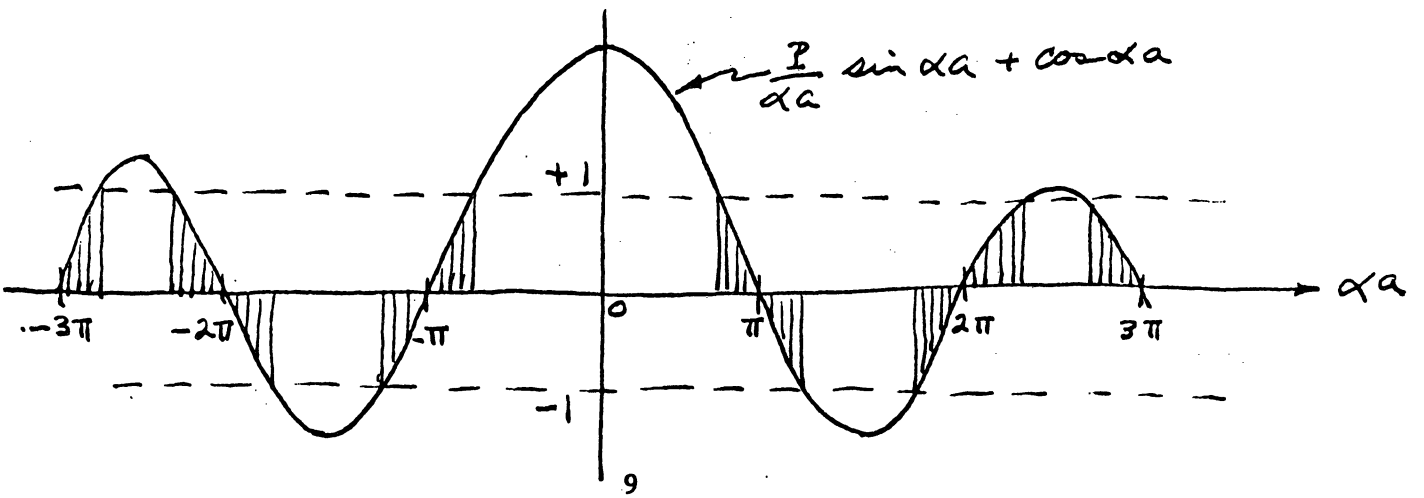

Figure 5.

Now 1) R. H. S. = cos ka $\therefore$ we can only have solutions when L.H.S. has values between $\pm$ 1

2) α^2 is proportional to energy

Therefore a) The energy spectrum consists only of a number of allowed energy bands separated by forbidden regions.

b) The width of the energy bands increases with increasing values of α a $\therefore$ increasing energy

c) The width of the allowed bands decrease with increasing P, i.e., increasing binding energy of the electrons.

Hence we can construct a diagram of the allowed energy bands

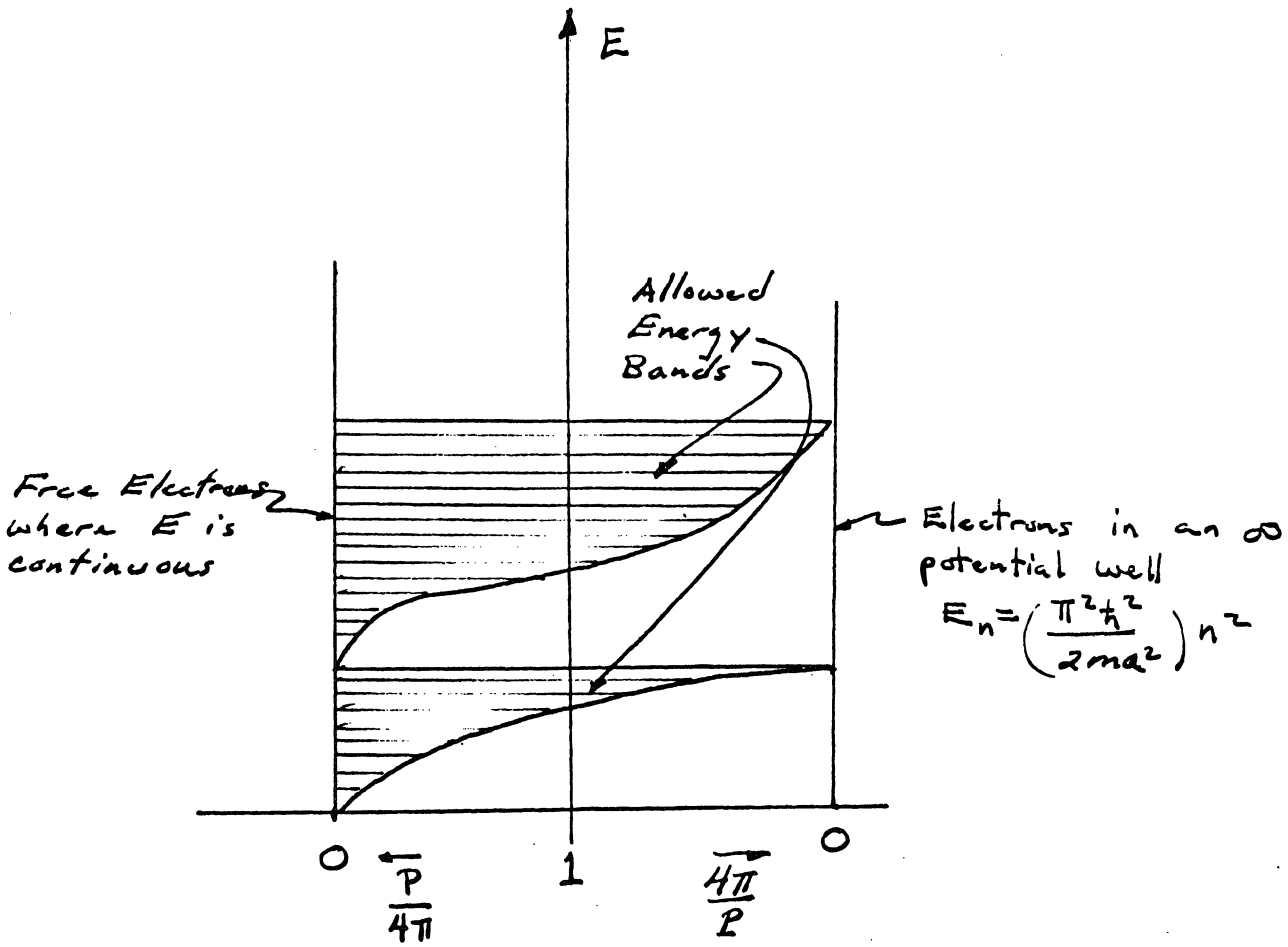

Figure 6.

Brillouin Zones:

We should recall that discontinuities in the E vis k curve occur for

$$\cos \alpha a = \cos ka = \pm 1$$

i.e. $$\alpha a = ka = n\pi$$

So the discontinuities occur at $k = \frac{n\pi}{a}$ $n = 1, 2, 3, \ldots$

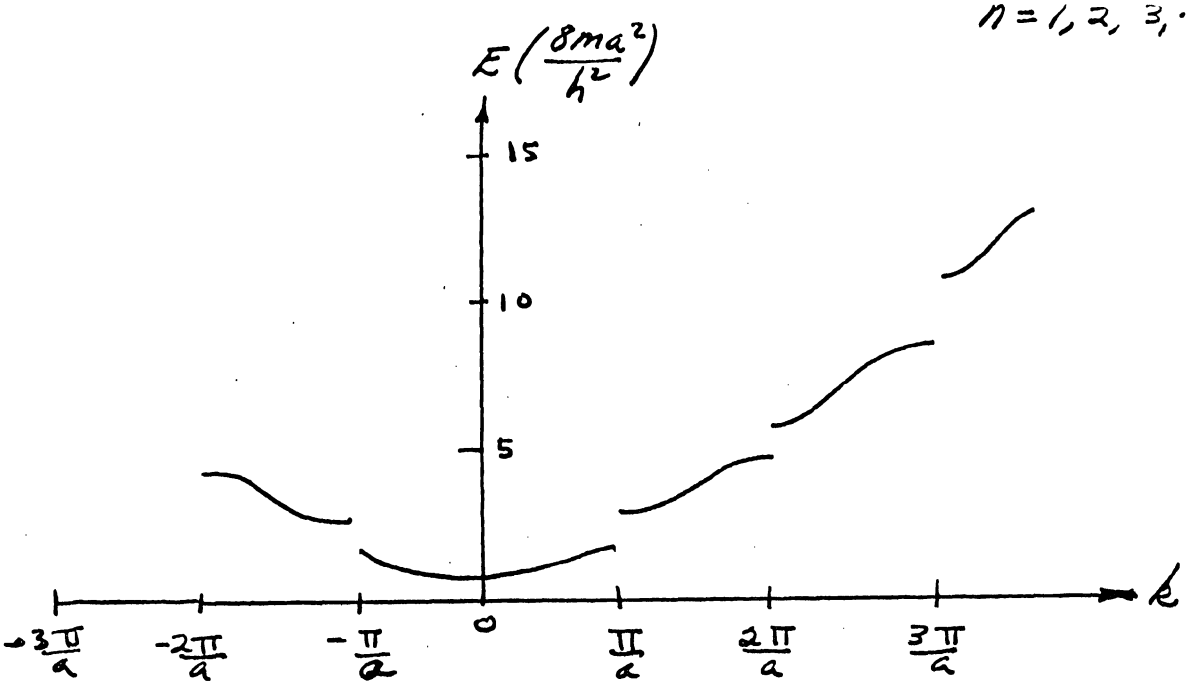

Figure 7.

Since $\left\{ \frac{P}{\alpha a} \sin \alpha a + \cos \alpha a = \cos ka = \cos \left(k + \frac{2\pi n}{a}\right) a \right\}$ which implies that the energy is a periodic function of k. In other words k is not uniquely defined it is therefore convienient to introduce a "Reduced Wave Vector" which is limited to the single region

$$-\frac{\pi}{a} \leq k \leq \frac{\pi}{a}$$

then we can plot E vis k

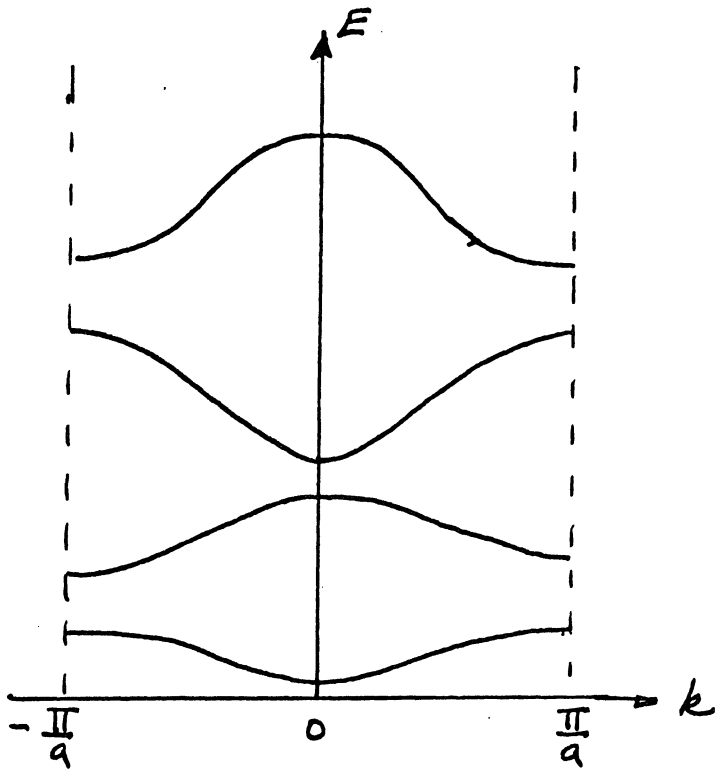

Figure 8.

The distinction between conductors, semiconductors can now be illustrated. To show this consider a particular energy band and assume it to be filled with electrons up to a certain wave number k_1. From the stand point of conductivity one would like to know how many "free" electrons exist in the energy band.

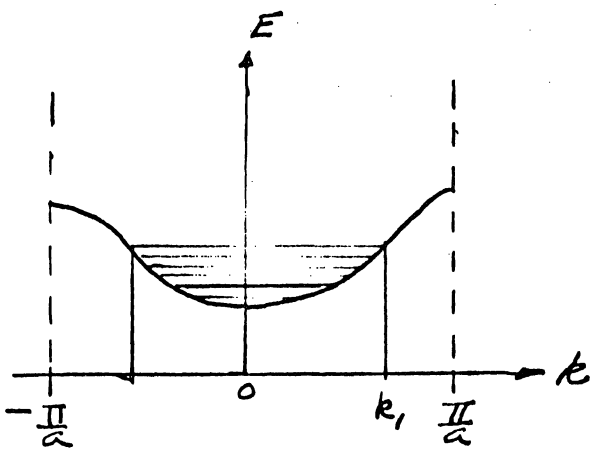

Figure 9.

It can be shown that the effective number of free electrons is given by

$$N_{eff} = \frac{2L}{\pi}\frac{m}{\hbar^2}\int_0^{k_1}\left(\frac{d^2E}{dk^2}\right)dk$$

$$N_{eff} = \frac{2L}{\pi}\frac{m}{\hbar^2}\left[\left.\frac{dE}{dk}\right|_{k_1} - \left.\frac{dE}{dk}\right|_{k=0}\right]$$

at $k=0$, $\frac{dE}{dk}=0$ so

$$N_{eff} = \frac{2L}{\pi}\frac{m}{\hbar^2}\left.\left(\frac{dE}{dk}\right)\right|_{k_1} \qquad (11)$$

Thus we note that

1. The effective number of electrons in a completely filled band is zero, since dE/dk = 0 at the top and bottom of the band.
2. The effective number of electrons reaches a maximum for a

band filled to the inflection point of the E (k) curve since dE/dk is a maximum.

From the above discussion of the properties of an electron in a periodic linear potential we can construct a simple model which posses many of the features of real solids. A more accurate picture is obtained if we applied the above technique to a three dimensional lattice having the symetry of the real crystal. However, from our simply theory we can conclude that the electrons can exist only in certain allowed energy bands.

Insulator: If the solid contains a certain number of energy bands which are completely filled and all the other bands completely empty, it is an insulator

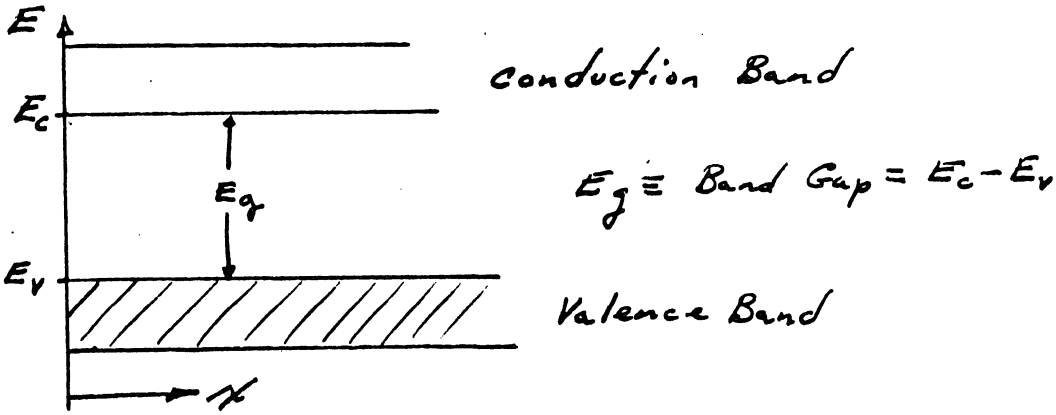

At T = o the valence band is completely filled and the conduction band is emply so that the material will be a perfect insulator. At temperatures not equal to zero some of the electrons will be thermally excited up into the conduction band. However if E_g is large compared to kT it effectively remains an insulator.

Conductor: From the above discussion it is indicative that a conductor will have a partially filled energy band @ T = 0

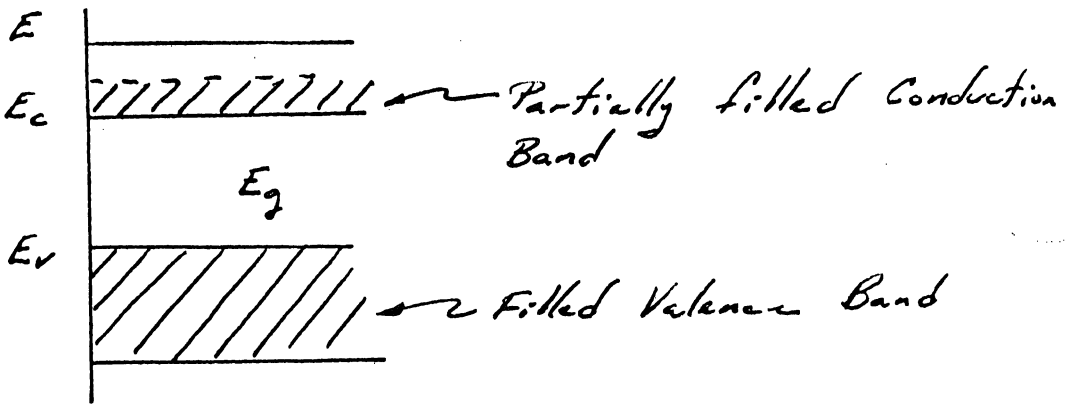

Intrinsic Semiconductor: A semiconductor can be represented as a material which has a completely filled valence band and an empty conduction band at T = 0. However, the band gap E_g is small compared to the insulator say of the order of 1 ev. Then as the temperature is raised to room temperature, electrons are excited thermally into the conduction band.

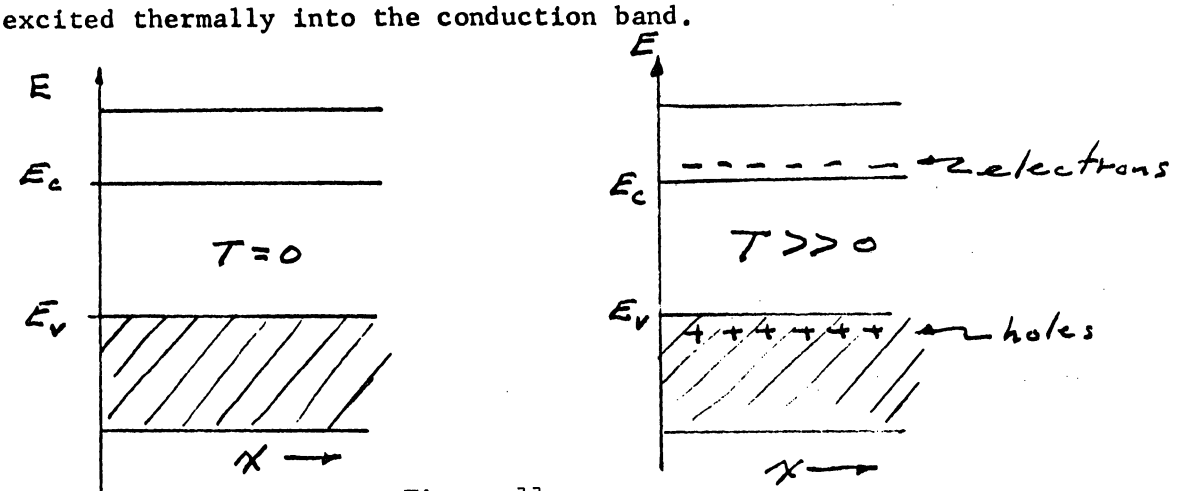

Figure 11.

When the electrons are excited into the conduction band they leave behind vacancies in the valence band called "holes". Both electrons and holes are mobile so that both contribute to the conductivity of the material.

Electrons and Hole Distributions in a Semiconductor

Since the properties of a semiconductor are determined partially by the number of effective electrons and holes in the conduction and valence bands respectively, it is necessary to determine quantitatively their number and temperature dependence. Let us define n(E)dE to be the number of electrons per unit volume occupying states in the energy range interval dE about E as shown in Figure 12 below.

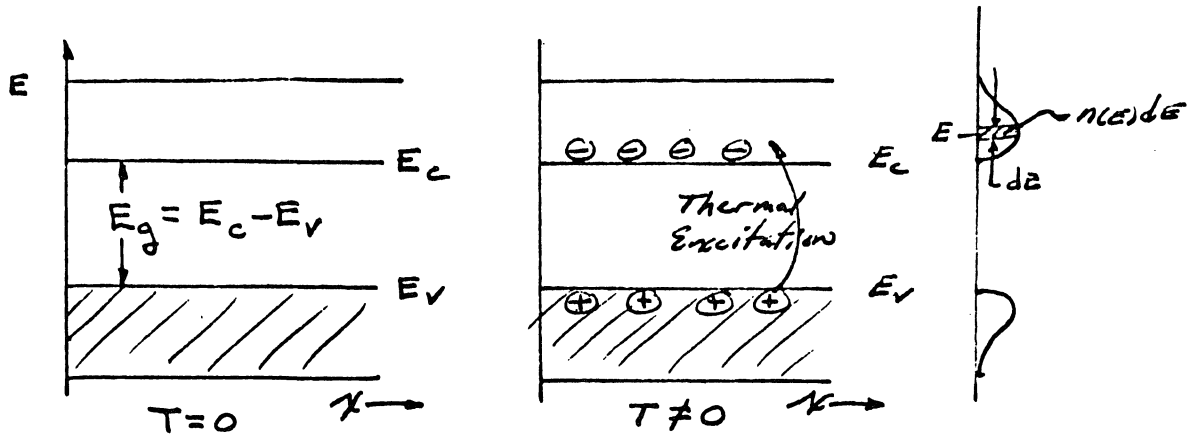

Figure 12

In addition we will define two functions Z(E) and F(E)dE. The function Z(E)dE is defined to be the number of possible states per unit volume at energy E. F(E) is defined to be the probability that a state in dE about E be occupied by an electron. Then the number of electrons with energies in dE about E, n(E), is given by the product of the number of allowed states times the probability of occupation as given by

The total number of electrons per unit volume in the conduction

band is given by

$$n_0 = \int_{E_c}^{E_{max}} n(E)\,dE = \int_{E_c}^{E_{max}} Z(E)\,F(E)\,dE. \qquad (13)$$

For an intrinsic semiconductor Z(E)dE is given approximately by

$$Z(E)\,dE = \frac{4\pi}{h^3}(2m_e^*)^{3/2}(E-E_c)^{1/2}\,dE \qquad (14)$$

for the density of states in the conduction band and

$$Z(E)\,dE = \frac{4\pi}{h^3}(2m_h^*)^{3/2}(E_v-E)^{1/2}\,dE \qquad (15)$$

for the density of states in the valence band. The distribution function F(E) is the well known Fermi function given by

$$F(E) = \frac{1}{e^{(E-E_f)/kT}+1} \qquad (16)$$

where E_F is the Fermi energy. This energy corresponds to that energy at which the probability of occupation is one half. The energy dependence of these functions are shown schematically below in Figure 13.

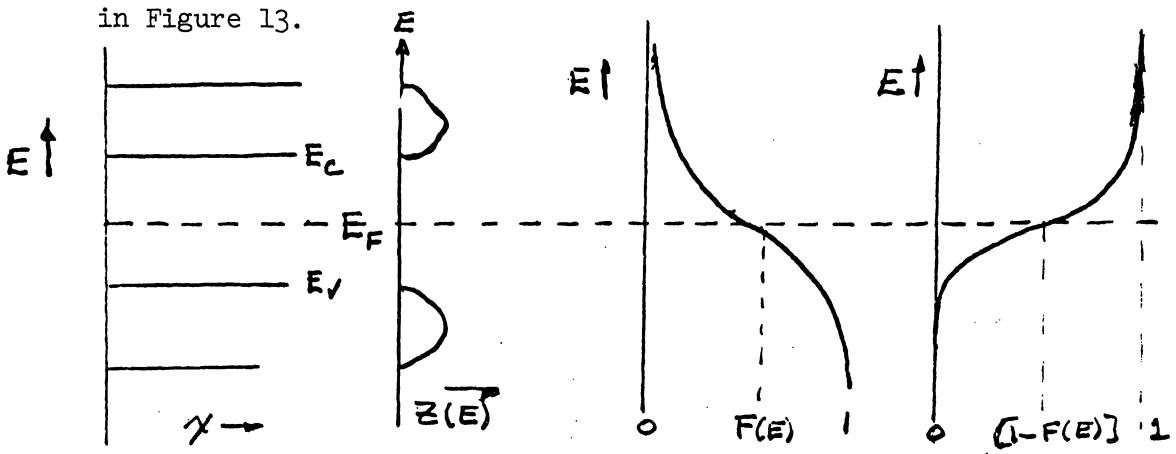

Figure 13.

Now the equilibrium density of electrons in the conduction band

can be obtained from

$$n_0 = \int_{E_c}^{E_{max}} N(E)\,dE = \int_{E_c}^{E_{max}} Z(E)\,F(E)\,dE$$

$$\doteq \left(\frac{4\pi}{h^3}\right)(2m_e^*)^{3/2} \int_{E_c}^{E_{max}} \frac{(E-E_c)^{1/2}\,dE}{e^{(E-E_F)/kT}+1} \qquad (17)$$

We will now let $E_{max} \to \infty$ which we justify by the fact that at E_{max}, $Z(E) = 0$ since $m_e^* = 0$. Furthermore we will assume that $E_c - E_F \geq 4kT$, then we can write

$$n_0 = \left(\frac{4\pi}{h^3}\right)(2m_e^*)^{3/2} \int_{E_c}^{\infty} \frac{(E-E_c)^{1/2}}{e^{(E-E_F)/kT}} \qquad (18)$$

since $e^{(E-E_F)/kT} >> 1$ for $E \geq E_c$.

The above expression can be rewritten as

$$n_0 = \frac{4\pi}{h^3}(2m_e^*)^{3/2}(kT)^{3/2} e^{(E_F-E_c)/kT} \int_{E_c}^{\infty} \frac{(E-E_c)^{1/2}}{(kT)^{3/2}} e^{-\frac{(E-E_c)}{kT}}\,dE$$

Since

$$\int_0^{\infty} x^{1/2} e^{-x}\,dx = \frac{\pi^{1/2}}{2} \qquad (19)$$

we have for the electron density in the conduction band

$$n_o = 2\left(\frac{2\pi m_e^* kT}{h^2}\right)^{3/2} e^{(E_F - E_c)/kT} \qquad (20)$$

or

$$n_o = N_c\, e^{(E_F - E_c)/kT} \qquad (21)$$

where N_c is the effective density of states in the conduction band.

For the equilibrium density of holes in the valence band, p_o we use the relationship

$$p_o = \int_{E_{min}}^{E_v} Z(E)[1 - F(E)]\, dE \qquad (22)$$

where

$[1 - F(E)]$ = the probability that a state of energy E be unoccupied

$$Z(E)\, dE = \left(\frac{4\pi}{h^3}\right)(2m_h^*)^{3/2}(E_v - E)^{1/2}\, dE \qquad (23)$$

and m_h^* represents the effective mass of the holes near the top of the valence band. We will assume that $E_F \geq E_V + 4kT$, then we can use the approximation that

$$[1 - F(E)] \simeq e^{(E - E_F)/kT} \qquad (24)$$

We will also use as the lower limit $E_{min} = 0$ since $[1-F(E)]$ goes to zero as $E < E_v$. Consequently we can write p_o as

$$p_o = \frac{4\pi}{h^3}(2m_h^*)^{3/2} \int_{-\infty}^{E_v} (E_v - E)^{1/2} e^{(E - E_F)/kT}\, dE \qquad (25)$$

and upon integrating we find

$$p_o = 2\left(2\pi m_h^* \frac{kT}{h^2}\right)^{3/2} e^{(E_v - E_F)/kT} \qquad (26)$$

or

$$p_o = P_v e^{(E_v - E_F)/kT} \qquad (26a)$$

where P_v = the effective density of states in the valence band

$$= 2\left(2\pi m_h^* \frac{kT}{h^2}\right)^{3/2}$$

Extrinsic Semiconductors

So far we have been talking about not only a pure but an ideal crystal. That is to say, we have assumed that the crystal has no impurity atoms and that all the lattice sites are occupied. This is a far cry from reality since the ideal crystal is an impossibility. In the real crystalline state both impurities, and structural effects occur. These defects contribute greatly to the conductivity of semiconductors. Experiments, show that there are two types of such defects, those that contribute electrons to the conduction band and those that tend to capture electrons from the valence band giving rise to free holes.

The impurities or defects which contribute electrons to the conduction band are called donors and the defects which capture electrons from the valence band giving rise to free holes are called acceptors. Impurity centers of these types possess allowed states which lie in the forbidden energy band as shown below

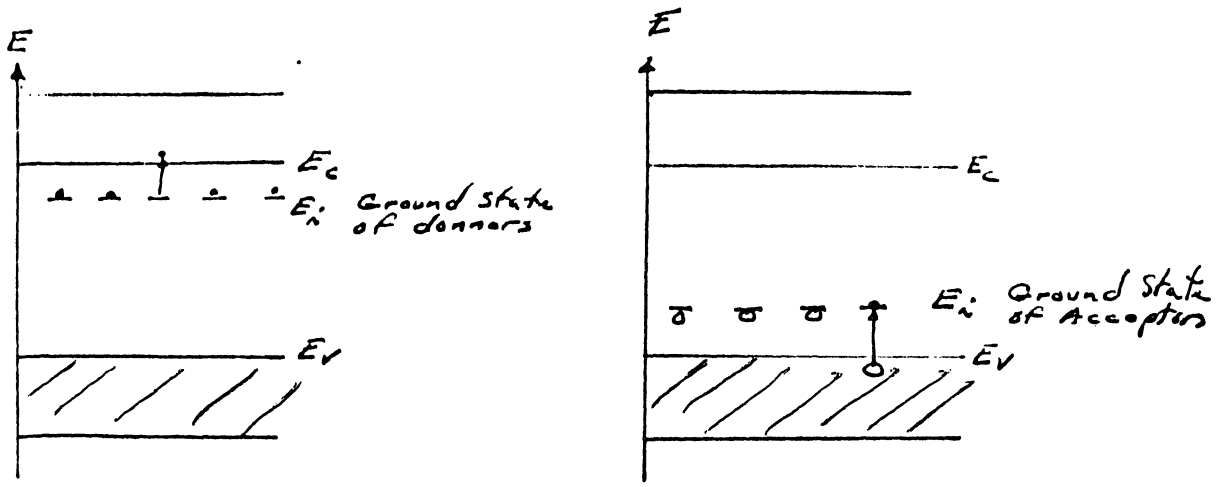

Figure 14.

Silicon and Germanium crystallize into the diamond structure with each atom forming four covalent bonds, one with each of its four nearest neighbors, corresponding to their chemical valence of four. If an impurity atom of valence five, such as phosphorous, arsenic or antimony, is substituted into the lattice in place of one of the Si or Ge atoms where will be an excess of one valence electron remaining after the formation of the four covalent bonds with the four nearest neighbors. The extra electron cannot fit into four bonds and as a result is only loosely bound to positive core of the impurity. The binding energy of the electron to these impurities in silicon is on the order of 0.1 ev. Consequently at room temperature these electrons are ionizied and free to move about the crystal. Near absolute zero the electrons would be bound to the positive core of the purity. Impurities which act to purduce free electrons are called donors and if the conduction band the material is called n-type.

Conversely, if the conductivity is determined by holes or positive carriers the materials is called p-type. In this case the added impurity is termed an acceptor. The simplist type of an impurity which will act as an acceptor is one of the elements of group III in a substitutional site. In this case the added impurity has a valence of three and therefore cannot

complete the valence bond structure surrounding it thus effectively creating a bound hole. This is depicted in Figure 26. The hole in one of the bonds to the group III impurity can now be filled by an electron from one of the adjacent bonds. The hole essentially becomes mobile leaving a localized site. This process is described in an analogous fashion to the ionization and motion of electrons produced by donors. At low temperatures the negative purity atom attracts the positively charged hole but as the temperature is raised the thermal energy produces excitation of the hole releasing it so that it is free to wander through the crystal contributing to the conductivity.

The density of states and the effective density of electrons and holes in an extrinsic material are governed by the same physical laws. However in contrast to the intrinsic material the Fermi level does not in general lie in the middle of the forbidden band. The distributions and densities for an n-type and p-type semiconductors are shown in Figure 15.

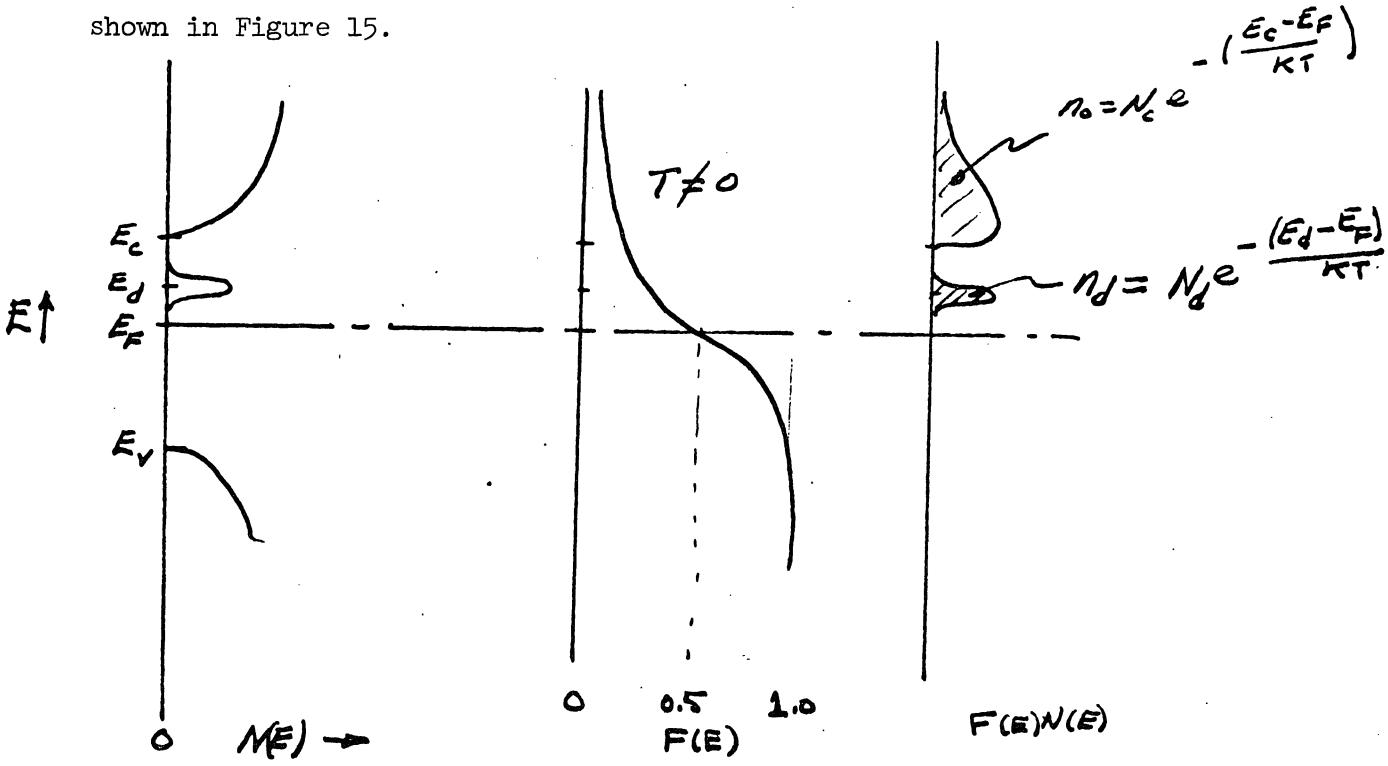

Figure 15.

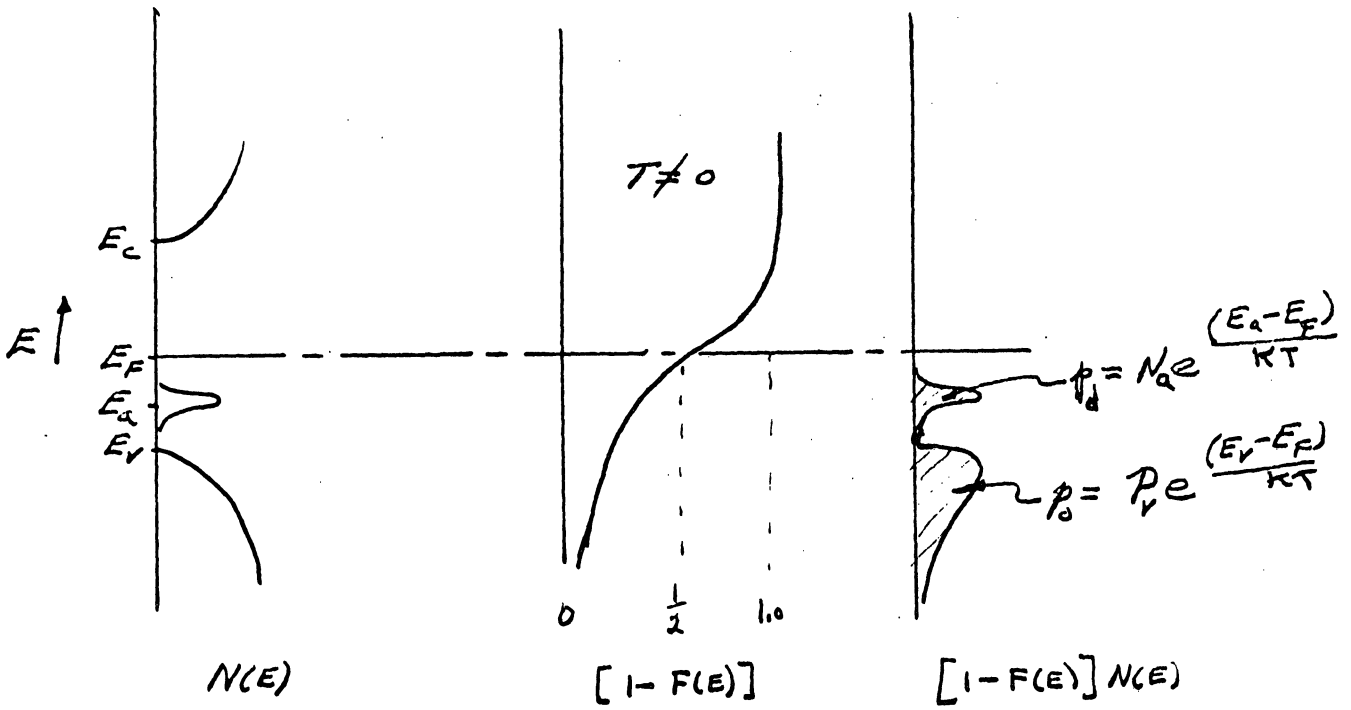

Figure 16.

As in the previous section the effective number of electrons in the conduction band is given by

$$n_0 = N_c\, e^{-(E_c - E_F)/KT}$$

and the effective hole density in the valence band by

$$p_0 = P_v\, e^{-(E_F - E_v)/KT}$$

The number of bound electrons at the donor sties in n-type material is given by the product of the number of sites, times the probability of occupation $F(E)$ or simply

$$n_d = N_d F(E_d)$$

$$= N_d \frac{1}{e^{(E_d - E_F)/kT} + 1} \qquad (26)$$

if E_d lies close to the conduction band $E_d - E_F > 4kT$ we can use the approximation that

$$n_d = N_d e^{-(E_d - E_F)/kT} \qquad (26a)$$

The number of holes trapped at acceptor sites N_a is given by

$$p_a = N_a [1 - F(E)]$$

$$= N_a \left(1 - \frac{1}{e^{(E_a - E_F)/kT} + 1}\right) \qquad (27)$$

but if $E_a < E_F$ then

$$\left[1 + e^{(E_a - E_F)/kT}\right]^{-1} = 1 - e^{(E_a - E_F)/kT}$$

consequently

$$p_a = N_a e^{-(E_F - E_a)/kT} \qquad (27a)$$

III. Ionization and the Generation of Free Carriers:

A. Quantum Yield:

As the result of the interaction of the radiation from a nuclear source, an accelerator or a space environment, free carriers are created through the ionization of atoms in the semiconductor. It is this effect which plagues the designer of electronic circuitry. Therefore the mechanisms by which the free carriers are produced and the subsequent behavior will be the area of interest in this present section. The primary manifestation of the transient radiation is the creation energetic electrons in the host material. Since the energy of the incident particles and quanta covers the range from a few ev to 20 Mev, the energy of the primary electrons produced will be several orders of magnitude greater than the fundamental band gap energy of the material. These electrons in turn create additional ionization through their interactions with lattice creating secondary, tertiary, etc, ionization effects. The net results is that for the abosrption or scattering of a single quanta we can create thousands of free carriers. The simple

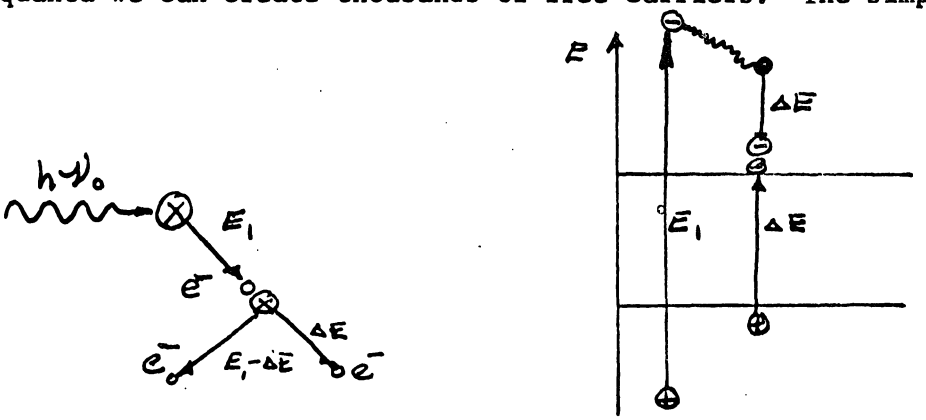

Figure 17.

case of the liberation of two free electrons and two free holes through the adsorption of one photon is illustrated in Figure 17.

We will define β to be the number of electrons and holes produced by a single absorbed photon or particle. It is reasonable to assume that for the production of more than one ion pair per absorbed photon the energy of the photon must exceed twice the energy gap of the solid i.e., $h\nu_0 \geq 2E_g$ However it is found that it requires more energy than 2 E_g before secondary ionization becomes important. A plot of β versus energy of the incident photons of low energy is shown in Figure 18 for germanium.

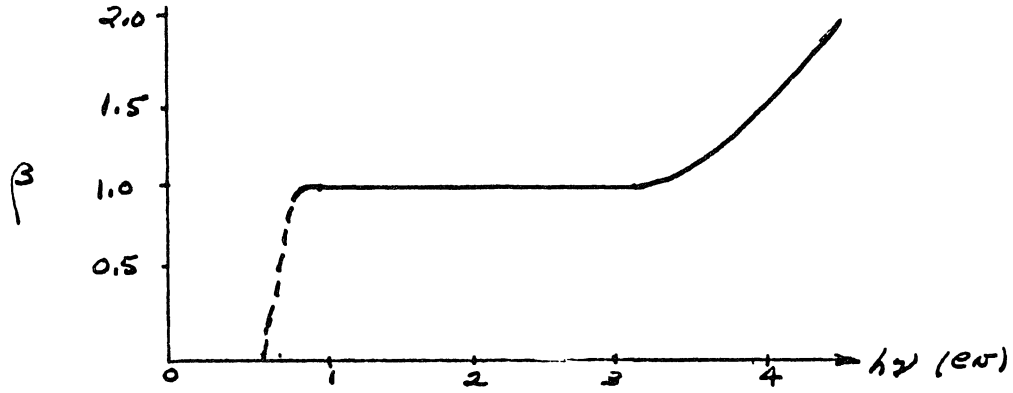

Figure 18.

From the information on germanium we see that secondary ionization does not become important until the energy of the incident radiation is greater than 4 E_g. At higher gamma energies the quantum yield increases with energy. Typical values for the energy expended per ion pair created in germanium and silicon are 3.0 to 4.5 ev. Thus the total absorption of a 1 mev gamma would produce from 2.2×10^5 to 3.3×10^5 ion pairs in Si or Ge. A plot of β is given for germanium and silicon for several types of incident particles in Figure 19.

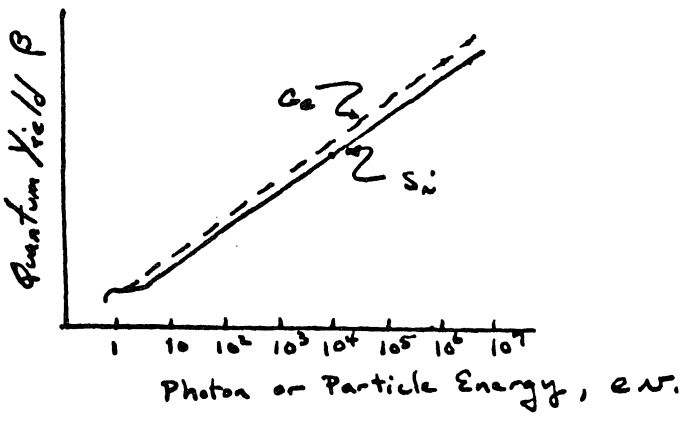

Figure 19.

The remaining absorbed energy which does not appear in the form of free carriers appears as lattice energy or phonon energy. This results from the collisions of the electrons with the lattice phonons and as a result appears as lattice heating.

It is apparent that as a result of the primary interaction we can create thousands of free electrons having an energy distribution varying from E_c up to the kev region. The time dependence of this electron energy distribution is also an important consideration. An examination of this question shows that distribution of excess

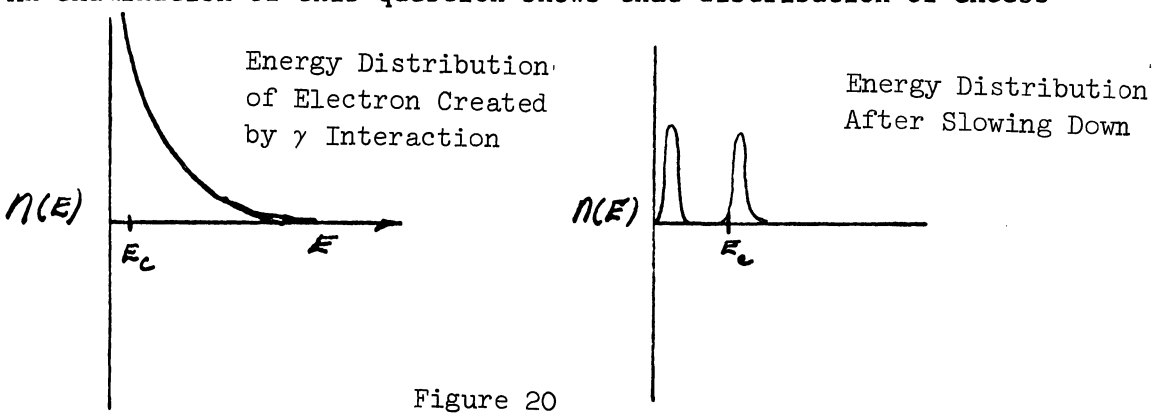

Figure 20

carriers produced by ionization will slow down in energy through collisions with the lattice to the conduction band energy in times of the order of 10^{-10} to 10^{-9} seconds in a semiconductor. Since most semiconductors have carrier lifetimes which lie between 10^{-3}sec and 10^{-7}sec it is as if the liberated carriers appear instantaneously as free carriers in the condition and valence bands with the corresponding energy distributions.

B. Interactions of Radiation with Matter:

1. Gammas and X-rays

The most significant contributor to the ionization effects produced by a weapon or a reactor environment is gamma radiation. This electromagnetic radiation interacts with matter

by three mechanisms a) the photoelectric effect b) the Compton effect and by c) pair production. The transmission of a columnated monoenergetic photon beam through is governed by the exponential law

$$I = I_0 e^{-\sigma x} \qquad (28)$$

where I_0 is the number of incident photons per cm^2, I is the number of photons which traverse a distance x without a scattering or an absorbing event, The linear absorption coefficient σ is given by

$$\sigma = \sigma_p + \sigma_c + \sigma_k \, . \qquad (29)$$

where σ_p, σ_c and σ_k represent the linear attenuation coefficient for the photon electric effect, Compton effect and pair production respectively.

a. Photoelectric Absorption:

In the photoelectric process all the energy, $h\upsilon$, of the incident photon is transferred to a bound electron which is ejected from the atom with kinetic energy T

$$T = h\nu - I \qquad (30)$$

where I = the ionization potential of the electron

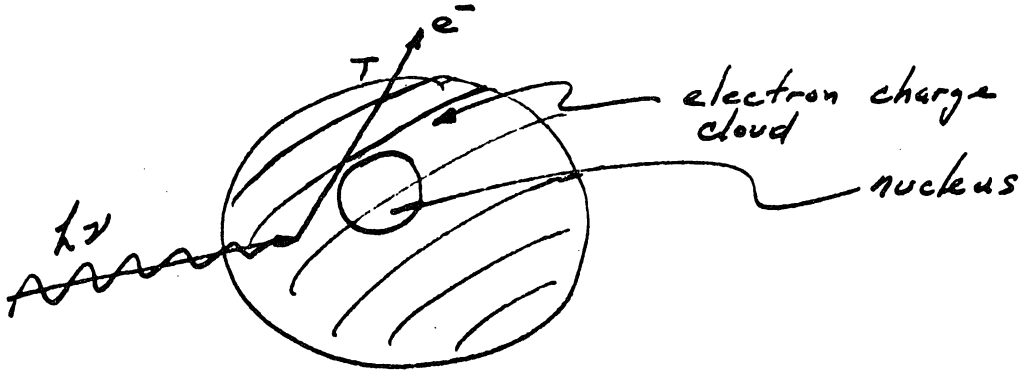

Figure 21.

Formulas for the probability that a photon of energy hυ will undergo photoelectric absorption have been devised by quantum mechanical methods. In reality several different relations must be used to cover the range from 0.1 - 10 mev. The main features are shown by the simplest relationship

$$\sigma_p = \phi_0 z^5 \left(\frac{1}{137}\right)^4 4\sqrt{2} \left(\frac{m_0 c^2}{h\nu}\right)^{7/2} \qquad (31)$$

where

$$\phi_0 = \frac{8\pi}{3}\left(\frac{e^2}{m_0 c^2}\right)^2 = 6.651 \times 10^{-25}\ cm^2$$

therefore,

$$\sigma_p \propto \left(\frac{z^5}{E_\gamma^{7/2}}\right)$$

where

$m_0 c^2$ = rest mass of the electron

z = atomic number of the material

$h\nu$ = energy of the incident photon

This applies to ejection from the k- shell which corresponds to 80% of the photoelectric interactions. We note that σ_p varies as z^5 thus for a given photon energy, the photoelectric absorption is much more important in heavy materials such as lead than in light materials such as aluminum or carbon.

Since σ_p varies as $(h\upsilon)^{-7/2}$ then for a given element, the effect is much greater at small photon energies than at higher energies.

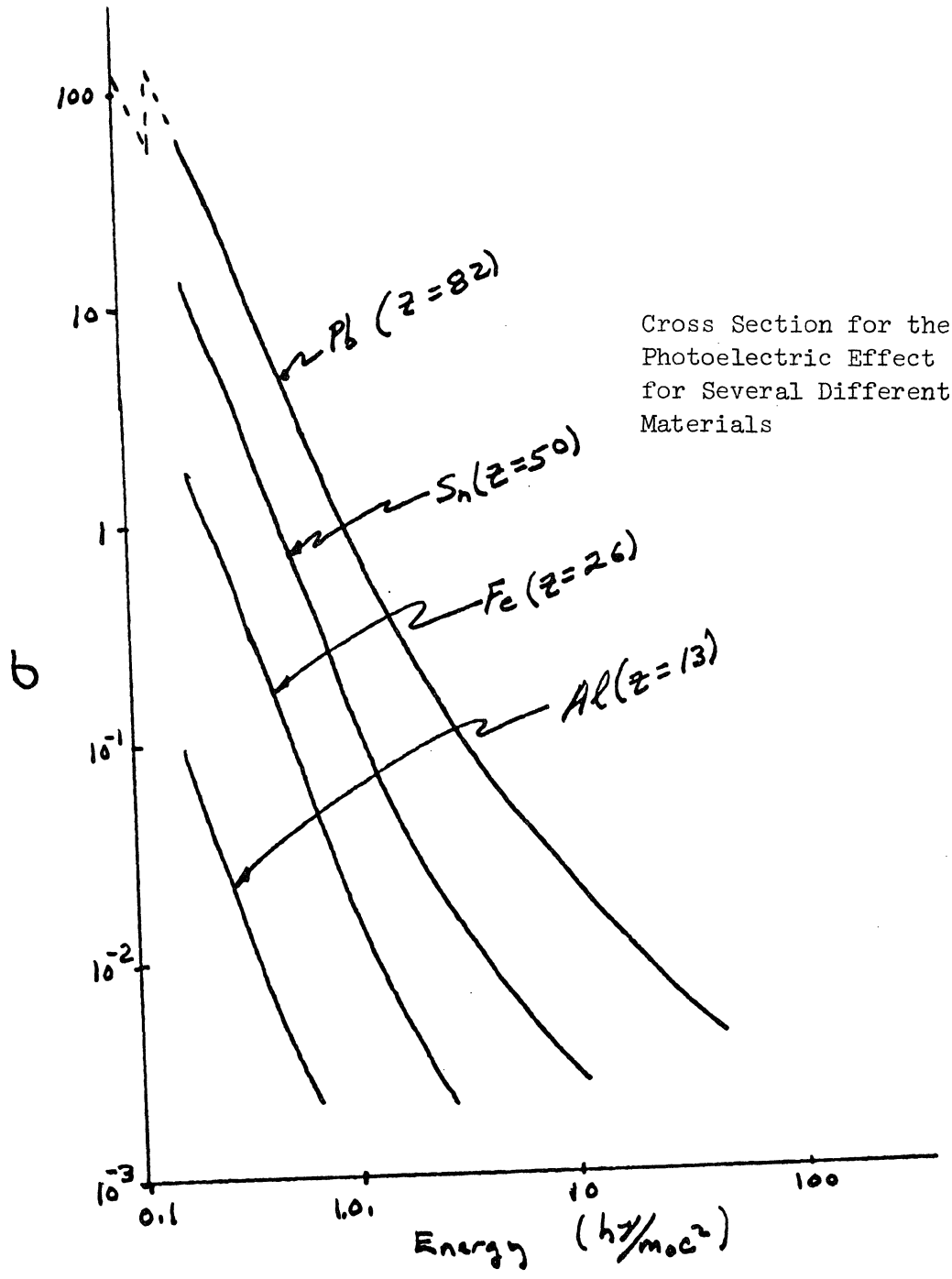

Cross Section for the Photoelectric Effect for Several Different Materials

Figure 22.

b. Compton Scattering:

In Compton scattering the incident photon is scattered by one of the atomic electrons and the latter is separated from its atom. The photon moves off at an angle with respect to its initial direction. This change in direction removes the photon from the incident γ beam

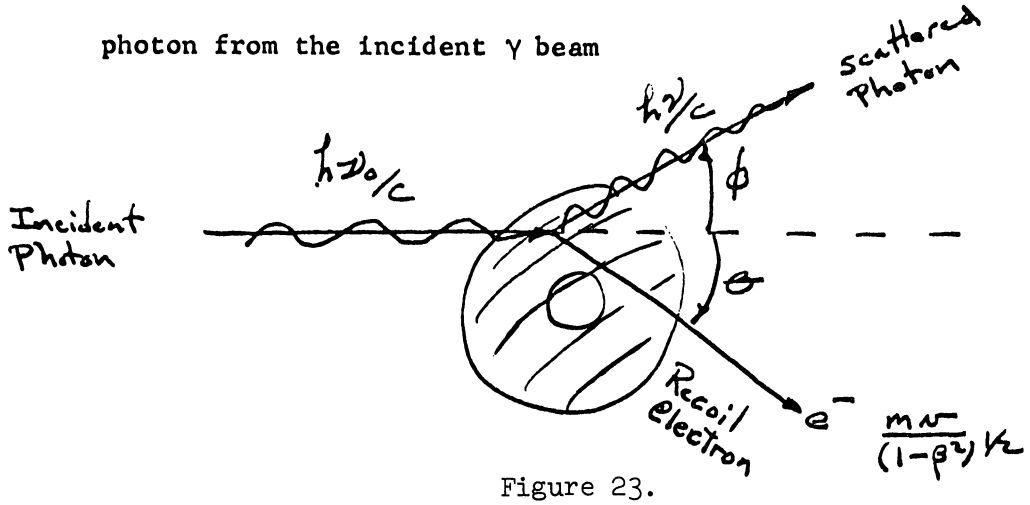

Figure 23.

The probability of γ scatter by the Compton process was calculated by Klein and Nishima. The cross-section per electron is given by

$$e\sigma_c = \frac{3}{4}\phi_0 \left\{ \frac{1+\alpha}{\alpha^2}\left[\frac{2(1+\alpha)}{1+2\alpha} - \frac{1}{\alpha}\ln(1+2\alpha) + \frac{1}{2\alpha}\ln(1+2\alpha) - \frac{1+3\alpha}{(1+2\alpha)^2} \right] \right\} \quad (32)$$

where

$$\alpha = \frac{h\nu_0}{m_0 c^2}$$

and

$$\phi_0 = \frac{8\pi}{3}\left(\frac{e^2}{m_0 c^2}\right)^2 = 6.651 \times 10^{-25}\ cm^2$$

To obtain σ_c we use the relationship $\sigma_c\ (cm^{-1}) = \rho N \left(\frac{Z}{A}\right) {}_e\sigma_c$, Thus σ_c is a measure of the total energy removed from the beam per centimeter of path length.

It is sometimes necessary to identify the energy carried by the scattered γ's and that which is absorbed. To account for this we let

$$ {}_e\sigma_c = {}_e\sigma_s + {}_e\sigma_a $$

- ${}_e\sigma_s$: Compton cross-section per electron for the energy absorbed
- ${}_e\sigma_a$: The Compton cross-section per electron for the energy of the scattered photon

where ${}_e\sigma_s$ = The Compton cross section per electron for the energy of the scattered photon

and ${}_e\sigma_a$ = Compton cross-section per electron for the energy absorbed.

The we can of course obtain the linear coefficient through

$$ \sigma_s = \rho N \left(\frac{Z}{A}\right) {}_e\sigma_s $$

and

$$ \sigma_a = \rho N \left(\frac{Z}{A}\right) {}_e\sigma_a $$

Hence, we find the Z dependence of σ_c is small since

$$ \left(\sigma_c/\rho\right) = N \left(\frac{Z}{A}\right) {}_e\sigma_c $$

and

$$ \left(\frac{Z}{A}\right) \sim \text{constant} $$

The cross-section does, however, vary inversely with photon energy since

$$ {}_e\sigma \propto \left(\frac{1}{h\nu_0}\right) $$

This behavior is depicted in Figure 24 below.

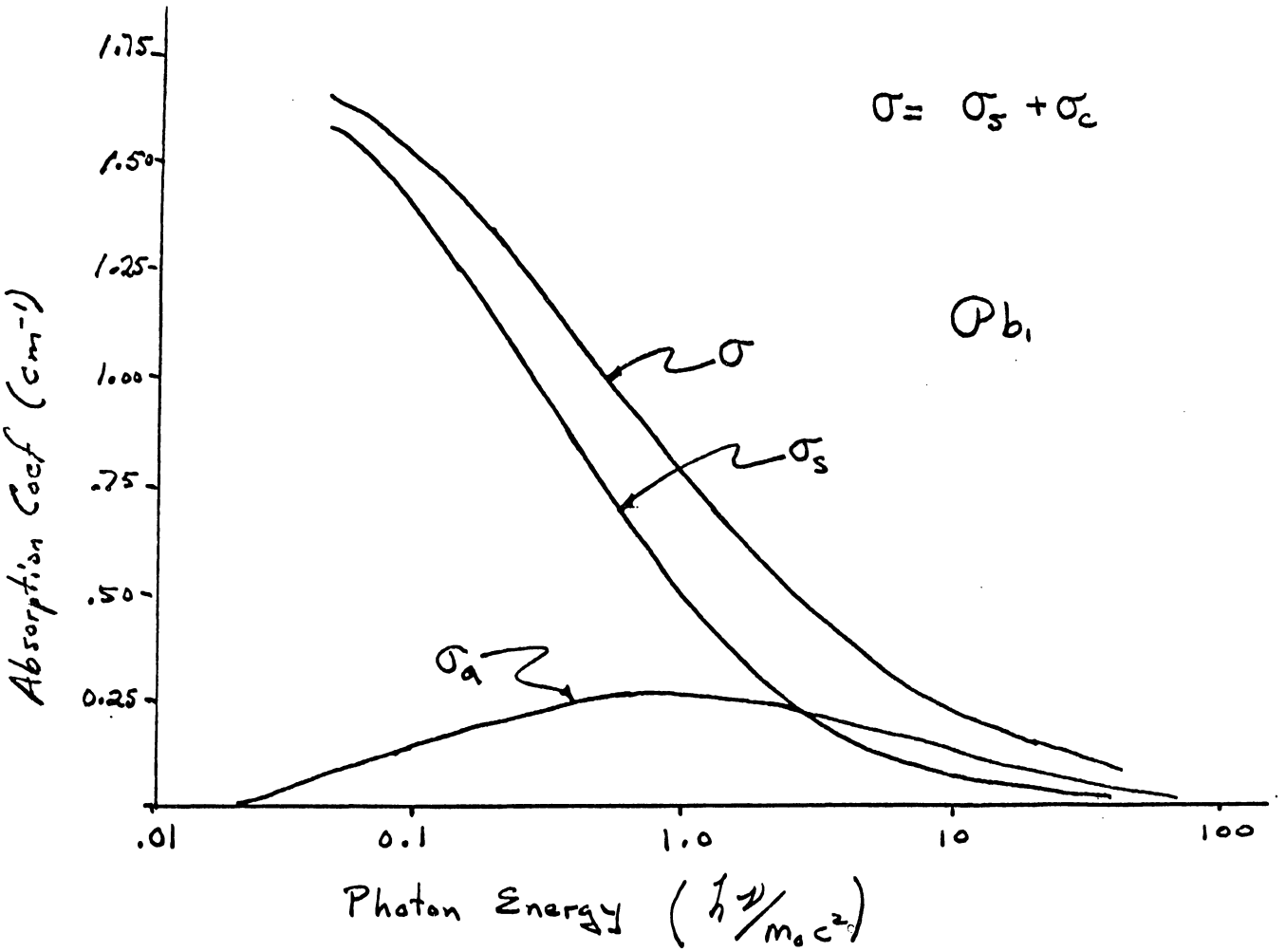

Figure 24.

The kinetic energy of the Compton scattered electron as a function of photon energy is given by

$$T_{elect} = h\nu_0 \left\{ \frac{(1-\cos\phi)\ \frac{h\nu_0}{m_0c^2}}{1+\frac{h\nu_0}{m_0c^2}(1-\cos\phi)} \right\} \qquad (39)$$

where $h\upsilon_0$ is the energy of the incident photon, m_0c^2 is the rest mass of the electron and ϕ is the angle between the direction of the incident photon and the electron. The range in electron energy for a given incident photon is from $T_{min} = 0$ corresponding to $\phi = o$ to

T_{max} corresponding $\phi = 180^{\circ}$, where T_{max} is given by

$$T_{max} = h\nu_0 \left\{ \frac{1}{1 + \frac{m_0 c^2}{2h\nu_0}} \right\} \qquad (34)$$

c. Pair Formation:

At high enough energies both the photoelectric and Compton effect become important compared with pair production. In pair production a γ ray with sufficient energy is annihilated. An electron and positron are created.

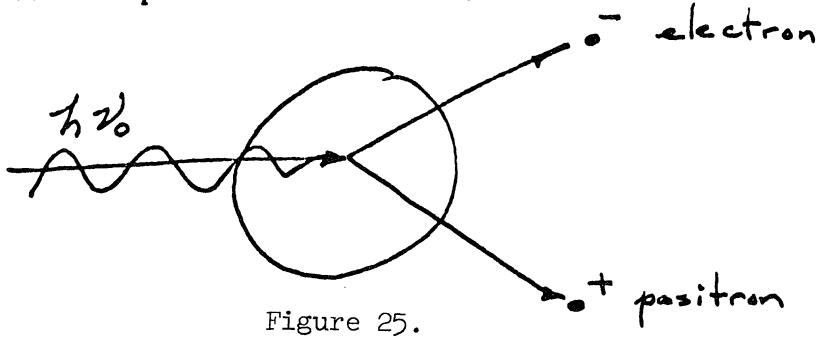

Figure 25.

The total energy of this pair is $h\upsilon$. Therefore, the kinetic energy of the pair is given by the difference between

$$T = h\nu - 2m_0 c^2 \qquad (35)$$

their rest mass and the energy of the photon. Consequently we must have

$$h\nu > 1.02 \text{ Mev} = 2m_0 c^2$$

Thus the cross-section is zero for $h\upsilon_0$ less than 1.02 mev

Thus the cross section is zero for $h\nu_o$ less than 1.02 and is proportional to $h\nu_o$ and z^2, i.e.,

$$\sigma_\kappa = 0 \qquad \text{for} \quad E = h\nu_o < 1.02 \text{ Mev}$$

$$\sigma_\kappa(E) \propto z^2 E \qquad \text{for} \quad E = h\nu_o \geq 1.02 \text{ Mev}$$

The total cross section is shown in Figure 26 for lead.

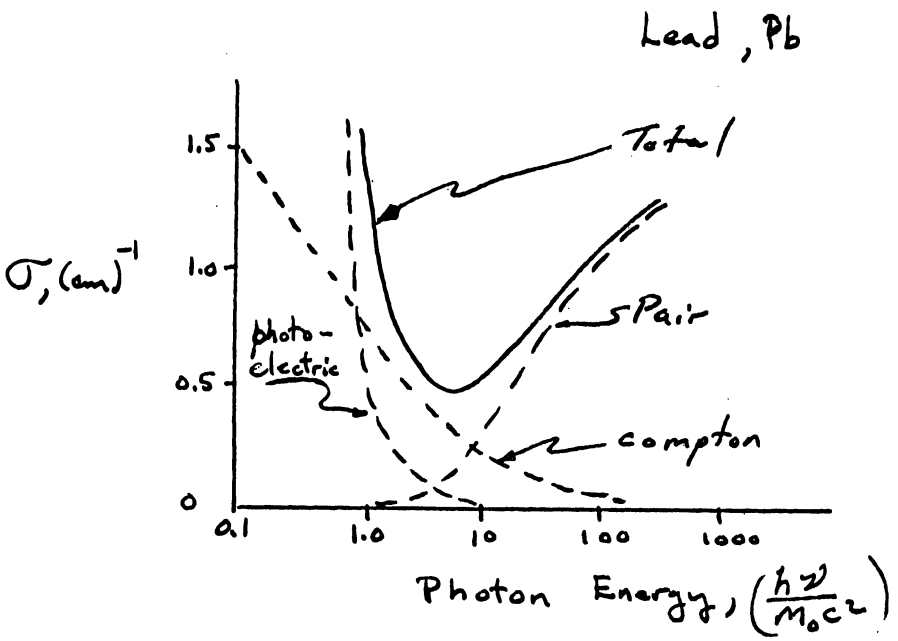

Figure 26.

2. Electrons:

When a material is irradiated with electrons, these negatively charged particles interact with the orbital electrons of atoms of the material. The interaction which occurs between the primary electron and the orbital electrons of the target is a coulomb interaction. The differential cross-section per atomic electron for energy transfer in dE about E is given by

$$d\sigma_i = \frac{2\pi z^2 e^4}{m_o v^2} \frac{dE}{E^2} \qquad (26)$$

where Ze is the charge of the incident particle, in this case Z=1. V is the velocity of the incident electron while m_o is its rest mass. The energy transfer is most probable for low values since the differential cross-section varies as $\frac{1}{E^2}$. Bethe has shown the from this differential cross-section a relationship for the specific energy loss from a relativistic electron is given by

$$-\frac{dE}{dx} = \frac{2\pi Ne^4}{mv^2} z \left[\ln \frac{mv^2 E}{2I^2(1-\beta^2)} + (2\sqrt{1-\beta^2} - 1+\beta^2) \ln 2 + 1-\beta^2 + \frac{1}{8}(1-\sqrt{1-\beta^2})^2 \right] + \cdots \qquad (27)$$

where E is the energy of the electron V is the electron velocity, c is the velocity of light and N is the number of atoms per cm^3.

The quantity I is average ionization potential for the material or the band gap energy for semiconductors.

For small values of β, $\frac{dE}{dx}$ reduces to $-\frac{dE}{dx} = \frac{4\pi N e^4}{mv^2} z \ln \frac{mv^2}{2I}\sqrt{\frac{e}{2}}$ (38)

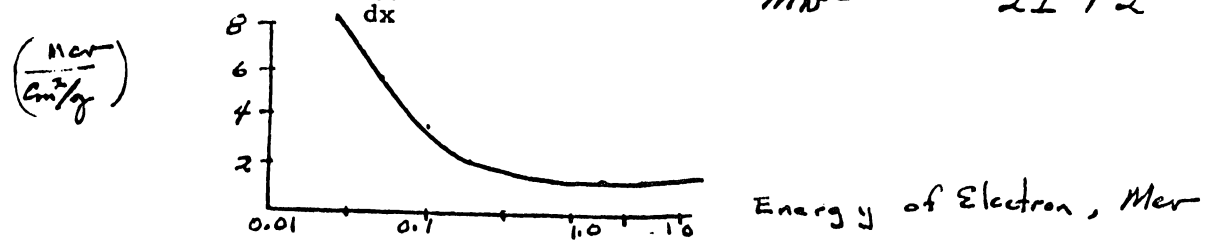

Figure 27.

Shown in Figure 27. is the variation in the specific ionization for silicon as a function of energy.

The above relationship for the specific energy loss does tell us the energy loss per unit path but the path actually followed by a electron through a material is very tortuous and thus this relationship does not give the energy deposition as a function of depth in a particular absorber. In most experimental cases one deals with a beam of monoenergetic electrons incident normally on the surface of a sample. On entering the sample, the electrons are scattered and the average distributinn of the ionization losses along the axis of the material differs greatly from the ionization produced by a single electron along its path. Spencer has developed a moments method for solving the transport equations and calculating the energy deposition as a function of the electron range for various materials and electrons energies. A plot of the relative energy deposition versus distance from the front surface normalizied to the range is shown below for silicon.

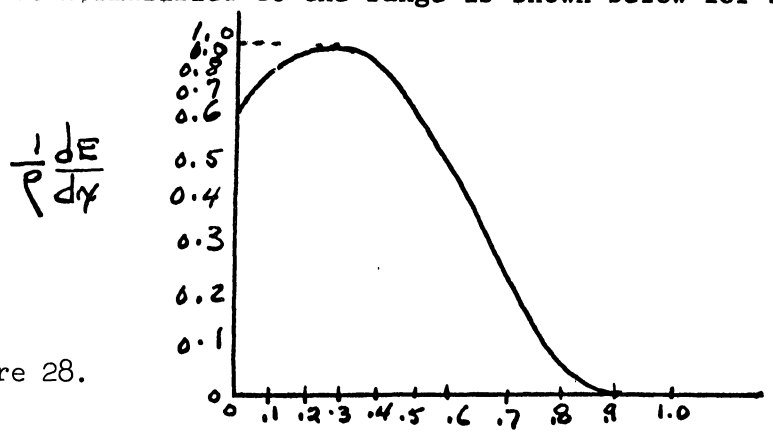

Figure 28.

3. Neutron-Induced Ionization

In the transport of neutrons through a material they undergo scattering and absorption collisions with the nuclei of the host lattice. These interactions with the nuclei of the irradiated material do not produce ionization directly. However, as a result of these interactions free carriers can be generated through the following mechanisms:

a) The Elastic scattering of a neutron by the host material can produce an energetic recoil atom which dissipates its energy by ionization and displacement collisions along its path.

b) Inelastic scattering of a neutron will produce an energetic recoil atom which can produce ionization as in elastic scattering but in addition a gamma is emitted. This emitted gamma is then an additional source of ionization.

c) The capture of a neutron will in general produce a nucleus in an excited state and in decaying to the ground state will emit ionizing radiation as a photon or charged particle.

Except for particular cases where the induced activity due to say an (n, α) reaction may be extremely high, this type of neutron induced ionization is neglected. As result neutron-induced ionization is considered to be important in only through the secondary gammas and recoil nuclei. The secondary gammas augment those present in the radiation field and those produced by neutron interactions in nearly all materials. Due to the difference

in speed between the prompt gammas from a weapon or other source and the fast neutrons, the secondary gammas may be separated in time from the primary gammas.

The recoiling nuclei producing ionization along their path. In general their energy is dissapipated in very small units of volume in the vicinity of the primary neutron-nuclei interaction. The ionization produced by neutrons in this manner is readily calculated by

$$\left(\frac{dE}{dV}\right)_{\substack{\text{neut} \\ \text{ionization}}} = \int_{0}^{E_{max}} \int_{E_R}^{E_{max}} f(E_R)\, E_R\, \phi(E)\, N_A\, \sigma(E_R, E)\, dE\, dE_R \qquad (39)$$

where N_A is the density of target atoms per cm^3, $\sigma(E_R, E)$ is the cross-section for producing a recoil particle of energy E_R by a neutron of energy E, $\phi(E)\,dE$ is neutron flux with energy in dE about E and $f(E_R)$ is the fraction of the recoil energy E_R that goes into ionization. For recoil nuclei $f(E_R)$ is generally less than unity. The function $f(E_R)$ is shown in Figure 29, for silicon. The solid curve is the predicted value by Lindhard while the measured value is shown by the solid data points are those of Sattler.

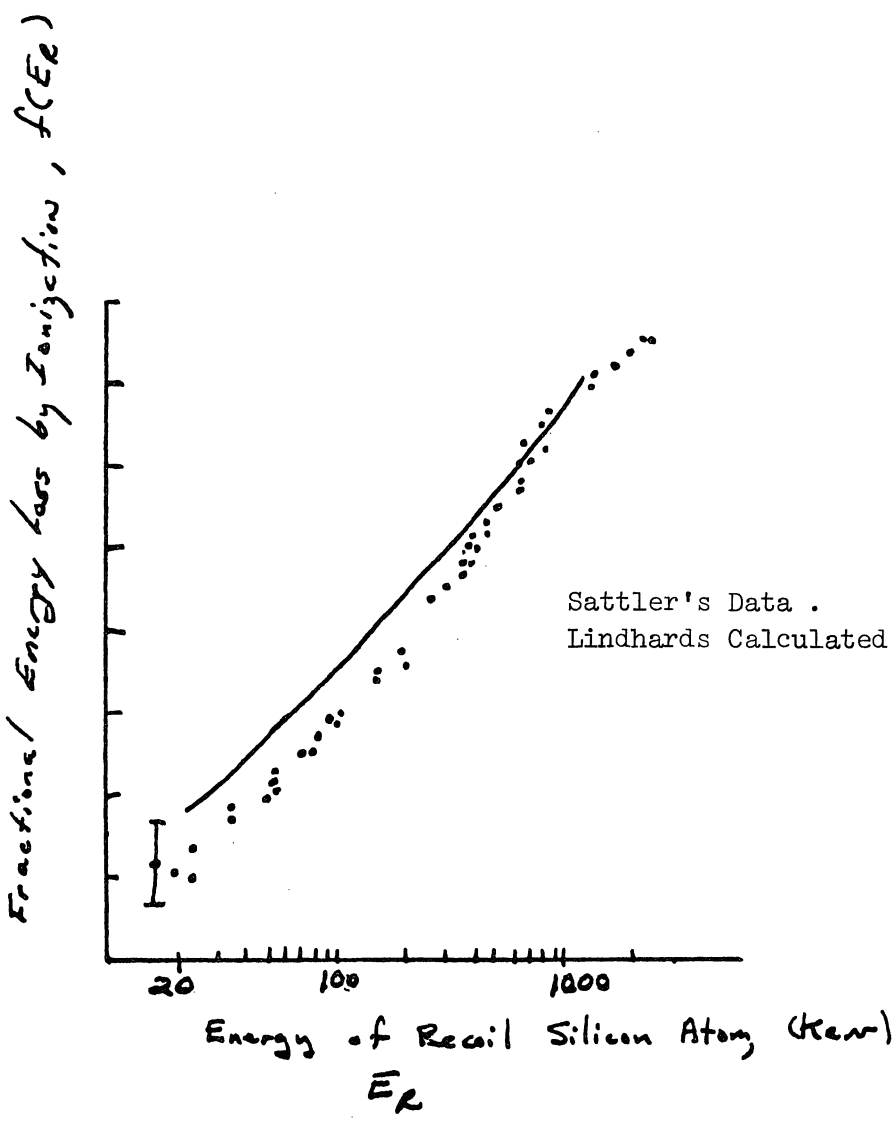
Fraction of Energy Loss by Ionization, f(E_R)
20
100
1000
Energy of Recoil Silicon Atom (kev)
E_R
Sattler's Data .
Lindhards Calculated Value -

Figure 29.

A. Photoconductivity:

Upon exposure of a semiconductor to external excitation, free electron and hole pairs will be created. The creation of these excess carriers will produce a corresponding increase in the conductivity, called photoconductivity. When the external excitation ceases, the thermal equilibrium between the lattice and electrons will in time be re-established. The process of re-establishing equilibrium between the lattice and electrons is generally considered to be that of recombination on nonequilibrium electrons and holes, while the temperature of the lattice and the whole crystal are considered to be unchanged. If we let n and p be the instaneous density of nonequilibrium electrons and holes respectively and assume that the application and removal of the excitation does not affect the equilibrium carrier densities, n_o and p_o, then we may write

$$n = n_o + \Delta n \tag{40}$$

and

$$p = p_o + \Delta p \tag{41}$$

where Δn and Δp are the instaneous changes in the electron and hole densities due to external excitation of injection.

As a result of the introduction of the nonequilibrium carriers, we produce a corresponding change in the conductivity of a semiconductor. The general case can be written in the form

$$\sigma = (\mu_n n_o + \mu_p p_o + \mu_n \Delta n + \mu_p \Delta p) \tag{42}$$

where e is the electronic charge and μ_n and μ_p are respectively the electron and hole mobility. Here, we have assumed that the nonequilibrium or photoexcited carriers have the same mobility

as the equilibrium carriers. Rewriting the above relationship for σ in terms of an equilibrium conductivity σ_o and an excess conductivity $\Delta\sigma$, we obtain

$$\sigma = \sigma_o + \Delta\sigma \tag{43}$$

where

$$\sigma_o = e(\mu_n n + \mu_p p) \tag{44}$$

and

$$\Delta\sigma = e(\mu_n \Delta n + \mu_p \Delta p) \tag{45}$$

Let us now determine what factors affect the values of Δn and Δp which govern the photoconductivity, $\Delta\sigma$. In general it is assumed that the number of electrons and holes generated per unit time per unit volume is proportional to the energy absorption in the unit of volume at that time. For example consider the case of excitation by photons. If I is the energy flux incident on an elemental slab dx in thickness, and 1 cm^2 inch area then the energy absorbed per unit time per cm^2 is given by

$$-dI = kIdx \tag{46}$$

where k is the energy absorption coefficient. The energy absorbed per cm^3 is given by

$$-\frac{dI}{dx} = kI$$

Under our assumption that the generation of excess electrons and holes should be equal and proportional to the absorbed energy, we can write

$$\frac{d(\Delta n)}{dt} = \frac{d(\Delta p)}{dt} = \beta k I \tag{47}$$

where β is the coefficient of proportionality and represents the

number of pairs formed by a single quantum. The energy of the photons and electrons which we are considering in this discussion is much greater than width of the forbidden bands of semiconductors consequently $\beta >> 1$. For example approximately 3.0 ev to 4.5 ev are expended in the production of a electron hole pair in silicon and germanium by energetic gammas and electrons. This is approximately twice the minimum energy required to produce an electron hole pair in these materials. The additional energy appears for the most part, as kinetic energy in the lattice.

If we assume no other processes take place other than carrier generation and that excitation began on time, t = 0, then the density of excess carriers would increase linearly with time according to the relation

$$\Delta n = \Delta p = \beta k I t \qquad (48)$$

Figure 30 shows the time dependence of Δ n as predicted by equation which increases with time without limit.

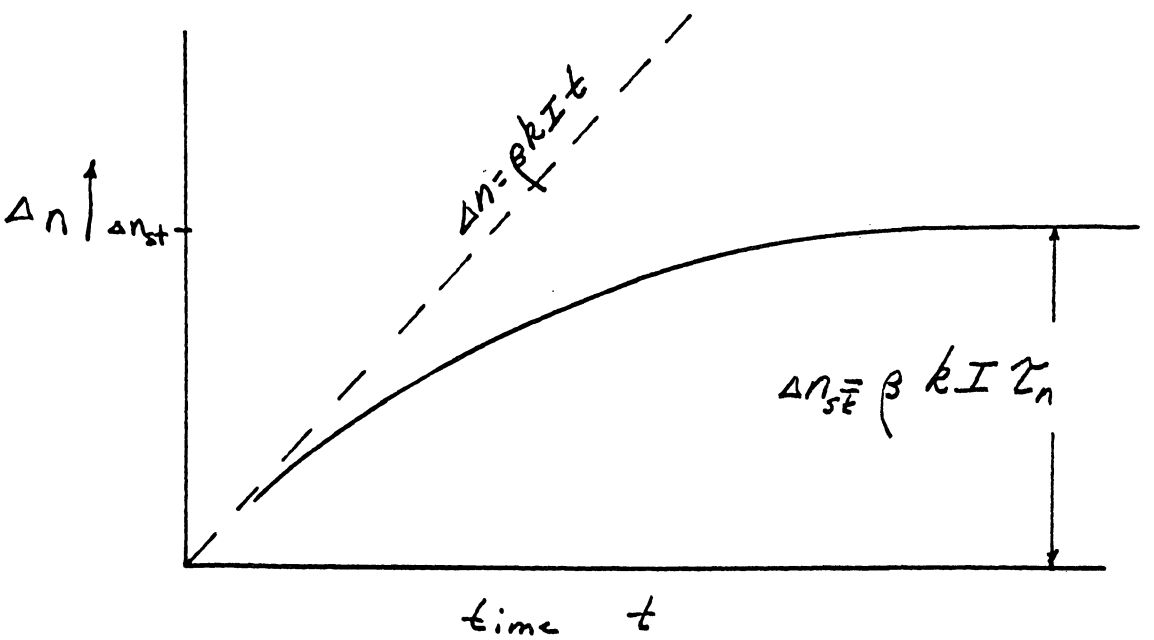

Figure 30.

However, experimental facts show that after a certain time from the initiation of steady-state excitation a constant steady-state photoconductivity $\Delta \sigma_{st}$ is reached. This steady-state photoconductivity corresponds to steady-state excess carrier densities Δn_{st} and Δp_{st}. Since the conductivity and carrier densities do not increase without limit, it follows that there must exist a process of carrier annihilation. Furthermore, the rate of annihilation is equal to the rate of generation when the steady-state is reached.

The annihilation process corresponds to the recombination of excess electrons and holes. The rate of recombination is directly proportional to the excess carrier densities. Thus the magnitude of the steady-state non-equilibrium electrons and holes will depend on the intensity of the excitation as shown in Figure 31 for two different steady-state excitations.

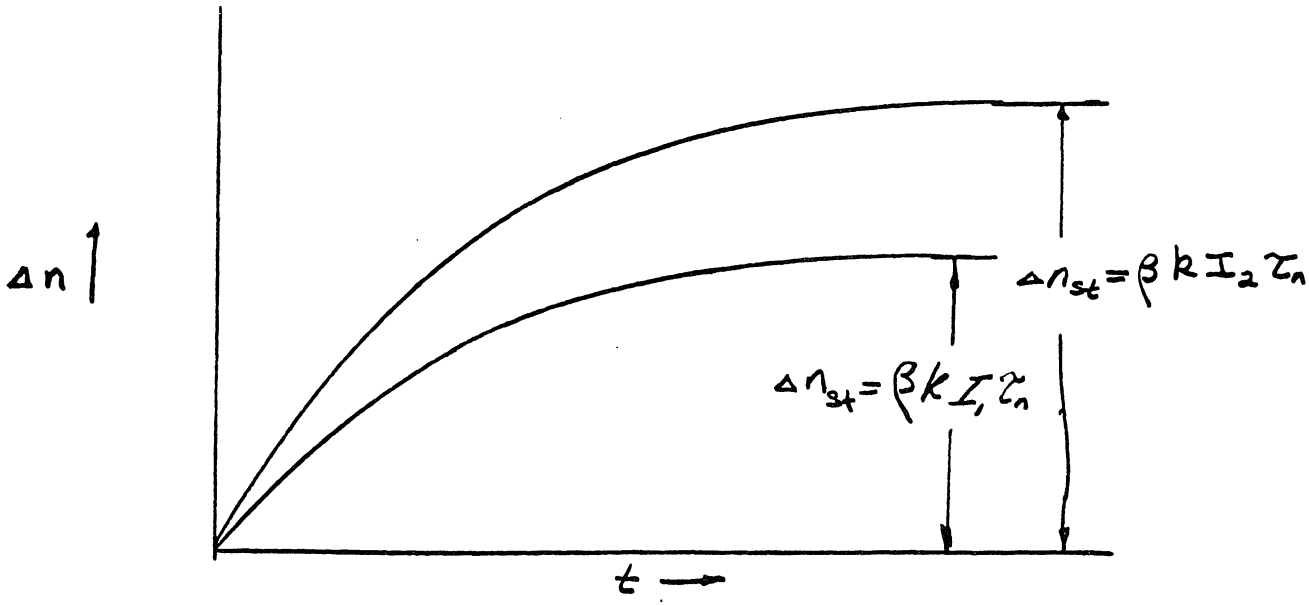

Figure 31. Time Dependence of Excess Electron Density During Steady State Excitation

The values of the steady-state carrier density are general expressed in terms of parameters representing the processes of generation and recombination. We now introduce the concept of the average lifetime of the excess carriers. Each nonequilibrium carrier excited by a photon or an ionizing particles can exist in a free state for a certain time until it recombines. This is the "free state" lifetime which is different for each type of carrier. Therefore, we introduce the "average life" and denote it by τ. The value of the average lifetime is dependent upon the particular material of interest and varries from 10^{-2} to 10^{-7} sec. The electron and hole densities corresponding to steady-state excitation can now be written as

$$\Delta n_{st} = \beta k I \tau_n \tag{49}$$

and

$$\Delta p_{st} = \beta k I \tau_p \tag{50}$$

where β k I represents the number of carriers liberated per unit volume while τ_n and τ_p are the average time of electron and hole existence in the conduction band before annihilation. By substitution of the above relationship into our relationship for excess conductivity, we have

$$\Delta\sigma_{st} = \Delta\sigma_{n_{st}} + \Delta\sigma_{p_{st}} = e\beta k I (\mu_n \tau_n + \mu_p \tau_p) \tag{51}$$

The photoconductivity as given above for steady-state excitation is governed by six parameters β, k, μ_n, τ_n, μ_p and τ_p.

Two of these β and k represent the interaction of radiation with matter and the rate at which carriers are generated. The remaining four parameters represent the interaction of carriers with the semiconductor and govern their motion and recombination.

B. Carrier Lifetime and Capture Cross-Section

As a result of the energy of each excess carrier they are free to move about in the crystal while remaining in the appropriate energy band. As a result of this motion they have a certain probability of encountering a carrier of the opposite charge and recombining. For example and electron while remaining in the conduction band under goes motion within the crystal lattice consequently it has a definite probability of being captured or recombining with a hole. In general the hole can be encountered in several different states such as a free hole in the valence band, a hole localizied at an impurity site or a hole localized at a structural defect. The probability of an electron encourting holes of a given type is proportional to their density in the crystal and to the magnitude of the average relative velocity between the holes and the electrons v_n. Generally the "capture cross-section" or "recombination cross-section", g_n, for the capture of an electron by a hole of a particular type is introduced. If p is the density of holes corresponding to the capture cross-section, g_n, for electrons with relative velocity v_n, then the average time between encounters between these two carriers is given by

$$\tau_n = \frac{1}{g_n v_n p} \qquad (52)$$

and since each encounter results in the capture of an electron by a hole and hence annihilation, the time τ_n is the average electron lifetime before capture by a given type hole.

Since a given semiconductor may contain several different means of electron hole recombination (i.e., electron hole recombination at an impurity center, or neutron induced structural defect) then for each type of recombination we can introduce a corresponding lifetime τ_{nk}. The lifetime τ_{nk} is given by:

$$\tau_n = \frac{1}{p_k g_{nk} v_{nk}} \tag{53}$$

where p_k is density of holes of the k th type, g_{nk} is the electron capture cross-section for holes of the k th type and v_{nk} is the magnitude of the relative velocity between the electrons and holes of the k th type. In this case, the total number of possible collisions per unit time is given by

$$\sum_k p_k v_{nk} g_{nk} \tag{54}$$

Hence the effective electron lifetime is

$$\tau = \frac{1}{\sum_k p_k v_{nk} g_{nk}} \tag{55}$$

Since

$$\tau_{nk} = \frac{1}{p_k v_{nk} g_{nk}} \tag{53}$$

then the electron lifetime for several recombination centers is given by

$$\frac{1}{\tau} = \sum_k \frac{1}{\tau_{nk}} \tag{56}$$

Obviously, the above concepts used to describe the electron lifetime are equally applicable in determining the hole lifetime Thus τ_p, the lifetime of a hole in the valence band, can be written as

$$\tau_{pj} = \frac{1}{n_j g_{pj} v_{pj}} \tag{57}$$

where n_j is the density of electrons of the j th type, q_{pj} is the hole capture cross-section by electrons of the j th type and v_{pj} is the magnitude of the relative velocity between holes and electrons of the j th type. Consequently we can also write for holes that

$$\frac{1}{\tau_p} = \sum_j \frac{1}{n_j g_{pj} v_{pj}} \tag{58}$$

C. Recombination Rate:

We are now able to express the rate at which recombination takes place within our semiconductor. Recall that product $p_k g_{nk} v_{nk}$ is the number of capture collisions per unit time made by an excess electron. Hence the recombination rate is given by

$$\int_0^{v_{max}} p_k g_{nk} v_{nk} \Delta n(v_{nk})\, dv_{nk} \tag{59}$$

This can be written as

$$\overline{g_{nk} v_{nk}}\, p_k \Delta n \tag{60}$$

where
$$\overline{g_{nk} v_{nk}} \equiv \frac{\int_0^{v_{max}} g_{nk} v_{nk} \Delta n(v_{nk})\, dv_{nk}}{\int_0^{v_{max}} \Delta n(v_{nk})\, dv_{nk}} \tag{61}$$

and
$$\Delta n = \int_0^{v_{max}} \Delta n(v_{nk})\, dv_{nk} \tag{62}$$

Thus the recombination rate for electrons due to capture by centers of the k th type is given by

$$\overline{g_{nk} v_{nk}}\, p_k \Delta n = \frac{\Delta n}{\overline{\tau}_{nk}} \tag{63}$$

Similarly for hole recombination at a single center

$$\overline{g_{pj} v_{pj}}\, n_j \Delta p = \frac{\Delta p}{\overline{\tau}_{pj}} \tag{64}$$

It is convenient to define the velocity averaged product of the carrier capture cross-section and relative velocity $\overline{g_{nk} v_{nk}}$ and $\overline{g_{pj} v_{pj}}$ as the capture coefficient γ_{nk} and γ_{pj} respectively, i.e.,

$$\gamma_{nk} = \overline{g_{nk} v_{nk}} \tag{65}$$

and
$$\gamma_{pj} = \overline{g_{pj} v_{pj}} \tag{66}$$

The values of the average lifetimes can now be written in the form

$$\overline{\tau}_{nk} = \frac{1}{\gamma_{nk} p_k} \tag{67}$$

and

$$\overline{\tau_{pj}} = \frac{1}{\gamma_{pj} n_j} , \qquad (68)$$

We should note here that the lifetimes τ_{nk} amd τ_{pj} are explicitly dependent on the carrier densities p_j and n_k, thus they cannot be constant for a given material. Instead they will vary with all the properties affecting the carrier concentrations, such as temperature, intensity of excitation, etc.

D. The Relaxation of Photoconductivity:

Here we wish to determine how the photoconductivity depends on time during excitation and darkness. Recall that upon excitation the photoconductivity $\Delta\sigma$ rise and approaches asymptotically a steady-state value which is proportional to the exposure. Similarly, upon cut-off of the excitation the photoconductivity decays and approaches asymptotically to zero as shown in Figure 32.

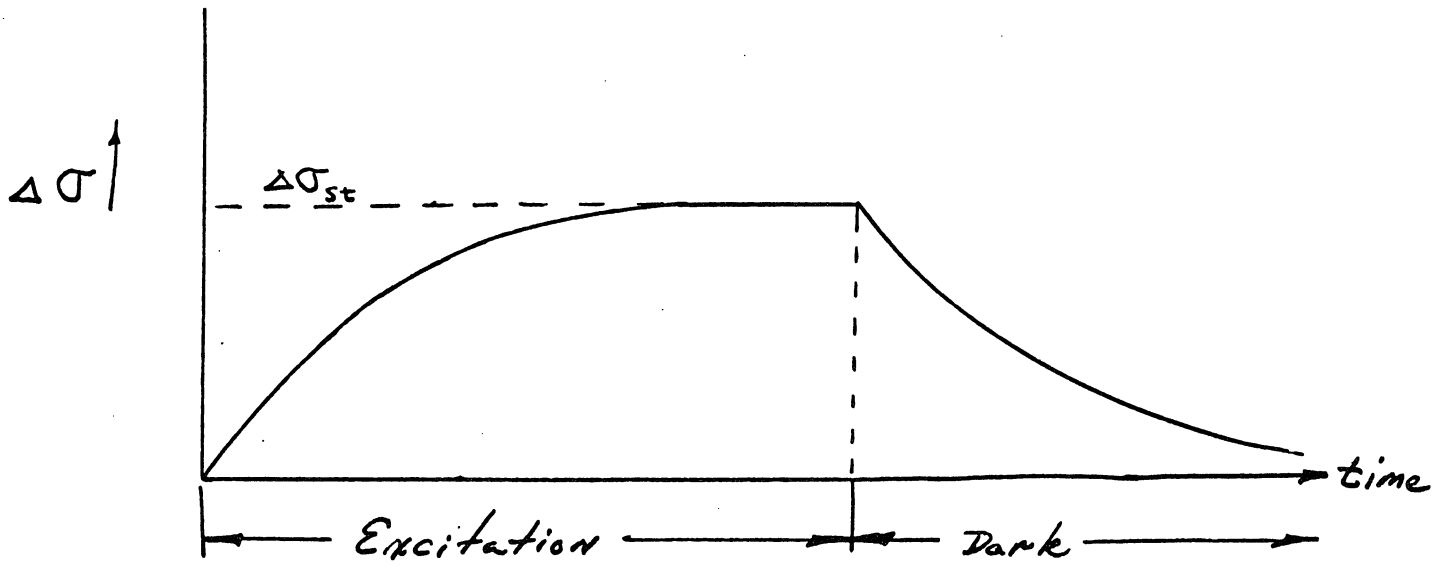

Figure 32.

Since the photoconductivity $\Delta\sigma$ is proportional to the excess hole and electron densities, Δn and Δp respectively, we consider their time dependence during excitation and relaxation as a means of understanding the nonequilibrium conductivity. In the following discussion we shall consider two important cases linear and quadratic recombination. We shall assume in each case that the recombination is either proportional to the first or second power of the excess carrier density and neglect for the moment the recombination mechanism.

1. Linear Recombination:

The change in the number of carriers of one type, say electrons, per unit time is given by a balance relation between the number of excess carriers generated and the number of excess carriers which are annihilated by recombination. In the case of linear recombination we will assume that the rate of recombination is proportional to the first power of the excess carrier density. Under this assumption we can write the following balance relation for the excess electron density as

$$\frac{d(\Delta n)}{dt} = \underbrace{\beta k I}_{\text{generation rate}} - \underbrace{\frac{\Delta n}{\tau_n}}_{\text{recombination rate}} \qquad (69)$$

We shall now drop the notation $\overline{\tau}$ for the average lifetime and simply use τ to represent this quantity.

Let us now assume that the sample is exposed to step function of illumination beginning at time t = 0 and determine the response of the excess electron concentration. Then equal to or

greater than zero

$$\frac{d(\Delta n)}{dt} + \frac{\Delta n}{\tau_n} = \beta k I_o \qquad (70)$$

where I_o is constant and Δn is zero at t equal zero. Therefore

$$\Delta n(t) = \tau_n \beta k I_o \left(1 - e^{-t/\tau_n}\right), \quad t \geq 0$$

$$\Delta n(t) = 0, \quad t \leq 0$$

Hence the rise of the excess carrier concentration is given by an exponential and is shown schematically in Figure 33a. Note that as $t \to \infty$

$$\Delta n(t) = \tau_n \beta k I_o = \Delta n_{st} \qquad (71)$$

Now let us ask the corallary; suppose the sample had been under steady-state illumination and its excess carrier concentration was at the steady-state value Δn_{st}, and at time t = o we instantainously cut-off the exposure, what is the time dependence of the excess carrier concentration $\Delta n(t)$? If the sample is not exposed I = 0 and we have for $t \geq 0$

$$\frac{d(\Delta n)}{dt} = -\frac{\Delta n}{\tau_n}, \quad t \geq 0 \qquad (72)$$

Using our initial condition that $\Delta n(o) = \Delta n_{st} = \tau_n \beta k I_o$ we have

$$\Delta n(t) = \tau_n \beta k I_o e^{-t/\tau_n} \qquad (73)$$

which is represented in Figure 33b.

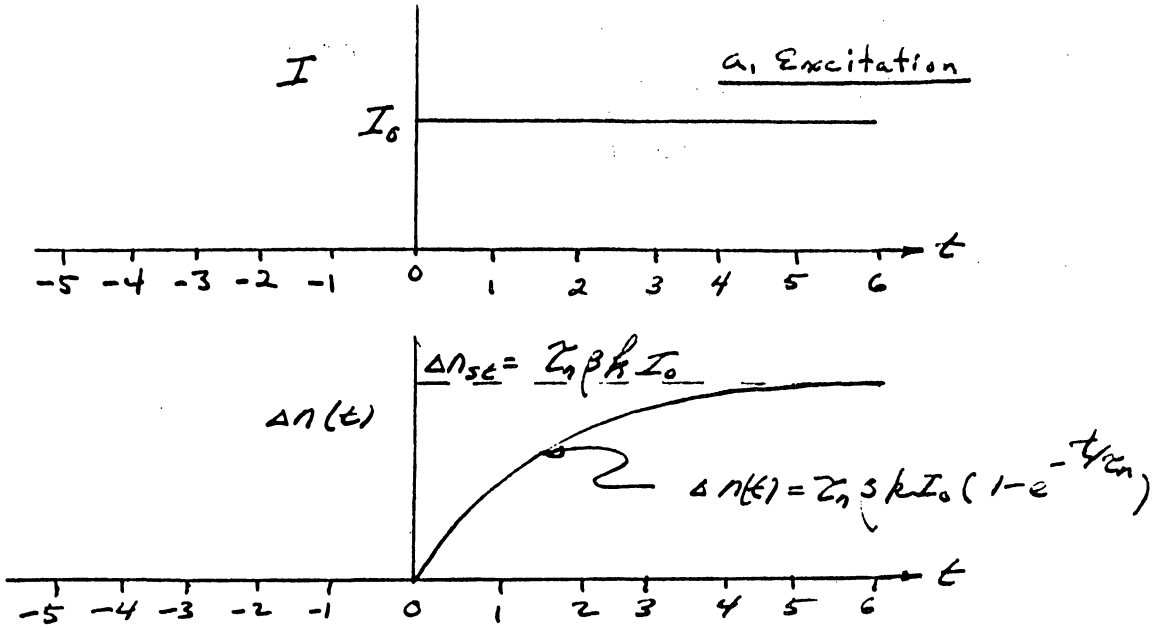

Figure 33. Excess Electron Concentration Produced by a Step Function Excitation and Cut-off For Linear Recombination.

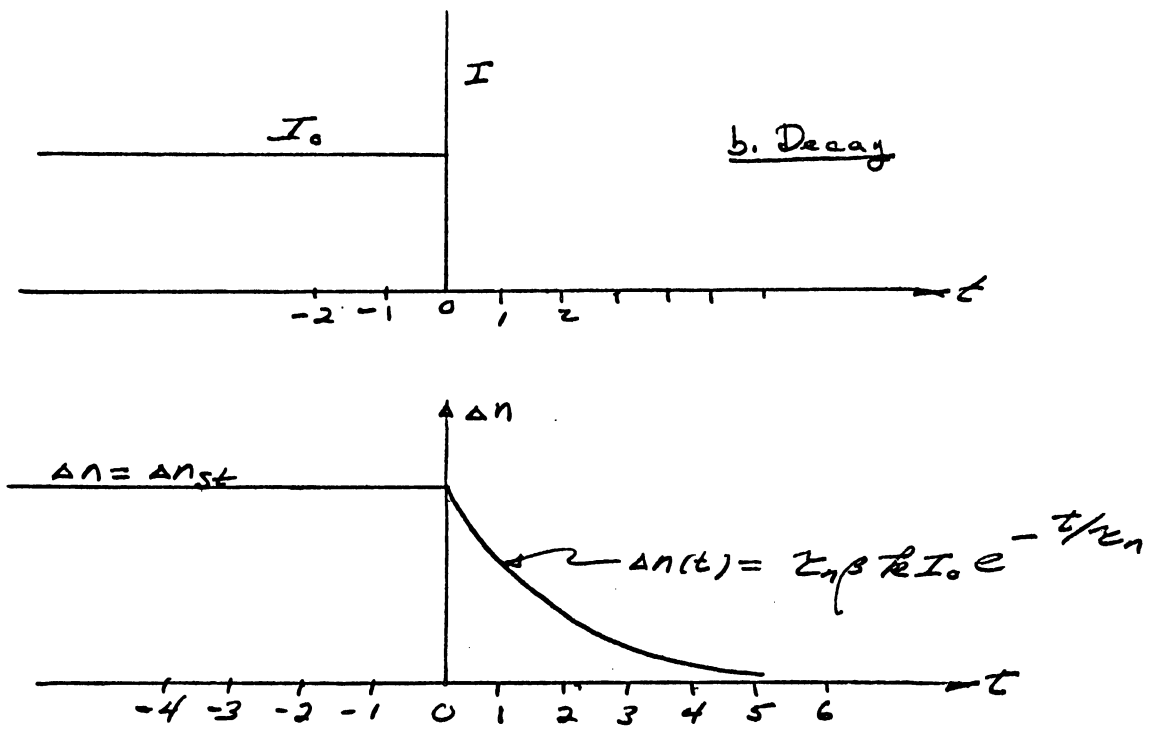

Figure 33.

From the above results we can infer the response to a square exposure pulse. For exposure to a square pulse with a pulse duration of time t_1, where t_1 is much greater than τ_n we would have the solution

$$\Delta n(t) = \Delta n_{st}\left(1 - e^{-t/\tau_n}\right), \qquad 0 \le t \le t_1$$

and

$$\Delta n(t) = \Delta n_{st}\, e^{-\frac{(t-t_1)}{\tau_n}}, \qquad t \ge t_1$$

Which is illustrated in Figure 34.

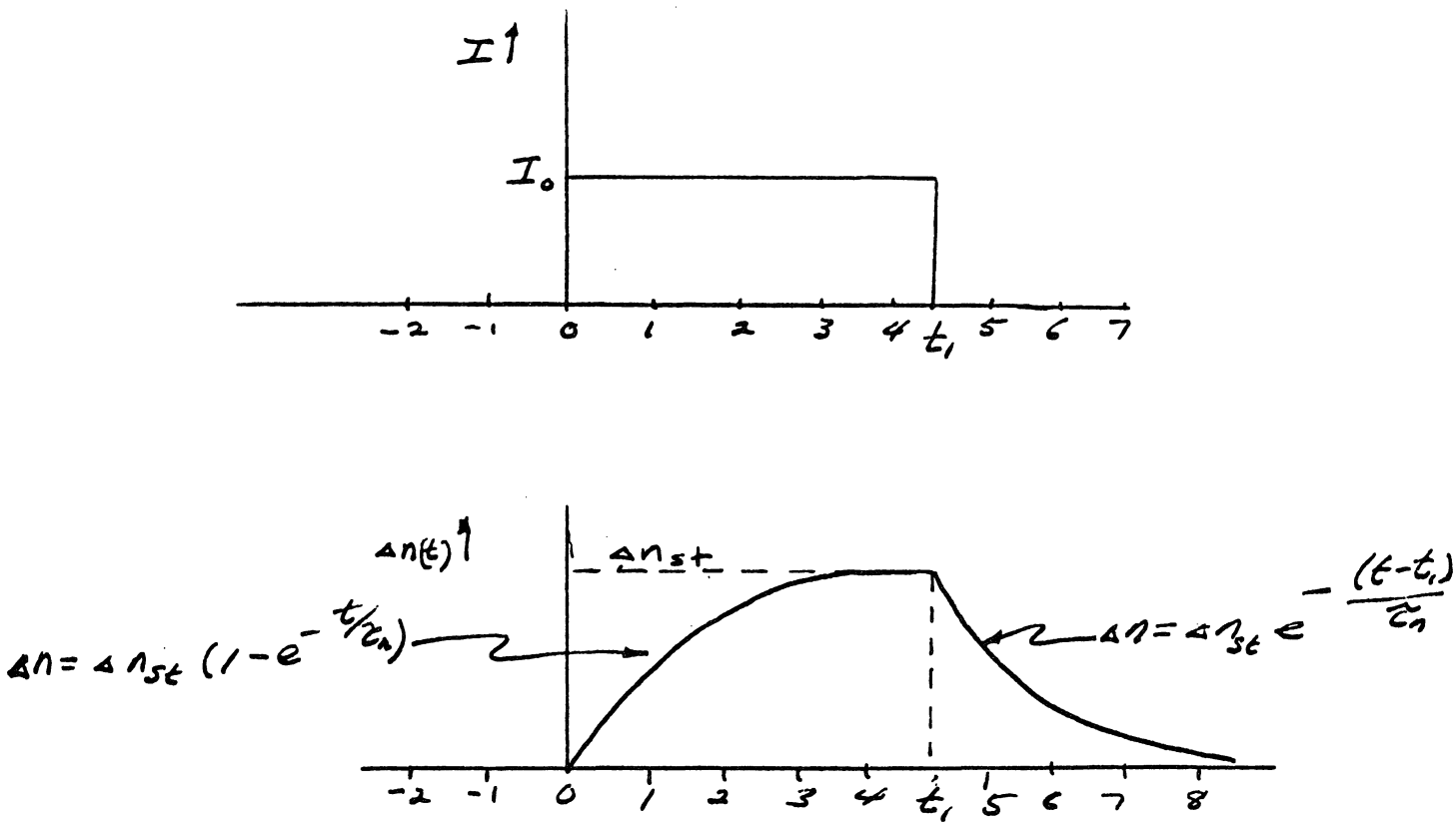

Figure 34. Response of the Excess Carrier Density to a Square Exposure Pulse.

From the above discussions of the linear recombination we can note that both the rise and decay of the excess carrier density would be exponential and that the time constant would be equal to the average lifetime. This simple case which assumed that the recombination was proportional to the first power of the excess carrier concentration Δn or Δp. This case does have practical significance such as the recombination of excess electrons with holes at a single recombination center and density of holes in these centers is initially very high relative to the change in concentration produced by excitation.

2. Quadratic Recombination:

As a second case, let us assume that the rate of recombination is proportional to the square of the excess carrier density. This might correspond to the situation where the density of the equilibrium carriers is small compared to excess carrier concentration produced by ionization. Then on excitation electrons are transferred to the conduction band leaving free holes in the valence band, then the excess hole and electron densities are equal and the rate of recombination would be given by

$$\gamma \Delta n \Delta p = \gamma (\Delta n)^2 = \gamma (\Delta p)^2 \qquad (74)$$

Under this assumption the balance relation for electrons would be

$$\frac{d(\Delta n)}{dt} = \beta k I - \gamma_n (\Delta n)^2 \qquad (75)$$

Let us now determine the time dependence of the nonequilibrium electron concentration for the examples used above (i.e., a step increase exposure and decrease in exposure) using a quadratic recombination rate. Again let us assume that the exposure begins at time, t = 0 and that the intensity remains constant at I_o. Also we will use the initial condition $\Delta n = 0$ at t = 0. Then for $t \geq 0$ the nonequilibrium electron density is described by

$$\frac{d(\Delta n)}{dt} = \beta k I_o - \gamma_n (\Delta n)^2 \quad , \quad t \geq 0 \qquad (76)$$

with the condition $\Delta n\,(t) = 0$ at t = 0. The solution is given by

$$\Delta n(t) = \left(\frac{\beta k I_o}{\gamma_n}\right)^{1/2} \tanh\left[t\,(\gamma_n \beta k I_o)^{1/2}\right] \qquad (77)$$

The rise of the excess electron density is not an exponential but is instead a hyperbolic tangent. This behavior is illustrated in figure 35a. In this case as $t \to \infty$ with obtain a steady-state density of

$$\lim_{t \to \infty} (\Delta n) = \left(\frac{\beta k I_o}{\gamma_n}\right)^{1/2} = \Delta n_{st} \qquad (78)$$

For decay let us again consider that we have a step cut-off of the exposure at time, t = 0, and that for all time $t \leq 0$ the exposure intensity was I_o. Then the nonequilibrium electron density is described as

$$\frac{d(\Delta n)}{dt} = -\gamma_n (\Delta n)^2 \quad , \quad t \geq 0 \qquad (79)$$

with the initial condition that $\Delta n = 0$ at t = 0. The solution

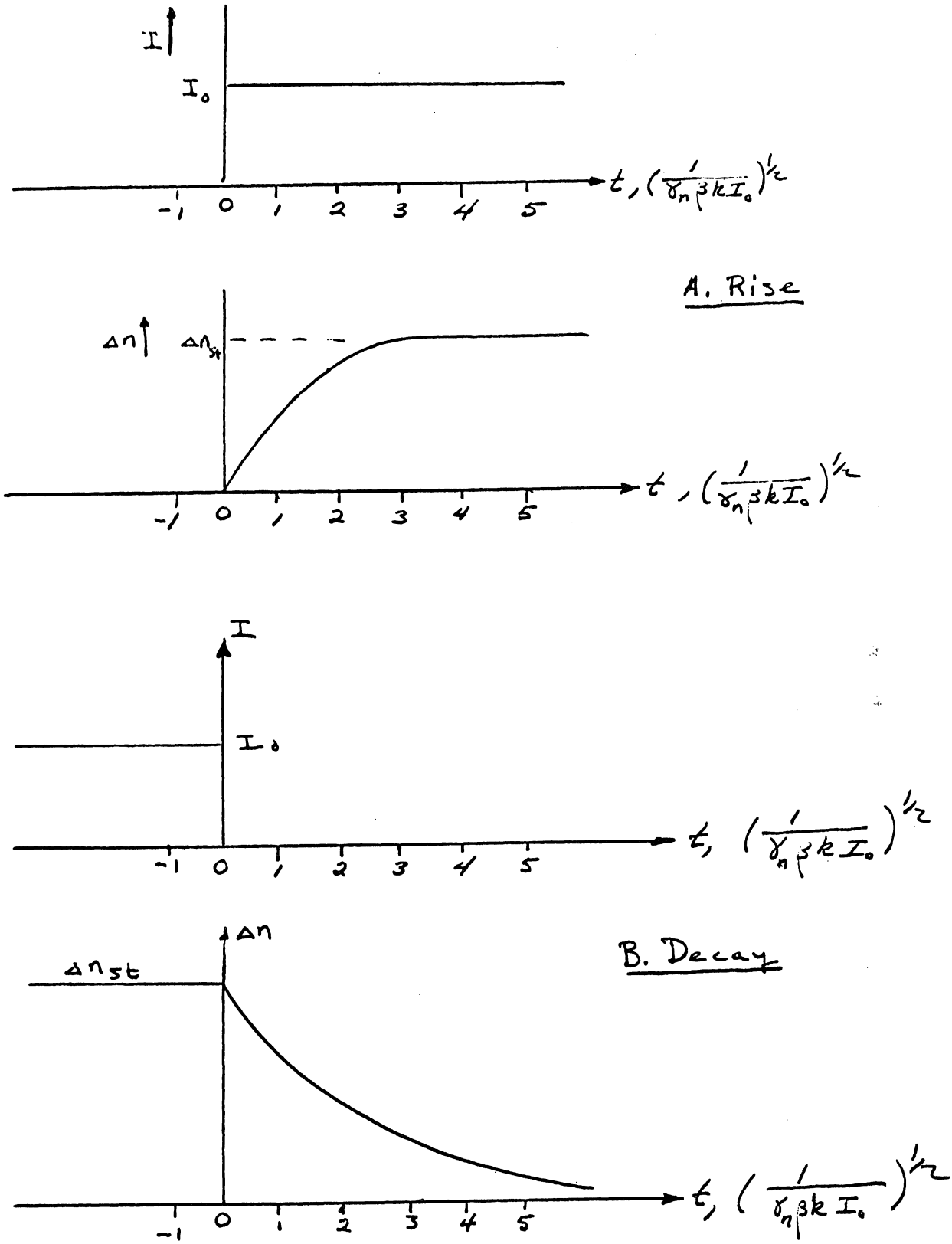

Figure 35. Nonequilibrium Electron Concentration for Quadratic Recombination.

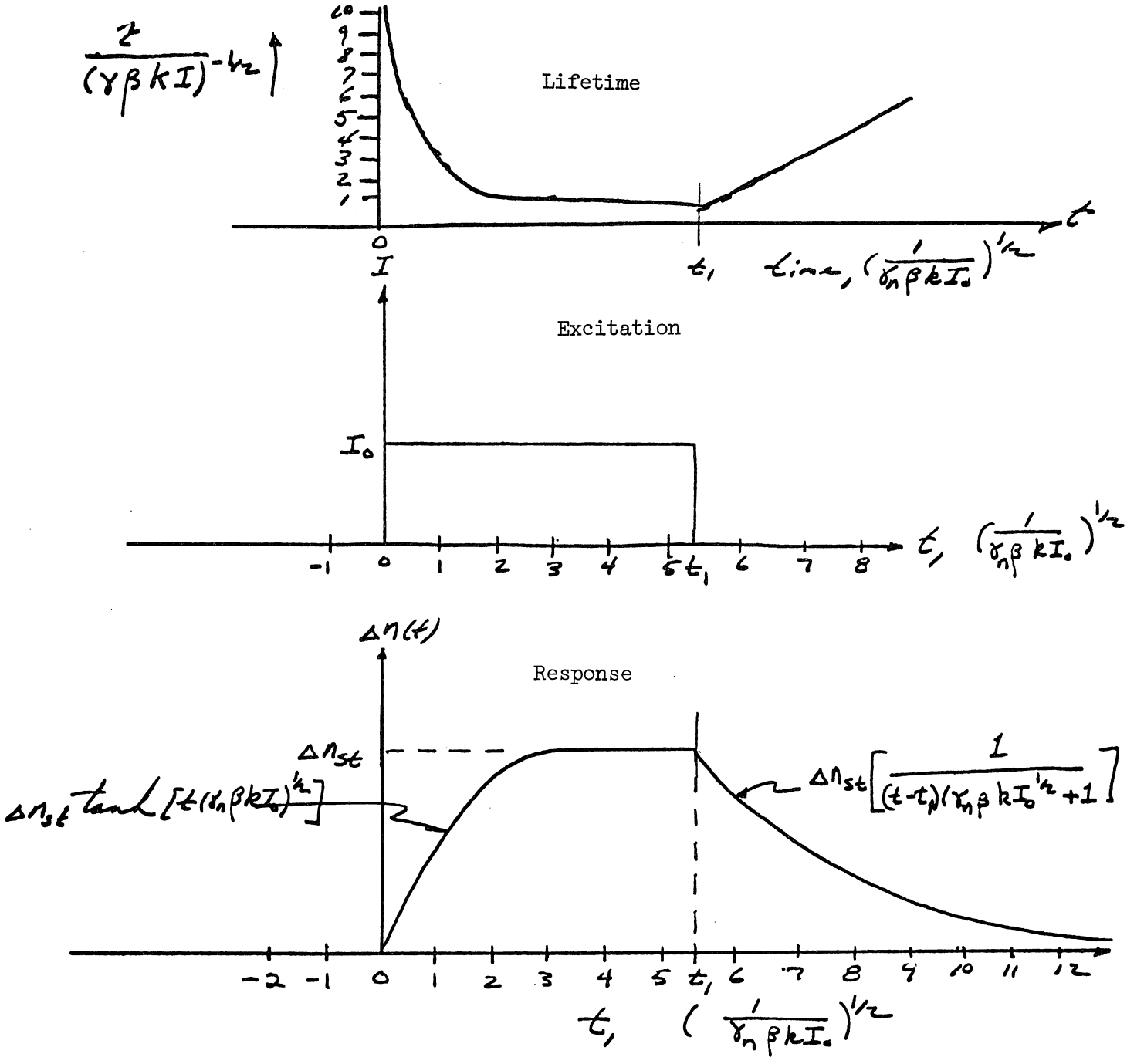

Figure 36. Excess Carrier Density Due to a Square Exposure Pulse for Quadratic Recombination.

is given by

$$\Delta n(t) = \left(\frac{\beta k I_o}{\gamma_n}\right)^{1/2}\left[\frac{1}{t(\gamma_n \beta k I_o)^{1/2}+1}\right] \quad (80)$$

or

$$\Delta n(t) = \Delta n_{st}\left[\frac{1}{t(\gamma_n \beta k I_o)^{1/2}+1}\right] \quad (80a)$$

Thus the decay is described by a hyperbola and is shown in Figure 35b.

Again we can infer the response to a square exposure pulse with a relatively long duration. The response to a square pulse initiated at time t = 0, with a duration t_1 and intensity I_o is given by

$$\Delta n(t) = \Delta n_{st} \tanh\left[t(\gamma_n \beta k I_o)^{1/2}\right], \quad 0 \le t \le t_1 \quad (81)$$

and

$$\Delta n(t) = \Delta n_{st}\left[\frac{1}{(t-t_1)(\gamma_n \beta k I_o)^{1/2}+1}\right], \quad t \ge t_1 \quad (82)$$

where

$$\Delta n_{st} = \left(\frac{\beta k I_o}{\gamma_n}\right)^{1/2} \quad (83)$$

This behavior is illustrated in Figure 36.

In the solution for quadratic recombination we did not find exponential rise or decay. Hence we no longer have a constant value for the lifetime but this does not mean that we can not use the concept of a lifetime. Recall that the average lifetime for an electron was given by

$$\tau_n = \frac{1}{\gamma_n \Delta p}$$

Since Δp is dependent upon excitation intensity and time, it is clear that τ_n is also a variable dependent on intensity and time. Thus in general $\tau = f(I,t)$. The general expression for the lifetime τ is given by solving the equations (69) for τ. That is

$$\frac{d(\Delta n)}{dt} = \beta k I - \frac{\Delta n}{\tau} \tag{69}$$

so

$$\tau = \frac{\Delta n}{k\beta I - \frac{d(\Delta n)}{dt}} \tag{84}$$

For the special case of quadratic recombination and we can use the equation $\tau_{(n_p)} = \frac{1}{\gamma_n \Delta n_{(p)}}$ to determine the lifetime as a function of time. We find that during the rise

$$\tau = \frac{1}{\gamma \Delta p} = \frac{1}{\gamma \Delta n} = \frac{1}{(\gamma \beta k I_0)^{1/2}} \coth\left[t(\gamma \beta k I_0)^{1/2}\right] \tag{85}$$

and during decay

$$\tau = \frac{1}{\gamma \Delta p} = \frac{1}{\gamma \Delta n} = \frac{1}{(\gamma \beta k I_0)^{1/2}} \cdot \left[t(\gamma \beta k I_0)^{1/2} + I_0\right] \tag{86}$$

where we assumed $p_o = n_o = 0$. The value of the lifetime when $\Delta n = \Delta n_{st}$ is given by

$$\tau_{st} = \frac{\Delta n_{st}}{\beta k I} \qquad (87)$$

which we obtained from equation 84 and the fact that $\frac{d(\Delta n)}{dt} = 0$ for the steady-state situation. The instantaneous values of the lifetime are included in Figure 36 for quadratic recombination.

Photoconductive Response of a Semiconductor with One Trap:

A. Introduction:

In the previous section we introduced many of the concepts used to describe the photoconductive response of semiconductors to the ionization produced by exposure to either a nuclear or space environment. Let us now introduce a realistic model which will illustrate more clearly the recombination mechanisms and the properties of the material.

As we discussed in an earlier section, impurities and defects such as neutron induced clusters play a dominant role in the recombination processes. These crystalline defects introduce levels which can act as recombination centers for electrons and holes. In the simplest cases these impurities are centers which may be in one of several charge states, i.e., neutral, singly charged, doubly charged, etc. These are labeled according to their charge state as donors, charged positive centers, and acceptors, charged negative centers. In this section we shall consider only the simplest impurities which have a single level in the forbidden band which can only be singly charged.

B. Recombination Through a Single Trap:

Let us now consider the transitions which can take place in a semiconductor having a single level in the forbidden gap. Then from these we will construct balance relations which describe

the kinetics of the holes and electrons in the material. The transitions which an electron can make in this system are illustrated in Figure 36.

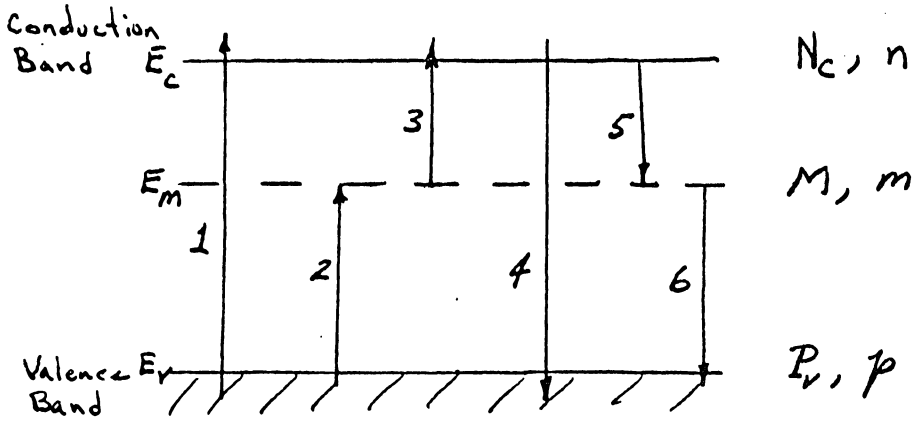

Figure 36. Electron Transitions in a Semiconductor With One Center.

In this system we shall consider six possible transitions as indicated. We will divide these transitions into two classes: a) absorption and excitation and b) trapping or capture leading recombination.

A. Transitions 1, 2 and 3 involve energy abosrption and are described in the following manner:

1. Transition 1 corresponds to absorption of energy by an atom of the crystal itself, creating free electrons and holes.
2. Transition 2 corresponds to energy absorption which raises an electron from the valence band to an unoccupied imperfection level, producing a free hole and a bound electron.
3. Transition 3 corresponds energy absorption at a crystal imperfection, creating a free electron and a bound hole.

B. Transitions 4, 5 and 6 are the capture and recombination processes and are accompanied by emission of thermal or optical energy.

1. Transition 4 corresponds to the direct recombination of free electrons and holes. The probability of this transition is very small. The transition energy generally appears as radiative energy.
2. Transition 5 corresponds to the capture or trapping of an electron by a crystal imperfection which may lead to recombination. The energy may appear either as radiative or thermal energy.
3. Transition 6 represents the capture of a hole by an imperfection leading to possible recombination. Again the energy released could appear as either radiative or thermal lattice energy

To describe the system we will let M be the total trap concentration and the number of electrons in these sites be m, which represents the number of filled centers. The free electron and hole concentrations will be given by n and p respectively. The effective density of states in the conduction and valence bands will be given by N_c and P_v. Furthermore, in this case each center will be represented by two capture cross-sections, g_n for electron capture, and g_p for hole capture. Essentially we are implying that g_n and g_p are not equal. In this model g_p might apply to the donor level when the center is in the neutral

state and its probability of capturing a hole. Then g_n would represent the positively charged state due to hole capture.

We would now like to determine the generation, release and capture rates for each of these six transistors.

a. Generation of Free Carriers due to Ionization

The generation rate of free electrons and holes due to external excitation may be written as in the previous section as

$$\left\{\begin{array}{l}\text{Generation rate of free electrons} \\ \text{and holes due to exposure to ionizing} \\ \text{radiation}\end{array}\right\} = \beta\, kI$$

where β = the number of ion pairs formed by the absorption of a single quanta of energy.

where k = the energy abosrption coefficient.

where I = the energy flux incident on an elemental slab

b. Capture rate of free electrons and holes by Traps:

We will let γ_n and γ_p be the coefficients for the capture of electrons by empty traps and γ_p be the capture of holes by occupied traps. Then the rate of capture of electrons by traps will be given as

$$\left\{\begin{array}{l}\text{Rate of removal of free electrons due} \\ \text{to capture by vacant traps}\end{array}\right\} = \gamma_n\, N(M-m)$$

This is the product of the number of available site (M-m), the probability of capture, γ_n, and the total number of electrons, n.

Similarly for holes we have

$$\left\{\begin{array}{l}\text{Rate of removal of free hole due to} \\ \text{capture by occupied traps.}\end{array}\right\} = \gamma_p\, pm \ .$$

c. Generation of Free Electrons and Holes by Thermal Excitation of Trapping Sites:

We will now determine the rate of thermal transitions from the trapping sites to each of the bands. However to do this we will digress a little in order to calculate the relationships between the recombination coefficients and the probability of thermal transitions from the traps to each band. We will first consider the kinetics which exist between the capture sites and the conduction band under equilibrium conditions without photoexcitation. For this case we can write a balance relationship for the change in electron density due to the capture and release of electrons by traps as

$$\frac{dn_o}{dt} = \alpha_n m_o - \gamma_n n_o (M-m) \qquad (88)$$

where $\alpha_n M_o$ = The thermal excitation rate of electrons into the conduction band from trapping sites

$\gamma_n N_o (M-m)$ = The rate of capture of electrons from the conduction band by empty traps.

Hence α_n represents the probability of thermal transitions from the trap to the conduction band and it is the unknown we wish to determine.

At equilibrium we can write

$$\frac{dn}{dt} = 0$$

hence $m_o = \frac{M}{\frac{\alpha_n}{\gamma_n n_o} + 1}$. But we also know that a equilibrium the number of occupied sites m is given by the product of the total number of sites M and the probability of occupation or the Fermi function. So we can write

$$m_o = M \left[\frac{1}{e^{\frac{(E_M - E_F)}{KT}} + 1} \right] \qquad (89)$$

Comparing like terms in express ( ) and ( ) we find

$$\alpha_n = \gamma_n n_o e^{\left(\frac{E_M - E_F}{KT}\right)} \qquad (90)$$

Recall the n_o is given by

$$n_o = N_c e^{-(E_F - E_c)/KT} \qquad (21)$$

Thus we obtain after substitution:

$$\alpha_n = \gamma_n N_c e^{\frac{-(E_c - E_M)}{KT}} \qquad (91)$$ and

we can write the thermal transition rate under equilibrium as

$$\alpha_n m_o = \gamma_n m_o N_c e^{-\frac{(E_c - E_M)}{KT}} \qquad (92)$$

Now we will argue that this is equally applicable to the nonequilibrium conditions if we replace m_o by m, since the nonequilibrium carriers in the conduction band have the same energy distribution as equilibrium carriers and hence are indistinguishable. The thermal transition rate for electrons

excited from traps is given by

$$\left\{\begin{array}{l}\text{Rate of thermal excitation of electrons}\\ \text{from the trapping sites to the conduction}\\ \text{band.}\end{array}\right\} = \gamma_n\, m\, N_c\, e^{\frac{-(E_M - E_v)}{kT}}$$

In a similar fashion we can obtain the transition rate of holes excited from the sites back to the valence band. It is given by

$$\left\{\begin{array}{l}\text{Rate of thermal excitation of hole}\\ \text{from the trapping sites to the valence}\\ \text{band}\end{array}\right\} = \gamma_p (M-m) P_v e^{\frac{-(E_M - E_v)}{kT}}$$

We can now write detailed balance relations for free electrons, trapped electrons and free holes. For free electrons in the conduction band,

$$\frac{dn}{dt} = \underbrace{k\beta I}_{\substack{\text{generation rate due to exposure of intensity I}}} - \underbrace{\gamma_n\, n\, (M-m)}_{\substack{\text{Removal rate due to electron capture by traps}}} + \underbrace{\gamma_n\, m\, N_c\, e^{\frac{-(E_c - E_M)}{kT}}}_{\substack{\text{Generation rate due to thermal excitation from traps.}}}, \qquad (93)$$

for free holes in the valence band,

$$\frac{dp}{dt} = \underbrace{k\beta I}_{\substack{\text{generation rate due to exposure at intensity I}}} - \underbrace{\gamma_p\, mp}_{\substack{\text{removal rate due to hole capture by traps}}} + \underbrace{\gamma_p\, (M-m)\, P_v\, e^{\frac{-(E_M - E_v)}{kT}}}_{\substack{\text{generation due to thermal excitation of holes from traps to the valence band.}}} \qquad (94)$$

and for the electron density in the centers we can write

$$\frac{dm}{dt} = \underbrace{\gamma_n n (M-m)}_{\text{Rate of capture of electrons by the trapping sites}} - \underbrace{\gamma_n m N_c e^{-\frac{(E_c-E_M)}{kT}}}_{\text{Excitation rate for electrons from the trapping sites to the conduction band}} - \underbrace{\gamma_p mp}_{\text{Rate at which electrons recombine with the holes at the centers}} + \underbrace{\gamma_p P_v e^{-\frac{(E_M-E_v)}{kT}} (M-m)}_{\text{Rate at which electrons are excited into the center releasing free holes in the valence band}} \quad (95)$$

If we define

$$N_{cM} = N_c e^{-\frac{(E_c-E_M)}{kT}} \quad (96)$$

$$P_{vM} = P_v e^{-\frac{(E_M-E_v)}{kT}} \quad (97)$$

then we can write the above relationships in a more concise manner as

$$\frac{dn}{dt} = k\beta I - \gamma_n n(M-m) + \gamma_n m N_{cM}, \quad (93)$$

$$\frac{dm}{dt} = \gamma_n n(M-m) - \gamma_n m N_{cM} - \gamma_p mp + \gamma_p P_{vM}(M-m), \quad (95)$$

$$\frac{dp}{dt} = k\beta I - \gamma_p mp + \gamma_p (M-m) P_{vM}. \quad (94)$$

In addition using charge neutrality we have a relationship for the number of excess electrons and holes

$$\Delta n + \Delta m = \Delta p. \quad (98)$$

Hence we now have a system of equations which completely describe the kinetics of electrons and holes in a system with a single recombination center or trap. Unfortunately even this simple system cannot be solved in a general closed form. However we can solve this system of equations for several situations of interest.

C. Relaxation of Photoconductivity in a Semiconductor with a Low Trap Concentration:

We shall now consider the nature of the relaxation of photoconductivity produced by a short pulse of radiation say the prompt gamma output of a nuclear weapon. In particular we shall determine the dependence of the nonequilibrium carrier density on time for a semiconductor with a low trap concentration. We shall assume that the number of traps M is so small that we can neglect the change in the concentration of charge in the traps Δ m relative to the changes which take place in the bands. Thus our neutrality condition may be rewritten as

$$\Delta p = \Delta n + \Delta m \simeq \Delta n$$

Since $\Delta n \cong \Delta p$, it is seen that during the main part of the relaxation process

$$\frac{dn}{dt} = \frac{dp}{dt}$$

Hence we can equate relationships (93) and (94), obtaining

$$k\beta I - \gamma_n n(M-m) + \gamma_n m N_{cM} = k\beta I - \gamma_p mp + \gamma_p (M-m) P_{vM} \qquad (99)$$

from which we can solve for m, the concentration of electrons in the traps. We find

$$m = \frac{\gamma_n nM + \gamma_p M P_{vM}}{\gamma_n (n + N_{cM}) + \gamma_p (p + P_{vM})} \qquad (100)$$

Now substituting into our relationship for $\frac{dn}{dt}$ we have

$$\frac{dn}{dt} = k\beta I - \gamma_n n M + m\gamma_n (n + N_{cm})$$

$$= k\beta I - \gamma_n n M + \frac{(\gamma_n n M + \gamma_p M P_{vm})}{\gamma_n (n + N_{cm}) + \gamma_p (p + P_{vm})} \cdot \gamma_n (n + N_{cm})$$

$$= k\beta I + \frac{(\gamma_p \gamma_n M P_{vm} N_{cm} - \gamma_n \gamma_p M np)}{\gamma_n (n + N_{cm}) + \gamma_p (p + P_{vm})}$$

hence

$$\frac{dn}{dt} = k\beta I + M \frac{\gamma_n \gamma_p (N_{cm} P_{vm} - np)}{\gamma_n (n + N_{cm}) + \gamma_p (p + P_{vm})} \qquad (101)$$

Now substituting the relationships

$$n = n_0 + \Delta n$$

$$p = p_0 + \Delta p \simeq p_0 + \Delta n$$

and

$$N_{cm} P_{vm} = n_0 p_0$$

we have

$$\frac{d(\Delta n)}{dt} = k\beta I + M \frac{\gamma_n \gamma_p (n_0 p_0 - n_0 p_0 - \Delta n p_0 - n_0 \Delta n - \Delta n \Delta n)}{\gamma_p (\Delta n + p_0 + P_{vm}) + \gamma_n (\Delta n + n_0 + N_{cm})} \cdot$$

(102)

Rewriting the above expression becomes

$$\frac{d(\Delta n)}{dt} + M \cdot \frac{\gamma_n \gamma_p (\Delta n + n_o + p_o)\Delta n}{\gamma_p(\Delta n + p_o + P_{VM}) + \gamma_n(\Delta n + n_o + N_{CM})} = k\beta I \qquad (102a)$$

Now let us consider the response of this material to a prompt gamma pulse from a nuclear weapon. Furthermore let us assume that we can approximate the intensity as a function of time with a square pulse. For the purposes of simplicity, let us assume that the pulse width is much longer than the carrier lifetime Later we will show the effect of pulse width on the response. The solution to this problem will be divided into two regions, the excitation and the decay.

Consider the response to the excitation due to a square gamma pulse of intensity, I_o, and width t where $t >> \tau$ as shown below

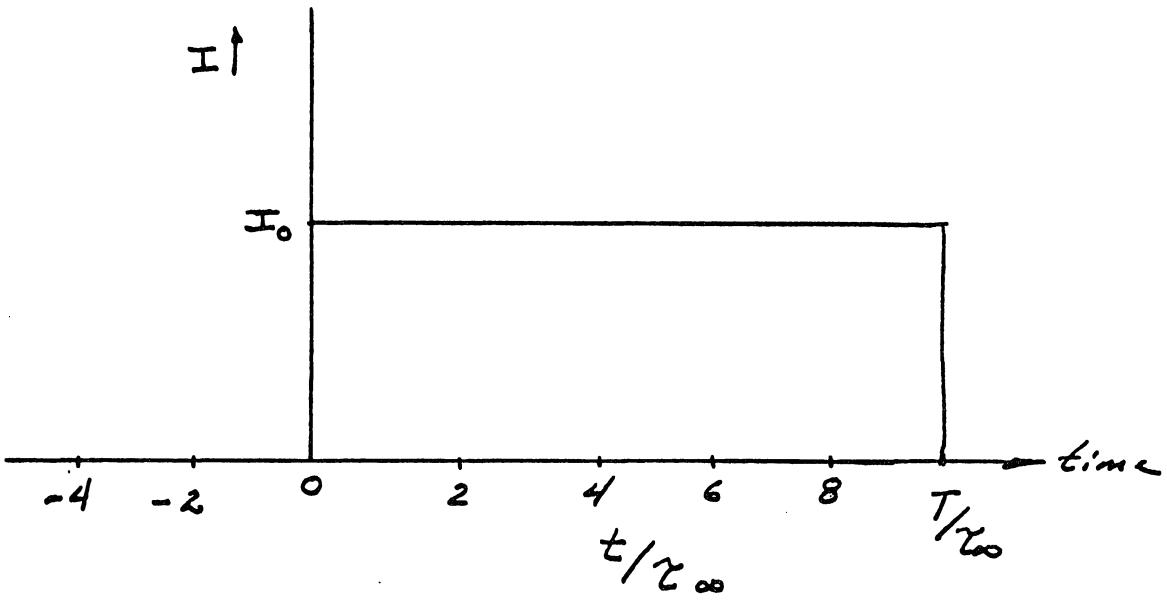

Figure 38.

1. Excitation or Rise, $t \leq t_1$

The differential equation describing the change in carrier concentration during this time is given by

$$\frac{d(\Delta n)}{dt} + \frac{M\gamma_n\gamma_p \Delta n(\Delta n + n_o + p_o)}{\gamma_p(\Delta n + p_o + P_{vm}) + \gamma_n(\Delta n + n_o + N_{cm})} = k\beta I_o, \quad \text{for } t \geq t_1. \tag{103}$$

Rearranging the above relation we have

$$\frac{d\Delta n}{dt} + \frac{\Delta n(\Delta n + n_o + p_o)}{\frac{(\gamma_p+\gamma_n)}{M\gamma_n\gamma_p}\Delta n + \frac{\gamma_p(p_o + P_{vm}) + \gamma_n(n_o + N_{cm})}{M\gamma_n\gamma_p}} = k\beta I_o$$

Now by defining

$$\tau_\infty = \frac{\gamma_p + \gamma_n}{M\gamma_n\gamma_p} \tag{104}$$

and

$$\tau_o = \frac{\gamma_p(p_o + P_{vm}) + \gamma_n(n_o + N_{cm})}{M\gamma_n\gamma_p(n_o + p_o)} \tag{105}$$

we can rewrite the above relationship for $\frac{d(\Delta n)}{dt}$ as

$$\frac{d(\Delta n)}{dt} + \frac{\Delta n(\Delta n + n_o + p_o)}{\tau_\infty \Delta n + \tau_o(n_o + p_o)} = k\beta I_o \tag{106}$$

If we change variables by letting

$$y = \frac{\Delta n}{(n_o + p_o)} \tag{107}$$

$$T = t/\tau_\infty \tag{108}$$

and define the constants

$$K = \frac{\tau_\infty k\beta I_o}{(n_o + p_o)} \tag{109}$$

and

$$m = \tau_o/\tau_\infty \tag{110}$$

then we get the differential equation

$$\frac{dy}{dT} + \frac{y(y+1)}{y+m} - K = 0. \tag{111}$$

Expanding we get

$$\frac{dy}{dT} + \frac{y^2 + y(1-k) - km}{y+m} = 0. \tag{112}$$

To solve this equation we simplify by letting

$$y^2 + y(1-k) - km = (y-a)(y+b) \qquad (113)$$

where both a and b are positive, therefore,

$$y^2 + y(1-k) - km = y^2 + (b-a)y - ab$$

and hence

$$ab = km$$
$$(b-a) = 1-k$$

so

$$a = \frac{(k-1) + \sqrt{(k-1)^2 + 4km}}{2} \qquad (114)$$

and

$$b = \frac{-(k-1) + \sqrt{(k-1)^2 + 4km}}{2}, \qquad (115)$$

Thus we can write

$$\frac{dy}{dT} = \frac{(y-a)(y+b)}{(y+m)} = 0 \qquad (116)$$

and after rearranging we have

$$-dT = \frac{(y+m)}{(y-a)(y+b)} = \frac{-(a+m)}{(b+a)} \frac{dy}{(a-y)} + \frac{(b-m)}{(b+a)} \frac{dy}{(y+b)} \qquad (117)$$

Now we can solve for T as a function of y by integrating from o to T and from 0 to y and we get

$$-T = \left[\left(\frac{a+m}{b+a} \right) \ln(a-y) + \left(\frac{b-m}{b+a} \right) \ln(y+b) \right] \Bigg|_0^y$$

thus either

$$-T = \left(\frac{a+m}{b+a}\right) \ln\left(1 - \frac{y}{a}\right) + \left(\frac{b-m}{b+a}\right) \ln\left(1 + \frac{y}{b}\right) \quad (118)$$

or

$$T = \left(\frac{a+m}{b+a}\right) \ln\left(\frac{a}{a-y}\right) + \left(\frac{b-m}{b+a}\right) \ln\left(\frac{b}{y+b}\right). \quad (118_a)$$

We have now a general solution which gives a relationship between time, t, and the excess carrier concentration Δ n, i.e.,

$$\frac{t}{\tau_\infty} = \left(\frac{a+m}{b+a}\right) \ln\left[\frac{a(n_o+p_o)}{a(n_o+p_o)-\Delta n}\right] + \left(\frac{b-m}{b+a}\right) \ln\left[\frac{b(n_o+p_o)}{b(n_o+p_o)+\Delta n}\right] \quad (119)$$

We note that at time, $\frac{t}{\tau_\infty} = o$, Δ n must be zero and as $\left(\frac{t}{\tau_\infty}\right)$ goes to large values Δ n must to the limiting value a $(n_o + p_o)$ as the first term on the RHS which controls the magnetude at large $\left(\frac{t}{\tau_\infty}\right)$.

$$\Delta n_{max} = a(n_o + p_o) = \left[\frac{(k-1) + \sqrt{(k-1)^2 + 4km}}{2}\right](n_o + p_o) \quad (120)$$

which after substitution becomes

$$= \frac{n_o+p_o}{2}\left[\frac{(\tau_\infty k\beta I_o - n_o - p_o)}{(n_o+p_o)} + \frac{\sqrt{(\tau_\infty k\beta I_o - n_o - p_o)^2 - 4k\frac{\tau_a}{\tau_\infty}(n_o+p_o)^2}}{(n_o+p_o)}\right]$$

or

$$\Delta n_{max} = \frac{1}{2}\left[(\tau_\infty k\beta I_o - n_o - p_o) + \sqrt{[\tau_\infty k\beta I_o - (n_o+p_o)]^2 - 4k\beta I_o \tau_o (n_o+p_o)}\right] \quad (121)$$

A plot of $\Delta n(t)$ is represented in Figure 39, the rise to square wave excitation

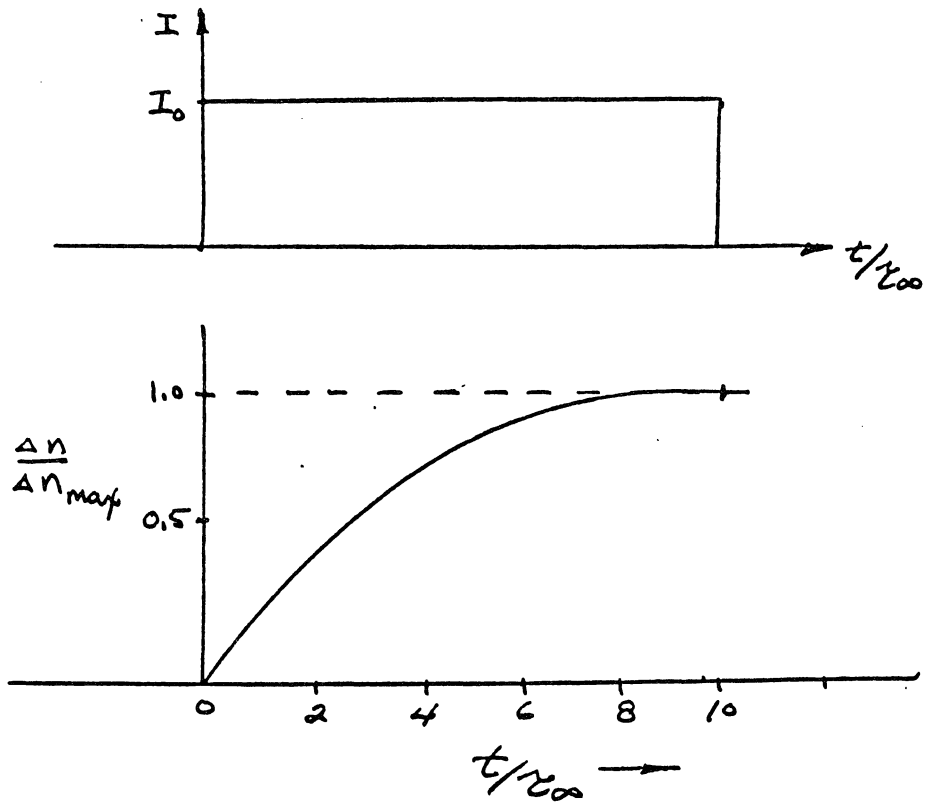

Figure 39.

The instantaneous value of the lifetime is given by

$$\tau_{inst} = \frac{-(\Delta n)}{\frac{d(\Delta n)}{dt}}$$

Upon substituting equation 106 for $\frac{d(\Delta n)}{dt}$ we have

$$\tau_{inst} = \frac{\Delta n}{\frac{\Delta n(\Delta n + n_0 + p_0)}{\tau_\infty \frac{\Delta n}{(n_0+p_0)} + \tau_0} - k\beta I_0} \qquad (122)$$

$$\tau_{inst} = \frac{\Delta n \left[\tau_\infty + \tau_0 \frac{(n_0+p_0)}{\Delta n} \right]}{(\Delta n + n_0 + p_0)(n_0 + p_0) - k\beta I_0 \tau_\infty - k\beta I_0 \tau_0 \frac{(n_0+p_0)}{\Delta n}}$$

2. Decay or Relaxation for $t \geq t_1$

Now let us determine the response of the material upon cutoff of the excitation at t = t. The system is now governed by the differential equation

$$\frac{d(\Delta n)}{dt} + \frac{M \gamma_n \gamma_p (\Delta n + n_0 + p_0) \Delta n}{\gamma_p (\Delta n + p_0 + P_{VM}) + \gamma_n (\Delta n + n_0 + N_{CM})} = 0 \qquad (123)$$

with the initial condition at time $t = t_1$ that

$$\Delta n (t_1) = \Delta n_1 \qquad (124)$$

We can now rewrite the above relationship as

$$\frac{d(\Delta n)}{dt} + \frac{\Delta n (\Delta n + n_0 + p_0)}{\tau_\infty \Delta n + \tau_0 (n_0 + p_0)} = 0 \qquad (125)$$

After separating we have

$$-dt = \left\{ \tau_\infty \left(\frac{1}{\Delta n + n_o + p_o} \right) + \tau_o (n_o + p_o) \left[\frac{1}{\Delta n (\Delta n + n_o + p_o)} \right] \right\} d(\Delta n)$$

Integrating over t from t_1 to t where $t \geq t_1$, and over on from the initial value Δn_1 to Δn (t), we get

$$-t \Big|_{t_1}^{t} = \tau_\infty \ln(\Delta n + n_o + p_o) \Big|_{\Delta n_1}^{\Delta n(t)} - \tau_o \ln\left(\frac{\Delta n + n_o + p_o}{\Delta n} \right) \Big|_{\Delta n_1}^{\Delta n(t)}$$

which gives

$$(t - t_1) = \tau_\infty \ln\left(\frac{\Delta n_1 + n_o + p_o}{\Delta n(t) + n_o + p_o} \right) - \tau_o \ln\left(\frac{\Delta n_1 + n_o + p_o}{\Delta n(t) + n_o + p_o} \right)$$

$$- \tau_o \ln\left(\frac{\Delta n_1}{\Delta n(t)} \right).$$

Thus we have for $t \geq t_1$

$$\left(\frac{t - t_1}{\tau_\infty} \right) = \left(1 - \frac{\tau_o}{\tau_\infty} \right) \ln\left(\frac{\Delta n_1 + n_o + p_o}{\Delta n(t) + n_o + p_o} \right) - \frac{\tau_o}{\tau_\infty} \ln\left(\frac{\Delta n_1}{\Delta n(t)} \right). \quad (126)$$

The decay in Δn (t) is shown below as a function of

as the solid trace.

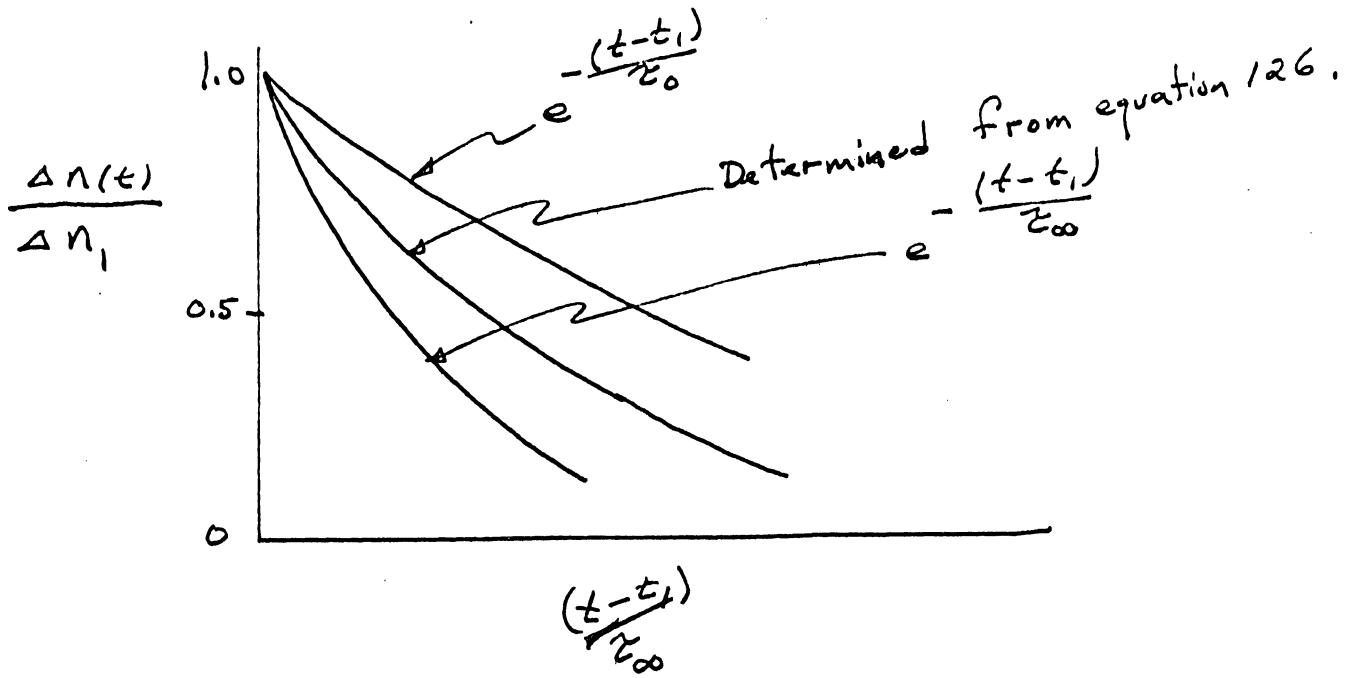

Figure 40.

Since $\tau_o > \tau > \tau_\infty$, these two special cases represent an upper and lower bound to the decay of the excess carrier concentration as shown in Figure 40.

For the case of exposure to a square wave with a pulse width much greater than, the excess electron concentration as a function of time is given by the system of equations which follows:

If the intensity of exposure is given by

$$I(t) = I_o \qquad \text{for} \quad o < t \leq t_1$$
$$I(t) = o \qquad \text{for} \quad t_1 < t < o$$

then a) for $(o \leq t \leq t_1)$ the excess electron density is given by:

$$\frac{t}{\tau_\infty} = \left(\frac{a+m}{b+a}\right) \ln\left[\frac{a(n_o+p_o)}{a(n_o+p_o)-\Delta n}\right] + \left(\frac{b-m}{b+a}\right) \ln\left[\frac{b(n_o+p_o)}{b(n_o+p_o)+\Delta n}\right]$$

where Δn has the limiting value of

$$\lim_{t \to \infty} (\Delta n) \longrightarrow a(n_o+p_o) = \Delta n_{max}$$

and b) for $(t_1 < t < o)$ the excess electron density is given by:

$$\left(\frac{t-t_1}{\tau_\infty}\right) = \left(1 - \frac{\tau_o}{\tau_\infty}\right) \ln\left(\frac{\Delta n_1 + n_o + p_o}{\Delta n(t) + n_o + p_o}\right) - \frac{\tau_o}{\tau_\infty} \ln\left(\frac{\Delta n_1}{\Delta n(t)}\right),$$

where $\Delta n_1 \simeq \Delta n_{max}$ for $t_1 \gg \tau_\infty$.

This solution is represented in Figure 41

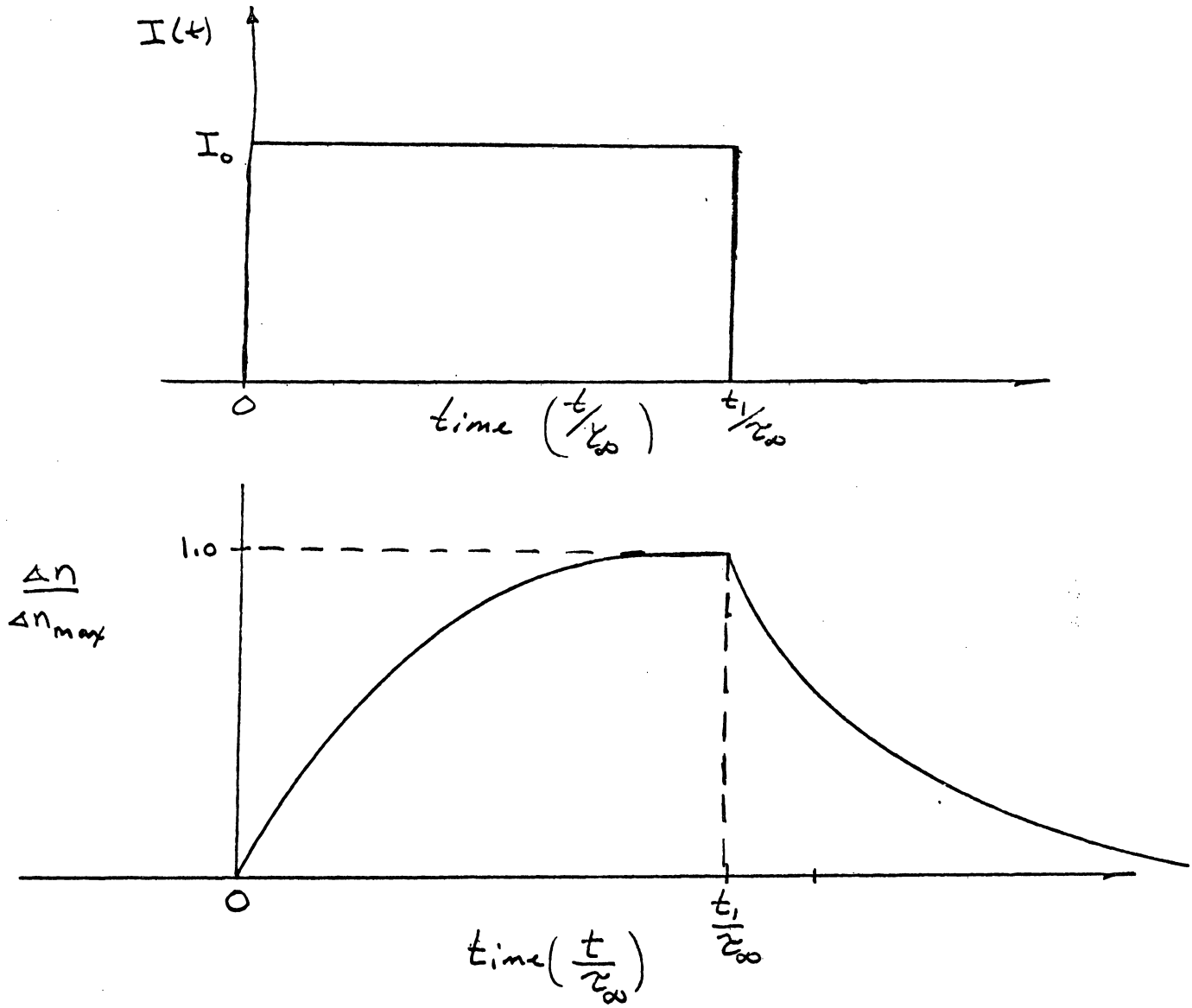
I(t)
I_o
0
time (t/τ_∞)
t_1/τ_∞
$\frac{\Delta n}{\Delta n_{max}}$
1.0
0
time $(\frac{t}{\tau_\infty})$
$\frac{t_1}{\tau_\infty}$

Figure 41.

The above solution was obtained for the hypothetical where t_1 the pulse width was much greater than lifetime of the carriers. But in general this will not be true, since the prompt gamma pulse may be of the order of 10^{-8} seconds while the lifetime of the carriers may be of the order of 10^{-7} to 10^{-2} sec. As a result the excess carrier concentration at the time of cutoff will not be Δn_{max} some value much less than this maximum as depicted in Figure 42.

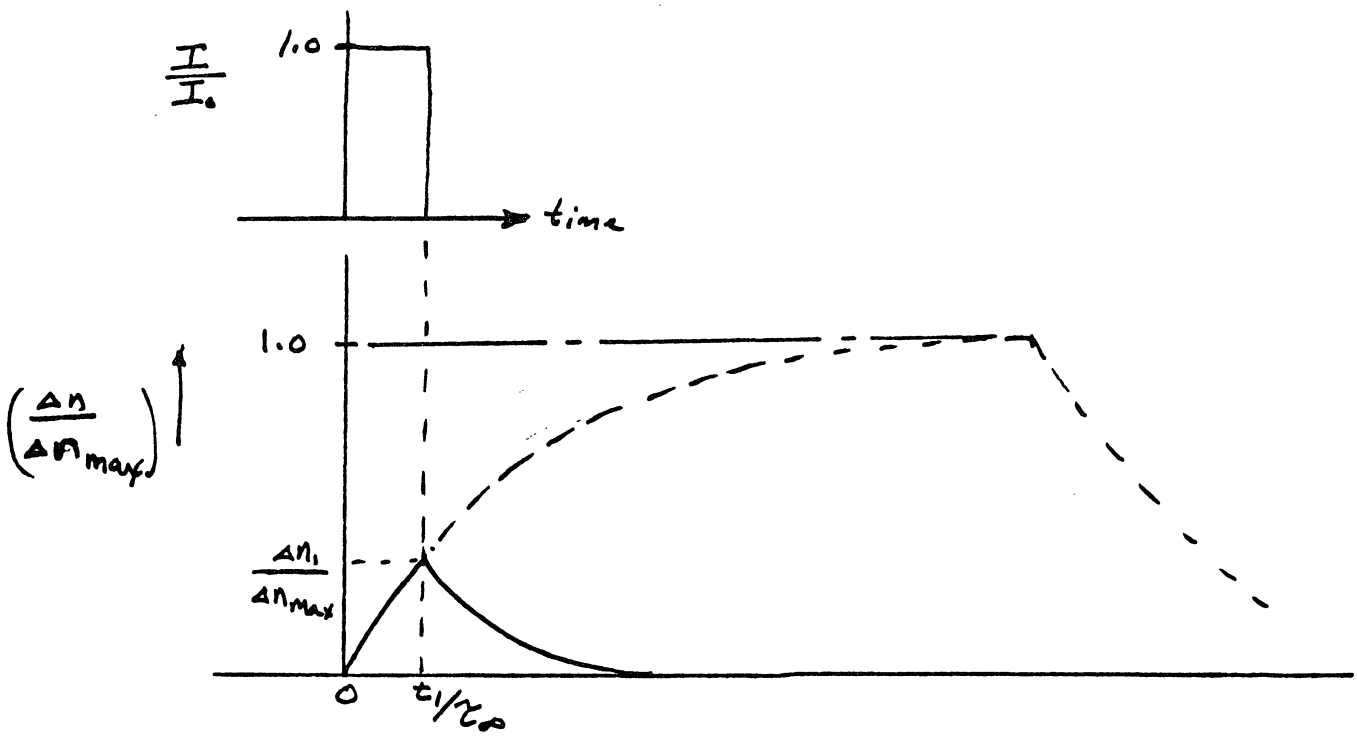

Figure 42.

Thus we see that the magnetude of the ionization, effects produced by radiation is determined by the mean lifetime of the free carriers, the pulse width of the exposure pulse, and the exposure rate. These features are illustrated in Figure 43 for two materials having two extreme values of mean lifetime exposed at two different exposure rates I_1 and I_2.

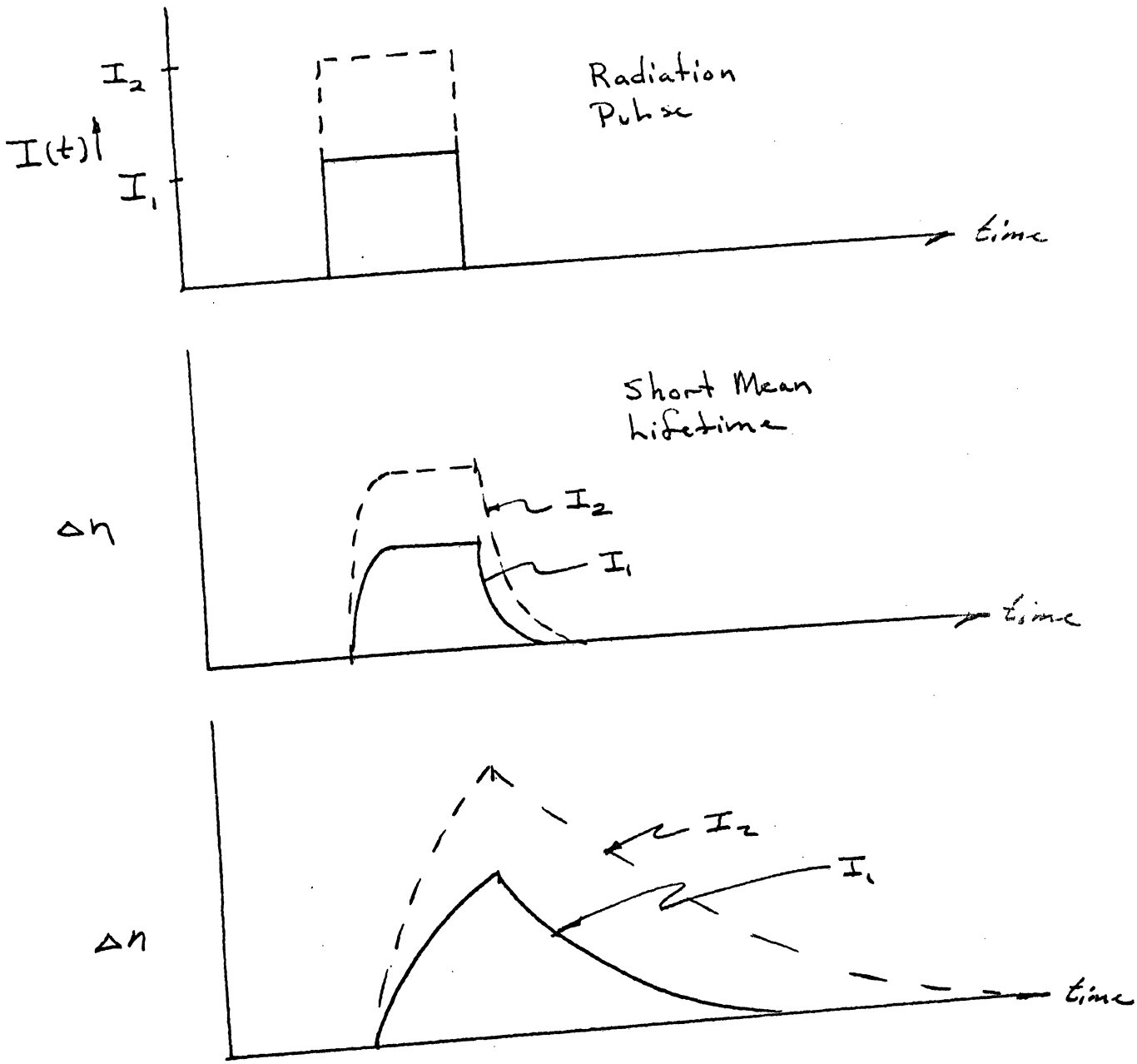
I_2
$I(t)$
I_1
Radiation Pulse
time
Short Mean lifetime
Δn
I_2
I_1
time
Δn
I_2
I_1
time

Figure 43.

SEMICONDUCTOR DEVICES

G. H. Hanson

SEMICONDUCTOR DEVICES

INTRODUCTION

The material in the succeeding pages is intended to cover those aspects of the theory and operation of p-n junction diodes and transistors that are essential to an understanding of their response to nuclear radiation. In order to present the information in a reasonable space, much detail has been omitted. In addition, there has been no attempt to develop a rigorous device theory. As a result, some simplifications have been introduced that must be accounted for when applying the results to specific problems or devices. A bibliography is included which constitutes a sound body of material for further study. Throughout these notes, references to texts are made wherever a more advanced treatment or more complete explanation would be helpful.

BACKGROUND

It is assumed that the reader is familiar with the concept of hole and electron conduction in solids and with the fact that the allowed energy states in a solid are grouped into bands as shown simply in one dimension in Figure 1.

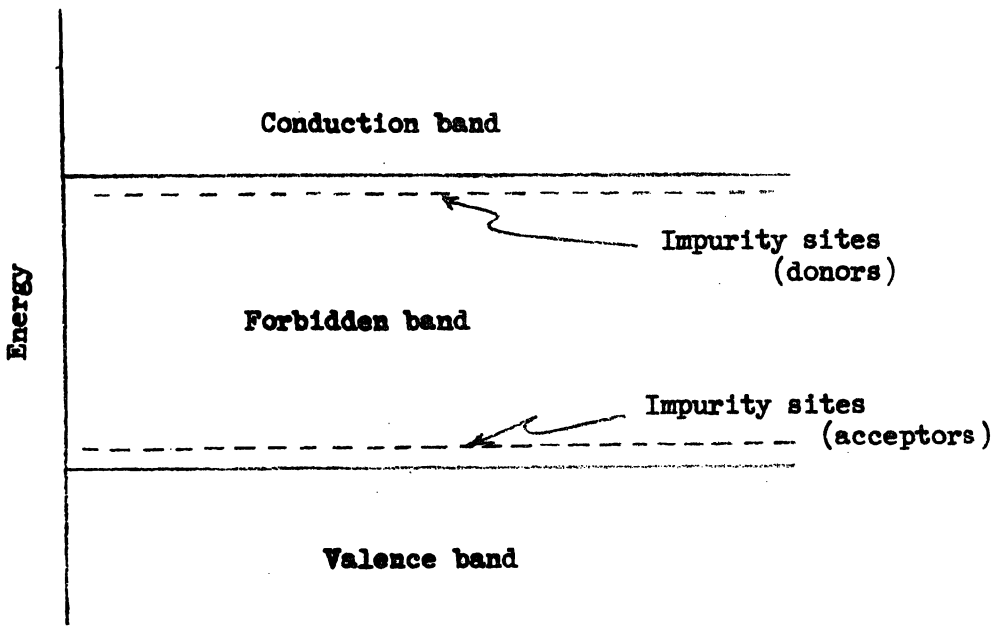

Figure 1

The essential features of the band theory that will be used later are:

a) The forbidden band in silicon is approximately 1.1 ev wide.

b) The population of electrons in the conduction band and of holes in the valence band is an exponentially decreasing function of distance from the band edge. exp (eV/kT)

c) The impurity sites are approximately 0.01 ev from the band edge and result from doping the semiconductor with such material as phosphorus, boron, antimony, etc.

d) Electrons may be excited into the conduction band from the donor sites or from the valence band provided enough energy is available to the individual electron to make the transition. Because of (c), almost all electrons on donor sites are thermally excited into the conduction band at room temperature. Because of (a) very few electrons are thermally excited from the valence band into the conduction band at room temperature.

e) When an electron leaves the valence band a hole is left behind.

f) Recombination of electrons in the conduction band with holes in the valence band occurs, usually with the help of some intermediate energy levels not shown in Figure 1.

g) At a fixed temperature there is an equilibrium concentration of electrons in the conduction band, and holes in the valence band resulting from the competing excitation and recombination processes.

Extensive treatments of the band theory of semiconductors and the applications to device design and use are given in References

CURRENT FLOW IN SEMICONDUCTORS

We now wish to consider a semiconductor under general conditions of current flow, i. e., into local sinks, (due to recombination processes), out of sources, (due to generation processes or across p-n junctions), and by diffusion and drift.

We first make use of the fact that there are a very large number of energy levels near the bottom of the conduction band and only a small number of electrons available to occupy them. Hence, all of these electrons are free to acquire energy and to contribute to the conduction.

Consider a sample of semiconduction in which there are n electrons per cm^3 and to which an electric field E is applied. The electrons will be accelerated by the field, collide with the lattice, alternately gaining and losing energy, but on the average they will drift against the field (holes will drift with the field) with an average velocity v_d that is proportional to E. That is

$$v_d = -\mu E \qquad (1)$$

The factor μ is called the mobility of the charge carrier and is measured in cm^2/volt second. Since the thermal velocity is very high compared with the drift velocity, there will be on the average many collisions of the carrier, hole or electron, with the lattice for each drift forward of one mean free path length. This means that the electron will have its forward component of velocity reduced to zero many times as a result of collisions. Consequently, the concept of an average drift velocity per unit field, i. e., a mobility, is a good one for small fields.

In a perfect lattice, i.e., one with no defects or impurities, and with its surfaces far removed, the average motion of charge carriers would be undisturbed by the uniformly periodic lattice potential so that the electron would move solely under the influence of the drift field. However, perfect lattices do not exist. At the higher temperatures, even for quite high levels of doping, the major contributor to the scattering of electrons is the thermal vibrations of the parent atoms. At lower temperatures, below 200°K for example, impurity effects begin to become dominant and at quite low temperatures where the lattice is essentially at rest, the imperfections due to the impurities and defects make the only effective contribution to the resistivity.

The electron charge density is

$$\rho = -ne \tag{2}$$

where (-e) is the electronic charge, and is exactly balanced locally everywhere by an equal positive charge density associated with the nucleii of the parent atoms. The current density per cm^2 in the material is therefore

$$J = \rho v_d = -\rho\mu E \tag{3}$$

Consequently

$$J = en\mu E = \sigma E \tag{4}$$

where σ is the conductivity. Thus

$$\sigma = ne\mu. \tag{5}$$

When an excess of majority carriers, that is, electrons in an n-type semiconductor, is injected into a semiconductor it will be redistributed very quickly over the surface as a result of the field corresponding to the mutual repulsion of the electrons. Only a small rearrangement of the electrons is necessary in order to achieve space charge neutrality inside. This process takes a time τ_r, termed the dielectric relaxation time, which is of the order of E/σ. For 1 ohm-cm silicon, commonly used in transistors, $\tau_r = 1.5 \times 10^{-12}$ sec. This means that local processes which are dependent only on the electromagnetic field for their completion take place in exceedingly short times compared with other processes and also with the normal time intervals involved in measurements. An injected pulse of majority carriers would disappear in only a small fraction of a cycle for any r-f signal so its presence would not be detected.

Let us compare this result for electrons with what happens when an excess concentration of holes is injected into n-type material. Two things will happen. First the electrons will redistribute themselves in a time τ_r (10^{-12} secs.) so as to maintain space charge neutrality in each small element of volume. Following this the holes will gradually spread out by diffusion and disappear by recombination. The time τ_p for the latter processes to occur will be much longer than τ_r, for the actual motion of holes across a large part of the semiconductor is involved. In a typical case, the concentration of electrons in silicon will be 10^{15} and that of holes will be 10^6. This means that only a very slight perturbation of the majority carrier system will take place. There will essentially be space charge neutrality with scarcely any change in the majority carrier distribution at all. As a result, the motion of the holes in the absence of an applied field will be by diffusion only.

We will now consider the case where there is a continuous flow of holes in an n-type semiconductor.

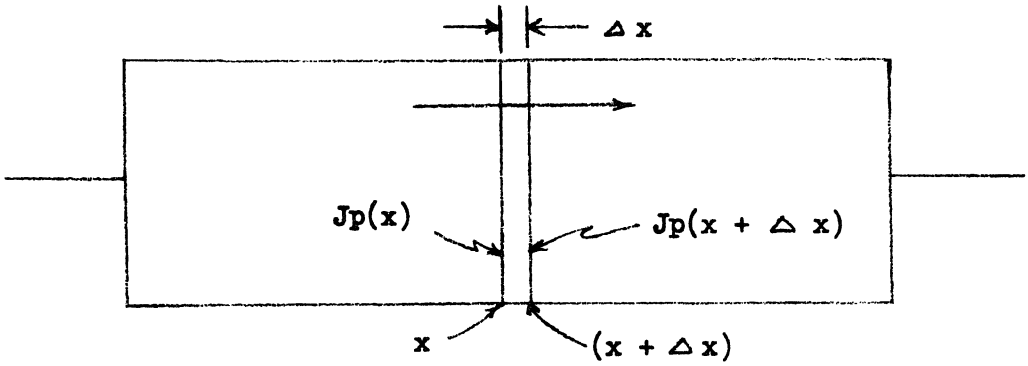

Figure 2

Suppose we have a cylinder of material of unit cross-section with ohmic contacts at the ends as shown in Figure 2. Suppose that holes are injected at the left contact and move toward the right. If $J_p(x)$ is the hole current density at a point x, then the current density at $(x + \Delta x)$ is

$$J_p\ (x + \Delta x) = J_p(x) + \frac{\partial J_p}{\partial x}\,\Delta x \qquad (6)$$

The rate of increase of holes due to current flow in a volume element of width Δx is therefore

$$-\frac{\partial J_p}{\partial x}\frac{\Delta x}{e}.$$

At the same time, the excess holes are recombining at a rate determined by the lifetime τ_p, and given by

$$\frac{(p - p_n)}{\tau_p} = \frac{\delta p}{\tau_p}$$

where $(p - p_n)$ is the excess hole concentration and p_n is the equilibrium hole concentration in n-type material.

We then have for the total rate of increase of the hole density

$$\frac{\partial p}{\partial t} = -\frac{(p - p_n)}{\tau_p} - \frac{1}{e}\frac{\partial J_p}{\partial x} + g_p \qquad (7)$$

where g_p is the rate of generation, if a generation process occurs.

The hole current J_p may occur for two reasons:

1) The application of an electric field E causes the holes to drift in the direction of the field and produce a current $J = \sigma E = +e\mu_p pE$.

2) The existence of a hole concentration gradient $\partial p/\partial x$ causes holes to move from regions of high concentration to regions of low concentration by diffusion. The rate of flow of holes is proportional to $\partial p/\partial x$ and may be written as $-D_p\,(\partial p/\partial x)$. The constant of proportionality D_p is called the diffusion constant for holes. The minus sign indicates that the net motion is from high to low concentration.

When both an electric field and a concentration gradient exist, we have for the hole current density

$$J_p = e\mu_p\, pE - eD_p\frac{\partial p}{\partial x} \qquad (8)$$

which may be substituted into (7) to give the rate of increase of hole density.

In the case where the field E is negligible we have then

$$\frac{\partial p}{\partial t} = -\frac{(p - p_n)}{\tau_p} + D_p \frac{\partial^2 p}{\partial x^2} + g_p \tag{9}$$

which is the continuity equation for holes in n-type material.

For many types of semiconductor devices equation (9), with appropriate boundary conditions, is sufficient to completely determine the current flow. In certain other devices where the field E is significant, equation (8) must be substituted in (7).

It is important to reemphasize here that we are dealing with minority carrier currents. J_p refers to the hole current density in n-type material, as in the base region of a pnp transistor.

In order to obtain a result which will be needed in our discussion of the junction diode we shall now solve the continuity equation for a particularly simple case.

With reference to Figure 3, assume that holes are introduced continuously from the left at $x = 0$ at such a rate that the hole concentration is p_o at $x = 0$ and that no generation occurs to the right of $x = 0$. Then, for $x > 0$, equation (9) is

$$\frac{\partial p}{\partial t} = -\left(\frac{p - p_n}{\tau_p}\right) + D_p \frac{\partial^2 p}{\partial x^2} \tag{10}$$

Since we have an equilibrium situation, $\frac{\partial p}{\partial t} = 0$. Therefore equation (10) becomes

$$\frac{\partial^2 P}{\partial x^2} = \frac{P}{D_p \tau_p} . \tag{11}$$

where $P = p - p_n$

This equation has the solution

$$P = C_1 e^{-\sqrt{\frac{x}{D_p \tau_p}}} + C_2 e^{+\sqrt{\frac{x}{D_p \tau_p}}}. \tag{12}$$

Since $P \to 0$ as $x \to \infty$, $C_2 = 0$

At $x = 0$, our point of origin, $p = p_o$, therefore $C_1 = p_o - p_n$. The solution of (11) is then

$$P = (p - p_n) = (p_o - p_n)\, e^{-\frac{x}{\sqrt{D_p \tau_p}}} \tag{13}$$

The term $L_p = \sqrt{D_p \tau_p}$ is called the diffusion length and is a measure of the distance holes will diffuse before recombining with an electron. In fact it is that distance in which an excess δp will have diminished to $\frac{1}{e}$ of its original value. See Figure 3.

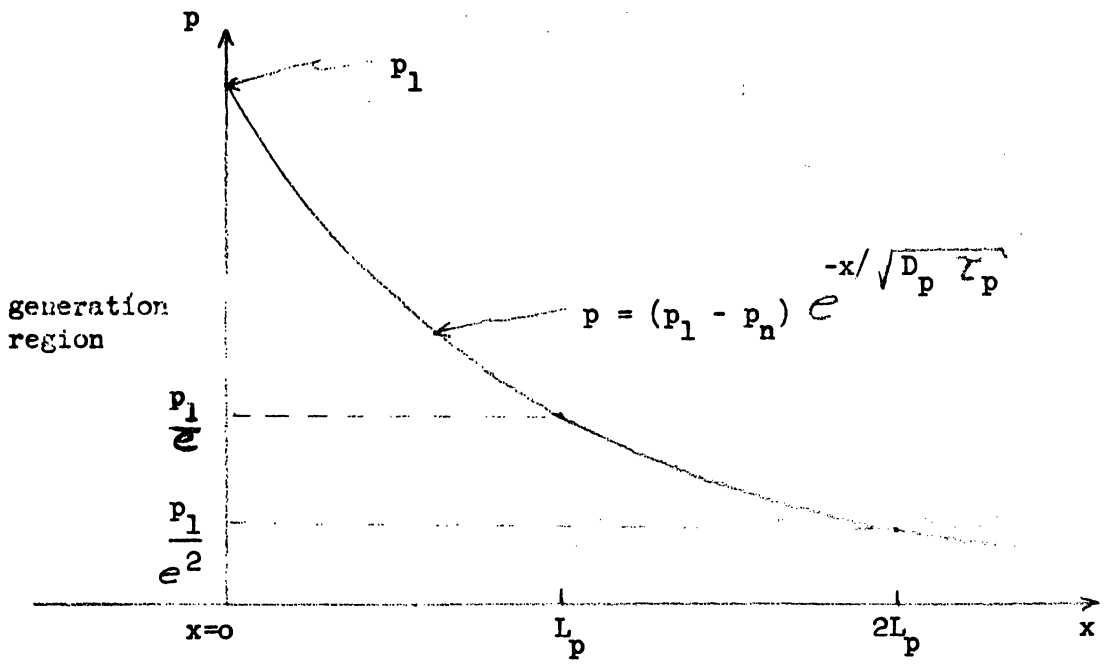

Figure 3

p-n JUNCTIONS

We are now in a position to discuss the formation of a junction between n and p type material and to derive the equations governing the current flow across a semiconductor junction.

Let us imagine that two pieces of silicon, one n type and one p type are brought together in intimate contact so that a regular lattice is formed throughout the material. (This is, of course, impossible. It serves, however, to illustrate clearly the idea of charge distribution at a junction.) Figure 4 illustrates typical hole and electron concentrations at the instant of contact.

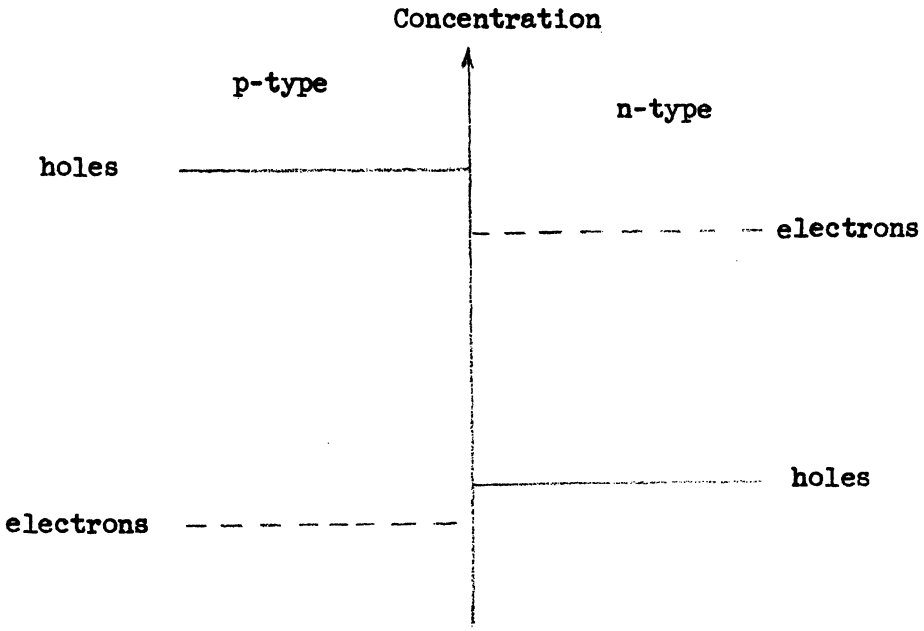

Figure 4

It is obvious that such a state of affairs cannot exist with the large differences in carrier concentrations across the junction unless there is a large force available to keep the charges separated. The holes and electrons, in the absence of such a force would simply mix by diffusion. For the condition drawn there is no such force. Consequently holes will diffuse from the p type material across the junction and electrons from the n type material will do the same. As they diffuse, a dipole layer will develop, composed of the fixed charges on the nuclei of the impurity atoms. Diffusion will continue until the electric field due to the dipole layer is just strong enough to prevent any more charge redistribution. The process is a local one and the charge redistribution will take place in a region of about 10^{-3} cms. The situation existing now can be represented as shown in Figure 5.

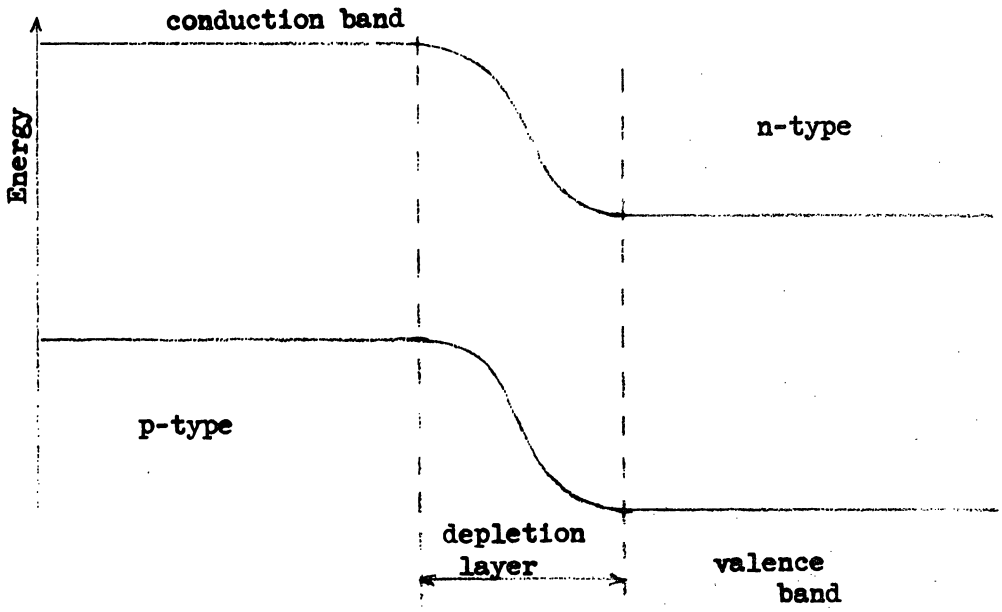

Figure 5

The central region from which the mobile charges have been removed is known as the depletion layer. This layer which stores charge on either side of it has the characteristics of a voltage dependent capacitor.

Since our imaginary junction is unbiased, there will be no net current flow. There will, however, be motion of individual holes and electrons across the junction. It is important to examine this charge motion so as to understand what happens when a bias is applied. In the n-region, a few electrons will gain enough (thermal) energy to permit them to pass across the potential barrier to the p-side, where they soon recombine with holes. At the same time, on the p-side, some hole-electron pairs are produced by thermal generation. If an electron so produced happens to diffuse to the junction, it is immediately accelerated across the junction by the field, where it becomes a majority carrier. In equilibrium these two currents are equal and so exactly compensate one another. The same situation exists for holes.

We are now in a position to bias the junction and demonstrate rectification action. For reverse bias the n region is made positive with respect to the p region so that the potential difference between the two regions is increased. (See Figure 6.) Now practically no holes or electrons can climb the potential hill and the recombination current density j_r drops to a very small value. Remember this is a small flow of current consisting of holes and electrons moving in opposite directions across the depletion region. The hole and electron generation current density j_g is not much affected by the reverse bias. Hence, the net current across the junction is essentially the generation current $-j_g$. When a forward bias V is applied (Figure 7), j_r increases according to the relation

$$j_r = j_g \, e^{eV/kT} \tag{14}$$

because of the exponential dependence of hole and electron population on the energy distance eV from the band edges. Note that for zero bias $j_r = j_g$, as required for equilibrium. The net current from the p region to the n region is given by the difference

$$j_r - j_g = j_g \, (e^{eV/kT} - 1). \tag{15}$$

This current is zero when V = 0, increases exponentially to large values for positive eV, and decreases when eV is negative toward a negative saturation value $-j_g$.

Let us now consider numerical values for some of the quantities discussed above. The mobility μ and the diffusion constant D are properties of the material. They are relatively slowly varying functions of temperature and impurity concentration in the ranges of interest. The lifetime τ of minority carriers is largely under the control of the device designer, for τ can be reduced by several orders of magnitude by the introduction of controlled amounts of gold into the silicon lattice. Because of the somewhat different nature of electron and hole motion, the values of μ, D and τ are different for holes and electrons under otherwise similar circumstances. Junction characteristics vary widely depending on the impurity concentration and the method of junction formation, so only typical values can be given.

The table below gives numerical values for the most commonly encountered conditions of temperature, impurity concentration and device design. Further details are given in the references.

Quantity	Symbol	Value	Units
Electron mobility	μn	1300	cm^2/volt-sec
Hole mobility	μp	500	cm^2/volt-sec
Diffusion constant (electrons)	D_n	40	cm^2/sec
Diffusion constant (holes)	D_p	12	cm^2/sec
Electron lifetime	τ_n	10^{-6} - 10^{-10}	sec
Hole lifetime	τ_p	10^{-6} - 10^{-10}	sec
Diffusion length (electrons)	L_n	6×10^{-3} - 6×10^{-5}	cm
Diffusion length (holes)	L_p	3×10^{-3} - 3×10^{-5}	cm
Junction potential (zero bias)	V_o	~ 0.7	volts
Junction width (zero bias)	W	$.25 \times 10^{-4}$	cm

CHARACTERISTICS OF p-n JUNCTIONS

In the last section we discussed the formation of a p-n junction and showed that a depletion layer exists in the neighbourhood of the junction. The hole and electron currents flowing across the junction were explained in terms of the carrier densities in the p and n regions and of other properties of the material, namely the diffusion length L, the diffusion constant D, and the lifetime τ. We showed how the current changes as the result of an applied D.C. potential, and thus explained the rectification properties of a p-n junction.

We will now extend the results by considering solutions of the differential equation which governs the potential distribution in the depletion layer. We will show how these solutions enable us to calculate the capacitance, width and electric field associated with the depletion layer. These calculations will be important for later discussion of radiation effects.

We will start with Poisson's equation which relates the potential $\psi(x)$ in a region to the charge density $\rho(x)$. We will discuss the case of a step junction, that is, one in which the acceptor density, N_a, of the p-region and the donor density, N_D, of the n-region are constant in the neighborhood of the junction. In many devices the impurity concentration is graded in the region of the junction. However, in that case the analysis is somewhat more complicated, so only the results will be given.

The space-charge distribution and corresponding potential distribution for a step junction are shown in Figure 8 below.

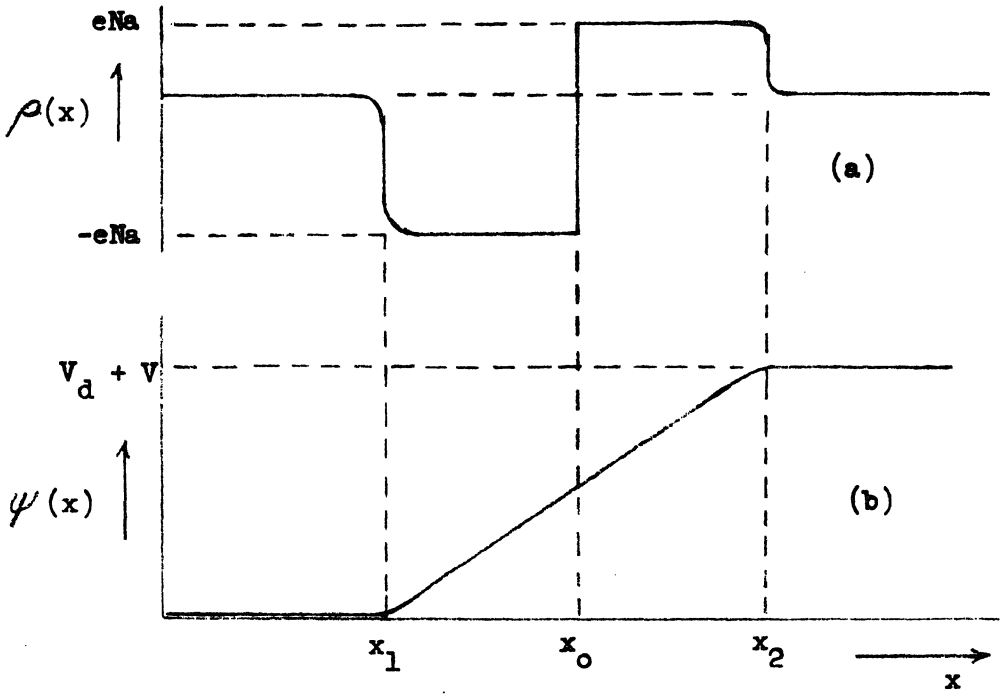

Figure 8

a) Space charge distribution in a p-n step junction.

b) Potential distribution in the same junction with an applied voltage V.

Poisson's equation for the potential ψ, is

$$\frac{d^2\psi}{dx^2} = -\frac{\rho(x)}{\varepsilon} \tag{16}$$

which must be solved subject to appropriate boundary conditions. With reference to Figure 8, we can state the following boundary conditions, assuming a voltage V is applied to the junction

$$\left.\begin{aligned} \psi(x) &= 0 \text{ at } x = x_1 \\ \psi(x) &= V_d + V \text{ at } x = x_2 \\ \frac{d\psi}{dx} &= 0 \text{ at } x = x_1 \text{ and } x = x_2. \end{aligned}\right\} \tag{17}$$

Here we have ignored any small voltage drops due to current flow in the body of the material.

The hole and electron densities in the area of the junction are given by

$$\left.\begin{aligned} p &= p_p\, e^{-e\psi/kT} \\ n &= n_n\, e^{-e(V_d+V-\psi)/kT} \end{aligned}\right\} \tag{18}$$

where p_p is the hole density in the region $x < x_1$ and n_n is the electron density for $x > x_2$.

The charge density $\rho(x) = -e(N_a - p + n)$ for $x < x_o$. However, n is very small for $x < x_o$, and p is also very small for $\psi > kT/e$ from (18), so it is a good approximation to put $\rho(x) = -eN_a$ for $x_1 < x < x_o$. Similarly we may put $\rho(x) = +eN_d$ for $x_o < x < x_2$. This is simply saying that the depletion layer has sharp boundaries and that the only charges in it are attached to the impurities in the lattice.

We can now solve Poisson's equation separately for the two regions $x_1 \leq x \leq x_o$ and $x_o \leq x \leq x_2$. If the solutions for these two regions are ψ_1 and ψ_2, we must have

$$\psi_1(x) = \psi_2(x), \quad \frac{d\psi_1}{dx} = \frac{d\psi_2}{dx} \text{ at } x = x_o \tag{19}$$

since both the potential ψ and the field $-d\psi/dx$ are continuous. For region 1 we may write (16) as

$$\frac{d}{dx}\frac{d\psi_1}{dx} = \frac{eN_a}{\varepsilon}. \tag{20}$$

Integrating with respect to x we have

$$\frac{d\psi_1}{dx} = \frac{eN_a}{\varepsilon}\, x + C_1 \tag{21}$$

Since, according to (17), $d\psi_1/dx = 0$ at $x = x_1$, we can determine that $C_1 = -(eN_a/\varepsilon)\, x_1$.

Therefore (21) becomes

$$\frac{d\psi_1}{dx} = \frac{eN_a}{\varepsilon} (x - x_1) \tag{22}$$

Integrating once more with respect to x_1 we have

$$\psi_1 = \frac{eN_a}{2\varepsilon} (x - x_1)^2 + C_2. \tag{23}$$

Since $\psi_1 = 0$ at $x = x_1$, from (17), we must have $C_2 = 0$.

Thus, the solution for $x_1 \leq x \leq x_o$ is

$$\left.\begin{aligned} \frac{d\psi_1}{dx} &= \frac{eN_a}{\varepsilon} (x - x_1) \\ \psi_1 &= \frac{eN_a}{2\varepsilon} (x - x_1)^2 \end{aligned}\right\} \tag{24}$$

Similarly, the solution for $x_o \leq x \leq x_2$ can be found to be

$$\left.\begin{aligned} \frac{d\psi_2}{dx} &= \frac{eN_d}{\varepsilon} (x_2 - x) \\ \psi_2 &= (V_d - V) - \frac{eN_d}{2\varepsilon} (x_2 - x)^2 \end{aligned}\right\} \tag{25}$$

Applying (19) we have

$$N_a (x_o - x_1) = N_d (x_2 - x_o) \tag{26}$$

and

$$\frac{eN_a}{2\varepsilon} (x_o - x_1)^2 = (V_d - V) - \frac{eN_d}{2\varepsilon} (x_2 - x_o)^2 \tag{27}$$

We may solve (26) and (27) simultaneously to determine $(x_o - x_1)$ and $(x_2 - x_o)$ and thus compute the width w of the transition region. We will omit the elementary algebra and write the result as

$$w = (x_2 - x_1) = \left[\frac{2\epsilon\ (V_d - V)\ (N_a + N_d)}{eN_aN_d}\right]^{1/2} \tag{28}$$

We have thus obtained the very important relation between the applied voltage V and the width w of the depletion layer. For $|V| >> V_d$, w = const. x $V^{1/2}$. At low voltages the dependence is less strong. Remember that for both germanium and silicon, V_d is less than one volt.

The transition region contains a positive charge + Q per unit area on the n-side, and a negative charge - Q per unit area on the p-side. From (26) and (27) this charge is

$$Q = eN_d(x_2 - x_o) = \left[\frac{2e\epsilon}{4}\ (V_d - V)\ \frac{N_aN_d}{N_a + N_d}\right]^{1/2} \tag{29}$$

We may now calculate the capacitance of the transition region per unit area,

$$C_T = \frac{dQ}{dV} = \left[\frac{e\ \epsilon}{2(V_d - V)}\ \frac{N_aN_d}{N_a + N_d}\right]^{1/2} = \frac{\epsilon}{W} \tag{30}$$

Note that the capacitance is the same as that of a parallel planar capacitor with a plate separation w.

We may also calculate the field strength - /dx. It attains a maximum value at $x = x_o$, as might be expected, at which point it is

$$\epsilon = \epsilon_{max} = -\left(\frac{d\psi}{dx}\right)_{x\ =\ x_o} = -\frac{eN_a}{\epsilon}\ (x_o - x_1) \tag{31}$$

$$= -\frac{2(V_d - V)}{w}$$

These formulas, (28), (30) and (31) hold for a step junction, such as occurs where the junction is made by the alloy technique. In most junctions, instead of a sudden step from N_a to N_d, we usually have a

more gradual transition. An analysis similar to the above, but somewhat more complicated gives the following results for the case of a uniformly graded junction.

$$w = \left[\frac{12\epsilon\ (V_d - V)}{ea}\right]^{1/3} \tag{32}$$

$$C_T = \left[\frac{ea\epsilon^2}{12\ (V_d + V)}\right]^{1/3} = \frac{\epsilon}{w} \tag{33}$$

Here 'a' is a measure of the grading of the junction; that is $N_d = N_d(0) + a_1(x - x_o)$, $N_a = N_a(0) - a_2(x - x_o)$ where $N_d(0)$ and $N_a(0)$ are the donor and acceptor concentrations at $x = x_o$, and $a = a_1 + a_2$ = slope of the impurity concentration.

There is thus a significant difference in the two types of junctions. In the step junction w and C_T vary as $V^{1/2}$, whereas in a uniformly graded junction they vary as $V^{1/3}$. If the change in impurity density is very slow ('a' small), the transition region will be much wider than for a step junction, and the capacitance and maximum field strength will be correspondingly smaller.

Most modern devices employ the technique of diffusion to introduce impurities into the lattice. Junctions formed by this means often have a transition region with properties midway between those of step and graded junctions. Thus in a diffused silicon transistor, the capacitance of the collector junction is of the form

$$C_T = \frac{\text{const}}{(V + V_d)^k} \quad , \tag{34}$$

where k is about 0.4.

When making calculations based on capacitance measurements, it is important to know the value of the diffusion potential V_d. It was indicated earlier that for silicon $V_d \approx 0.7$ volts. Having chosen a value for V_d, one may plot C_T vs $(V_d + V)$. If log-log paper is used, the resulting straight-line graph has a slope equal to the exponent in equation (34).

Current Flow in p-n-p Transistors

Now let us turn to the p-n-p transistor under normal bias. See Figure 9.

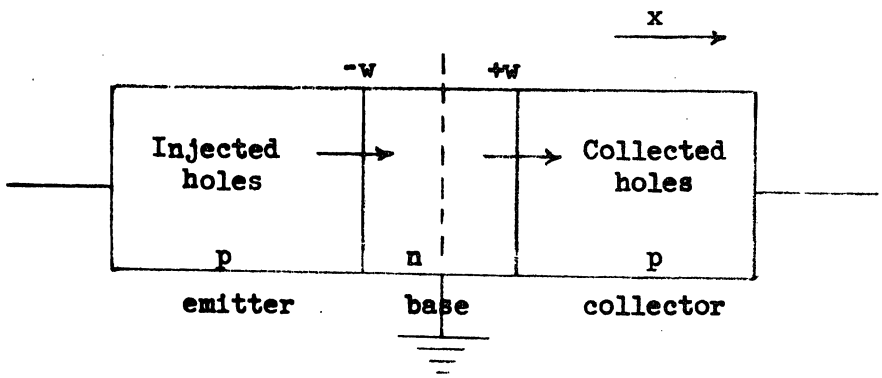

Figure 9

For normal transistor operation the emitter junction is forward biased and the collector junction is reverse biased. Holes are injected into the base by the emitter, diffuse across the base into the reverse biased collector junction and are then swept into the collector region where they become majority carriers. The base region is narrower than the diffusion length L_p so that very nearly all of the holes which get into the base also get to the collector. The holes which leave the emitter are balanced in the external circuit at the emitter contact by electrons leaving the transistor. Likewise, holes arriving at the collector are balanced by electrons entering the transistor at the collector contact. The electrons in the base which are lost by injection (diffusion) into the emitter and collector, and by recombination with holes are supplied through the base lead.

The transfer of holes from emitter to collector constitutes transistor action. Since the emitter junction is forward biased and hence has a very low resistance (R = 26/current in milliamperes), and the collector is reverse biased with a very high impedance, the passage of the same quantity of holes from emitter to collector produces a considerable power gain. Typical values are from one to several hundred.

Now let us examine the transistor under an applied d.c. potential. We will solve the continuity equation for holes in the n region (the base).

The continuity equation has the equilibrium form

$$\frac{\partial^2 (p - p_n)}{\partial x^2} - \frac{p - p_n}{L_p^2} = 0 \qquad (35)$$

The origin of the coordinate system will be chosen at the center of the base. The width of the base region is 2W with the emitter and collector junctions at -W and +W, respectively. The necessary boundary conditions are the hole concentrations at x = ±W. They are related to the equilibrium hole concentration pn in the n region by

$$\left.\begin{aligned} p_{eo} = p(-W) &= p_n\, e^{eV_e/KT} \qquad (p_e \text{ for emitter}) \\ \text{and} \quad p_{co} = p(+W) &= p_n\, e^{eV_c/KT} \qquad (p_c \text{ for collector}) \end{aligned}\right\} \tag{36}$$

It turns out to be simpler not to use the earlier exponential solution of our second order equation but rather to use a hyperbolic form (Recall $e^x = \cosh x + \sinh x$)

$$p - p_n = A \sinh\left(\frac{W - x}{L_p}\right) + B \sinh\left(\frac{W - x}{L_p}\right) \tag{37}$$

Substitution of the two boundary conditions into equation (37) leads to the complete solution for the hole density in the base

$$p_o - p_n = \frac{(p_{eo} - p_n) \sinh[(W - x)/L_p] + (p_{co} - p_n) \sinh[(W + x)/L_p]}{\sinh (2W/L_p)} \tag{38}$$

Again making use of the earlier techniques, we find the d.c. hole current density in the base to be

$$J_{po} = \frac{eD_p}{L_p} \frac{(p_{eo} - p_n) \cosh[(W - x)/L_p] - (p_{co} - p_n) \cosh[(W + x)/L_p]}{\sinh (2W/L_p)} \tag{39}$$

The emitter and collector hole current densities are obtained by evaluating J_{po} at the junctions, i.e., at x = -W and = +W.

Thus

$$J_{peo} = (eD_p/L_p)[(p_{eo} - p_n) \coth(2W/L_p) - (p_{co} - p_n) \operatorname{csch}(2W/L_p)] \tag{40}$$

$$J_{pco} = (eD_p/L_p)[(p_{eo} - p_n) \operatorname{csch}(2W/L_p) - (p_{co} - p_n) \coth(2W/L_p)] \tag{41}$$

Now let us plot the hole densities and currents in the transistor under various conditions to see what the above equations mean, since at first glance they don't appear to be very intelligible

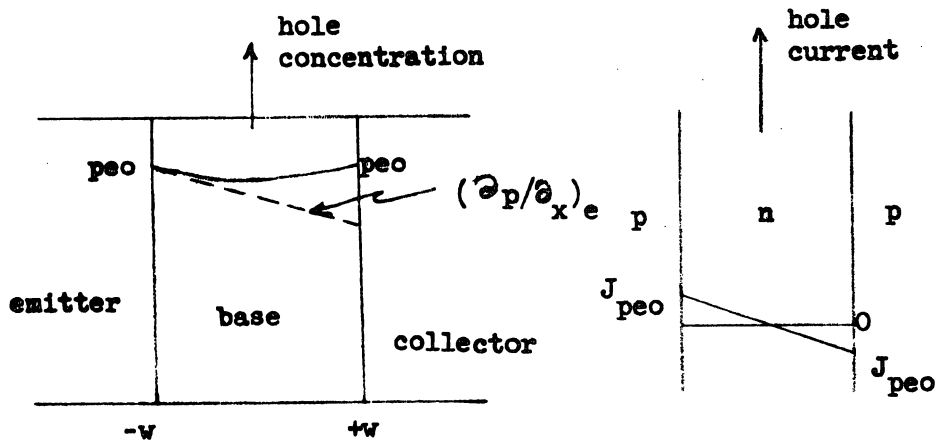

Figure 10

Case 1. Emitter and collector both forward biased, $v_e = v_c$ (biases given with respect to the base). See Figure 10.

In this case $p_{eo} = p_{co}$ with both junctions injecting into the n region. Note the very slight dip in the center due to recombination.

The current is given by

$$J_p = \frac{eD_p}{L_p} \frac{\partial p}{\partial x} \tag{42}$$

so that it is determined at the junctions by the initial slope $(\partial p/\partial x)_{x=\pm W}$ there. The current for this bilaterally operating device is quite low when W is small. It does, however, increase with W. At the center of the base the hole current is zero.

If the collector is moved off to infinity, then the charge concentration at both junctions in the base falls off more rapidly ($\partial p/\partial x$ is greater) and the junctions are independent of one another. In this case there is no feedback from the collector to the emitter. Since $\partial p/\partial x$ is larger, the current is also larger.

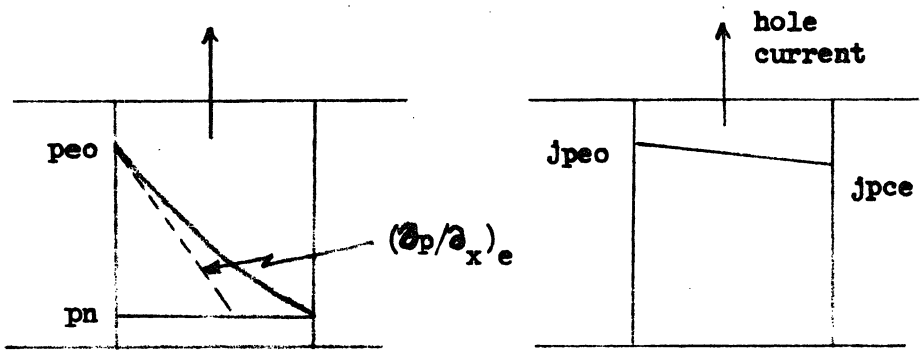

Figure 11

Case 2. Emitter forward biased, collector zero biased. See Figure 11.

p_{eo} will remain the same as in the earlier case but $p_{co} = p_n$ since $p_{co} = p_n\, e^{eV_c/KT}$. The emitter hole current will be increased appreciably, however, over that corresponding to any base width of the forward biased collector case. The increase may be by as much as a factor of 20.

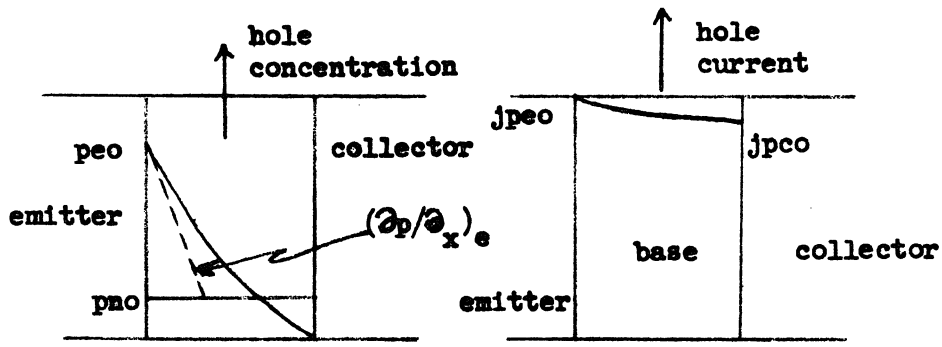

Figure 12

Case 3. Emitter forward biased, collector reverse biased. This situation corresponds to normal operation. See Figure 12.

In this case the hole concentration at the collector drops below p_n because of the reverse bias. This means that $(\partial p/\partial x)$ is increased over any of the other cases; hence, the hole current is the highest. When this is coupled with the increased drop at the collector, the highest power gain is obtained; consequently, we have the normal operating condition for the transistor.

As is shown in all three sets of figures, the current across the base is only slightly diminished from emitter to collector. The excess goes out the base.

Although the only current linking the collector to the emitter is the base minority carrier current, in the case of the p-n-p hole current, there are small majority carrier currents in the base. These currents are between base and emitter and between the base and collector. They do not contribute to the transistor action and do, in fact, detract from the device efficiency.

Frequency Response of Transistors

We will consider briefly the factors that determine the frequency response of a transistor. This may be done in a rigorous way by solving the continuity equation in the base region subject to appropriate boundary conditions at the junctions. However, this must be an a.c. solution; that is, the hole concentrations are of the form $p_o \exp(j\ wt)$. The complete solution is complicated even in the simplest case, and is contained in several of the references so will not be given here. The result is an approximation to the well-known changes in amplitude and phase with frequency. Another result is the important fact that the frequency cut-off of a transistor is reciprocal to the square of the base width.

It is possible to understand the reason for the dependence of cut-off frequency on base width by recalling that signal transfer from emitter to collector is through the mechanism of diffusion. Since any signal propagates through the base as a succession of changes in hole density, there is a natural tendency for the signal to lose strength, because the diffusion process is inherently one of average motion from regions of high concentration to low. Evidently the farther the signal has to travel across the base, the greater will be the loss due to smoothing of variations in hole concentration. A mathematical treatment gives the result quoted above.

At very high frequencies, transistor performance is determined in part by the capacitance of the emitter and collector junctions. These capacitances are area dependent. Consequently, for high-frequency transistors there is a reciprocal relation between frequency response and the dimensions in the plane of the junctions.

RADIATION EFFECTS IN SEMICONDUCTORS

James H. Crawford, Jr.

RADIATION EFFECTS IN SEMICONDUCTORS

James H. Crawford, Jr.
Physics Department, University of North Carolina
Chapel Hill, North Carolina

Introduction

Nearly all of the properties that make semiconductors interesting to study and valuable for applications in solid-state electronics are strongly dependent upon the presence of imperfections in the crystalline structure. Therefore, they are excellent materials in which to investigate damage to the crystal lattice produced by high-energy radiation. This modulation of electronic behavior, which we call "Radiation Effects," is a clue to the type of damage introduced and, if we are clever enough to connect specific defect structures with the various qualitative and quantitative changes in properties, we should be able to construct a complete picture of the lattice damage introduced by various types of energetic radiation. Studies of radiation effects in semiconductors have an additional advantage: From them we learn much about radiation sensitivity of properties vital to the operation of semiconductor devices, as well as various factors which affect this sensitivity. Now many potential applications of semiconductor devices may involve radiation environment, space vehicle communication gear, for example. Therefore, knowledge pertaining to radiation sensitivity will be invaluable in developing devices with longer service lives in outer space or when used near a nuclear power source.

As a field of study, radiation effects in semiconductors is not new. The first work in this field was done on germanium and silicon nearly 20 years ago at Purdue University and Oak Ridge National Laboratory, and the late Karl Lark-Horovitz[1] was an outstanding leader in these investigations. But although the field is not new, its present complexion is vastly different from what it was six or seven years ago. Before that time the main emphasis was colored by what turned out to be a vain attempt to test quantitatively in terms of defect yield the simple theory of radiation damage, and by a valiant but equally vain attempt to account for the multitude of defect energy levels in terms of simple interstitials and vacancies. Beginning in 1959, several developments occurred[2] which revealed without doubt that in the room-temperature range both the yield and nature of radiation defects in silicon and germanium are strongly influenced by the type and amount of impurity present. Since this discovery much effort has been devoted to the determination of the complex structures of defects, involving both impurities and simple vacancies, which are responsible for changes in electronic behavior. These studies have employed properties such as optical absorption of polarized light and electron spin resonance to reveal the symmetry and composition of the photon and microwave absorption centers. In addition, annealing studies have given some insight into the defect-complex structure through the kinetics of the various relaxation processes, leading to both their formation and decomposition.

In this brief summary, I would like to discuss the types of defects that result from irradiation with various types of energetic particles and photons; to indicate briefly the way in which imperfections

influence semiconducting behavior; to present evidence for the various defect-impurity interaction products that are produced as a result of the migration of simple defects; and, finally, to mention recent interesting developments in the area of compound semiconductors.

The Nature of Radiation Defects

In elemental systems such as germanium and silicon, which will be our primary concern, defects are not created in the perfect lattice by ionization through radiochemical processes as they are in the alkali halides. Instead, elastic collisions between the incoming particles and lattice atom are required. Moreover, the recoil energy imparted to the lattice atom must be greater than some minimum value E_d, called the displacement energy, which is required to create a stable interstitial-vacancy pair. In the early, naive damage theory,[3] the displacement probability was assumed to be a step function: 0 if $T < E_d$, and unity or greater if $T > E_d$. Using this simple concept E_d is usually measured by exposing a crystal to a prescribed dose of Van de Graaff electrons and increasing the energy until a change in a radiation sensitive property is first detected. E_d is related to this threshold electron energy by the relativistic expression for the maximum energy imparted in an elastic collision, namely,

$$E_d = 2(E + 2\ mc^2)\ E/Mc^2 \qquad (1)$$

where E and m are the energy and rest mass of the electron, and M is the mass of the target atom.

The naive theory does not account for the ordered arrangement of atoms. Obviously, if the lattice structure is considered, the ease of displacement will depend upon the direction of the impulse: In open directions E_d will be much smaller than in the direction of a neighboring ion. Also, in determining E_d care must be taken that the defects created are stable enough for experimental detection. Such a complication is encountered in germanium. Low-temperature electron bombardment experiments (1 to 4.5 MeV electrons at 4°K) of MacKay and Klontz[4] have shown that conduction electrons are required to stabilize close interstitial-vacancy pairs. These defects, which act as acceptors and hence remove conduction electrons, are therefore produced in higher yield the higher the concentration of conduction electrons. In fact, in p-type specimens where the current is carried by positive holes instead of electrons the yield is almost below detection. From an experimental point of view then, the electronic state of the semiconductor (whether an electron or hole conductor) would appear to have a strong influence upon the apparent value of E_d for low-temperature (<10°K) irradiations with electrons since even at liquid helium temperature these close-pair defects are unstable in the absence of conduction electrons.

Another complication which may also be encountered in other solids as well but for which there is direct evidence in silicon is the creation of divacancies by electron bombardment. This occurs when the impulse is along the appropriate crystallographic direction and the recoil energy high enough. Using electron spin resonance techniques, Corbett and Watkins[5] have found that divacancies are formed in silicon

during bombardment with 0.7 to 1.5 MeV electrons at 20°K, and that the yield is highest for the bombarding beam parallel to the Si-Si bond direction. These results indicate that the divacancy is formed by a single collision event and that divacancies are a primary radiation defect.

As the energy of the primary recoil increases to many times E_d, the recoil acts as a bombarding particle and secondary, and even tertiary, displacements are created as it collides with other lattice atoms. This results in what is called a displacement cascade in which the defects are closely spaced and have a high local concentration. Damage produced by fast neutron bombardment in a nuclear reactor consists predominantly of regions of high defect density (disordered regions) of this type. Typically, these regions are roughly spherical with a diameter of ~100 Å and these have been resolved in germanium by electron micrography.[6] These disordered regions have a rather unusual effect on the electrical behavior of n-type germanium. Since the dominant effect of radiation defects in germanium is acceptor action, the disordered regions are p-type islands in an n-type matrix and as such they must be isolated from the matrix by a potential barrier and an electrical double layer,[7] such as shown in Fig. 1. The radial extent of the space-charge zone in the junction surrounding the disordered region is roughly given by the Debye-Hückel length.

$$L_{DH} = \left(\frac{kT\epsilon}{q^2 N_D} \right)^{1/2} \qquad (2)$$

where q is the electronic charge, ϵ is the dielectric constant, and N_D is the donor density. For reasonable purity n-type germanium (donor concentration of 10^{14} to 10^{15}), this distance is between one and two orders of magnitude larger than the radius of the disordered region itself. The potential gradient extending over this region denudes it of mobile charge so that the entire space-charge zone acts as an insulator blocking current flow. The situation is shown schematically in Fig. 2. Because of this double-layer, disordered regions markedly reduce the conductivity and for non-overlapping space-charge zones[8] the conductivity is approximately

$$\sigma \simeq \sigma_o \, (1 - f)/(1 + \tfrac{1}{2}f) \tag{3}$$

where σ_o is the true bulk conductivity and f is the fraction of the volume occupied by non-overlapping insulating zones, which is given approximately by

$$f = \overline{V}_{sc} \, N^o \, \sigma_s \, \phi_d t, \tag{4}$$

where $\overline{V}_{sc}$ is the average volume of the region affected by space-charge zones, N^o is the density of lattice sites, σ_s is the scattering cross section for high-energy electrons, and $\phi_d t$ is the integrated flux of neutrons with energies (>0.7 MeV) sufficient to create a disordered region large enough to support a space-charge zone. Solution of Poisson's equation for the spherical case yields

$$V_{sc} = \psi_p \, \epsilon \, r_1/q \, N_2 \tag{5}$$

where ψ_p is the difference in electrochemical potential between the disordered region and the unperturbed matrix, r_1 is the radius of the disordered region, and N_2 is the net donor concentration in the matrix. This model of disordered regions and associated space-charge zones has been verified for neutron-bombarded n-type germanium by several investigators in terms of electrical properties alone[7,9,10] and the disordered regions are found to have a radius of 50 to 100 Å. The electrical results have been confirmed by means of thermal conductivity measurements recently made by Van Dong.[11] He found the mean disordered region radius to be 70Å. More recently, Bertolotti and coworkers[12] have identified both the disordered region and the space-charge on electron micrographs of replicas of etched surfaces of germanium after bombardment with 14 MeV neutrons. Figure 3a shows a micrograph on which the space-charge zone (1000 to 1500 Å radius) is clearly visible. Figure 3b shows an enlargement of one of the etch figures, and at the center is detectable a crater of radius 150 to 200 Å which is presumably the disordered region. Interestingly enough, presumably because of its smaller atomic mass and different defect energy level structure, neutron-irradiated silicon shows no definite evidence of disordered regions.[13]

Not all the energy of primary recoils is consumed in the displacement cascade. It was mentioned earlier that ionization is not effective in creating lattice defects in elemental solids. In fact, energy lost through "inelastic" ionization and excitation processes is not available for the displacement of lattice atoms.[3] The higher the velocity and the larger the charge of the primary recoil, the greater the amount of energy lost in these inelastic processes. Another mechanism of fruitless

dissipation of recoil energy is through "focusing" or focused collisions[14] down a close-packed row in a crystal. The succession of energy transfers in a focused chain interaction in effect drains energy away from the region of primary impact or the cascade region. An additional mode of energy loss for energetic recoils or incident ions is called "channeling".[15] This occurs when the high energy particles find themselves in an open channel or crystallographic direction. Small energy losses occur through ionization or very small angle collisions with the rows of atoms defining the channel. The most open direction and hence the most probable channel in the diamond structure is along any of the <110> directions. This is clearly shown in Fig. 4. In contrast, views along the [100] direction in Fig. 5, and the [111] direction in Fig. 6 show very little open space. That this is indeed the channel direction for the diamond lattice is shown by the dependence of the range of 40 keV xenon ions in silicon in Fig. 7. These measurements by Davies and coworkers[16] show quite dramatically that ions penetrate much more deeply along this direction than any other low index direction. Also shown for comparison is the range in single-crystal aluminum which has a face-centered cubic structure with a [110] channel direction.

Another very effective demonstration of channeling is afforded by the response of silicon p-n junction fission detectors. One problem that arises in using junction detectors in fission-fragment spectroscopy is the failure of the pulse-height absorbed energy calibration for high energy massive particles, which is designated by the term pulse-height defect. The smaller than expected pulse of current indicates that some other process besides ionization is available for dissipating a portion of the

energy. Recently, Moak and coworkers[17] have investigated the influence of crystal orientation upon pulse-height response of a detector to ^{127}I ions with energies in the range of 10 to 100 MeV. When the detector was aligned such that the incident beam was parallel to a <111> direction, the pulse-height defect for the channel ions virtually disappeared. Therefore, one is lead to the conclusion that the pulse-height defect is caused by energy losses in elastic collisions which displace atoms. When the ions are channeled the probability of displacement collisions is much reduced and nearly all of the particle energy appears as ionization current in the p-n junction.

Influence of Defects on Semiconducting Behavior

Defects, like impurity atoms, are capable of introducing local energy states into the band structure of semiconductors. Depending upon their nature and the electronic characteristics of the host lattice, defect centers may act as (a) donors, yielding electrons on thermal excitation in n-type material or capturing holes in p-type; (b) acceptors, in which capacity they may thermally ionize to produce holes in p-type conductors and capture electrons in n-type; or (c) as amphoteric centers capable of capturing electrons in n-type and holes in p-type. Moreover, it is common for radiation defects to possess two or more energy levels. In consequence, introduction of defects by irradiation can produce profound and often complicated changes in the electronic behavior. Not only is the carrier concentration altered even to the extent of inducing conversion from n- to p-type (or conversely), but carrier scattering is affected by the introduction of charged centers and the influence upon

non-equilibrium minority-carrier processes such as trapping and recombination by the deep level defects which act both as efficient recombination centers and traps is very large. In short, all semiconducting properties are influenced in some degree by exposure to energetic particles or photons capable of displacing lattice atoms.

In studies of radiation effects[18] use is made of the influence of defects on properties to gain quantitative information about the position and relative numbers of energy levels produced by a given exposure to various types and energies of incident particles. The most common investigation involves the temperature dependence of the carrier concentration and the mobility which are obtained from measurements of Hall coefficient and mobility. This approach yields the position of the thermally accessible energy levels and information on their charge state. Other electronic properties that have been useful in locating energy levels of radiation defects not readily detected by the above approach include excess carrier lifetime, trapping of minority carriers, and the spectral dependence of photoconductivity. Both electron spin resonance and optical absorption have been very valuable tools in gaining detailed information about defect structure.

Additional information on defect stability and the tendency for various defects to interact with other imperfections (point defects, impurities, and dislocations) is obtained from the thermal annealing of radiation defects. By employing a radiation sensitive property as an index of the defect content, the kinetics governing the restoration of initial conditions through some annealing cycle (isochronal or isothermal) may be examined to yield values of defect motion energies or the binding energies for defects in certain complexes.[18]

The Structure of Radiation Defects

As we have already indicated above, defects remaining in germanium or silicon irradiated with electrons in the 0.5 to 5 MeV range, or even more massive particles such as protons or neutrons in the room-temperature range, are not simple interstitials and vacancies but rather are invariably complexes formed by the interaction of simple point defects with other imperfections, notably impurity atoms and vacancy pairs as well as more complex clusters of defects.

The first clue to this state of affairs came in 1959 when Bemski[19] and Watkins and coworkers[20] observed that irradiation of oxygen containing n-type silicon gave rise to an imperfection with both a spin-resonance spectrum and an ionization energy that are quite different from that observed in specimens containing little oxygen. It was concluded and subsequently confirmed by optical absorption of polarized light[21] that the defect in the oxygen-containing material is a silicon vacancy associated with an interstitial oxygen atom. The model for this defect is shown in Fig. 8, and it is distinguished by the fact that it acts as an acceptor center with an energy level located 0.17 eV below the conduction band. Conclusive identification[21] of this center with an oxygen-vacancy complex was accomplished via an optical absorption band at 12μ, which is produced by electron irradiation under the same conditions that the defect resonance is produced. This band is made birefringent by uniaxial pressure in the same way that certain equivalent orientations of the paramagnetic center become more heavily populated by the application of pressure and, significantly, the thermal annealing of both the birefringence and the imbalance in the spin system follows the same path. The

final point of evidence that the center responsible for the 12μ band contains oxygen is the observation that specimens doped with oxygen enriched in ^{18}O exhibit second band shifted to lower frequencies by the amount expected for the increase in isotopic mass to influence an antisymmetric stretching vibration.

Since this early discovery, a number of defect complexes have been identified in both n- and p-type silicon after irradiation with electrons. Figure 9 shows the model[22] of the vacancy-phosphorous complex which in n-type silicon is responsible for at least one acceptor level located 0.43 eV below the conduction band. This center can be identified by ESR alone since the hyperfine interaction of the unbalanced spin with the movement of the phosphorous demonstrates conclusively that phosphorous impurity is a part of the defect structure.

In Fig. 10 we see the model of the divacancy,[5] the production of which as a primary defect by electron bombardment along a <111> direction we have already discussed. This rather complex-looking center is responsible for three energy levels: An acceptor state ~0.4 eV below the conduction band; an acceptor state quite near the center of the forbidden energy gap (~0.5 eV above the valence band); and a donor level quite near the top of the valence band.

More recent studies[23] on p-type silicon have revealed the existence of a vacancy-acceptor complex (specifically a vacancy attached to an aluminum atom), interstitial acceptor impurity (both gallium and aluminum), and complexes one component of which is an interstitial acceptor atom. An example of the latter is a Ga_2^+ molecular complex, with one of the gallium atoms in a substitutional site and the other occupying an interstitial

position. The energy levels that have been attributed to these defects are summarized in Fig. 11.

We must now ask by what mechanism are these complexes formed? The divacancies[5] have already been discussed and it was shown that they are primary defects formed directly by a single collision. However, the same cannot be said for the impurity-containing complexes because the impurity concentration is so small ($<10^{-4}$ mole fraction) that the probability that these can be created directly by the irradiation for the exposures employed is vanishingly small. Therefore, it must be concluded that these are formed by the interaction of mobile simple defects (interstitials and vacancies) with these imperfections. A study of the ESR spectra of silicon irradiated at low temperature shows that this is indeed the case. Watkins[23,24] has observed the ESR spectrum for the isolated vacancy in p-type silicon after electron bombardment at both 4° and 20°K. However, the vacancy resonance disappears as the crystal is warmed to the vicinity of 170°K, presumably because the vacancy migrates to and forms complexes with other imperfections or annihilates at vacancy sinks. Pulse annealing studies reveal that the activation energy for motion is 0.33 ± 0.03 eV. In n-type silicon the vacancy is not detectable by an ESR signal presumably because it contains only paired electrons when the Fermi level is in the upper half of the forbidden energy gap. However, the motion and trapping of vacancies can be detected through the formation of phosphorous-vacancy pairs which are formed during annealing of n-type silicon after low-temperature irradiation. It is noteworthy that the vacancies move with a much smaller activation energy in n-type material, confirming the hypothesis put forth many years ago[25] that the charge state

of defects should influence their ease of motion. From consideration of the energy level structure of the vacancy, it is concluded that the neutral vacancy is the form that moves in p-type Si with the 0.33 eV motion energy while both the V^- and V^{--} forms expected to exist in n-type Si (Fig. 9) have appreciably smaller activation energies of migration.[23]

All attempts at detecting isolated interstitials by ESR methods have failed. Although one might conclude from this that they may always be present in a nonmagnetic form and therefore escape detection, careful experiments with p-type silicon irradiated at 4°K indicate quite another cause for their absence. Watkins[23] has identified a resonance associated with interstitial aluminum ions (Al^{++}) and measurements of the relative intensities of microwave absorption show that their concentration is virtually the same as the isolated vacancy concentration. These interstitial impurities are tightly lodged in the lattice and begin to move only upon heating to the vicinity of 200°C when they also interact with other imperfections to form complexes. In gallium-doped material post-irradiation anneals near 200°C there appear gallium pairs, one member of which is interstitial adjacent to the other member in a substitutional site.[22]

As a result of these observations, it is concluded that the interstitial silicon moves rapidly through the lattice by some type of interstitialcy mechanism (the interstitial propagates by interchange with substitutional atoms) and at temperatures even as low as 4°K when impurities such as Al, Ga, or perhaps even donor atoms are encountered, these are ejected into interstitial sites, thus breaking the interstitialcy chain process. The interstitial impurities can now migrate only by a normal interstitial diffusion and a much higher activation energy. (Note

that the activation energy of interstitial motion for Li^+, the smallest ion studied, is 0.66 eV in silicon.[26])

It should be mentioned here that these defect structures account for only a fraction of the resonances that have been isolated from the complex spectra of electron-irradiated silicon. In addition, other resonances including those for S = 1 states have been obtained on fast neutron-irradiated silicon[27] and an oxygen containing state in p-type silicon[28] has been reported.

As a result of this outstanding series of ESR investigations, we are now in a position to understand the full complexity of the problem of identifying the imperfections responsible for the various acceptor and donor states not only in irradiated silicon but in germanium and other semiconductors as well. Rather than attempting to force experimental observations into a conceptual framework in which only the existence of simple defects is admitted, we have learned to accept the principle that the products of irradiation will include nearly every conceivable complex between vacancies and impurities that are present as well as numerous interstitial-impurity complexes. This new point of view has led to quite rapid progress in understanding striking differences in behavior in specimens with slightly different impurity content. For example, we show in Fig. 12 the effect of oxygen impurity on the radiation response of the excess carrier lifetime τ in n-type silicon.[29] Although the two specimens have nearly the same initial lifetime and conductivity, the oxygen-free material is much more strongly affected than crystals which contain 10^{17} to 10^{18} oxygen atoms per cm^3. The difference can be readily explained: The deep acceptor state associated with the phosphorous-vacancy complex, which is the dominant radiation defect in the oxygen-free

crystal, is a much more efficient recombination center than the shallow state associated with the oxygen-vacancy complex. Interestingly, the higher purity specimen is more sensitive to radiation with respect to this particular property than the less pure one, and since excess carrier lifetime is so important to the operation of most devices, it would appear that, other things being equal, a diode or transistor fabricated from quartz-crucible grown silicon would have a better radiation resistance than the less highly oxygen contaminated floating-zone grown crystals.

Let us now see what the results obtained on silicon can tell us about germanium. Unfortunately, defects in germanium are not so amenable to study by ESR techniques and one is therefore forced for the most part to infer the nature of the processes associated with electrical property changes resulting from irradiation and subsequent annealing, in terms of defect structures analogous to those found in silicon. The possibility of defect-impurity complexes in irradiated germanium was first pointed out by Brown and coworkers[30] who found that radiation defects were thermally more stable in n-type specimens doped with small donor atoms (As and P) than those doped with antimony. The recovery is much more rapid in the antimony-doped specimens than in the others. A naive interpretation of this observation would be that the smaller donor atoms, i.e. arsenic or phosphorous, trap and stabilize a simple defect. Subsequent work[31,32] has shown this view to be untenable since the rate of recovery in this temperature range increases as the antimony concentration increases, indicating that the impurity must either be directly involved in the unstable defects or participate in the annealing stages. The

influence of antimony concentration on the recovery of excess carrier lifetime is shown in Fig. 13. Arsenic-doped material shows only a very slight influence of concentration.

Until recently there was no direct evidence that point defects might exhibit a similar behavior and form similar complexes with impurities in germanium as they do in silicon. However, Whan[33] has presented conclusive evidence that vacancies begin to move in germanium near 65°K and form a series of oxygen complexes which can be detected through their vibronic infrared absorption spectra. Armed with this vital piece of evidence, analysis of annealing data in terms of vacancy-impurity complexes and perhaps even interstitial-impurity complexes can be carried out with reasonable confidence. Indeed such defects have been invoked in interpreting the isochronal recovery of electron concentration and reciprocal mobility in n-type germanium which had been exposed to ^{60}Co γ rays at 78°K. Evidently, even at this temperature vacancies are able to migrate and form donor-vacancy complexes, and the mutual annihilation of interstitial donors and vacancies.

It should be pointed out that Whan's results as well as those of Watkins' on the ease of vacancy motion confront us with a serious paradox concerning the mechanism underlying self-diffusion in these materials. The self-diffusion energy for germanium as measured by Letaw and coworkers[34] is 3 eV while recent studies on silicon[35,36] yield 5.1 eV. If the diffusion is assumed to proceed through the motion of vacancies this energy is the sum of the energy of formation and the energy of motion of the vacancies. Now these component energy values can be separately determined by quenching and subsequent annealing experiments which have

been carried out in the case of germanium.[37] The temperature dependence of the quenched-in vacancy concentration as reflected by changes in Hall coefficient yields a formation energy of ~1.9 eV, and the annealing of the excess vacancy concentration which should reflect the activation energy of motion gives a value of ~1.2 eV. The sum of these values is in good agreement with the self-diffusion energy. However, the motion energy determined thermally is at least a factor of five larger than that observed in irradiated specimens, as inferred from the results of Whan. An attractive solution to the paradox would be to say that the diffusion-current at high temperature is carried by divacancies. If the motion energy for the divacancy in germanium is comparable to its value in silicon determined experimentally[22] (1.3 eV), it would certainly be consistent with the observed activation energy for the annealing of quenched-in defects. In fact, Seeger[38] pointed out a number of years ago on the basis of the behavior of deformed germanium that the motion energy of germanium divacancies should be in the neighborhood of 1.5 eV. Another factor favoring this viewpoint is the dislocation jog structure in the diamond lattice. Haasen and Seeger[39] have pointed out that the shortest jog produced by the displacement of an edge dislocation from one glide plane to the next adjacent one is two atoms high. Now in many solids vacancies are known to be created in the bulk thermally by evaporation from dislocation jogs (evaporation of a vacancy causes the jog to advance a unit spacing along the dislocation) and these jogs which also act as sinks for the deposition of defects as the crystal is cooled from high temperature. Consequently, if in the diamond lattice the energy to move a jog by removing a pair of vacancies one at a time is much larger than removing the pair as a unit, one would expect

them to be produced bound together in pairs. If now the binding energy holding this pair together is large enough to prevent thermal breakup, the predominant thermal defects will be divacancies rather than single vacancies. This is just another way of stating that the formation energy of divacancies is smaller than that of single vacancies. In order for divacancy motion to dominate self-diffusion, the following relation must hold:

$$E_F'' + E_M'' < E_F' + E_M' \tag{5}$$

where the double-primes refer to the divacancies and the single primes to single vacancies. In view of the small value of E_M' (~0.1 eV) indicated by the experiments of Watkins[23] and Whan[33], the self-diffusion energies would then require that $E_F' > 3$ eV for germanium and 5 eV for silicon. It should be pointed out, however, that theoretical calculations of E_F[40-42] all yield values for germanium that are consistent with the accepted single vacancy model for self-diffusion, i.e., ~2 eV. Consequently, unless it can be shown that the excellent agreement between these calculations and experiment is fortuitous, it appears doubtful that the paradox can be resolved on the basis of divacancies being responsible for self-diffusion.

Another possible way of accounting for the disparity between the motion energies of radiation vacancies and thermal vacancies is the influence of charge state. However, inspection of the energy level structure of vacancies as shown in Fig. 11 indicates that this suggestion would hardly be valid since at high temperature the vacancy would have an appreciable probability of being negative (the Fermi level lies in

the center of the gap near the position of the acceptor level) and this is the charge state of highest mobility.[23] Evidently, a careful re-examination of our ideas concerning the mechanism of self-diffusion in the diamond structure is required.

Compound Semiconductors

Because of the binary nature of III-V or II-IV semiconductors, the complexity of defect structures that might be expected to result from irradiation is considerably greater than that encountered in elemental semiconductors. Because of mutual interaction between radiation defects, interaction of two types of interstitials and vacancies with chemical impurity and a new type of defect—the misplaced atom (a Group III atom on a Group V lattice site and conversely)—the number of defect structures in these materials is perhaps nearer N^2 than 2N, where N represents the number of prominent defect structures in the elemental case. In view of this seemingly overwhelming complexity, one might question whether the experimental results could be interpreted in terms of any realistic defect models or yield any physical insights into the nature of radiation effects in these materials. For a review of the variety of results on the III-V compounds, the reader is directed to Aukerman's comprehensive review.[43] Although in many instances complexity is indeed an obstacle, in some cases it works to our advantage and I would like to present briefly two such cases.

The first of these concerns a peculiarity of the zinc-blende structure in a material such as indium antimonide. Each In atom is covalently bound to four Sb atoms, each being situated at the corners of a regular tetrahedron and the inverse of course holds for each Sb atom.

If these atoms could be transformed into identical atoms without any change in position or binding, the lattice would assume the diamond structure, which indeed is a highly symmetrical structure. But let us now examine the environment of each In atom or each Sb atom situated on a given {111} plane. It is immediately evident that the lattice is unsymmetrical with respect to this plane. For example, one covalent bond extends from each In atom to the left and three to the right, whereas this configuration is inverted from the Sb atoms. This suggests that there are two possible {111} surfaces, each containing a single type of atom, and a polarization direction, namely, the <111>. The existence of this unsymmetrical situation has important consequences for many properties of III-V compounds: cleavage, piezoelectric effect, chemical behavior both with respect to oxidation and etching, a variety of electronic transport effects, and even crystal growth.[44]

As might be expected this polarized structure is also reflected in the ease of defect creation by fast electrons. Eisen[45] has determined the threshold energy and the defect yields in indium with the electron beam in the two senses of <111> direction. In the "minus" direction, examining those atom pairs parallel to the beam, the electron sees first the In atom immediately behind which is the Sb atom and immediately behind that there is an open interstitial site. The "plus" direction is the inverse, i.e., the Sb atom, followed by the In atom, followed by the interstitial site. The results indicate that not only is the displacement energy E_d different for the two directions but that the thermal stability of the defects is quite different. For the beam direction into the (111) face (the plus direction), it is seen

from Fig. 14 that there is an open interstitial site immediately behind the In atom; hence, this should be the direction for easy In-atom displacement. On the other hand, an Sb atom receiving an impulse in this direction would have to collide with an indium atom before reaching the interstitial site. The situation is, of course, inverted for the beam into the $(\bar{1}\bar{1}\bar{1})$ face, which corresponds to the direction for easy Sb-atom displacement. An analysis of the effect of irradiation on the Hall coefficient reveals that the displacement energy $E_d(In)$ for In in the easy direction is 6.4 eV and the resulting defect is thermally more stable than the structure created by displacement of Sb atoms for which $8.5 < E_d(Sb) < 9.9$ eV. Although the precise structure of these defects which decrease the electron concentration by capturing electrons cannot be described, this investigation indicates that a displaced In atom plays a dominant role in the one which is thermally stable up to 128°K, and Sb-atom displacement is involved in the one that is stable only up to 83°K.

A second series of experiments by R. O. Chester[46] has employed nuclear characteristics of the atoms comprising the compound semiconductor to throw light upon the defects responsible for acceptor and donor action. She studied the response of cadmium sulfide and cadmium telluride to gamma irradiation employing different γ-ray sources, namely, ^{60}Co with E_γ = 1.17 and 1.33 MeV, and ^{137}Cs with E_γ = 0.66 MeV. Because of the markedly different mass and atomic numbers of the Cd and S atoms, it can be demonstrated from simple collision theory that the 0.66 MeV photon from ^{137}Cs decay displaces S atoms and the ^{60}Co photons predominantly displace Cd atoms. The situation is reversed in cadmium telluride

for which the smaller energy photon preferentially displaces Cd atoms but because of the greater similarity of atom mass the distinction is not as great as in cadmium sulfide. Investigation of the behavior of Hall coefficient of gamma-irradiated n-type cadmium sulfide and both n- and p-type cadmium telluride shows that preferential Cd-displacement leads to the introduction of acceptor states while displacement of the electro-negative constituent leads to donor action. Because of the propensity of simple defects for forming complexes with other imperfections, one cannot infer from these results the precise structure of the defects responsible for the dominant electronic states. Nevertheless, this study indicates what are the dominant ingredients of the radiation acceptors and donors in the II-VI compounds.

REFERENCES

1. For an early review, see K. Lark-Horovitz, Semiconducting Materials, ed. by H. K. Henisch (Academic Press, New York) 1951, p. 47.
2. These developments were first reported at the Gatlinburg Conference on Radiation Effects in Semiconductors in 1959, and the Proceedings were published in J. Appl. Phys. 30, No. 8 (1959).
3. For a review, see D. S. Billington and J. H. Crawford, Radiation Effects in Solids (Academic Press, New York) 1950, Chap. II.
4. J. W. MacKay, E. E. Klontz, and G. W. Gobeli, Phys. Rev. Letters 2, 146 (1959); J. W. MacKay and E. E. Klontz, J. Appl. Phys. 30, 1269 (1959); E. E. Klontz and J. W. MacKay, J. Phys. Soc. Japan 18, Suppl. III, 216 (1963).
5. J. W. Corbett and G. D. Watkins, Phys. Rev. Letters 7, 314 (1961).
6. J. R. Parsons, R. W. Balluffi, and J. S. Koehler, Appl. Phys. Letters 1, 57 (1962).
7. B. R. Gossick, J. Appl. Phys. 30, 1214 (1959); J. H. Crawford, Jr., and J. W. Cleland, J. Appl. Phys. 30, 1204 (1959); J. W. Cleland and J. H. Crawford, Jr., Proc. International Conf. on Semiconductor Physics, Prague, 1960 (Academic Press, New York) 1961, p. 299.
8. H. J. Juretschke, R. Landauer, and J. A. Swanson, J. Appl. Phys. 27, 838 (1956).
9. H. J. Stein, J. Appl. Phys. 31, 1309 (1960).
10. W. H. Closser, J. Appl. Phys. 31, 1693 (1960).
11. N. Van Dong, J. Appl. Phys. 36, 3450 (1965). See also, N. Van Dong, P. Ngu Tung, and M. Vanderyner, Compt. Rend. 236, 1722 (1963).

REFERENCES (Con't)

12. M. Bertolotti, T. Papa, D. Setti, V. Grosso, and G. Vitali, Nuovo Cimento 29, 1200 (1963); J. Appl. Phys. 36, 3506 (1965).

13. For a summary of recent developments, see F. L. Vook, Radiation Damage in Semiconductors, ed. by P. Baruch (Academic Press, New York) 1965, p. 51.

14. R. H. Silsbee, J. Appl. Phys. 28, 1246 (1957).

15. M. T. Robinson and O. S. Oen, Appl. Phys. Letters 2, 30 (1963); Phys. Rev. 132, 2385 (1963).

16. J. A. Davies, G. C. Ball, F. Brown, and B. Domeij, Canadian J. Phys. 42, 1070 (1964).

17. C. D. Moak, J. W. T. Dabbs, and W. W. Walker, Bull. Am. Phys. Soc. 11, 101 (1966); to be published in Rev. Sci. Inst.

18. For a coverage of radiation sensitive properties and thermal annealing of radiation defects in semiconductors, the reader is directed to recent review papers: J. H. Crawford, Jr., Interaction of Radiation with Solids, ed. by R. Strumane, J. Nihoul, R. Gevers, and S. Amelinckx (North Holland Publishing Co., Amsterdam) 1964, p. 421; V. S. Vavilov, phys. stat. sol. 11, 447 (1965). An excellent coverage of recent work is also to be found in Radiation Damage in Solids, ed. by P. Baruch (Academic Press, New York) 1965.

19. G. Bemski, J. Appl. Phys. 30, 1195 (1959).

20. G. D. Watkins, J. W. Corbett, and R. M. Walker, J. Appl. Phys. 30, 1198 (1959).

21. J. W. Corbett, G. D. Watkins, R. M. Chrenko, and R. S. McDonald, Phys. Rev. 121, 1015 (1961).

REFERENCES(Con't)

22. G. D. Watkins and J. W. Corbett, Disc. Faraday Soc. 31, 86 (1961).

23. G. D. Watkins, Radiation Damage in Semiconductors, ed. by P. Baruch (Academic Press, New York) 1965, p. 97.

24. G. D. Watkins, J. Phys. Soc. Japan 18, Suppl. II, 22 (1963).

25. H. Y. Fan and K. Lark-Horovitz, Semiconductors and Phosphors, ed. by M. Schon and H. Welker (Interscience, New York) 1958, p. 113.

26. J. Maita, J. Phys. Chem. Solids 4, 68 (1958).

27. Mun Jung and G. S. Newell, Phys. Rev. 132, 648 (1963).

28. N. Almeleh and B. Goldstein, Bull. Am. Phys. Soc. 11, 16 (1966).

29. K. Matsuura and Y. Inuishi, J. Phys. Soc. Japan 16, 339 (1961); Y. Inuishi and K. Matsuura, J. Phys. Soc. Japan 18, Suppl. III, 240 (1963).

30. W. L. Brown, W. M. Augustyniak, and T. R. Waite, J. Appl. Phys. 30, 1258 (1959).

31. O. L. Curtis, Jr., and J. H. Crawford, Jr., Phys. Rev. 124, 173 (1961); 126, 1342 (1962).

32. J. C. Pigg and J. H. Crawford, Jr., Phys. Rev. 135, A1141 (1964).

33. R. E. Whan, Appl. Phys. Letters 6, 221 (1965); Phys. Rev. 140, A690 (1965).

34. H. Letaw, W. M. Portnoy, and L. Slifkin, Phys. Rev. 102, 636 (1956).

35. W. R. Wilcox and T. J. LaChapelle, J. Appl. Phys. 35, 240 (1964).

36. B. J. Masters and J. M. Fairfield, Appl. Phys. Letters 8, 380 (1966).

37. For a recent assessment of this matter, see A. Hiraki, J. Phys. Soc. Japan 21, 34 (1966).

REFERENCES (Con't)

38. A. Seeger, Solid State Physics in Electronics and Telecommunications, ed. by M. Desirant and J. L. Michiels (Academic Press, New York) 1960, Vol. I, p. 61.

39. P. Haasen and A. Seeger, Halbleiterprobleme, ed. by W. Schottky (Vieweg and Solm, Braunschweig) 1958, Vol. IV, p. 68.

40. R. A. Swalin, J. Phys. Chem. Solids 18, 290 (1961).

41. A. Scholz and A. Seeger, phys. stat. sol. 3, 1480 (1963); Radiation Damage in Solids, ed. by P. Baruch (Academic Press, New York) 1965, p. 315.

42. K. Bennemann, Phys. Rev. 137, 1497 (1965).

43. L. Aukerman, Semiconductors and Semimetals, ed. by R. K. Willardson and A. C. Beer (Academic Press, New York) Vol. 4, Physics of III-V Compounds (to be published).

44. J. W. Faust, Semiconducting Compounds, ed. by R. K. Willardson and H. L. Goering (Reinhold Publishing Corp., New York) 1962, p. 445.

45. F. H. Eisen, Phys. Rev. 135, A1394 (1964).

46. R. O. Chester, to be published. See also, Ph.D. thesis from the University of Tennessee, ORNL-3767 (unpublished).

ORNL-LR-DWG 45249R

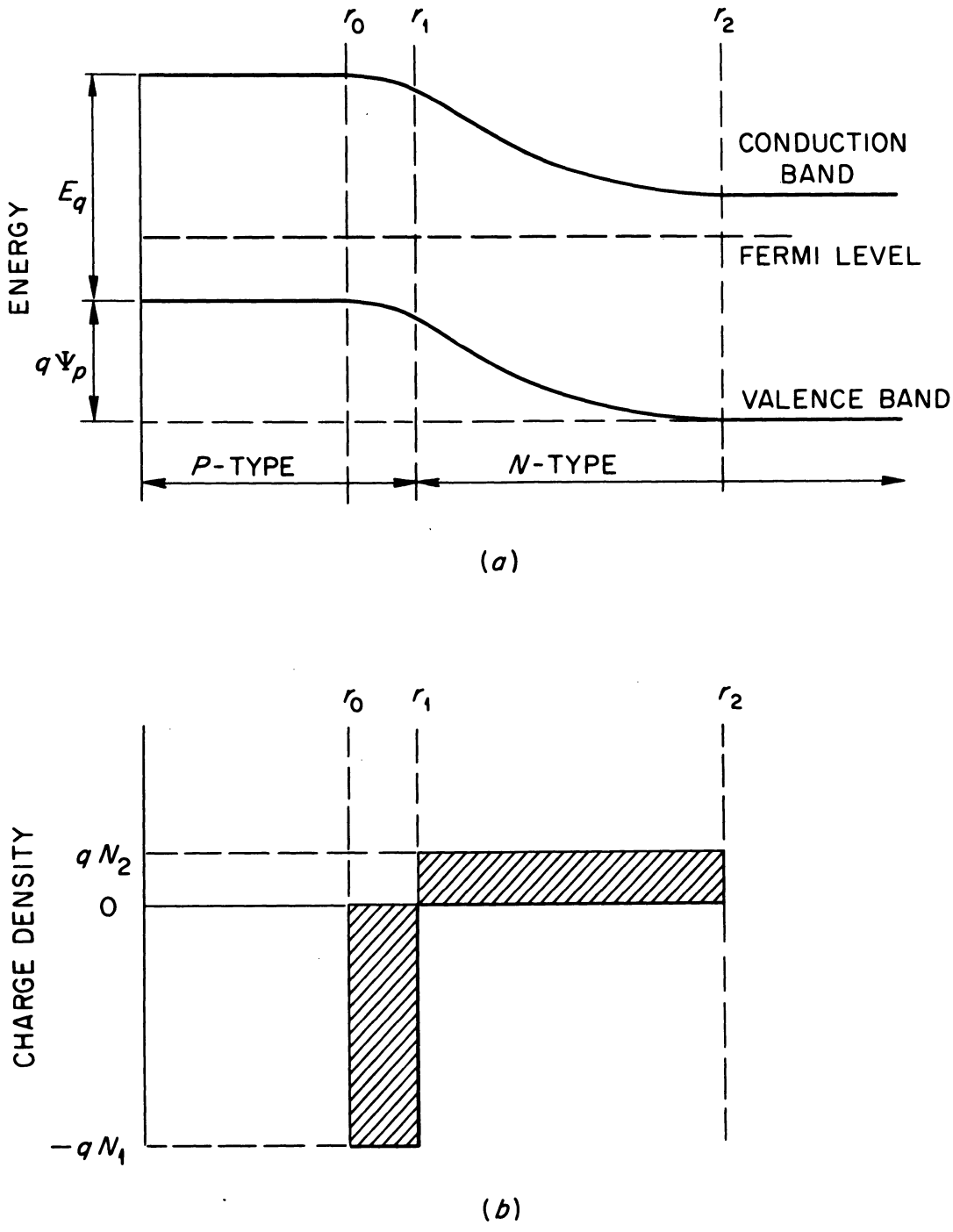

Fig. 1. The structure of the electrical double layers (space-charge zone) associated with a disordered region in germanium.

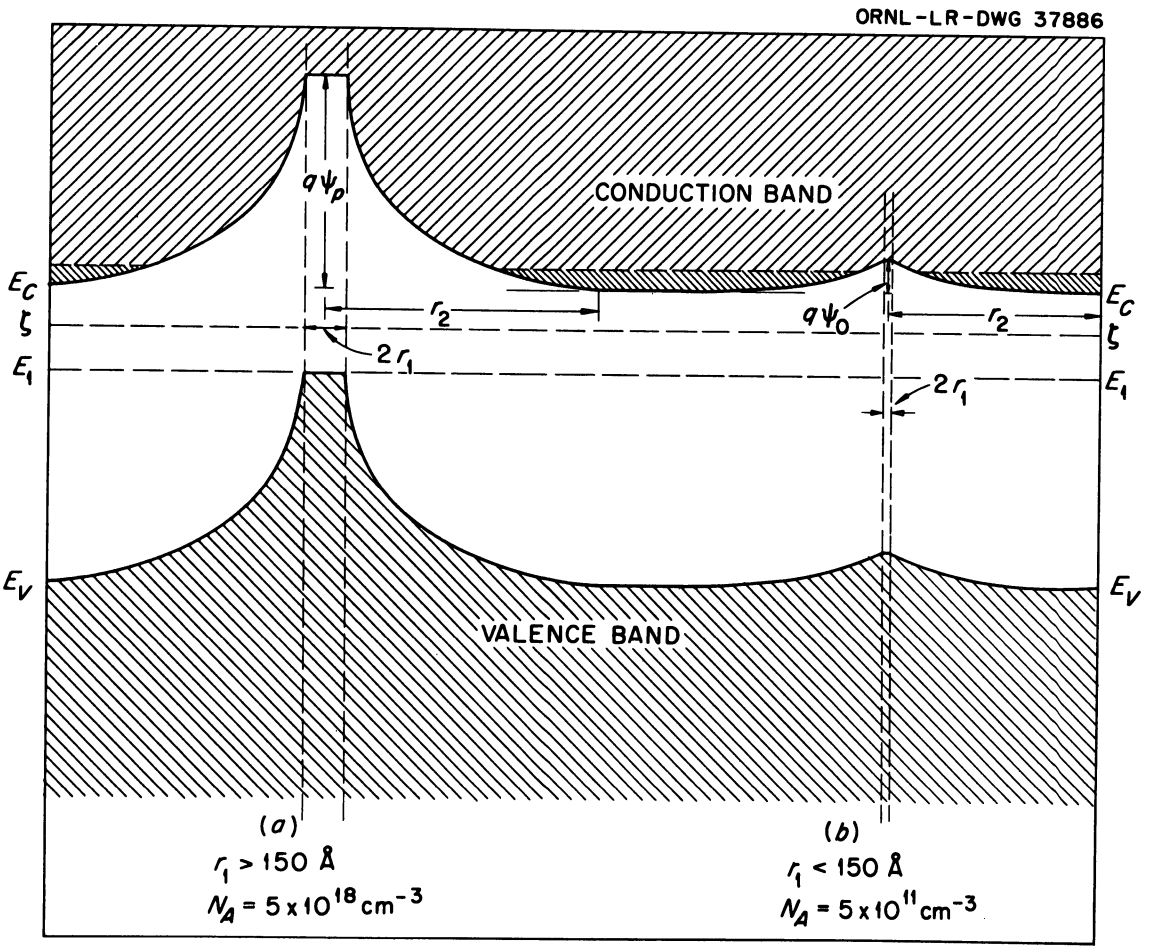

Fig. 2. Schematic drawing of the disordered region and its associated space-charge zone. Part (a) refers to a disordered region large enough to support a double layer of maximum radial extent. Part (b) shows the relatively minor perturbation of the band edges by a small disordered region.

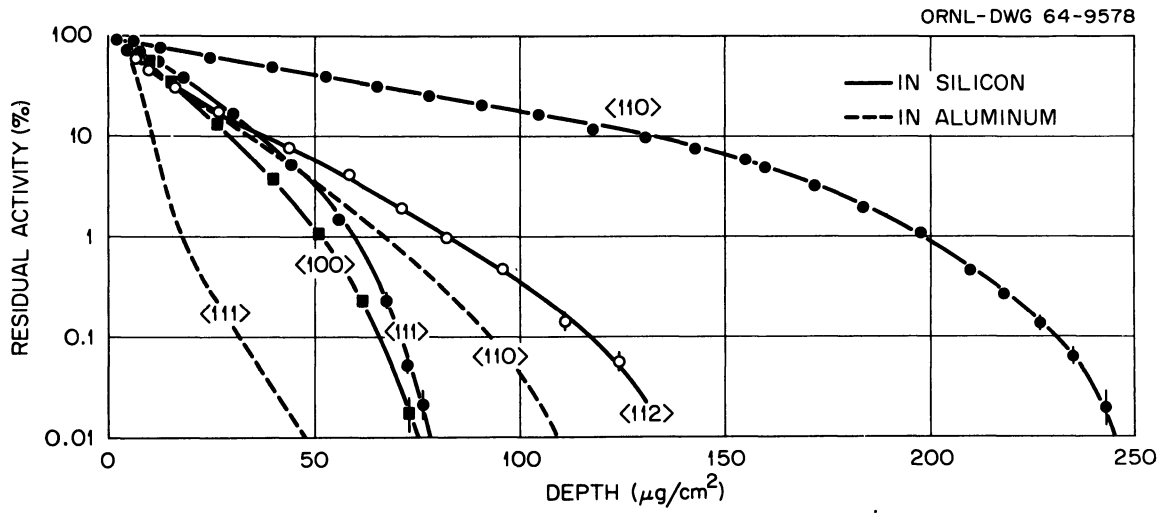

Fig. 7. Penetration of 40 keV ^{125}Xe ions into single crystals of silicon and aluminum. (After Davies et al., Ref. 20.)

ORNL-LR-DWG 51380

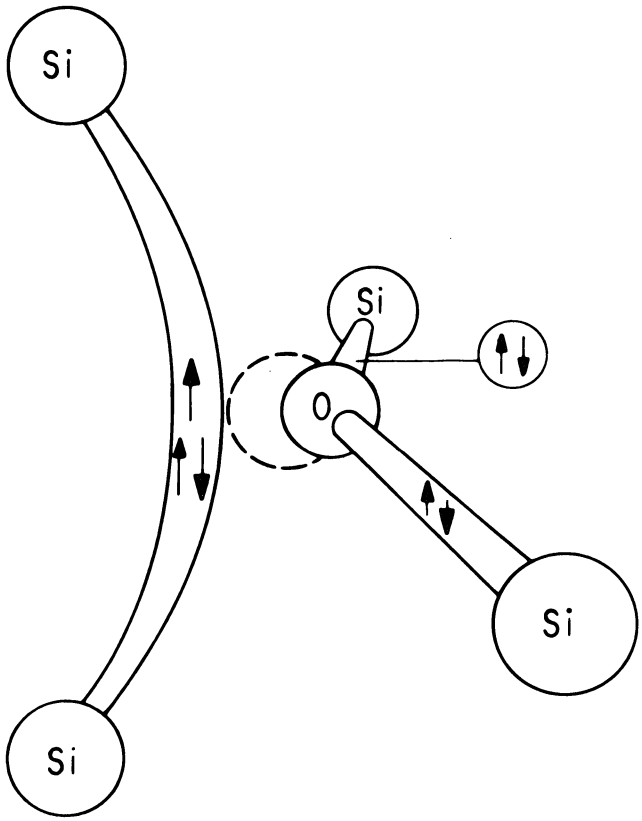

A CENTER

Fig. 8. Model for oxygen-vacancy center in electron-irradiated silicon. (After Watkins and Corbett, Ref. 20.)

ORNL—LR—DWG 51381

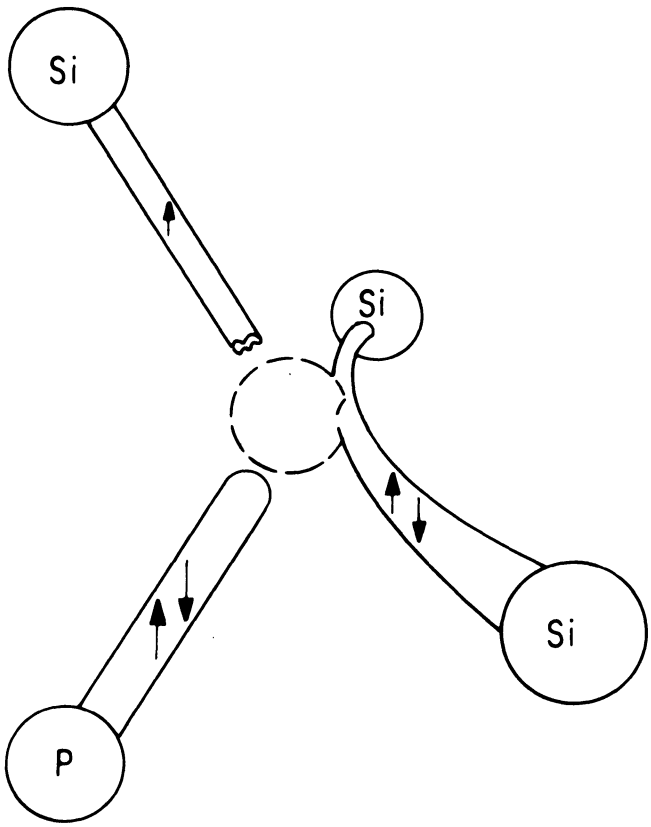

Fig. 9. Model for the phosphorous-vacancy center in electron-irradiated silicon. (After Watkins and Corbett, Ref. 22.)

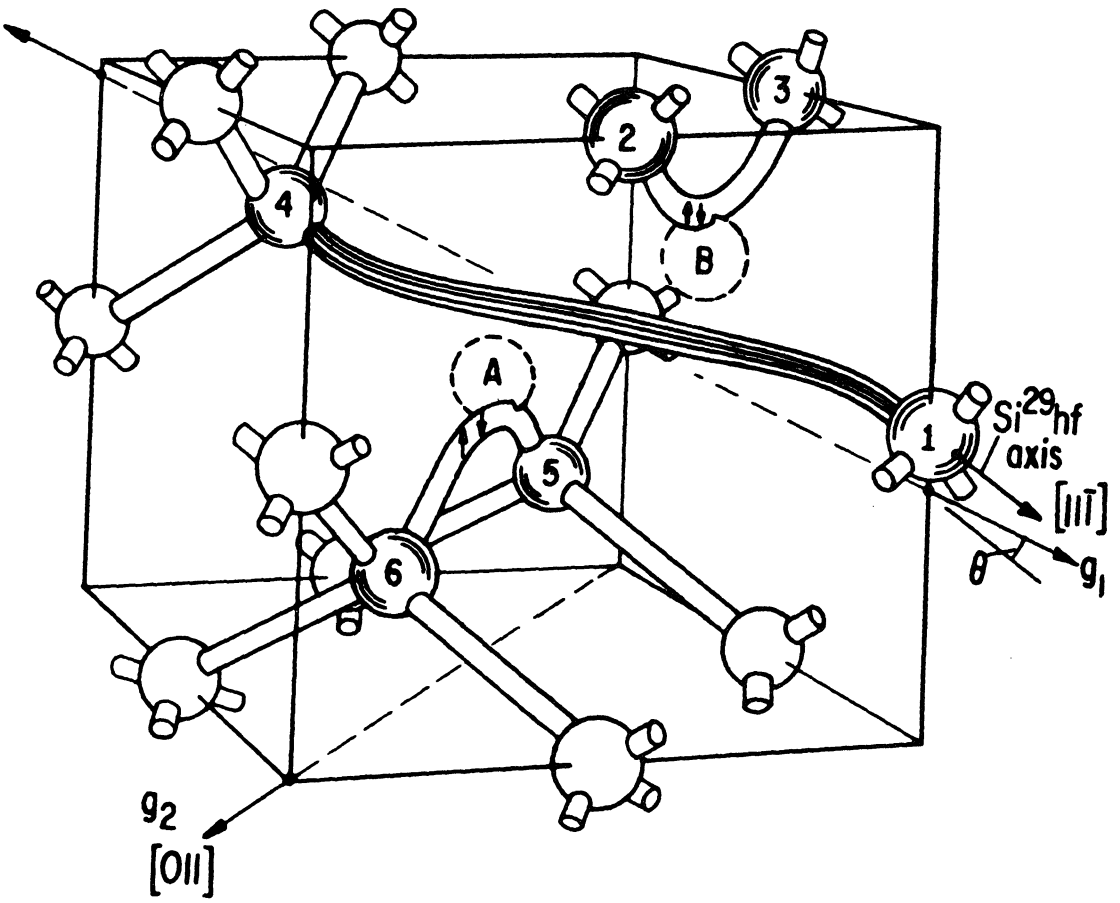

Fig. 10. Model of the divacancy in electron-irradiated silicon. (After Corbett and Watkins, Ref. 5.)

ORNL-DWG 66-7636

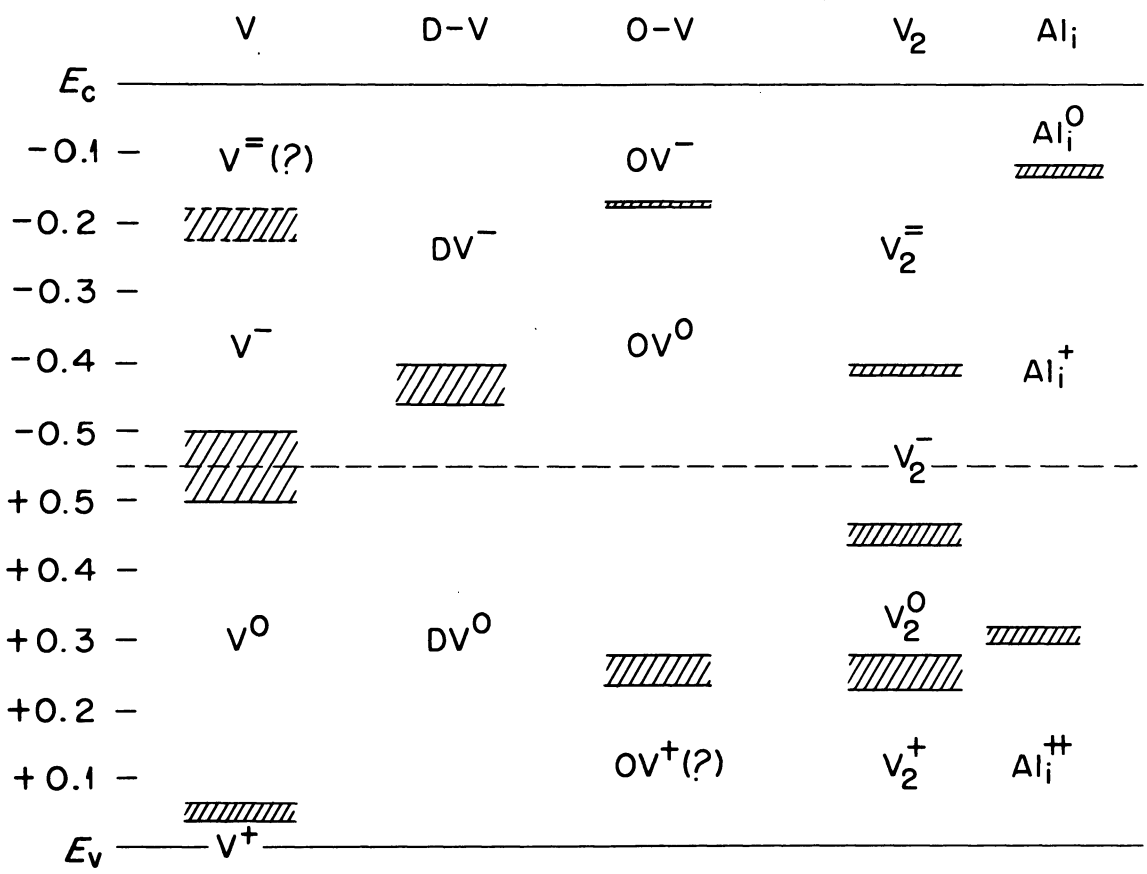

Fig. 11. Position in the band gap of energy levels associated with defect complexes as identified by ESR in electron-irradiated silicon.

V - vacancy
D-V - donor-vacancy complex
O-V - oxygen-vacancy complex
V_2 - divacancy
Al_i - interstitial aluminum

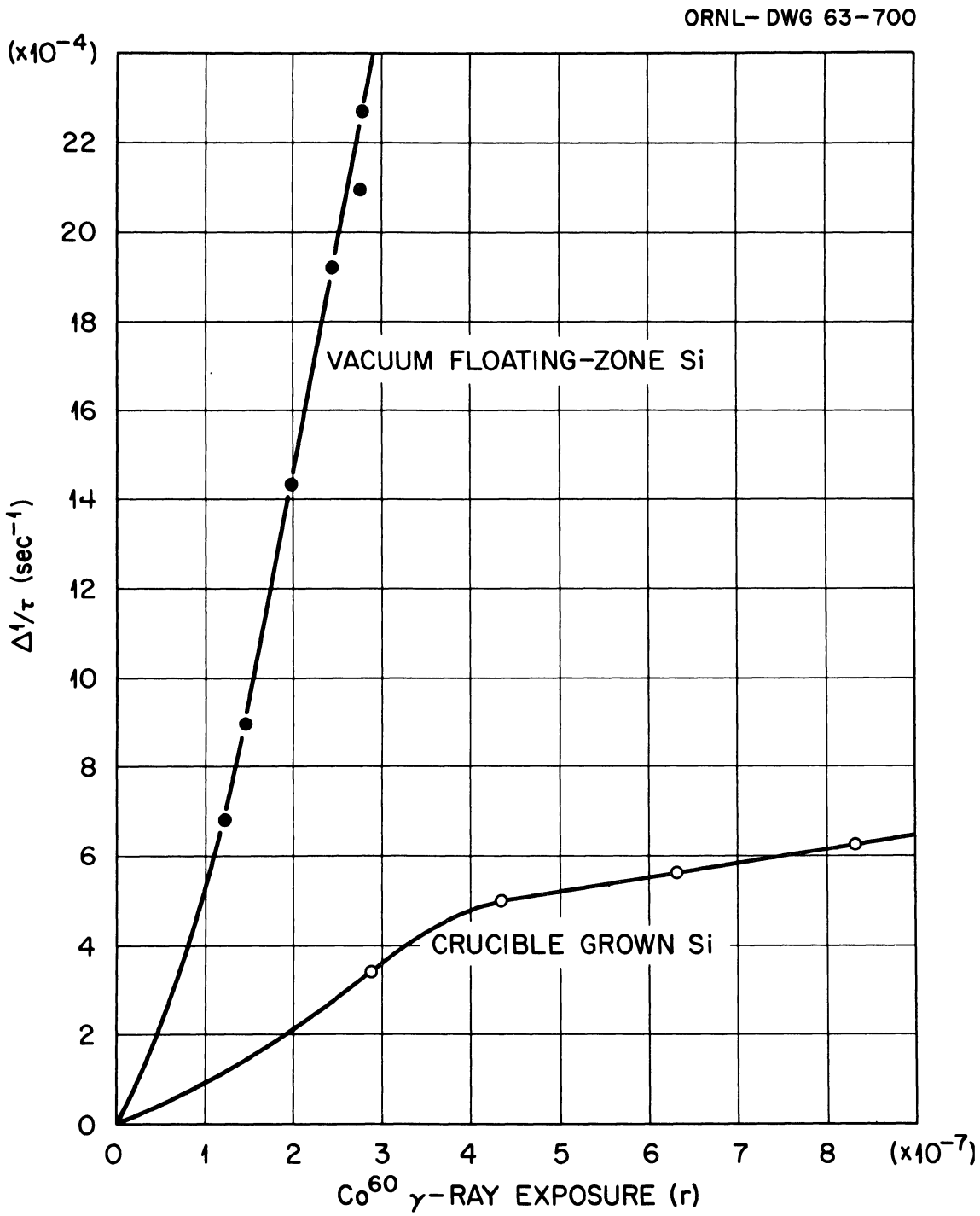

Fig. 12. Change in reciprocal of lifetime of excess carriers in n-type silicon exposed to γ rays, showing the difference in response of oxygen-free (vacuum floating zone) and oxygen containing (crucible grown) material. (After Matsuura and Inuishi, Ref. 29.)

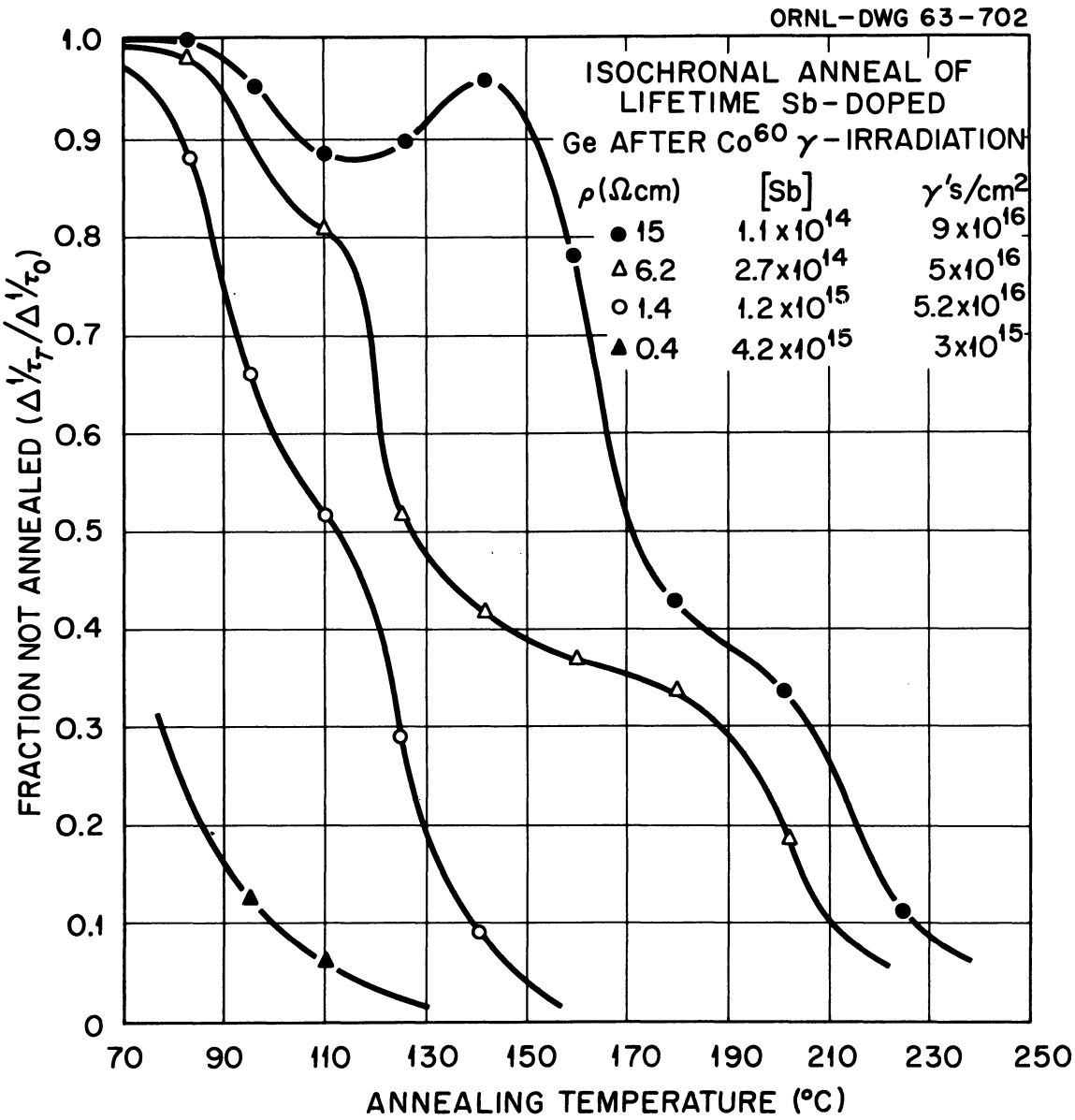

Fig. 13. The influence of antimony concentration on the recovery of excess carrier lifetime in γ-irradiated n-type germanium. (After Curtis and Crawford, Ref. 31.)

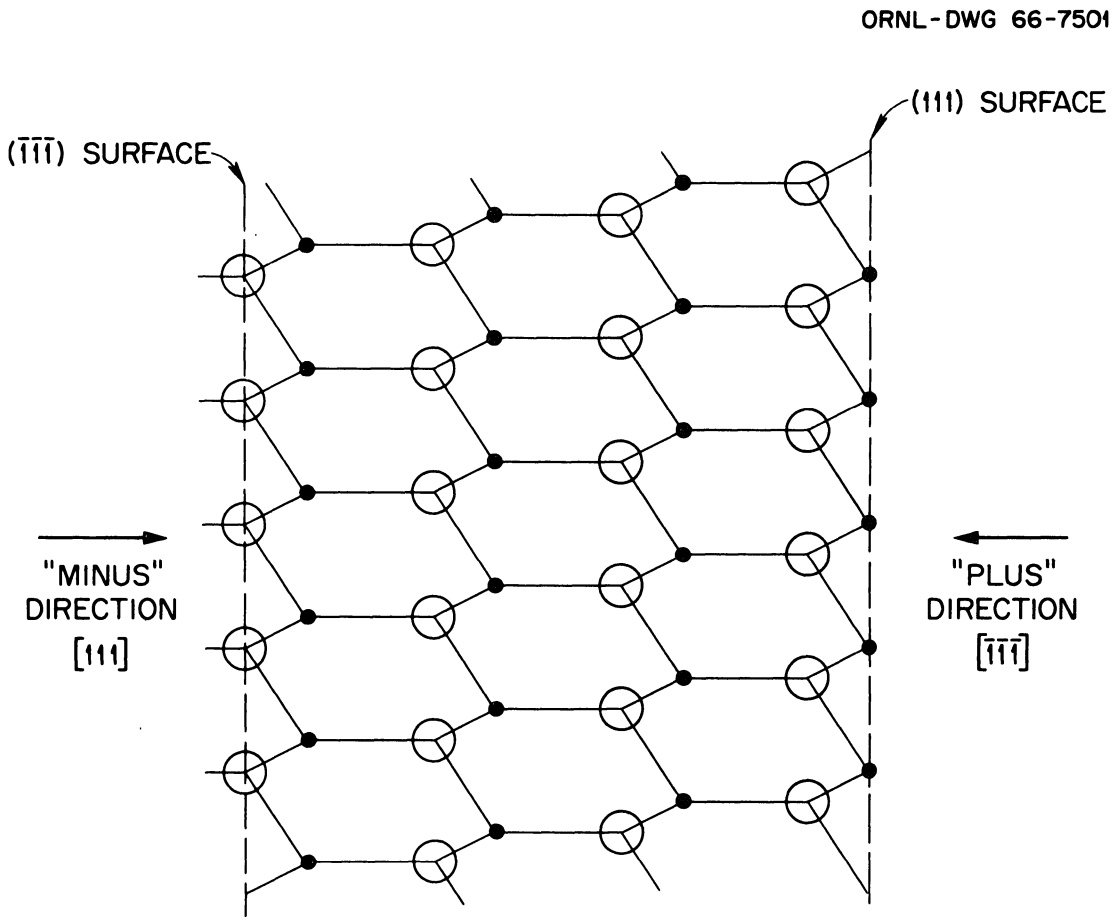

Fig. 14

Fig. 14. A projection of the xinc-blende lattice onto a $\{110\}$ plane.

RADIATION EFFECTS ON TRANSISTORS

George C. Messenger

I INTRODUCTION

A. LIFETIME REDUCTION OF DOMINANT IMPORTANCE

1. Current Gain Reduction

2. Changes in Other Parameters Related to Current Gain

2.1 Storage Time

2.2 Saturation Voltage

B. SECONDARY RADIATION EFFECTS

1. Surface Potential and Surface Recombination Velocity Changes

2. Carrier Removal or Addition

3. Reduction of Carrier Mobility

C. ESTABLISHMENT OF TRANSISTOR EQUATIONS IN TERMS OF RADIATION DEPENDENT PARAMETERS

1. General Admittance Matrix

2. Low Injection Level Effects

3. High Injection Level Modifications

D. FUNCTIONAL DEPENDENCE OF LIFETIME, CARRIER DENSITY, CARRIER MOBILITY, AND SURFACE RECOMBINATION VELOCITY ON RADIATION FLUENCE

E. TRANSISTOR EQUATIONS AS A FUNCTION OF RADIATION FLUENCE

1. Admittance Matrix

2. Current Gain

F. VARIOUS RADIATION ENVIRONMENTS

G. MICROCIRCUITS

II. ESTABLISHMENT OF GENERAL ADMITTANCE MATRIX

A. BASIC ONE DIMENSIONAL STRUCTURE (Reference 2 and 3)

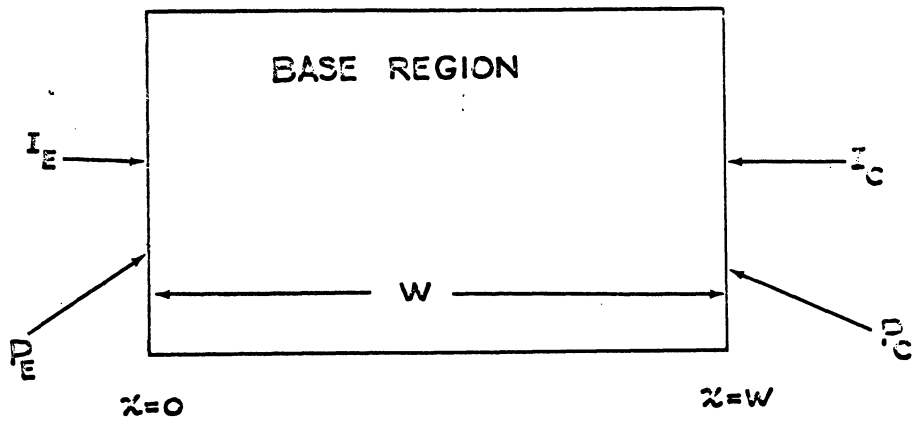

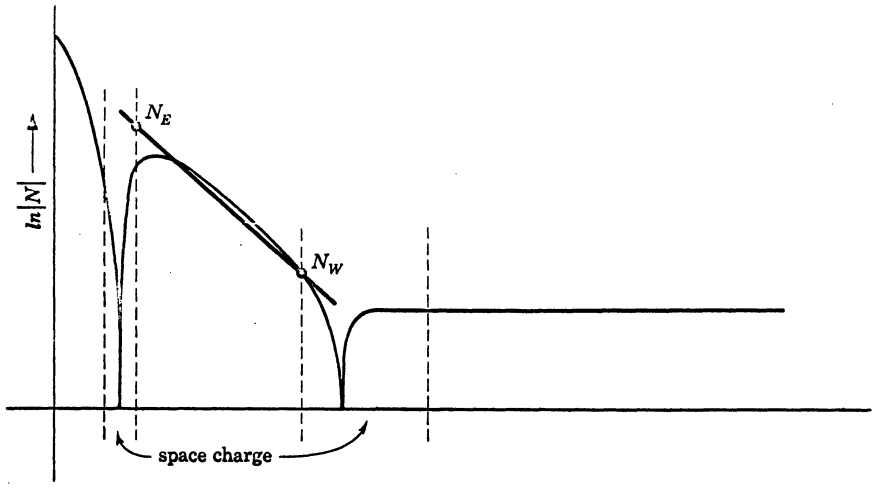

1. Discussion of General Applicability

1.1 Constant Field in Base

1.1.1 Graded Base

1.1.2 Homogeneous Base

1.2 Other Base Distributions such as Error Function (Reference 1)

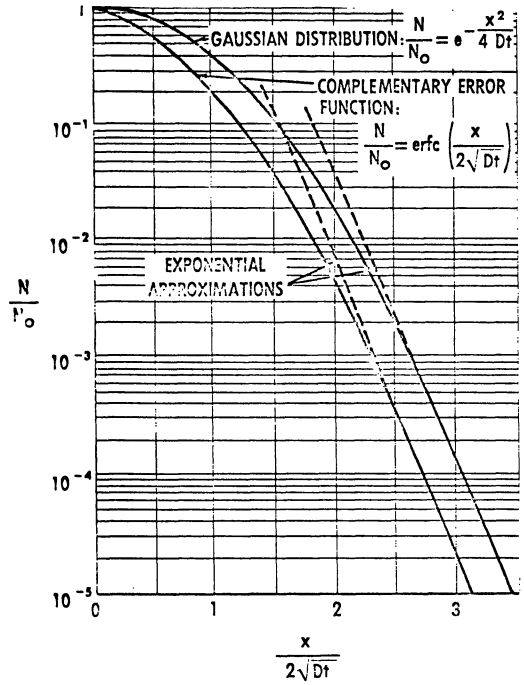

1.3 Two Dimensional Effects

1.4 Emitter Area Often Smaller than Collector Area

2. Basic Differential Equations (Reference 4)

2.1
$$\frac{\partial n}{\partial t} = g - R + \frac{1}{q}\frac{\partial J_n}{\partial x}$$

$$\frac{\partial p}{\partial t} = g - R - \frac{1}{q}\frac{\partial J_p}{\partial x}$$

2.2
$$J_p = q\mu_p\, pE - q\, D_p \frac{\partial p}{\partial x}$$

$$J_n = q\mu_n\, nE + q\, D_n \frac{\partial n}{\partial x}$$

2.3
$$\nabla^2\phi = -\frac{p - n + N_D - N_A}{\kappa\epsilon_o}$$

3. Discussion of Required Assumptions

3.1 τ_p, τ_n Shockley Read functions of resistivity. Assumed constant for solving equations and the solution subsequently multiplied by Shockley Read function. (Reference 5)

3.2 μ_n, μ_p, D_n, D_p assumed constant. They are actually related to impurity density by the Conwell-Weisskoff or Brooks-Herring functions (Reference 6).

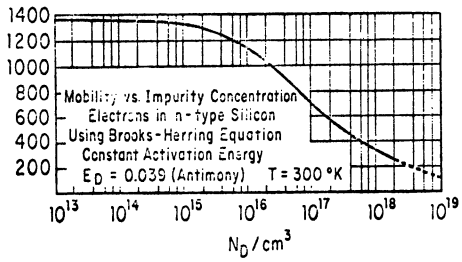

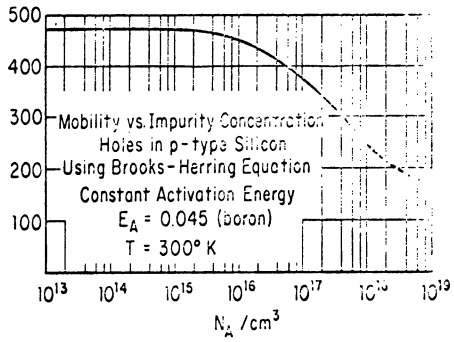

Effect of transition from low level to high level conditions modifies diffusion constants by a factor of 2. This is taken account of by the factor

$f'(Z) = \frac{1 + \frac{Z}{2}}{1 + 2}$ applied after the integration (Reference 7)

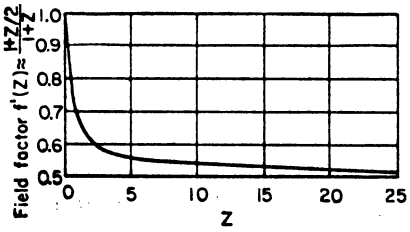

3.3 Space Charge Neutrality assumed.

3.4 $n_b = N_D$ assumed.

4. Discussion of Boundary Conditions (Reference 8)

4.1 Lifetime τ_E, τ_B, τ_C

4.2 Finite Emitter Region

4.3 $N_B = N_B^W \, e^{(1 - \frac{X}{W})\ln k}$

4.4 $p_E = p_n^o \, e^{\frac{qV_E}{kT}}$; $p_C = p_n^W \, e^{\frac{qV_C}{kT}}$.

5. Low Frequency Admittance Matrix

5.1

$$I_e = a_{11} \psi_E - a_{12} \psi_C$$

$$I_c = a_{21} \psi_E + a_{22} \psi_C ,$$

$$\psi_{E,C} = e^{\frac{qV_{E,C}}{kt}} - 1 ,$$

5.2

Matrix Element Function	Exact Form	Approximate Form
$\frac{a_{11}}{AD_p\, q\, p_n^o}$	$\sigma \coth \sigma W + \frac{n}{2W}$	$\frac{1 + \frac{W^2}{2L_p^2} + \frac{n}{2} + \frac{n^2}{8}}{W}$
$\frac{a_{12}}{AD_p\, q\, p_n^W}$	$\frac{\sigma \operatorname{csch} \sigma W}{\sqrt{k}}$	$\frac{1}{W\sqrt{k}} \left(1 + \frac{W^2}{6L_p^2} + \frac{n^2}{24}\right)$
$\frac{a_{21}}{AD_p\, q\, p_n^o}$	$\sqrt{k}\, \sigma \operatorname{csch} \sigma W$	$\frac{\sqrt{k}}{W} \left(1 + \frac{W^2}{6L_p^2} + \frac{n^2}{24}\right)$
$\frac{a_{22}}{AD_p\, q\, p_n^W}$	$\sigma \coth \sigma W - \frac{n}{2W}$	$\frac{\frac{W^2}{2L_p^2} - \frac{n}{2} + \frac{n^2}{8}}{W}$

$$\sigma = \frac{1}{2}\sqrt{\left(\frac{n}{W}\right)^2 + \left(\frac{4}{L_p}\right)^2}, \quad k = \frac{N_{DE}}{N_{DC}}, \quad n = \ln k, \quad L_p = \sqrt{D_p \tau},$$

$$k = p_n^W / p_n^o$$

$$\gamma_{E,C} = 1/1 + \frac{j_{n\ E,C}}{j_{p\ E,C}}$$

B. LOW INJECTION LEVEL CASE (Silicon only)

1. Recombination in Base Emitter Field Region (Reference 9)

$$j_{RG} = \frac{2W_S\, qn_i}{2\tau_o} \frac{kT}{q(\psi_o - V)} e^{qV/kT}$$

2. $$\gamma_E = 1/\left(1 + \frac{I_{RG}}{a_{11}}\right) = 1/\left(1 + \frac{A}{I_E^{\frac{1}{2}}}\right) \quad I_E \neq 0$$

3. Homogeneous base

$$\gamma_E = 1/\left(1 + \frac{W_S\, kT}{q(\psi_D - V)} \frac{n_1}{p_n^o} \frac{W^2}{L^2} e^{-\frac{qV_E}{2kT}}\right)$$

C. HIGH INJECTION LEVEL CASE

1. Built-in field slowly disappears as injection increases

2. $$\gamma_E = 1/\left(1 + \frac{n_p^o\, D_n \left(\sigma_E \coth \sigma_E W_E + \frac{\ln k_E}{2\, W_E}\right)}{p_n^o\, D_p\, (\sigma \coth \sigma W + \ln K/2W)}\right)$$

3. Effect of emitter lifetime. $W_E >> L_E$

$$n_p^o\, D_n\, (\sigma_E \coth \sigma_E\, W_E + \ln k_E/2W_E) \approx \frac{n_p^o\, D_n}{L_n^E}$$

4. Homogeneous base conductivity modulation

$$\gamma_E = 1/\left(1 + \frac{j_{neo}\, W\, (1 + \frac{Z}{2})}{q\, n_1^2\, D_p}\right), \quad Z = \frac{j_E\, W}{q\, D_p N_D}$$

5. Graded base conductivity modulation

5.1 Modification to Differential Equation for Determining a_{11} (Reference 10)

$$\frac{d\hat{p}}{dx} N_D + 2\hat{p} \frac{d\hat{p}}{dx} + \hat{p} \left(\frac{J_p}{qD_p} - N_{DE} \frac{\eta}{W} e^{-\eta x/W}\right) + N_{DE} e^{-\eta x/W} \frac{J_p}{qD_p} = 0$$

5.2 $$\gamma_E = \frac{1}{1 + A(1 + bI_E)}$$

6. Emitter Crowding

D. SURFACE RECOMBINATION EFFECTS

$$j_S = q\, Sp_B^o$$

$$\gamma_S = 1/1 + \frac{I_S}{a_{11}}$$

III DEPENDENCE OF LIFETIME AND OTHER PARAMETERS ON FLUENCE

1. Lifetime (Reference 11, 12, and 13)

$$\frac{1}{\tau} = \frac{1}{\tau_i} + \frac{\phi}{K(\rho_b, E_n)} .$$

$\tau \approx K/\Phi$ when $K/\Phi \ll \tau_i$ Defines Lifetime Damage Constant "Radiation Lifetime"

2. Carrier Density (Reference 14)

2.1 $$n = n_o \pm \Phi \frac{dn}{d\Phi}$$

2.2 $\frac{dn}{d\phi}$ is a function of ϕ (Reference 15)

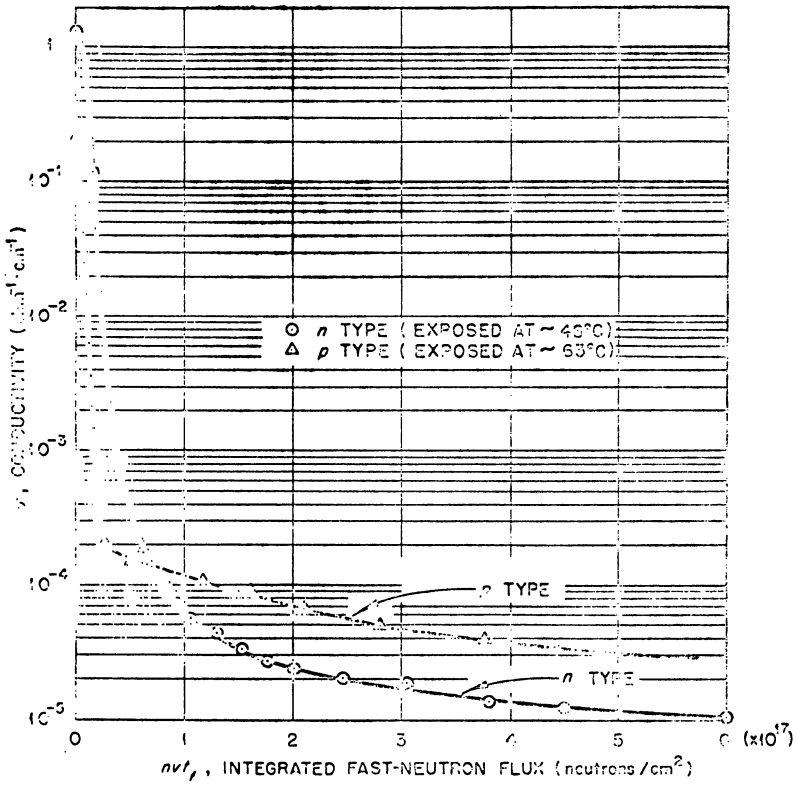
n TYPE (EXPOSED AT ~ 40°C)
p TYPE (EXPOSED AT ~ 65°C)
p TYPE
n TYPE
0
1
2
3
4
5
6 (x10^17)
nvt, INTEGRATED FAST-NEUTRON FLUX (neutrons/cm²)

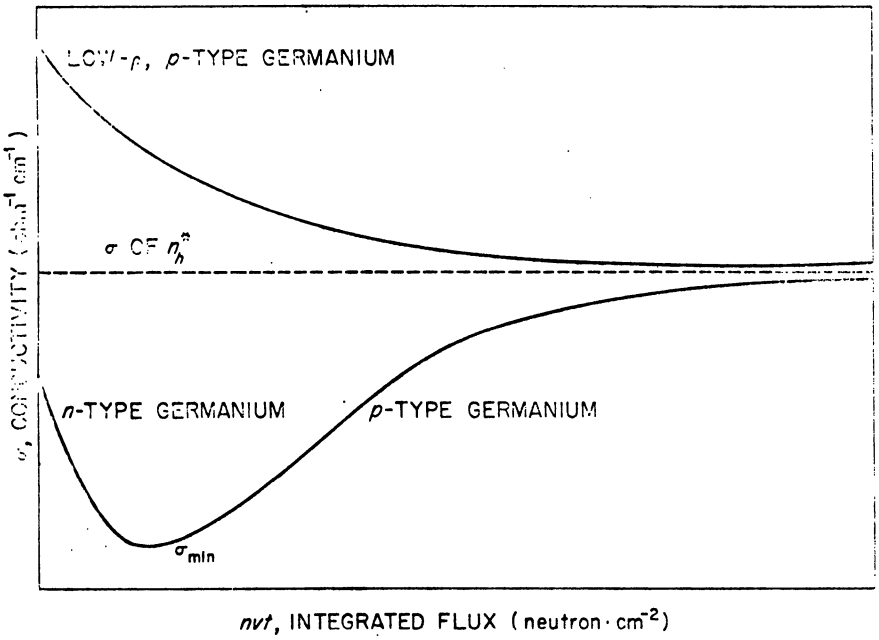
LOW-ρ, p-TYPE GERMANIUM
σ OF n_i^*
n-TYPE GERMANIUM
p-TYPE GERMANIUM
σ_{min}
nvt, INTEGRATED FLUX (neutron·cm⁻²)

2.3 Silicon approaches intrinsic; germanium approaches low resistivity p-type

3. Surface Recombination Velocity and Surface potential (Reference 16)

3.1 S versus ϕ

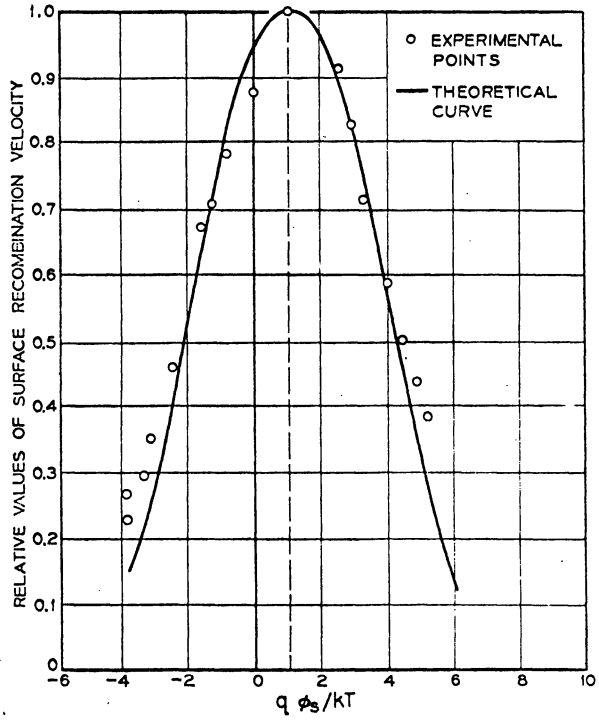

(Reference 25)

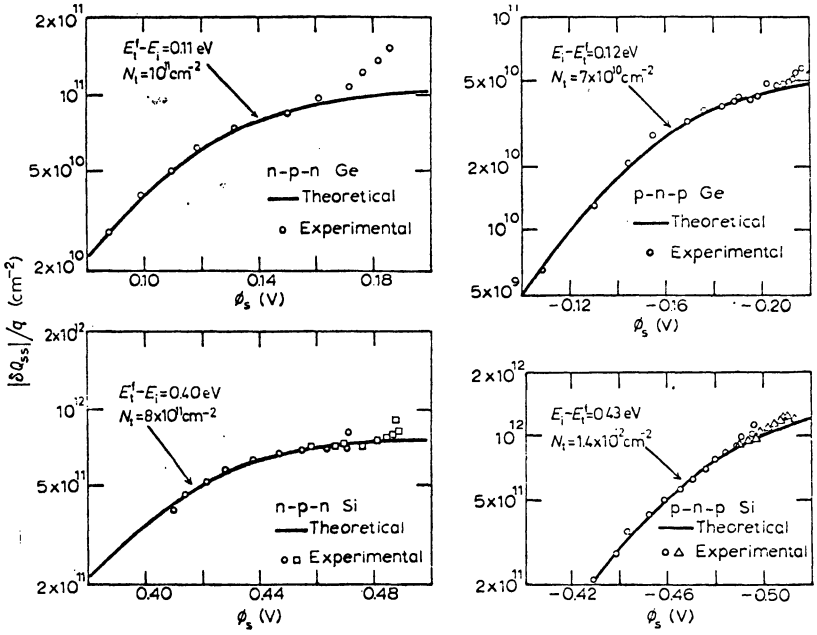

3.2 ϕ_S versus Φ (Reference 17)

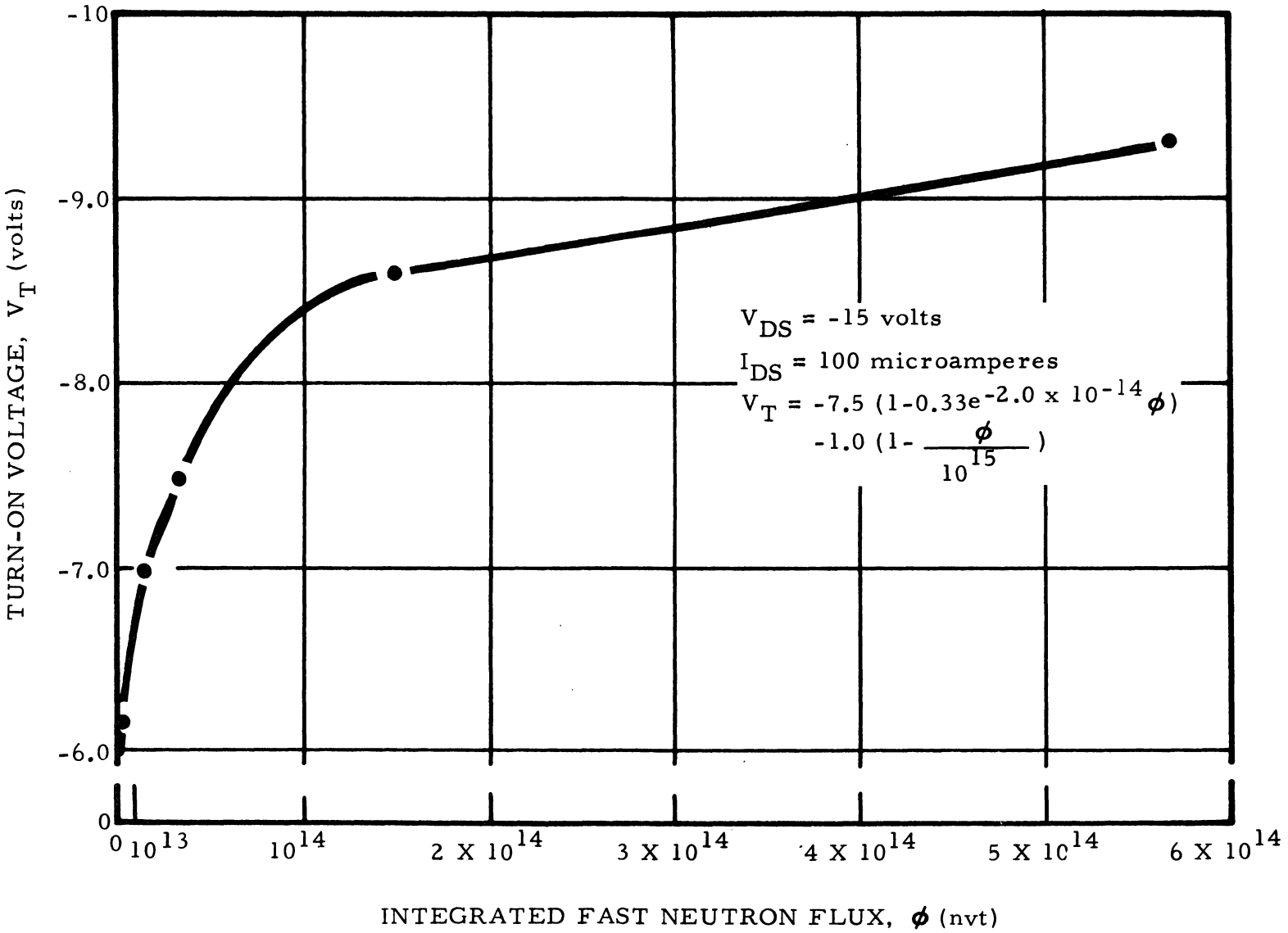

$$V_T \propto Q_{SS} \propto V_S \propto \phi_S$$

$$\phi_S = \frac{qV_S}{kT}$$

4. Carrier Mobility (Reference 18)

4.1 $\mu = \mu_o - \Phi \, d\mu/d\phi$

4.2 $d\mu/d\phi$ is a function of Φ

IV DEPENDENCE OF CURRENT GAIN ON FLUENCE

A. CONTRIBUTIONS TO CURRENT GAIN AND MINORITY CARRIER LOSS

1. Description of Recombination Processes

1.1 Finite Emitter Current due to majority carriers

1.2 Recombination in emitter field region

1.3 Recombination on peripheral emitter surface

1.4 Bulk Recombination

1.5 Collector multiplication

2. $\alpha = \gamma \, \alpha_S \, \alpha_T \, \alpha^*$

$$\gamma = 1 - \epsilon_1$$
$$\alpha_S = 1 - \epsilon_2$$
$$\alpha_T = 1 - \epsilon_3$$
$$\alpha^* = 1 + \epsilon_4$$

3. $$\frac{1}{\beta} = \frac{1 - \alpha}{\alpha} = \epsilon_1 + \epsilon_2 + \epsilon_3 - \epsilon_4$$

4. $$\frac{1}{\beta} = \frac{S \, A_S}{D_p A(\sigma \coth \sigma W + \ln k/2W)} F'(Z) \quad \text{Surface Term}$$

$$+ K^{-\frac{1}{2}} (1 + n^2/8 + W^2/2L_p{}^2)$$

$$+ n/2K^{-\frac{1}{2}} \left(1 + \frac{n^2}{24} + \frac{W^2}{1L_p^2}\right) - 1 \quad \text{Bulk Recombination}$$

$+ \frac{j_{neo}}{j_{peo}} (1 + bI_E)$ Emitter Efficiency and Bulk Conductivity Modulation

$+ \frac{A}{I_E^{\frac{1}{2}}}$ Recombination in Base Emitter Field Region

5. Homogeneous Base Transistor (Reference 12)

$$\frac{1}{\beta} = \frac{SWA_s}{D_p A_e} g(Z) + \frac{\sigma_b W}{\sigma_e L_e} \left(1 + \frac{Z}{2}\right) + \frac{1}{2} \frac{W^2}{L_b^2} h(Z) + \frac{dI_{RE}}{dI_E}$$

6. Volume Recombination Dominant (Reference 8)

6.1 $$\frac{1}{\beta} = [\frac{1}{\sqrt{k}} (1 + \frac{n^2}{8} + \frac{W^2}{2L_p^2}) + \frac{n}{2\sqrt{k}} (1 + \frac{n^2}{24} + \frac{W^2}{6L_p^2})] - 1$$

6.2 $$\tau = K/\Phi$$

6.3 $$\frac{\beta^{-1} - \beta_i^{-1}}{\Phi} = (\frac{W^2}{2D_p K})(\frac{1}{\sqrt{k}} + \frac{n}{6\sqrt{k}})$$

6.4 $$\frac{W^2}{2D_p} = \frac{0.2[1 + (\frac{n}{2})^{4/3}]}{f_\alpha}$$

6.5 $$K = \frac{(\frac{1}{\sqrt{k}} + \frac{n}{6\sqrt{k}})[1 + (\frac{n}{2})^{4/3}]\Phi}{f\alpha(\beta^{-1} - \beta_i^{-1})}$$

$$= \frac{0.2F(n)\Phi}{f_\alpha(\beta^{-1} - \beta_i^{-1})}$$

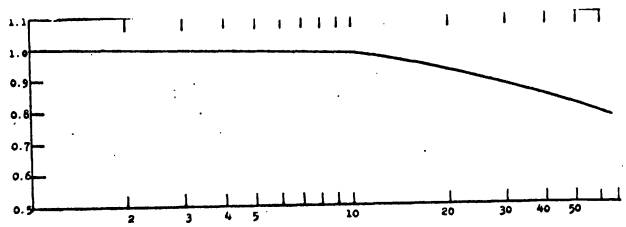

Fig. 1. $F(n)$ as a function of k.

6.6 $$\frac{1}{\beta} = \frac{1}{\beta_i} + \frac{0.2\Phi}{f_\alpha K}$$

6.7 $f_\alpha^* = \alpha_o K_B f_t^*$ (Reference 19)

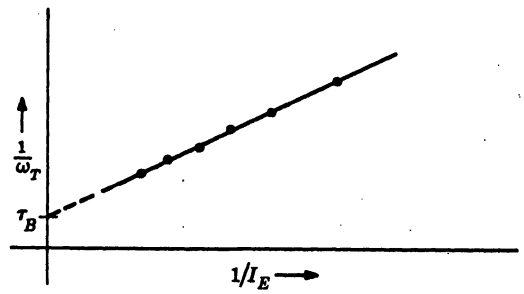

7. Surface Recombination Dominant

7.1 $$\frac{1}{\beta} = \frac{1}{\beta_i} + \frac{A_S\ S(\Phi)}{D_p A\ (\sigma \coth \sigma W + \ln K/2W}$$

7.2 $$\Delta\frac{1}{\beta} = \frac{W\ A_S}{D_p\ A} \quad \frac{\partial S}{\partial \phi}\ \Phi$$ Homogeneous Base

7.3 (Reference 20)

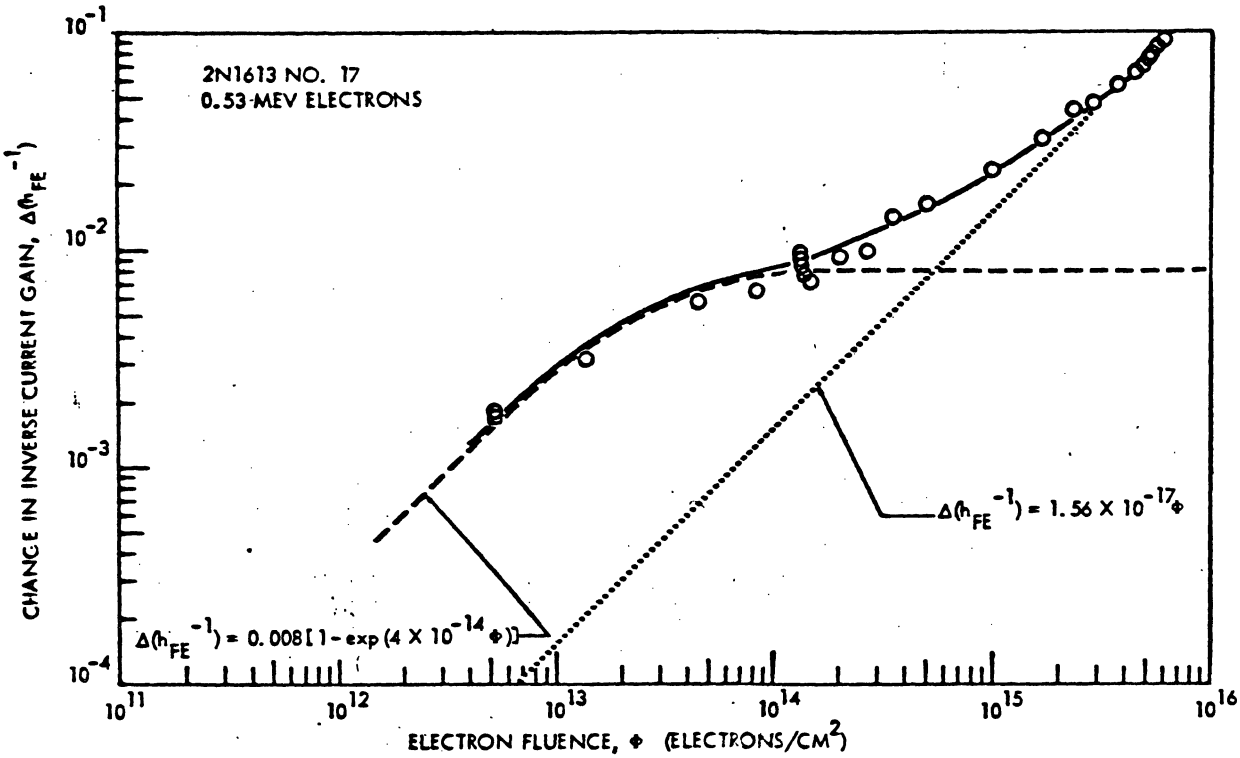

V ENVIRONMENTS

A. NEUTRONS

1. Clusters (Reference 21)

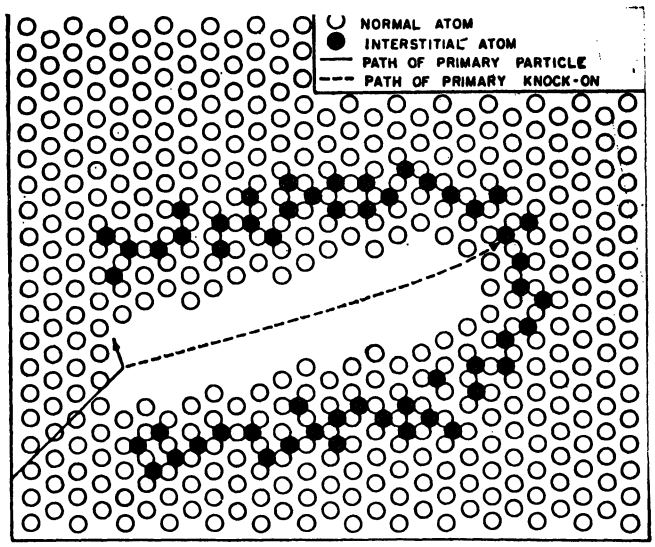

1.1 Carrier Removal

1.2 Two Recombination Centers

1.3 Hard Sphere Scattering

2. Fast Annealing (Reference 22)

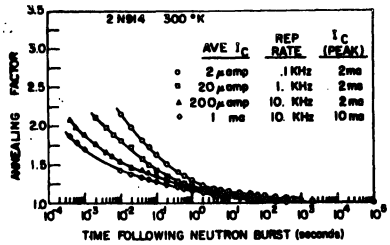

Curves of Annealing Factor Versus Time for a 2N914 Transistor, at 300°K, Comparing Different Injection Levels for the Same Temperature

3. Slow Annealing (Reference 23)

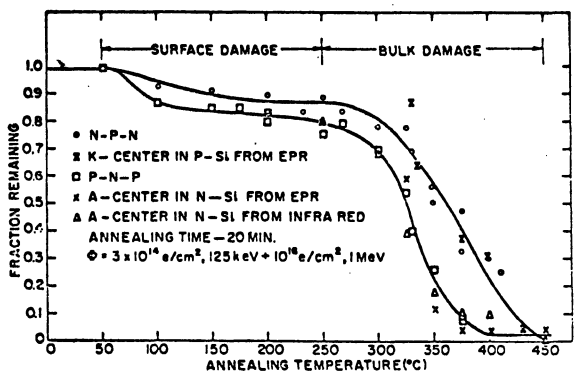

Isochronal annealing curves for base-current recovery (I_c = 1 ma) of 2N2102 n-p-n and 2N1132 p-n-p transistors damaged with 125 keV electrons followed by 1 MeV electrons. Curves compared with data from annealing of A and K-centers in bulk silicon from refs. 25 and 26.

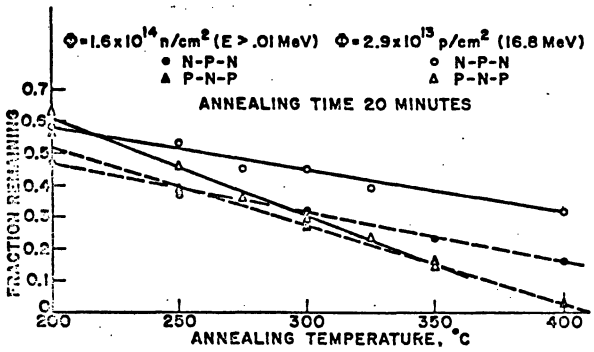

Isochronal annealing curves for base-current recovery (I_c = 1 ma) of 2N2102 n-p-n and 2N1132 p-n-p transistors damaged with 125 keV electrons followed by either 16.8 MeV protons or reactor neutrons.

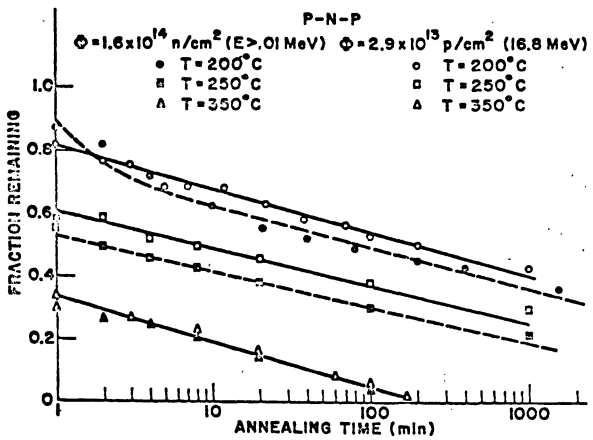

Isothermal annealing curves for base-current recovery (I_c = 1 ma) of 2N1132 p-n-p transistors damaged with 125 keV electrons followed by either 16.8 MeV protons or reactor neutrons.

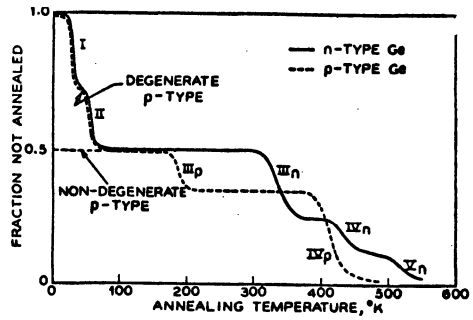

— Schematic diagram of the stages of annealing in germanium.

B. PROTONS

1. Clusters and Point Defects

2. Rutherford Scattering

C. ELECTRONS

1. Major Surface Effect in Space Environments

2. Rutherford Scattering and Point Defects

D. GAMMA'S

1. Create High Energy Electron by Compton Scattering

2. Rutherford Scattering and Uniform Point Defects

E. MIXED ENVIRONMENT

F. BULK DAMAGE EQUIVALENCE (Reference 20)

Particle-Type Displacement Equivalences, $\Delta(h_{FE}^{-1})$

Particle Type and Energy	Alpha Particle (5 Mev)	Proton (1 Mev)	Neutron (Reactor Spectrum)	Electron (1 Mev)	Gamma Ray (Co^{60})
Alpha Particle (5 Mev)	1	3.5	1.4×10^{2}	$*7 \times 10^{3}$	1.5×10^{5}
Proton (1 Mev)	2.9×10^{-1}	1	4×10^{1}	$*2 \times 10^{3}$	4.3×10^{4}
Neutron (Reactor)	7.1×10^{-3}	2.5×10^{-2}	1	$*5 \times 10^{1}$	1.1×10^{3}
Electron (1 Mev)	$*1.4 \times 10^{-4}$	$*5 \times 10^{-4}$	$*2.0 \times 10^{-2}$	1	$*2.2 \times 10^{1}$
Gamma Ray (Co^{60})	6.7×10^{-6}	2.3×10^{-5}	9.1×10^{-4}	$*4.5 \times 10^{-2}$	1

*Transistor cans of 0.17 gm cm^{-2}.

VI DEPENDENCE OF DAMAGE CONSTANT ON RESISTIVITY, INJECTION LEVEL AND TEMPERATURE (Reference 24)

A. RETURN TO $\Delta\frac{1}{\beta} = \frac{0.2\ \phi}{f_\alpha K}$ where $K = K(\rho, \frac{\delta_n}{n}, T)$

B. RECOMBINATION THROUGH A CENTER IN THE FORBIDDEN BAND

1. $$\tau = \frac{K}{\phi} = \frac{\tau_{no}(p_o + p_1 + \Delta n) + \tau_{po}(n_o + n_1 + \Delta n)}{(p_o + n_o + \Delta n)}$$

2. Let $\tau_{no} = \frac{1}{C_n R \phi}$ and $\tau_{po} = \frac{1}{C_p R \Phi}$

3. $$K = \frac{1}{C_n R}\ \frac{p_o + p_1 + \delta_n}{p_o + n_o + \delta_n} + \frac{1}{C_p R}\ \frac{n_o + n_1 + \delta_n}{p_o + n_o + \delta_n}$$

C. TWO LEVEL MODEL

1. $\frac{1}{\tau} = \frac{\Phi}{K} = \frac{1}{\tau_1} + \frac{1}{\tau_2}$

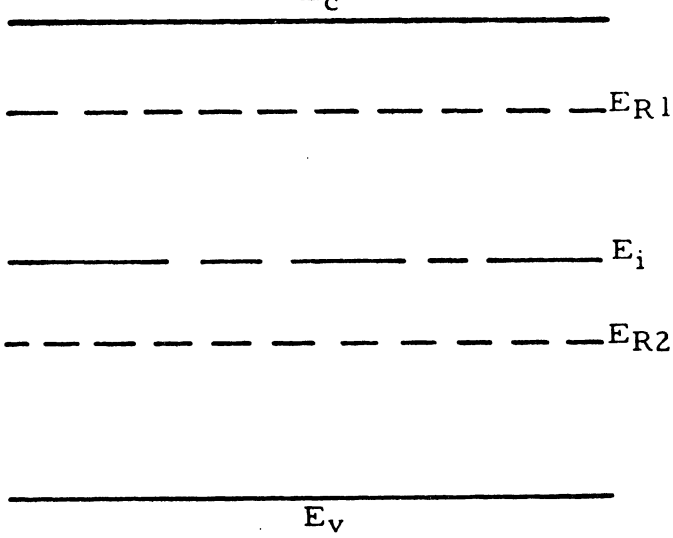

2. $$\frac{1}{K} = \frac{1}{\frac{1}{C_{p1}R_1}\left(\frac{n_0 + n_1 + \delta_n}{n_0 + p_0 + \delta_n}\right) + \frac{1}{C_{n1}R_1}\frac{(p_0 + p_1 + \delta_n)}{(n_0 + p_0 + \delta_n)}}$$

$$+ \frac{1}{\frac{1}{C_{p2}R_2}\left(\frac{n_0 + n_2 + \delta_n}{n_0 + p_0 + \delta_n}\right) + \frac{1}{C_{n2}R_2}\frac{(p_0 + p_2 + \delta_n)}{(n_0 + p_0 + \delta_n)}}$$

3. $$\frac{1}{K_H} = \frac{C_{n1}R_1}{\frac{C_{n1}}{C_{p1}}+1} + \frac{C_{p2}R_2}{\frac{C_{p2}}{C_{n2}}+1}$$

4. $$\frac{1}{K_{LN}} = \frac{C_{p1}R_1}{1+\frac{n_1}{n_0}} + \frac{C_{p2}R_2}{1+\frac{C_{p2}}{C_{n2}}\frac{p_2}{n_0}}$$

5. $$\frac{1}{K_{LP}} = \frac{C_{n1}R_1}{1+\frac{C_{n1}}{C_{p1}}\frac{n_1}{p_0}} + \frac{C_{n2}R_2}{1+\frac{p_2}{p_0}}$$

6. Dependence on injection level

$$\frac{1}{K_p} = \frac{C_{n1}R_1}{1 + \frac{C_{n1}}{C_{p1}}\left(\frac{n_1 + \delta_n}{p_o + \delta_n}\right)}$$

$$+ \frac{C_{p2}R_2}{\frac{\delta_n}{p_o+\delta_n} + \frac{C_{p2}}{C_{n2}}\left(\frac{p_o + p_2 + \delta_n}{p_o + \delta_n}\right)}$$

7. Temperature Dependence

7.1 $$n_1 = AT^{3/2} \exp-(E_c - E_1)/kT$$

$$P_2 = BT^{3/2} \exp-(E_2 - E_v)/kT \quad .$$

7.2

$$\frac{1}{K_N} = \frac{C_{p1}R_1}{\frac{C_{p1}}{C_{n1}}\left(\frac{\delta n}{n_o + \delta_n}\right) + 1 + \left(\frac{n_o}{n_o + \delta_n}\right)\left(\frac{n_1}{n_o}\right)_{T_1}\left(\frac{T}{T_1}\right)^{3/2}\exp\left[38.6\left(1 - \frac{T_1}{T}\right)\Delta E_1\right]}$$

$$+ \frac{C_{n2}R_2}{\frac{C_{n2}}{C_{p2}} + \frac{\delta n}{n_o + \delta_n} + \left(\frac{n_o}{n_o + \delta n}\right)\left(\frac{p_2}{n_o}\right)_{T_1}\left(\frac{T}{T_1}\right)^{3/2}\exp\left[38.6\left(1 - \frac{T_1}{T}\right)\Delta E_2\right]}$$

8. Low Temperature Assymptote

$$\frac{1}{K_n^{**}} = \frac{C_{p1}R_1}{\frac{C_{p1}}{C_{n1}}\left(\frac{\delta n}{no + \delta n}\right) + 1} + \frac{C_{n2}R_2}{\frac{C_{n2}}{C_{p2}} + \frac{\delta n}{no + \delta n}}$$

9. Calculated Curves

9.1

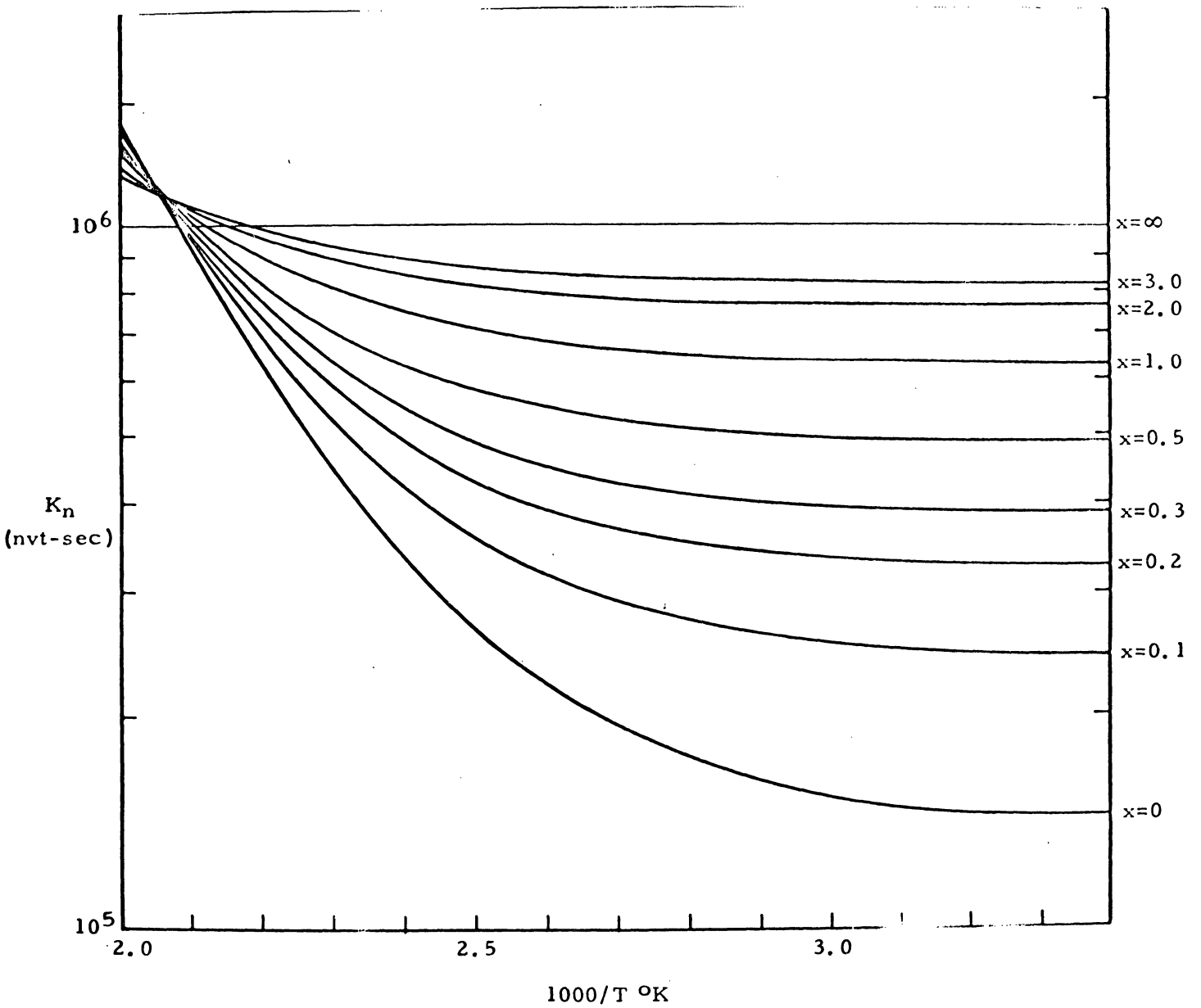

9.2

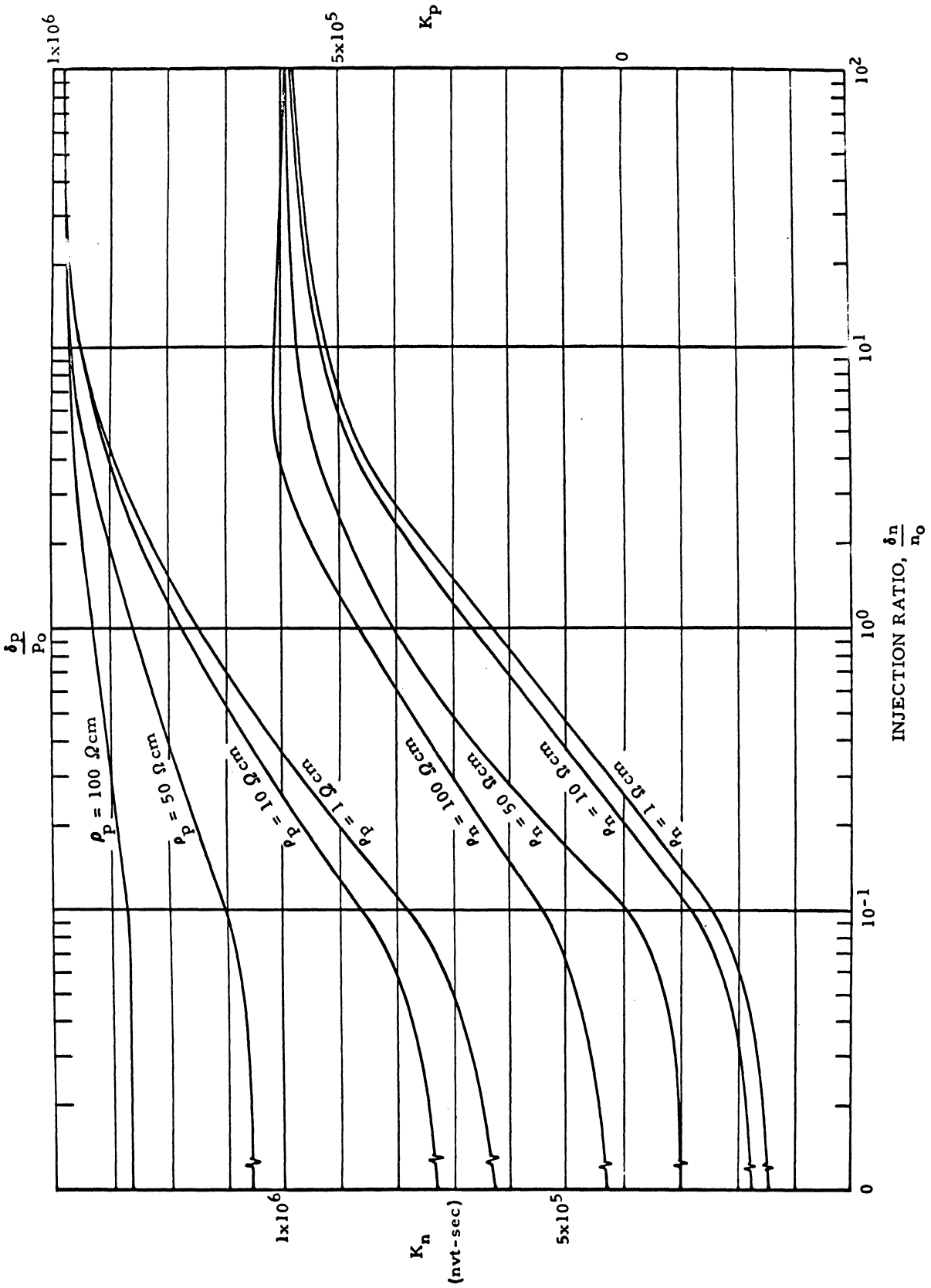
$\frac{\delta p}{p_o}$
K_p
K_n (nvt-sec)
INJECTION RATIO, $\frac{\delta n}{n_o}$
ρ_p = 100 Ωcm
ρ_p = 50 Ωcm
ρ_p = 10 Ωcm
ρ_p = 1 Ωcm
ρ_n = 100 Ωcm
ρ_n = 50 Ωcm
ρ_n = 10 Ωcm
ρ_n = 1 Ωcm
1x10^6
5x10^5
0
10^2
10^1
10^0
10^-1

10. Silicon Constants

$$R_1C_{p1} = 0.37 \times 10^{-6} \text{ (sec-n/cm}^2\text{)}^{-1}$$

$$R_1C_{n1} = 0.40 \times 10^{-5} \text{ (sec-n/cm}^2\text{)}^{-1}$$

$$R_2C_{p2} = 0.68 \times 10^{-5} \text{ (sec-n/cm}^2\text{)}^{-1}$$

$$R_2C_{n2} = 0.76 \times 10^{-6} \text{ (sec-n/cm}^2\text{)}^{-1}$$

$$n_1 = 2.0 \times 10^{14} \text{ cm}^{-3}$$

$$p_2 = 1.3 \times 10^{13} \text{ cm}^{-3}$$

$$K_{LN} = \frac{1.4 + 8.6 \cdot 10^{-2}\rho + 1.2 \cdot 10^{-3}\rho^2}{1 + 3.8 \cdot 10^{-2}\rho}$$

$$K_{LP} = \frac{2.1 + 0.18\rho + 9.0 \cdot 10^{-5}\rho^2}{1 + 1.4 \cdot 10^{-2}\rho}$$

11. Germanium Constants

$$R_1C_{p1} = 4.4 \times 10^{-8}$$

$$R_2C_{p2} = 92 \times 10^{-8}$$

$$R_1C_{N1} = 35 \times 10^{-8}$$

$$R_2C_{N2} = 0.9 \times 10^{-8}$$

$$E_1 = 0.28 \text{ ev}$$

$$E_2 = 0.32 \text{ ev}$$

VII DEPENDENCE OF DAMAGE PROCESS ON RADIATION PARTICLE ENERGY (Reference 12 and 13)

A. NEUTRONS

1. Threshold Energy E_d 10 to 30 ev

2. Let $E_d = E_{p(MAX)} = \frac{4E_n Mm}{(M+m)^2} \approx \frac{4E_n}{A}$

$E_N \sim 200$ ev for silicon

3. Above 200 ev $N_D \alpha E_n$ up to $\approx$ 1 Mev then slowly saturates

4. As E_N increases, point defects give way to clusters. $\overline{E}_p = E_{p(MAX)}/2$

5. First order theory $N_d = \frac{N_A \sigma_d \phi E_{p(MAX)}}{4E_d}$ $E_p < E_i$

$$N_d = \frac{N_A \sigma_d \phi E_i}{2E_d} \quad E_p \geq E_i$$

$$N_d = N_A \sigma_d \phi \overline{\nu}$$

6. $\overline{n}(E) + \overline{\nu}(E) = E$

6.1 $\overline{n}(E)/E$ versus E_n

6.2 $\overline{\nu}(E)/E$ versus E_n

ENERGY GOING INTO ATOMIC PROCESSES AND NORMALIZED RECIPROCAL LIFETIME DAMAGE CONSTANT AS A FUNCTION OF INCIDENT NEUTRON ENERGY

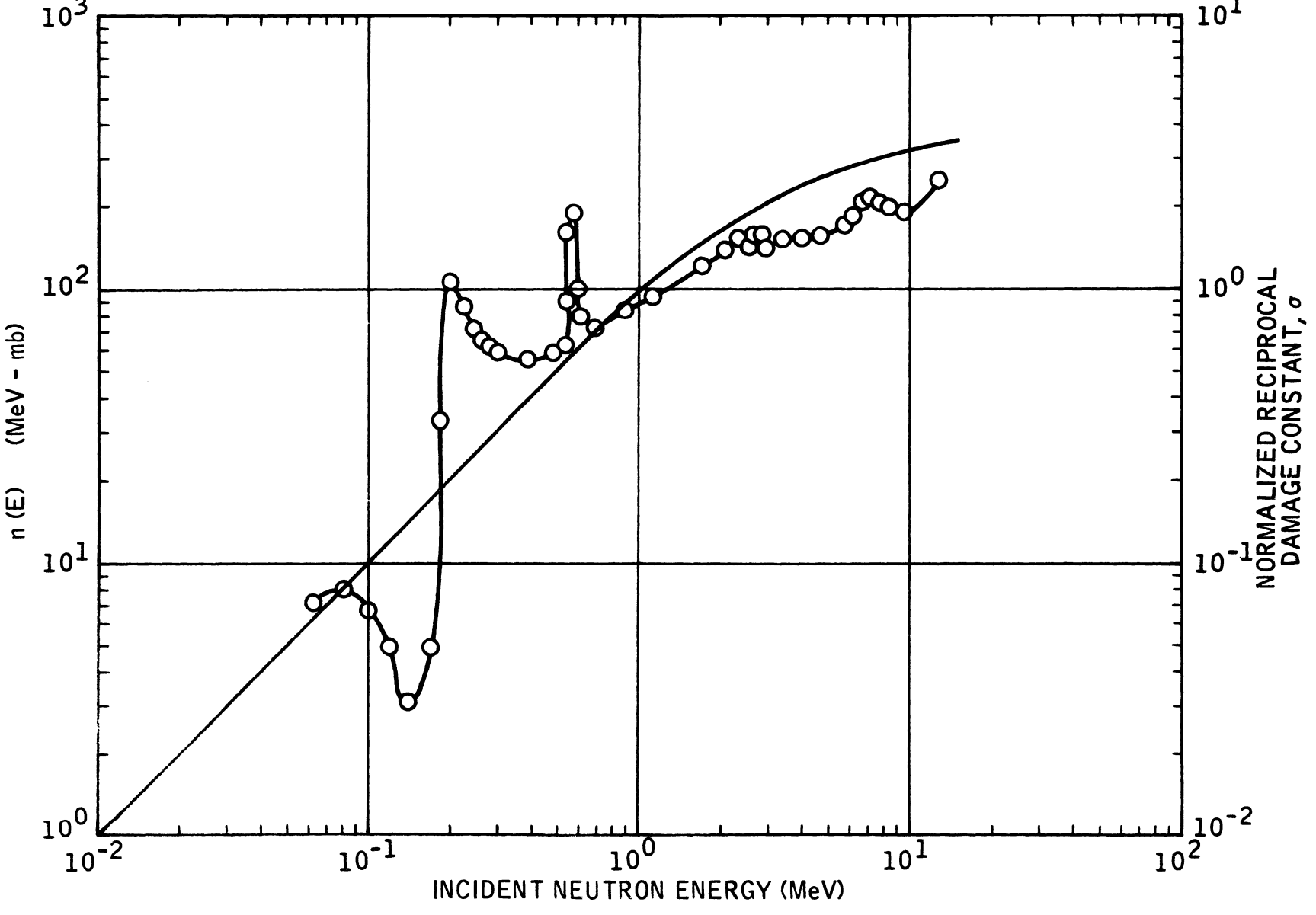

$\bar{\nu}$(E) vs NEUTRON ENERGY

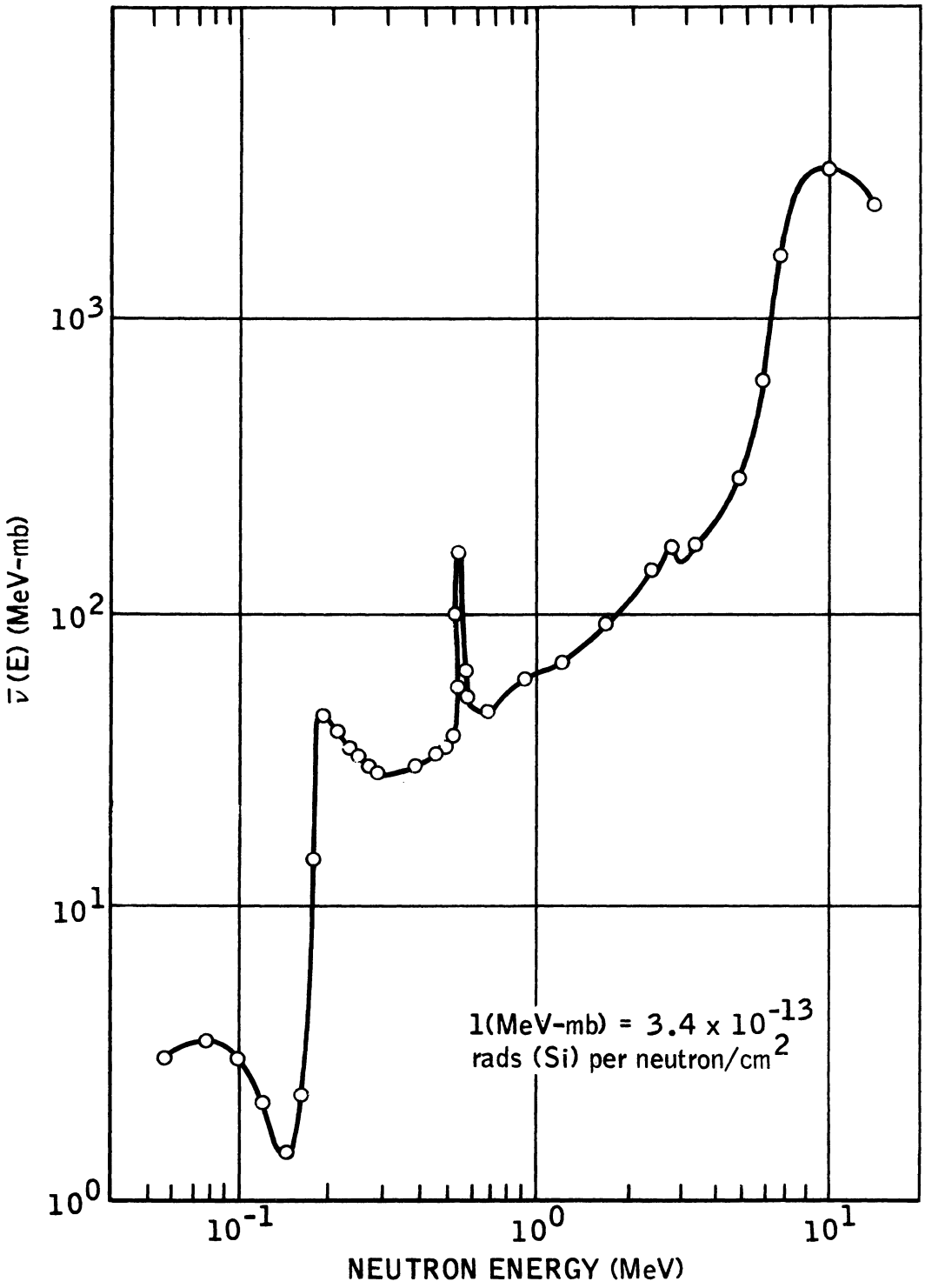

7. Assume N_R α to $\overline{n}(E)$

8. Neutron Spectra

$$K^{-1} = \sigma = \frac{\int_{0.01\ Mev}^{\infty} \sigma(E)N(E)dE}{\int_{0.01\ Mev}^{\infty} N(E)dE}$$

$$\sigma = aE_n(1 - e^{-A/E_n}).$$

$a = 1.02/MeV$ and $A = 3.6$ MeV

B. ELECTRONS

1. Threshold for Bulk Damage ~ 0.4 Mev

2. Necessity for relativistic correction

3. Rutherford Scattering

$$\overline{E}_p = E_d \ln E_{p(MAX)}/E_d$$

4. Point Defects

5. Differential cross section inversely proportional to electron energy (Reference 22)

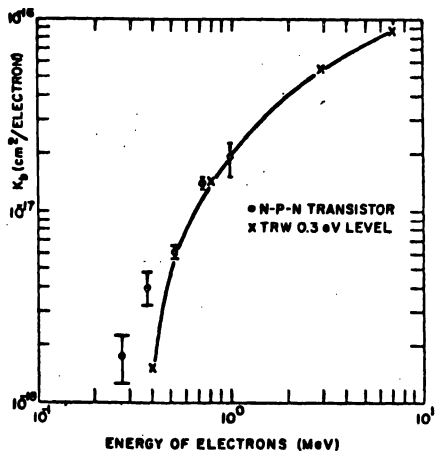

FIG. 4 Average value of the damage constant K_p versus electron energy for the 2N2102 n-p-n transistor. Results compared with energy dependence of damage introduction rate for the 0.3 eV energy level from reference 21.

7. Shielding

8. Gamma Radiation

C. PROTONS

1. Rutherford Scattering

2. Non-relativistic

3. Shielding

4. Energy dependence (Reference 20)

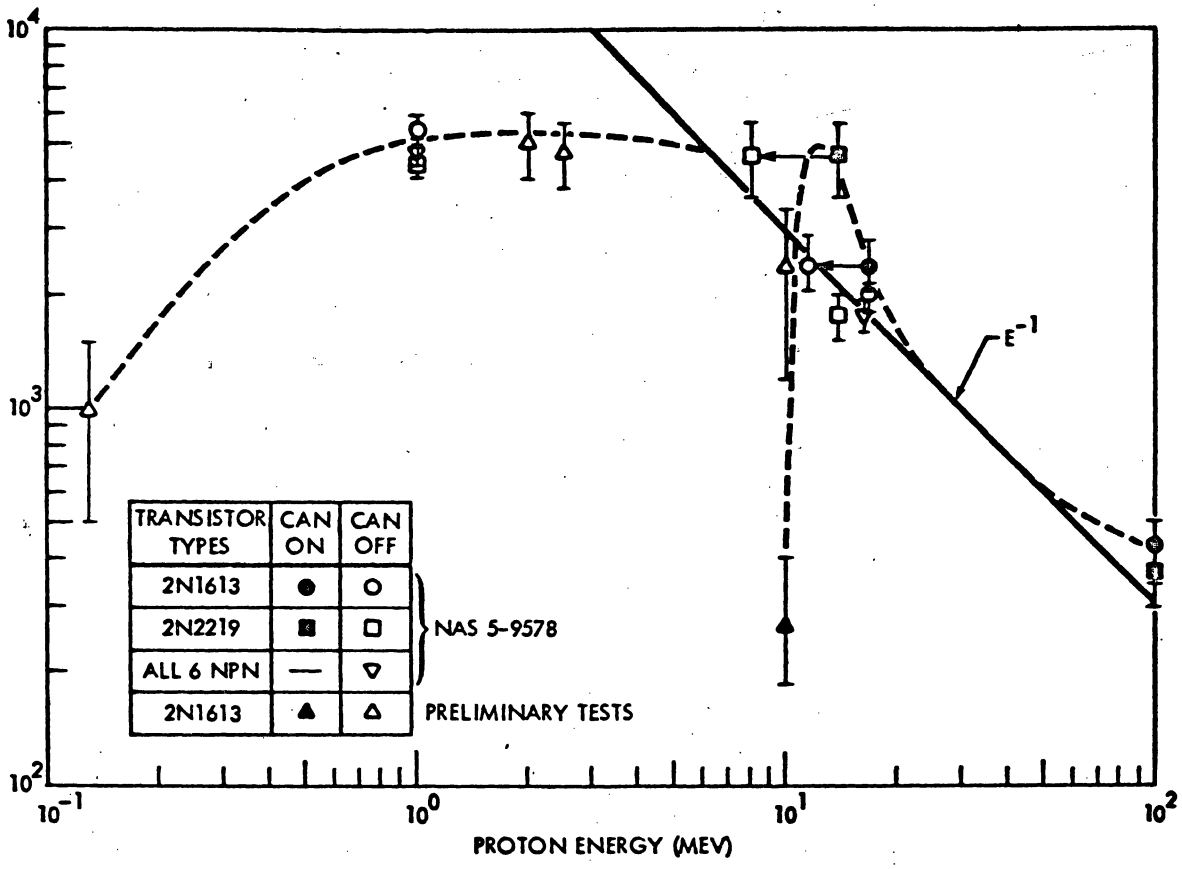

Proton Energy Dependence of Displacement Damage (npn Transistors)

D. IONIZATION

1. $\frac{\partial n}{\partial t} = g - R + \frac{1}{q}\frac{\partial J_n}{\partial t}$

$\frac{\partial p}{\partial t} = g - R - \frac{1}{q}\frac{\partial J_p}{\partial t}$

2. $R = \frac{n - n_o}{\tau_n}$, P-type material

$R = \frac{p - p_o}{\tau_p}$, N-type material

$R = \frac{pn - p_o n_o}{\tau_{p_o}(n+n_1) + \tau_{n_o}(p+p_1)}$

3. $g = k\dot{\gamma}$

3.1 Neutrons $\left[k \approx 4 \times 10^{13} \text{ eh p/cm}^3 \text{ rad(Si)}\right.$

3.2 Charged particle $\left.k \approx 10^{14} \text{ eh p/cm}^3 \text{ rad(Ge)}\right]$

4. $I_{drift} = qgAw_{sc}$ $\quad t \leq t_p$

$I_{diff} = qgAL \operatorname{erf}\left(\frac{t}{\tau}\right)^{1/2}$ $\quad t \leq t_p$

$I_{diff} = qgAL\left[\operatorname{erf}\left(\frac{t}{\tau}\right)^{1/2} - \operatorname{erf}\left(\frac{t - t_p}{\tau}\right)^{1/2}\right]$ $\quad t \geq t_p$

$I_{total} = qgA(w_{sc} + L_n + L_p)$.

5. $I_c = I_{cl} + \beta i_{pp\ effective}$

VII MICROCIRCUITS (Reference 13)

A. CLASSIFICATION SCHEME

1. Monolithic
   - 1.1 p-n junction isolated
   - 1.2 S_1O_2 isolated
2. Multiple chip
3. Compatible
4. Hybrid

B. PERMANENT DAMAGE EFFECTS

1. General
2. Gates
3. Flip-Flops
4. Amplifiers

C. IONIZATION EFFECTS

1. General
   - 1.1 p-n junction isolation
   - 1.2 Dielectric isolation
   - 1.3 Other
2. Gates
3. Flip-Flops
4. Amplifier

TABLE I DEVICES STUDIED

	Monolithic Diffused Active and Passive Devices. p-n junction isolation.	Multiple Chip Several interconnected chips containing diffused active and passive devices.	Compatible Diffused Active Devices with thin film passive devices. p-n junction isolation.	Monolithic Diffused Active and passive Devices. SiO_2 isolation	Hybrid Diffused Active devices with thin film interconnects and passive devices.
GATES	[1]MC-201G - 8 (units tested) [1]MC-201F - 3 " " [2]SE-115G - 2 " " [3]RC-1031 - 6 " " [4]PF-801T - 2 " " [4]PF-800T - 2 " "	[5]A7WA - 8 (units tested)	[8]A11 - 8 (units tested) [3]RC401 - 8 " "	[1]XC201-G - 8 (units tested) [9]RD111 - 2 (units tested) [8]WX-1 - 1 (unit tested)	[10]M8214 - 8 (units tested)
FLIP FLOPS	[1]MC209G - 2 " " [2]SE124K - 2 " " [3]SE124G - 6 " " [5]SN337A - 2 " "	[7]PC-8 - 8 " "	[8]A16 - 8 " "	Not available	[10]M8107 - 8 (units tested)
AMPLIFIERS	[1]MC1525G - 9 " " [2]SE500K - 2 " " [5]SN3514 - 2 " " [6]NM1024 - 3 " " [6]NM2002 - 2 " "	[7]PC-12 - 8 " "	[1]MC1527-G - 8 (units tested) [6]NM2021 - 8 (units tested)	[6]NM3401 - 8 (units tested)	[10]M8201 - 8 (units tested)

Note: The superscript before the device description refers to the following manufacturer:
[1]Motorola, [2]Signetics, [3]Raytheon, [4]Signetics, [5]Texas Instruments, [6]Norden, [7]General Instruments, [8]CBS, [9]Radiation Incorporated, [10]Varo.

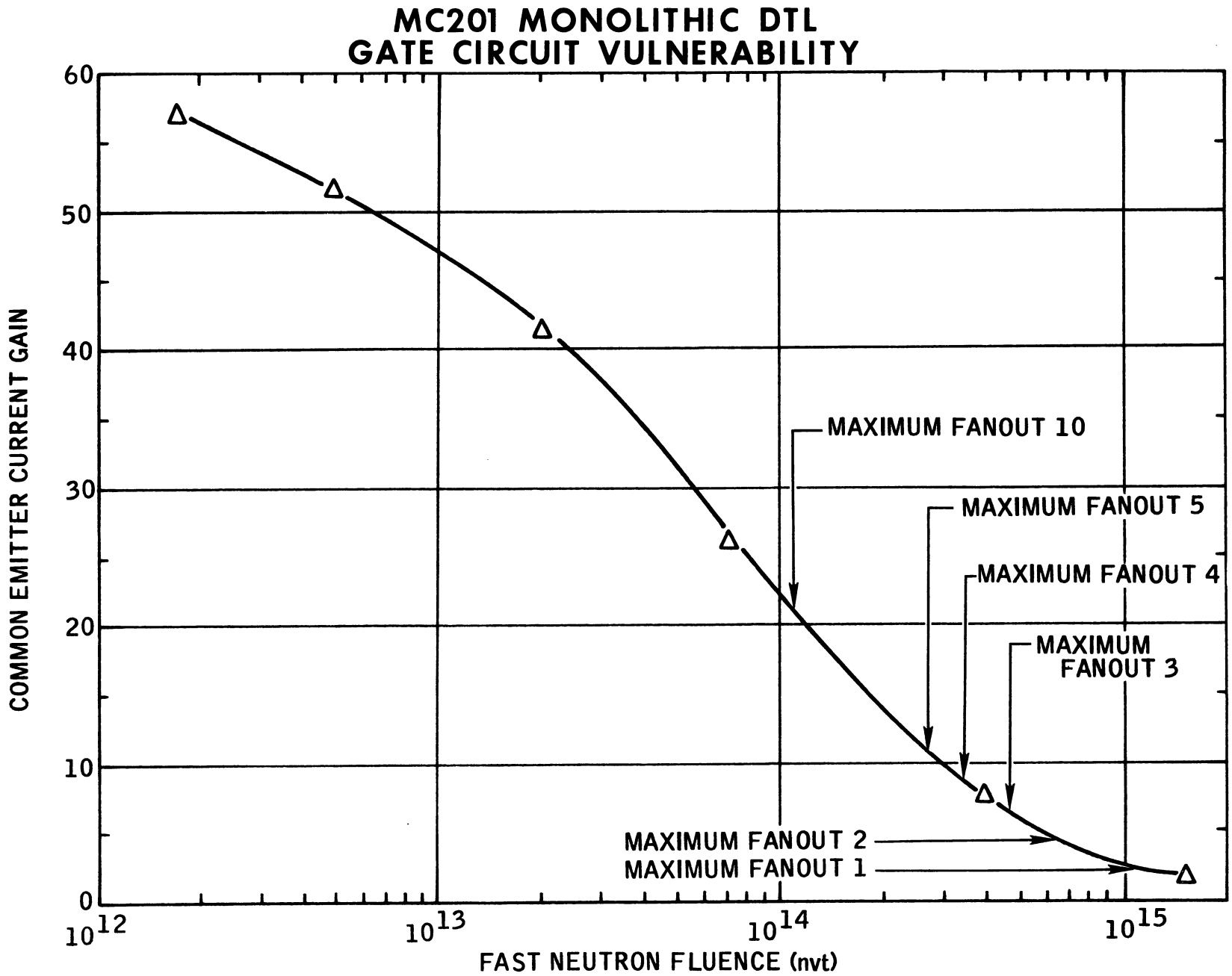
MC201 MONOLITHIC DTL
GATE CIRCUIT VULNERABILITY
COMMON EMITTER CURRENT GAIN
60
50
40
30
20
10
0
MAXIMUM FANOUT 10
MAXIMUM FANOUT 5
MAXIMUM FANOUT 4
MAXIMUM
FANOUT 3
MAXIMUM FANOUT 2
MAXIMUM FANOUT 1
10^{12}
10^{13}
10^{14}
10^{15}
FAST NEUTRON FLUENCE (nvt)

NEUTRON DEGRADATION OF SE124K-1 "OFF" VOLTAGE, SATURATION VOLTAGE AND MINIMUM PULSE AMPLITUDE TO SWITCH Q OUTPUT

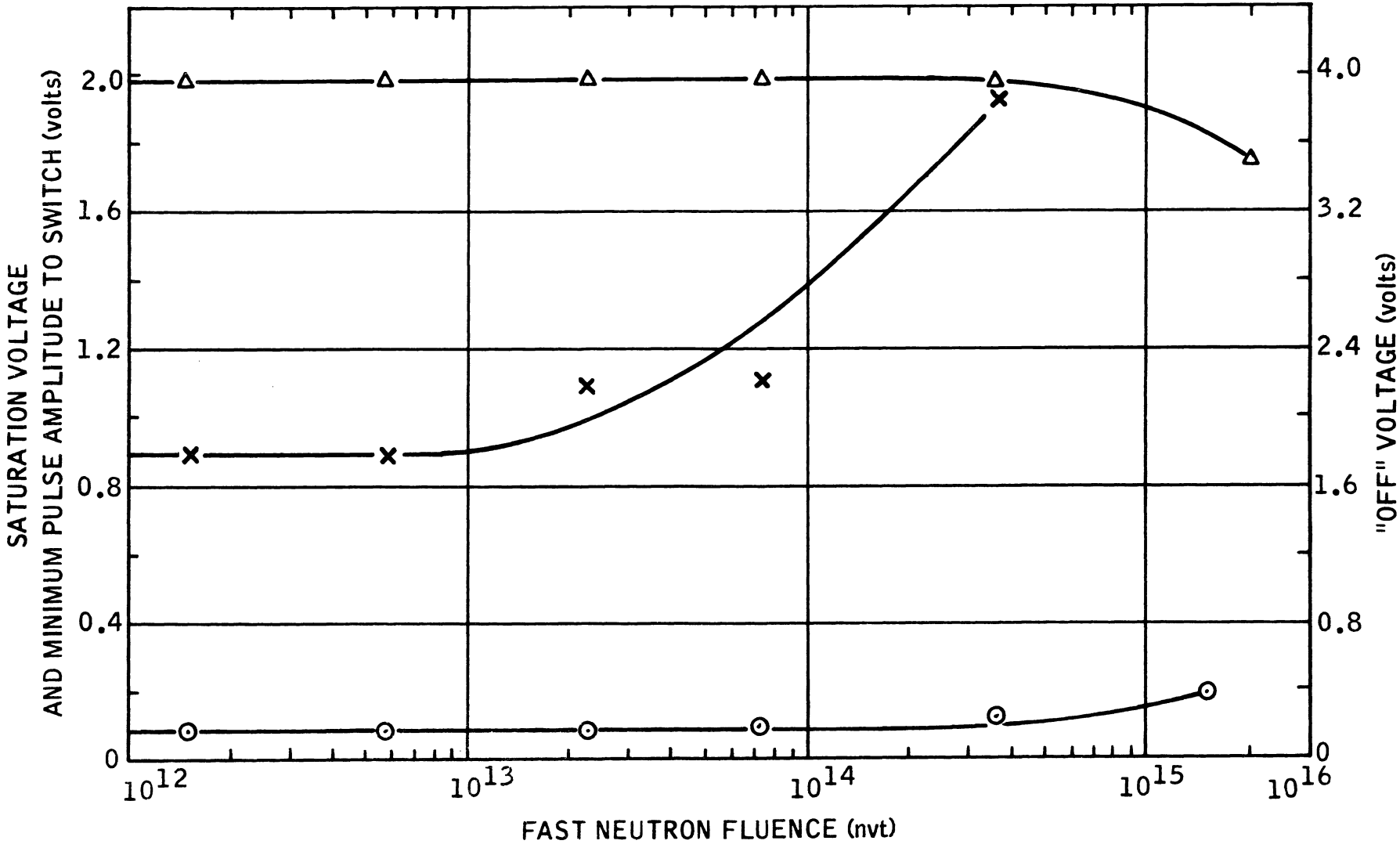

MC1525 GAIN vs NEUTRON DOSE

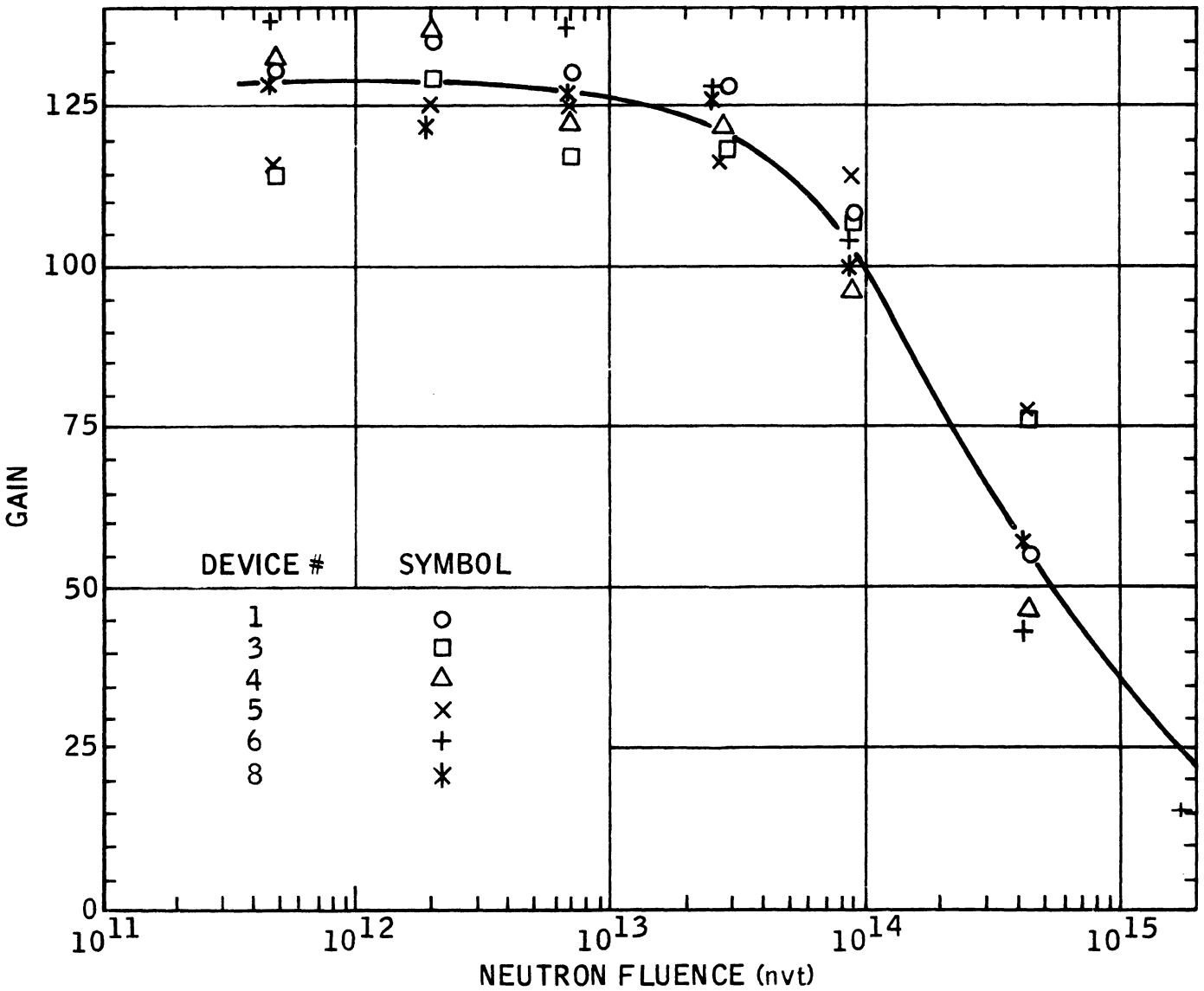

COMPARISON OF PHOTOCURRENTS AS A FUNCTION OF DOSE RATE IN A MICROCIRCUIT TRANSISTOR ELEMENT AND AN EQUIVALENT DISCRETE TRANSISTOR

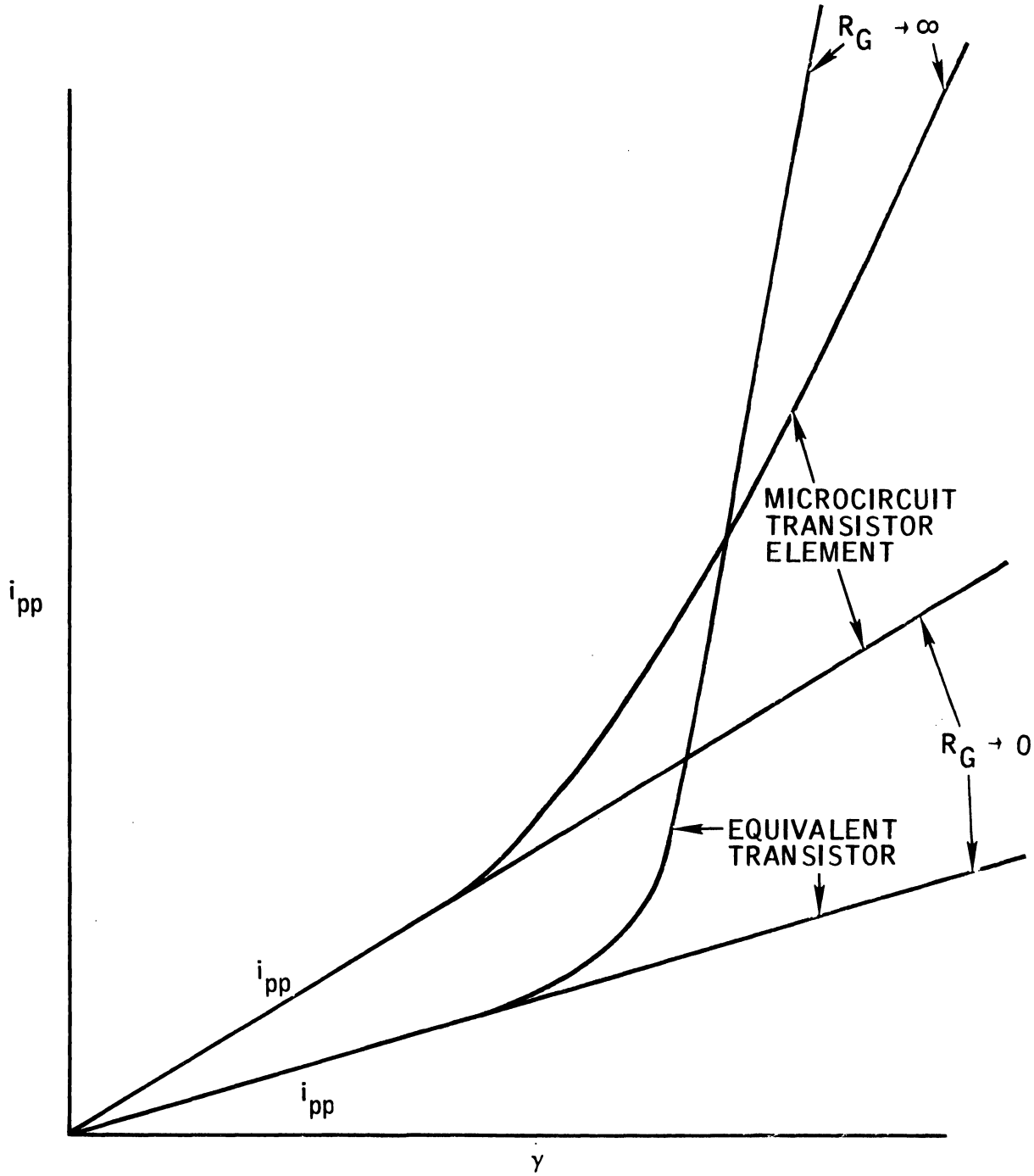

μL 945 RADIATION-INDUCED CHANGE-OF-STATE VULNERABILITY

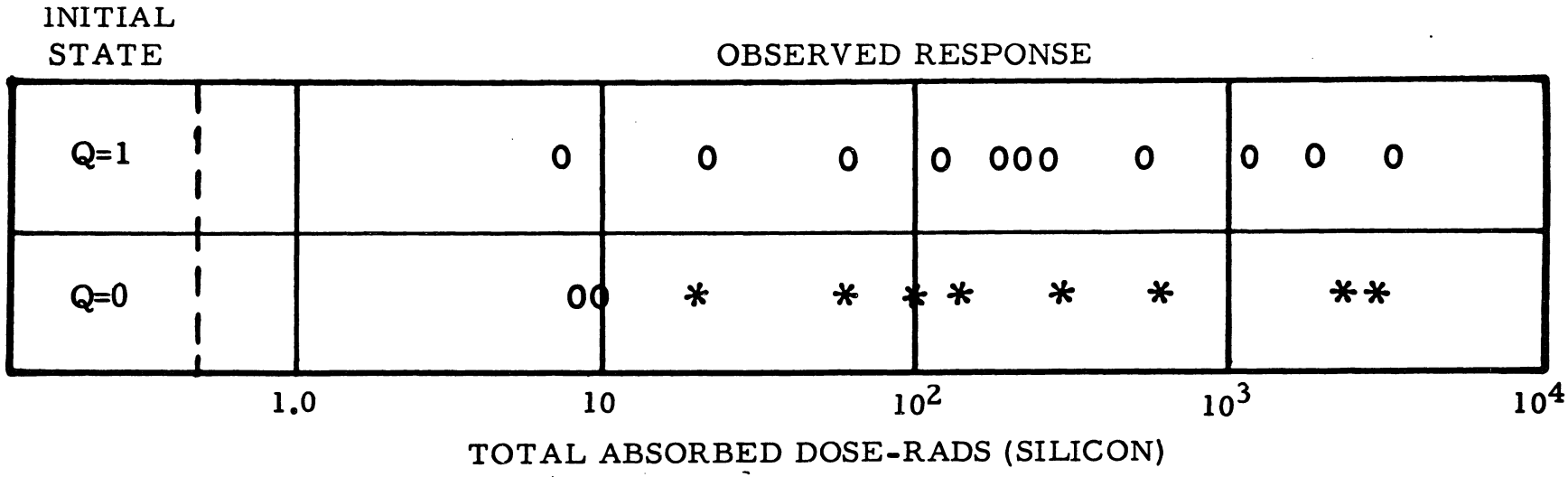

FSE 124 RADIATION-INDUCED CHANGE-OF-STATE VULNERABILITY

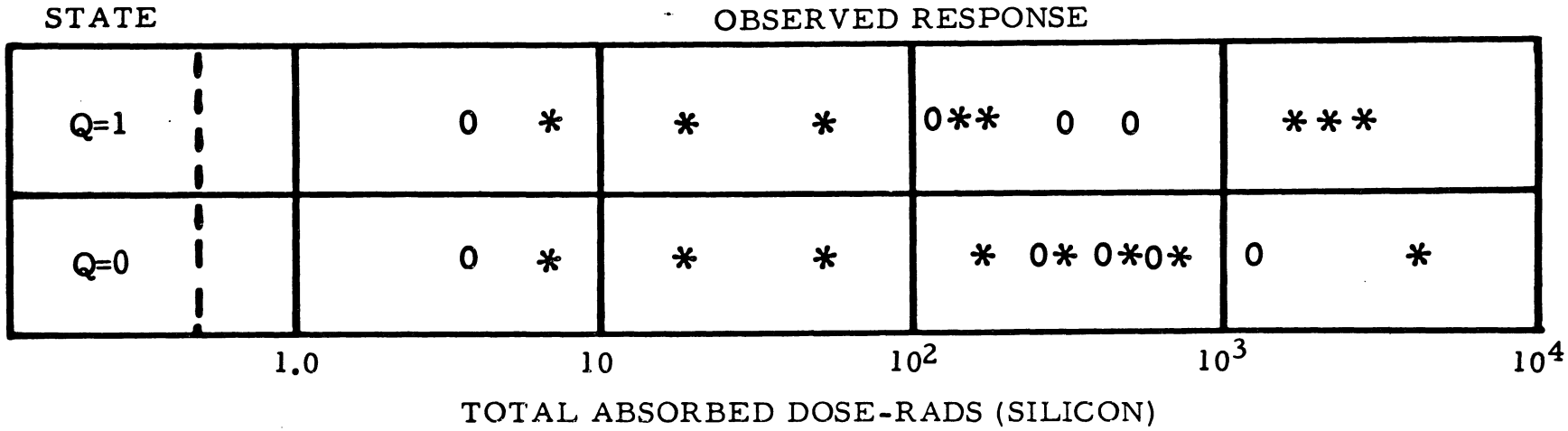

REFERENCES

1. "Integrated Circuits" R. Warner and J. Fordemwalt McGraw Hill, 1965 pp 88

2. Motorola Integrated Circuit Course (1964) Vol. II, Chapter 19 and pp 19-6

3. "Fundamentals of Semiconductor Devices" Lindmayer and Wrigley, D. Van Nostrand Co. 1966 p 143

4. "Electrons and Holes in Semiconductors" W. Shockley, Van Nostrand Co. Aug. 1956, Chapter 12

5. "Statistics of the Recombination of Holes and Electrons" W. Shockley and W. Read, Phys. Rev. Vol. 87, No. 5, Sept 1952 pp 835 - 842

6. "Silicon Semiconductor Technology" W. Runyan, McGraw Hill, 1965, pp 177

7. "Transistor Engineering" A. Phillips, McGraw Hill, 1962, Chapter 10

8. "Current Gain Degradation due to Displacement Damage for Graded Base Transistors" G. C. Messenger, Proc. IEEE, Mar 1967, p 413

9. "Carrier Generation and Recombination in P-N Junctions" C. Sah and R. Noyce, Proc. IRE, Sept 1957, pp 1228-1243

10. "Fundamentals of Semiconductor Devices" Lindmayer and Wrigley, D. Van Nostrand Co. 1966, p 241 and Chapter 7 Section 3

11. "The Effects of Neutron Irradiation on Germanium and Silicon" G. Messenger and J. Spratt, Proc. IRE June 1958, pp 1038-1044

12. "Displacement Damage in Silicon and Germanium Transistor" G. C. Messenger, IEEE Trans. on Nuc. Sci. NS-12, No. 2, April 1965

13. "Radiation Effects on Microcircuits" G. C. Messenger, IEEE Trans on Nucl Sci, NS-13, No. 6, pp 141-159

14. TREE Handbook, Battelle Memorial Institute, July 1966 Section E

15. "Radiation Damage to Solids" Billington and Crawford, Princeton Univ. Press, 1961, Chapter 7

16. "Surface Effects of Radiation on Semiconductor Devices" J. Mitchell and K. Wilson, BSTJ, January 1967, pp 1-80

17. "Displacement Damage in MOS Transistors" G. C. Messenger and E. J. Steele, IEEE Trans. on Nucl Sci, NS-12, No. 5, Oct 1965, pp 78-82

18. "Radiation Damage in Solids" Billington and Crawford Princeton Univ. Press, 1961, Section 9.9 pp 344-348

19. "Fundamentals of Semiconductor Devices" Lindmayer and Wrigley, D. Van Nostrand Co., 1966, pp 178.

20. "Energy Dependence ..... Semiconductor Devices" R. Brown Conf. on Radiation Effects on Semiconductor Devices, Toulouse, France, Mar 7-10, 1967.

21. "Disordered Regions in Semiconductors.... Neutrons" B. Gossick, JAP 30 p 1214 (1959)

22. "Correlation of Radiation Damage....." S. Brucker Conf. on Radiation Effects on Semiconductor Devices, Toulouse, France, Mar 7-10, 1967.

23. "Transient Annealing ....." H. Sander and B. Gregory, IEEE Trans. on Nuc. Sci., NS-13, No. 6, pp 53-62.

24. "A Two Level Model....." G. C. Messenger, Conf. on Radiation Effects on Semiconductor Devices, Toulouse, France, Mar 7-10, 1967.

25. "Semiconductor Surfaces" Many Goldstein and Grover, John Wiley, 1965

CURRENT GAIN DEGRADATION DUE TO DISPLACEMENT DAMAGE FOR GRADED BASE TRANSISTORS

George C. Messenger

Introduction

Current gain reduction for graded base transistors due to displacement damage has been discussed using homogeneous base design equations.[1] An effective basewidth

$$W^1 = \frac{W}{1 + \ln \frac{N_{DE}}{N_{DC}}}$$

was suggested as an appropriate first order correction factor to include the contribution of the built in field. A consequence of this assumption was that lifetime damage constant could be determined for both homogeneous and graded base transistors by measuring the change of reciprocal current gain as a function of flux and using the relationship

$$K = \frac{0.2\ \Phi}{f_\alpha(\beta^{-1} - \beta_i^{-1})} \quad .$$

An accurate expression for intrinsic current gain applicable to both homogeneous and graded base transistors will now be obtained. The difference between the radiation response of graded base and homogeneous base transistors will be discussed in this light. Using the same relationship to determine lifetime damage constant for both graded and homogeneous base transistor will be shown to permit a very good approximation.

Theoretical Development

At low frequencies the intrinsic transistor is described by[2]

$$I_e = a_{11}\ \psi_E - a_{12}\ \psi_C \qquad (1)$$

$$I_c = -a_{21}\ \psi_E + a_{22}\ \psi_C \ ,$$

where

$$\psi_{E,C} = e^{\frac{qV_{E,C}}{kT}} - 1 \ ,$$

$I_{E,C}$ are emitter and collector currents, $V_{E,C}$ are emitter and collector voltages and the a's are admittance matrix parameters. The matrix parameters are shown in Table I.

TABLE I

Functions of the Conductance Matrix Elements Applicable to Both Homogeneous Base and Graded Base Transistors

$\frac{a_{11}}{AD_p\, q\, p_n^o}$	$\sigma \coth \sigma W + \frac{n}{2W}$	$\frac{1 + \frac{W^2}{2L_p^2} + \frac{n}{2} + \frac{n^2}{8}}{W}$
$\frac{a_{12}}{AD_p\, q\, p_n^W}$	$\frac{\sigma \operatorname{csch} \sigma W}{\sqrt{k}}$	$\frac{1}{W\sqrt{k}} \left(1 + \frac{W^2}{6L_p^2} \quad \frac{n^2}{24}\right)$
$\frac{a_{21}}{AD_p\, q\, p_n^o}$	$\sqrt{k}\, \sigma \operatorname{csch} \sigma W$	$\frac{\sqrt{k}}{W} \left(1 + \frac{W^2}{6L_p^2} \quad \frac{n^2}{24}\right)$
$\frac{a_{22}}{AD_p\, q\, p_n^W}$	$\sigma \coth \sigma W - \frac{n}{2W}$	$\frac{1 + \frac{W^2}{2L_p^2} - \frac{n}{2} + \frac{n^2}{8}}{W}$

In Table I, $\sigma = \frac{1}{2}\sqrt{\left(\frac{n}{W}\right)^2 + \left(\frac{4}{L_p}\right)^2}$, $k = \frac{N_{DE}}{N_{DC}}$, $n = \ln k$, $L_p = \sqrt{D_p \tau}$, W is transistor base width, N_{DE} is donor density in the base near the emitter, N_{DC} is donor density in the base near the collector, L_p is hole diffusion length in the base, D_p is hole diffusion constant in the base, and τ is lifetime in the base. Current gain

$$\alpha = \frac{a_{21}}{a_{11}} = \frac{\beta}{1 + \beta} .$$

Using the expressions in Table I, an expression for $1/\beta$ can be obtained.

$$\frac{1}{\beta} = \left[\frac{1}{\sqrt{k}} \left(1 + \frac{n^2}{8} + \frac{W^2}{2L_p^2}\right) + \frac{n}{2\sqrt{k}} \left(1 + \frac{n^2}{24} + \frac{W^2}{6L_p^2}\right)\right] - 1 \qquad (2)$$

This expression applies for homogeneous base transistors ($k = 1$, $n = 0$) and graded base transistors ($k \approx 10$, $n \approx 2.3$).

Application to Displacement Damage

For a transistor whose base lifetime has been substantially degraded by displacement damage, $\tau = K/\Phi$ where K is lifetime damage constant and Φ is radiation fluence. Now,

$$\frac{(\beta^{-1} - \beta_i^{-1})}{\Phi} = \left(\frac{W^2}{2D_p K}\right)\left(\frac{1}{\sqrt{k}} + \left(\frac{n}{6\sqrt{k}}\right)\right) \tag{3}$$

Usually, $W^2/2D_p$ is calculated using a measured value of current gain cut-off frequency, f_α. An expression[3] applicable to both homogeneous and graded base transistors is,

$$\frac{W^2}{2D_p} = \frac{0.2\ [1 + (\frac{n}{2})^{\frac{4}{3}}]}{f_\alpha} \tag{4}$$

Therefore, for both homogeneous and graded base transistors, lifetime damage constant is given by

$$K = \frac{0.2\ (\frac{1}{\sqrt{k}} + \frac{n}{6\sqrt{k}})[1 + (\frac{n}{2})^{\frac{4}{3}}]\Phi}{f_\alpha\ (\beta^{-1} - \beta_i^{-1})} \tag{5}$$

$$= \frac{0.2\ F(n)\ \Phi}{f_\alpha\ (\beta^{-1} - \beta_i^{-1})}$$

The function $F(n)$ is unity for homogeneous base transistors as expected. The variation of $F(n)$ with k is shown in Figure 1. Notice that $F(n)$ is approximately unity for values of k up to ten and has only dropped to 0.72 for a k value of one hundred. Thus,

$$K = \frac{0.2\ \Phi}{f_\alpha\ (\beta^{-1} - \beta_i^{-1})}$$

is a valid approximation for graded base transistors.

Conclusion

An admittance matrix and a current gain expression valid for both homogeneous and graded base transistors in the radiation environment has been obtained. Examination of the determination of lifetime damage constant K from the rates of change of current gain with flux has shown that the relationship previously used for homogeneous base transistor can be extended to graded base transistors without appreciable error.

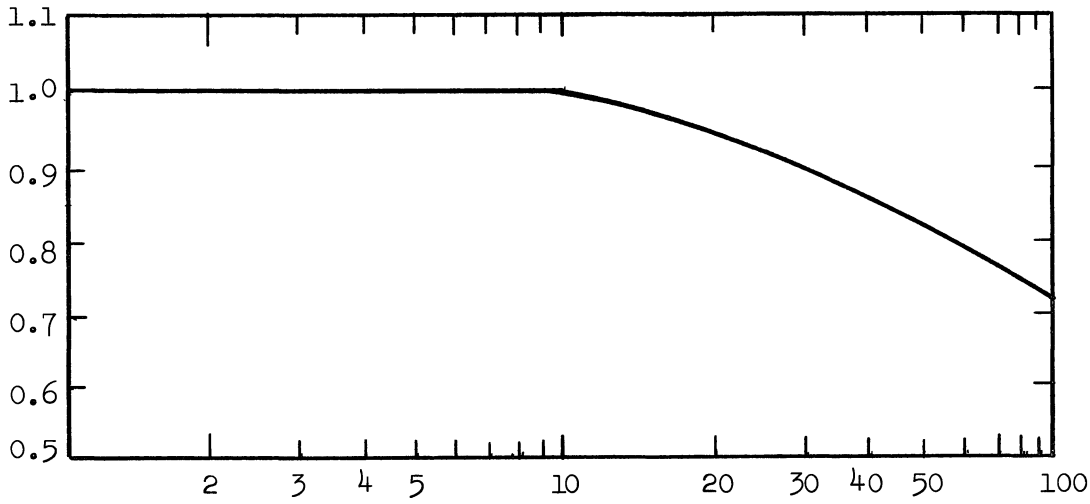

Figure 1. F(n) as a Function of k.

A TWO LEVEL MODEL FOR LIFETIME REDUCTION PROCESSES IN NEUTRON IRRADIATED SILICON

George C. Messenger

Introduction

A two level model for recombination processes in neutron irradiated bulk silicon and silicon devices is proposed. This model explains the large body of published experimental data much better than the previously used single level models.

Previous investigators have established that damage centers produced by fast neutrons are complicated defect clusters which give rise to a number of energy levels within the forbidden band[1,2,3].

Recombination processes have usually been analyzed in terms of a single recombination level. The two levels most frequently discussed are at approximately 0.18 eV below the conduction band and 0.31 eV above the valence band[4,5]; although other levels have been occasionally mentioned.

Curtis[4] has recently shown that lifetime degradation does not depend on the type of dopant or the oxygen concentration; further, damage constant vs resistivity curves do not obey the single one-level Hall-Schockley Read theory.

The two level model will be developed by assuming that the net effect of all the levels in the upper half of the band can be approximated by a single level and, similarly, all the levels in the lower half of the band can be approximated by another discrete level. In keeping with the experimental results, these levels are assumed to be independent of dopant and oxygen concentration and therefore must operate simultaneously in both p- and n-type material. They will be assumed to act independently so that reciprocal lifetimes are additive.

The statistical data recently reported by Curtis is used to determine the constants of these two "average" recombination centers. A level is found 0.265 eV below the conduction band and another level 0.31 eV above the valence band. Previously an 0.265 eV level has been observed from photoconductivity measurements[1]; it has not been determined from recombination measurements. It therefore, seems likely that this is an "average" level which in effect integrates the contribution of several levels in the upper half of the band. Several experimenters have attributed recombination effects to a level 0.31 eV above the valence load, and this level has been found in photoconductivity measurements. It seems probable that this is a dominant discrete level, even in the highly disordered cluster region.

Calculated curves of lifetime damage constant as a function of resistivity, temperature and injection levels for the two level model are presented. The higher values of damage constant deduced by device experiments as compared to those found by material experiments are adequately explained by the variation of lifetime damage constant with injection level.

Development of the Two Level Model

If the reciprocal lifetime after irradiation $\frac{1}{\tau}$ is used to define a lifetime damage constant K, resulting from two recombination centers

$$\frac{1}{\tau} = \frac{\Phi}{K} = \frac{1}{\tau_1} + \frac{1}{\tau_2} \quad .$$

A straightforward application of Shockley-Read statistics[6] leads to a general formulation for the damage constant:

$$\frac{1}{K} = \frac{1}{\frac{1}{C_{p1}R_1}\left(\frac{n_o + n_1 + \delta_n}{n_o + p_o + \delta_n}\right) + \frac{1}{C_{n1}R_1}\left(\frac{p_o + p_1 + \delta_n}{n_o + p_o + \delta_n}\right)} + \frac{1}{\frac{1}{C_{p2}R_2}\left(\frac{n_o + n_2 + \delta_n}{n_o + p_o + \delta_n}\right) + \frac{1}{C_{n2}R_2}\left(\frac{p_o + p_2 + \delta_n}{n_o + p_o + \delta_n}\right)} \qquad (1)$$

Here n_o and p_o are the equilibrium electron and hole densities in the silicon n_1, p_1, n_2 and p_2 are electron and hole densities resulting if the Fermi level coincides with the recombination centers. Notice that the combined effects of injection level, resistivity and temperature are implicity contained in this expression.

Experimental Determination of the Constants

The variation of damage constant with resistivity at low injection levels has been measured by Curtis. Equation (1) simplifies to

$$\frac{1}{K_{LN}} = \frac{C_{p1}R_1}{1 + \frac{n_1}{n_o}} + \frac{C_{p2}R_2}{1 + \frac{C_{p2}}{C_{n2}}\frac{p_2}{n_o}} \qquad (2a)$$

$$\frac{1}{K_{LP}} = \frac{C_{n1}R_1}{1 + \frac{C_{n1}}{C_{p1}}\frac{n_1}{p_o}} + \frac{C_{n2}R_2}{1 + \frac{p_2}{p_o}} \qquad (2b)$$

for the low injection level case in n- and p-type silicon respectively. Figures 1 and 2 show Curtis' experimental data fitted to equations (2a) and (2b).

Values of the experimental constants determined by a least square analysis are shown in Table I.

Variation of Damage Constant with Resistivity and Injection Level

Using the experimentally determined constants, a plot of damage constant as a function of resistivity and injection level is made for both n- and p-type silicon in Figure 3.

Damage constant has an asymptotic value at very low resistivities and then tends to increase as resistivity increases. The maximum dependence on resistivity occurs at very low injection levels; at very high injection levels damage constant approaches 10^6 nvt-sec independent of resistivity. The low resistivity low injection level damage constant asymptote for n-type material is $(C_{p1}R_1 + C_{p2}R_2)^{-1}$ whereas the asymptote for p-type material is $(C_{n1}R_1 + C_{n2}R_2)^{-1}$. This is the source of the basic difference in damage constant for n- and p-type silicon material; p-type material is basically more resistant to neutron radiation damage.

Damage constant increases with increasing injection level for resistivities less than about 100 ohm cm. This includes most material of interest to device manufacturers. Experimenters have usually deduced lifetime damage constant on material samples by determining the degradation rate of low level lifetime with flux whereas device experimenters have measured the rate of current gain degradation with flux usually at injection ratios in the neighborhood of one. The higher values of damage constant consistently reported by device experimenters compared to material investigators are expected based on the increase in damage constant with injection level.

Variation of Damage Constant with Temperature

Temperature dependence is introduced explicitly in equation (1) by expanding n_1 and p_2. The resulting equations are normalized to room temperature yielding,

$$\frac{1}{K_P} = \frac{C_{p1}R_1}{\frac{C_{p1}}{C_{n1}} + \frac{\delta n}{p_o+\delta n} + \left(\frac{p_o}{p_o+\delta n}\right)\left(\frac{n_1}{p_o}\right)T_1 \left(\frac{T}{T_1}\right)^{3/2} \exp\left[38.6\left(1 - \frac{T_1}{T}\right)\Delta E_1\right]} \quad (3a)$$

$$+ \frac{C_{n2}R_2}{\frac{C_{n2}}{C_{p2}}\left(\frac{\delta n}{p_o+\delta_n}\right) + 1 + \left(\frac{p_o}{p_o+\delta_n}\right)\left(\frac{p_2}{p_o}\right)T_1 \left(\frac{T}{T_1}\right)^{3/2} \exp\left[38.6\left(1 - \frac{T_1}{T}\right)\Delta E_2\right]}$$

$$\frac{1}{K_N} = \frac{C_{p1}R_1}{\frac{C_{p1}}{C_{n1}}\left(\frac{\delta n}{n_o+\delta n}\right) + 1 + \left(\frac{n_o}{n_o+\delta n}\right)\left(\frac{n_1}{n_o}\right)T_1 \left(\frac{T}{T_1}\right)^{3/2} \exp\left[38.6\left(1 - \frac{T_1}{T}\right)\Delta E_1\right]} \quad (3b)$$

$$+ \frac{C_{n2}R_2}{\frac{C_{n2}}{C_{p2}} + \frac{\delta n}{n_o+\delta n} + \left(\frac{n_o}{n_o+\delta n}\right)\left(\frac{p_2}{n_o}\right)T_1 \left(\frac{T}{T_1}\right)^{3/2} \left[\exp 38.6\left(1 - \frac{T_1}{T}\right)\Delta E_2\right]}$$

These equations are relatively complicated. Therefore, a computer run was made at a number of different resistivities varying both temperature and injection level. A typical set of curves is shown in Figure 4 where K_N , and K_p are plotted against $\frac{1000}{T(°K)}$ for various resistivities and injection levels.

Several important characteristics are evident in these curves. As the injection level increases the value of K at low temperature increases and the value of K at high temperature decreases. The apparent slope decreases as a function of increasing injection level. Therefore, in experiments where the slope of this line is used to deduce an activation energy, one must be sure to consider the effect of injection level.

Substantially different values of energy levels result when experimental curves are fitted to a two level model rather than a one level model even after injection level effects are properly considered.

The variation of lifetime damage constant with temperature increases substantially as resistivity increases. At very low resistivities, lifetime damage constant becomes relatively independent of temperature in the temperature range from 250°K to 500°K.

Previously, data showing relatively constant values of lifetime below room temperature have been attributed to trapping effects. Equations (5a) and (5b) show that both a finite injection level and a second recombination center can cause this effect. It is instructive to examine the low level asymptote for several approximations*.

$$\frac{1}{K_n^{**}} = \frac{C_{p1}R_1}{\frac{C_{p1}}{C_{n1}}\left(\frac{\delta n}{no+\delta n}\right)+1} + \frac{C_{n2}R_2}{\frac{C_{n2}}{C_{p2}}+\frac{\delta n}{no+\delta n}} \qquad \text{(no approximations} \qquad (4a)$$

$$\frac{1}{K_n^{**}} = C_{p1}R_1 + C_{p2}R_2 \qquad \left(\frac{\delta n}{no} = 0\right) \qquad (4b)$$

$$\frac{1}{K_n^{**}} = \frac{C_{p1}R_1}{1+\frac{C_{p1}}{C_{n1}}\left(\frac{\delta n}{no+\delta n}\right)} \qquad \text{(one level model)} \qquad (4c)$$

$$\frac{1}{K_n^{**}} = C_{p1}R_1 \qquad \text{(one level model and } \frac{\delta n}{no} = 0) \qquad (4d)$$

Experimental Verification

The two level model has been used to compare experimental and calculated results for low level lifetime vs. temperature on a number of different samples. The agreement is generally good and reflects the same degree of scatter as is inherent in the basic data in Figure 1 and 2 which were used to derive the constants. An example of this is shown in Figure 5.

The two level model has been used to compare experimental and calculated results for transistor current gain as a function of injection level and temperature for both p and n base units. Again, the degree of scatter between calculated and experimental results is consistent with the accuracy of the basic determination reflected in Figures 1 and 2. In addition, however, there seems to be a systematic error which results in the calculated damage exceeding the measured damage by a factor of about 1.5. An example of this is shown in Figure 6.

*This will be done for n-type material; the extension to p-type is obvious.

Summary

A two level recombination model for neutron irradiated silicon has been set forth which adequately explains the temperature, resistivity and injection level dependence of recombination processes both for transistor and material samples. The level in the upper half of the band appears to be an "average" level as opposed to a discrete level and probably indicates that contributions from several levels are important. The lower level has been previously identified as a dominant recombination level; this analysis strengthens that conclusion. Predictions based on this model are probably good within a factor of two which is all that is expected within the present state-of-the-art.

REFERENCES

1. R. F. Kornopleva, et al, Soviet Phys. Solid State 8, 264 (1966).

2. A. K. Ramdas and M. G. Rao, Phys. Rev. 142, 451 (1966).

3. B. R. Gossick, J. Appl. Phys. 30, 1214 (1959).

4. O. L. Curtis, Jr., "Effects of Oxygen and Dopant on Lifetime in Neutron Irradiated Silicon," IEEE Conf. on Nuclear and Space Radiation Effects, Stanford University, July 1966.

5. G. C. Messenger, IEEE Trans. on Nuclear Sci. NS-12, 53 (1965)

6. W. Shockley and W. J. Read, Jr., "Statistics of Recombination of Holes and Electrons," Phys. Rec. 87, 835 (1952).

TABLE I

Parameters for the Recombination Centers Determined by a Least Square Fit to Curtis' Low Level Lifetime Damage Constant Data

$$R_1 C_{p1} = 0.37 \times 10^{-6} \ (\text{sec-n/cm}^2)^{-1}$$

$$R_1 C_{n1} = 0.40 \times 10^{-5} \ (\text{sec n/cm}^2)^{-1}$$

$$R_2 C_{n2} = 0.68 \times 10^{-5} \ (\text{sec-n/cm}^2)^{-1}$$

$$R_2 C_{n2} = 0.76 \times 10^{-6} \ (\text{sec-n/cm}^2)^{-1}$$

$$n_1 = 2.0 \times 10^{14} \ \text{cm}^{-3}$$

$$p_2 = 1.3 \times 10^{13} \ \text{cm}^{-3}$$

$$K_{LN} = \frac{1.4 + 8.6 \cdot 10^{-2} \rho + 1.2 \cdot 10^{-3} \rho}{1 + 3.8 \cdot 10^{-2} \rho}$$

$$K_{LP} = \frac{2.1 + 0.18\rho + 9.0 \cdot 10^{-5} \rho^2}{1 + 1.4 \cdot 10^{-2} \rho}$$

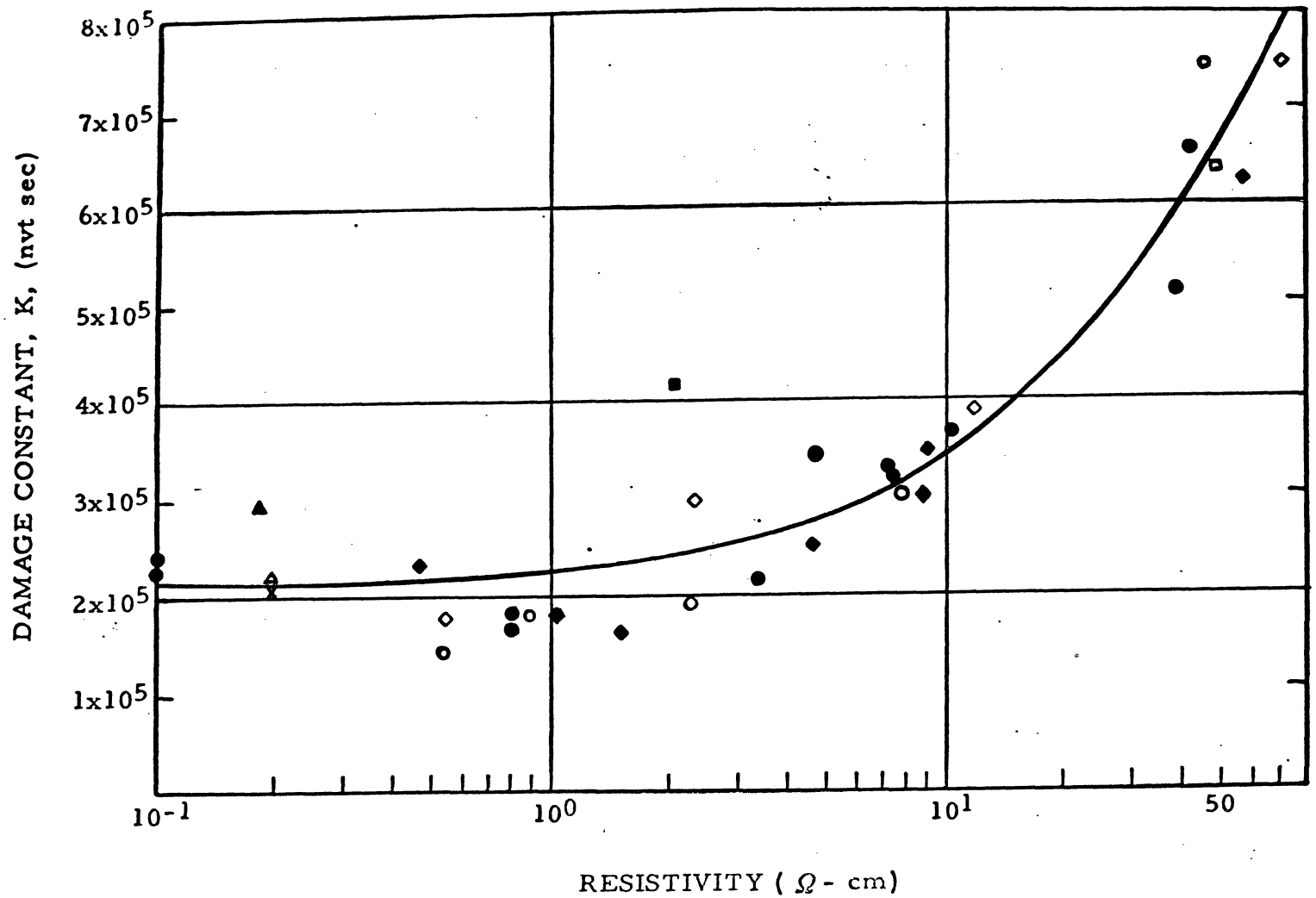

Figure 1. Damage Constant vs Resistivity for p-type Silicon. Curtis' data are given, showing least squares fit to Eq. (2b). Constants determined by the least equares fit are shown in Table 1.

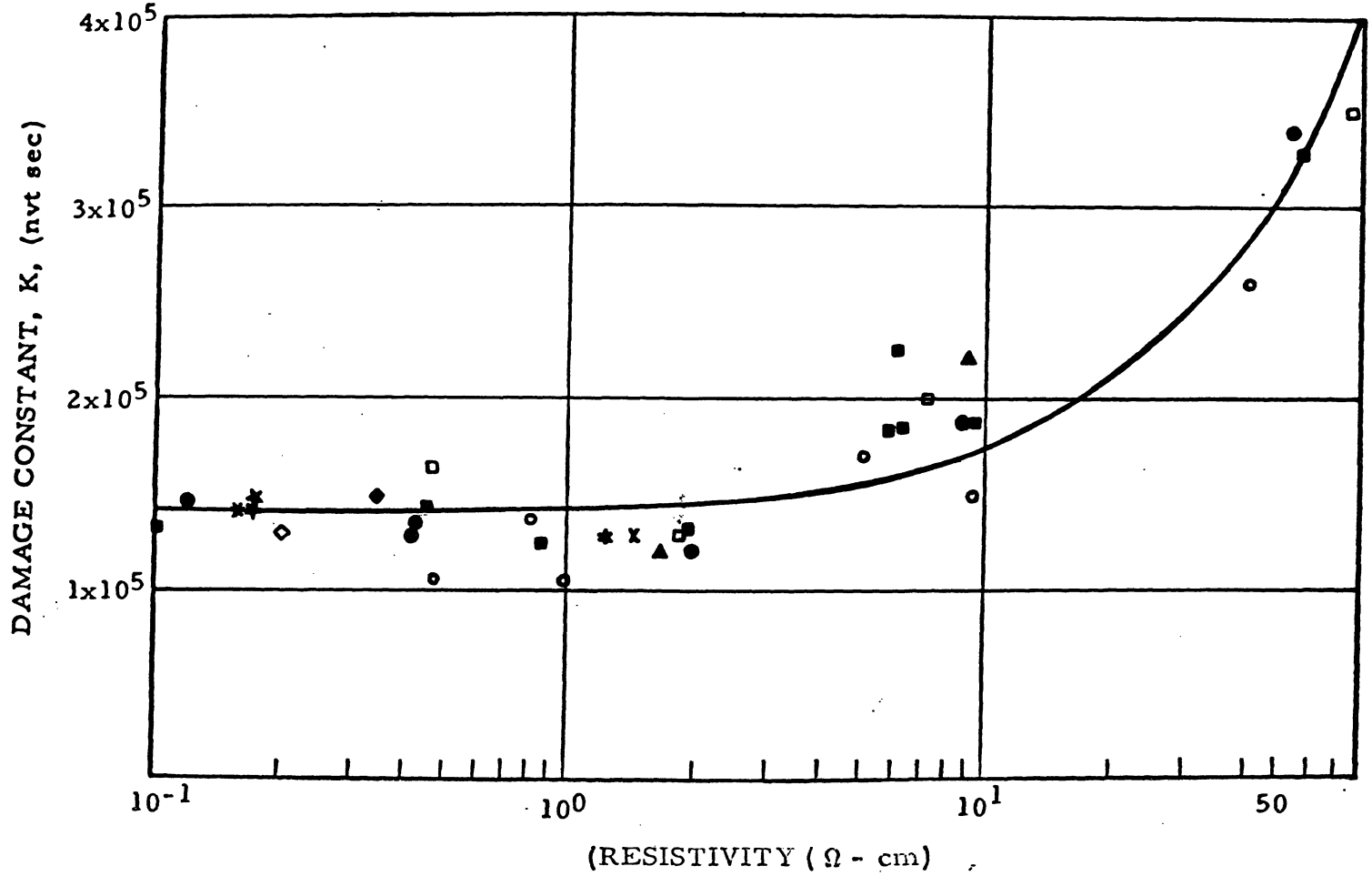

Figure 2. Damage Constant vs Resistivity for n-type Silicon. Curtis' experimental data are given, showing least equares fit to Eq. (2a). Constants determined by the least squares fit are shown in Table 1.

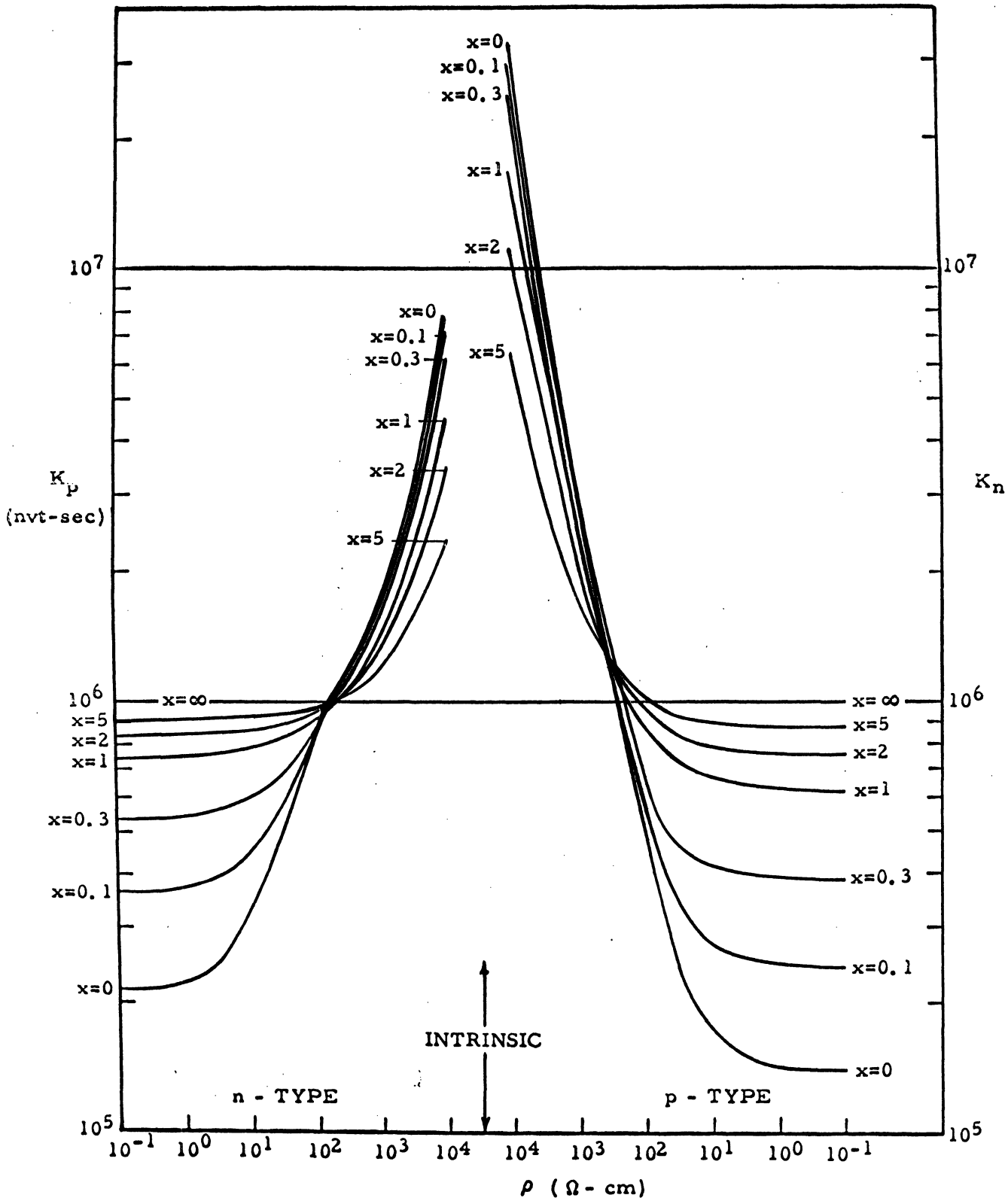

Figure 3. Lifetime Damage Constant K_n, K_p vs Resistivity for Various Injection Ratios, $x = \frac{\delta n}{n_o}, \frac{\delta p}{p_o}$. Equation (1) is plotted with constants from Table I. $\rho_n = 5.0 \times 10^{15}/n_o$ and $\rho_p = 2.5 \times 10^{16}/p_o$.

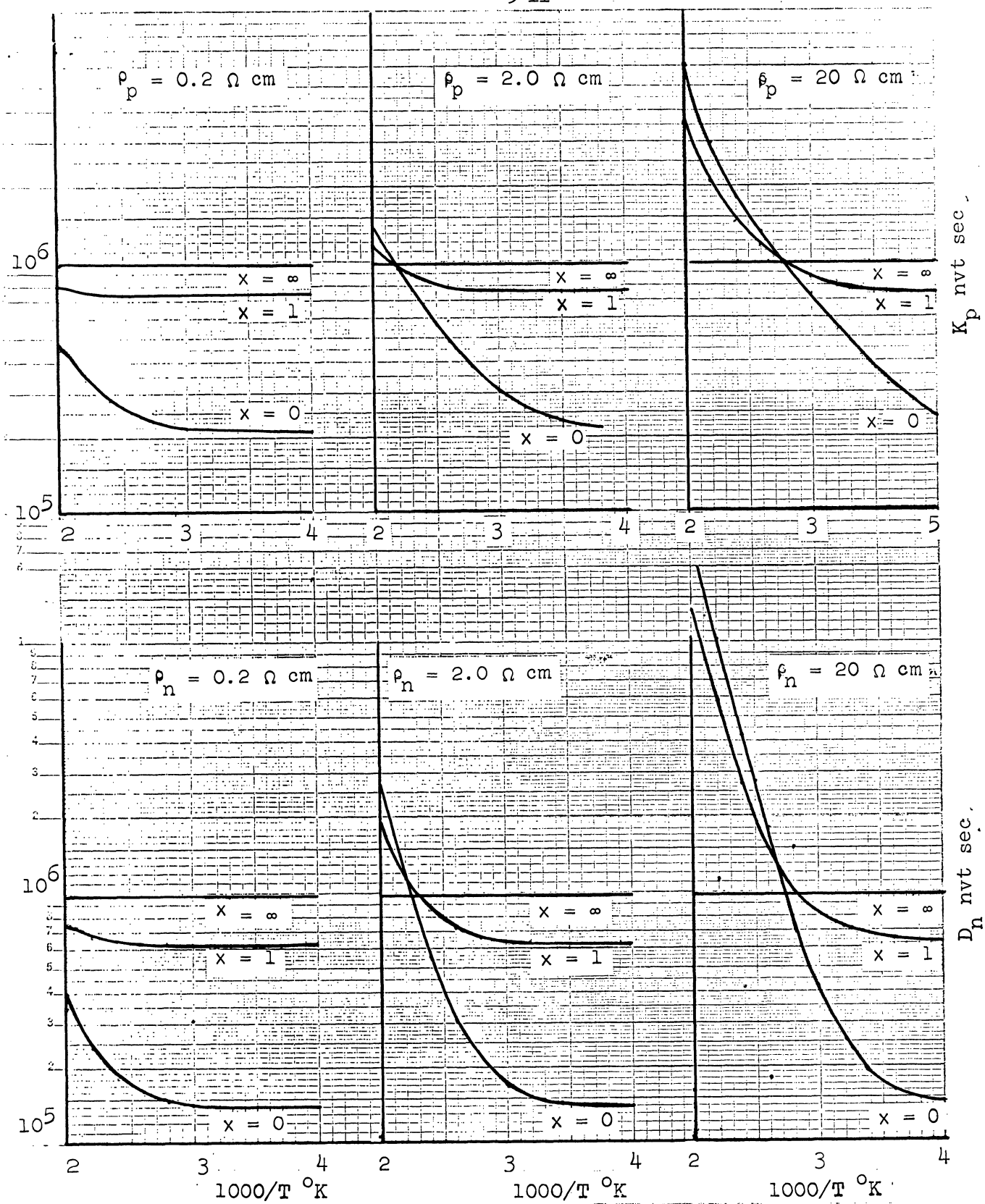

Figure 4. Lifetime Damage Constants K_n and K_p as a Function of Reciprocal Temperatures for Various Values of Resistivity and Injection Level.

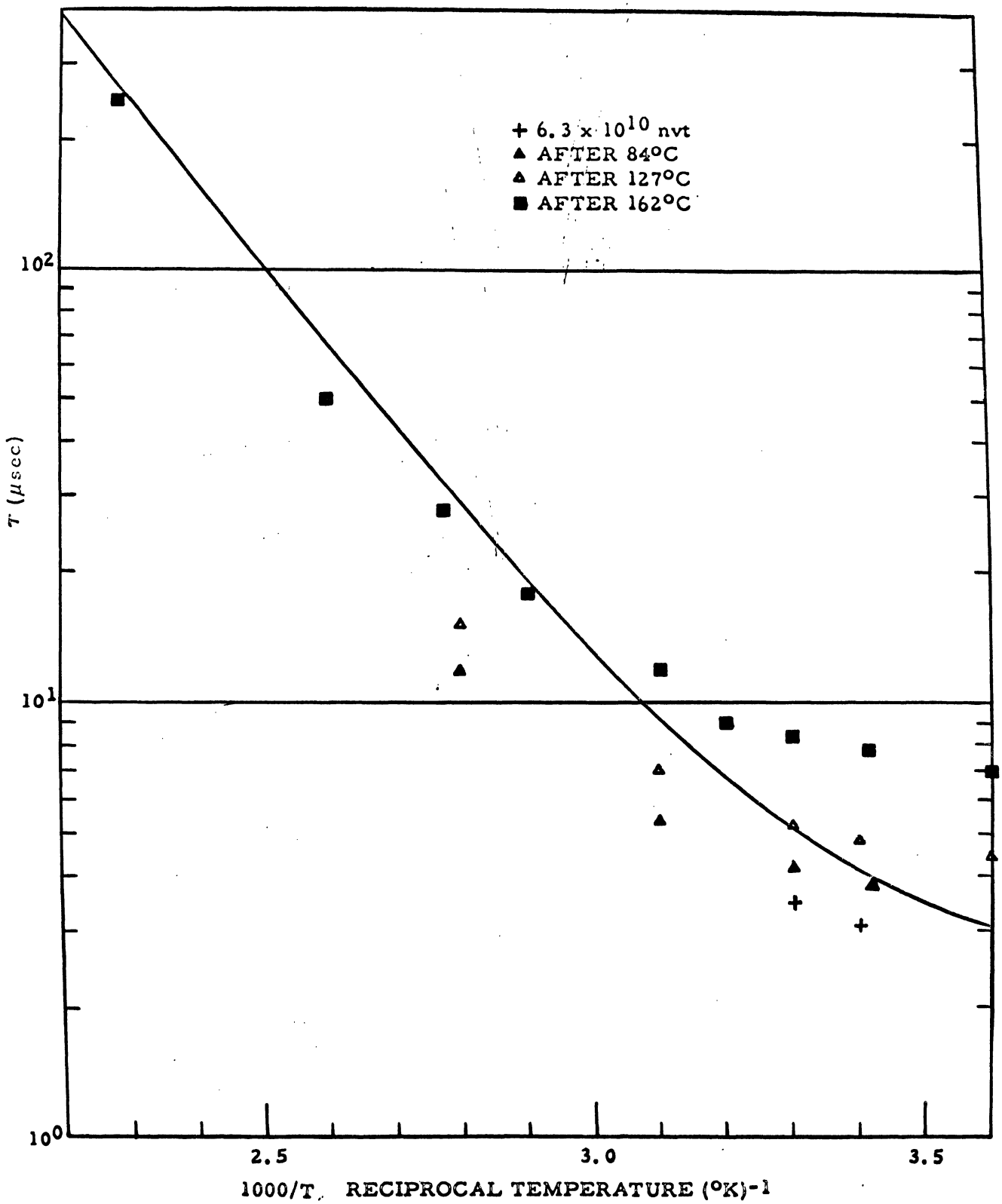

Figure 5. A Comparison of Curtis' Measured Lifetime Data with Eq. (3b) using the Constants of Table I. ρ_n = 58 ohm-cm.

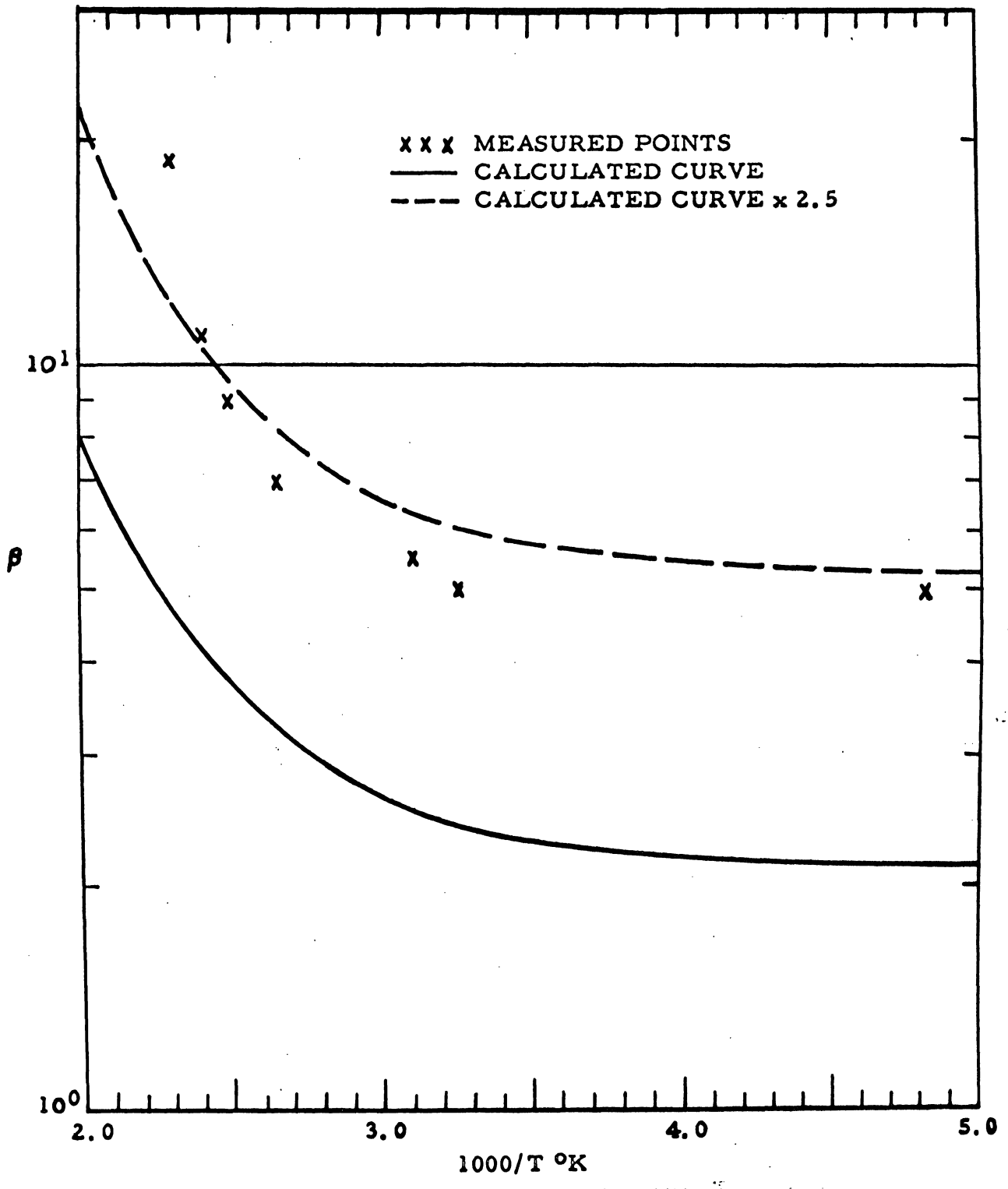

Figure 6. A Comparison of Messenger's β vs $10^3/T^oK$ Measured Data with Eq. (3a) using the Constants of Table I and the Auxiliary Relation $\beta = 4.2 \times 10^{-6}K$. Transistor is 2N335 npn grown; $\delta p/p_o \approx 0.3$, V_{CE} = 2.0V, I_E = 8.0 ma, $\phi = 8.6 \times 10^{13}$ n/cm^2, and $\rho_b \approx 5.0$ ohm-cm.

TRANSIENT ANNEALING OF NEUTRON DAMAGE IN SEMICONDUCTOR DEVICES

H. H. Sander
B. L. Gregory

SC-R-66-923A

TRANSIENT ANNEALING OF NEUTRON DAMAGE IN SEMICONDUCTOR DEVICES*

H. H. Sander and B. L. Gregory, 5212
Sandia Laboratory, Albuquerque, New Mexico

Introduction

When a silicon transistor is exposed at room temperature to a pulse of fast neutrons, the common emitter current gain is initially reduced to a value considerably lower than the stable gain to which the transistor recovers within several seconds or minutes after irradiation.[1] These results are especially significant to the circuit designer since it is evident that circuits required to function immediately after a pulsed neutron exposure must not only be designed to function properly with the reduced gain value that exists shortly after irradiation but also to function under transient gain conditions. These design requirements place significant limitations on the radiation tolerance that can be achieved in certain classes of electronic circuits and systems; consequently, it is very important that these effects be quantitatively related to device operating conditions, e. g., temperature and injection level, and understood in terms of fundamental annealing processes in bulk materials. An attractive aspect of this study is that it provides an additional tool to probe the nature of neutron damage in silicon. The kinetics of the annealing processes involved can convey much information about the initial and final damage present following neutron irradiation.

In this work, experiments will be discussed which conclusively show the transient annealing (rapid annealing) observed in neutron-irradiated devices to be due to bulk, rather than surface, processes. Additional experiments are discussed wherein transient annealing has been studied in silicon transistors, solar cells, and other semiconductor devices as a function of both temperature and injection level. For the convenience of circuit and systems designers, the transistor data in this paper are presented in the form of an Annealing Factor[1] which may be defined as the ratio of the radiation-induced defect density at the time t to the density of stable defects that do not anneal. This is equivalent to defining this parameter as $\Phi^*(t)/\Phi$, the ratio of the effective neutron fluence, $\Phi^*(t)$, required to produce the damage observed at time t, to Φ, the actual fluence. Consequently, transistor current gain at time t can be obtained from existing gain degradation curves by utilizing the effective fluence, Φ^*, which is the product of the actual fluence Φ and the annealing factor at time t.

The existing information about neutron damage in silicon is summarized and employed, along with present results, to obtain a preliminary prediction of the processes important in annealing of neutron damage. These processes are subsequently employed to derive a model for transient annealing in silicon. Various kinetic processes are discussed in this derivation, including both diffusion-limited and generation-limited processes. The results of this model are then compared with experimental data presented in this paper. The successes and failures of this model are also discussed.

*This work was supported by the United States Atomic Energy Commission.

Experimental Annealing Investigations

Since transient annealing in devices is a relatively new field, experiments have been conducted to (1) deduce the origin of the annealing phenomenon, i.e., differentiate between bulk and surface annealing, and (2) provide detailed experimental data from which the fundamental nature of the annealing mechanisms can be ascertained.

A. Bulk Annealing Versus Surface Effect Experiments

In the original disclosure of transient annealing, several experiments were described which supported the conclusion that the observed damage recovery is the result of defect annealing in the bulk silicon and not a surface effect. First, transient annealing results were compared for transistors with gas-filled encapsulations and transistors with evacuated encapsulations. These experiments indicated that the transient annealing characteristics of both the evacuated and gas-filled devices were nearly identical and, therefore, showed that surface effects produced by gas ion contamination at the surface were not significant. Second, the possibility that a surface effect produced by ionization in the oxide layer is responsible for the observed recovery was explored by varying the neutron-to-gamma ratio of radiation source. Although this ratio was varied by a factor of 3, no difference in the annealing characteristic was observed.

To validate further the results reported earlier, two additional experiments have been performed. If the transient annealing effects observed in transistors were due to ionized particles trapped on the transistor surface, thereby producing surface channels, the transient effects should also be observed following exposure to a pulse of X rays. To check this possibility, both irradiated and unirradiated transistors were exposed to 30-nanosecond X-ray pulses from a 2 MeV flash X-ray machine. These exposures produce the same dose $(\sim 1200$ rads (Si)$)$ as that achieved at the Sandia Pulsed Reactor (SPR)* during a typical transient annealing experiment. No evidence of transient gain recovery was observed in these experiments.

The solar cell, which may readily be employed to measure radiation changes in diffusion length, is known to be much more independent of surface problems than transistors because of its large active-volume-to-perimeter-area ratio. Consequently, measurements were made of the short circuit current output of illuminated P on N and N on P silicon cells as a function of time following exposure to neutron bursts. The result of a typical room temperature exposure, shown in Figure 1, illustrates that solar cells also exhibit transient annealing and require nearly 10^4 seconds to reach a stable condition. This extremely long time for completion of the transient recovery is similar to that obtained for transistors operated at similarly low injection levels.

For penetrating illumination, the short circuit current of a solar cell is linearly related to the base region minority carrier diffusion length, L. Assuming only small changes in carrier mobility upon irradiation, diffusion length may be related to the effective recombination center density, N_{eff}, by the expression

$$\frac{1}{L^2} \sim N_{eff} \cdot \qquad (1)$$

*The SPR is a bare, critical assembly providing an intense, 50-microsecond pulse of fission spectrum neutrons.

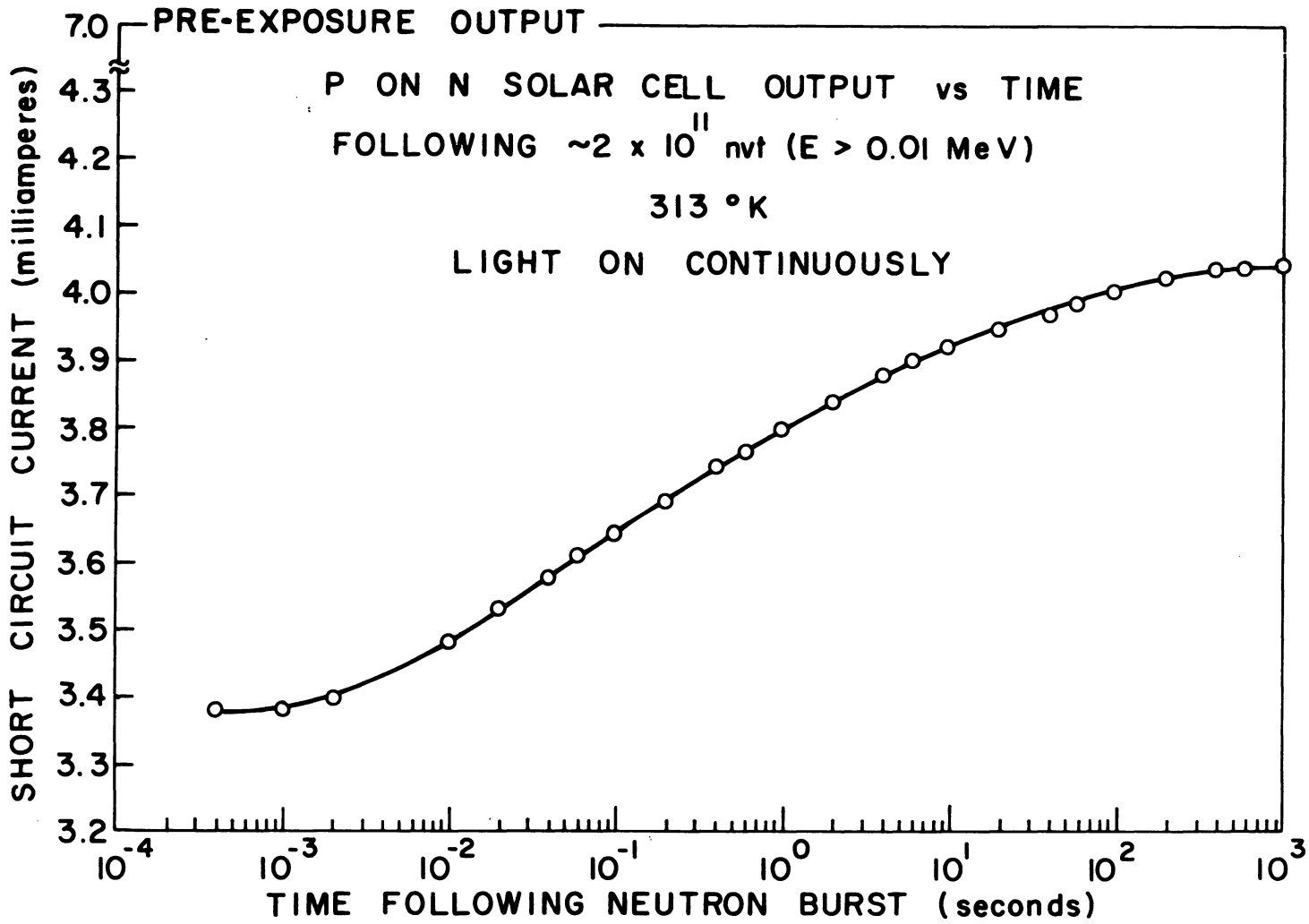

Figure 1. Transient Annealing in a P on N Silicon Solar Cell Following a Neutron Burst Exposure

If the data shown in Figure 1 is reduced according to the inverse square function indicated in Equation 1, one observes an approximate 40-percent reduction in effective defect density during transient annealing. This value is consistent with the amount of annealing typically seen in transistors at this temperature and injection level.

Although a solar cell is relatively free from surface problems, there are ways in which surfaces can influence these measurements. In this device, recombination at the peripheral surfaces may be neglected. However, front surface recombination may not be negligible if measurements are made with light containing nonpenetrating wavelengths. This light is strongly absorbed in the diffused surface region of the cell and produces a surface component of current which can be modulated by changes in the front surface recombination velocity. Experimentally, no difference is found in the relative magnitudes of the transient and permanent damage for penetrating or full spectrum tungsten light. Hence, one can conclude that changes in surface recombination are not responsible for the observed transient annealing and that it must be a bulk effect.

B. Temperature and Injection Dependence of Transient Annealing

As stated in the introduction, it is necessary to understand both the temperature and injection dependences of the transient annealing phenomena in order to predict the importance of this effect in any particular device operating condition. Furthermore, the variation of the annealing curves with these two parameters is an important key to understanding the physical processes involved.

In order to separate the temperature and injection dependences, experiments were performed where the collector current was applied in constant amplitude pulses of 10 μs duration. By varying the magnitude and repetition rate, the average injection level could be varied over a wide range while maintaining essentially equal junction and case temperatures. Base current measurements were obtained for three repetition rates (100 Hz, 1 KHz, and 10 KHz) at four temperatures (213, 268, 300, and 348°K) with a peak collector current of 2 ma. These measurements were also performed at room temperature with a peak collector current of 10 ma.

Typical results for the Fairchild 2N914 NPN silicon transistor are shown in Figures 2 and 3. Figure 2 shows annealing factors versus time following a 1.8×10^{13} NVT (E > 0.01 MeV) exposure at each of the four temperatures. Figure 3 shows results for the same temperature and fluence but with a repetition rate of 10 KHz instead of the 100 Hz rate used to obtain Figure 2. The rather strong temperature dependence at the lower temperature is clearly shown in each of these figures. Figure 3, for example, shows that at 348°K, an Annealing Factor of approximately 2 exists at 10^{-4} seconds. However, at 213°K, the Annealing Factor at 10^{-4} seconds is approximately 5. These data indicate that a system designed to operate at temperatures below room temperature must accommodate a much larger Annealing Factor than had been reported previously. This result is especially significant when it is recognized that the temperature range reported here is nearly identical to the standard Military Specifications (-55 to +75°C).

To obtain an estimate of the annealing which occurs in the absence of injection, experiments were performed where the collector current was terminated from +1 second to +101 seconds after the neutron exposure. At all four temperatures, annealing was observed to continue, although at a much reduced rate, in the absence of injection. A sample of these results is shown in Figure 4. For an average collector current of 20 μa, approximately 65 percent of the transient annealing at 300°K appears to be due to injection dependent processes.

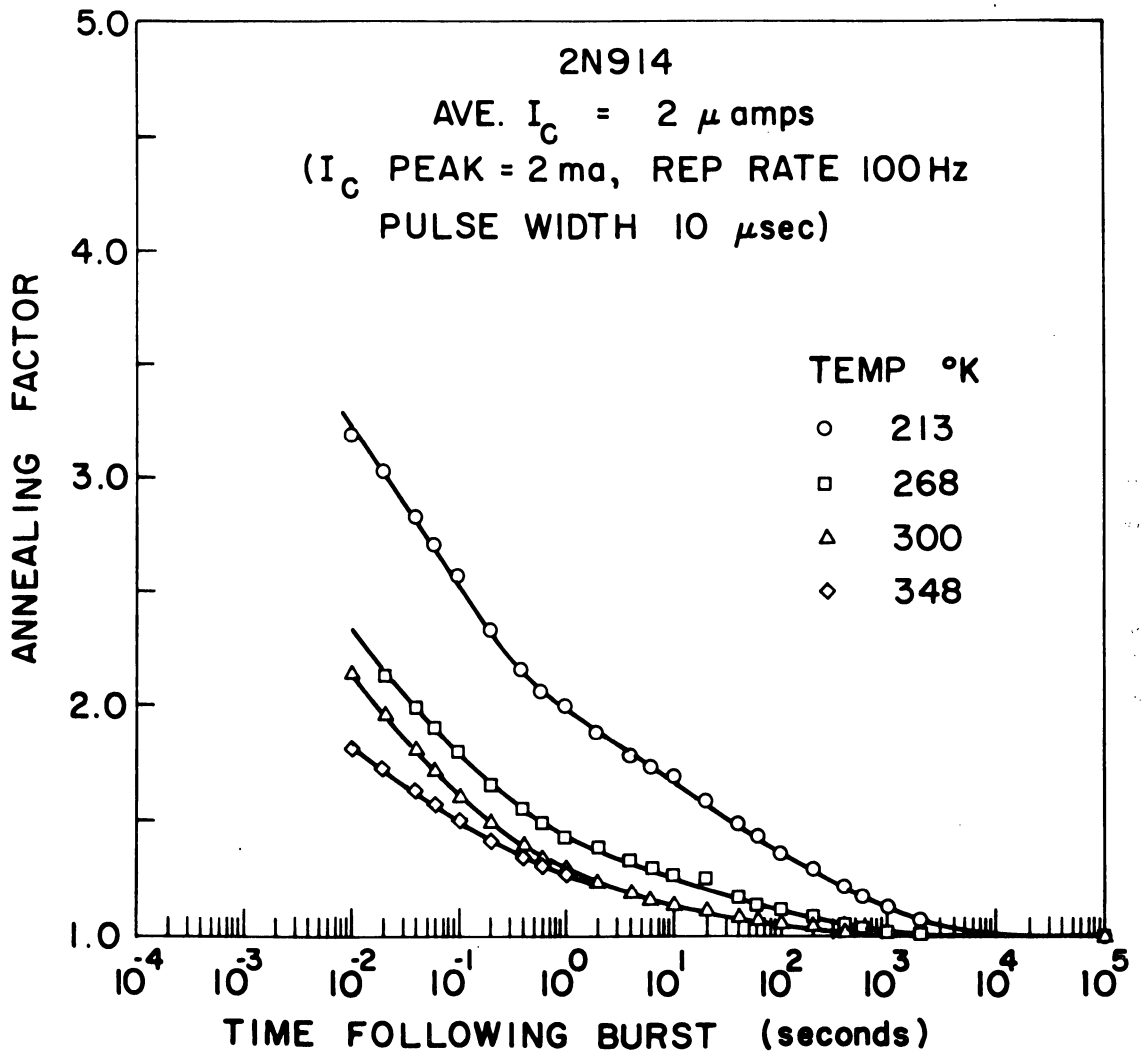

Figure 2. Curves of Annealing Factor Versus Time Following a Neutron Burst Exposure for a 2N914 Transistor, for 2 ma Peak I_C, Repetition Rate of 100 Hz (Average Current Density of 0.025 A/cm^2), at Four Temperatures

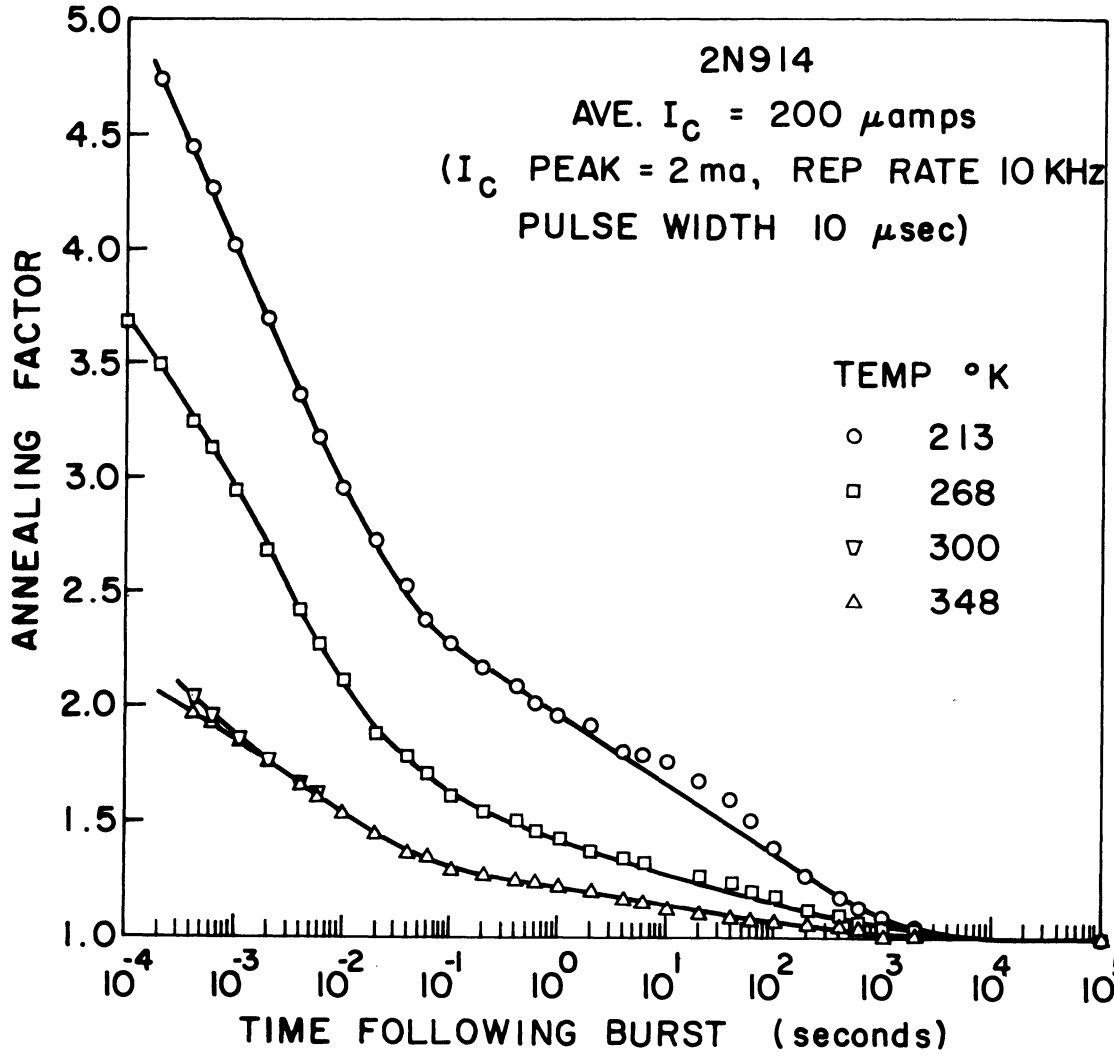

Figure 3. Curves of Annealing Factor Versus Time Following a Neutron Burst Exposure for a 2N914 Transistor, for 2 ma Peak I_C, Repetition Rate of 10 KHz (Average Current Density 2.5 A/cm^2), at Four Temperatures

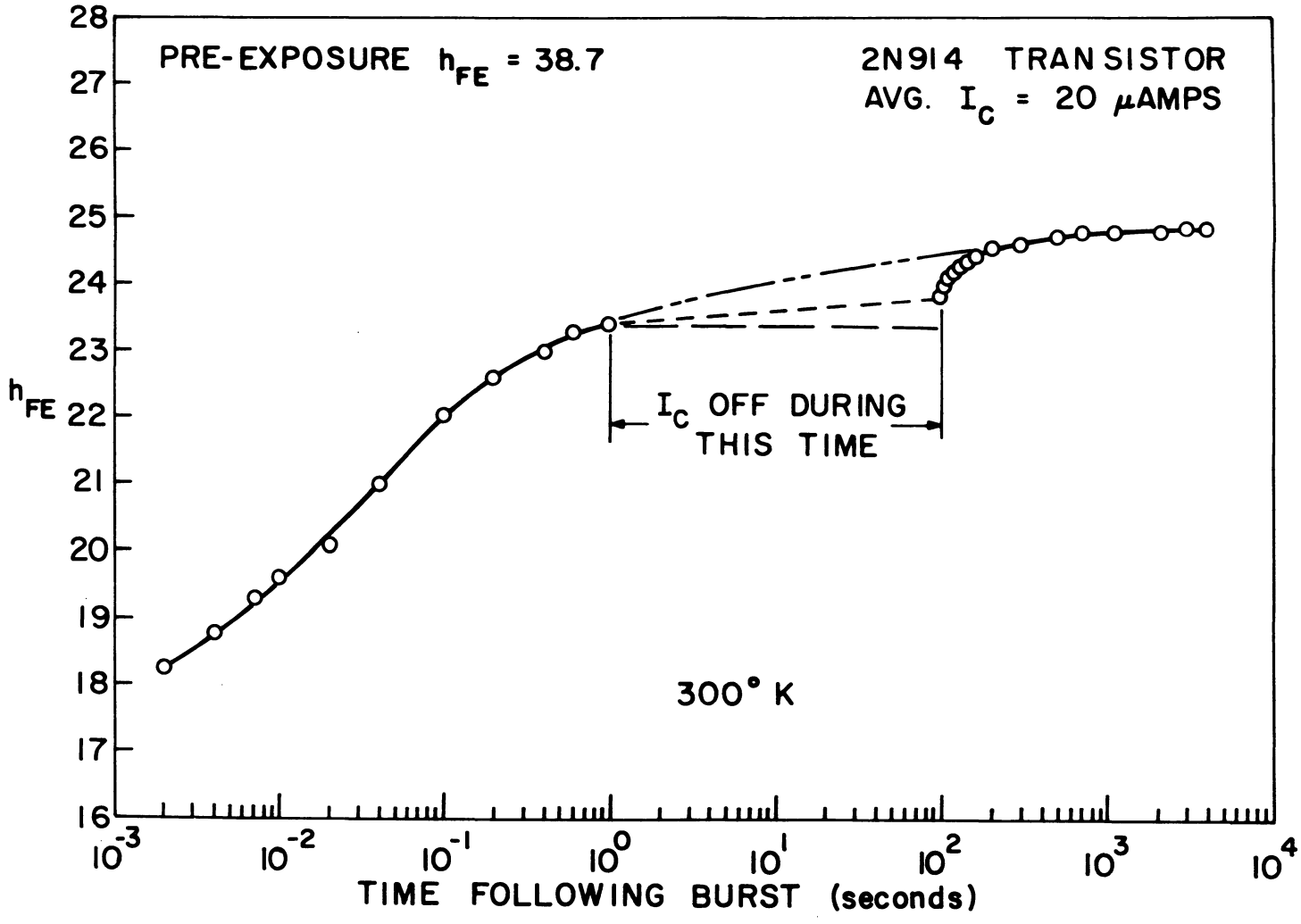

Figure 4. h_{FE} Versus Time Following a Neutron Burst Exposure at Room Temperature, with I_C Off from +1 to +101 Seconds. (The dashed lines indicate the reduced rate of annealing when injection is removed.)

The results of pulsed measurements using both 2 ma and 10 ma peak collector currents are compared in Figure 5. These data also indicate that the rate at which annealing takes place is strongly dependent upon the average injection level. For an average current of 2 μa, one observes annealing rates which are approximately 100 times smaller than for an injection level of 1 ma average current. It should be emphasized that devices which are in the nonconducting state will anneal quite slowly and, therefore, recovery in some classes of electronic circuits can require relatively long annealing times.

C. Low-Temperature Studies

An experiment which illustrates the effects of injection at low temperatures was performed employing a transistor capable of operation in liquid nitrogen. This device, having a pre-exposure current gain of approximately 40 at 76°K, was exposed to a neutron burst, and its transient gain recovery was observed at 76°K. The collector current was then terminated for a time interval of several seconds. The gain recovery ceases during the time the injection current is thus removed. When current is again applied, the gain recovery (annealing) continues.

Similar results are obtained with silicon solar cells. Two P on N solar cells, one cell operating at 76°K and the other at 313°K, were exposed to the same neutron burst and their output currents observed. Illumination (injection) was then terminated shortly after the neutron exposure. During the absence of illumination, no recovery was observed in the cell at 76°K. However, the cell at 313°K annealed appreciably during this same time period. These results, shown in Figure 6, are nearly identical to those observed for N on P solar cells.

It can be seen in Figure 6 that the low-temperature curve is still changing rather rapidly at 10^3 seconds, much more so than the 313°K curve. Therefore, to compare the total amounts of observable annealing at these two temperatures, the device held at 76°K was warmed to room temperature, and then returned to 76°K for a final measurement. Although the total observed recovery is considerably greater in the device irradiated at 76°K than in the device held at 313°K, it should be emphasized that annealing takes place more rapidly at the higher temperature and a considerable amount of annealing could take place before the earliest 313°K measurement.

At 76°K, results of gamma irradiation[2] of silicon solar cells indicate that injection of minority carriers following irradiation also produces recovery in the device diffusion length. Recent transient experiments have been performed following gamma irradiation of such devices to compare (or contrast) the form of the annealing in this case to the neutron results at the same temperature. These gamma irradiation experiments were performed by irradiating the sample in the dark and then observing the transient annealing after the sample is exposed to an illumination source. In Figure 7 the transient annealing of both gamma and neutron damage is shown for P/N devices. One observes a striking difference in the two curves. The gamma damage annealing looks very much like a simple kinetic process, such as one might expect for the annealing of point defects. The neutron annealing, however, is a much more slowly varying function which obviously cannot be described by a single first or second order process.

An attempt was also made to observe transient annealing following exposure of solar cells to intense 30-nanosecond pulses of 1.5 MeV electrons (~5×10^{13} electrons/cm^2) at room temperature. No annealing was observable following such irradiations of 315°K for times greater than 50 μs. Noise problems associated with the pulse generation and lifetime effects prevented observation of the device output at times less than 50 μs.

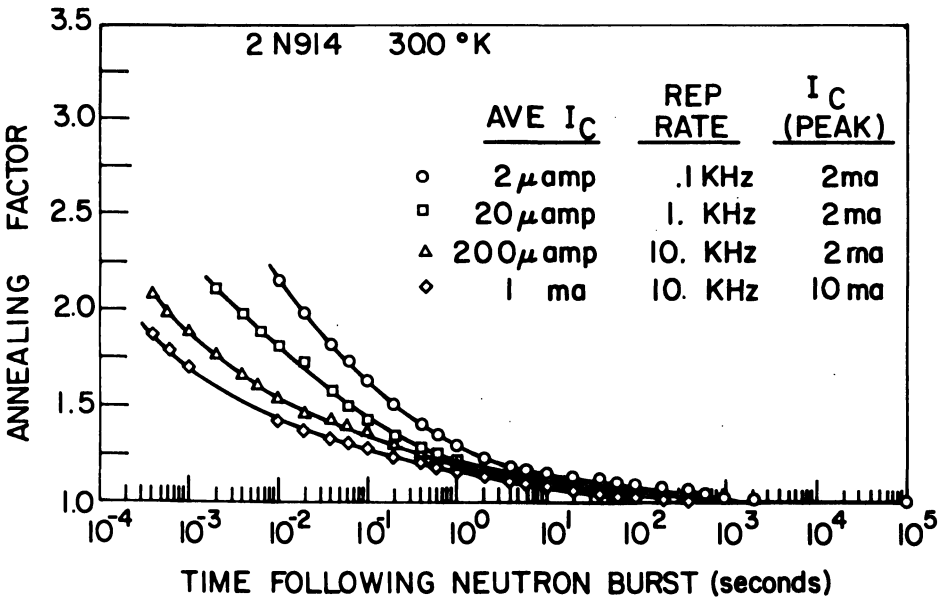

Figure 5. Curves of Annealing Factor Versus Time for a 2N914 Transistor, at 300°K, Comparing Different Injection Levels for the Same Temperature

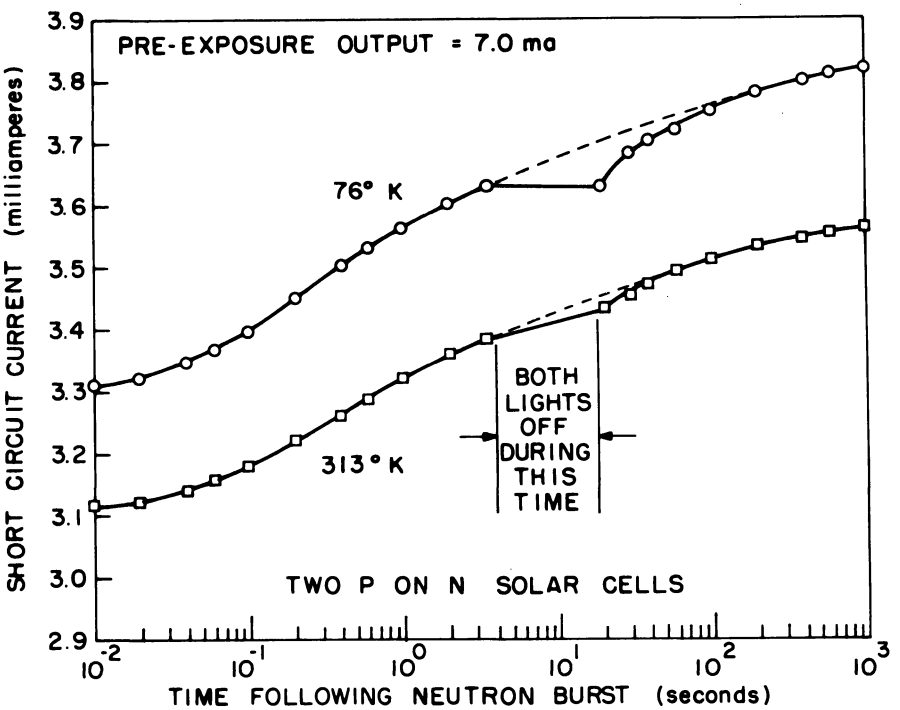

Figure 6. Comparison of Transient Annealing for Silicon Solar Cells at 76°K and 313°K, With and Without Injection

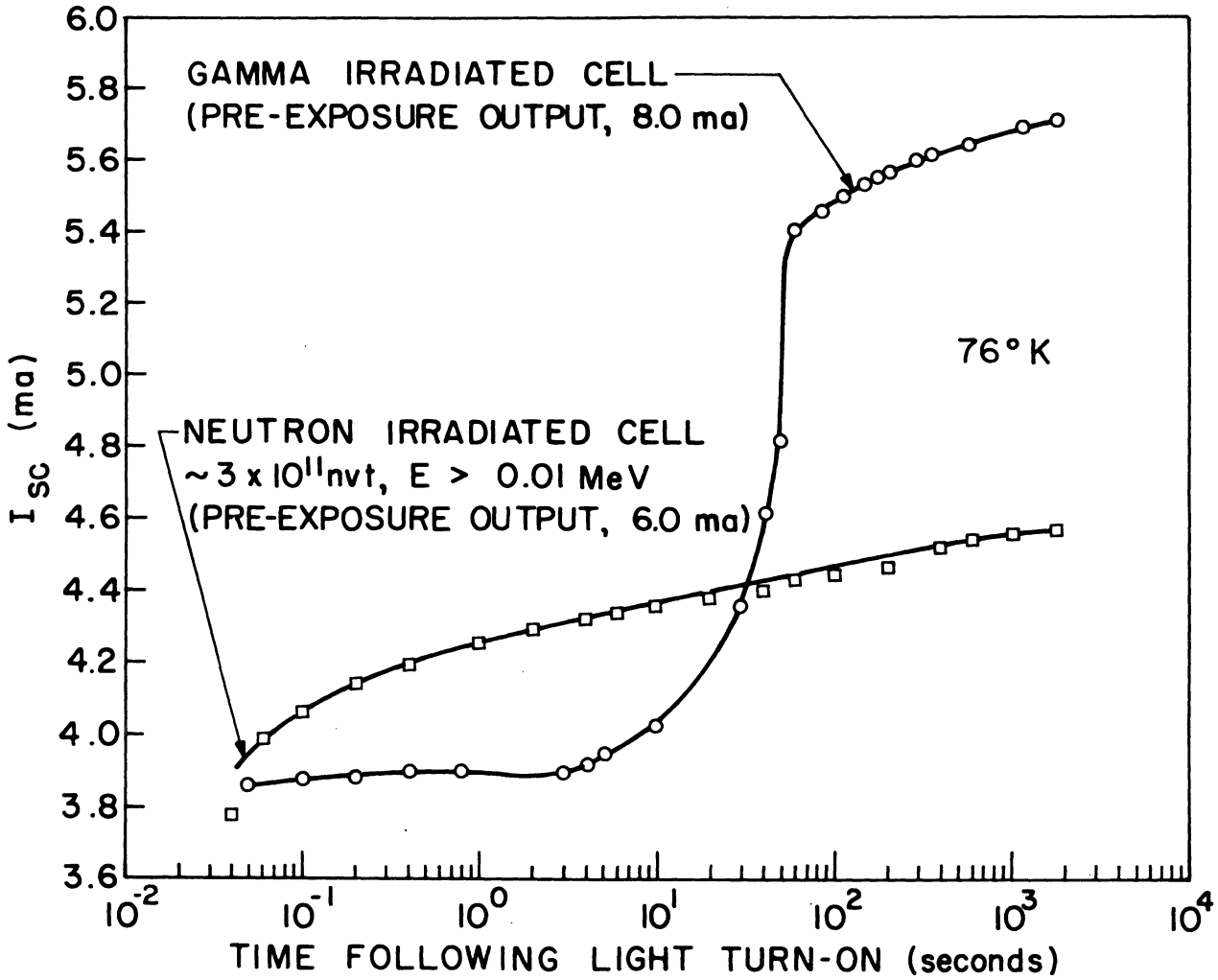

Figure 7. Comparison of Transient Annealing for P on N Silicon Solar Cells Following Gamma and Neutron Irradiation, at 76°K

D. Other Factors Influencing Transient Annealing

Annealing factors have been found to differ for various device codes, even for devices operating at essentially the same current density. This difference appears largest when comparing high-power, low-frequency devices to the lower power, high-frequency devices. As both doping level and impurity content may differ in the high- and low-power devices, these parameters may be significant in influencing transient annealing. Presently, however, insufficient data exist to justify any conclusions concerning a doping level or impurity effect.

E. Transient Annealing in Other Semiconductor Devices

Transient annealing is also observed in silicon controlled rectifiers. A plot of both "on" and "off" firing voltages versus time during the transient annealing period is shown in Figure 8 for an SCR, as obtained by the circuit in the inset of the figure. The exposure was carried out at room temperature. While no attempt has been made to reduce these data into the form of annealing factors, it is evident that annealing factors prepared from these data would be comparatively high, due in part, no doubt, to the relatively low current density employed in this experiment. Note that the time for recovery compares with that for transistors and solar cells.

The Nature of Neutron Damage

The previous sections clearly illustrate that transient annealing does occur in neutron-irradiated silicon at temperatures near room temperature. Furthermore, the experiments show this effect to be of bulk origin and to be unique to neutron damage at room temperature. To understand the phenomenon fully, it is most important to understand the difference between neutron damage and 2 MeV electron or gamma ray damage since this difference must be responsible for much of the behavior characteristic of neutron-damaged materials.

When a semiconductor crystal is exposed to a fluence of fast neutrons, it is known that a certain fraction of the neutrons will collide with crystalline atoms while transiting the crystal and produce high-energy recoil atoms. These energetic recoils then dissipate their energy by displacing and ionizing other crystalline atoms. The secondary and higher order displacements associated with a neutron encounter will be distributed over a distance in the crystal approximating the "range" of the primary recoil atom. Therefore, one observes that "regions" of disorder may be created in the crystal by neutron encounters. The physical details of such a "cluster" of damage depend primarily on the range and energy of the primary recoil atom. If said range is short, such as is appropriate for a high-Z semiconductor, the cluster region will be reasonably small. In this case, the host material may actually melt in the region of the encounter and subsequently regrow, leaving behind only a small amorphous region.

This is believed to be the case for germanium since electron diffraction patterns of germanium given large doses of energetic heavy ions, approximating Ge recoils from neutron encounters, are characteristic of amorphous material.[3] Such clusters have been seen directly in n-type germanium by electron microscopy and observed to be approximately 100 to 200 Å in diameter.[4]

Although there is little direct evidence for the existence of damage clusters in silicon, a wealth of electrical data supports the cluster theory. For example, it is known that the carrier removal produced by

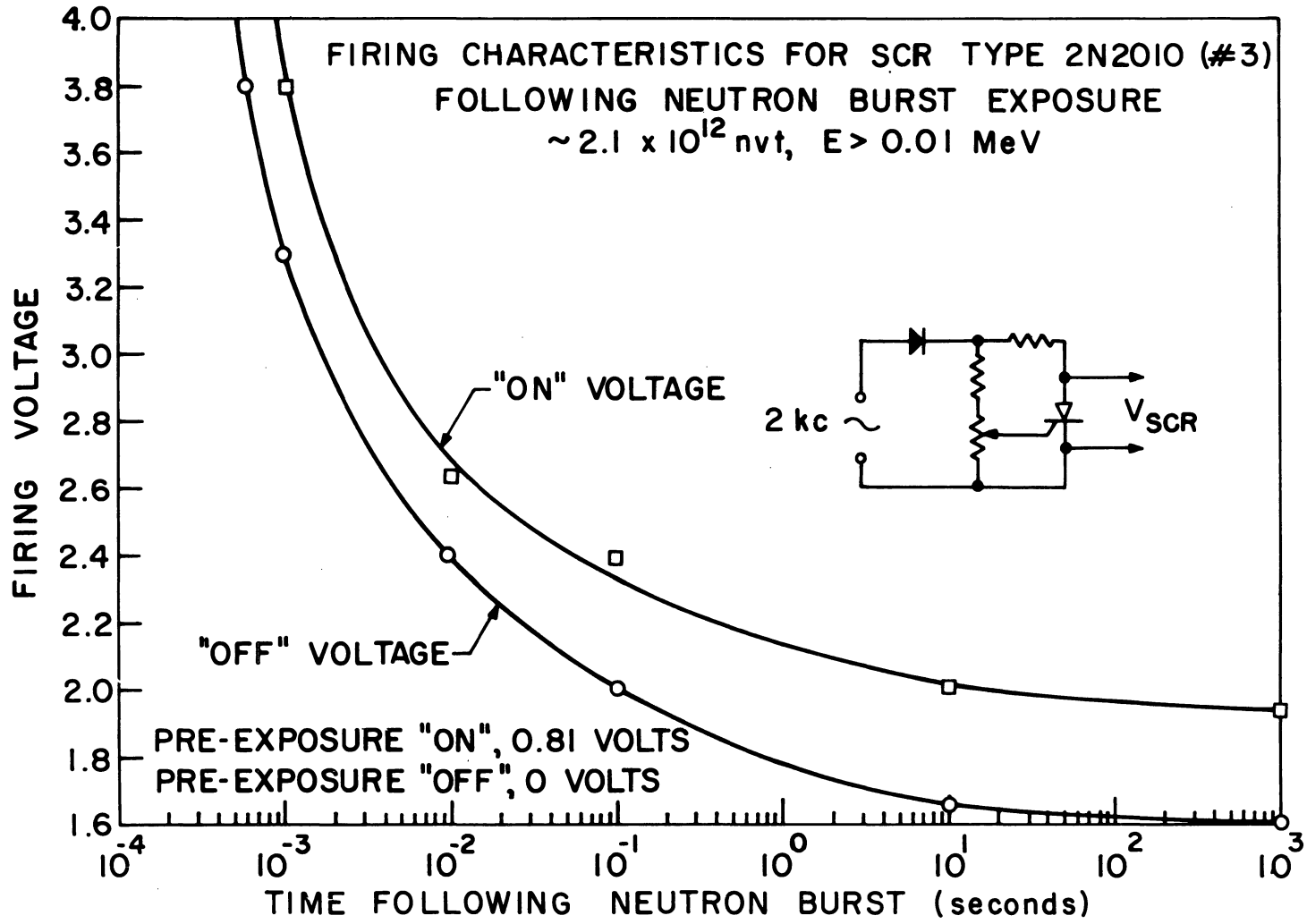

Figure 8. Transient Annealing in a Silicon Controlled Rectifier, at 300°K, as Obtained Using the Circuit in the Inset

neutron irradiation at 76°K is independent of crystalline impurity content in both p- and n-type material.[5] This result is in direct contrast to the case for 2 MeV electron-irradiated, n-type silicon,[6] where the defects are known to be introduced predominantly as point defects. Furthermore, the carrier removal rate remains essentially independent of impurity content even at temperatures up to 270°K.[7] The one exception to this impurity independence occurs in n-type silicon, where the carrier removal rate varies by approximately 50 percent with varying oxygen concentration,[4] the higher rate being applicable to material with low oxygen concentration. However, even this difference is small compared with that found for electron irradiation[7] in the same materials. Other evidence supporting the impurity independence of neutron damage has been obtained by Curtis and co-workers[8] in room temperature lifetime degradation studies.

Also supporting the cluster theory is the very slow minority carrier trap observed in neutron-irradiated silicon at temperatures below approximately 180°K.[9] This effect, which appears as a slow decay of the excess conductivity following the termination of excess carrier generation, is not found in 2 MeV electron or gamma-irradiated materials. Such behavior can be qualitatively explained by a cluster model for silicon similar to that proposed by Gossick[10] for germanium.

Considering the electrical evidence to be sufficient to justify the cluster model, several statements can be made about cluster annealing. As indicated above, observations of carrier removal in neutron-irradiated, n-type silicon at 270°K show a slight dependence on oxygen concentration. Presumably this dependence is an indication of partial cluster decomposition even at this temperature. Other evidence that such decomposition of clusters does occur below room temperature results from IR absorption studies. In these studies, Whan[11] has neutron-irradiated silicon samples at -50°C and monitored the silicon A center (836 cm^{-1} band) as a function of annealing temperature following irradiation. The observations show a steady growth in A center density as the temperature is raised, indicating that vacancy generation occurs in the crystal, probably at the cluster.

Consistent with these results, one observes that the above discussed minority carrier trapping effect in neutron-irradiated silicon becomes less important upon isochronal annealing to room temperature. Stein has observed that the trap begins to anneal at 130°K and continues to anneal until approximately 400°K, where it is virtually gone. If this phenomenon is cluster associated, as presently believed, its annealing is strong evidence that the cluster does break up over this temperature range.

Theoretical Models for Cluster Annealing

The above electrical measurements on neutron-irradiated silicon indicate that clusters probably do exist in this material. From range calculations, it can be shown that the maximum dimension of such a cluster in silicon is approximately 1000 Å immediately after its creation.[12] However, there are many details about the cluster, such as its shape, defect density, and initial defect nature, which are virtually unknown. It may be, for example, that the damage cluster is in the shape of a cigar with its long axis approximating the primary recoil range. Such a structure was hypothesized by Truell[13] to explain results of ultrasonic attenuation measurements in neutron-irradiated silicon. An additional complication may exist in the form of a melted and subsequently regrown region at the end of the primary recoil track. This region could be amorphous, as is thought to be the situation in germanium, and could, for example, supply defects to the surrounding material as it annealed.

If one first treats the case where the neutron cluster consists purely of displacement damage, the type of defects which should be present initially in and around the cluster can be postulated. The simplest defects would, of course, consist only of isolated silicon vacancies and interstitials. Close vacancy-interstitial pairs will probably not exist for any significant time since these are known to be unstable even at temperatures as low as 76°K.[13] Defect complexes, e.g., divacancies, di-interstitials, etc., may also be created directly during irradiation because of the production of adjacent displacements inside the cluster. The number of defects which are created as complexes relative to the number created as isolated defects depends on the number and distribution of defects created by each encounter of a recoil atom with the crystal. Since these details are unknown, both complexes and isolated defects should be initially allowed inside the cluster.

In addition to the defects initially present inside the cluster, there will probably be a certain number created simultaneously outside the cluster. For example, a fraction of the silicon interstitial atoms will channel out of the immediate cluster region and create a cloud of interstitials around the cluster. Also, a small number of vacancies may have been created in this region by long-range energetic recoil atoms. In Figure 9, the primary defects are shown as they might exist immediately after creation of the cluster along with possible reactions involving these defects.

Since the simple defects inside the cluster are known to be unstable at room temperature, these defects will react with each other and with other complexes. The likely reactions are:

(1) $V + V \rightarrow VV$ (divacancy formation),

(2) $V - I$ (recombination),

(3) $VV + I \rightarrow V$, $II + V \rightarrow I$, etc. (complex annihilation),

(4) $V + O \rightarrow VO$ (A center formation), and

(5) higher order complex formation, including trivacancy, VOV centers, di-interstitials, etc.

Although these processes are probably all allowed, they are not equally important in determining cluster reordering. Process (2), for example, will depend on the fraction of the interstitial population which does not channel, while process (4) depends both on the cluster size and oxygen concentration. The process of complex annihilation, (3), depends upon the number of complexes formed initially. Process (5) will be less probable than the others, but the defect complexes formed could represent a source which slowly evolves defects to the bulk and account for the slowly varying portion of the transient annealing curves.

Examining the kinetic processes likely to be involved in the annealing of a displacement cluster, one observes that the initial stages should be dominated by the internal reordering processes since the reacting defect densities are highest inside the cluster. Of the processes listed above, the first three will undoubtedly be most significant. (Process 4 may be significant in a very dilute cluster.) All should exhibit second order behavior since the reactions are all bimolecular. However, the reactant concentrations will not necessarily change according to the simple form given by

$$1/C - 1/C_o = K_A t, \qquad (2)$$

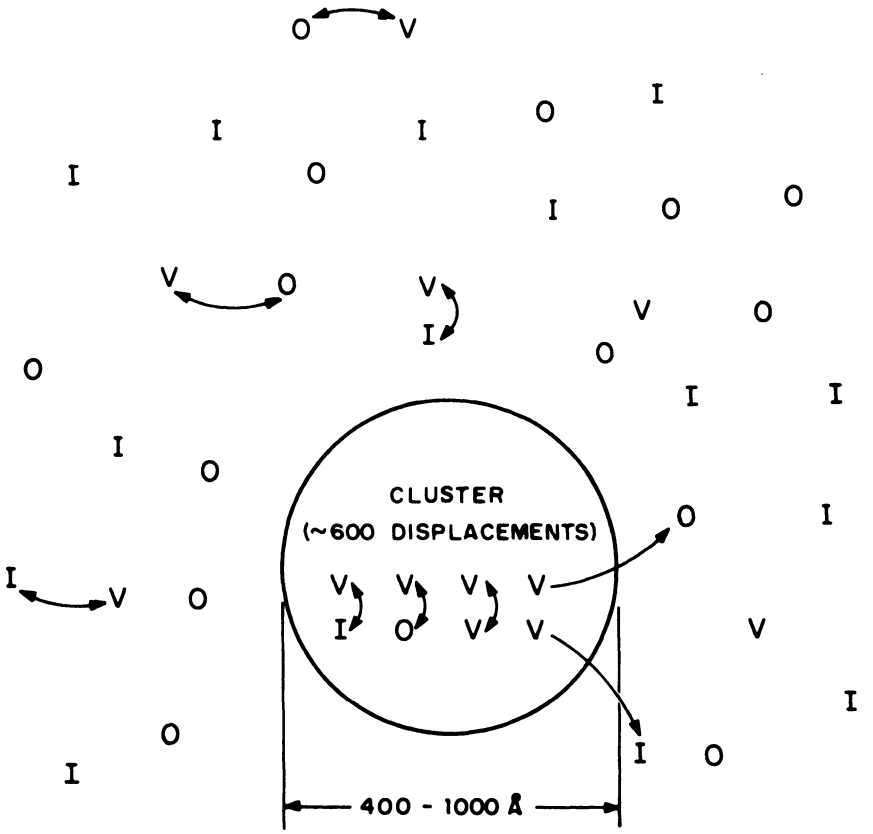

Figure 9. Simple Spherical Model for a Pure Displacement Defect Cluster Showing a Possible Initial Defect Distribution and Defect Reactions

where C_o is the initial concentration, C is the total concentration, K_A is the rate constant and t is the time. This form holds only for equal reactant concentrations. Although many of the details of these processes are unknown, the first approximation would be to merely lump them together into a single process which is assumed to follow simple second order kinetics. This assumption can be checked by comparing the experimental results with Equation 2.

A. Discussion of Experimental Results

If the transient annealing data shown in Figure 3 is examined carefully, there appears to be a distinct annealing stage occurring in the 213°K curve at times earlier than approximately 5×10^{-2} seconds. This process appears to be responsible for the annealing which occurs between the initial annealing factor and an annealing factor of approximately 2.5. If the kinetic behavior in this region is characterized by a simple second order process, then the annealing should be described by the expression

$$\frac{1}{AF(t) - 2.5} - \frac{1}{AF(o) - 2.5} = Mt, \tag{3}$$

where the slope M is the product of the stable defect density and the rate constant of the process. In Figure 10, the inverse defect density $(1/(AF(t) - 2.5))$ is plotted as a function of time for the 2N914 at 212°K. Note that the data falls reasonably close to a straight line as predicted by Equation 3. As an illustration of particular second order process, the solid curve shown in this figure represents a prediction based on vacancy-to-divacancy conversion (assuming vacancies and divacancies to be equally effective as recombination centers). In this case, the theoretical equation is[15]

$$\frac{1}{AF(t) - \frac{AF(o)}{2}} - \frac{1}{\frac{AF(o)}{2}} = 8/3\pi r_o \nu X_J^2 N_{NA} \exp\left(\frac{-E_A}{KT}\right) t. \tag{4}$$

To obtain the illustrated curve, the following parameter values were assumed:

E_A (activation energy) = 0.33 eV (vacancy in p-type Si),

r_o (defect interaction distance) = 4.7×10^{-8} cm (two interatomic distances),

ν (frequency factor) $\cong 2.10^{12}$ (from Watkins),

X_J (jump distance) = 2.35×10^{-8} cm, and

N_{NA} (stable defect density) = 6.3×10^{19} cm^{-3}.

For this value of N_{NA}, the initial vacancy concentration would be approximately 2.9×10^{20} cm^{-3}, predicting a cluster diameter (if spherical) of approximately 169 Å for a 600-defect cluster (the most probable number for the SPR spectrum). For a cigar-shaped cluster, a larger maximum dimension would be necessary to include the same number of defects.

This vacancy concentration inside the cluster is considerably greater than expected. However, there is doubt as to the validity of using the 0.33 eV vacancy activation energy since inside the highly disordered cluster region the vacancy charge state is likely to be different than in bulk material. In fact, an activation energy of approximately 0.26 eV is obtained from an analysis of the first stage in the 213°K and 268°K

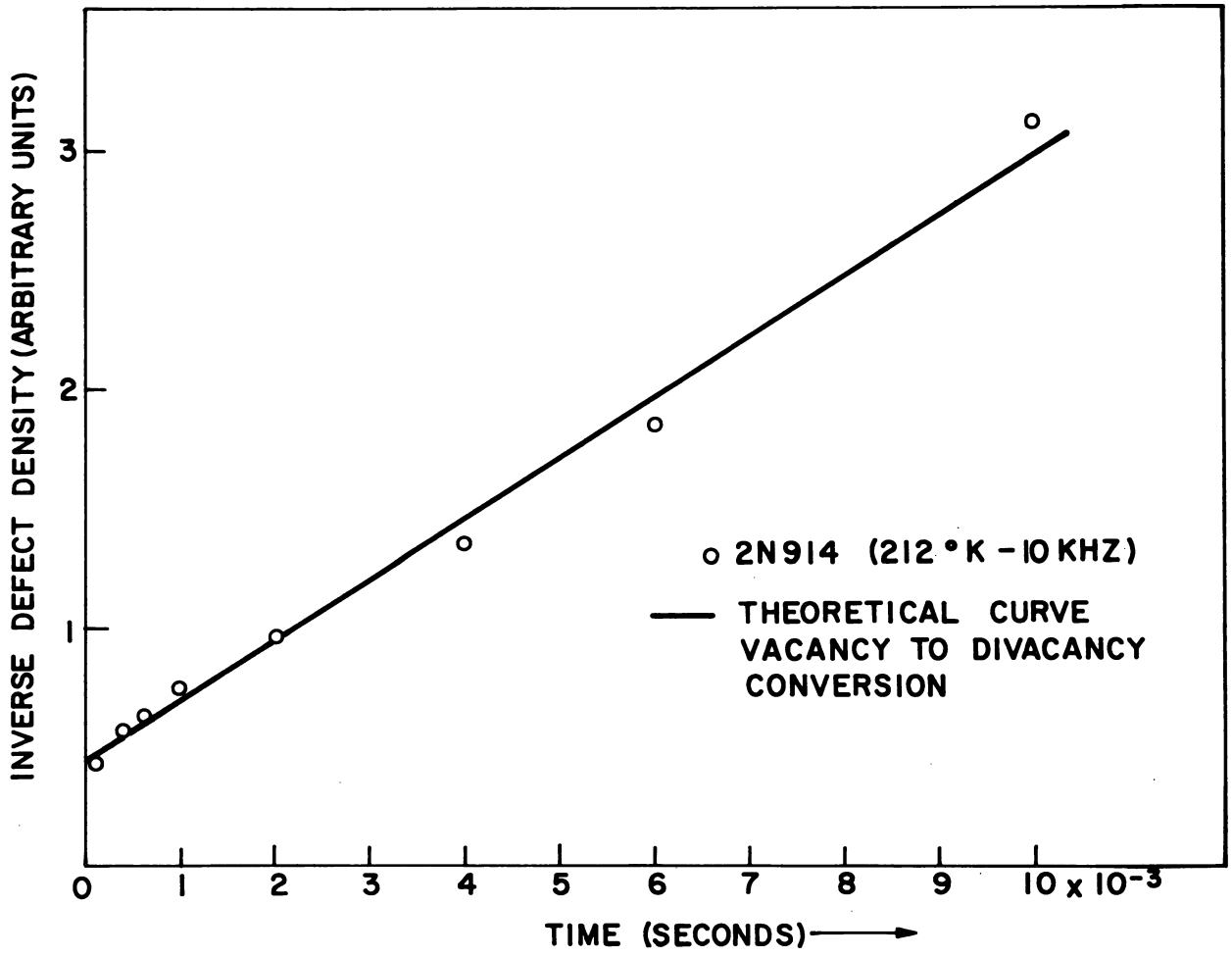

Figure 10. The Inverse Density of Defects Which Anneal in the First Stage at 212°K Versus Time

curves shown in Figure 3. For this activation energy, a more reasonable initial vacancy density, 5×10^{18} cm^{-3}, yields the calculated curve shown in Figure 10.

Outside the cluster, interstitials and vacancies undergo reactions similar to those discussed above; however, the concentrations of these defects are undoubtedly lower in this region than inside the disordered region itself. Consequently, the relative probabilities of the above reactions may be quite different than inside the cluster. If, for example, the concentration of radiation produced defects is comparable to or smaller than the impurity density, the most significant reaction may be the pairing of defects with impurities, i.e., process 4. These reactions will become significant in the reordering when the higher order reactions inside the cluster have neared completion.

In this study, the dominant impurity present is undoubtedly oxygen since most silicon devices are fabricated from pulled crystals. The solar cells employed in these measurements contained a measured oxygen concentration of approximately 10^{18} cm^{-3}.

It is observed, then, that the initial phase of cluster reordering should involve processes inside the cluster where the defect density is greatest, but that later phases of the reordering should be dominated by processes external to the cluster. One such process is A center formation due to migration of isolated vacancies to interstitial oxygen atoms. The kinetics of this process have been studied by Watkins[14] through EPR measurements of oxygen containing silicon. The vacancy activation energy (0.33 eV - p-type silicon) and pre-exponential factor (2×10^{12} sec^{-1}) obtained by Watkins predict halftimes which are within an order of magnitude of those observed experimentally for the latter stage of the 2N914 annealing characteristic shown in Figure 3. However, if the vacancy concentration is much smaller than the oxygen concentration, as in Watkins' measurements, such annealing should be characterized by first order kinetics and an exponential time dependence. This is not observed experimentally, as can be seen in Figure 3. The actual annealing curve varies much more slowly with time than a simple exponential. Furthermore, if vacancy motion is involved in this stage of the annealing, such motion should be charge state dependent. In n-type silicon the vacancy moves much faster than in p-type[14] silicon and, consequently, the annealing should proceed more rapidly in n-type material. Also, the effect of minority carrier injection on the annealing should differ in p- and n-type materials. No such results have been observed. The halftimes for this annealing stage are approximately equal in both material types. In addition, minority carrier injection has a similar effect in both material types, i.e., it speeds up the process. It appears, then, that the annealing in this stage is inconsistent with simple vacancy migration to oxygen. Although other, more elaborate, models involving vacancy motion could possibly be formulated to eliminate the disagreement between experimental and predicted curve shapes, these models will still be inconsistent with the observed injection dependences. Consequently, these models will not be pursued further until this inconsistency is substantiated or resolved.

An alternative explanation for this annealing stage could be the migration of interstitial silicon atoms back to their parent cluster. Upon reaching the cluster, the interstitial could recombine with a vacancy complex formed during the initial stage of reordering, releasing vacancies to the bulk in agreement with the previously discussed optical absorption experiments. The migration of interstitials back to the cluster would be a diffusion-limited process. Hence, the number which would return in a given time interval would depend both on the initial interstitial distribution and the interstitial diffusion constant, D_I.

Evidence substantiating the feasibility of this model has been provided by the quenching experiments of Bemski and Dias.[16] In these experiments, quenching of silicon samples introduced a defect which annealed at room temperature with an activation energy of approximately 0.3 eV. The dependence of the observed annealing on sample dimensions, even in oxygen containing materials, led Bemski and Dias to believe that the silicon interstitial was being observed. In the interstitial diffusion models the time-varying defect density inside the cluster can be obtained by solving the problem of defect diffusion into a spherical sink for a particular initial defect distribution outside the sink. This involves solving the diffusion equation in spherical coordinates. Simple solutions to this problem, which is discussed extensively in Crank,[17] can be obtained only for certain very simple initial distributions. For example, a solution can be obtained for the case where the initial interstitial density, $N_I(r)$, is given by the expressions

$$N_I(r) = N_{IO}\left(\frac{r_o}{r}\right); \quad r_o \leq r \leq d \tag{5}$$

and

$$N_I(r) = 0; \quad r > d, \tag{6}$$

where r_o is the cluster (sink) radius, and d is the radius bounding the interstitial distribution. For this distribution, the total number of defects in the cluster, T_c, is given by the expression

$$T_c = T_{co} - \frac{2 r_o (d - r_o)}{d^2 - r_o^2} \frac{IX}{\sqrt{\pi}}\left[1 - \exp\left(-\frac{1}{X^2}\right) + \frac{\sqrt{\pi}}{X} \operatorname{erfc}\left(\frac{1}{X}\right)\right], \quad X = \frac{2(D_I t)^{1/2}}{(d - r_o)} \tag{7}$$

and

I = total number of interstitials.

For a fixed number of interstitials distributed over the region $r_o \leq r \leq d$, the average interstitial-cluster separation in the above distribution is larger than if the initial interstitial density varies more rapidly with r. Consequently, this model predicts a slower annealing rate than would be predicted for a more rapidly varying distribution over the same total distance d.

The temperature dependence of this process should, of course, be characteristic of interstitial motion. If the interstitial is quite mobile at room temperature, as required in this model, the temperature dependence is much less pronounced than for a first or second order process involving a higher activation energy of motion and a much smaller number of jumps.

Consequently, the temperature dependence of the experimental transient annealing is significant in distinguishing between the above model and one involving possible evolution of defects from large defect complexes. This latter model could be characterized by a spectrum of first order processes with varying activation energies. Such a model would be considerably more temperature-dependent than the diffusion-limited model, since the process activation energies necessary to match a generation-limited model and

experimental kinetic data would be much larger than the corresponding activation energy required when the defect is allowed to travel large distances before recovery occurs.

If the initial process at 213°K is subtracted from the total, the remaining process encompasses approximately 50 percent of the annealing, but it requires much longer times to reach completion. Figure 11 shows a plot of this long time process, as observed in the 2N914 at 268°K. Here most of the initial process is completed before 0.1 ms. Also plotted in this figure is the prediction of the theoretical interstitial migration model discussed above. In this plot, the unannealed fraction (F) of the process is plotted versus normalized time where the normalization factor for each curve is the process halftime. The experimental curve is observed to vary more slowly with time than the calculated curve. This would be expected for a distribution of interstitials around the cluster varying more rapidly with r than assumed above. Also shown in this figure are data for the 2N914 at 300°K and solar cell data for a P/N device at 313°K. When normalized in the manner shown in this plot, all the data show a similar time dependence.

In Figure 12, the temperature dependence of the 2N914 data has been plotted in terms of the second stage halftime versus inverse temperature. Although considerable scatter exists in these data, the process activation energy can be extracted from the slope of the most probable line drawn between the points. By doing so, a value of approximately 0.28±0.05 eV is obtained for E_A. The data in this plot were for the 100 Hz measurements, the lowest average injection level available. The higher injection level measurements predicted similar values for E_A; however, the experimental scatter in the data was much more severe.

To check the consistency of this value of E_A with the time dependent annealing observations, the value of D_I necessary to equate the experimental and theoretical processes at their halftime points can be calculated. If d is assumed to be much greater than r_o, Equation 5 reduces to

$$D_I = \frac{0.238d^2}{t_{1/2}} \tag{8}$$

at $t = t_{1/2}$, the process halftime. Substituting the halftime value obtained from the 268°K curve of Figure 2, the relation

$$D_I \cong 2d^2 \tag{9}$$

is obtained. If D_I is approximated by the expression[18]

$$D_I = \nu \frac{(X_J)^2}{6} Z \exp\left(-\frac{E_A}{KT}\right), \tag{10}$$

the value of d necessary to make the experimental data consistent with the activation energy of 0.28 eV, obtained in Figure 12, can be calculated by using appropriate values of X_J, ν and the coordination number Z.

For $\nu = \frac{KT}{h}$, $X_J = 3.8 \times 10^{-8}$ cm and Z = 4 (appropriate for diamond lattice) a value of 8×10^{-5} cm is obtained for the distance parameter, d. This value is quite large compared to the likely cluster size ($<10^{-5}$ cm). Such a large value of d is questionable since it is greater than the average separation for the neutron fluence employed. (For 1.8×10^{13} NVT, the cluster separation is approximately 0.37×10^{-4} cm.) However, the value of ν used in the above calculation is valid only to within an order of magnitude. For vacancy motion, for example, Watkins has observed a value of $\nu Z = 2 \times 10^{12}$ sec^{-1}. If interstitial motion

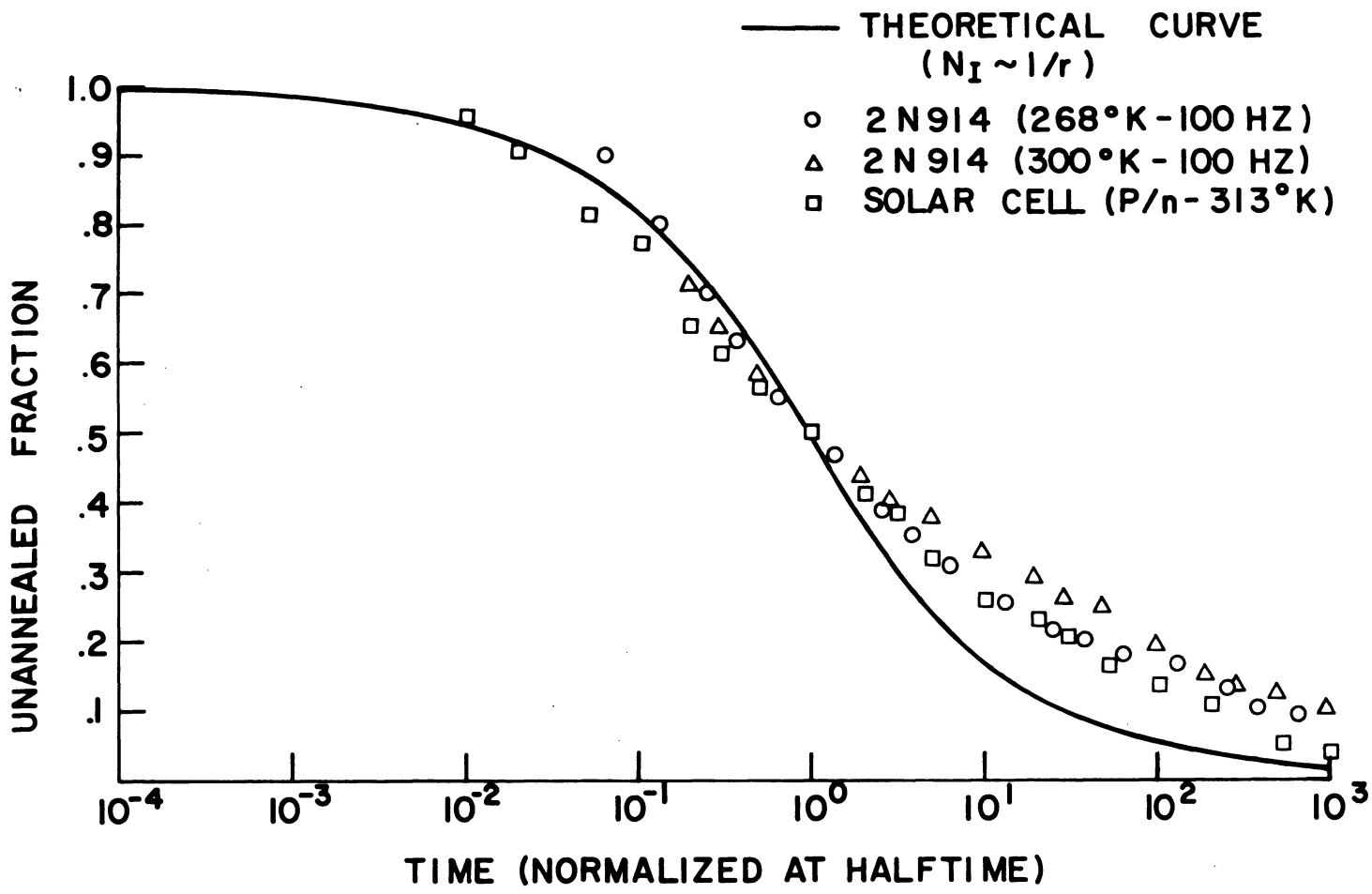

Figure 11. The Unannealed Fraction of Defects in Second Stage Annealing Versus Time. (The theoretical curve is obtained assuming a distribution of mobile defects around the cluster whose density varies as 1/r.)

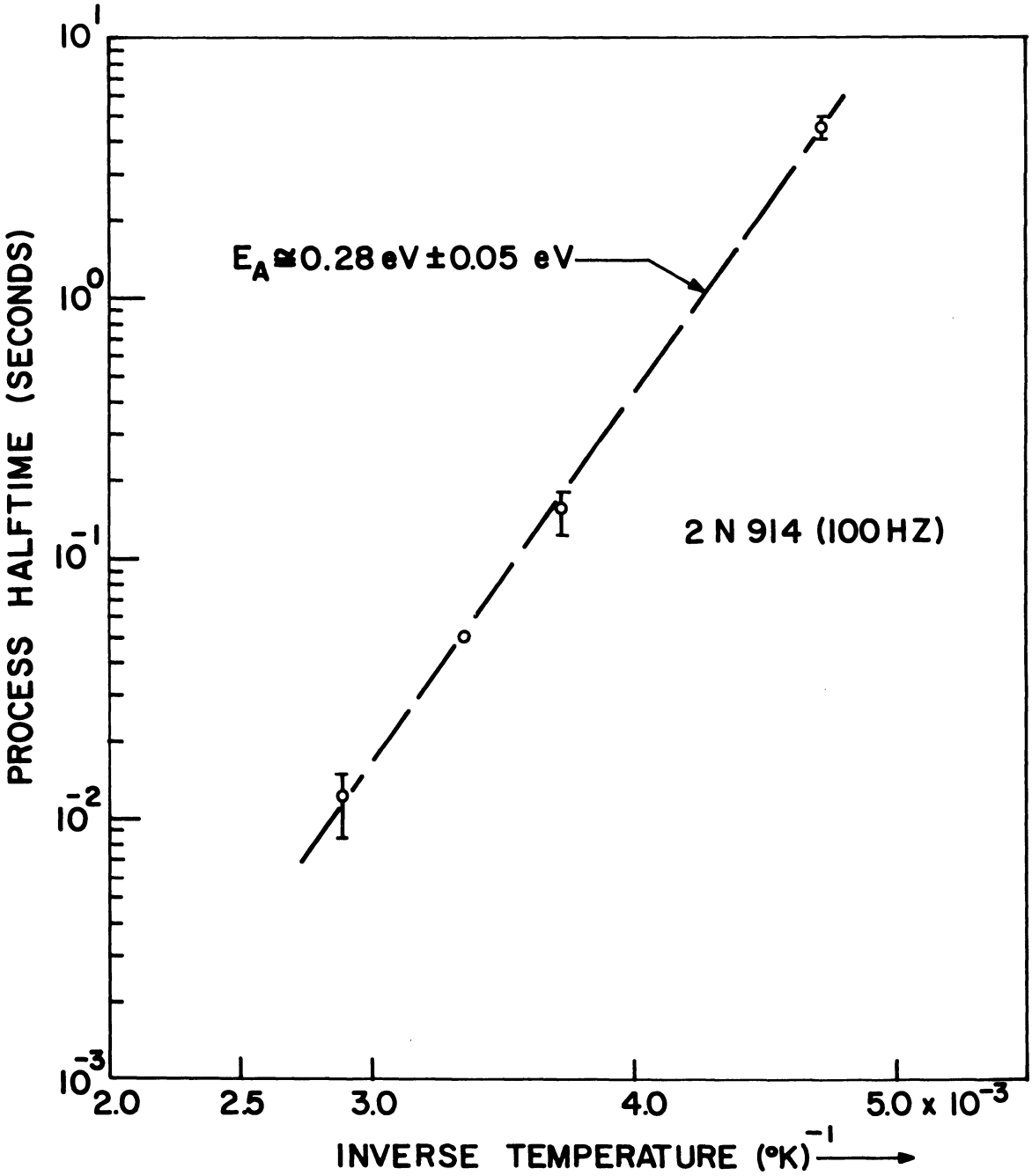

Figure 12. The Halftime of the Second Annealing Stage Versus Inverse Temperature for the 2N914 Transistor (100 Hz Measurements)

were also characterized by this smaller value of νZ, a value of approximately 2 x 10^{-5} cm would result for the distance d. It can be concluded from these calculations that the value of d necessary to equate the theoretical and experimental processes at their halftime points is not unreasonable. Unfortunately, it is not possible to determine this parameter precisely due to lack of knowledge of constants in Equation 10. It is satisfying, however, that this model with its many assumptions can be made to fit the experimental results reasonably well. It is believed that the agreement will be increased when more realistic interstitial distributions are employed in the diffusion analysis.

It is possible, however, that interstitial diffusion may be a more complex process than pictured above, since recent infrared absorption studies[11] indicate that the silicon interstitial may also be trapped by oxygen in the crystal. Since the average distance between such oxygen complexes is likely to be much less than the distance d, derived above, any interstitials at the proper distance from the cluster to satisfy this model would be trapped before they could arrive at the cluster. However, these absorption studies also indicate that the complex thus formed is thermally unstable near room temperature. This is significant since it means that the diffusion of interstitials back to their parent cluster may be characteristic of trap-limited diffusion where the interstitial spends part of the time trapped on an oxygen atom and part of the time diffusing.

B. Injection Dependence

At the present time the least understood aspect of transient annealing is the injection dependence. The data shown earlier for the 2N914 shows that this dependence definitely does exist and that it is quite significant, even at 300°K. By varying the pulse repetition rate in the measurements on this device, the average injection level was varied without varying the measurement injection level. When the results of these measurements are superimposed for various repetition rates, as in Figure 5 (300°K), the second annealing stage, the dominant stage near room temperature, is seen to be quite injection dependent. In the 2N914 (NPN), the annealing rate in this stage depends strongly on the injection level in the base of the device (p-type region). An increase in either the injection level (pulse height) or pulse repetition rate is observed to increase the rate of annealing. Only a very small change in E_A is required to produce the observed dependence of process halftime on repetition rate. Unfortunately, values for E_A within the experimental error shown in Figure 12 would be sufficient. Such a change in defect activation energy with injection level could be explained in terms of a charge state dependent activation energy, similar to that proposed for the vacancy by Watkins[14] and observed by Gregory[2] in gamma ray damage annealing studies. Recent studies of injection dependent annealing in both P and N type materials in silicon solar cells (N on P and P on N devices respectively) have yielded results consistent with such a model. These studies also indicate that minority carrier injection increases the annealing rate in p-type silicon, greatly reducing the annealing factor at any given time. Furthermore, as the model requires, in n-type material carrier injection has a much smaller effect and the small dependence which does exist is in the opposite sense, i.e., an increase in injection level produces a decrease in annealing rate, or larger annealing factors.

As this discussion indicates, the injection dependence of transient annealing is not yet understood. However, it is recognized that these effects are significant in semiconductor devices and that they must be included in any model which explains the transient annealing of neutron damage.

BIBLIOGRAPHY

1. Sander, H. H., Room Temperature Annealing of Silicon Transistor Parameters Degraded by a Burst of Neutrons, SC-R-64-192, Sandia Laboratory, Albuquerque, July 1964.

2. Gregory, B. L., JAP, 36, pp. 3765-3769, December 1965.

3. Parsons, J. R., Phil. Mag (G.B.), 12, pp. 1159-1178, December 1965.

4. Bertolotti, M., Papa, T., Sette, D., and Vitali, G., JAP, 36, pp. 3506-3512, November 1965.

5. Stein, H. J., Personal Communication.

6. Stein, H. J., Bul. Am. Phys. Soc., 11, p. 194, February 1966.

7. Stein, H. J., IEEE Nuclear Radiation Effects Conf., (1965), SC-R-65-938, Sandia Corporation, Albuquerque, New Mexico.

8. Curtis, O. L., Jr., Bul. Am. Phys. Soc., 11, p. 193, February 1966.

9. Stein, H. J., IEEE Nuclear Radiation Effects Conf. (1966).

10. Gossick, B. R., JAP, 30, pp. 1214-1218, August 1959.

11. Whan, R. E., to be published, JAP.

12. Schmitt, R. A., and Sharp, R. A., Phys. Rev. Letters, 1, pp. 445-447, December 15, 1958.

13. Truell, R., Teutonico, L. J., and Levy, P. W., Phys. Rev., 105, pp. 1723-1729, 1957.

14. Watkins, G. D., J. Phys. Soc. Japan, 18, pp. 22-27, 1963.

15. Waite, T. R., Phys. Rev., 107, pp. 463-470, July 15, 1957.

16. Bemski, G. and Dias, C. A., JAP, 35, pp. 2983-2985, October 1964.

17. Crank, J., The Mathematics of Diffusion, p. 84, Oxford, 1956.

18. Reiss, H. and Fuller, C. S., Semiconductors, ed. Hannay, N.B., Reinhold Publishing Corp., New York (1959), p. 223.

19. Gregory, B. L. and Sander, H. H., IEEE Nuclear Radiation Effects Conf., Columbus, Ohio (1967).

OTHER ARTICLES AND REPORTS ON TRANSIENT ANNEALING

1. Binder, D. and Butcher, D. T., Rapid Annealing in Silicon Transistors, Air Force Weapons Laboratory Report AFWL-TR-66-145, February 1967.

2. Wikner, E. G., Nichols, D. K., Naber, J., Flanagan, T., Horiye, H., and Van Lint, V. A. J., Transient Radiation Effects, Harry Diamond Laboratories Report DA-49-186-AMC-65(X)-1, February 1967.

3. Curtis, O. L., Jr., Bass, R. F., and Germano, C. A., Radiation Effects in Silicon and Germanium, Harry Diamond Laboratories Report DA-49-186-AMC-235(X)-2, November 1966.

4. Stein, H. J. and Vook, F. L., Transient Radiation Defects, Symposium on Radiation Effects in Semiconductor Components, Toulouse, France, March 7-10, 1967, SC-R-67-1048, Sandia Corporation, Albuquerque, New Mexico.

5. Barnett, B., Langsam, L. M., Schoch, C. B., and Schow, D. A., Temporary Neutron Damage in Transistors, Symposium on the Physics of Failure of Devices, Douglas Aircraft Company Technical Report, Columbus, Ohio, November 1966.

RADIATION SOLID STATE PHYSICS

Chihiro Kikuchi

TABLE OF CONTENTS

RADIATION SOLID STATE PHYSICS

Chihiro Kikuchi
Department of Nuclear Engineering
University of Michigan

I. INTRODUCTION

The purpose of the following lectures will be to provide an introduction to solid state physics to students of nuclear science and engineering. Solid state physics as a discipline has been known for many years, but it is only recently that the general public has become aware of its importance. Thanks to the press, popular scientific articles and others, terms such as transistors, Esaki diode, parametric amplifiers, masers, lasers, etc. Words such as molecular electronics, micro-electronics and quantum electronics have been coined to describe this facinating new field of applied solid state physics.

Many solid state devices have already found application in nuclear instrumentation and no doubt many more will be found. It is hoped that through the discussion to follow, students will get an insight into effects produced by nuclear radiations in solids, and through this understanding to anticipate future developments in radiation solid state physics.

To limit the scope of the discussion, we shall center our attention upon the effects of high energy radiation in

solids, as presented schematically in the following diagram.

Neutrons
α, β, γ

Target

The target material can be a solid of some kind or another, such as a solar battery, a NaI crystal, a piece of cadmium sulfide, or NaF doped with uranium. For our discussions we shall be concerned primarily with materials such as germanium, silicon, silicon P-N junctions, cadmium sulfide, and NaI.

A variety of radiations can be used, such as neutrons, α-particles, β-particles, and gamma rays. The bulk of our discussions will be centered about neutron effects, so that some of the neutron properties are listed below.

1.	Mass	:	1.008982
		=	1.6747×10^{-24} gm
2.	Charge	:	0
3.	Half-life	:	1288 min.
4.	Spin (angular momentum)	:	$\hbar/2$
5.	Magnetic moment	:	-1.913148
6.	Wave Length	:	$\lambda = h/p$

Because of the zero charge and heavy mass, the neutron can penetrate deep into solids and impart appreciable linear momentum and energy to nuclei upon collisions. Property (3) is

probably unimportant for most experiments in terrestrial laboratories in which the neutron transit time is very short in comparison to its half-life. Properties (4), (5), and (6) are important in neutron diffraction.

We plan in particular to emphasize the effects produced by thermal neutrons. The bulk of the radiation damage studies to date have been done by using fast neutrons. However, effects produced by thermal neutrons in solids, such as NaF doped with uranium or compounds containing cadmium have not been thoroughly investigated. It is hoped that a detailed examination of the thermal neutron effects will open up new areas of research.

And finally, a few comments about the fluorescence and scintillation of NaI and possibly other alkali halides will be made. One reason for this is to correct the erroneous impression that the mechanisms for energy transport and energy conversion in NaI are similar to those in such semiconductors as silicon, zinc sulfide, and cadmium sulfide. The other reason is that the discussion of the fluorescence and scintillation of NaI will give us an opportunity to introduce the concept of excitons, which are the solid-state analogues of the electron-positron pair. The importance of excitons in energy transfer and energy conversion mechanisms is just beginning to be appreciated, and in the future we will no doubt be hearing more about it.

II. SEMICONDUCTOR FUNDAMENTALS

Since the interpretation of radiation effects will depend upon such terms as conduction and valence bands, electrons and holes, excitons, donors and accepters, substitutional and interstitial sites, etc., we shall first present a brief review of some of the concepts and properties of semiconductors.

2.1 Crystal Structure, Substitutional and Interstitial Sites

The crystal of germanium or silicon has the so-called diamond structure, which can be most easily visualized as consisting of two inter-penetrating face-centered cubic lattices, in which the two lattices are displaced by 1/4 of the distance along the body diagonal of the cell. We notice that the atoms belonging to one sub-lattice are bonded tetrahedrally to 4 atoms belonging to the other sub-lattice.

Possibly some additional insight to the relation of different crystal structures can be obtained by examining the crystal structure of zinc blende, or cubic zinc sulfide. In this crystal, the zinc atoms form a face-centered cubic, and so do the sulfur atoms. Furthermore it is easy to see that the Zn-sub-lattice is displaced from the S-sub-lattice by 1/4 of the body diagonal. If in this structure, the two atoms are made identical, then we will have the diamond structure. The so-called NaCl-structure is somewhat closely related to the zinc blende structure. As in zinc blende, in NaCl, there are

the two face-centered cubic lattices of Na and Cl atoms, but in this case, the two sub-lattices are displaced by 1/2 of the body diagonal.

The crystal lattice sites that are occupied by atoms in an ideal crystal are called substitutional sites, and those that are not occupied are called interstitial sites. It is clear that in a real crystal, some atoms might be missing from substitutional sites, and atoms might be present in interstitial sites. Chemical impurities might occupy substitutional and/or interstitial sites. A germanium struck by neutron can become displaced from its substitutional site and subsequently become trapped in an interstitial site. These crystal defects, due to chemical impurities or other means have profound effects upon semiconductor properties.

2.2 Energy Level in Atoms and in Solids. The Band Model

Experiments show that solids have a very wide range of resistivities, varying from about 10^{-6} ohm-cm for metals to about 10^{12} ohm-cm for crystalline insulators. This is hard to understand from the classical standpoint because all solid materials for a given volume have comparable numbers of electrons. To account for these differences in electrical resistivity, it is customary to appeal to the so-called band model.

Consider an atom with energy levels as represented by the horizontal lines to the left.

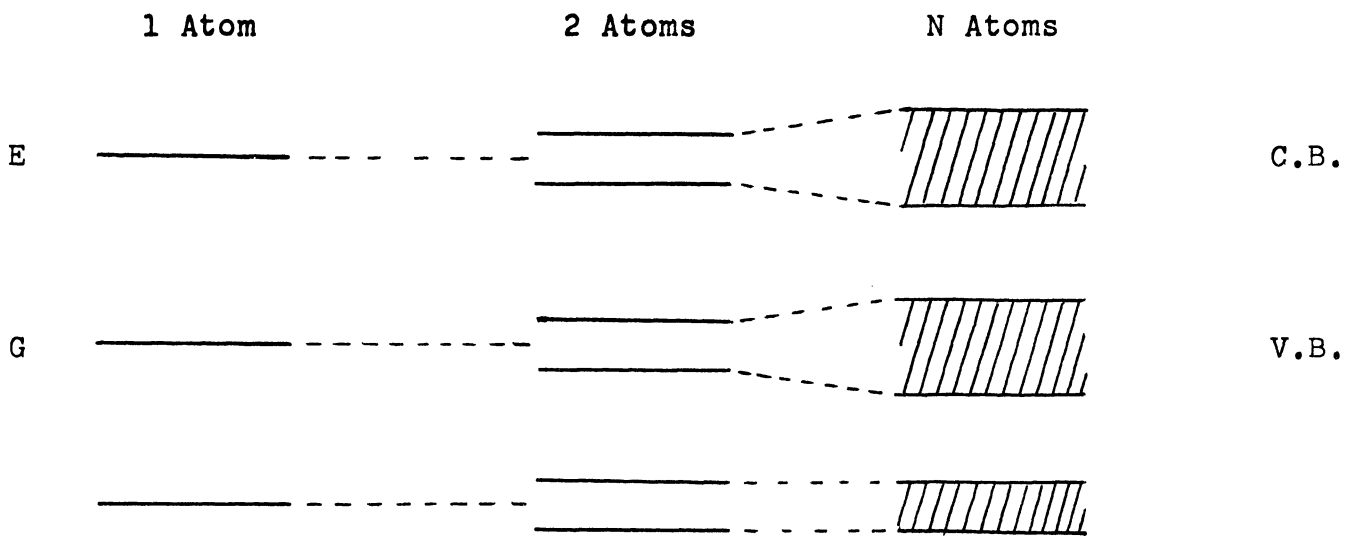

Figure 2.1

Quantum mechanics shows that if two such atoms are placed close together, the energy levels will be split as shown in the second column. Extrapolating to N particles, we should expect the atomic levels to fan out into a band of N levels spaced close together. Consider now the energy bands arising from the atomic levels G and E, which are the ground and first excited states respectively. The band labelled V.B., for Valence Band, comes from G, and C.B., for Conduction Band, comes from E. At T = 0, the atomic state G is occupied, so that for the solid, we should expect the valence band to be full. Similarly, at T = 0, both E and C.B. are empty.

Let us now see how these bands can contribute to the conductivity of the material. We need to consider only the valence and the conduction band. The separation between the bands is called the band gap. The following diagrams depict the situation at T = 0 and T $\neq$ 0:

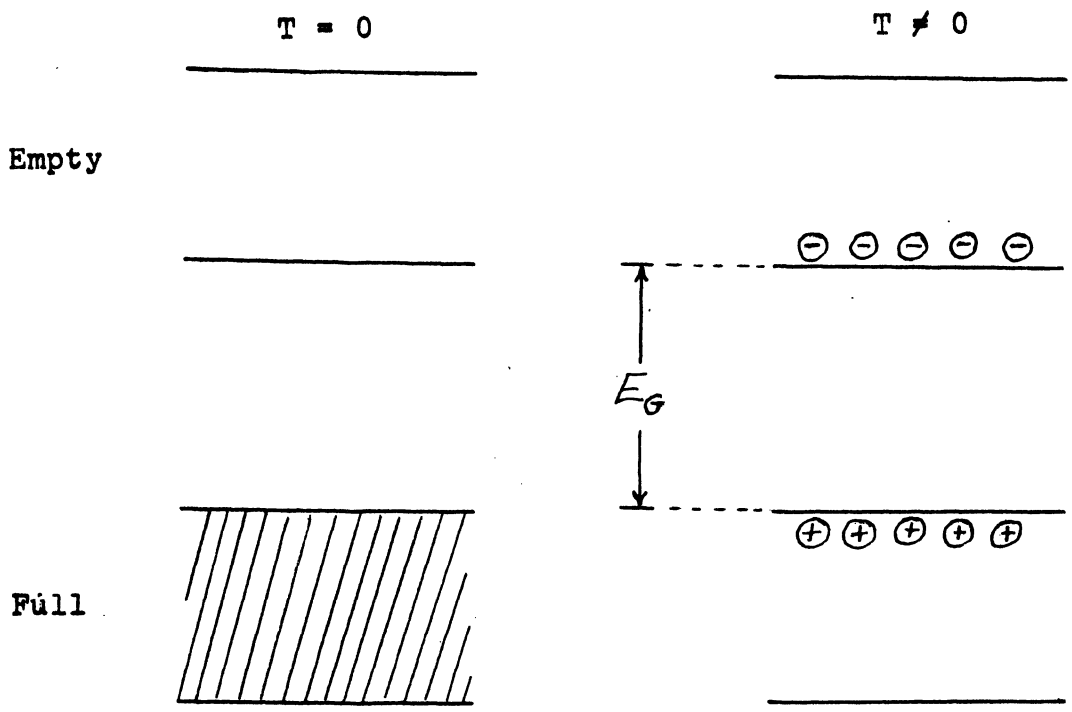

Figure 2.2

At T = 0, the valence band is full and the conduction band is empty, so that this material will be a perfect insulator. On the other hand T = 0, some of the electrons will be excited thermally into the conduction band, leaving behind vacancies called holes. The electrons and holes can move around, so that they can now contribute to the conductivity of the material. For the ideal pure material under consideration, we see that

$$n = p \tag{2.1}$$

in which n and p are the electron and hole concentrations. Also because of the Boltzmann factor, we expect n and p to increase with increasing temperature, or for a given temperature, n and p are larger for smaller band gap, E_G. In fact we shall show

that

$$np \propto e^{-E_G/kT} \tag{2.2}$$

For the ideal, perfect, and pure crystal

$$n = p$$

so that

$$n_i = p_i \propto e^{-E_G/2kT} \tag{2.3}$$

in which the subscript i is added to denote that this carrier concentration is a property of a pure sample. We need to note that (2.2) applies not only to a pure sample, but also when chemical impurities and imperfections are present. In fact, it can be shown that

$$np = n_i p_i = n_i^2 \qquad (n_i = p_i) \tag{2.4}$$

So far we have assumed that the electron and hole concentrations arise from thermal agitation. It is however important to keep in mind that free electrons and holes can be created by photons, with sufficient energy to push an electron into the conduction band; when this happens, photoconductivity takes place. Also the electrons can be put into the conduction band by means of an ionizing particle, such as an alpha-particle. When this happens, an electrical pulse can be produced in the external circuit. Again, excess electrons

and holes can be injected; then later action can take place.

2.3 Comparison of Water and Semiconductor (Germanium)

Superficially water and germanium look very different. But let us consider some of the similarities.

Pure water contains H^+ and OH^- ions. Also it is known that the acidity and alkalinity of water can be controlled by adding acids and bases. Chemists have shown that the ionization product, or the product of the hydrogen and hydroxyl ion concentrations in moles/liter, for water is

$$[H^+]\,[OH^-] = 10^{-14} \tag{2.5}$$

In pure water

$$[H^+] = [OH^-] = 10^{-7} \text{ moles/liter} \tag{2.6}$$

Physicists, on the other hand, prefer to work in concentrations expressed in atoms or ions/cm^3. Since

$$1 \text{ mole} = 6.03 \times 10^{23} \text{ ions}$$

$$[OH^-] = 10^{-7} \text{ moles/liter} = 10^{-10} \text{ moles/cm}^3$$

$$= (6.03 \times 10^{23})(10^{-10}) = 6 \times 10^{13} \frac{\text{ions}}{\text{cm}^3}$$

As we shall see presently this concentration is very close to the electron and hole concentration in germanium at room temperature. If acid, such as HCl, is added, then

$$\begin{aligned} H_2O &\longleftrightarrow H^+ + OH^- \\ HCl &\longleftrightarrow H^+ + Cl^- \end{aligned} \qquad (2.8)$$

so that the increase in the hydrogen ion concentration causes a decrease in the hydroxyl ion concentration. Consider next the enthalpy for the reaction. According to McDougall, Thermodynamics and Chemistry, p. 322, at T = 300°K,

$$H = 13{,}300 \text{ cal/mole}$$

In physics, electron-volt is often used as the unit of energy. The conversion factor is

$$\begin{aligned} 1 \text{ ev/molecule} &= 1.60 \times 10^{-12} \text{ erg/molecule} \\ &= (1.6 \times 10^{-12})(6.03 \times 10^{23}) \text{ ergs/mole} \\ &= \frac{(1.6 \times 10^{-12})(6.03 \times 10^{23})}{4.185 \times 10^{10}} = 23.05 \frac{\text{k Cal}}{\text{Mole}} \\ \frac{\Delta H}{N_o} &= 0.88 \text{ ev /ion} \end{aligned} \qquad (2.9)$$

For germanium, this value is about 0.72 ev.

For pure germanium, the electron and hole concentrations are

$$[h^+] = [e^-] = 2 \times 10^{13}/cm^3 \qquad (2.10)$$

The electron hole association and dissociation processes can be represented by

$$(h^+ \; e^-) \longleftrightarrow h^+ + e^- \qquad (2.11)$$

Now, boron, as an example, behaves like a semiconductor acid, i.e.,

$$B \longleftrightarrow h^+ + B^- \qquad (2.12)$$

So the addition of boron increases the hole concentration and thus makes the material p-type.

The following table then perhaps can serve to illustrate the relation of water and germanium.

TABLE 2.1

Water	Germanium
H	h^+
OH	e^-
$[OH]\ [H^+] = 10^{-14}$	$[h^+][e^-] = 10^{-13}$
Pure H_2O	Pure Ge
$H^+ = 10^{-7}$	$h^+ = 1/3 \times 10^{-7}$ moles/liter
Acid: HCl	p-type: Boron
Base: NaOH	n-type: Phosphorus
H = 13.3 K cal/mole	H = 16.6 K cal/mole

2.4 Donors and Acceptors

The semiconductor analogues of acids and bases in chemistry are the acceptors and donors. Acceptors tend to increase the hole concentration, just as acids added to water will increase the hydrogen ion (positive) concentration. Donors, on the other hand, increase the electron concentration and suppress the hole concentration, just as a base in water will increase the negative hydroxyl ion concentration while suppressing the hydrogen ion concentration. In the Group IV semiconductors,

elements that give rise to donors are those in Group V, such as F, As and Sb, and those that give rise to acceptors are the Group III elements such as B, Al, Ga. The donor and acceptor centers can be produced by irradiation.

If the electron concentration n is larger in comparison with the hole concentration the material is said to be N-type.

2.5 Semiconductor Transport Properties

We shall then explore some of the transport properties of carriers--the electrons and holes--as affected by the applied electric and magnetic fields.

a. Electric Field

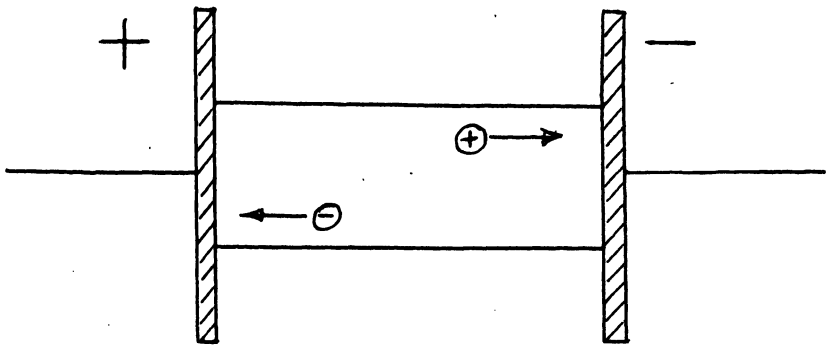

Figure 2.3

Suppose that a potential difference is applied across a semiconductor, as shown in the figure. The electrons will then stream to the left and the holes to the right. Consider for the moment, the motion of the holes. These are subject to two types of forces, one due to the accelerating action of the electric field, and the other due to the retarding effects

of collisions. We can write

$$m \frac{dV}{dt} = F_{acc} + F_{net} \tag{2.13}$$

where, obviously

$$F_{acc} = q \mathcal{E} \tag{2.14}$$

For the retarding forces, we shall assume that it is proportional to the velocity. Thus we shall set

$$F_{net} \propto \bar{V} \qquad F_{net} = -\frac{m}{\tau} V \tag{2.15}$$

where τ is proportionality constant, having the dimension of the time, and is to be associated with the mean time between collision of the streaming electrons. Then (2.13) becomes

$$m \frac{dV}{dt} = e\mathcal{E} - \frac{m}{\tau} V$$

Experimentally it is observed that a <u>constant</u> current flows through the material when the voltage is applied. This implies that the velocity reaches a steady state value. In other words

$$\frac{dV}{dt} = 0$$

So that

$$e\mathcal{E} - \frac{m}{\tau} V = 0$$

or

$$V = \frac{e\tau}{m}\mathcal{E} = \mu\mathcal{E} \tag{2.16}$$

where

$$\mu \equiv \frac{e\tau}{m} \tag{2.17}$$

is referred to as the mobility. Now the current density is given by

$$\begin{aligned} J_p &= (\text{Charge density})(\text{Velocity}) \\ &= q\,V\,P = q\,P\,\mu_p\,\mathcal{E} \end{aligned} \tag{2.18}$$

where p is the hole density. Furthermore, Ohm's law states that the current density is proportional to the electric field, i.e.

$$J_p = \sigma_p\,\mathcal{E} \tag{2.19}$$

where σ_p is the conductivity. Comparing (2.18) and (2.19) we find that

$$\sigma_p = q\,P\,\mu_p \tag{2.20}$$

Similarly for electrons

$$J_n = q\,n\,\mu_n\,\mathcal{E} \tag{2.21}$$

$$\sigma_n = q\,n\,\mu_n \tag{2.22}$$

and the <u>total</u> current density clearly is

$$J = J_p + J_n = q(n\mu_n + p\mu_p)\mathcal{E} \qquad (2.23)$$

and

$$\sigma = q(n\mu_n + p\mu_p) \qquad (2.24)$$

b. Magnetic Field

This is important because it becomes possible to distinguish the effects of the electrons from those of the holes. Consider the following simple-minded picture. In figure 2.3, suppose that a magnetic field B is applied at right angles to and into the plane of the paper. Then the holes streaming to the right will tend to be deflected towards the top of the page, but the well-known relation that the force on a charged particle moving in a magnetic field with velocity $\underline{v}$ is

$$q\,\underline{v} \times \underline{B} \qquad (2.25)$$

where q is the charge. Similarly, the electrons will be deflected downwards. As a result there will be a transverse potential developed across the semiconductor. Roughly speaking, the lower edge will be positive if the charged carriers are predominantly holes, and negative, if the electrical conductivity arises primarily from the motion of the electrons. This is the so-called Hall effect. The Hall current is

$$\mu_p \underline{J}_p \times \underline{B} \qquad (2.26)$$

for holes and

$$\mu_n \underline{J}_n \times \underline{B} \tag{2.27}$$

for the electrons.

c. Concentration Effects

If there are variations in carrier concentrations, the charged carriers will tend to move in the direction of decreasing concentrations, giving rise to the diffusion current. For the holes this is

$$-q D_p \nabla p \tag{2.28}$$

and for the electrons

$$q D_n \nabla n \tag{2.29}$$

in which D_p and D_n are the diffusion coefficients of holes and electrons respectively. The diffusion coefficient and the mobility are related by

$$\mu = \frac{q}{kT} D \tag{2.30}$$

in which q, k, and T are the elementary charge, Boltzmann constant, and the absolute temperature respectively.

Diffusion plays an important part in photoconductivity, photomagnets-electric effect, and in thermo-electric effects in semiconductors.

The total current is then given by

$$J_p = q p \mu_p \underline{E} + \mu_p \underline{J}_p \times \underline{B} - q D_p \nabla p \tag{2.31}$$

$$J_n = q n \mu_n \underline{E} - \mu_n \underline{J}_n \times \underline{B} + q D_n \nabla n \tag{2.32}$$

Semiconductor transport properties such as electrical conductivity, magnetoconductivity, and photomagnetoelectric effects can be derived from the above with equations, subject to appropriate boundary conditions.

c.1 Magneto-resistivity and the Hall Effect

Let us consider the consequences of (2.26) and (2.27). As an example, assume that a sample of semiconductor is placed in a magnetic field, whose direction is the Z - axis, and a D.C. voltage along the x-axis. As the electrons and holes stream through the semiconductor sample, they will tend to be deflected upward or downward, along the y-axis, resulting in the change of the resistivity of the sample or the development of the transverse emf.

To carry out a quantitative formulation of these ideas, we shall turn to Eq. (2.31) and (2.32) and restrict our discussion to the case in which concentration gradient is negligible. Then, these equations can be written

$$J_{px} = q p \mu_p \mathcal{E}_x + \mu_p J_{py} \underline{B} \tag{2.33}$$

$$J_{py} = q p \mu_p \mathcal{E}_y - \mu_p J_{px} \underline{B}$$

$$J_{nx} = q n \mu_n \mathcal{E}_x - \mu_n J_{ny} \underline{B}$$

$$J_{ny} = q n \mu_n \mathcal{E}_y + \mu_n J_{nx} \underline{B} \qquad (2.34)$$

Let us first see how the resistivity is affected by the magnetic field. The experimental conditions are such $\mathcal{E}_y = 0$. Then eliminating the y-components or the electron and hole currents and solving for the x-components we find

$$J_{px} = \frac{q p \mu_p}{1 + \mu_p^2 B^2} \mathcal{E}_x \qquad (2.35)$$

$$J_{nx} = \frac{q n \mu_n}{1 + \mu_n^2 B^2} \mathcal{E}_x \qquad (2.36)$$

giving

$$J_x = J_{px} + J_{nx} = \frac{q p \mu_p \mathcal{E}_x}{1 + \mu_p^2 B^2} + \frac{q n \mu_n \mathcal{E}_x}{1 + \mu_n^2 B^2} \qquad (2.37)$$

Suppose that the material is such that only one type or carrier contributes to the conductivity, say, N-type, i.e. $n >> p$. Then

$$J_x \cong J_{nx} = \frac{q n \mu_n \mathcal{E}_x}{1 + \mu_n^2 B^2} \qquad (2.38)$$

$$\sigma = \frac{q n \mu_n}{1 + \mu_n^2 B^2} = \frac{\sigma_o}{1 + \mu_n^2 B^2} \tag{2.39}$$

where σ_o is the conductivity in zero magnetic field. The resistivity, by definition, is the reciprocal of the conductivity. Hence

$$\rho = \rho_o (1 + \mu_n^2 B^2) \tag{2.40}$$

and therefore

$$\frac{\rho - \rho_o}{\rho_o} = \mu_n^2 B^2 \tag{2.41}$$

Experimental results should then yield the following plot

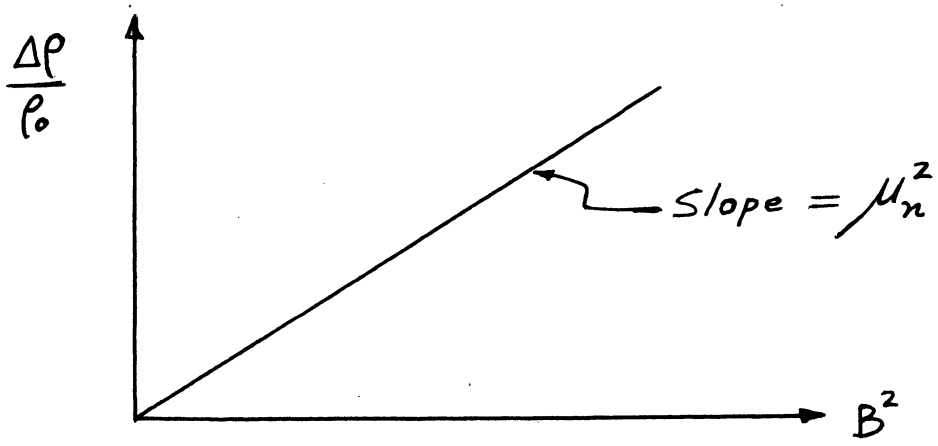

Figure 2.4

In the Hall measurement, a transverse potential (along the y-axis) is applied to balance out the transverse current, i.e.

$$J_y = J_{py} + J_{ny} = 0 \tag{2.42}$$

Furthermore, to reduce further the necessary algebra, assume again that the sample is N-type. Then (2.36) gives

$$\begin{aligned} J_{nx} &= q n \mu_n \mathcal{E}_x - \mu_n J_{ny} B \\ 0 &= q n \mu_n \mathcal{E}_y + \mu_n J_{nx} B \end{aligned} \tag{2.43}$$

so that

$$E_y = -\frac{B}{qn} J_{nx} \tag{2.44}$$

Now the Hall coefficient is define as

$$R \equiv \frac{E_y}{B J_x} = -\frac{1}{qn} \tag{2.45}$$

Thus the Hall measurement provides a method for the measurement of carrier concentration.. Now, the Hall voltage V_H is

$$V_H = E_y w \tag{2.46}$$

where w is the sample width, and

$$J_x = \frac{I}{A} \tag{2.47}$$

where I is the current through the sample, and A is the Cross sectional area of the sample.

If two types of carriers are present, Eqs. (2.33) and (2.34) lead to

$$R = \frac{(P\mu_P^2 - n\mu_n^2)}{q(n\mu_n + P\mu_P)^2} \tag{2.48}$$

provided $\mu_n B$ and $\mu_P B$ are small in comparison to 1.

d. Thermoelectric Effect

From the preceding discussion, it is clear that the Hall effect can be used to determine the sign of the charged carriers, i.e. whether the semiconductor is N- or P-type. Thus suppose that the material is N-type, biased along the x-axis, and the magnetic field along the z-axis, as shown in the following figure:

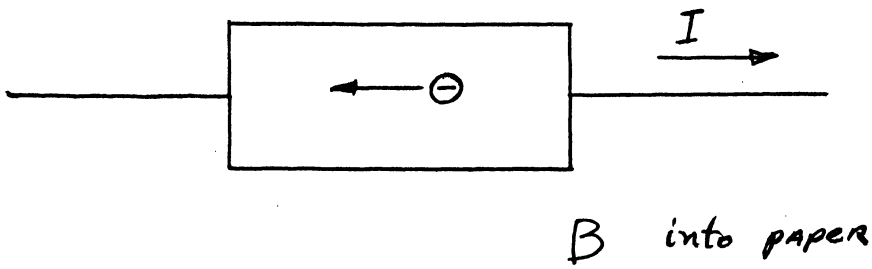

Figure 2.5

Since the Lorentz force on a negative charge is given by

$$-q\,\underline{V} \times \underline{B} \tag{2.49}$$

we see that the electrons will tend to be deflected upwards, so

that the upper edge will need to be negative to counteract this tendency. Suppose next that the material is P-type. The Lorentz force is

$$q\,\underline{V} \times \underline{B} \tag{2.50}$$

so that the deflection of the carrier is again upward, so that in this case the upper edge will need to be made positive with respect to the lower one.

There is however another method to determine the carrier sign, namely the thermoelectric effect. The theory is a little more complicated, but the essential physical results can be seen very easily. Suppose first we have an N-type material, with one end hot and the other end cold, as shown in the following figure

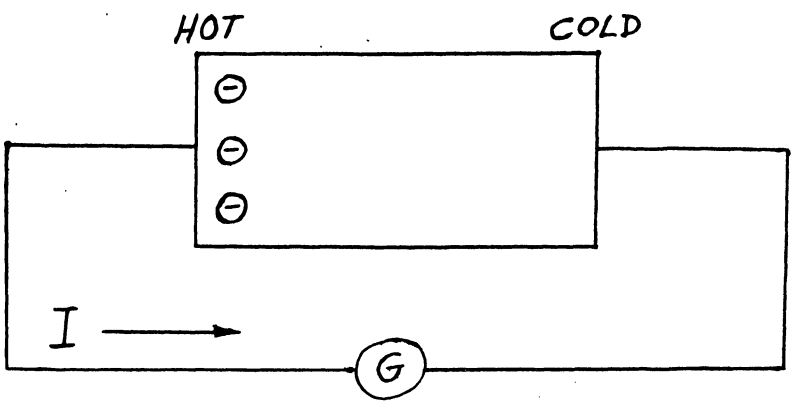

Figure 2.6

Because the electrons at the hot end will have a greater average kinetic energy than those at the cold end, the electrons will drift from the hot to the cold end. This will result in a

current through the galvanometer from left to right, as shown. On the other hand, if the material is p-type, the holes will still drift from the hot to the cold end, but this will result in a current in the external circuit from right to left.

2.6 Solid State Ionization Detector

As an example of the application of Eq. (2.18), let us consider the solid-state ionization detector. The advantages of such a detector are (a) compactness, and (b) possibly a small value for the energy required for the production of an electron hole pair. The compactness stems from the fact that density in a solid is of the order of 1000 times greater than in a gas, so that the linear dimension of a solid-state device can be about one order of magnitude smaller than the gaseous counterpart, provided other factors remain the same. In air, for example, the energy required for the production of an ion pair by an ionizing particle is 30 ev. and is about a factor of two larger than the ionization energy. In solids, such as germanium and silicon, the band gap is about 1 ev., and the energy per electron hole pair is known to be about 3 ev. This means then that an ionizing particle going through a solid can produce about ten times as many electron-hole pair as in gases. However, because this implies that the density of charged pairs in a solid is about 1000 times larger, so that the loss of signal through recombinations might be correspondingly more significant.

Consider then a semiconductor, with contacts applied as shown in Figure 2.7. For simplicity

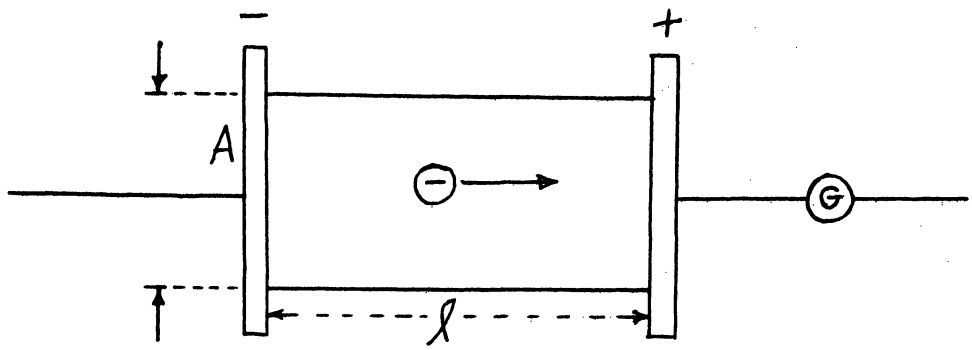

Figure 2.7

let us determine the effect of an electron moving towards the positive plate. The length and the cross-sectional area of the semiconductor are ℓ and A respectively. In addition, a galvanometer will be inserted in the circuit to make the necessary observations. According to Eq. (2.21)

$$J_n = q n \mu_n \mathcal{E}$$

Since we have 1 electron in volume $A\ell$.

$$n = \frac{1}{A\ell} \tag{2.51}$$

The current I_n is

$$I_n = J_n A = q \frac{\mu_n \mathcal{E}}{\ell} = \frac{q}{\ell} V_n \tag{2.52}$$

If the electron moves ΔX in time τ, the charge flowing through G is

$$\Delta Q = I_n \tau = \frac{q}{\ell} V_n \tau = \frac{q \Delta X}{\ell} \tag{2.53}$$

$$\Delta X = \mu_n \tau \mathcal{E} = V_n \tau \tag{2.54}$$

which is the expression often referred to as Heckt's relation in the literature. If G is the capacitance, then voltage pulse is given by

$$\Delta V = \frac{\Delta Q}{C} = \frac{q \Delta X}{C \ell} \tag{2.55}$$

If the incoming ionizing particle produces N electrons, then the voltage pulse is

$$\Delta V = \frac{q \Delta X}{C \ell} N \tag{2.56}$$

if the electron travels only the fraction ΔX between the contacts. On the other hand, if they travel the entire distance, then clearly,

$$V = \frac{q}{C} N \tag{2.57}$$

Thus if

$N \sim 10^6$

$q \sim 10^{-19}$ coulombs

$$C = \frac{KA}{4\pi d} = 0.0885 K \frac{S}{t} \ \mu\mu f$$

$$C \sim 10^{-12} \ \text{farads}$$

$$\Delta V \sim \frac{10^{-19}}{10^{-12}} (10^{6}) \sim \underline{\underline{0.1 \ \text{volt}}}$$

Thus the signal can be appreciable.

From Eqa. (2.53), (2.54), and (2.55) we see that to produce a large pulse, the produce $\mu_n \mathcal{E} \tau$ must be large and C must be small. For insulating crystals such as diamond, CdS, etc., $\mathcal{E}/\ell$ can be made large, but $\mu_n \tau$ is small. For semiconductor such as germanium and silicon, $\mu_n \tau$ is large, but $\mathcal{E}/\ell$ is small. But McKay of the Bell Telephone Laboratories suggested a way to circumvent this problem by using a P-N junction.

2.7 Semiconductor Statistics

Concepts such as electron and hole concentrations n and p have been discussed, and it was pointed out that the product np is a constant at a given temperature. Consequently we shall look into these a little more carefully, as an introduction to semiconductor statistical thermodynamics.

Consider then the statistical distribution of electron in the conduction band. This can perhaps be visualized as follows.

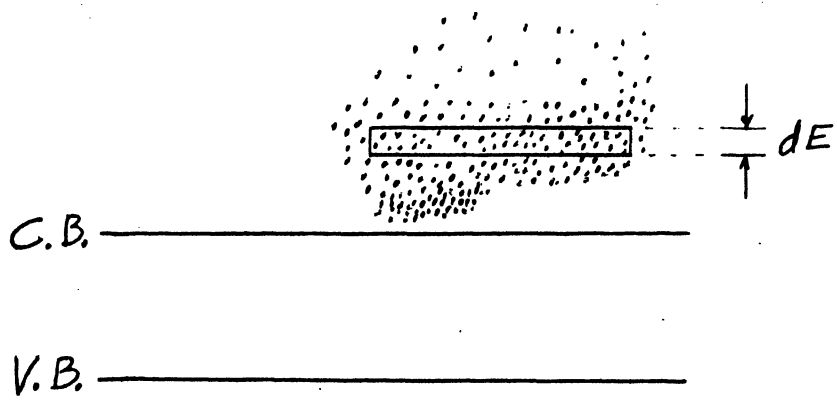

Figure 2.8

Clearly we can expect the electron concentration to be larger somewhere near the edge of the conduction band and to taper off as the energy increases. Suppose then we consider the electron in the range dE about E. The number of electrons in this range as is well known depends on two factors, the density of states and probability of occupation of the states. Thus

$$dN = (\text{Density of States})(\text{Probability of Occupation}) \qquad (2.58)$$

The density of states arises from the fact that electrons moving in different directions can have the same energy. If the electrons in the conduction band are assumed to be like a free electron gas, then

$$E = \frac{1}{2m} p^2 \qquad (2.59)$$

so that all states in the shell about dp at p will be associated with the same energy.

$$D(p)\,dp = \frac{4\pi p^2 dp\, V}{h^3} \qquad (2.60)$$

and since

$$D(p)\,dp = D(E)\,dE \tag{2.61}$$

we obtain

$$D(E) = D(p)\frac{dp}{dE} = \frac{4\pi p^2 V}{h^3}\,\frac{dp}{dE} \tag{2.62}$$

But

$$E = E_c + \frac{p^2}{2m} \tag{2.63}$$

so that

$$D(E)\,dE = \frac{4\pi V}{h^3}\sqrt{2(E-E_c)}\; m^{3/2}\,dE$$

$$= \frac{V}{\sqrt{\pi}}\,\frac{N_c}{2}\left[\frac{E-E_c}{kT}\right]^{1/2}\frac{dE}{kT} \tag{2.64}$$

where

$$N_c = 2\left[\frac{2\pi m kT}{h^2}\right]^{3/2} \tag{2.65}$$

The electron spin is 1/2, giving a multiplicity of 2, so that the expression in (2.64) needs to be multiplied by 2. Thus

$$D(E)\,dE = \frac{V}{\sqrt{\pi}}\,N_c\left[\frac{E-E_c}{kT}\right]^{1/2}\frac{dE}{kT} \tag{2.64}'$$

The result of (2.60) can be obtained by another argument. Consider a free electron gas in a box. Then inside the box, the electrons satisfy

$$-\frac{\hbar^2}{2m}\nabla^2\psi = E\psi \tag{2.66}$$

so that the solutions are given by

$$\psi \sim e^{i\underline{p}\cdot\underline{r}/\hbar}$$

Since the electrons are confined in the box, to fit the boundary conditions, ψ must be periodic in L. Thus

$$\begin{aligned} \frac{p_x L}{\hbar} &= 2\pi n_x \\ \frac{p_y L}{\hbar} &= 2\pi n_y \\ \frac{p_z L}{\hbar} &= 2\pi n_z \end{aligned} \tag{2.67}$$

so that the number of states in n_x and $n_x + dn_x$ is

$$dn_x = \frac{L}{2\pi\hbar}dp_x = \frac{L}{h}dp_x \tag{2.68}$$

and similarly for dn_y, and dn_z

$$dn_y = \frac{L}{h} dp_y$$

$$dn_z = \frac{L}{h} dp_z$$

so that

$$dn = dn_x\, dn_y\, dn_z = \frac{V}{h^3} dp_x\, dp_y\, dp_z = \frac{V}{h^3} 4\pi p^2 dp \tag{2.69}$$

The probability of occupation of these states is given by the Fermi-Dirac distribution function

$$f(E) = \frac{1}{\exp\left[\frac{E-E_F}{kT}\right]+1} \tag{2.70}$$

where E_F is the so-called Fermi energy, and

$$f(E_F) = \frac{1}{2} \tag{2.71}$$

We can get a graphical construction of the electron distribution as follows

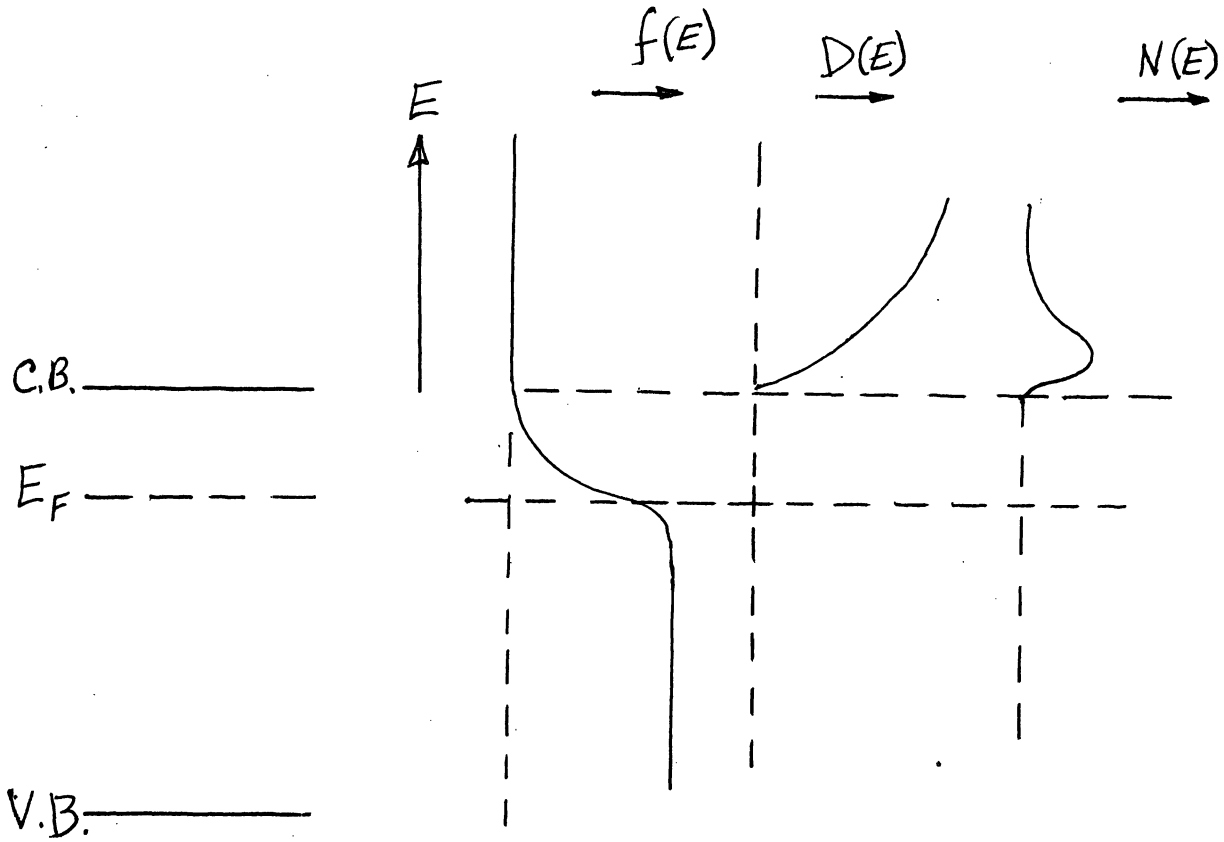

Thus

$$n = \frac{N}{V} = \frac{1}{V}\int_{E_c}^{\infty} N(E)\,dE \qquad (2.72)$$

If we put

$$\eta = \frac{E - E_c}{kT} \qquad \xi \equiv E_F - E_c \qquad (2.73)$$

then

$$\frac{n}{N_c} = \frac{2}{\sqrt{\pi}}\int_0^{\infty} \frac{\sqrt{\eta}\,d\eta}{e^{(\eta - \xi/kT)} + 1} \qquad (2.74)$$

To carry out this integration, let us examine ξ/kT. At room

temperature kt $\sim$ 1/40 ev, so that even if the Fermi level is only 0.2 ev below the edge of the conduction band $\xi/kT \sim -10$, and η is a positive quantity.

$$e^{(\eta - \xi/kT)} >> 1 \tag{2.75}$$

Therefore we can approximate the integral by

$$\frac{n}{N_c} = \frac{2}{\sqrt{\pi}} \int_0^\infty e^{-\eta + \xi/kT} \sqrt{\eta}\, d\eta = \frac{2}{\sqrt{\pi}} e^{\xi/kT} \int e^{-\eta} \sqrt{\eta}\, d\eta \tag{2.76}$$

$$= \frac{2}{\sqrt{\pi}} e^{\xi/kT} \Gamma(3/2) = e^{\xi/kT} \tag{2.77}$$

Similarly it can be shown that

$$\frac{p}{N_v} = e^{-(E_F - E_v)/kT} \tag{2.78}$$

where

$$N_v \equiv 2 \left[\frac{2\pi m_h kT}{h^2} \right]^{3/2} \tag{2.79}$$

One consequence of (2.77) and (2.78) is

$$np = N_c N_v e^{-(E_c - E_v)/kT} = N_c N_v e^{-E_G/kT} \tag{2.80}$$

If the material is intrinsic, i.e. pure, then

$$n = p = n_i = \sqrt{N_c N_v}\, e^{-E_G/2kT} \tag{2.81}$$

Also

$$E_F = \frac{1}{2}(E_c + E_v) + \frac{1}{2} kT \ln \frac{n}{p} + \frac{3}{4} kT \ln \frac{m_{ph}}{m_{ne}} \tag{2.82}$$

Thus, for n = p, an $m_h = m_e$, the Fermi level lies exactly midway between the conduction and valence band edges. Another consequence of (2.77) is the Fermi level approaches the conduction band edge as the material becomes more N-type, as can be seen from

$$E_F = E_c + kT \ln \frac{n}{N_c} \tag{2.83}$$

and the Fermi level approaches the valence band edge as the material becomes more P-type, which follows from

$$E_F = E_v - kT \ln \frac{p}{N_v} \tag{2.84}$$

For the results discussed so far, we have assumed that $\xi/kT << -1$, and the results that followed apply to the so-called non-degenerate semiconductors. The other degenerate case arises when $\xi/kT >> 1$. For this case the exponential term is small in comparison to 1 as long as $\eta < \xi/kT$. As soon as $\eta > \xi/kT$, the exponential term very soon outweights the term 1, and greatly reduces the value of the integrand. Hence

as an approximation, we can put 1 for the denominator on the range $0 < \eta < \xi/kT$ and in the range $\xi/kT < \eta < \infty$, the denominator can be approximated by ∞. Then

$$\frac{2}{\sqrt{\pi}} \int_0^{\xi/kT} \sqrt{\eta}\, d\eta = \frac{n}{N_c}$$

so that

$$\frac{n}{N_c} = \frac{2}{\sqrt{\pi}} \left(\frac{2}{3}\right) \left(\frac{\xi}{kT}\right)^{3/2} = \frac{4}{3\sqrt{\pi}} \left[\frac{E_F - E_c}{kT}\right]^{3/2} \tag{2.85}$$

This case becomes important in tunnel diodes and semiconductor injection laser.

Chapter III

P-N Junction

Because of the importance of this concept to such devices as transistors, tunnel-diodes, solid-state detectors, solar and nuclear batteries, etc., we shall first present a detailed discussion of the P-N Junction theory. As indicated earlier, a semiconductor specimen may be N- or P- type depending on whether electrons or holes make the dominant contribution to the electrical conductivity. N-type samples are made by dissolving small quantities of P, As, or Sb in germanium or silicon, and for P-type samples, impurities such as B, Al, Ba, and In are used.

Our problem is to see what effects are to be expected by putting N- and P- samples together. We shall first consider the P-N junction in thermal equilibrium. Furthermore, for sake of definiteness we shall assume that both the P- and N-type materials are non-degenerate, i.e. the Fermi level lies somewhere in the forbidden gap.

The P-N junction system under consideration is one consisting of two phases. And for such systems as is well known, the thermodynamic potentials at our disposal are the Helmholtz free energy, given by

$$F = U - TS \tag{3.1}$$

or sometimes called the thermodynamic potential at constant volume, because of its importance in isothermal processes at constant

volume, and the Gibbs free energy, given by

$$G = U - TS + pV \tag{3.2}$$

or the thermodynamic potential at constant pressure, because of its usefulness in isothermal processes at constant pressure. Since volume changes for solids are small, the Holmholtz free energy F is normally used in the discussion of solid-state thermodynamics. If in the thermodynamical system charges are present, thereby contributing to the internal energy U, then the term "chemical potential" or "electrochemical potential" is used. In solid-state theory, where the approach is microscopic, it is preferable to speak about the energy of a single carrier and of the thermodynamic potential per charged carrier. The so-called Fermi energy is such a quantity and is just the chemical potential per charged carrier. Being then a thermodynamic potential, the Fermi energy E_F is then a constant throughout the semiconductor P-N junction system. This Fermi level provides an energy reference level for all levels in the P- and N-regions.

Consider then the effects that will take place upon bringing a P- and N-type materials, such as shown in the following figure, into intimate contact.

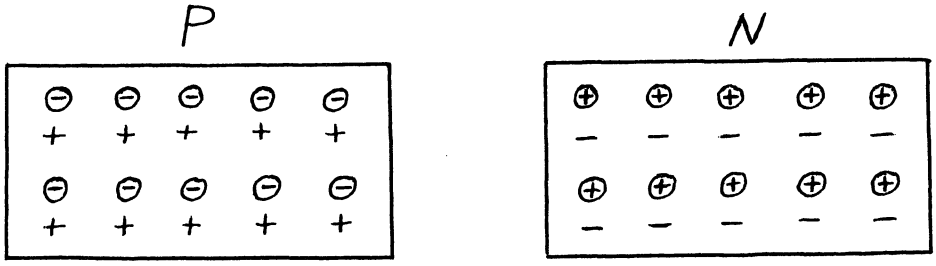

Fig. 3.1

The ionized acceptors and donors are represented by ⊖ and ⊕ , and the charged carriers by + and -. If the two materials are brought into intimate contact, because of the higher concentration of holes in the P-region, there will be a tendency for such carriers to diffuse across the boundary into the N-region, and a similar diffusion of electrons from the N-region into the P-region, so that in the P-side of the junction, there will be a net negative charge, and a net positive charge on the N-side, as shown in Fig. 3.2 a.

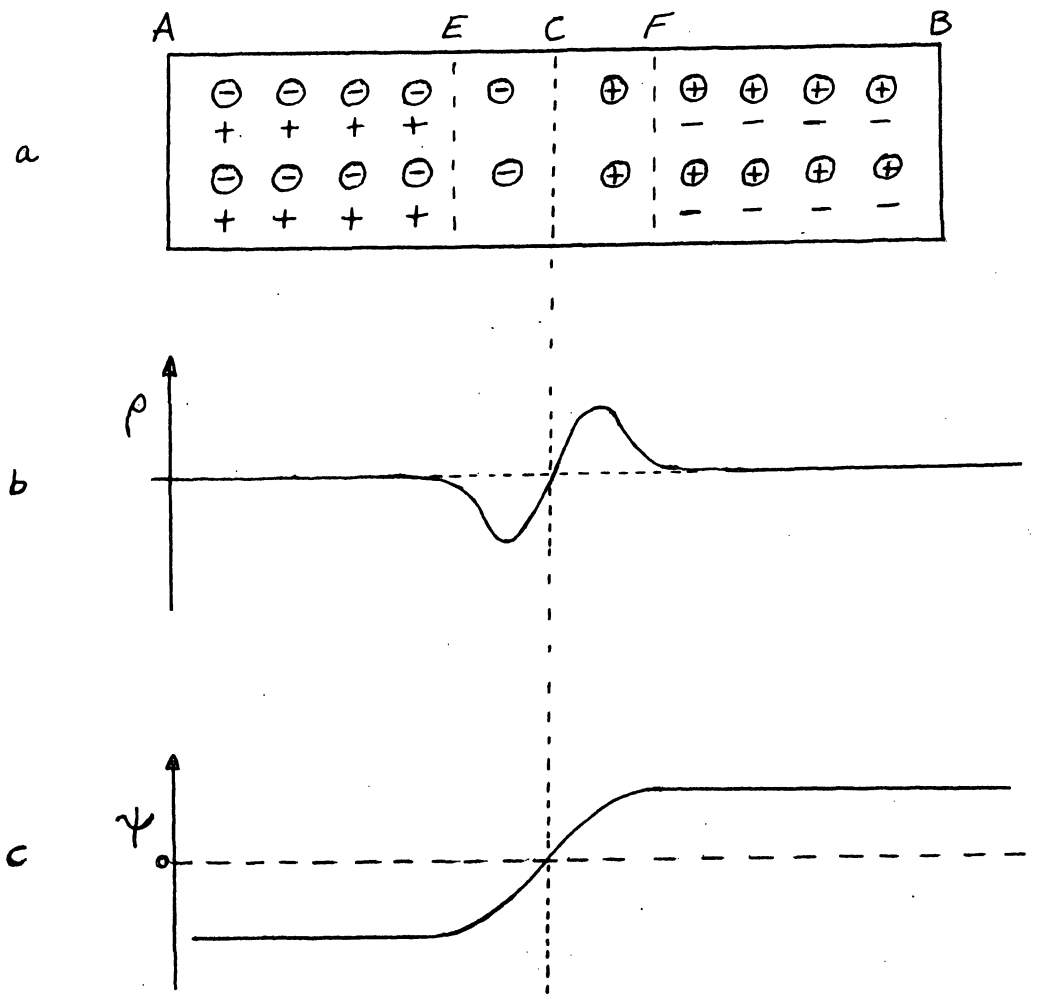

Fig. 3.2

Fig. 3.2 b gives the charge density resulting from such a reshuffling of the carriers. Now, the electrostatic potential ψ and the charge density ρ are related by the Poisson's equation

$$\nabla^2 \psi = -\rho/\epsilon \tag{3.3}$$

A "mental" integration of this equation leads to a potential function indicated in Fig. 3.2 c. For, in the region from A to E, the charge density is zero, so that the potential is a constant. In the region E to C, the charge density is negative, so that the right-hand side of (3.3) is positive, so that the cm value of the potential function must be upward. And at C, the charge density is again zero, corresponding to the inflection point of the potential function.

We are now ready to construct the energy level diagram. This is accomplished as follows:

1. Draw a horizontal line representing the Fermi level E_F
2. At points far away from the junction, locate the positions of the conduction and valence band edges using the relations

$$E_c - E_F = -kT \ln \frac{n}{N_c} \tag{3.4}$$

and

$$E_F - E_v = -kT \ln \frac{p}{N_v} \tag{3.5}$$

An alternative construction is as follows. We have

$$n = N_c e^{\frac{E_F - E_c}{kT}} \tag{3.6}$$

$$p = N_V e^{\frac{E_V - E_F}{kT}} \tag{3.7}$$

Suppose that E_i is the Fermi level of an intrinsic sample. Then

$$n_i = N_c e^{\frac{E_i - E_c}{kT}} \tag{3.8}$$

$$p_i = N_V e^{\frac{E_V - E_i}{kT}} \tag{3.9}$$

so that

$$E_i = \frac{E_c + E_V}{2} + \frac{1}{2} kT \ln \frac{N_V}{N_c} \tag{3.10}$$

As commented earlier, if the sample is intrinsic, and the effective masses of the electrons and holes equal, the Fermi level will lie exactly midway between the conduction and valence band edges. Also note that

$$E_G = E_c - E_V \tag{3.11}$$

Therefore it follows that

$$E_c = E_i + \frac{1}{2} E_G - \frac{1}{2} kT \ln \frac{N_V}{N_c} \tag{3.12}$$

and

$$E_V = E_i - \frac{1}{2} E_G - \frac{1}{2} kT \ln \frac{N_V}{N_c} \tag{3.13}$$

3. To plot the space variation near the junction, note that the electron energy E and the electrostatic

potential ψ are related by

$$E = -\mathcal{E}\psi \tag{3.14}$$

Thus we get the following plot

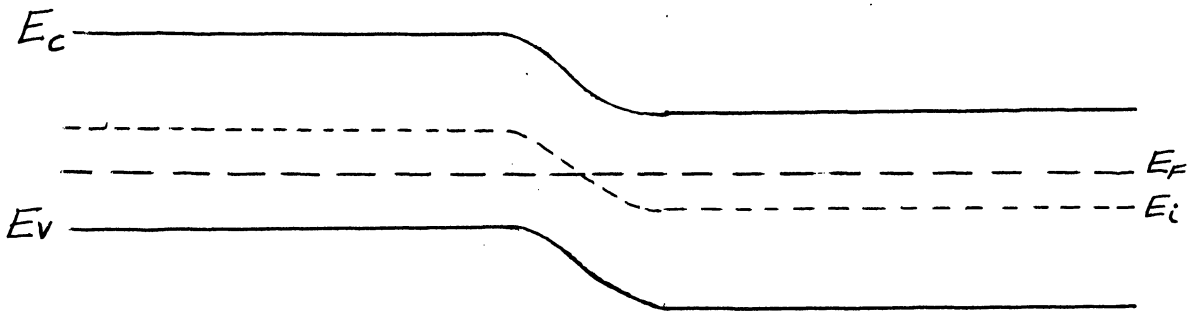

Fig. 3.7

The rise in potential, often called the diffusion voltage, can be readily estimated. Since

$$E_c^{(P)} = E_F - kT \ln \frac{n_p}{N_c} \tag{3.15}$$

$$E_c^{(N)} = E_F - kT \ln \frac{n_N}{N_c} \tag{3.16}$$

so that

$$E_c^{(P)} - E_c^{(N)} = kT \ln \frac{n_N}{n_p}$$

Suppose for example the function is made of materials such that

$$n_N = p_p = 10^{16}/cm^3$$

Then, since

$$n_i = 2.5 \times 10^{13} / cm^3$$

we find that

$$n_p = \frac{n_i^2}{P_p} = 6.25 \times 10^{10}$$

Also, at room temperature, kT is about .025 ev, so that

$$V_B = .025 \ln \frac{10^{16}}{6 \times 10^{10}} = 0.36 \ v \qquad (3.17)$$

Furthermore, as we shall see presently, this rise in potential occurs in a distance of about 10^{-4} cm, so that there is a very large built in electrostatic field at the junction.

Let us now scrutinize the depletion region near the junction. As indicated in Fig. 3.2 b, the true charge distribution is no doubt a smooth function of the distance. However, to simplify the numerical analysis we shall make a few simplifying assumptions, as shown below, in Fig. 3.4

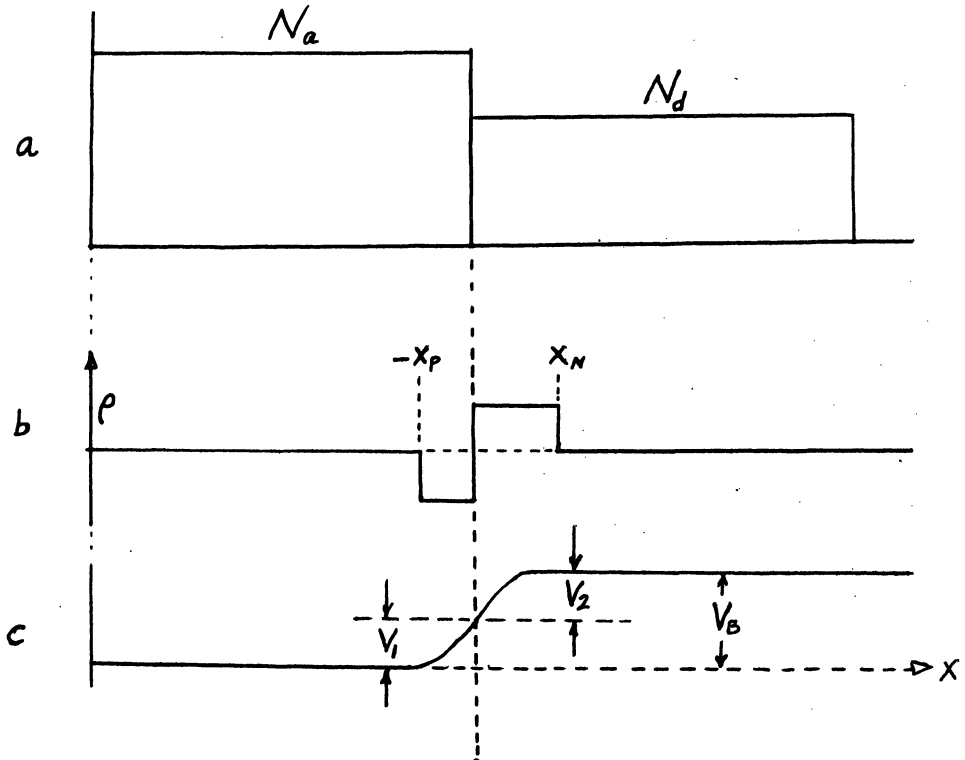

Fig. 3.4

First, we shall assume that the junction is abrupt, having uniform acceptor concentration N_a and donor concentration N_d in the P- and N-type regions respectively. Furthermore we shall assume that the holes are depleted to a depth of x_p and the electrons to x_N. Since the total charge must be zero, for overall charge neutrality, we have

$$X_p N_a = X_N N_d \tag{3.18}$$

Poisson's equation applied to the P-side ($X<0$) gives

$$\frac{d^2\psi}{dX^2} = -\frac{\rho}{\epsilon} = \frac{qN_a}{\epsilon} \quad \text{for } X<0 \tag{3.19}$$

Integrating,

$$\frac{d\psi}{dX} = \frac{qN_a}{\epsilon} X + C \tag{3.20}$$

For $x = -x_p$, the electric field E is to be zero.

$$\frac{d\psi}{dX} = \frac{qN_a}{\epsilon} (X + X_p) \tag{3.21}$$

Integrating again

$$\psi = \frac{qN_a}{\epsilon} \left(\frac{X^2}{2} + X_p X \right) + C_2 \tag{3.22}$$

Letting $\psi = 0$, for $x = -x_p$, we find

$$\psi = \frac{qN_a}{\epsilon} \left(\frac{X^2}{2} + X_p X + \frac{X_p^2}{2} \right) \tag{3.23}$$

so that at $x = 0$,

$$\psi = \psi_1 = \frac{qN_a X_p^2}{2\epsilon} \tag{3.24}$$

Similarly it can be shown that the rise in potential on the N-type side is

$$\psi_2 = \frac{q N_d X_N^2}{2\epsilon} \tag{3.25}$$

so that

$$V_B = \psi_1 + \psi_2 = \frac{q}{2\epsilon}\left(N_a X_P^2 + N_d X_N^2\right) \tag{3.26}$$

Combining with (3.18), we find

$$X_P = \left[\frac{2\epsilon V_B}{q N_a (1 + N_a/N_d)}\right]^{1/2} \tag{3.27}$$

$$X_N = \left[\frac{2\epsilon V_B}{q N_d (1 + N_d/N_a)}\right]^{1/2} \tag{3.28}$$

We note that the depletion zones extend into the two regions, in inverse relation to the impurity concentration of those regions, and in proportion to the square root of the barrier voltage. Often in abrupt junction devices, the impurity concentration of one region is very much larger than that of the other. In such cases, the depletion region extends almost entirely within the region of lower impurity concentration. Suppose for example

$$N_a >> N_d$$

Then the depletion width X_D

$$X_D = X_P + X_N \cong X_N = \left[\frac{2\epsilon V_B}{q N_d}\right]^{1/2} \tag{3.29}$$

But the conductivity σ is given by

$$\sigma = q n \mu_n = q N_d \mu \tag{3.30}$$

so that

$$X_D \cong \left[\frac{2 \epsilon \mu V_B}{\sigma} \right]^{1/2}$$

We next need to examine the effect of these devices under the so-called "forward bias" and "reverse bias". Under forward bias, the conduction band on the N-side is raised with respect to the P-side, and under "reverse bias" the N-type side is lowered. Clearly then, the forward bias is the direction of easy conduction, whereas reverse bias is the direction of hard conduction.

If the P-N junction is biased, forward or reverse, the system is no longer in thermal equilibrium so that the usual concepts of thermodynamics, strictly speaking, no longer apply. However, it turns out that the time required for the electrons and/or holes to approach equilibrium is most frequently very short in comparison to the observation time. The time required for the electrons in a semiconductor to reach equilibrium through collisions with the lattice is estimated to be about 10^{-12} sec., which is very short in comparison to the characteristic time needed for most P-N junction devices. This means then, that the electrons come into thermal equilibrium in a very short period of time, and so do the holes. It should be remembered, however, that the electrons may <u>not</u> be in thermal equilibrium with the holes, because the time required

to approach true equilibrium may be quite long, say 10^{-7} sec. This has some important implications to the semiconductor injection laser.

Because of this very rapid approach to quasi-equilibrium, the electrons and the holes can be described by the so-called quasi-Fermi levels for the electrons and holes respectively. For sake of definiteness consider the case of forward bias. At points very far away from the junction, the electron and holes distributions are effectively unaffected by the bias. Consequently the difference in the quasi-Fermi levels on the two sides will be just the forward bias, as shown in the following figure.

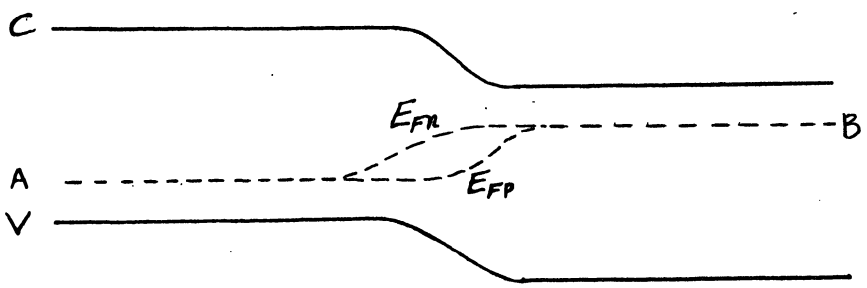

Fig. 3.5

Both the electrons and holes are very nearly in thermal equilibrium with each other so that effectively, the quasi-Fermi levels for the electrons and holes are coincident. This is indicated in the diagram by the points A and B. Near the junction, however, there will be a copious number of holes

injected into the N-type region, and electrons into the P-type region. The time required for the excess carriers to combine with the majority carriers in the two regions is quite long, so that the original distribution of carriers may persist for an appreciable distance beyond the junction.

The assumption that has been made so far in calculating the Fermi energies in Eqs. (3.15) and (3.18) is that the impurity concentration is low, i.e. $n << N_c$ and $p << N_v$ On the other hand if the impurity is so high that $n >> N_c$ and $p >> N_v$, then it can be shown that

$$E_F = E_c + kT\left(\tfrac{3}{4}\right)^{2/3}\pi^{1/3}\left(\frac{n}{N_c}\right)^{2/3}$$
$$= E_c + 1.209\left(\frac{n}{N_c}\right)^{2/3} \qquad (3.31)$$

and similarly for the valence band

$$E_F = E_v - 1.209\left(\frac{p}{N_v}\right)^{2/3} \qquad (3.32)$$

The important point to note is that the Fermi level in the N-type sample lies <u>above</u> the conduction band edge, and for the P-type material, <u>below</u> the valence band edge. The energy-level diagram for the P-N junction of heavily doped materials is as follows:

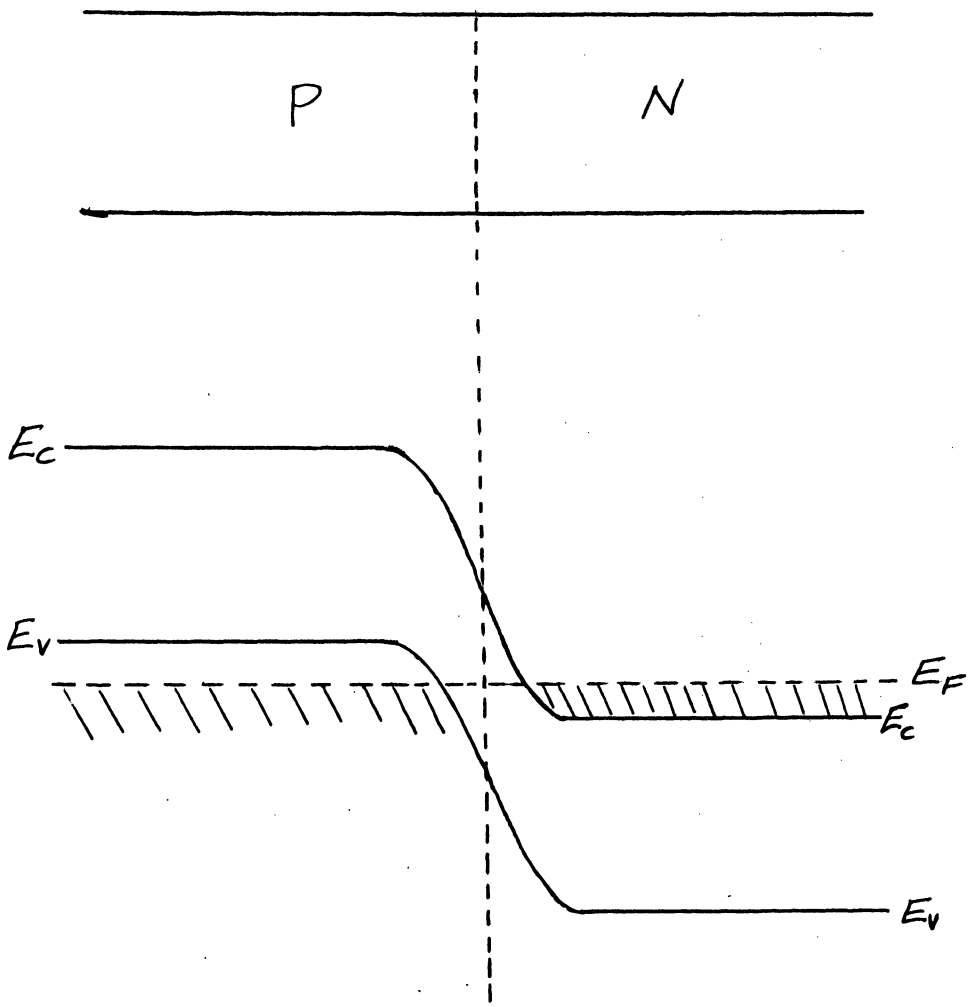

Fig. 3.6

The hashed area below the Fermi level E_F indicates that the electron states are approximately full, and above E_F the electron states are approximately empty. The physical significance of this type of junction was first recognized by L. Esaki, and is referred to in the literature as the tunnel or the Esaki diode.

Certain qualitative results can be deduced immediately from this diagram. In this device the electrons "tunnel" through the potential barrier. It should be recalled that in

this tunneling process, there is no change in energy, so that in this diagram, an electron moves horizontally to the other side to a position not already occupied by an electron. We see then, that the behavior of this device under forward and reverse bias is very different from the ordinary P-N junction. Consider first the reverse bias. Then the quasi-Fermi level of the N-side is lowered with respect to the P-type side. Then the electrons under the hashed area can move across to the energy levels above the quasi-Fermi level. As the reverse bias is increased more electrons in the valence band will face more empty levels in the conduction band of the N-type side, so that the reverse bias is the direction of easy conduction. Under forward bias, however, the device shows some sticking characteristics. As the forward bias is increased, the electrons in the N-type side will face empty states in the P-type side. This trend will continue until the E_F of the N-side becomes even with the valence band edge on the P-type side. Beyond this value of the forward bias, increasing number of electrons will face the forbidden gap of the P-region, so that the current will decrease. This then results in the S-shaped I-V curve discovered first by Esaki.

Chapter IV P-N Junction Devices

The theory of the P-N junction will be applied to a few typical junction devices important in nuclear instrumentation. These are the semiconductor detector, nuclear and solar battery, and the tunnel diode, as examples of devices operated under reverse, zero, and forward bias respectively. The tunnel diode actually is operated under only a small forward bias. Perhaps a better example of a forward bias junction is the semiconductor injection laser.

4.1 Semiconductor Nuclear Radiation Detector

From the earlier discussion it is clear that if a reverse bias is applied to a P-N junction, it will develop a very high resistance, and virtually all of the voltage drop along the sample will be concentrated across the P-N barrier. Thus, very crudely speaking, the barrier can be compared to a very thin insulator (10^{-4} cm) with the main portion of the P- and N-regions acting like the condenser plates. If the bombarding particle strikes the barrier itself so that the resulting holes and electrons are produced in this high resistance and high field region, the holes and electrons will be swept across the barrier, thereby registering in the external circuit.

In the experiments by K. G. McKay (Phys. Rev. 84, 829 (1951) Nov. 15) of the Bell Telephone Laboratories, a germanium crystal about 2 cm long and having a square cross-sectional area of 1 mm^2 was used. The junction was bombarded with

Po-214 5.298 Mev alpha particles. The barrier width was estimated at 5×10^{-4} cm so that a few volts of reverse bias will result in an electric field of the order of 10,000 v/cm. in the barrier. The charged carrier mobilities are of the order of 1000 $cm^2/v/sec$ ($\mu_n = 3600$, $\mu_p = 1700$). The carrier drift velocities in the barrier is then about 10^7 cm/sec., so that the barrier traversal time is of the order of 10^{-11} sec. Experiment showed that this time is certainly not more than 2×10^{-8} sec. McKay's experimental value was limited by the slowness of the electronics.

Measurements show that the charge collected per incident alpha-particle is

$$Q = 1.77 \times 10^6 \, e$$

so that the energy per electron-hole pair is

$$\frac{5.298 \times 10^6}{1.77 \times 10^6} = 3.0 \text{ ev}$$

This is to be compared with the value of about 30 ev. required for ion pair production in air.

Typical of the subsequent research developments are the investigations carried out by S. S. Friedland, J. W. Mayer, and J. S. Wiggens (Nucleonics 18, 54 (Feb. 1960)). These investigators explored the uses of silicon. Some of the properties important in the design of the devices are listed below.

Table 4.1 Properties of Silicon

Group IV b

$Z = 14$

At. Wt. = 28.09

Crystal: Diamond

Co = 5.42 A

$N = 4.96 \times 10^{22}/cm^3$

$D = 2.33$ gm/cm^3

M.P. = 1420°C

B.P. = 2600°C

K = 12 (Dielectric Const.)

n = 3.5 at 12μ

$E_G = 1.106$ ev

$\rho_i = 230{,}000$ Ω-cm (300°K)

$n_i = 1.5 \times 10^{10}/cm^3$ (300°K)

$\mu_n = 1350$ cm^2/V/sec. (300°K)

$\mu_p = 480$ "

Another fact that needs to be kept in mind is that the range of ionizing particles, such as a 5 Mev. alpha particle, is of the order of 100μ . This follows from the fact that the specific ionization is directly proportional to the atomic density of the medium so that the range of the ionizing particle in a solid is about 1/1000 that in air. Typically, an alpha particle of energy 7.68 Mev. has a range of about 7 cm in air, so that its range in a solid can be expected to be about 70/1000 = 70μ . This means then that the depletion layer,

which is effective in detecting the particle should possibly be a few hundred microns. Furthermore to avoid excessive energy dissipation, the depletion layer should be as close to the detector surface as possible.

To achieve this, a high resistivity P-type silicon is doped on the surface with phosphorus, to produce low resistivity N-type layer. If the donor concentration N_D is made large in comparison with N_A, then the total depletion width x is given essentially by the depletion width in the high resistivity material. Thus

$$x \cong x_D = \left[\frac{2 \epsilon (V_B + V_r)}{q N_A} \right]^{1/2}$$

$$= [2 \epsilon \rho \mu_p (V_B + V_r)]^{1/2} \qquad (4.1)$$

$$= 3.2 \times 10^{-5} (\rho V_r)^{1/2}$$

where

$$\rho = qp \mu_p \cong q N_A \mu_p \qquad (4.2)$$

The junction capacitance is given by

$$C = \frac{\epsilon A}{x} = A \left[\frac{\epsilon q N_A}{2 V_r} \right]^{1/2} \qquad (4.3)$$

This is important because the signal voltage developed, as the result of an ionizing particle is given by

$$V = \frac{Q}{C} \qquad (4.4)$$

Typically, with $\rho = 10^4$ ohm cm, and for 100 v reverse bias, the depletion width is about 300 μ and the capacitance about 30 pf/cm^2.

As the ionizing particle enters the depletion layer (Fig. 4.1) electrons and holes are liberated, which are swept in the directions indicated by the arrows. The energy per electron-hole pair for all types of radiations appear to be very close to 3.5 ev. A 5.5 Mev alpha particle thus will produce approximately 1.6×10^6 electron-hole pairs.

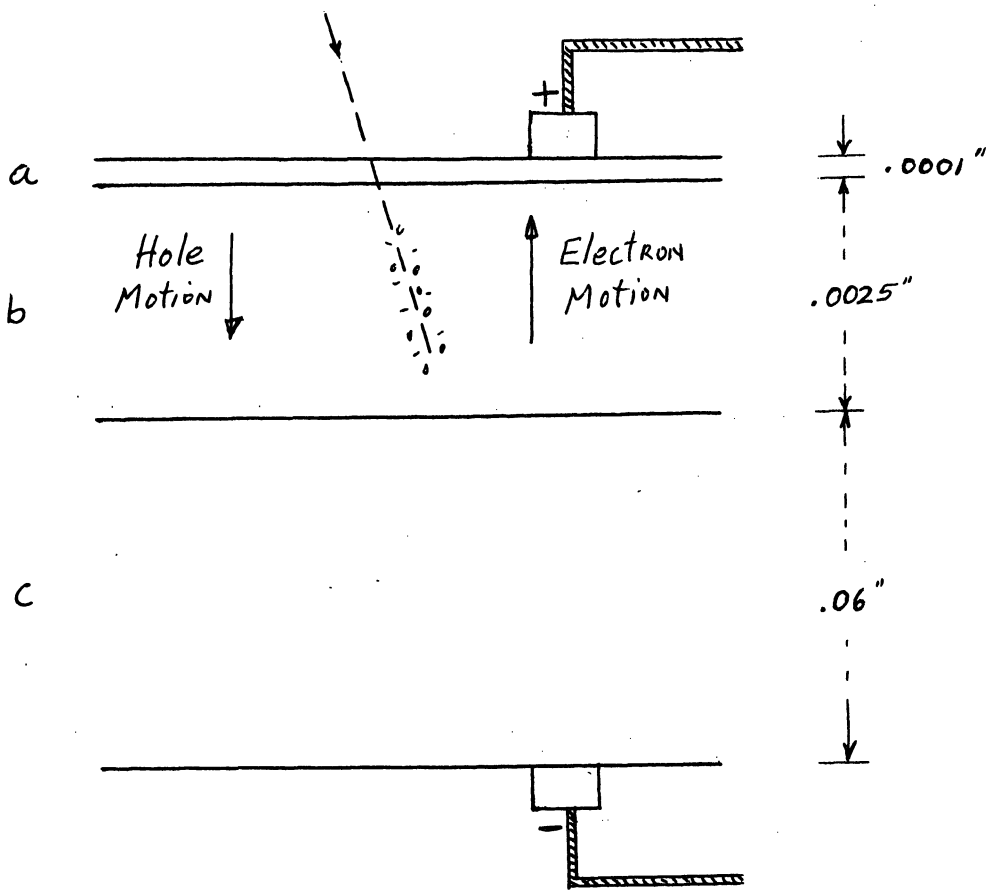

Fig. 4.1

The charge Q given in (4.4) produced by the ionizing particle is a statistical quantity, and is subject to fluctuation, thereby contributing to the width of the ionization pulse. Apparently there are a number of processes contributing to the

fluctuation, or the noise. An excellent discussion can be found in the paper by D. C. Northrop and O. Simpson, "Semiconductor Counters I. Theory", Proc. Phys. Soc. 80, 262 (1962). We shall here, however present a brief discussion of three of the processes, namely the effects of ionization fluctuations, thermal noise, and current noise.

The procedure in determining the effects of noise upon the pulse width is to first calculate the standard deviation for the particular process and then to identify it with the Gaussian distribution, given by

$$dP = \frac{1}{\sigma\sqrt{2\pi}} \, e^{-\frac{(x-m)^2}{2\sigma^2}} \tag{4.5}$$

where dP is the probability that x will lie between x and x + dx, m is the mean value of x and σ is the standard deviation. It can be easily verified that

$$\int (x-m)^2 \, dP = \sigma^2 \tag{4.6}$$

and that the F W H M (full width at half maximum) is

$$FWHM = 2\sigma\sqrt{2\ln 2} = 2.35\sigma \tag{4.7}$$

Hence, if several processes contribute to the pulse width, then

$$\sigma^2 = \sum_i \sigma_i^2 \tag{4.8}$$

Consider, then first, the ionization fluctuation. If E_α is the energy of the ionizing particle, and w the energy required per electron-hole pair, then the average number $\bar{N}$

of electron-hole pairs produced is

$$\bar{N} = E_\alpha / w \tag{4.9}$$

The ionization produced can be thought of as a "Yes-No" random walk problem, for which the standard deviation is known to be simple $\sqrt{\bar{N}}$. (See. R. B. Lindsay, Introduction to Physical Statistics, John Wiley). The energy that would produce a signal equal to the standard deviation is

$$\sqrt{N}\ w = \sqrt{w\ E_\alpha} \tag{4.10}$$

For a 1 Mev. alpha particle in silicon (W = 3.6 ev), the standard deviation is

$$\sqrt{wE_\alpha} = 1.9 \text{ Kev} \tag{4.11}$$

giving about 4.5 Kev FWHM. We note from (4.10) that the standard deviation is proportional to the square root of the energy of electron-hole pair production. For air, the energy for ion pair production is about 10 times larger. Consequently, the ultimate pulse width is about 3 times larger in a gaseous ionization detector compared with a solid state detector.

Another contributing factor is the thermal noise (Johnson or Nyquist, of Johnson-Nyquist) which stems from the fact that a resistor can be thought of as a voltage or a current generator. Consider

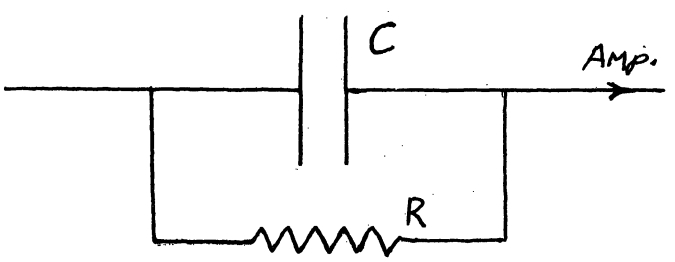

The shunt resistance R is equivalent to a voltage generator.

$$\overline{V^2(f)\,df} = 4\,kT\,R\,df \tag{4.12}$$

Now the current through the capacitance is given by

$$I = \frac{V}{\sqrt{R^2 + \frac{1}{\omega^2 C^2}}} \tag{4.13}$$

so that the capacitance voltage V_c

$$V_c = \frac{I}{\omega C} = \frac{V}{\sqrt{1 + \omega^2 C^2 R^2}}$$
$$\therefore \quad \overline{V^2}_c = \frac{\overline{V^2}}{1 + \omega^2 C^2 R^2} \tag{4.14}$$

If this signal is fed into a broad-band amplifier, then the total thermal noise signal is

$$\int_{\text{bandwidth}} \overline{V^2}_c\,df \cong \int_0^\infty \overline{V^2}_c\,df = \int_0^\infty \frac{4\,kT\,R\,df}{1 + \omega^2 C^2 R^2} = \frac{kT}{C} \tag{4.15}$$

giving an effective charge fluctuation of

$$\overline{Q^2} = C^2\,\overline{V^2} = k\,CT \tag{4.16}$$

Thus the <u>energy</u> giving this deviation is

$$\sigma_{th} = \sqrt{k\,CT}\,\frac{w}{q} = w\sqrt{\frac{kT}{q}\,\frac{C}{q}} \cong w\sqrt{\frac{1}{40}\left(\frac{C_{pf} \times 10^{-12}}{1.6 \times 10^{-19}}\right)}$$
$$= 1.4\,C_{pf}^{1/2}\ \text{Kev.} \tag{4.17}$$

at room temperature. This then gives a contribution

$$\text{FWHM} = 3.2\left(\frac{T}{300}\right)^{1/2} C_{pf}^{1/2} \tag{4.18}$$

If the capacitance is about 16 pf, the above (4.18) becomes

$$\text{FWHM} \cong 13 \left(\frac{T}{300}\right)^{1/2} \text{Kev.} \qquad (4.18')$$

At room temperature then the thermal noise contribution to the pulse width is possibly an order of magnitude larger than the ionization width.

Another source of noise is the current noise. If n represents the average number of electrons in the conduction band, then for a random fluctuation, the standard deviation is proportional to the square root of n. Hence the contribution of the carrier fluctuation is given by

$$\sigma \sim w\sqrt{n_i} \qquad (4.19)$$

At room temperature for intrinsic silicon

$$n_i \sim 10^{10}/\text{cm}^3 \qquad (4.20)$$

so that (4.19) gives about 350 Kev. Thus at room temperature the pulse width is expected to be too broad to detect. At liquid nitrogen temperature n_i is expected to be about $10^6/\text{cm}^3$, so that the contribution to the width from this source of noise is about 3.5 Kev. The above analysis points to the importance of cooling the semiconductor junction detectors to liquid nitrogen temperature and of selecting materials for which the electron-hole production energy is small.

References

K. G. McKay, "A Germanium Counter," Phys. Rev. 76, 1537 (1949).

"Electron-Hole Production in Germanium by Alpha Particles", Phys. Rev. 84, 829 (Nov. 15, 1951).

G. Derrnaley-D. C. Northroy, "Semiconductor Counters for Nuclear Radiation", John Wiley, 1953.

D. A. Bromley, "Nuclear Instrumentation with Semiconductor Detectors", Nucleonics 20, 55 (May 1962).

J. W. Mayer, "Semiconductor Detectors: How Have They Improved?", Nucleonics 20, 60 (May 1962).

A. I. Yavin, "Detection of Alpha Particles with Commercially Available Transistors", RSI 31, 351 (1960).

C. S. Ananiades and J. W. Dewdney, "Transistor Alpha Particle Detector", Am. J. Phys. 29, 329 (May 1961).

S. S. Friedland, J. W. Mayer, J. S. Wiffens, "Tiny Semiconductor in Fast Linear Detector", Nucleonics 18, 54 (Feb. 1960).

D. C. Northroy and O. Simpson, "Semiconductor Counters I, Theory", Proc. Phys. Soc. 80, 262 (1962).

R. B. Lindsay, "Introduction to Physical Statistics", John Wiley, 1941.

J. B. Birks, "Proceedings of the Symposium on Nuclear Instruments", Academic Press, 1962.

4.2 Esaki Tunnel Diode

A brief discussion of this device will be given here because this device offers the possibility of obtaining information about deep-lying impurity states due to chemical impurities or radiation damage, in semiconductors, in addition to the many potential electronic applications. Furthermore, it is interesting to note that the discovery of this device came about as the result of deliberately heavily doping semiconducting materials, in contrast to the general trend at that time, in 1957, of working with highly purified materials.

This device was first reported by L. Esaki in 1957, who prepared a narrow P-N junction of width of about 150 A, made of P-type acceptor concentration of about $1.6 \times 10^{19}/cm^3$, and N-type donor concentration of about $10^{19}/cm^3$ prepared by mixing 0.025 to 0.26 gm of gallium in 100 gm of Ge, and .45 to .5 gm of InP in 100 gm of Ge to prepare the P- and N-type materials respectively. Because of the high impurity concentration, the P-N junction consists of degenerate P- and N-type materials. The positions of the Fermi levels and the band edges, as given by Esaki is shown below.

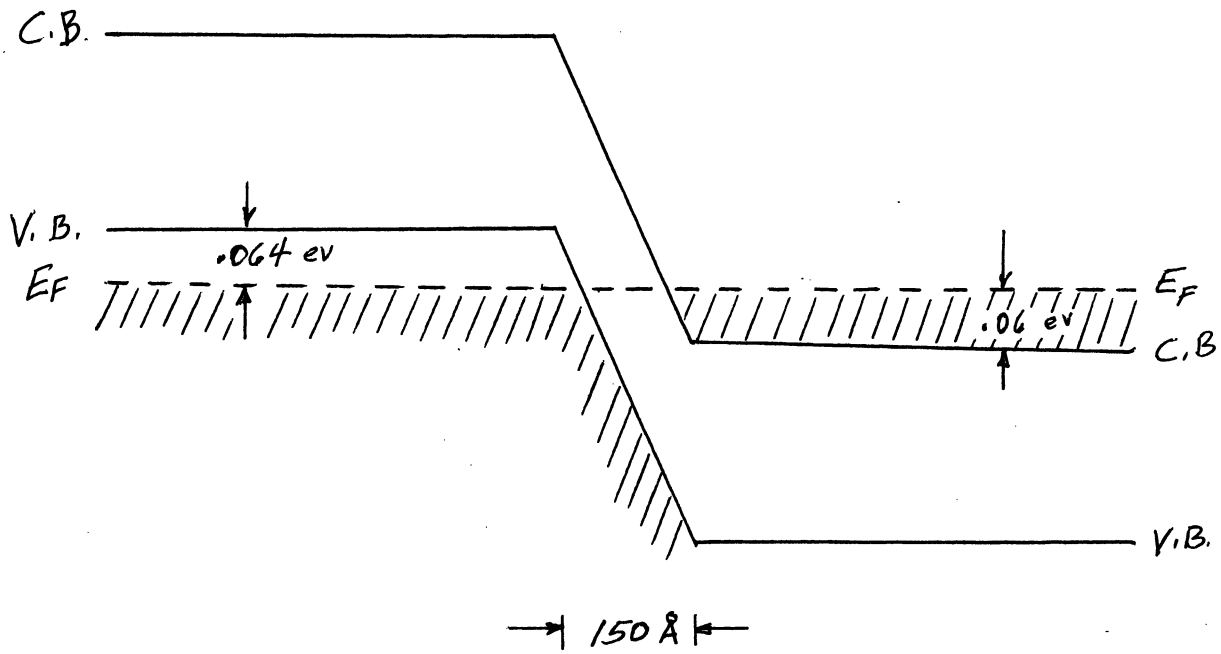

The built-in field at the junction is estimated to be about 5×10^5 v/cm. The current-voltage curve is shown below.

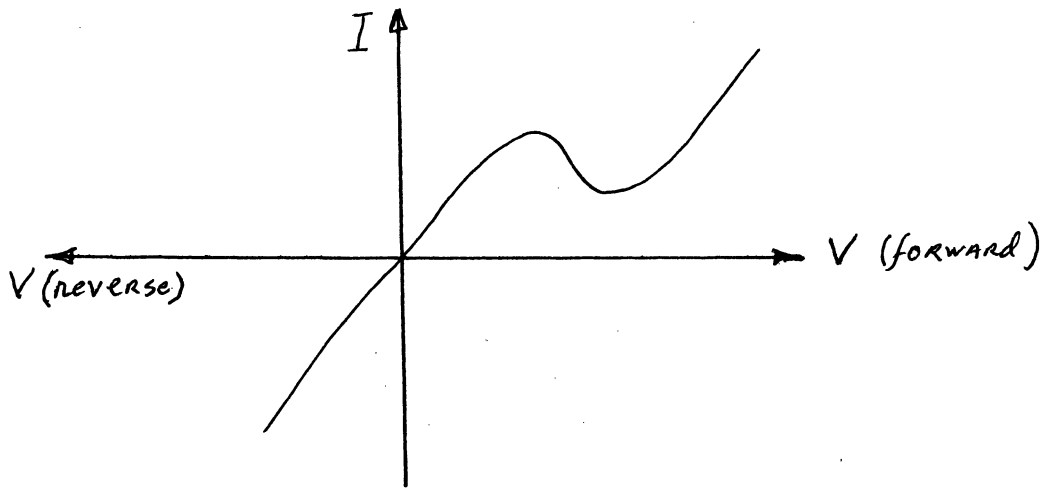

There are several interesting features to this curve. One is that, in contrast to the usual P-N junction, the direction of easy conduction is from N to P, i.e. under reverse bias.

Another is the bump occurring under forward bias. The current reaches a maximum at about 0.035 v, and upon further increase of voltage, the current decreases. In other words, the resistance is negative. For larger forward bias, the current increases, and experiments indicate that this portion of the current-voltage curve is given the usual diode equation

$$I = I_s \left[e^{\frac{qV}{kT}} - 1 \right]$$

The operation of the tunnel diode is based on quantum mechanical tunnel effect--a well-known phenomenon invoked sometime ago to explain alpha-decay, field emission from solids, and breakdown in dielectrics. Consider the potential barrier function q V (x) indicated in the following figure.

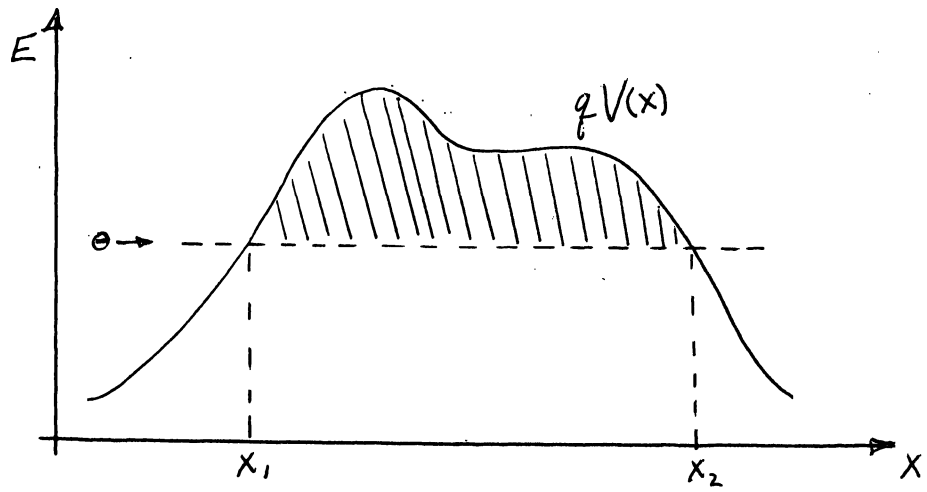

An electron of energy E and charge -q is confronted with the above potential barrier. Classically, as the electron moves towards the barrier, its motion will be slowed, stop at the barrier, and then reflected. Quantum mechanics, however

shows that there is a finite probability of penetrating a barrier lighter than its own energy. This probability is given by

$$Z = \exp\left[-2\int_{x_1}^{x_2} \frac{(2m)^{1/2}}{\hbar}(q\,V - E)^{1/2}\,dx\right]$$

where $x_1 - x_2$ is the interval in space over which the energy of the barrier exceeds that of the electron.

The situation encountered in solid insulators or in tunnel diodes is indicated in the following figure.

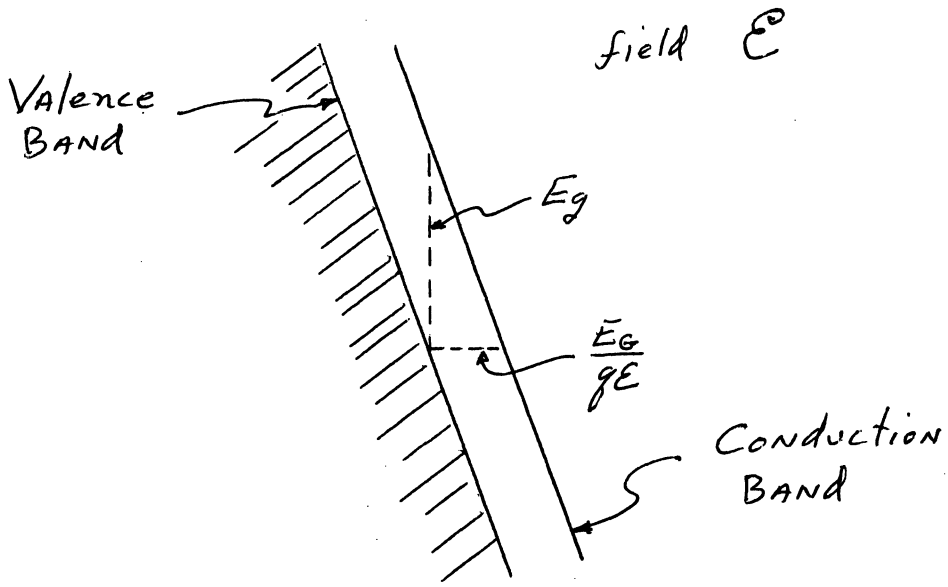

In the depletion region

Under a high applied electric field or built-in electric field the energy bands are sloping and a valence band electron at

level faces a triangular potential barrier of height E_G and thickness $E_G/q\mathcal{E}$. For this barrier we obtain

$$Z = \exp\left[-\frac{4}{3}\frac{(2m^*)^{1/2}}{\hbar q}\frac{E_G^{3/2}}{\mathcal{E}}\right]$$

One difference between an insulator and a tunnel diode is that whereas in the former all valence electrons face <u>unoccupied</u> electron states in the conduction band, in the latter the electrons in valence and the conduction bands do not always face empty electron states. This can perhaps be made clearer from the following diagram

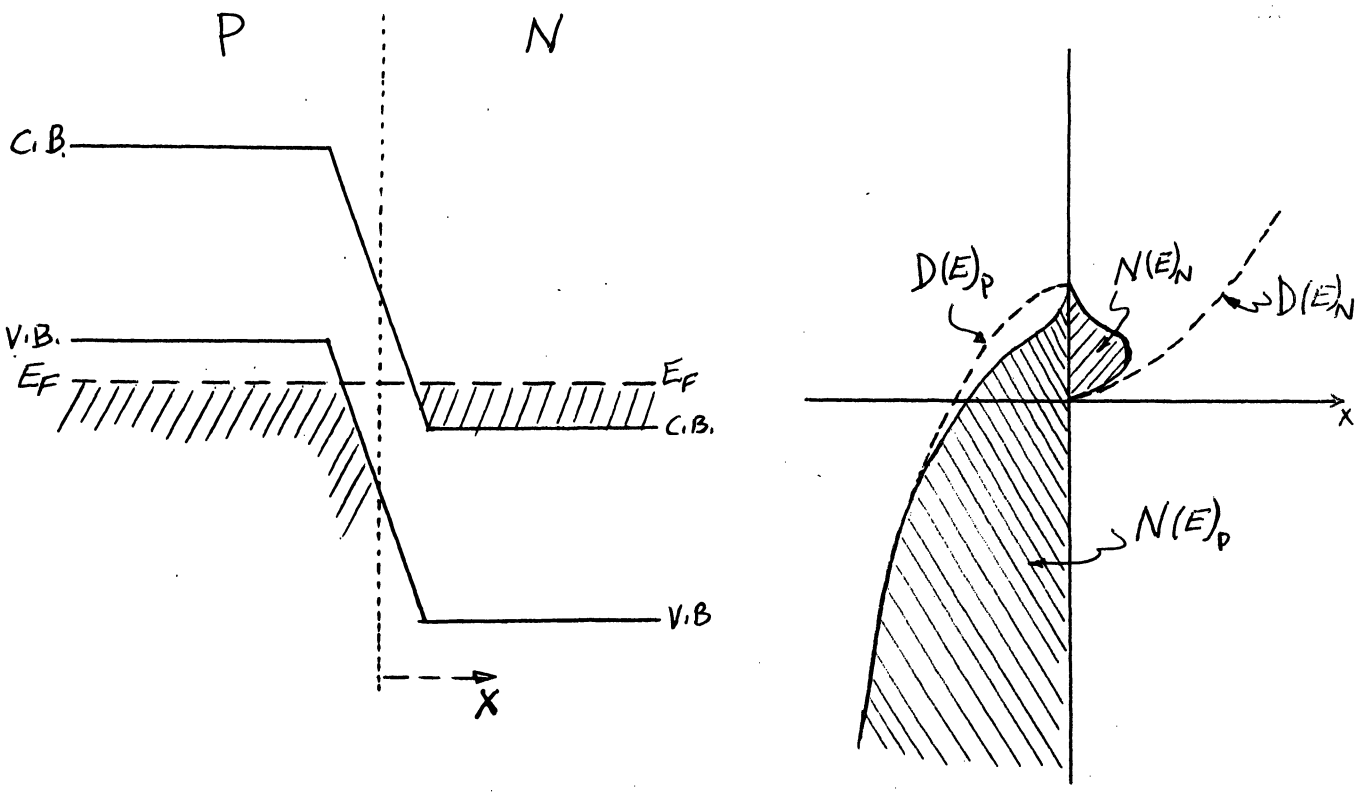

On the left we have shown the conventional energy level diagram of a P-N junction. On the right we indicate the density of states, shown by the cotted curves, and the occupied states,

in the shaded area. The current from one region into the other is proportional to (1) probability of barrier penetration, (2) the density of electrons, and (3) the density of unoccupied electron states. Thus

$$I_{P\rightarrow N} = A \int_{E_C}^{E_V} Z\, f_V(E)\, D_V(E)\, [1 - f_C(E)]\, D_C(E)\, dE$$

and

$$I_{N\rightarrow P} = A \int_{E_C}^{E_V} Z\, f_C(E)\, D_C(E)\, [1 - f_V(E)]\, D_V(E)\, dE$$

The net current is the difference of the two, or

$$I = I_{N\rightarrow P} - I_{P\rightarrow N}$$

$$= A \int_{E_C}^{E_V} [f_C(E) - f_V(E)]\, ZD_C(E)\, D_V(E)\, dE$$

Thus the current is proportional to the quantity

$$g \equiv \int_{E_C}^{E_V} [f_C(E) - f_V(E)] \sqrt{E - E_C}\, \sqrt{E_V - E}\, dE$$

Under zero bias, the current clearly is equal to zero. The effect of the forward bias can be most easily visualized by shifting the electrons and density of states on the N-side upwards with respect to the P-side. As this takes place, more and more of the electrons in the conduction band will face empty states near the top of the valence resulting in an increase in the diode current. The peak in this current

is to be expected when the quasi Fermi level of the N-side is somewhere near the edge of the valence band of the P-side. Beyond this bias, the current is expected to decrease because increasing number of electrons will be facing the forbidden gap on the P-type side. This, then, results in the decrease of diode current, and the current should drop to zero when the bias is such as to make the lower edge of the N-side conduction band coincide with the upper edge of the P-side valence band.

It was first noted, however, by Esaki, that the current does not drop to zero but remains appreciable for all values of forward bias. This current in the valley region is referred to as the excess current, and investigations conducted to date indicate that it is a property of the defect structure of the tunnel diode. The first direct evidence that this excess current is due to deep impurity states was given by Largo, who investigated the effects of deep drops in germanium produced by electron bombardment upon I-V curve of tunnel diodes. Subsequently excess current induced by electron irradiation has been studied in silicon junction by Logan and Chnometh; in germanium, silicon and gallium arsenide by Classen. The effects of impurity states in Ga As and InP has been investigated by Holonyak, and in Si and Ge by Sah and Tremore.

References

P. Franzini, "Tunnel Diode Nonosecond Coincidence Circuit," RSI 32, 1222 (Nov. 1961).

M. Kanter and U. Golil, "Simple Tunnel Diode Coincidence Circuit for Liquid Scintillation Counting", RSI 32, 1259 (Nov. 1961).

N. Ur, "Tunnel-Diode Binary Counter Circuit", Proc. IRE 49, 1092 (June 1961).

A. K. Jouscher, "The Physics of the Tunnel Diode", Brit. J. Appl. Phys. 12, 634 (Dec. 1961).

I. G. Cressell, "Proceedings of the Symposium on Tunnel Diodes", Bul J. Appl. Phys. 12, 646 (Dec. 1961).

L. Esaki, "Properties of Heavily-Doped Germanium and Narrow P-N Junction", Solid State Physics and Telecommunication, Vol. I, Semiconductors Part I, p. 514.

J. W. Easley and R. R. Blair, "Fast Neutron Bombardment of Germanium and Silicon Esaki Diodes", Phys. Rev. 31, 1772 (Oct. 1960).

C. T. Sah, "Electronic Processes and Excess Currents in Gold-Doped Narrow Silicon Junction", Phys. Rev. 123, 1594 (Sept. 1, 1961).

L. Esaki, "New Phenomenon in Narrow Germanium P-N Junctions", Phys. Rev. 100, 603 L (1958).

T. Yamiji and L. Esaki, "Excess Noise in Narrow Germanium P-N Junctions" J. Phys. Soc. Japan 13, 1281 (1958).

L. Esaki, "New Phenomenon in Narrow Germanium P-N Junctions", Phys. Rev. 109, 603 (1958).

"Solid State Physics in Electronics and Telecommunication", Vol. 1, 514 (Acad. Press 1960).

A. G. Chynoweth, W. L. Feldman, and R. A. Logan, "Excess Tunnel Current in Silicon Esaki Junctions", Phys. Rev. 121 ~~181~~, 684 (1961).

S. L. Miller, M. I. Nathan, and A. C. Smith, "Pressure Dependence of the Current-Voltage Characteristics of Esaki Diodes", Phys. Rev. Letters 4, 60 (1960).

T. Yajima and L. Esaki, "Excess Noise in Narrow Germanium P-N Junction", J. Phys. Soc. Japan 13, 1281 (1958).

L. Esaki and Y. Miyohara, "A New Device Using the Tunneling Process in Narrow P-N Junctions", Solid State Electronics, 1, 13 (1960).

T. A. Longo, "On the Nature of the Maximum and Minimum Currents in Germanium ~~and Silicon Esaki~~ Tunnel Diodes", ~~J. App. Phys. 31, 1772 (1960).~~ Bull. Am. Phys. 5, 160 (1960)

R. A. Longan, W. M. Augustyniak, and J. F. Gilbert, "Electron Bombardment Damage in Silicon Esaki Diodes", J. App. Phys. 32, 1201 (1961).

R. S. Classon, "Excess and Hump Current in Esaki Diodes", J. App. Phys. 32, 2372 (1961).

C. B. Pierce and A. D. Kantz, "Defects Introduced in Neutron-Irradiated Esaki Diodes", J. App. Phys. 34, 1496-1503.

A. Ashkin and M. Gershonzar, "Reflection and Grinding of Light at P-N Junctions", J. App. Phys. 34, 2116-19 (July 1963).

R. F. Schaufele, H. Statz, J. M. Lavine, and A. A. Iannini, "Donor-Acceptor Pair Absorption in BaAs Diodes at 2.1 K", App. Phys. Letters 3, 40-1 (Aug. 1963).

Logan and Chynoweth, "Temperature Dependence of Current in Esaki Diodes", Bull. Am. Phys. Soc. 5, 160 (1960)

R.R. Blair and J.W. Easley, "Fast neutron Bombardment of Germanium and Silicon Esaki Diodes", J. App. Phys. 31, 1772 (1960)

4.3 Junction Energy Convesters. The Photo- and Electron-Voltoic Effect.

Here we present a review of the theory and application of the photovoltaic effect with special emphasis on solar energy conversion. A testimonial to the importance of this field today, is the use of these cells in artificial satellites. As the need for power becomes greater and conventional energy sources such as fossil fuel and fissionable materials are used up, the direct conversion of solar energy striking the waste lands of the world could become an important source power.

A step towards the solution of this difficult problem has been achieved by the photovoltaic cell. Cells have already been made that can convert the sun's radiated energy directly into electrical energy with an efficiency of up to 14%.

Becqueral in 1839 first discovered that a photo voltage was developed when light was directed on to one of the electrodes in an electrolytic solution. Adams and Day were the first to observe the effect in a solid (silenium) about forty years later. A number of other early solid-state workers including Lange, Grondahl, and Schottky did pioneering work on silenium and cuprous oxide photovoltaic cells. The work eventually resulted in the photoelectric exposure meter that has become important in photography. It was not until about 1954 when there was a revival of interest in the photovoltaic effect. In that year, an RCA group demonstrated that practical efficiencies could be achieved in converting radioactive radiation into

electrical energy using a silicon P-N junction photovoltaic cell. Using a similar method, Chapin, Fuller, and Pearson reported a solar conversion efficiency of about 6%. Another paper appeared in 1954, by Reynolds, Leies, Antes, and Marburger, who reported about 6% solar-conversion efficiency in cadmium sulfide P-N junctions.

The photovoltaic effect can be defined as the generation of a potential when radiation ionizes the region in or near the built-in potential barrier of a semiconductor. It is characterized by a self-generated emf and the ability to deliver power to a load, the primary power coming from the ionizing radiation. Photons with energy greater than the band gap (1.1 ev for Si) will create electron-hole pairs. At a given temperature the product np is a constant ($np \sim 10^{21}$ for silicon at room temperature). For N-type highly conducting silicon, n can be $10^{17}/cm^3$ and p therefore will be about $10^4/cm^3$. When sunlight strikes this semiconductor, those photons having energy greater than the forbidden gap energy produce both types of carriers in equal numbers. The net effect is that an intense light source can increase the minority-carrier density by many orders of magnitude while the effect on the majority-carrier density is negligible. These photo-induced carriers are in excess of the thermal equilibrium number and they will diffuse randomly about the semiconductor and recombine in times of the order of tenths of microseconds.

If the N- and P-type semiconductors are brought together a P-N junction having a potential barrier is formed because thermodynamics requires that the average energy of the carriers (the Fermi level) be the same in the two materials. Now, excess carriers that are within a diffusion length (the average distance that minority carriers diffuse before they recombine) of the potential barrier will be trapped by the barrier and caused to flow across it in an attempt to reduce their energy. The excess electrons flow to the right and the excess holes to the left.

A typical commercially available silicon solar cell is shown below

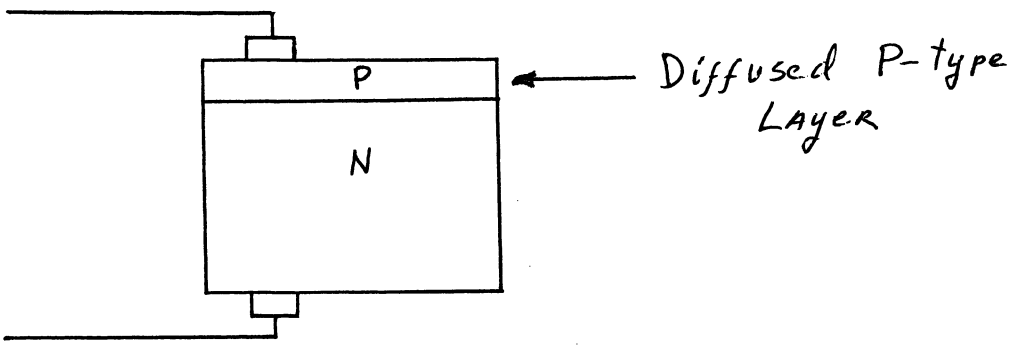

Boron is diffused into an N-type wafer at about 1100°C for 20 minutes, causing a P-type skin a few micron thick to form on all exposed surfaces. All surfaces are etched or lapped down to the N region except the top face. Ohmic contact

is made to the top and bottom by first nickel plating the surface and then soldering.

To achieve high conversion efficiency it is desirable to produce electron-hole pairs within a diffusion length of the junction. For short diffusion length material it is therefore desirable to absorb most of the photons in the region where the field exists.

The following "ball park" figures will serve to obtain further insight into the solid state voltaic processes. Consider a P-N junction being irradiated with beta particles or with photons. From

$$n = N_C \, e^{-\frac{E_C - E_F}{kT}} \tag{4.27}$$

we find that

$$E_C^{(P)} = E_F - kt \, ln \frac{n_P}{N_C} \tag{4.28}$$

and

$$E_C^{(N)} = E_F - kt \, ln \frac{n_N}{N_C}$$

so that

$$E_C^{(P)} - E_C^{(N)} = kT \, ln \frac{n_N}{n_P} \tag{4.29}$$

For a typical donor and acceptor concentrations of about $10^{16}/cm^3$, we find that

$$n_N \sim 10^{16}, \quad n_P = 10^{20}/10^{16} \sim 10^4$$

so that the rise in potential going from the P side to the

N side is from (4.29)

$$V_B = \frac{E_C^{(N)} - E_C^{(P)}}{-q} = \frac{kT}{q} \ln \frac{n_N}{n_P} \sim .4 \text{ volt}$$

The thickness of the transition layer in which this rise in potential takes place can be estimated from

$$x_P = \left[\frac{2 \epsilon V_B}{q N_A \left(1 + \frac{N_A}{N_D}\right)} \right]^{1/2}$$

$$x_N = \left[\frac{2 \epsilon V_B}{q N_D \left(1 + \frac{N_D}{N_A}\right)} \right]^{1/2} \qquad (4.30)$$

Upon putting $N_A = N_D \sim 10^{16}$ and using appropriate numerical values, we find that $x = x_P + x_N \sim 10^{-4}$cm. Thus a charged carrier finding itself in this barrier region is subject to a built-in electric field of about

$$\frac{0.4}{10^{-4}} \sim 4000 \text{ volt/cm}$$

We need next to estimate the excess electron-hole pairs created by the incident radiation. As an example, the solar radiation is typically 0.1 w/cm^2 or about 10^6 ergs/cm^2/sec. Hence, from

$$I = c\mu$$

we find that

$$\mu \sim 10^6/(3 \times 10^{10}) \sim \frac{1}{3} \times 10^{-4} \text{ ergs/cm}^3$$

and the photon flux Φ is given by

$$\Phi = \frac{I}{h\nu} = I \left(\frac{\lambda}{Ch}\right) \sim 10^6 \left(\frac{10^{-4}}{(3\times10^{10})(6\times10^{-27})}\right)$$

$$\sim 10^{18} \text{ photons/cm}^2\text{/sec} \qquad (4.31)$$

If the cell is illuminated from the P-side as shown in the following figure

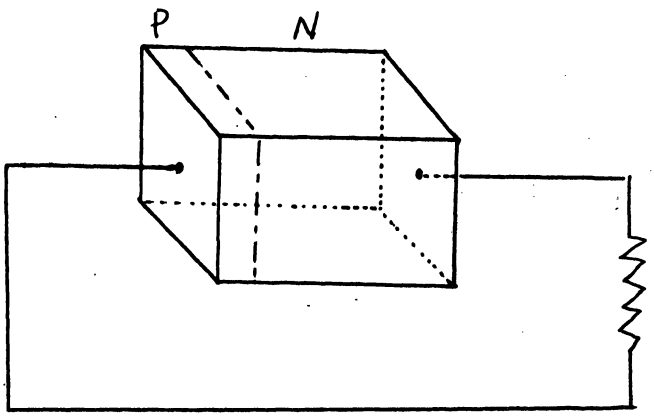

the rate of excess electron generation is about $10^{18}/\text{cm}^3/\text{sec.}$, compared to the normal electron concentration of about $10^{10}/\text{cm}^3$. These excess electrons will then diffuse into the transition region, if generated within a diffusion length from the junction, and then pulled in by the electric field.

The device then is basically a current generator, giving

$$I_s = q\, g\, L \qquad (4.32)$$

where g is the rate of generation of free carriers, and L is the diffusion length given by

$$L = \sqrt{D_n \tau} \qquad (4.33)$$

Now

$$D_n \sim 35 \text{ cm}^2/\text{sec.}$$

$$\tau \sim 100 \times 10^{-6} \text{ sec.}$$

so that

$$L \sim \sqrt{35 \times 10^{-4}} \sim 6 \times 10^{-2} \text{cm}$$

$$I \sim 10^{-19}(6 \times 10^{-2})(10^{18}) \sim 10^{-2} \text{ amp/cm}^2$$

From the above analysis, it is quite clear that the excess carrier concentration must be produced on one side of the P-N junction. This means that the incident radiation must be absorbed on one side, at distances not larger than 10^{-2}cm from the junction. Consequently the following procedure is used for the fabrication of the device. An N-type sample of silicon is heated in an atmosphere of boron trichloride, so that boron diffuses in to form a skin of P-type material about 10^{-4}cm thick. Later a part of the P-type layer is ground away, and one of the contact is made directly to the N-type base as shown in the following figure.

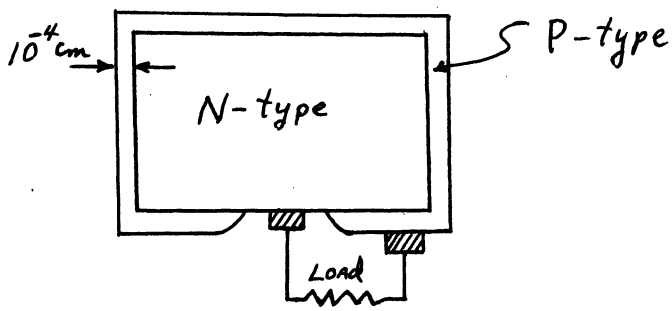

For the electron-voltaic cell, or the so-called nuclear battery a P-N junction is made into a well as shown in the following figure.

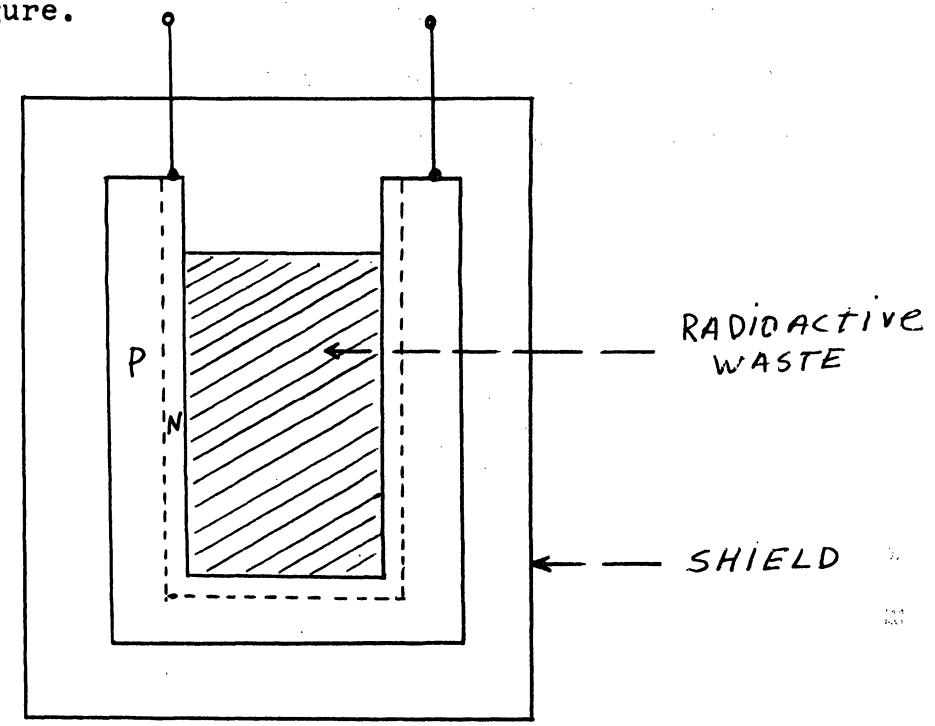

The nuclear radiation striking the N-region are absorbed, thereby creating excess electrons and holes. The mechanism for this device is similar to that of the solar cell. P. Rappaport (Phys. Rev. 93, 246 (1954) Jan. 1) of RCA bombarded a germanium and silicon P-N junction of 1/4 cm^2 cross-sectional area with beta particles from a 50 millicurie Sr^{90} - Y^{90} source. For silicon, a maximum open-circuit voltage of 200 mv and a short-circuit current of 10^{-5} amp were observed. From a 50 millicurie source (about 200 microwatt) electrical power of 0.8 microwatt was delivered to a matched load of about 10,000 ohms. This represents a conversion efficiency of about 0.5 per cent. One of these devices was used as a generator to drive a transistor audio-oscillator.

Such a power supply has potentially a long life because the half-life of Sr-90 is known to be 28 years. However, radiation damage due to the energetic 2.26 Mev beta particles from Y-90 might reduce the useful life of the device. The decay scheme for Sr-90-Y-90 is as follows:

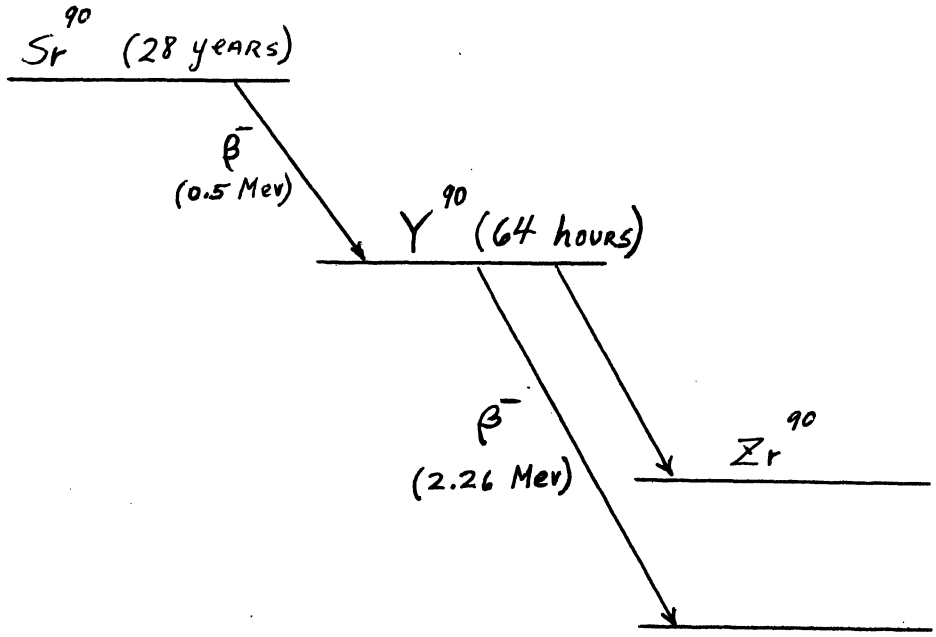

According to Loferski and Rappaport (Phys. Rev. 98 1861 L (1955) June 15) the threshold for atomic displacement in germanium produced by electrons is about 0.6 Mev.

As indicated by (4.32) a quantity of critical importance in the operation of these devices is the diffusion length. This as seen from (4.33) depends upon the minority carrier lifetime τ, which as we shall see is very sensitive to the effects of radiation.

The above discussion provides a brief qualitative description of the voltaic effects. We shall return to a more detailed discussion of the theory later, in conjunction

with the measurement of the threshold energy for atomic displacement.

References

F. A. Junga and G. M. Anslow, "Radiation Effects in Silicon Solar Cells", IRE Trans NS-6, 49 (June 1959).

R. V. Bobcack, "An Explanation of the Superior Radiation Resistance of P-Type Bru Si Solar Cells", J. Electrochem Sa 1081, 1119 (1961).

R. L. Cummerow, "Photovoltaic Effect in P-N Junctions", Phys. Rev. 95, 16 (July 1, 1954).

P. Rappaport, "The Photovoltaic Effect and Its Unilization", RCA Rev. 20, 373 (1950).

M. B. Prince and M. Wolf, "New Developments in Silicon Photovoltaic Devices", J. Bri IRE 18, 583 (Oct. 1958).

E. Becquerel, "On Electric Effects Under the Influence of Solar Radiation", Compt. Rend. 9, 561 (1839).

W. G. Adams and R. E. Day, "The Action of Light on Silenium", Proc. Roy. Soc. 25A, 113 (1877).

B. Lange, "New Photoelectric Cell", Zeit. Phys. 31, 139 (1930).

L. O. Crandahl, "Copper-Cuprous-Oxide Rectifier and Photoelectric Cell", Rev. Mod. Phys. 5, 141 (1933).

W. Scheltky, "Cuprous Oxide Photoelectric Cell", Zs. Phys. 31, 913 (1930).

P. Rappaport, "The Electron Voltaic Effect in P-N Junctions Induced by Beta=Particle Bombardment", Phys. Rev. 93, 246, (Jan. 1954).

P. Rappaport, J. J. Loferski, and E. G. Linder,"The Electron-Voltaic Effect in Germanium and Silicon P-N Junctions", RCA Rev. 17, 100 (1956).

D. M. Chapin, C. S. Fuller, and G. L. Pearson, "A New Silicon P-N Junction Photocell for Converting Solar Radiation into Electrical Power", J. App. P hys. 25, 676 (May 1954).

M. B. Prince, "Silicon Solar Energy Converters", J. App. Phys. 26, 534 (1955).

D. C. Reynolds, G. Leies, L. L. Antes, and R. E. Marburger, "Photovoltaic Effect in Cadmium Sulfide", Phys. Rev. 96, 533 (Oct. 1954).

W. G. Phann and W. Van Roosbroeck, "Radiactive and Photo-Electric P-N Junction Power Sources", Transistor Techn. 2, P. 472-497 (J. App. Phys. 25, Nov. 1954).

M. B. Prince, "Silicon Solar Energy Converters", Transistor Technology 2, 497-511 (J. App. Phys. 26, (May 1955)).

CHAPTER V.

RADIATION DAMAGE

We shall now consider the chain of events that will be triggered by a neutron striking a lattice atom. We shall first consider specifically the effects of fast neutrons and reserve the discussion of the effects of thermal neutron to a later chapter. Also to limit the scope of the discussion, we shall limit ourselves primarily to radiation damage in germanium and silicon.

Before plunging into the details, let us compare the nuclear and internuclear distances to astronomical distances, in order to obtain an appreciation for the rarity of nuclear encounters. Nuclear radii are of the order of 10^{-12} cm and internuclear distances in solids are about 10^{-8} cm so that

$$\frac{\text{Internuclear Distance}}{\text{Nuclear Radii}} \sim 10{,}000$$

Now the earth's diameter is about 8,000 miles, and the distance to the sun is about 93,000,000 miles so that the ratio of the distance to the sun to the earth's diameter is also about 10,000. In other words, if a nucleus were magnified to the size of the earth, then other nuclei in solids will be at distances comparable to the distance to the sun.

Imagine then that the nuclei are magnified to the size of the earth. Then neighboring nuclei will be at distances

comparable to the sun's distance. A reasonable value for the target-source distance in nuclear experiments is of the order of 1 cm, and this distance on the magnified scale (taking 1 A equivalent to 100,000,000 miles) would correspond to $10^8 \times 10^8 = 10^{16}$ miles, or about 17,000 light years (1 light year is about 6×10^{12} miles). The nearest star Proxima Centauri is only 4.27 light years away. The diameter of the Milky Way is estimated at 100,000 light years, and its center is supposed to be about 30,000 light years from the solar system. This means then that the problem of hitting a germanium nucleus with neutrons is like trying to hit the solar system from the center of the Milky Way, with projectiles about the size of the earth.

This comparison I think makes clear that nuclear encounters are most rare events. The ionization tracks produced by recoiling nuclear particles appearing on the nuclear horizon are like the comets we see once or twice in a century.

Another point to note is that neutrons are actually quite harmless until it collides with a nucleus. Because the neutron is massive, the struck nucleus will receive an appreciable amount of kinetic energy. As this struck atom, called the primary knock-on, moves through the lattice, it will produce ionization and then other atomic displacements.

5.1 Primary Knock-Ons

Consider then a neutron of energy E_o colliding with a germanium atom. We wish to show that

$$\text{(a)}\quad T_{max}\ (\text{recoil}) = \frac{4Mm}{(M+m)^2}\,E_o \tag{5.1}$$

in which M and m are the masses of the target nucleus and neutron replacements.

(b) The differential cross section for transfer of energy between T and T + dT to the target nucleus is

$$d\sigma = \frac{\sigma_s}{T_m}\,dT \tag{5.2}$$

and

$$\text{(c)}\qquad \overline{T} = \frac{1}{2}T_m \tag{5.3}$$

Consider first a neutron moving with velocity v_o to the right in the laboratory coordinate system (L-system). The target nucleus M is then stationary. Let the neutron and the target recoil as shown in the figure.

From the principles of conservation of energy and linear momentum we obtain

$$E_o = \frac{1}{2} m v_o^2 = \frac{1}{2} m v^2 + \frac{1}{2} M V^2 \tag{5.4}$$

$$m v_0 = MV \cos\theta + m v \cos\alpha$$

$$0 = MV \sin\theta - m v \sin\alpha \tag{5.5}$$

Solving these equations, we find that the recoil energy T of M is

$$T = \frac{1}{2} M V^2 = \frac{4Mm}{(M+m)^2} E_0 \cos^2\theta \tag{5.6}$$

This is maximum when $\theta = 0$ corresponding to a head-on collision.

To determine the distribution in energy of the primary knock-ons, it is simplest to go to the center of mass system (C-system). The velocity of the center of mass is

$$V_c = \frac{m v_0}{(M+m)} \tag{5.7}$$

to the right. In the C-system, the velocity of the incoming neutron then is

$$v_0 - V_c = \frac{M}{(M+m)} v_0 \tag{5.8}$$

and that of the target nucleus is

$$V = -V_c \tag{5.9}$$

The minus sign indicates that the motion of the target nucleus is to the left.

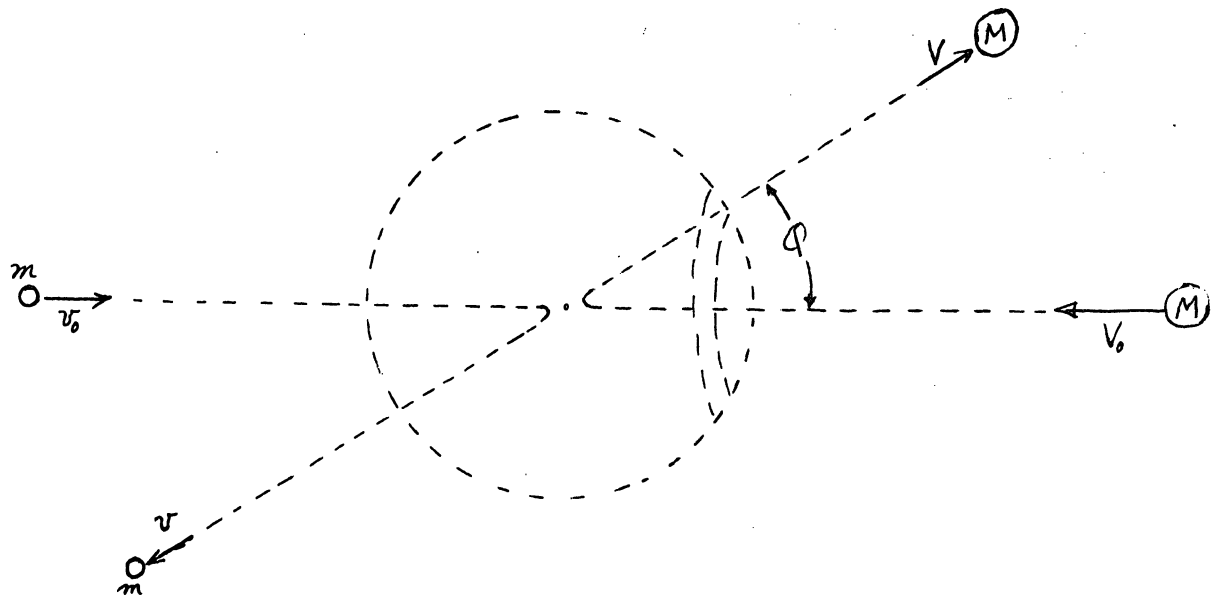

It can be easily shown that the C-system, the colliding particles merely undergo change in direction of motion (along a straight line) after collision. Thus, if v_0 and V_0 are the velocities of the colliding particles before collision, and v and V are the corresponding quantities after collision, then

$$|v| = |v_0| \tag{5.10}$$

and

$$|V| = |V_0|$$

Thus the kinetic energy of M in the C-system remains unchanged, and is equal to

$$T_c = \frac{1}{2} M V_0^2 = \frac{Mm}{(M+m)^2} E_0 = \frac{1}{4} T_m \tag{5.11}$$

If θ and φ are the recoil angles of the struck nucleus in the L- and C-systems respectively, and T and T_C the kinetic energies in the L- and C-systems, the relations among these quantities can be readily deduced from the following vector diagram:

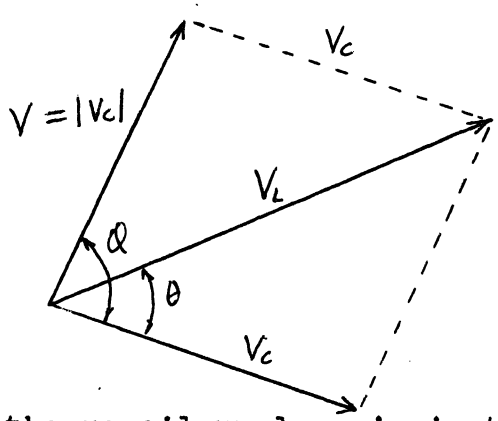

The velocity of the recoil nucleus is just the resultant of the velocities of the center of mass and of the recoil nucleus in the C-system. The magnitudes of these two vectors are equal, so that

$$\theta = \frac{\varphi}{2} \tag{5.12}$$

and

$$T = \frac{1}{2} M V_L^2 = \frac{1}{2} M \left[2V_c^2 + 2V_c^2 \cos\varphi \right]$$

$$= \frac{2Mm}{(M+m)^2} E_0 (1+\cos\varphi) = \frac{1}{2} T_{max} (1+\cos\varphi) \tag{5.13}$$

so that the recoil energy T in the L-system is determined by the recoil angle φ in the C-system.

Now let us assume that the scattering in the C-system is

isotropic. This means that if N_o is the total number of recoil nuclei in all directions, the number scattered in any direction depends only upon the solid angle subtended by that area. Consider then the particles recoiling between φ and $\varphi + d\varphi$. The number scattered into this zone is

$$dN = N_o \frac{2\pi \sin\varphi \, d\varphi}{4\pi} = \frac{1}{2} N_o \sin\varphi \, d\varphi \tag{5.14}$$

But the recoil nuclei in this zone have energies between T and T - dT, in which

$$dT = \tfrac{1}{2} T_{MAX} \sin\varphi \, d\varphi \tag{5.15}$$

$$\therefore dN = N_o \frac{dT}{T_{MAX}} \tag{5.16}$$

But by the definition of scattering cross section

$$N_o = I \sigma_s \tag{5.17}$$

in which I is the incoming neutron flux and σ_s the total cross section, which is assumed to be very close to the scattering cross section. Therefore

$$d\sigma = \frac{\sigma_s}{T_{MAX}} dT \tag{5.18}$$

Furthermore

$$\overline{T} = \frac{\int T \, dN}{\int dN} = \frac{\int_0^{T_{MAX}} T \, dT}{\int_0^{T_{MAX}} dT} = \frac{1}{2} T_{MAX} \tag{5.19}$$

Consider eq. (5.3). Calculations of irradiation effects have usually been made under the assumption that all neutrons possess a single effective energy, lyin g somewhere between 1 and 2 Mev. For sake of simplicity, we shall assume that

$$E_o = 2 \text{ Mev.}$$

Then (5.3) becomes

$$\bar{T} = \frac{4A}{(A+1)^2} \sim \frac{4}{A} \quad (Mev) \tag{5.20}$$

in which A is the mass number of target nucleus, assumed to be large in comparison to 1. Representative recoil energies are

Nucleus	A	$\bar{T}$ (Mev)
Si	28	.143
Cu	65	.061
Ge	72	.050

Next we shall consider the effects produced by the recoiling primaries.

5.2 Limiting Energy of Ionization (E_i)

Next we need to determine the physical processes brought about by the primary knock-ons. For this, we shall review the effects produced by α particles in air.

a. Alpha Particles in Air

The α-particle cloud chamber tracks, shown in such books as I. Kaplan, Nuclear Physics, (Addison Wesley) p. 256,

are typically as follows:

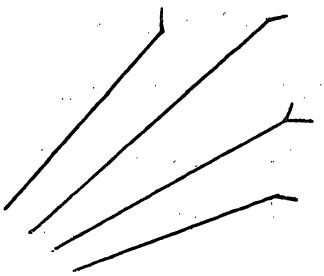

That is, tracks show high ionization near the end of the track, with little kinks at the end. Specific ionization of α-particles has been studied in considerable detail and the results are typically as follows:

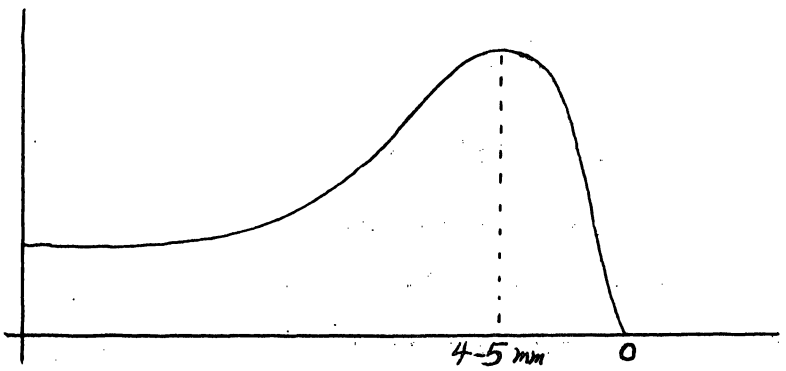

When the particle is just starting it produces about 2,200 ion pairs per mm. The specific ionization increases very slowly at first, as the α-particle loses energy, and the ionization reaches 2,700 ion pairs/mm at about 3.0 cm, from the end of the range. It then increases more rapidly reaching a maximum of about 7,000 ion pairs/mm when the particle is about 4 or 5 mm from the end of its range. The specific ionization decreases very rapidly in the last few millimeters of its range. For the Ra C' (P_o^{214}) 7.68 Mev α-particle, the range is known to be about 6.95 cm, producing a total of 2.2×10^5 ion pairs in air at 15°C and 760 mm of Hg. It follows that the particle

loses about 35 ev on the average for each ion pair. The kinks in the ionization tracks indicate nuclear collisions.

That electron collision rather than nuclear collision is the dominant mechanism for α-particle energy dissipation initially can be seen from the following argument. Consider an α-particle going from left to right as shown in the following figure:

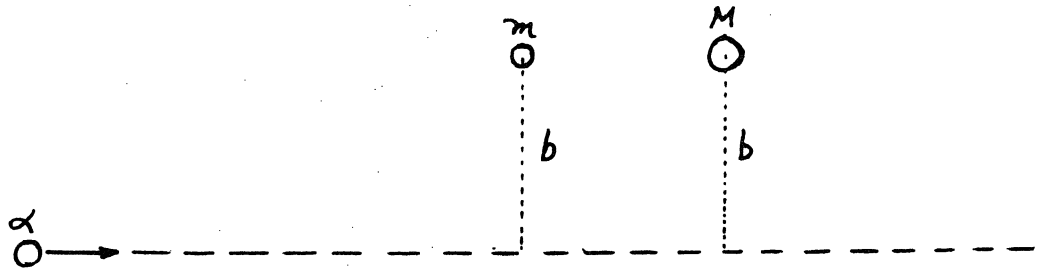

Consider then two particles, one an electron and the other a nucleus having the same impact parameter b. As the α-particle sweeps by, a force $F_\perp$ is exerted on the particle, arising from the Coulomb interaction. The net momentum imparted to the particles m and M is

$$\Delta p = \int F_\perp \, dt$$

Therefore

$$\Delta E \text{ (electron)} = \frac{1}{2m} (\Delta p)^2$$

and

$$\Delta E \text{ (ion)} = \frac{1}{2M} (\Delta p)^2$$

so that the ratio of the energies is

$$\frac{\Delta E\,(\text{electron})}{\Delta E\,(\text{ion})} \sim \frac{M}{m} \sim 10^3$$

This suggests then that very little of the α-particle energy is taken up by nuclei by Coulomb collisions..

The reason for the rapid rise in specific ionization near the end of the particle can also be seen by similar arguments. The imparted impulse is given by

$$I_\perp = \int F_\perp(t)\,dt = \int q E_\perp(t)\,dt$$

$$= q\int E_\perp \frac{dx}{v} = \frac{q}{v}\int E_\perp\,dx$$

Now according to Gauss' theorem

$$\int \underline{E}\cdot d\underline{\sigma} = 4\pi z_1 q$$

so that

$$\int_{-\infty}^{\infty} E_\perp(x)\,2\pi b\,dx = 4\pi z_1 q$$

$$\int_{-\infty}^{\infty} E_\perp\,dx = \frac{2 z_1 q}{b}$$

Consequently

$$I_\perp = \frac{2 q^2 z_1}{b}\,\frac{1}{v}$$

Therefore the energy transferred is

$$\Delta E \propto \frac{1}{v^2}$$

showing that greater specific ionization is to be expected for lower energies, i.e., near the end of the track.

Near the end of the track another mechanism of electron pick-up will become important, i.e.,

$$\alpha + e \longrightarrow He^{+}$$

$$He^{+} + e \longrightarrow He$$

These processes should become important when the nuclear velocity is such that the electrons can stay on the nucleus. This means that

$$v_{\alpha} \sim v \text{ (orbital electron)}$$

Now since

Electron energy ~ Hydrogen ionization energy ~ 10 ev

we see that

$$E_{\alpha} = \frac{1}{2} M v_{\alpha}^{2} = \frac{M}{m}\left(\frac{1}{2} m v_{\alpha}^{2}\right) \sim 10^{3}(10) \sim 10 \text{ Kev}$$

This means that the α-particle will pick up electrons when its energy is reduced to about 10 Kev. By this time the α-particle is a neutral helium atom. These neutral helium atoms can now make very close enounters with other neutral atoms, so that nuclear collisions become important only at the very end of the range.

Theory shows that the rate of energy loss is given

$$\frac{dE}{dx} = -\frac{4\pi z^2 e^4 N}{m_e v^2} Z \ln\left(\frac{2 m_e v^2}{I}\right)$$

where

ze, v . . . charge and speed of the particle

m_e . . . electron mass

Z . . . atomic number of substance

N . . . number of electrons/cm^3 of the substance

I . . . average excitation potential

Now the range R of the particle is given

$$R = \int_0^R dx$$

so that it follows immediately that

$$R \propto \frac{1}{N}$$

That is, the range is inversely proportional to the material density. Since solids are about 1000 times more dense than gas, the α-particle range in solids is expected to be about 1/1000 that in air.

Range of Ra C' (P_o^{214}) 7.68 Mev α-Particle

Air (15°C, 760 mm Hg)	6.953 cm
Mica	.0036
Aluminum	.00406
Copper	.00183
Gold	.00140

b. Ionizing Particles in Solids

The recoil atoms moving through matter with energies of the order of 100 Kev is slowed down by numerous collisions, some of which impart appreciable energy to target atoms but most of which impart energy to individual electrons of the target. Such a moving atom would be expected to be heavily ionized when it is moving at high speeds and to acquire electrons as it slows down. Roughly speaking, those electrons whose orbital velocities are greater than the velocity with which the atom is moving will remain attached; those electrons which have an orbital velocity lower than that of the atom will be stripped away. This means that Mev protons or deuterons will be completely ionized, while the knock-on atoms will be only rarely ionized, except for the lightest elements.

The collisions by the moving atoms can be elastic or inelastic. In an elastic collision, the moving particles merely transfer a part or whole of its kinetic energy to another lattice atom, without producing electronic excitation. In an inelastic collision, part of the kinetic energy is used in producing electronic excitation.

In general, inelastic collisions are much more frequent while the energy of the moving atom is high, and elastic collisions become more probable as the moving atoms slows down. To simplify the analysis, the following assumption will be made: If the moving atom has a velocity much less than that

of an electron in the target, that electron will be left without excitation; if the velocity is greater, then the electron will be excited. The energy at which elastic collision will predominate over an inelastic collision is called the limiting energy of ionization, E_i. Seitz suggests that for insulators

$$E_i = \frac{1}{8} \frac{M}{m} I \qquad (5.21)$$

where M is the mass of moving atom, m is the electron mass, and I is the optical excitation energy.

For many insulators I is about 5 ev, so that the above expression becomes approximately

$$E_i \sim 1000 A \text{ ev} \qquad (5.22)$$

i.e. the limiting energy of ionization is equal to the atomic weight in Kev. Using this rule, E_i for germanium should be about 70 Kev.

5.3 Threshold Energy of Atomic Displacement

According to the picture presented so far, a neutron collides with a lattice atom, and the recoil atom will dissipate its energy by producing ionization until its energy is reduced to E_i. For example, the average kinetic energy of recoiling silicon is about 140 Kev when struck by a 2 Mev neutron. According to our estimate E_i for silicon is about 28 Kev.

Consequently, much of the energy of the primary knock-on is used up in producing ionization. For germanium, on the other hand, the estimated E_i is 70 Kev. in comparison to its recoil energy of 50 Kev. Therefore, according to our simplified theory, the primary knock-on germanium atom will lose its energy principally through elastic collisions. We need to find out how much energy on the average is required to produce an atomic displacement and the number of atomic displacements produced by one primary knock-on. The energy for atomic displacement, called the threshold energy, has in the past been more or less arbitrarily set at 25 ev. This value was given first by F. Seitz by the following argument. The energy required to remove a typical atom from a lattice and interstitial path interior site in a solid in an adiabatic and reversible manner is about 2 E_c, where E_c is the energy of sublimation. If, however, the process is carried out dynamically, as in the fast collision, the process is highly irreversible and the energy required is expected to be of the order of $4E_c$. Since E_c in tightly bound solids is of the order of 5-6 ev, a value of 25 ev for E_d is suggested.

The experimental value for the displacement threshold energy can be determined by bombarding N-type germanium with variable high-energy electrons. In these experiments the electron energy is changed but the total number of incident particles per bombardment is kept constant. The change in conductivity is then plotted as a function of electron energy. For low electron energy, conductivity electron energy curve is horizontal (conductivity is not affect by the bombardment),

followed by a sharp decrease in the conductivity. The energy at which the conductivity. The energy at which the conductivity begins to change is taken as the displacement energy.

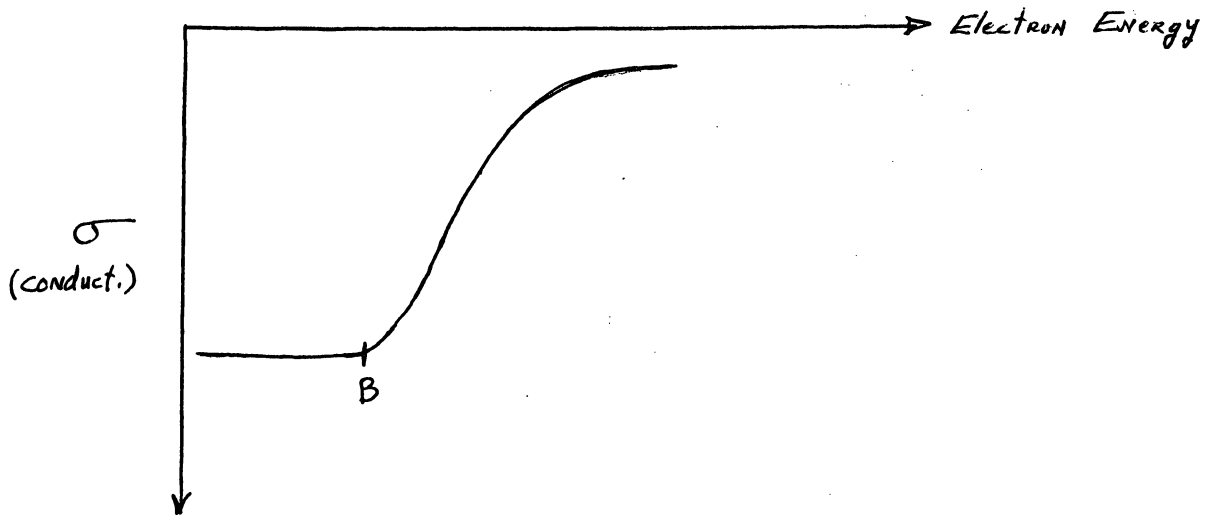

The break in the curve, indicated by B, comes at about 0.63 Mev. Under electron bombardment, the maximum energy transferred to the struck nucleus of mass M is given by

$$E_m = \frac{2T(T+2m_0c^2)}{Mc^2} \tag{5.23}$$

in which T is the kinetic energy of the incoming electrons. The above result can be easily proved as follows.

$$E = c\sqrt{p^2 + m_0^2c^2}$$

$$E = T + m_0c^2$$

$$\therefore p^2 = \frac{E^2}{c^2} - m_0^2c^2 = \frac{1}{c^2}T(T+2m_0c^2) \tag{5.24}$$

But since the struck nucleus is massive compared to the

electron, so that the momentum P of the heavy nucleus is

$$P = 2p$$

Furthermore

$$E = \frac{1}{2M} P^2 \tag{5.25}$$

so that $E_m = \frac{1}{2M} \frac{4}{c^2} T(T + 2m_0c^2)$

$$E_m = \frac{2T(T+2m_0c^2}{Mc^2} \tag{5.26}$$

Now

$$T = 0.63 \text{ Mev}$$
$$2m_0c^2 = 1.022 \text{ Mev}$$
$$Mc^2 = 931 \text{ A Mev}$$

For germanium A is about 73. Therefore

$$E_m = \frac{2(0.63)(1.65)}{931\ (73)} \text{ Mev}$$
$$= 31 \text{ ev}$$

More recently Loferski and Rappaport have made a careful determination of the threshold displacement energy in silicon and germanium using the electron-voltnic effect. The experiment carried out by them revelas another important aspect of radiation damage, namely, the reduction of carrier lifetime. This is a critical quantity that determines the performance

of such devices as the solar and the nuclear batteries. Therefore their experiments will be described in detail.

Consider then a P-N junction being irradiated by ionizing particles such as β-particles, or even photons. In the experiment by Loferski and Rappaport, a Sr = 90 source was used. As these particles strike and penetrate into the junction, a cloud of electron-hole pairs will be created. Since the energy level for the P-N junction is as shown in the following figure

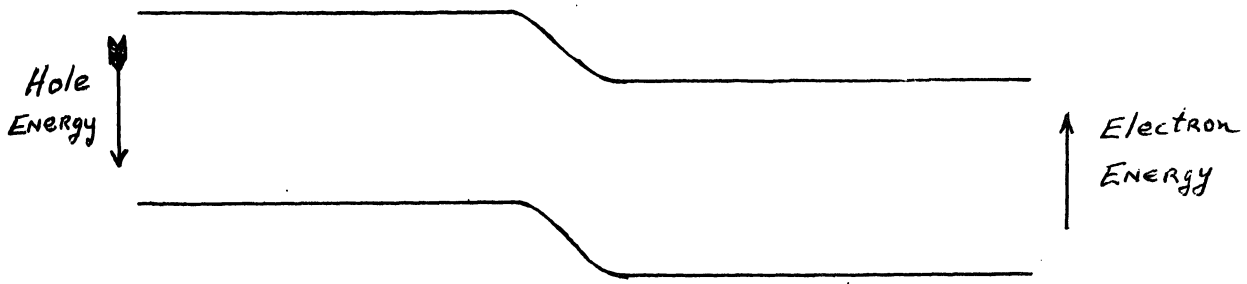

with the electron and hole energies respectively increasing in the direction indicated by the arrows, the electrons will drift into the N-region and the holes in the P-region. If then the device is shorted through an a meter A, then there will be a flow of current through the external circuit from left to right. In other words, the β -irradiated P-N junction is a current generator.

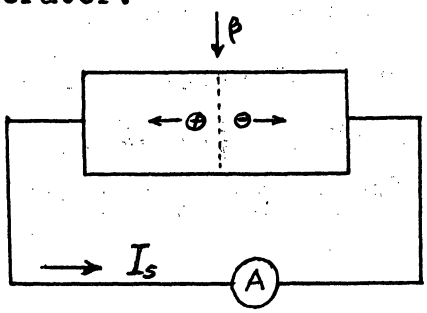

Unfortunately from the standpoint of device application, but fortunately for threshold energy measurements, the damage produced by the β -particles is appreciable. The Sr-90 decay scheme is shown below:

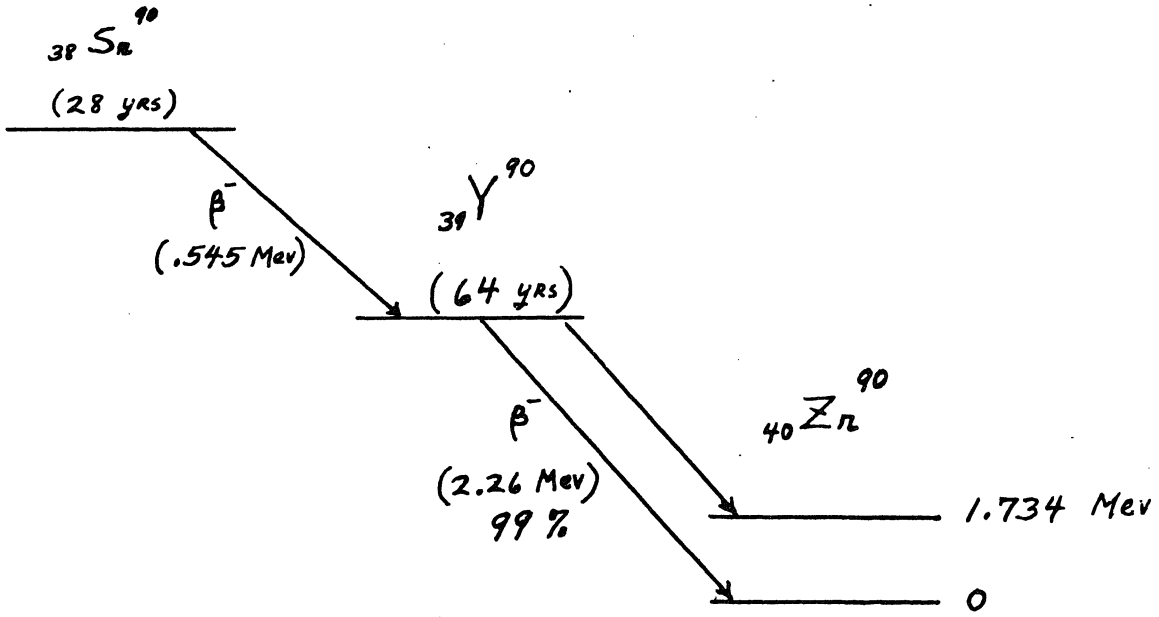

From an earlier discussion, it was noted that the threshold for electron bombardment damage is about 0.6 Mev. Consequently the 2.26 Mev β -particles emitted in the Y^{90} - Zr^{90} decay will certainly contribute to the damage, and so possibly will the .545 Mev β -particles emitted in the Sr^{90} - Y^{90} dacay.

Suppose now we focus our attention on the holes. During the bombardment process, holes are generated, and at the same time, recombination with electrons takes place, according to the relation

$$\frac{dP}{dt} = g - \frac{P - P_0}{\tau}$$

where g is the hole generation rate. Under steady-state condition, we find

$$P = P_0 + g\tau$$

showing that the bombardment corresponds to hole injection of $g\tau$. In the P-type region, away from the bombardment region, the diffusion equation gives

$$D_P \frac{\partial^2 P}{\partial x^2} = \frac{\partial P}{\partial t}$$

and since

$$\frac{\partial P}{\partial t} = - \frac{P - P_0}{\tau}$$

we find that

$$D_P \frac{\partial^2 P}{\partial x^2} = - \frac{P - P_0}{\tau}$$

Solving this equation, and noting that x is negative on the P-type side (x = 0 at junction) we find

$$P - P_0 = C e^{x/L_P}$$

where the diffusion length L_P is defined by

$$L_P \equiv \sqrt{\tau D_P}$$

Since

$$p - p_o = g\tau \qquad \text{at } x = 0$$

we obtain

$$p - p_o = g\tau\, e^{x/L_p}$$

Now

$$J_p = -q D_p \frac{dp}{dx}$$

so that

$$J_p = \frac{q D_p g \tau}{L_p} = q g L_p = q g \sqrt{\tau D_p}$$

Consequently

$$\tau = \frac{J_s^2}{q^2 g^2 D_p}$$

where we have used J_s for the short-circuit current density. Thus under constant β-particle irradiation a constant current generation is to be expected if such bombardment does not alter the carrier lifetime τ.

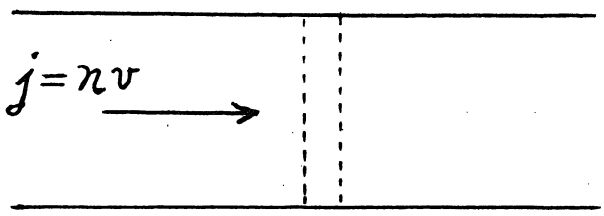

To determine the dependence of the carrier lifetime upon the bombardment time, consider the trapping out of carriers due to bombardment produced defect. The rate of trapping out

is given by

$$\frac{dn}{dt} = j\sigma_c$$

(No. of empty trapping centers)

where σ_c is the electron capture cross section of the trapping center. If N_r represents the density of trapping centers produced by radiation, at level E_r, then the concentration of occupied traps is

$$\frac{N_r}{e^{\frac{E_r - E_F}{KT}} + 1}$$

and the concentration of empty traps is

$$N_r - \frac{N_r}{e^{\frac{E_r - E_F}{KT}} + 1} = N_r f(E_r - E_F)$$

so that we can write

$$\frac{dn}{dt} = j\sigma_c N_r f(E_r - E_F)$$

Since

$$j = nv$$

we have

$$\frac{1}{\tau} = \frac{1}{n}\frac{dn}{dt} = v\sigma_c N_r f(E_r - E_F)$$

Now, since N_r is the concentration of centers produced by irradiation,

$$N_r = \Phi \Delta(E_B)$$

where ϕ is the integrated irradiation particle flux and Δ is the cross section for the trap center formation.

$$\therefore \quad \frac{d}{dt_B}\frac{1}{\tau} = v\sigma_c f(E_n - E_F)\frac{d\phi}{dt}\Delta(E_n)$$

The quantities on the right-hand side are constant so that the plot of $1/\tau$ should show an increase linear in bombardment time if the trapping centers are produced. As shown earlier, the carrier lifetime is proportional to the square of the short-circuit current so that a suitable plot is the reciprocal square of the short-circuit current against bombardment time.

The experimental plots obtained by Loferski and Rappaport are as follows:

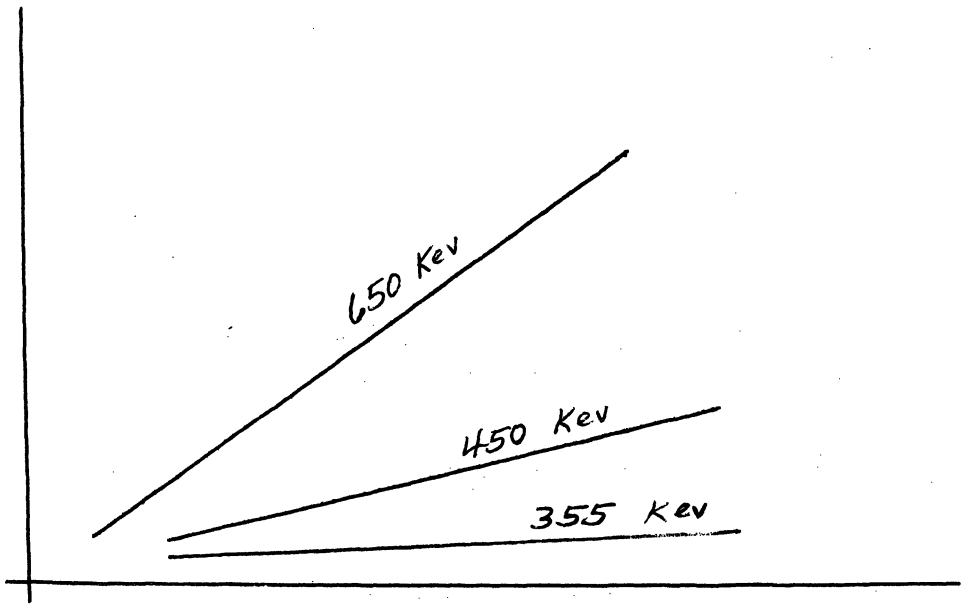

The threshold bombardment energy. . . i.e., the electron energy for which there is no change in the short-circuit current. . . was found to be about 355 KV for Ge, and 140 KV for silicon. This value leads to

$$E_D = \frac{2(.355)(1.37)}{72(931)} = 14.5 \text{ ev}$$

The displacement energy for Si is given as 13 ev.

More recent investigations by Arnold and Compton indicate that the constituent atoms of a diatomic material have different displacement energy. According to their brief report (Phys. Rev. Letters 4, 66 (1960) Jan. 15), a thin sample of α-Al_2O_3 (curundum, sapphire) was bombarded with electrons and the growth of the absorption band at 2040 A was studied. This band is not produced by x-rays or gamma-rays, and is presumed to arise from the trapping of charges at defects which occur under atomic displacement. Arnold and Compton indicate that the values best fitting their data are 50 ev for aluminum and 90 ev for oxygen.

5.4 Theory of Displacement Production

The next problem is to estimate the average number of atomic displacements produced by a primary knock-on. The total number of displaced atoms per unit volume is N_d as given by

$$N_d = n_p \bar{\nu} \tag{5.28}$$

in which n_p is the number of primary knock-ons produced, given by

$$n_p = \phi t n_o \sigma \tag{5.29}$$

where ϕ is the neutron flux, n_o is the density of target nuclei, and t is the irradiation time.

We wish to show now that

$$\begin{aligned} \nu(E) &= 1 && 0 < E < 2E_d \\ \nu(E) &= \frac{E}{2E_d} && 2E_d < E < E_i \\ \nu(E) &= \frac{E_i}{2E_d} && E > E_i \end{aligned} \tag{5.30}$$

The following assumptions will be made:

1) The knock-ons loses energy entirely by ionization until its kinetic energy falls below the limiting energy of ionization E_i.

2) All knock-ons with kinetic energies below E_i lose energy only by elastic collisions with lattice atoms, and in these collisions they behave as hard spheres.

3) An atom will invariably be displaced from its lattice site if by collision it receives kinetic energy greater than some threshold energy E_d and will never be displaced if it receives less than E_d.

4) The striking atom will remain behind at the collision site if the struck atom receives energy greater than E_d and

the incoming atom is left with energy less than E_d. Thus, there will be a net increase in the number of displaced atoms only if both atoms have kinetic energies greater than E_d after the collision.

Let $\nu(E_1)$ be the mean number of displaced atoms, including the primary knock-on itself, produced by a primary knock-on of energy E_1. Further assume that $2E_d < E_1 < E_i$. In the next collision, the energy E_1 is shared by two atoms, such that

$$E_1 = E_1' + E_2'$$

Now the probability that a particle having initially energy E_1 will have energy between E_1' and $E_1' + dE_1'$ is

$$P(E_1')\,dE_1' = \frac{dE_1'}{E_1} \tag{5.31}$$

or

$$N(E_1')\,dE_1' = N(E_1)\,\frac{dE_1'}{E_1} \tag{5.32}$$

If $\nu(E_1')$ represents the average number of displacements produced by atoms with energy between E_1' and $E_1' + dE_1'$, then

$$\nu(E_1')\,N(E_1')\,dE_1' = \nu(E_1')\,N(E_1)\,\frac{dE_1'}{E_1}$$

Gives the contribution to the atomic displacements by those atoms in this energy range after one collision. Consequently, total number of displacements produced by atom 1 after the first collision is

$$\int_{E_d}^{E_1} \frac{1}{E_1} \nu(E_1') N(E_1)\, dE_1' \qquad (5.33)$$

Similarly, for the second atom

$$\int_{E_d}^{E_1} \frac{1}{E_1} \nu(E_2') N(E_1)\, dE_2'$$

so that

$$N(E)\nu(E_1) = \int_{E_d}^{E_1} \frac{1}{E_1} \nu(E_1') N(E_1)\, dE_1' + \int_{E_d}^{E_1} \frac{1}{E_1} \nu(E_2') N(E_1)\, dE_2' \qquad (5.34)$$

Therefore

$$\nu(E) = \frac{2}{E} \int_{E_d}^{E} \nu(E')\, dE' \qquad (5.35)$$

Multiplying both sides by E and differentiating we obtain

$$\nu(E) + E\frac{d\nu}{dE} = 2\nu(E)$$

or

$$E\frac{d\nu}{dE} = \nu(E)$$

$$\nu(E) = CE$$

But

$$\nu(2E_d) = 1$$

so that

$$C = \frac{1}{2E_d} \tag{5.36}$$

$$\therefore \quad \nu(E) = \frac{E}{2E_d}$$

REFERENCES

Billington and Crawford, "Radiation Damage in Solids".

Dienes and Vineyard, "Radiation Effects in Solids".

Seitz and Koehler, Solid State Physics, Vol. 2, 305, (1956).

Kinchin and Pease, "The Displacement of Atoms in Solids", Rep. Prog. in Phys. 18, 1 (1955).

A. N. Goland, "Atomic Displacements In Solids by Nuclear Radiation", Ann. Rev. Nuc. Sci. 12, 243 (1962).

H. Brooks, "Nuclear Radiation Effects in Solids", Ann. Rev. Nuc. Sci. 6, 215 (1956).

Chapter VI Radiation Effects in Germanium and Silicon

We shall now apply the concepts developed so far to investigate the effects of radiation in semiconductors such as germanium and silicon. Perhaps a descriptive name for this is "Fermi Level Engineering" because, as we shall see, radiation provides us with an easy method to alter the Fermi level in these materials. Before going into the subject, we shall take up one topic on the statistical distributions, going beyond what is found in the usual textbooks.

6.1 Distribution Functions

The general procedure is to calculate the thermodynamical probability W, from which the entropy is calculated using

$$S = k \ln W \tag{6.1}$$

where k is the Boltzmann constant, by means of which the Helmholtz free energy

$$F \equiv U - TS \tag{6.2}$$

can be constructed. If i and j denote parts of the system in thermodynamical equilibrium, then

$$dF_i + dF_j = 0 \tag{6.3}$$

and furthermore

$$dF_i = -dF_j = -E_F dn_j \tag{6.4}$$

Consider then first the distribution of free electron,

which as is well known is given by the Fermi-Dirac function

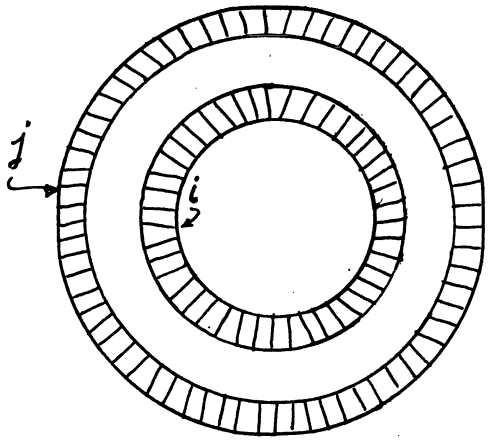

If Z_i represents the number of cells in the shell i, and N_i the number of electrons in this shell, then the number of ways that the N_i electrons can be distributed in the cells is given by

$$W_i = \frac{Z_i !}{N_i ! (Z_i - N_i)!} \tag{6.5}$$

The free energy for the electrons in this shell then is

$$F_i = N_i E_i - kT \ln W_i \tag{6.6}$$

and for the total system

$$F = \sum F_i \tag{6.7}$$

At equilibrium, the free energy has a stationary value, so that the transfer of electrons among two shells, say the i-th and j-th, does not change the total free energy, i.e.

$$dF = \sum dF_i = dF_i + dF_j = 0 \tag{6.8}$$

Hence

$$dF_i = E_i dN_i - kTd \ln W_i = E_F dN_i \tag{6.9}$$

But, by Stirling's approximation

$$\begin{aligned} d \ln W_i &= -d \ln N_i ! - d \ln (Z_i - N_i) ! \\ &= - \ln N_i dN_i + \ln (Z_i - N_i) dN_i \end{aligned} \tag{6.10}$$

given

$$E_i = kT \ln \frac{Z_i - N_i}{N_i} = E_F$$

$$\frac{N_i}{Z_i} = \frac{1}{1 + \exp\left(\frac{E_i - E_F}{kT}\right)} \tag{6.11}$$

which is the usual Fermi-Dirac function. In the above derivation it was assumed that a cell can accept an electron with positive and/or negative spin. This is, a single cell can be empty, have an electron of positive or negative spin, or even contain two electrons of opposite spins.

Now in going to the case for donors, we need to be a little more careful because a donor can accept only <u>one</u> electron at most, i.e. the donor can take on an electron of either spin but <u>not</u> both.

Let then

N_o .... donors

n_+ .... electrons of + spins localized on donors

n_- .... electrons of - spin localized on donors

Then the number of ways that the electron of + spin can be distributed among the "boxes" representing donors is

$$\frac{N_D !}{(N_D - n_+) ! \; n_+ !} \tag{6.12}$$

and the negative spin electrons among the remaining "boxes" is

$$\frac{(N_D - n_+)!}{(N_D - n_+ - n_-)!\ n_-!} \tag{6.13}$$

Thus the total number of ways that electrons of positive and negative spins can be distributed among the free electron gas cells and the donors is given by

$$W = \frac{N_D!}{(N_D - n_+)!\ n_+!} \quad \frac{(N_D - n_+)!}{N_D - n_+ - n_-)!} \quad x \tag{6.14}$$

$$\prod_i \frac{Z_i}{N_i^+!\ (Z_i - N_i^+)!} \quad \frac{Z_i}{N_i^-!\ (Z_i - N_i^-)!}$$

Therefore

$$kd\ln W = -k\ln n_+ \ dn_+ - k\ln n_- \ dn_- + k\ln(N_D - n_+ - n_-)(dn_+ + dn_-)$$

$$+ k \ln \frac{Z_i - N_i^+}{N_i^+} \ dN_i^+ + k\ln\frac{Z_i - N_i^-}{N_i^-} \ dN_i^- \tag{6.15}$$

$$E_F = \frac{\partial F}{\partial n^+} = E_D - kT \ln\frac{N_D - n_+ - n_-}{n_+}$$

$$N_D \frac{-n_+ - n_-}{n+} = \exp\left(\frac{E_D - E_F}{kT}\right) \tag{6.16}$$

But

$$n_- = n_+ = \frac{n}{2}$$

so that

$$\frac{n+}{N_D} = \frac{/}{2 + \exp\left(\frac{E_D - E_F}{kT}\right)} \tag{6.17}$$

$$n = \frac{N_D}{1 + 1/2 \exp\left(\frac{E_D - E_F}{kT}\right)}$$

For the distribution function among the acceptors let N_A represent the concentration of acceptors, n_o the number of occupied acceptors, and n_+ and n_- the number of unoccupied acceptors with either + or - spin. The electron entering an acceptor neutralizes the spin of the unoccupied acceptor. Then the thermodynamical probability for the acceptor electron alone is

$$W_A = \frac{N_A\,?}{n_o!\; n_+!.(N_A - n_+ - n_o)\;!} \tag{6.18}$$

which gives

$$E_F = \frac{\partial F}{\partial n_o} = E_A + kT \frac{N_A - n_+ - n_-}{n_o}$$

Now

$$n_+ = n_-$$

so that

$$n_+ = 1/2(N_A - n_o)$$

leading to

$$\frac{n_o}{N_A} = \frac{1}{1 + 2 \exp\left(\frac{E_F - E_A}{kT}\right)} \tag{6.19}$$

Clearly

$$P_A = \frac{N_A - n_o}{N_A} = \frac{1}{1 + (1/2)\exp\left(\frac{E_F - E_A}{kT}\right)} \tag{6.20}$$

The above arguments can be readily extended to the case of localized centers with arbitrary spin. Thus if the statistical weight stemming from the spin is β , then

$$W_D = \frac{N_D !}{n_1! n_2! \ldots \ldots \ldots n_\beta!} \tag{6.21}$$

with

$$n_1 + n_2 + \ldots \ldots + n_\beta = n_D \tag{6.22}$$

From the free energy

$$F_D = E_D \sum_{i=1}^{\beta} n_i - kT \ln W_D \tag{6.23}$$

upon varying n_i, we obtain

$$E_F = E_D - kT \ln n_i + kT \ln (N_D - n_D)$$

$$\frac{n_D}{N_D} = \frac{1}{1 + \beta \exp \left(\frac{E_D - E_F}{kT}\right)} \tag{6.24}$$

6.2 Defects by Thermal Quenching

The behavior of germanium under neutron bombardment is in many ways analogous to that observed with appropriate heat treatment. If N-type Ge is quenched from temperature near the melting point (800°C), P-type Ge is produced. This conversion of type is presumably due to Frenkel type lattice defects which act as acceptors. By annealing at 450°C and cooling slowly the original N-type character is restored.

We shall therefore present a brief discussion of Frenkel and Schottky defects. (See N. F. Mott and R. W. Gurney, "Electronic Processes in Ionic Crystals," Clarendon Press) Consider first Frenkel defects. These defects arise when an atom in a normal lattice site goes into an interstitial site, such as by having atom in site a going into the interstitial site b, as shown in figure.

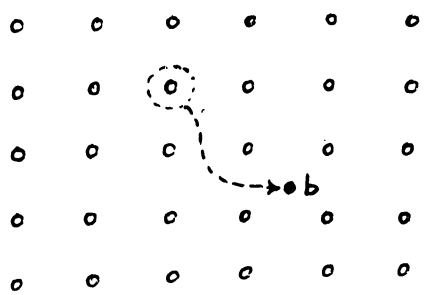

Let N be the total number of atoms and let N' be the total number of possible interstitial sites. If n atoms have left their lattice sites, then the number of ways that such atoms can be arranged in the interstitial sites is

$$W' = \frac{N'!}{(N' - n)!\, n!} \tag{6.25}$$

and the number of ways of arranging the lattice vacancies is

$$W = \frac{N!}{(N - n)!\, n!} \tag{6.26}$$

If the energy to produce a Frenkel pair is E then

$$F = nE - kT \ln W\, W' \tag{6.27}$$

At equilibrium

$$\frac{\partial F}{\partial n} = 0$$

so that

$$E = kT \ln \frac{N' - n}{n} + kT \ln \frac{N - n}{n} \tag{6.28}$$

giving therefore

$$\frac{n^2}{(N - n)(N' - n)} = e^{-E/kT} \tag{6.29}$$

In practice $n << N, N'$, so that

$$n = \sqrt{N N'}\; e^{-E/2kT} \tag{6.30}$$

The Schottky defects differ from the Frenkel defects in that the atoms removed from the lattice sites move to another lattice on the surface

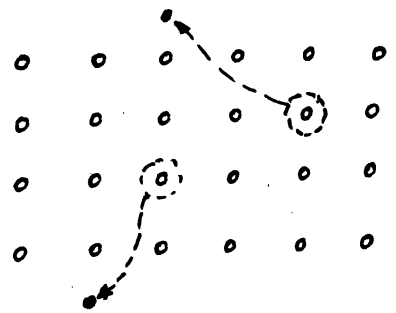

The number of ways that the n vacancies can be arranged is

$$W = \frac{N!}{(N - n)!\, n!} \tag{6.31}$$

so that

$$F = n E_g - kT \ln \frac{N!}{n!(N - n)!} \tag{6.32}$$

giving

$$\frac{n}{N - n} = e^{-E_s/kT} \tag{6.33}$$

Thermally induced acceptors have been studied by C. A. Logan (Phys. Rev. 91, 757 (1953), S. Mayburg and L. Rotondi (Phy. Rev. 91, 1015, Aug. 15, 1953), and by S. Mayburg (Phys. Rev. 95, 38 (July 1, 1954)). These investigators found 1.8 ev and 2.15 ev. for the defect activation energy.

6.3 Fast Neutron Effects in Germanium

Let us now apply the ideas presented so far to interpret the changes in the electrical properties of germanium reproduced by fast neutron bombardment. Much of this work was carried out by Lark-Horovitz and his students at Purdue University, and by Cleland and his associates at the Oak Ridge National Laboratory (See for example J. W. Cleland et al, Phys. Rev. 83, 312 (July 15, 1951).

When P-type Ge is bombarded with fast neutrons, the conductivity increases monotonically. The conductivity of N-type Ge, on the other hand, first decreases, passes through a minimum and increases with further bombardment. Hall coefficient measurement proves that the bombarded N-type material has been converted to P-type. These changes in the electrical properties are too large to be explained by impurities introduced by nuclear reaction. The number of impurity atoms produced by transmutation is, in general, quite small, although there are special cases, such as in InSb, in which appreciable effects can be produced. On the other hand,

appreciable lattice disordering and lattice displacements are produced by collisions of the incoming neutrons with the lattice atom, resulting in energetic primary knock-ons, followed by a cascade of other atomic displacements. The production of lattice vacancies and interstitials results in a large number of electron traps and acceptors. These traps or acceptors neutralize the donors in N-type Ge thus decreasing the current carrier concentration, and in the case of P-type Ge, if they are sufficiently deep-lying, they may augment the concentration of positive carriers in the filled band.

All of the electrical effects of lattice disordering may be removed by annealing the crystal at about 450°C. It is to be noted that the behavior following neutron bombardments is similar to effects produced by heat treatment. If N-type Ge is quenched from temperatures near the melting point (about 800°C). P-type Ge is produced. This conversion is presumably due to Frenkel defects which act as acceptors. Be annealing at 450°C and cooling slowly, the original N-type Ge is obtained.

The introduction of vacant states deep in the forbidden gap of the N-type material will cause the Fermi level to be lowered toward the filled band. During this process increasing number of electrons will be removed from the conduction band. If the irradiation proceeds and the number of vacant slates increases, then these states will begin to behave like acceptors, i.e. remove electrons from the valence band, causing the material to become P-type. Consequently, a

constant rate of introduction of a distribution of low-lying vacant states may be visualized as causing (1) a rapid lowering of the Fermi level toward the center of the forbidden gap, corresponding to the initial removal of electrons from the conduction band, (2), a further lowering of the Fermi level across the center of the gap, corresponding to the redistribution of electrons to traps of lower energy and transition to P-type, and (3) the asymptotic approach of the Fermi level to a position near the top of the valence band.

Addition of acceptors to P-type Ge has the same effect as phase (3) of N-type Ge. High-resistivity P-type Ge is readily affected, since the Fermi level is well above the top of the filled band. But in low resistivity P-type Ge the Fermi level may already be below the limiting position mentioned in (3). If such is the case, the only effect produced by bombardment on the conductivity will be through a decrease in the mobility.

The neutron bombardment dependence of conductivity, as shown in the following figure,

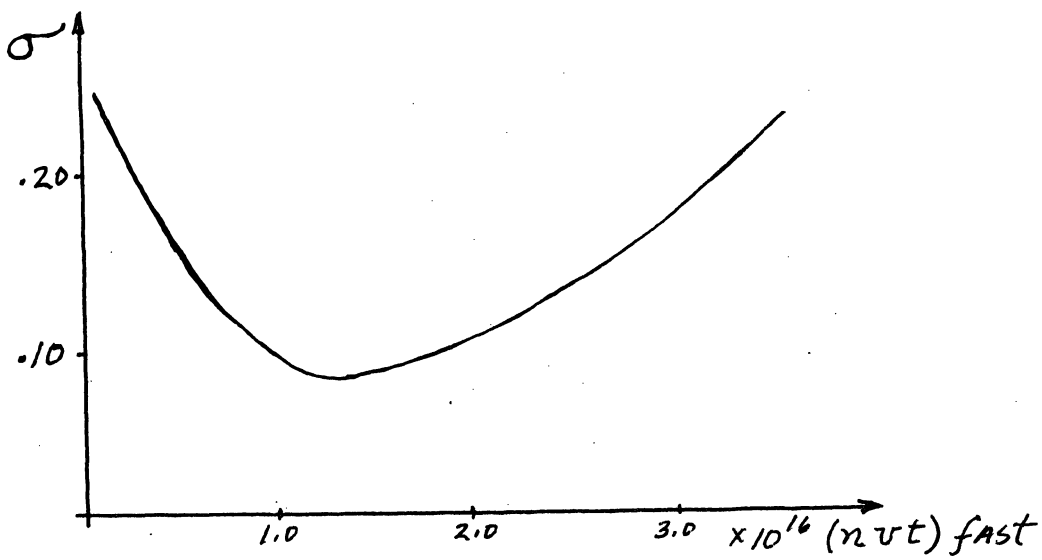

can be explained in terms of the simple semiconductor model discussed earlier. As shown earlier, the conductivity is given by

$$\sigma = q(n\mu_n + p\mu_p) = q\mu_p(bn + p) \tag{6.34}$$

in which

$$b \equiv \frac{\mu_n}{\mu_p} \tag{6.35}$$

Furthermore

$$np = n_i^2 \tag{6.36}$$

so that

$$\frac{d\sigma}{dn} = q\mu_p\left(b - \frac{n_i^2}{n^2}\right) = 0 \tag{6.37}$$

Consequently the minimum in the conductivity occurs for

$$n = \frac{n_i}{\sqrt{b}}$$

The minimum conductivity then is given by

$$\sigma_{min} = 2q\mu_p\sqrt{b}\, n_i \tag{6.38}$$

The samples used by Cleland et. al. had electron concentrations of the order of $10^{14} - 10^{15}$. Since

$$n_i \sim 10^{13}$$

this means that the neutron bombardment should decrease the conductivity by a factor of 10 to 100.

From the initial slope of the conductivity vs. neutron bombardment it is possible to determine K, the average number

of electron traps produced per incident neutron. Thus

$$K \equiv \frac{dn}{d(nvt)_{fast}} = \frac{1}{q\mu_n} \frac{d\sigma}{d(nvt)_{fast}} \qquad (6.39)$$

since

$$\sigma = q \mu_n n$$

upon neglecting the contribution from holes, which is negligible for N-type Ge.

For example, consider the following result reported by J. H. Crawford and K. Lark-Horovitz (Phys. Rev. 78, 815L (1950) June 15). The initial resistivity was 0.77 ohm/cm.

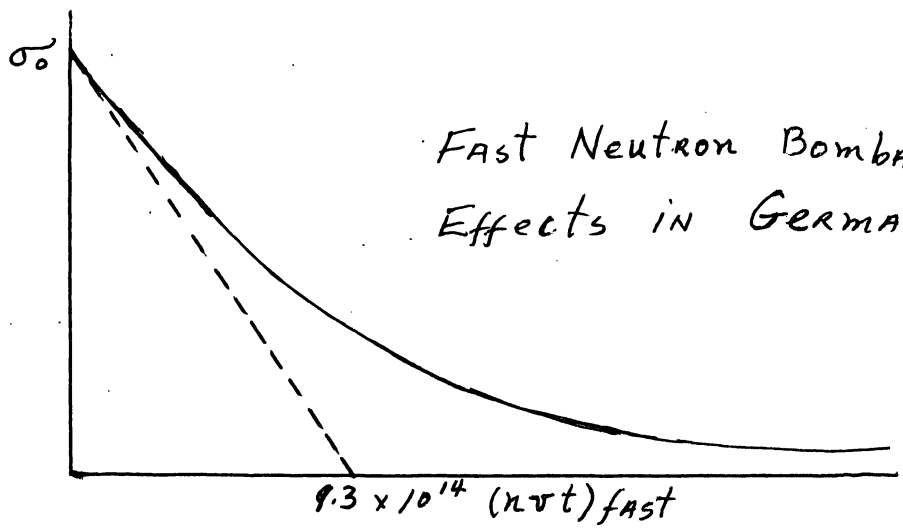

with $\mu_n = 2920$ cm^2/v/sec. Consequently

$$\frac{d\sigma}{d(nvt)} = \frac{.77}{9.3 \times 10^{14}} \frac{dn}{d(nvt)} = \frac{1}{(1.6 \times 10^{-19})(2920)} (8.3 \times 10^{-16}) \qquad (6.40)$$

$$= 1.78$$

Average of the measurements such as indicated here (see, for example, Cleland and Crawford, Phys. Rev. 98, 1742 (1955) June 15), point to

$$k = 2.5 \text{ traps/incident fast neutron}$$

This value is in reasonable agreement with the theory of atomic displacement outlined earlier. From Eq. (5.28)

$$\frac{Nd}{(nvt)_f} = n_o \sigma \bar{\nu} \tag{6.41}$$

Here we are identifying the number of traps with the number of atomic displacements. The density of germanium is 5.36 gm/cm^3, so that

$$n_o = 6 \times 10^{23}\left(\frac{5.36}{72.6}\right) = 4.4 \times 10^{22} \tag{6.42}$$

From (5.36) we find

$$\bar{\nu} = \frac{\bar{E}}{2Ed} = \frac{50{,}000}{50} = 1000 \tag{6.43}$$

Taking

$$\sigma = 10^{-25} cm^2$$

we find

$$\frac{Nd}{(nvt)_f} = 4.4 \times 10^{22} \, (10^{-25})(1000) = 4 \tag{6.44}$$

If Ed is taken to be 13 ev., the above value will be about 80. Thus the theoretically predicted value is about one order of magnitude too large.

6.4 James and Lark-Horovitz Model

One of the puzzling features of early studies of radiation effects was the markedly different behavior of germanium and silicon. N-type germanium was converted to P-type and P-type specimen increased in conductivity with exposures, whereas both N- and P-type silicon tended towards intrinsic. The behavior of germanium could be explained qualitatively on the basis of acceptor introduction alone, which in silicon it was necessary to postulate the introduction of both deeplying acceptors and donors to account for the removal of carriers of both signs. In view of the close chemical and electronic similarity of these materials, this apparent difference in defect energy level structure was not to be expected. James and Lehman, however, pointed out that donors or hole traps in germanium might escape detection if they lay near the top of the valence band. Further investigation of low-resistivity P-type germanium indeed demonstrated their presence. Moreover a closer examination of conductivity v. bombardment curves of initially N-type germanium revealed that the initial linear slope extrapolated to zero conductivity at an exposure only about one-half that required to cause conversion to P-type.

Earlier ideas concerning energy levels associated with lattice defects were based on single ionization of lattice vacancies and interstitial atoms. Hence a vacancy was expected to behave as an acceptor or an electron trap, whereas an interstitial atom was expected to behave as a donor or a hole

trap. However, examination of the conductivity σ vs. bombardment time curves for N-type Ge revealed that extrapolation of the initial linear slope to zero conductivity gave a value of exposure only about one-half that required to produce the conductivity minimum or intrinsic behavior. This behavior would seem to indicate the presence of two electron trapping centers, of which one is rather shallow. It was on the basis of this observation that James and Lark-Horovitz considered the possibility of multiple ionization. They find that in a lattice with as high a dielectric constant as that of Ge, one might indeed expect states corresponding to the first and second ionization energies of the interstitial atom to lie in the forbidden energy band. Similarly the energy required to put as many as two electrons into a vacant site is expected to lie in the forbidden gap. When both the interstitial and vacancy are present simultaneously, the electrons arising from the interstitial atoms are redistributed among all the localized states to positions of lowest energy. Hence for Ge they find the following levels of localized states:

(1) A shallow vacant level corresponding to the first ionization of the interstitial atom which is estimated to lie $\sim$ 0.05 ev. below the conduction band;

(2) A deep vacant level below the middle of the conduction band which arises from either the second ionization of the interstitial or the second ionization of the vacancy; and

(3) The two remaining levels, which are occupied and which lie near the top of the valence band.

For the analysis of bombarded N-type Ge, only the vacant levels are considered. Namely one shallow level of electron traps which is only partly effective in removing electrons and a deep level which is completely effective. It is assumed that all chemical impurities are completely ionized and that the intrinsic process is negligible over the whole range of consideration. The electron concentration is given by

$$n = n^{o} - N_{s}^{-} - N \tag{6.45}$$

where n^{o} is the initial electron concentration, N_s^- is the concentration of occupied shallow traps, and N is the concentration of deep traps. Suppose then

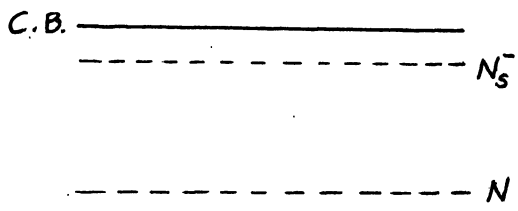

The rate at which electrons are trapped by the shallow traps is proportional to $n(N-N_s^-)$, where n is the electron concentration in the conduction band, and $N-N_s^-$ is the concentration of unoccupied shallow traps. The rate at which electrons leave the shallow traps to enter the conduction band is proportional to N_s^-. Hence for the reaction.

electrons + shallow traps $\rightleftharpoons$ Electrons in shallow traps

we obtain

$$n(N - N_s^-)K_s = N_s^- \tag{6.46}$$

giving

$$N_s^- = \frac{n N K_s}{1 + nK_s} \tag{6.47}$$

Here K_s is the mass-action proportionality constant, and can be determined in the following way.

$$N_s^- = \frac{N}{1 + \gamma_t \exp\left(\frac{E_t - E_F}{kT}\right)} \tag{6.48}$$

$$\frac{N - N_s^-}{N_s^-} = \gamma_t \exp\left(\frac{E_t - E_F}{kT}\right) \tag{6.49}$$

$$\therefore \quad K_s = \frac{N_s^-}{n(N - N_s^-)} = \frac{1}{\gamma_t N_c} \exp\left(-\frac{E_t - E_c}{kT}\right) \tag{6.50}$$

Using the above model, the workers at Oak Ridge National Laboratory established the existence of two vacant states, one located below the middle of the forbidden energy gap and the other located 0.2 ev. below the conduction band.

For 0.2 ev. level the conduction band, the arguments are as follows. From (6.45) and (6.47), we find

$$2K_s n = (n^\circ - 2N) K_s - 1 + \sqrt{\left[(n^\circ - 2N)K_s - 1\right]^2 + 4K_s(n^\circ - N) + 1} \tag{6.51}$$

The validity of the above model was established by determining K_s and hence ϵ_s, where

$$\epsilon_s \equiv E_c - E_t \tag{6.52}$$

by three independent approaches. These are (1) the variation

of the initial slope as a function of n^o of the n vs. bombardment curve, (2) the application of (6.51) to the bombardment curve over the entire n-type range, and (3) the temperature dependence of the electron concentration in bombarded Ge.

Differentiating (6.51) with respect to N we find for the initial rate of change of n with Frenkel defect concentration

$$\left[\frac{dn}{dN}\right]_{N=0} = -\frac{1 + 2K_s n^o}{1 + K_s n^o} \tag{6.53}$$

Thus

$$K_s = -\frac{1 + \left(\frac{dn}{dN}\right)_o}{n^o \left[1 + 2\left(\frac{dn}{dN}\right)_o\right]}$$

and using (6.50) and

$$m_e = [w_s^2 m_x m_y m_z]^{1/2} = 0.51\, m_o$$

$$\left(\frac{2\pi m_o k}{h^2}\right)^{3/2} = 2.42 \times 10^{15}/cm^3/^oK^{3/2}$$

$$\frac{\epsilon_s}{kT} = 34.42 + \ln(k_s T^{3/2})$$

$$\epsilon_s = 8.65 \times 10^{-5} T \left[34.42 + \ln(K_s T^{3/2})\right]$$

The average of measurements gave

$$\epsilon_s = 0.197 \text{ ev.}$$

Next they fitted the n vs. N curve given (6.51) over the entire N-type range. A plot such as shown below is obtained.

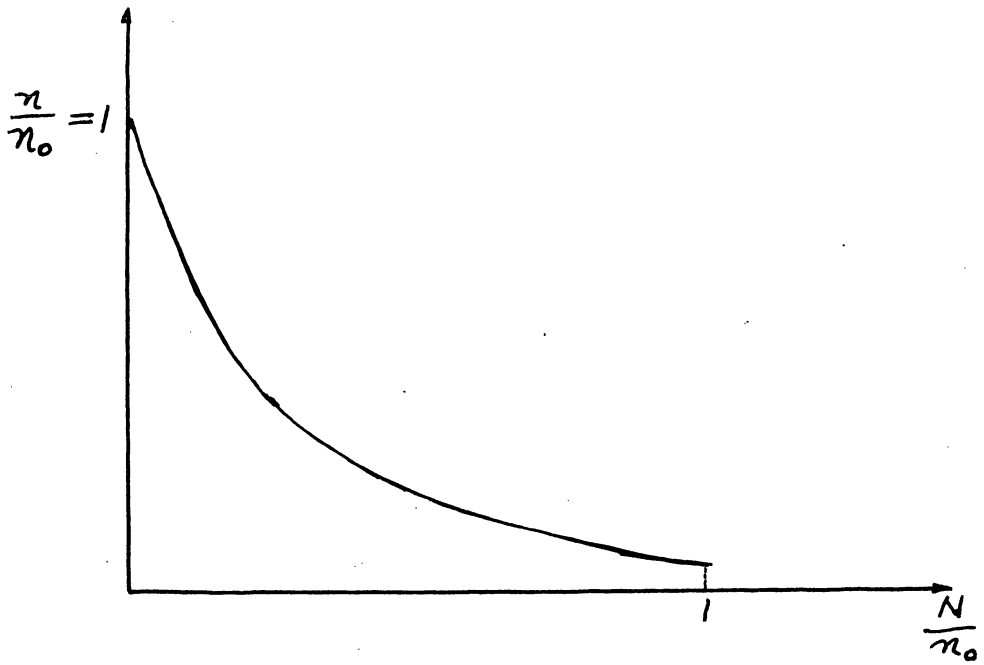

A rather good fit to the curve was obtained using $K_s = 3.6 \times 10^{-6}$ cm^3, which corresponds to $\epsilon_s = .199$ ev.

6.5 Hall Effect

We shall present here a brief discussion of the Hall effect to show how such measurements can provide information about semiconductors.

When semiconductors are subjected to nuclear radiations, defects are produced. So that the semiconductor defect properties, rather than the intrinsic properties, i.e. the properties of the pure material, become important. Consequently, we shall investigate the effects of donors and acceptors, lying close to the allowed energy bands. Consider then a semiconductor, say germanium, containing N_D donors at E_D' below the edge of the conduction band i.e.

$$E_D' = E_c - E_D \tag{6.54}$$

According to (6.17), the concentration of occupied donors is

$$\frac{N_D}{1 + 1/2 \exp\left(\frac{E_D - E_F}{kT}\right)} = \frac{N_D}{1 + 1/2 \exp\left(\frac{-E_D' + E_F'}{kT}\right)} \tag{6.55}$$

where we have put

$$E_F' \equiv E_c - E_F \tag{6.56}$$

Consequently the number of electrons in the conduction must be just equal to the unoccupied donors, i.e.

$$n = \frac{N_D}{1 + 2 \exp\left(\frac{E_D' - E_F'}{kT}\right)} \tag{6.57}$$

Suppose that the conditions are non-degenerate over the entire temperature range. Then

$$n = N_c \exp\left(-\frac{E_F'}{kT}\right) \tag{6.58}$$

Combined with (6.57) gives

$$n \left[1 + \frac{2n}{N_c} \exp \epsilon_D'\right] = N_D \tag{6.59}$$

where

$$\epsilon_D' = \frac{E_D'}{kT} \quad , \quad \epsilon_F' \equiv \frac{E_F'}{kT}$$

Solving for n we find

$$n = \frac{2 N_D}{1 + \sqrt{1 + \frac{8N_D}{N_c} \exp \epsilon_D'}} \tag{6.60}$$

Suppose that $N_D = 10^{16}/cm^3$, and $E_D' = .01$ ev. Then $\epsilon_D' \sim .4$, and since $N_c \sim 10^{19}$, the second term under the radical is small in comparison to unity. Therefore at room temperature

$$n \cong N_D \tag{6.61}$$

that is, the donors are essentially completely ionized. On the other hand at low temperatures the second term under the radical is large in comparison to unity, so that

$$n = \frac{2 N_D}{1 + 2\sqrt{\frac{2 N_D}{N_c}} \exp \frac{\epsilon_D'}{2} \left[1 + \frac{N_c}{8 N_D} \exp(-\epsilon_D')\right]^{1/2}}$$

$$\cong \sqrt{\frac{N_c N_D}{2}} \exp\left(-\frac{\epsilon_D'}{2}\right) \tag{6.62}$$

Thus the plot of $\ln n$ vs. 1/T will be as follows:

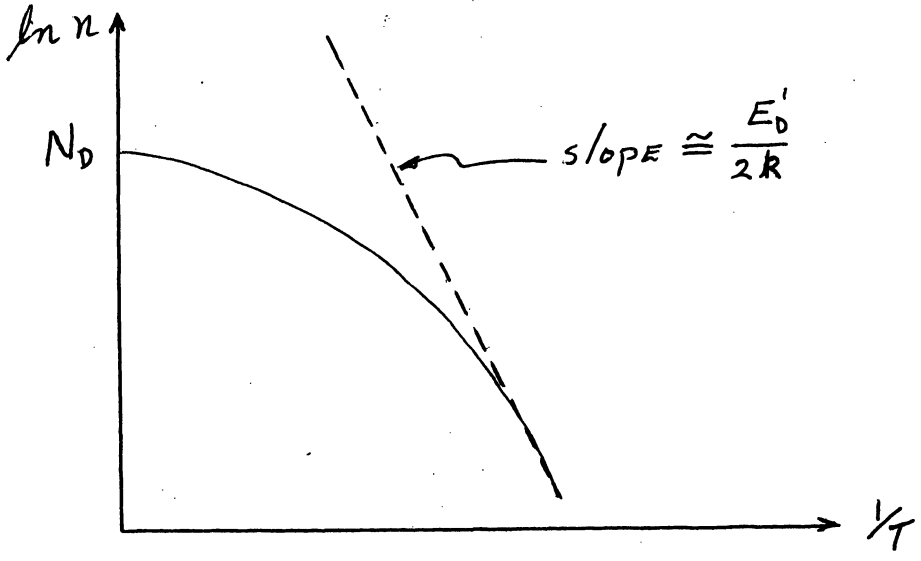

At low temperatures, $\ln n$ will fall linearly with 1/T and a high temperature such that $E_D' \cong kT$, the curve will flatten out to the saturation value of N_D. Experimentally, this means that Hall measurement at "high temperature" will give the donor concentration N_D and that the low temperature Hall

measurement gives information about the position of the donor level with respect to the conduction band.

To see what is meant by "high" and "low" temperatures, we need to examine the temperature dependence of the Fermi level. We need merely to recall that if the Fermi level is several kT below E_D, then the donor levels are essentially empty; and if the Fermi level is several kT above E_D the donor levels are almost completely occupied. From (6.57) for

$$E_D' = E_F'$$

we have

$$n = \frac{N_D}{3} \tag{6.63}$$

so that from (6.58)

$$\frac{E_F'}{kT} = \ln \frac{N_c}{n} = \ln \frac{3N_c}{N_D} \simeq 10 \tag{6.64}$$

Thus the Fermi level should cross the donor energy level around 30°K. Thus to determine the donor energy level it would be necessary to make measurements at liquid hydrogen temperature and lower. A little more detailed analysis will reveal that in going from room temperature down to 100°K, the carrier concentration will change at most by 10%.

Consider next the effect of introducing N_t electron states upon the conduction electron concentration. Then

$$N_D = n + \frac{N_t}{1 + 1/2 \exp\left(\frac{-E_t' + E_F'}{kT}\right)} \tag{6.65}$$

Since the conduction electron concentration will be changing most rapidly with temperature when the Fermi level is at the trapping level, we shall attempt to estimate the value of this Fermi level. Then (6.65) becomes simply

$$N_D = n + \frac{N_t}{1 + 1/2} = n + \frac{2}{3} N_t \qquad (6.66)$$

so that

$$E_F' = -kT \ln \frac{N_D - 2/3 N_t}{N_c} = kT \left[\ln \frac{N_c}{N_D} - \ln(1 - 2/3 \alpha)\right] \qquad (6.67)$$

where we have put

$$N_t = \alpha N_D \qquad (6.68)$$

The order of magnitude of the quantity in the square brackets is about 10, so that

$$kT \cong \frac{E_t'}{10} \qquad (6.69)$$

If E_t' is about 0.2 ev below the conduction band the above analysis suggests a very rapid decrease in the conduction electron concentration around 240°K.

The qualitative difference in the temperature dependence of the electron concentration, as measured by the Hall effect, before and after the introduction of traps is as shown in the following figure.

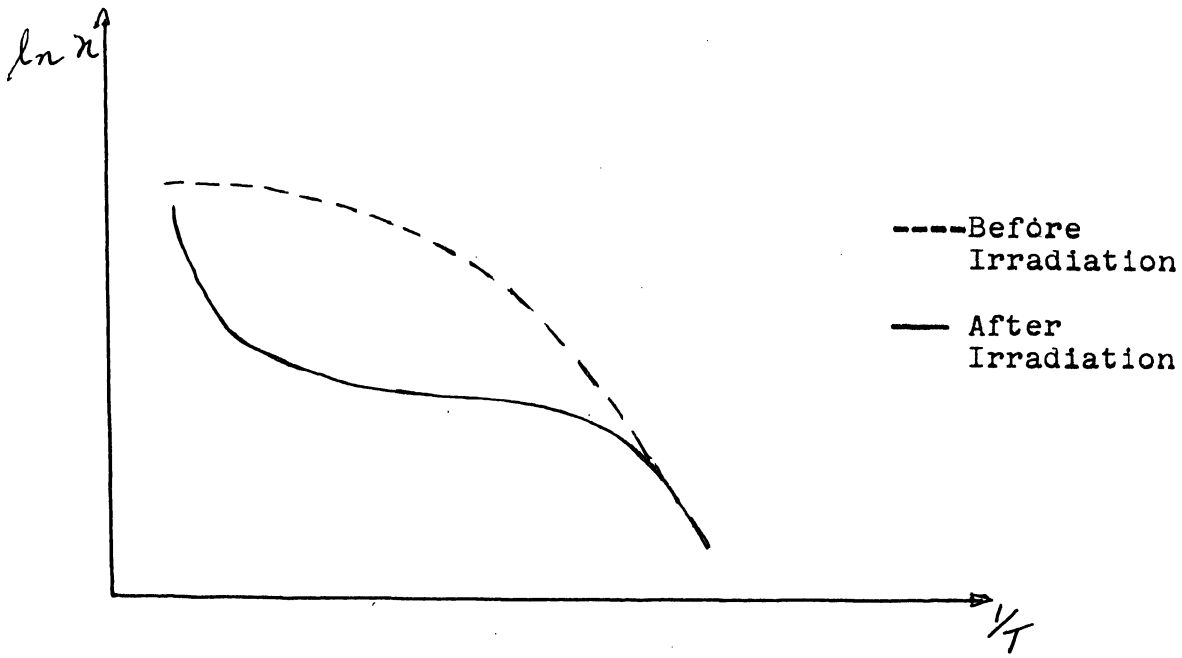

6.6 Bombardment of P-type Germanium

It was shown by Cleland, Crawford, Lark-Horovitz, Pigg and Young (Phys. Rev. 84, 861 (1957)) that both the magnitude and the sign of the initial rate of change of hole concentration $[dp/d(nvt)]_t = 0$ are dependent on the initial hole concentration P_o and the temperature of exposure T_e. This result is consistent with the proposed model of energy levels associated with Frenkel defects, since both occupied and vacant localized states above the top of the valence band are predicted by this model. Consequently, the situation is characterized by two competing processes: production of hole vacant states (acceptors) and trapping of holes by the occupied states (donors). Under conditions of thermal equilibrium, the effect of Frenkel defect introduction depends on the position of the initial Fermi level E_F° relative to the limiting value E_F^+ which is determined solely by the positions

of the defect energy levels and the temperature. According to the model, two occupied levels and one vacant level are expected. If it is assumed that all of the chemical acceptors are completely ionized, then the hole concentration is given by

$$P = P_o' + N_1^- - N_2^+ - N_3^+ \qquad (6.70)$$

where N_1^- is the concentration of ionized acceptors (hole vacancies) and N_2^+ and N_3^+ are the concentration of holes in the deep and shallow traps respectively. From the law of mass action, then,

$$\begin{aligned} p\ N_1^- &= K_1(N - N_1^-) \\ P(N - N_2^+) &= K_2 N_2^+ \\ p(N - N_3^+) &= K_3 N_3^+ \end{aligned} \qquad (6.71)$$

giving

$$\begin{aligned} N_1^- &= \frac{NK_1}{p + K_1} \\ N_2^+ &= \frac{pN}{p + K_2} \\ N_3^+ &= \frac{pN}{p + K_3} \end{aligned}$$

It is easy to show that the equilibrium constants K_i are given by

$$K_i = \frac{N_v}{\gamma_i} e^{-\epsilon_i/kT} \qquad (6.72)$$

For example, consider K,

$$N_1^- = \frac{N}{1 + \gamma_1 \exp\left(\frac{E_1 - E_F}{kT}\right)} \doteq \frac{N}{1 + \gamma_1 \exp\left(\frac{\epsilon_1 - \epsilon_F}{kT}\right)} \qquad (6.73)$$

where we have put

$$\begin{aligned} \epsilon_1 &= E_1 - E_v \\ \epsilon_F &= E_F - E_v \end{aligned} \tag{6.74}$$

Then

$$N - N_1^- = \frac{N \gamma_1 \exp\left(\frac{\epsilon_1 - \epsilon_F}{kT}\right)}{1 + \gamma_1 \exp\left(\frac{\epsilon_1 - \epsilon_F}{kT}\right)}$$

so that

$$\frac{N_1^-}{N - N_1^-} = \frac{1}{\gamma_1} \exp\left(-\frac{\epsilon_1 - \epsilon_F}{kT}\right) \tag{6.75}$$

Now

$$P = Nv\, e^{-\epsilon_F/kT} \tag{6.76}$$

Therefore

$$K_1 = \frac{N_v}{\gamma_1} \exp\left(-\frac{\epsilon_1}{kT}\right) \tag{6.77}$$

Consequently (6.70) gives

$$P = P_o + N\left[\frac{K_1}{p + K_1} - \frac{P_o}{p + K_2} - \frac{p}{p + K_3}\right] \tag{6.78}$$

Where N represents the Frenkel defect concentration produced by neutron bombardment. It follows immediately that the initial rate of change of p is given by

$$\left(\frac{dP}{dN}\right)_{N=0} = \frac{K_1}{P_o + K_1} - \frac{P_o}{P_o + K_2} - \frac{P_o}{P_o + K_3} \tag{6.79}$$

To simplify the analysis we should neglect the effect of the last term. This is justified by experimental results. Then (6.79) becomes simply

$$\left(\frac{dP}{dN}\right)_{N=0} = \frac{K_1}{P_o + K_1} - \frac{P_o}{P_o + K_2} \qquad (6.79')$$

Thus the sign of initial slope is dependent upon the initial hole concentration P_o. Furthermore, this becomes zero when

$$\frac{K_1}{P_o + K_1} = \frac{P_o}{P_o + K_2} \qquad (6.80)$$

or

$$P_o^2 = K_1 K_2 \qquad (6.81)$$

From

$$P_o = N_v \exp\left(-\frac{E_F - E_v}{kT}\right)$$

and (6.72) we find that the initial slope is expected to be zero, if

$$\epsilon_F^* = \frac{\epsilon_1 + \epsilon_3}{2} + \frac{1}{2} kT \ln \gamma_1 \gamma_2 \qquad (6.83)$$

since

$$\gamma_1 \gamma_2 = 1 \qquad (6.84)$$

Thus the initial slope will be positive if the initial Fermi level is above E_F^*; and negative, if below. From such measurements, the hole concentration p for which the initial slope is zero, was found to be $1.5 \times 10^{15}/cm^3$, and the corresponding

Fermi level E_F^* to be 0.123 ev above the valence band. This value however, represents merely the midpoint between the acceptors and hole traps. To determine and ϵ_1, (6.79) is plotted, assuming a variety of values. The values giving the best fit to the data are $\epsilon_1 = 0.180$ ev. and $\epsilon_2 = 0.066$ ev.

References

R. A. Logan "Thermally Induced Acceptors in Single Crystal Germanium", Phys. Rev. 91, 757 (1953).

S. Mayburg and L. Rotondi, "Thermal Acceptors in Vacuum Heat-Treated Germanium", Phys. Rev. 91, 1015 (Aug. 15, 1953).

S. Mayburg, "Vacancies and Interstitials in Heat Treated Germanium", Phys. Rev. 95, 38 (July 1, 1954).

W. E. Johnson and K. Lark-Horovitz, "Neutron Irradiated Semi-Conductors", Phys. Rev. 76, 442 (Aug. 1, 1949).

J. W. Cleland, J. H. Crawford, and J. C. Pigg, "Fast-Neutron Bombardment of N-type Ge", Phys. Rev. 98, 1742 (June 15, 1955).

J. W. Cleland, K. Lark-Horovitz, and J. C. Pigg, "Transmutation-Produced Germanium", Phys. Rev. 78, 814 (1950).

J. W. Cleland, J. H. Crawford, Jr., K. Lark-Horovitz, J. C. Pigg, F. W. Young, "Evidence of Production of Hole Traps in Germanium by Fast Neutron Bombardment", Phys. Rev. 84, 861 (Nov. 15, 1951).

G. W. Lehman, "Fermi Levels in Semiconductors", Phys. Rev. 81, 321 (1951).

H. Brooks, "Nuclear Radiation Effects in Solids", Ann. Rev. of Nuclear Sci. 6, 215 (1956).

J. W. Cleland, J. H. Crawford, Jr., and J. C. Pigg, "Fast Neutron Bombardment of P-type Germanium," Phys. Rev. 99, 1170 (Aug. 15, 1955).

CHAPTER VII DEFECTS BY NUCLEAR TRANSMUTATIONS

In the previous chapter, the defects produced by displacements following nuclear collisions were discussed. For this, we shall take germanium as an example, and also discuss some of the results obtained at the University of Michigan.

7.1 Nuclear Transmutation in Germanium

This work, reported first by J. W. Cleland, K. Lark-Horovitz, and J. C. Pigg, (Phys. Rev. 78, 814 (1950)) is interesting in that a study of the semiconducting properties of germanium led to the discovery of an error in neutron capture cross section measurements.

In addition to the atomic displacement defects, which can be annealed out, there are other effects which cannot be annealed out, when the samples have been irradiated with neutrons of $nvt \sim 10^{18}$ or more. The reason for this is that the thermal neutron capture by Ge^{70} leads to the formation of Ga^{71}, an acceptor, and the neutron capture by Ge^{74} to the formation of As^{75}, a donor. The net effect, clearly will depend upon the thermal neutron capture cross-sections of Ge^{70} and Ge^{74}. The following table summarizes the results as were known at the time the investigations were carried out.

Isotope	Abundance	Cross Section		End Product
		Isotopic	Atomic	
Ge^{70}	21.2	0.073 .45	0.0155 .095	Ga
Ge^{74}	37.1	0.38	0.14	As

These results suggested that germanium would become N-type upon prolonged neutron irradiation. For

$$N(Ga^{71}) = (nvt)\,\sigma(Ge^{70})\,N(Ge^{70})$$

$$N(As^{75}) = (nvt)\,\sigma(Ge^{74})\,N(Ge^{74})$$

where $N(Ga^{71})$ and $N(As^{75})$ are the concentrations of Ga^{71} and As^{75} produced by nuclear transmutation and $N(Ge^{70})$ and $N(Ge^{74})$ are the concentrations of Ge^{70} and Ge^{74} in the original germanium sample. If N_A is the number of germanium atoms per unit volume, then the excess of Ga formed over As is given by

$$N(Ga^{71}) - N(As^{75})$$
$$= (nvt)\,N_A\left[.212\,\sigma(Ge^{70}) - .371\,\sigma(Ge^{74})\right]$$
$$= (nvt)\,N_A\,(.0155 - .14)$$

showing that the As formation exceeds Ga formation, so that the final sample should be N-type. Experimentally, after prolonged irradiation and careful annealing the sample becomes P-type. This discrepancy led to the redetermination of the neutron cross sections. The revised data are as follows:

Isotope	Abundance	Cross Section Isotopic	Cross Section Atomic	End Product
Ge^{70}	21.2	3.25	0.69	Ga
Ge^{72}	27.3	0.94	0.26	Ge
Ge^{73}	7.9	13.69	1.08	Ge
Ge^{74}	37.6	0.60	0.22	As
Ge^{76}	6.1	0.35	0.02	Se

These revised values of cross sections lead to

$$N(Ga^{71}) - N(As^{75}) = 2.05 \times 10^{-2} (n v t)$$

leading to results that are in good agreement with carrier concentration measurements. For example, the initial, the calculated, and the measured carrier concentrations of two samples are shown below

n_o	n_x (calc)	n_f (meas)
-5.25×10^{14}	6.16×10^{15}	8.82×10^{15}
-2.28×10^{16}	3.21×10^{16}	2.92×10^{16}

7.2 Thermal Neutron Effects in Cadmium Compounds.

The idea that thermal neutron capture by Cd^{113} may lead to observable effects occurred to this author while lecturing to a class of beginning students in nuclear physics. The basic idea is as follows. When Cd^{113} captures a neutron, the compound nucleons $[Cd^{114}]^*$ is formed, which has about 9.044 Mev above the Cd^{114} ground state.

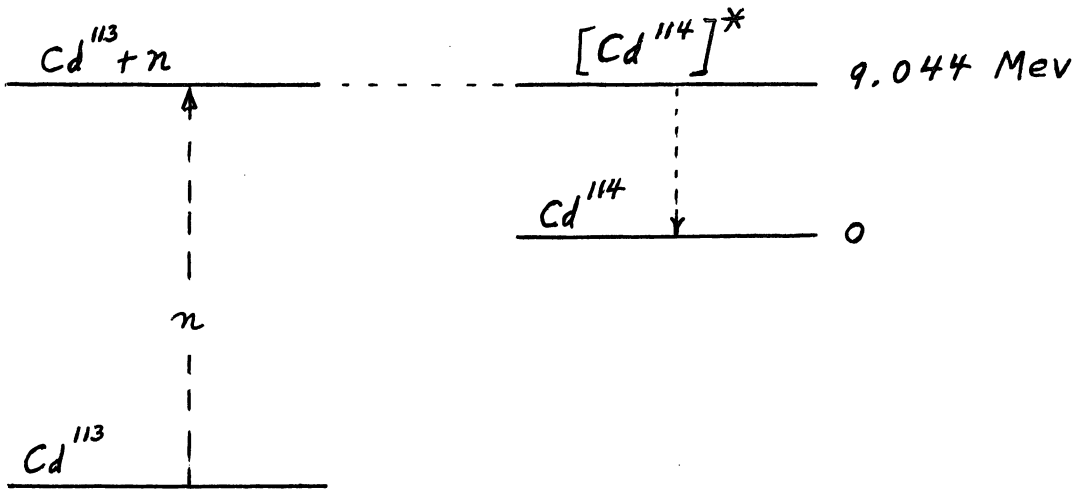

The transition to the ground state can occur with the emission of a single gamma ray or more. The details of the capture gamma ray spectra have been studied by many. If a single gamma ray is emitted, then the Cd^{114} recoil momentum is given by

$$p = \frac{h\nu}{c} = \frac{E_\gamma}{c}$$

so that the recoil energy is

$$E = \frac{1}{2M} p^2 = \frac{1}{2M} \frac{E_\gamma^2}{c^2} = \frac{537}{A} E_\gamma^2$$

For the 9.044 Mev gamma ray, the recoil energy is 380 ev. Thus the recoil energy will vary from this maximum value down to zero. This 380 ev. recoil energy is more than adequate to produce atomic displacement.

We discuss first the calculation of damage production by thermal neutron (n, γ) reactions and this will compare with damage production by fast neutrons.

If all the excitation energy of a captured neutron is released as a single γ-ray of energy E (Mev) then the

recoil atom has a unique energy T given from momentum conservation as

$$T = \frac{537}{A} E^2 \times 10^{-6} \tag{7.1}$$

where A is the atomic mass. E is generally about 6 Mev so that T can be several hundred electron volts. Since the threshold for atomic displacement is about 25 ev, such energetic recoils can produce extensive damage.

If ϕ_t is the thermal neutron flux, σ_t the capture cross section, and ν_t is the average number of atomic displacements produced by each recoiling nucleus, then

$$F_t = \phi_t \sigma_t \nu_t \tag{7.2}$$

where F_t is the rate of defect production. Now

$$\nu_t \cong \frac{\overline{T}}{2E_d} \tag{7.3}$$

so that

$$F_t = \frac{270 E^2 \phi_t \sigma_t}{A T_d} \times 10^{-6} \tag{7.4}$$

Unfortunately, the excitation energy is not usually released as a single gamma-ray. Instead many gamma-rays are emitted. If their emission time is short compared to the recoil atom collision time, the final recoil energy is determined by both the magnitude and angular correlation of the various γ-rays. On the other hand, if the emission times are longer than the collision times, then the individual γ-rays in the cascade can be treated separately. Since, however, the details

of the transitions are not known, the following scheme can perhaps be adopted. In a cascade process, if the initial γ-ray has an energy between E_{max} and $(1/2)E_{max}$, then it must be followed by lower energy γ-rays. These low energy γ-rays serve only to broaden the nuclear recoil energy characteristic of the initial high energy γ-ray. As a simplification in calculating the damage, only those captures in which such a high energy gamma ray is present is counted.

Then

$$F_t \cong 2.7 \times 10^{-4} \frac{\Phi_t \sigma_t}{A T_d} \int_{\frac{1}{2}E_{MAX}}^{E_{MAX}} E^2 N(E)\, dE \qquad (7.5)$$

where $N(E)dE$ represents the number of γ-rays having energies between E and $E + dE$

The defects produced by fast neutron knock-ons are given by

$$F_f = \Phi_f \sigma_f \bar{\nu}_f$$

Now

$$\bar{\nu}_f = \frac{\bar{T}}{2E_d}$$

where

$$\bar{T} \cong \frac{2E_o}{A}$$

so that

$$F_f = \frac{E_o}{AE_d} \Phi_f \sigma_f = \frac{\Phi_f \sigma_f}{AE_d}$$

upon putting E_o = 1 Mev. Taking the ratio of (7.5)

to (7.6) we find

$$R \sim 3 \times 10^{-4} \left(\frac{\Phi_t}{\Phi_f}\right) \frac{\sigma_t}{\sigma_f} \int_{\frac{1}{2}E_{MAX}}^{E_{MAX}} E^2 N(E) dE \qquad (7.7)$$

For most nuclei the ratio of thermal neutron defects to fast neutron defects is about unity. The exceptions are Cd, Gd, and Sm, as shown below.

Element	σ_t/σ_f	R
Cd	500	20
Gd	5400	81
Sm	1400	26

A more detailed study of the thermal neutron damage in CdS has been carried out recently at the University of Michigan. Some of the nuclear properties of Cd isotopes are listed below.

Isotope	Abundance		Nuclear Reaction
Cd^{106}	1.22%	1.0 ± 0.5	$Cd^{106}(n,\gamma)Cd^{107} \xrightarrow[6.7\ hr]{\beta^-} Ag^{107}$
Cd^{108}	0.87%	- - -	
Cd^{110}	12.39%	0.2 ± 0.1	$Cd^{110}(n,\gamma)Cd^{111}$
Cd^{111}	12.75	- - -	
Cd^{112}	24.07	0.030 ± 0.15	$Cd^{112}(n,\gamma)Cd^{113}$
Cd^{113}	12.26	20,000 ± 300	$Cd^{113}(n,\gamma)Cd^{114}$
Cd^{114}	28.86	0.14 ± .03	$Cd^{114}(n,\gamma)Cd^{115} \xrightarrow[43\ days]{\beta^-} In^{115}$
		1.1 ± .3	$Cd^{114}(n,\gamma)Cd^{115} \xrightarrow[2-3\ days]{\beta^-} In^{115}$
Cd^{116}	7.58	1.5 ± 0.3	$Cd^{116}(n,\gamma)Cd^{117} \xrightarrow[50\ min;\ 2.9\ hrs]{\beta^-} In^{117} \xrightarrow[45\ min;\ 1.9\ hrs]{\beta^-} Sn^{117}$

From the γ-ray spectrum of Cd^{114} it is estimated that the average recoil energy is about 140 ev. To study the effects of such recoils CdS was selected because of the earlier luminescence studies of the material and the changes of such properties under particle bombardment. R. J. Collins (J. App. Phys. 30, 1135 (1959)) produced edge emission in CdS with a 200-Kev beam of electrons, and on the basis of the effect of heat treating in a sulfur atmosphere, concluded that edge emission was a result of sulfur vacancies. B. A. Kulp and R. H. Kelley (J. App. Phys.) measured the threshold for the production of edge emission by electron bombardment as being 115 Kev and proposed that edge emission was a result of sulfur interstitials. Kulp proposed that sulfur vacancies are the center for the fluorescence band at 7200 A at 77°K.

The "edge" emission mentioned above refers to the emission in the green appearing just outside the fundamental absorption edge, when excited by ultraviolet radiation. The highest energy peak in the edge emission occurs at 5140 A and is followed by regularly spaced peaks separated by an energy difference equal to the energy of the longitudinal optical phonon. The emission is believed to arise through the recombination of a free carrier with a trapped carrier.

In addition, CdS shows the blue luminescence centered about 4850 A, when excited by ultraviolet radiation at liquid nitrogen temperature. This blue emission is considered to be

due to exciton recombination near the surface of the crystal.

The particular radiation on which attention was focused was the red luminescence at 7200°A. This is the radiation that becomes particularly prominent following thermal neutron radiation.

Cadmium sulfide is a semiconductor having band gap of 2.5 ev. Pure cadmium sulfide is therefore expected to be an insulator at room temperature and below. However, because of deviation from stoichiometry and possibly impurities, the "as-grown" exhibit a wide range of conductivities, varying from the almost metallic crystals, having resistivity of about 0.1 ohm-cm., to insulating samples having resistivities as high as 10^9 ohm-cm. The "bulk" crystals from which suitable samples were prepared by cleaning, were of the low-resistivity type, and the dendritic of the "platelet" crystals had the high resistivity.

Under ultraviolet excitation at 78°K the bulk-type crystals show the usual blue exciton emission at 4880 A and a very low intensity band around 7200 A. After about 36 megawatt-minute thermal neutron irradiation the exciton intensity is reduced, accompanied by a dramatic increase in the 7200 A red luminescence. Similar effects are observed for the platelet-type crystals.

The following analysis provides an estimate of the numbers needed for the design of the experiment. Suppose that a crystal of CdS is exposed to a neutron beam of flux Φ_o ,

then its attenuation inside the crystal is given by

$$\Phi = \Phi_0 e^{-N_0 \sigma x}$$

where σ is the thermal neutron capture cross section of Cd^{113}, and N_0 is the Cd^{113} concentration in the crystal. The thermal neutron capture cross section is about 20,000 barns. The Cd^{113} concentration N_0 can be estimated from the density of CdS (3.09 gm/cm^3) and the isotopic abundance (12.26%). Thus

$$N_0 = 6.03 \times 10^{23} \times \frac{3.09}{144.48}(.1226) = 1.6 \times 10^{21} / cm^3$$

Hence the mean penetration into the crystal is

$$\lambda = \frac{1}{N_0 \sigma} = \frac{1}{1.6 \times 10^{21}(2 \times 10^{-20})} = 0.03 \text{ cm}$$

Thus a crystal of thickness 1 mm will abosrb thermal neutrons completely. If the thermal neutron flux is about 10^{12} cm^2/sec., and assuming one atomic displacement per neutron, we find that the estimated density of atomic displacements will be produced. Hence the effects due to thermal neutrons can be readily observed by conventional semiconductor techniques.

The thermal neutron irradiation has a marked effect upon the temperature dependence of conductivity. To interpret the result, suppose that the neutron capture leads to the formation of a electron trapping centers E_t below the edge of the conduction band.

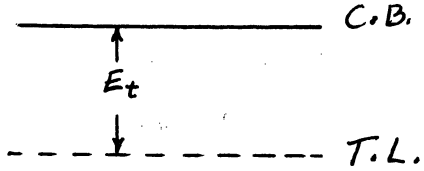

Then

$$n^{\circ} = n + \frac{N_t}{1 + \frac{1}{2}\exp\left(\frac{E_F' - E_t}{kT}\right)}$$

where

$$E_F' \equiv E_c - E_F$$

Using

$$n = N_c e^{-E_F'/kT}$$

we obtain

$$n^{c} = n + \frac{N_t}{1 + 1/2 \frac{N_c}{n}\exp\left(-\frac{E_t}{kT}\right)}$$

$$\frac{n(N_t - n^{\circ} + n)}{n^{\circ} - n} = \frac{1}{2} N_c \exp\left(-\frac{E_t}{kT}\right)$$

In the above expression N_t is the density of trapping centers introduced by thermal neutron captures, n° is the initial electron concentration, and E_t is the depth of the trapping level below the conduction band. If the sample has been irradiated a sufficient length of time so that $N_t > n^{\circ}$ and suppose furthermore that $n < N_t - n^{\circ}, n^{\circ}$ Then

$$n = \frac{1}{2} \frac{n^{\circ}}{N_t - n^{\circ}} N_c \exp\left(-\frac{E_t}{kT}\right)$$

The conductivity is given

$$\sigma = q \mu_n n$$

Theory shows that the temperature dependence of the mobility, due to thermal scattering is proportional to $T^{-3/2}$. This temperature dependence is just cancelled by the factor $T^{+3/2}$ in the

effective density of state N_c . Thus we can write

$$\sigma = \sigma_0 e^{-E_t/kT}$$

Hence the slope of the semilog plot of the conductivity gives the depth of the trapping level. Measurements seem to show that E_t is about 1.1 ev.

CHAPTER VIII MINORITY CARRIER LIFETIME

Although high energy radiations have pronounced effect upon the semiconductivity of semiconductors, such radiations have an even more important effect in the operation of many semiconductor devices. Consequently we shall here first discuss the so-called Hall-Shockley-Read mechanism, and show the effects of radiation upon the minority carrier lifetime.

8.1 Hall-Shockley-Read Mechanism

Our principle task here is to derive the relation

$$\tau = \frac{\frac{1}{C_p}(n_0 + n_1) + \frac{1}{C_n}(p_0 + p_1)}{n_0 + p_0} \tag{8.1}$$

where

$$C_p = N_t \sigma_p v_p \tag{8.2}$$

$$C_n = N_t \sigma_n v_t$$

$$n_1 = N_c \exp\left(-\frac{E_c - E_t}{kT}\right) \tag{8.3}$$

$$p_1 = N_v \exp\left(-\frac{E_t - E_v}{kT}\right) \tag{8.4}$$

(8.5)

C_n .... capture rate per electron when the electron trap is empty

C_p .... capture rate of holes where traps are fully occupied

The sequence of events presumed to occur in the HSR-mechanism is as follows. First the trapping center captures an electron, and subsequently, the electron in this trapping center is annihilated by combining with a hole. Thus the recombination center is ready to repeat the cycle for electron-hole recombination.

Consider then the electron trapping part of the recombination process

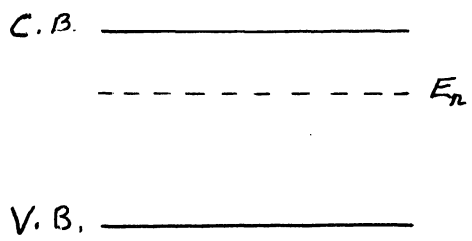

If the energy of the trapping center is E_r, then the rate at which electrons will fall into the traps will be given by

$$R_c = C_n n (1 - f_n) \tag{8.6}$$

where $1 - f_n$ represents the fraction of trapping centers that are not occupied. The rate at which electrons are leaving the trapping centers to go into the conduction band is

$$R_e = C_n' f_n \tag{8.7}$$

and at equilibrium

$$R_c = R_e \tag{8.8}$$

so we obtain

$$C_n' = C_n \frac{n_0 (1 - f_{n0})}{f_{n0}} = C_n n_0 \exp\left(\frac{E_n - E_F}{kT}\right) \tag{8.9}$$

Furthermore

$$n_c = N_c \exp\left(-\frac{E_c - E_F}{kT}\right) \tag{8.10}$$

so that (8.9) becomes

$$C_n' = C_n N_c \exp\left(-\frac{E_c - E_n}{kT}\right) \equiv n_1 C_n \tag{8.11}$$

where we have put

$$n_1 \equiv N_c \exp\left(-\frac{E_c - E_n}{kT}\right) \tag{8.12}$$

From (8.6), (8.7) and (8.11), we obtain for the net rate of electron capture the expression

$$R_n \equiv R_c - R_e = C_n \left[(1 - f_n) n - n_1 f_n\right] \tag{8.13}$$

Similarly for the net rate of hole capture we have

$$R_p = C_p \left[f_n p - p_1 (1 - f_n)\right] \tag{8.14}$$

Under steady state conditions

$$R_n = R_p \tag{8.15}$$

so that

$$f_n = \frac{n C_n + p_1 C_p}{C_n (n + n_1) + C_p (p + p_1)} \tag{8.16}$$

Inserting (8.16) into (8.13) and (8.14), we find

$$R = R_n = R_p$$

$$= \frac{C_n C_p (np - n_1 p_1)}{C_n (n+n_1) + C_p (p+p_1)} \tag{8.17}$$

Now $$n_1 p_1 = n_0 p_0$$

$$\therefore \; np - n_1 p_1 = np - n_0 p_0 = (n_0 + p_0)\Delta n \tag{8.18}$$

for small Δn

$$\tau = \frac{\frac{1}{C_p}(n_0+n_1) + \frac{1}{C_n}(p_0+p_1)}{n_0 + p_0} \tag{8.19}$$

If we write

$$C_n = N_n C_n$$
$$C_p = N_n C_p$$

where C_n and C_p are the capture probabilities of electrons and holes per vacant center and per occupied center, then (8.19) can be written as

$$\tau = \frac{1}{N_n} \frac{\frac{1}{C_p}(n_0+n_1) + \frac{1}{C_n}(p_0+p_1)}{n_0 + p_0} \tag{8.20}$$

Several consequences follow immediately. From (8.20), for several trapping centers we have

$$\frac{1}{\tau} = \sum_n N_n \frac{n_0 + p_0}{\frac{1}{C_{pn}}(n_0 + n_{1n}) + \frac{1}{C_{nn}}(p_0 + p_{1n})}$$

(8.21)

$$\frac{1}{\tau} = \frac{1}{\tau_o} + N_t \frac{n_o + p_o}{\frac{1}{C_{pt}}(n_o + n_{1t}) + \frac{1}{C_{nt}}(p_o + p_{1t})}$$

where the centers introduced by irradiation has been singled out. Eq. (8.21) then shows that the plot of $\ln\left(\frac{1}{\tau} - \frac{1}{\tau_o}\right)$ and $\ln N_t$ should be linear, and hence linear with the $\ln(nvt)$ Such measurements have been reported by O. L. Custis, J. W. Cleland, J. H. Crawford, and J. C. Pigg (J. App. Phys. 28, 1161 (Oct. 1967)). The log-log plot of the reciprocal lifetime against the integrated neutron flux and integrated gamma flux yield straight lines with slopes very nearly equal to unity.

Let us next see what information can be obtained by examining the temperature dependence of the lifetime, suppose the specimen is N-type, such that $n_c >> p_o$, $n_1 >> p_1$. Then (8.21) gives

$$\tau = \frac{1}{N_t C_p}\left(1 + \frac{n_1}{n_o}\right) \qquad (8.22)$$

In this expression the only appreciable variation of τ with temperature arises from n, since over the range of measurement (220°K to 350°K) n_o is expected to remain essentially constant. For electron concentration such that $n_1/n_o >> 1$, (8.22) predicts a linear $\ln \tau$ vs. $1/T$ curve. The slppeoof this curve yields $E_c - E_t$ since

$$n_1 = N_c \exp\left(\frac{E_t - E_c}{RT}\right) \qquad (8.23)$$

The slope of this curve indicates that

$$E_c - E_t = 0.23 \text{ ev}$$

REFERENCES

O. L. Curtis, J. W. Cleland, J. H. Crawford, Jr., and J. C. Pigg, "Effect of Irradiation on the Hole Lifetime of N-type Germanium", J. App. Phys. 28, 1161 (Oct. 1957).

O. L. Curtis, J. W. Cleland, and J. H. Crawford, Jr., "Radiation Induced Recombination Centers", J. App. Phys. 29, 1722 (Dec. 1958).

F. A. Junga and G. M. Enslow, "Radiation Effects in Silicon Solar Cells", IRE Trans. NS-6, 49 (June 1959).

IX. ELECTRON SPIN RESONANCE IN SEMICONDUCTOR RESEARCH

The purpose of this chapter will be to provide a brief introduction to electron spin resonance in order to point out the potential usefulness of this research tool for the study of semiconductors and radiation effects in semiconductors. Some of the possible uses for the study of radiation effects are given in a University of Michigan Phoenix Memorial Project Report by C. Kikuchi, S. Yip, and I. Chen.

The usefulness of electron spin resonance stems from the fact that the electrons and nuclei in a solid can be thought of as microscopic electric and magnetic probes, and as such can be used to explore the electric and magnetic fields in microscopic regions of a solid. In semiconductors those paramagnetic centers have most frequently electron spin S of 1/2. Consequently we shall examine this case in great detail.

Consider then, an electron of spin angular momentum of 1/2 and magnetic moment μ located in a magnetic field. The energy of this bar magnet is given by

$$E = -\underline{\mu} \cdot \underline{H} = -\mu H \cos\theta \tag{9.1}$$

where θ is the angle between the magnetic moment and the magnetic field. Thus the energy is lowest when $\theta = 0$, i.e. when the magnetic fields are parallel, but largest when $\theta = 180°$, i.e. when the magnetic moment and the magnetic field

are anti-parallel. The difference in energy or the energy needed to go from parallel to anti-parallel orientation then is

$$\Delta E = 2\mu H \tag{9.2}$$

If this is to be supplied by the electromagnetic field, then

$$h\nu = \Delta E = 2\mu H = 2\beta H \tag{9.3}$$

where we have used β for the electron magnetic moment. Since

$$h = 6.625 \times 10^{-27} \text{ erg sec}$$
$$\beta = 0.9273 \times 10^{-20} \text{ erg/gauss}$$

we find that

$$\nu = 2.8 \text{ H} \quad \text{Mc/sec}$$

If in particular H = 3300 gauss, we find that resonance absorption is to be expected at ν = 9,250 Mc/sec.

The above simple classical analysis then suggests the following experimental procedure.

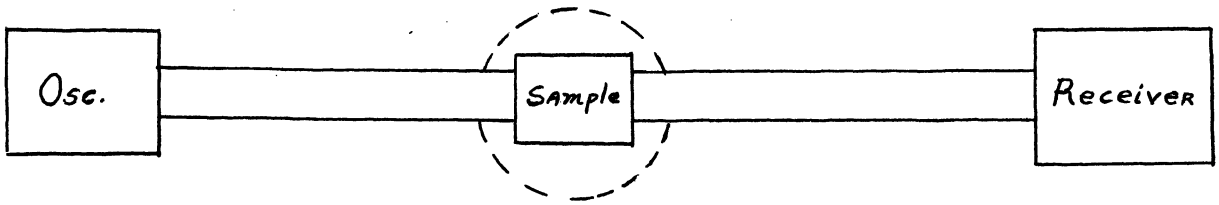

Suppose the oscillator puts out a constant power at ν = 9,250 Mc/sec. The experimental arrangement is to be such that this power is incident on the sample, and that the receiver is to

measure the transmitted power. Furthermore, suppose that the electromagnet is such that it is possible to sweep through resonance magnetic field, H, given by (9.3). If the magnetic field is below this value there will be no appreciable absorption of microwave, and this condition will continue as the magnetic field is slowly increased. However, when the magnetic field reaches H_o, there will be a sudden absorption of power, resulting in the decrease of the transmitted microwave power. In these experiments we need merely record the transmitted power as a function of the applied magnetic field.

1. Spin Quantum Mechanics

Although the above arguments provide an intuitive insight into electron spin resonance, we need to have the result of quantum mechanics to interpret the details of the experimental results. Accordingly we shall give here some of the fundamentals of quantum mechanics relevant to electron spin resonance.

The basic equation in quantum mechanics is

$$\mathcal{H}\Psi = i\hbar \frac{\partial \Psi}{\partial t} \tag{9.4}$$

where the Hamiltonian H can be written in the form

$$\mathcal{H} = \mathcal{H}_o + \mathcal{H}_{int} \tag{9.5}$$

consisting of time-independent part H_o and time-dependent part H_{int} respectively. The time-independent part consists of several parts, such as the interaction with the external magnetic field, called the Zeeman term, the electron-nuclear interaction

term, etc. Furthermore, a point to note is that the Hamiltonian is an invarient. Consequently, the invarients that can be constructed from the magnetic field vector $\underline{H}$, the spin angular momentum vectors S and I, for the electron and nucleus respectively, are such as to suggest the following phenomenological Hamiltonian

$$\mathcal{H}_0 = \beta \underline{H} \cdot \underline{\underline{g}} \cdot \underline{S} + \underline{I} \cdot \underline{\underline{A}} \cdot \underline{S} - \beta_n \underline{H} \cdot \underline{\underline{g}}_n \cdot \underline{I} \tag{9.6}$$

where $\underline{\underline{g}}$, $\underline{\underline{A}}$ and $\underline{\underline{g}}_n$ are tensors of rank two. In the usual electron spin resonance experiments, the experimental conditions are such that the nuclear spin undergoes no change. Then the last term in (9.6) is a constant, we shall hereafter omit this from any explicit discussion. In (9.6) there should be another term giving the contribution of the crystalline electric field stemming from the crystal lattice ions. But this term gives no contribution, except indirectly, to the electron energy.

The time dependent part of the Hamiltonian can be written in the form

$$\mathcal{H}_{int} = \beta \underline{H}(t) \cdot \underline{\underline{g}} \cdot \underline{S} - \beta_n \underline{H}(t) \cdot \underline{\underline{g}}_n \cdot \underline{I} + H'(\text{cryst.}) \tag{9.7}$$

The second term giving the nuclear Zeeman term can again be omitted from most of our discussions. The last term, giving the time-dependent perturbation stemming from the crystal lattice vibrations provides the mechanism for spin-lattice relaxation. Again, to simplify our analysis this term will

not be considered here. Consequently for our purposes we shall consider the static part of the Hamiltonian to be given by the first two terms in (9.6) and that the transitions among the different states are induced by the first term in (9.7).

2. Energy Levels

To solve the quantum mechanical problem for the Hamiltonian (9.6), we need to recall a theorem in quantum mechanics which states that for two commuting operators Q and R there exists a complete set of simultaneous eigenstates for both Q and R. (See for example Dicke and Wittke, Introduction to Quantum Mechanics, p. 97). That is, if

$$Q\psi_j = q\psi_j \tag{9.8}$$

where q is assumed to be non-degenerate, and if

$$[Q, R] = 0 \tag{9.9}$$

then

$$R\psi_j = r_j\psi_j \tag{9.10}$$

On the other hand, if q is degenerate, such that

$$Q\psi_j = q\psi_j \tag{9.8'}$$

with more than one eigenfunction belonging to the eigenvalue q, then the theorem asserts the possibility of finding a linear combination μ_k, such that

$$\mu_k = \sum c_{kj} \psi_j \tag{9.11}$$

$$Q \mu_k = q \mu_k \tag{9.8''}$$

and

$$R \mu_k = r_k \mu_k \tag{9.10'}$$

The Hamiltonian that we shall be concerned with are functions of the electron and nuclear spin operators. For this reason the Hamiltonian is often referred to as the spin-Hamiltonian. We shall therefore, summarize the properties of the spin operators and functions. The spin operators have the following properties:

$$S^2 \equiv S_x^2 + S_y^2 + S_z^2 \tag{9.12}$$

$$\begin{aligned} [S_x, S_y] &= i S_z \\ [S_y, S_z] &= i S_x \\ [S_z, S_x] &= i S_y \end{aligned} \tag{9.13}$$

It can be easily shown that S_x, S_y, and S_z commute with S^2, i.e.

$$[S^2, S_x] = [S^2, S_y] = [S^2, S_z] = 0 \tag{9.14}$$

The spin functions Φ_M have the following properties

$$S^2 \Phi_M = s(s+1) \Phi_M \tag{9.15}$$

$$S_z \Phi_M = M \Phi_M \tag{9.16}$$

$$S_+ \varphi_M = \sqrt{S(S+1) - M(M+1)}\ \varphi_{M+1} \tag{9.17}$$

$$S_- \varphi_M = \sqrt{S(S+1) - M(M-1)}\ \varphi_{M-1} \tag{9.18}$$

where

$$M = -S, -S+1, \cdots, +S$$

Similar results apply to the nuclear spin operators I_x, I_y, and I_z, and

$$I^2 \equiv I_x^2 + I_y^2 + I_z^2 \tag{9.19}$$

To demonstrate how the above results are to be used, consider first the Zeeman effect of an electron whose magnetic moment is parallel to its spin. Then

$$\underline{\mu} = -g\beta\,\underline{S} \tag{9.20}$$

so that

$$\mathcal{H} = -\underline{\mu}\cdot\underline{H} = g\beta\,\underline{S}\cdot\underline{H} \tag{9.21}$$

and the quantum equation is

$$g\beta\,\underline{S}\cdot\underline{H}\,\psi = E\psi \tag{9.22}$$

If the magnetic field is taken along the z-axis, then (9.21) becomes

$$\mathcal{H} = g\beta H S_z \tag{9.21'}$$

Clearly

$$[\mathcal{H}, S_z] = 0 \tag{9.23}$$

so that according to the stated theorem for non-degenerate eigenvalue and the result of (9.16), we find that Φ_M is also the eigenfunction for (9.22).

$$\therefore g\beta H S_z \Phi_M = g\beta H M \Phi_M = E\Phi_M$$

$$\therefore E = g\beta H M \tag{9.24}$$

Thus if an electron of spin S is placed in a magnetic field, the ground state splits up into 2S + 1 equally spaced energy levels. The spacing is given by

$$\Delta E = g\beta H(M+1) - g\beta H M = g\beta H \tag{9.25}$$

As another example consider an electron whose magnetic moment is a <u>linear function</u> of the spin operator, i.e.

$$\underline{\mu} = -\beta \underline{\underline{g}} \cdot \underline{S} \tag{9.26}$$

and the Hamiltonian and the quantum equation are

$$\mathcal{H} = \beta \underline{H} \cdot \underline{\underline{g}} \cdot \underline{S} \tag{9.27}$$

$$\beta \underline{H} \cdot \underline{\underline{g}} \cdot \underline{S} \Psi = E\Psi \tag{9.28}$$

If the coordinate axes are taken along the principal axes of the g-tensor, then (9.27) can be written

$$\mathcal{H} = \beta(H_x g_x S_x + H_y g_y S_y + H_z g_z S_z) \tag{9.29}$$

$$= \beta\left[g_z H_z S_z + \tfrac{1}{2}(g_x H_x - i g_y H_y) S_+ + \tfrac{1}{2}(g_x H_x + i g_y H_y) S_-\right]$$

where we have written

$$g_{xx} = g_x \quad , \quad g_{yy} = g_y \quad , \quad g_{zz} = g_z \tag{9.30}$$

We note (9.29) no longer commutes with S_z, but does commute with S^2, as can be seen from (9.14). But there are 2S + 1 eigenfunctions ϕ_M belonging to the operator S^2, i.e.

$$S^2 \phi_M = s(s+1)\, \phi_M$$

Consequently to construct the simultaneous eigenfunctions for the Hamiltonian of (9.29) and (9.15), we need to take a linear combination of the ϕ_M's. To simplify the analysis we shall take S = 1/2, then M = -1/2 and 1/2, so that if we take

$$\mu = a\, \phi_{1/2} + b\, \phi_{-1/2} \tag{9.31}$$

we find that

$$S^2 \mu = \frac{3}{4} \mu \tag{9.32}$$

and the results of the stated theorem asserts that

$$\beta \left[g_z H_z S_z + \tfrac{1}{2} (g_x H_x - i g_y H_y) S_+ + \tfrac{1}{2} (g_x H_x + i g_y H_y) S_- \right] \mu = E \mu \tag{9.33}$$

From (9.17) and (9.18) we note that for S = 1/2,

$$S_+ \phi_{1/2} = 0 \qquad S_- \phi_{1/2} = \phi_{-1/2}$$

$$S_+ \phi_{-1/2} = \phi_{1/2} \qquad S_- \phi_{-1/2} = 0 \tag{9.34}$$

Hence (9.33) gives

$$\frac{1}{2}g_z H_z (a\alpha_{1/2} - b\alpha_{-1/2}) + \frac{1}{2}(H_x g_x - iH_y g_y) b\alpha_{1/2} + \frac{1}{2}(g_x H_x + i g_y H_y) a\alpha_{-1/2}$$

$$= \frac{E}{\beta}(a\alpha_{1/2} + b\alpha_{-1/2}) \tag{9.35}$$

Since the α_m's are ortho-normal, we find that

$$\begin{aligned} \frac{1}{2}g_z H_z a + \frac{1}{2}(H_x g_x - i g_y H_y) b &= a\frac{E}{\beta} \\ \frac{1}{2}(g_x H_x + i g_y H_y) a - \frac{1}{2} g_z H_z b &= b\,E/\beta \end{aligned} \tag{9.36}$$

Hence, for the existence of non-trivial values of a and b, we find that

$$\begin{vmatrix} \frac{1}{2}g_z H_z - \frac{E}{\beta} & \frac{1}{2}(H_x g_x - i g_y H_y) \\ \frac{1}{2}(g_x H_x + i g_y H_y) & -\frac{1}{2} g_z H_z - E/\beta \end{vmatrix} = 0 \tag{9.37}$$

$$\therefore\quad E = \pm\frac{1}{2}\beta\sqrt{g_x^2 H_x^2 + g_y^2 H_y^2 + g_z^2 H_z^2} \tag{9.38}$$

As the third example, consider the Zeeman effect of an electron and a nucleus coupled by an isotropic election nuclear spin-spin interaction. Taking the z-axis along the magnetic field, the appropriate Hamiltonian can be written in the form

$$(g\beta H S_z - g_n \beta_n H I_z + A\,\underline{I}\cdot\underline{S})\psi = E\psi \tag{9.39}$$

with

$$\mathcal{H} \equiv g\beta H S_z - g_n \beta_n H I_z + A\,\underline{I}\cdot\underline{S} \tag{9.40}$$

It is easy to verify that

$$[\mathcal{H}, S^2] = [\mathcal{H}, I^2] = 0 \tag{9.41}$$

and

$$[\mathcal{H}, S_z + I_z] = 0 \tag{9.42}$$

The results of (9.41) suggest that the eigenfunctions of (9.39) are of the form

$$\mathcal{Q}_M \chi_m \tag{9.43}$$

where

$$I^2 \chi_m = i(i+1)\chi_m$$
$$I_z \chi_m = m \chi_m \tag{9.44}$$

Furthermore, according to (9.42)

$$(S_z + I_z)\mathcal{Q}_M \chi_m = (M+m)\mathcal{Q}_M \chi_m \tag{9.45}$$

so that the eigenfunctions of (9.39) are to be constructed from the set of $\mathcal{Q}_M \chi_m$ giving the same eigenvalue $M+m$. To simplify the analysis again take S = 1/2. Then, clearly

$$(S_z + I_z)\mathcal{Q}_{1/2} \chi_m = (\tfrac{1}{2} + m)\mathcal{Q}_{1/2} \chi_m$$
$$(S_z + I_z)\mathcal{Q}_{-1/2} \chi_{m+1} = (\tfrac{1}{2} + m)\mathcal{Q}_{-1/2} \chi_{m+1} \tag{9.46}$$

Then

$$\psi = a\,\mathcal{Q}_{1/2} \chi_m + b\,\mathcal{Q}_{-1/2} \chi_{m+1} \tag{9.47}$$

Carrying through the analysis as before we find that

$$\tfrac{1}{2}(g\beta H + mA)a + \tfrac{1}{2}Ab\sqrt{I(I+1)-m(m+1)} = Ea$$

$$\tfrac{1}{2}Aa\sqrt{I(I+1)-m(m+1)} - \tfrac{1}{2}\left[g\beta H + A(m+1)\right]b = Eb \qquad (9.48)$$

$$\begin{vmatrix} \tfrac{1}{2}(g\beta H + Am) - E & \tfrac{1}{2}A\sqrt{I(I+1)-m(m+1)} \\ \tfrac{1}{2}A\sqrt{I(I+1)-m(m+1)} & -\tfrac{1}{2}g\beta H - \tfrac{1}{2}A(m+1) - E \end{vmatrix} = 0$$

$$E = -\frac{A}{4} \pm \frac{1}{2}\sqrt{\left(g\beta H + A(m+\tfrac{1}{2})\right)^2 + A^2\left[I(I+1)-m(m+1)\right]} \qquad (9.49)$$

3. Transition Probabilities and Selection Rules

Before considering the applications of the results just derived, we shall consider transition probabilities and selection rules because these are important in the design of experiments. For this we shall again consider the Zeeman effect of an electron, subject to an oscillating as well as a steady magnetic field. The basic quantum mechanical equation is

$$\mathcal{H}\psi = i\hbar\frac{\partial\psi}{\partial t} \qquad (9.3.1)$$

where

$$\mathcal{H} \equiv \mathcal{H}_0 + \mathcal{H}_{int} \qquad (9.3.2)$$

where $\mathcal{H}_0$ is the time-independent part of the Hamiltonian, given by

$$\mathcal{H}_0 \equiv g\beta H_0 S_z \qquad (9.3.3)$$

and $\mathcal{H}_{int}$ represents the interaction of the electron with the applied oscillating magnetic field, i.e.

$$\mathcal{H}_{int} = g\beta \underline{H}'(t) \cdot \underline{S} = g\beta \underline{H}' \cdot \underline{S} \cos \omega t \tag{9.3.4}$$

Our task is to see what conditions $\underline{H}'(t)$ must satisfy to induce transitions among the Zeeman levels.

To obtain the solution of (9.50), we write

$$\psi = \sum a_{M'}(t)\, \varphi_{M'}\, e^{-\frac{i E_{M'} t}{\hbar}} \tag{9.3.5}$$

where φ_M is satisfy the equation

$$\mathcal{H}_0 \varphi_M = E_M \varphi_M \tag{9.3.6}$$

From (9.54) we see that

$$\mathcal{H}_0 \psi = \sum_{M'} a_{M'}(t) E_{M'} \varphi_{M'} e^{-\frac{i E_{M'} t}{\hbar}} \tag{9.3.7}$$

$$\frac{\partial \psi}{\partial t} = \sum_{M'} \dot{a}_{M'}(t) \varphi_{M'} e^{-\frac{i E_{M'} t}{\hbar}} - \frac{i}{\hbar} \sum_{M'} E_{M'} a_{M'}(t) \varphi_{M'} e^{-\frac{i E_{M'} t}{\hbar}} \tag{9.3.8}$$

Consequently, substituting into (9.50) we find that

$$\sum_{M'} a_{M'}(t) \varphi_{M'} e^{-\frac{i E_{M'} t}{\hbar}} E_{M'} + \sum_{M'} a_{M'}(t) \mathcal{H}_{int} \varphi_{M'} e^{-\frac{i E_{M'} t}{\hbar}} \tag{9.3.9}$$

$$= i\hbar \sum_{M'} \left[\dot{a}_{M'}(t) - \frac{i}{\hbar} E_{M'} a_{M'}(t) \right] \varphi_{M'} e^{-\frac{i E_{M'} t}{\hbar}}$$

$$\therefore i\hbar \sum_{M'} \dot{a}_{M'}(t) \varphi_{M'} e^{-\frac{i E_{M'} t}{\hbar}} = \sum_{M'} a_{M'}(t) \mathcal{H}_{int} \varphi_{M'} e^{-\frac{i E_{M'} t}{\hbar}} \tag{9.3.10}$$

$$\therefore \dot{a}_M(t) = \frac{1}{i\hbar} \sum_{M'} \langle M | \mathcal{H}_{int} | M' \rangle a_{M'}(t)\, e^{-\frac{i(E_{M'} - E_M)t}{\hbar}} \tag{9.3.11}$$

From (9.3.4) we see that

$$\mathcal{H}_{int} = \frac{1}{2} g \beta \underline{H}' \cdot \underline{S} \left(e^{i\omega t} + e^{-i\omega t} \right) \tag{9.3.12}$$

Furthermore, if it is assumed that at t = 0

$$a_{M_0}(0) = 1 \quad , \qquad a_M(0) = 0 \quad (M \neq M_0)$$

then the integration of (9.3.11) leads to

$$a_M(t) = \left[\frac{e^{\frac{i(E_M - E_{M_0} + \omega\hbar)t}{\hbar}} - 1}{\frac{i(E_M - E_{M_0} + \omega\hbar)}{\hbar}} + \frac{e^{\frac{i(E_M - E_{M_0} - \omega\hbar)t}{\hbar}} - 1}{\frac{i(E_M - E_{M_0} - \omega\hbar)}{\hbar}} \right] \frac{g\beta}{2i\hbar} \langle M | \underline{H}' \cdot \underline{S} | M_0 \rangle$$

$$a_M(t) = \frac{g\beta}{2} \langle M | \underline{H}' \cdot \underline{S} | M_0 \rangle \left[\frac{e^{\frac{i(E_M - E_{M_0} + \omega\hbar)t}{\hbar}} - 1}{E_M - E_{M_0} + \omega\hbar} + \frac{e^{\frac{i(E_M - E_{M_0} - \omega\hbar)t}{\hbar}} - 1}{E_M - E_{M_0} - \omega\hbar} \right] \tag{9.3.13}$$

We note that the term $e^{i\omega t}$ gave rise to the first term in the square brackets, which is large if

$$E_M = E_{M_0} - \omega\hbar$$

that is, if the final energy is less than the initial energy by $\omega\hbar$. Thus this term gives rise to an emission of photon of energy $\omega\hbar$. Similarly, the term $e^{-i\omega t}$ which leads to the second term in the square brackets is associated with photon absorption.

Let us now look at the matrix elements

$$\langle M | \underline{H}' \cdot \underline{S} | M_0 \rangle$$

$$= \langle M | H_z' S_z + \tfrac{1}{2} H_+' S_- + \tfrac{1}{2} H_-' S_+ | M_0 \rangle \qquad (9.3.14)$$

The first term involving S_z gives rise to transitions among Zeeman levels with the same magnetic quantum number M. But according to our previous analysis, the different Zeeman levels have different magnetic quantum numbers. Consequently it follows that the component of the oscillating magnetic field parallel to the steady magnetic field gives no contribution to photon absorption or emission. In other words, for the Hamiltonian of (9.3.1), (9.3.3), and (9.3.4), the oscillating magnetic field must be perpendicular to the steady magnetic field.

To see how the polarization is related to the emission and absorption processes, consider the last two terms in (9.3.14). To simplify it, take the x-axis along the direction

of the oscillating magnetic field. Then, upon re-introducing the time dependence we find that

$$\frac{1}{2} H'_{+} S_{-} + \frac{1}{2} H'_{-} S_{+} = H' S_x \cos \omega t \tag{9.3.15}$$

This can be resolved into "clockwise" and "anti-clockwise" rotating magnetic field as follows:

$$H_x^{(a)} = \frac{1}{2} H' \cos \omega t \qquad H_x^{(c)} = \frac{1}{2} H' \cos \omega t$$

$$H_y^{(a)} = \frac{1}{2} H' \sin \omega t \qquad H_y^{(c)} = -\frac{1}{2} H' \sin \omega t \tag{9.3.16}$$

$$\therefore \underline{S} \cdot \underline{H}^{(a)} = \frac{1}{2} S_{+} H_{-}^{(a)} + \frac{1}{2} S_{-} H_{+}^{(a)}$$

$$= \frac{1}{4} H' \left[S_{+} e^{-i\omega t} + S_{-} e^{i\omega t} \right] \tag{9.3.17}$$

$$\underline{S} \cdot \underline{H}^{(c)} = \frac{1}{4} H' \left[S_{+} e^{i\omega t} + S_{-} e^{-i\omega t} \right] \tag{9.3.18}$$

It is to be recalled that S_{+} gives rise to transitions in which angular momentum is absorbed from the electromagnetic field, i.e. the angular momentum of the electron increases. Similarly S_{-} is responsible for the emission of angular momentum. Then the several terms in (9.3.17) and (9.3.18) have the following significance:

	Operator	Energy	Angular Momentum	
$H^{(a)}$	$S_{+} e^{-i\omega t}$	Absorption	Absorption	(9.3.19)
	$S_{-} e^{i\omega t}$	Emission	Emission	

	Operator	Energy	Angular Momentum
$H^{(c)}$	$S_+ e^{i\omega t}$	Emission	Absorption
	$S_- e^{-i\omega t}$	Absorption	Emission

Now for negative and positive magnetic moments, the energy level arrangements for S = 1/2 are as follows:

Negative		Positive
M = 1/2	———	——— M = -1/2
M = -1/2	———	——— M = 1/2

For negative magnetic moment then angular momentum is absorbed during the energy absorption process, whereas for positive magnetic moment, angular momentum is emitted when a photon is absorbed. Thus for negative magnetic moments, the anti-clockwise induces the transitions, whereas for the positive magnetic moment, the clockwise component is the operative one.

From the above analysis then it is clear that the selection rules are given by

$$\Delta M = \pm 1 \tag{9.3.20}$$

that is, the transitions will take place between adjacent Zeeman levels. Since the Zeeman energy levels are given by

$$E_M = g\beta HM$$

we see that the photon needed to induce the transitions must be such that

$$h\nu = \Delta E = g\beta H \tag{9.3.21}$$

in agreement with the semiclassical result given earlier.

So far we have neglected the effects of the nuclear spin. If this is included (9.3.3) becomes

$$\mathcal{H}_o \equiv g\beta H S_z - g_n \beta_n H I_z + A \underline{I}\cdot\underline{S} \tag{9.3.3'}$$

and

$$\mathcal{H}_{int} = \underline{H}'\cdot(g\beta \underline{S} - g_n \beta_n \underline{I}) \cos \omega t \tag{9.3.4'}$$

so that the matrix element occurring in (9.3.13) becomes

$$\langle M, m \mid \mathcal{H}_{int} \mid m_o, M_o \rangle$$

The transition probability is proportional to the square of this matrix element. Then from (9.3.4') it is clear that the leading term will be about β^2 in comparison to $\beta\beta_n$ and β_n^2 for the remaining two terms. The nuclear magnetron β_n is roughly 10^{-3} smaller than the Bohr magnetron. Thus the electron spin operator S will determine principally the transition probability, so that the selection rules when nuclear spins are present are given by

$$\Delta M = \pm 1$$
$$\Delta m = 0 \tag{9.3.20'}$$

Furthermore the relative intensities of the allowed transitions are proportional to the square of the matrix elements.

Therefore, the relative intensities for $M \leftrightarrow M+1$ are given by

$$\left| S(S+1) - M(M+1) \right|$$

The result of (9.3.13) shows how the amplitudes of the state $M = M_0 \pm 1$ change with the time. Suppose we consider the emission process. Then the probability that the electron is in state M, when initially in M_0 is given by

$$\left|a_M(t)\right|^2 = \frac{g^2\beta^2}{4} \left|\langle M | \underline{H}' \cdot \underline{S} | M_0 \rangle\right|^2 \left(\frac{t}{2\hbar}\right)^2 \frac{\sin^2 \frac{t}{2\hbar}(E_M - E_{M_0} + \omega\hbar)}{\left\{\frac{t}{2\hbar}(E_M - E_{M_0} + \omega\hbar)\right\}^2} \tag{9.3.22}$$

In many physically important situations, we are not concerned with transitions to only a single sharp final state. Hence we need to sum over all possible final states. Then the transition probability is given by

$$\begin{aligned} w &= \frac{1}{t} \sum \left| a_M(t) \right|^2 \\ &= \frac{g^2\beta^2 t}{16\hbar^2} \int \frac{\sin^2 \frac{t}{2\hbar}(E_M - E_{M_0} + \omega\hbar)}{\left\{\frac{t}{2\hbar}(E_M - E_{M_0} + \omega\hbar)\right\}^2} n(E_M - E_{M_0})\, dE_M \\ &= \frac{g^2\beta^2 t}{16\hbar^2} n(E_M - E_{M_0}) \frac{2\hbar}{t} \int \frac{\sin^2 X}{X^2}\, dX \qquad (9.3.23) \\ &= \frac{\pi g^2 \beta^2}{8\hbar} n(E_M - E_{M_0}) \left|\langle M | \underline{H}' \cdot \underline{S} | M_0 \rangle\right|^2 \end{aligned}$$

A similar result holds for the reverse process.

4. Radiative and Relaxation Processes

The expression for the transition probability just derived, however, does not yet provide a complete link with experiment. The reason for this is that the transition probability applies to a single electron, whereas the experimental results depend upon a large number N of electrons distributed among different energy states. We shall then see what additional concepts are needed to relate theory to the observed results.

Again for sake of simplicity, consider an electron of spin S = 1/2, which, as we have seen, split into two Zeeman levels separated by $g\beta H$. Thus

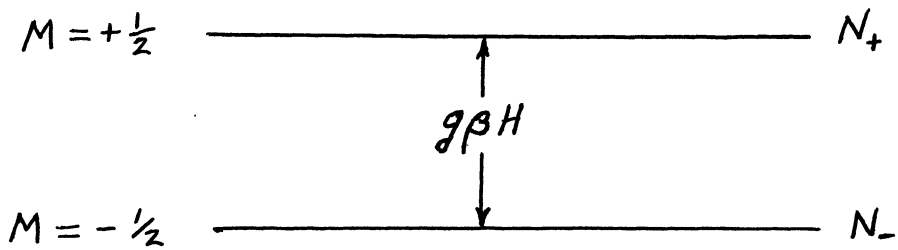

And of the N electrons, we shall assume that N_+ and N_- are in the upper and lower states respectively. Clearly

$$N = N_+ + N_- \tag{9.4.1}$$

If w, derived in the previous section, denotes the transition probability, then the rate equations for the populations are

$$\begin{aligned} \frac{dN_+}{dt} &= N_- w - N_+ w = (N_- - N_+) w \\ \frac{dN_-}{dt} &= (N_+ - N_-) w = -(N_- - N_+) w \end{aligned} \tag{9.4.2}$$

If, furthermore

$$n \equiv N_- - N_+ \tag{9.4.3}$$

then subtracting the two equations in (9.4.2) we find

$$\frac{dn}{dt} = -2nw \tag{9.4.4}$$

which gives

$$n(t) = n(0)e^{-2wt} \tag{9.4.5}$$

Thus, under the assumption that the electrons are coupled to the photon field only, the population difference with decreased exponentially upon turning on the resonance magnetic field. The experimentally observable quantity is the absorbed power given by

$$P = h\nu[N_- w - N_+ w] = h\nu(N_- - N_+)w = h\nu w n \tag{9.4.6}$$

Thus absorbed power P will vanish exponentially with time.

However, we have neglected the fact that the electrons are also coupled to the phonon field, or to the crystal lattice vibrations. The crystal lattice vibrations provide a sink for the energy fed into the electron spin system. The contribution to the rate equation, from this mechanism alone can be written in the form

$$\frac{dN_+}{dt} = N_- R_+ - N_+ R_- \tag{9.4.7}$$

where R_+ and R_- are the transition probabilities for the electrons to upward and downward transitions, due to coupling with the

phonon field. Also

$$\frac{dN_-}{dt} = -(N_- R_+ - N_+ R_-) \tag{9.4.8}$$

so that

$$\begin{aligned}\frac{dn}{dt} &= -2(N_- R_+ - N_+ R_-) \\ &= (n+N)R_+ + (N-n)R_- \\ &= N(R_- - R_+) - n(R_+ + R_-)\end{aligned} \tag{9.4.9}$$

At thermal equilibrium, $\frac{dn}{dt} = 0$ and $n = n_0$ so that (9.4.9) gives

$$n_0 = N\left(\frac{R_- - R_+}{R_- + R_+}\right) \tag{9.4.10}$$

Consequently, if we put

$$\frac{1}{T_1} \equiv R_+ + R_- \tag{9.4.11}$$

then (9.4.9) can be written in the form

$$\frac{dn}{dt} = \frac{n_0 - n}{T_1} \tag{9.4.12}$$

The solution is clearly

$$n = n_0\left(1 - e^{-t/T_1}\right) \tag{9.4.13}$$

showing that the population difference approaches the thermal equilibrium with a time constant T_1. Combining (9.4.4) and (9.4.12) we find that the photon and Phonon coupling leads to the rate equation

$$\frac{dn}{dt} = -2nw + \frac{n_0 - n}{T_1} \tag{9.4.14}$$

Under steady-state condition, $\frac{dn}{dt}=0$ so that (9.4.14) gives

$$n = \frac{n_0}{1+2w T_1} \tag{9.4.15}$$

The steady-state absorbed power P is then

$$P = h\nu w n = \frac{n_0 h\nu w}{1+2w T_1} \tag{9.4.16}$$

showing that power absorption exhibits the saturation effects. The quantity w is proportional to the incident microwave power. Thus, (9.4.16) shows that initially the power absorption is proportional to the incident power. However, for very large incident powers, the absorbed power will reach the saturation value

$$P_{SAT} = \frac{n_0 h\nu}{2T_1} \tag{9.4.17}$$

5. Spin Statistical Thermodynamics

The macroscopic magnetic moment M due to the electrons is given by

$$M = \frac{N\left[-\frac{1}{2}g\beta e^{\frac{1}{2}g\beta H/kT} + \frac{1}{2}g\beta e^{-\frac{1}{2}g\beta H/kT}\right]}{e^{\frac{1}{2}g\beta H/kT} + e^{-\frac{1}{2}g\beta H/kT}}$$

$$= -\frac{Ng\beta}{2}\frac{\sinh\frac{g\beta H}{2kT}}{\cosh\frac{g\beta H}{2kT}} = -\frac{Ng\beta}{2}\tanh\frac{g\beta H}{2kT}$$

For small H or high T, $g\beta H/2kT$ is small. Now for small x

$$\tanh x \simeq x$$

so that

$$M = -\frac{Ng\beta}{2}\frac{g\beta H}{2kT}$$

6. Microwave Circuit Design

A few comments on the microwave components needed for electron spin resonance spectrometer will be made here. For this the Maxwell equations are fundamental. The basic equations are

$$\nabla \cdot \underline{D} = \rho \qquad \nabla \cdot \underline{B} = 0$$

$$\nabla \times \underline{E} = -\frac{\partial \underline{B}}{\partial t} \qquad \nabla \times \underline{H} = \underline{J} + \frac{\partial \underline{D}}{\partial t} \tag{9.6.1}$$

$$\underline{D} = \epsilon \underline{E}$$

$$\underline{B} = \mu \underline{H}$$

where

$$\epsilon_0 = \frac{1}{36\pi} \times 10^{-9} \quad \text{farad/m}$$

$$\mu_0 = 4\pi \times 10^{-7} \quad \text{henry/m}$$

As an example we shall consider the rectangular cavity. First consider a wave propagating along the z-axis in a wave

guide. Assume that the medium is non-conducting and neutral. Then

$$\rho = \underline{J} = 0 \tag{9.6.2}$$

Furthermore, for the TE-mode, $E_z = 0$, and if the time dependence is given by $e^{-i\omega t}$

then

$$\nabla \times \underline{E} = i\mu\omega \underline{H}$$

$$\nabla \times \underline{H} = -i\epsilon\omega \underline{E}$$

or

$$-\frac{\partial E_y}{\partial z} = i\mu\omega H_x \tag{9.6.2}$$

$$\frac{\partial E_x}{\partial z} = i\mu\omega H_y \tag{9.6.3}$$

$$\frac{\partial E_y}{\partial x} - \frac{\partial E_x}{\partial y} = i\omega\mu H_z \tag{9.6.4}$$

$$\frac{\partial H_z}{\partial y} - \frac{\partial H_y}{\partial z} = -i\omega\epsilon E_x \tag{9.6.5}$$

$$\frac{\partial H_x}{\partial z} - \frac{\partial H_z}{\partial x} = -i\omega\epsilon E_y \tag{9.6.6}$$

$$\frac{\partial H_y}{\partial x} - \frac{\partial H_x}{\partial y} = -i\omega\epsilon E_z = 0 \tag{9.6.7}$$

and

$$\frac{\partial E_x}{\partial x} + \frac{\partial E_y}{\partial y} = 0 \tag{9.6.8}$$

$$\frac{\partial H_x}{\partial X} + \frac{\partial H_y}{\partial y} + \frac{\partial H_z}{\partial z} = 0 \qquad (9.6.9)$$

The additional condition that the wave is propagating along the z-axis means that all vectors are of the form

$$e^{-i(\omega t - kz)}$$

so that all derivatives with respect to z are to be replaced by ik. From (9.6.2), (.6.3), (9.6.5), and (9.6.6) we find that

$$H_x = -\frac{k}{\omega\mu} E_y \qquad (9.6.10)$$

$$H_y = \frac{k}{\omega\mu} E_x \qquad (9.6.11)$$

$$E_x = \frac{\omega\mu}{i(k^2 - k_0^2)} \frac{\partial H_z}{\partial y} \qquad (9.6.12)$$

$$E_y = -\frac{\omega\mu}{i(k^2 - k_0^2)} \frac{\partial H_z}{\partial X} \qquad (9.6.13)$$

where

$$k_0^2 = \omega^2 \epsilon \mu \qquad (9.6.14)$$

Inserting into (9.6.4) we obtain

$$\frac{\partial^2 H_z}{\partial X^2} + \frac{\partial^2 H_z}{\partial y^2} = (k^2 - k_0^2) H_z$$

As a further simplification, assume that $E_y = 0$. Then

$$H_x = 0$$

so that from (9.6.6)

$$\frac{\partial H_z}{\partial x} = 0$$

$$\frac{\partial^2 H_z}{\partial y^2} = (k^2 - k_0^2) H_z$$

$$H_z = H_0 \left\{ \begin{matrix} \sin \\ \cos \end{matrix} \right\} \sqrt{k_0^2 - k^2}\, y$$

According to boundary conditions at a perfectly conducting surface, the tangential electric field must be zero. This means that

$$E_x = 0 \qquad @ \; y = 0 \;,\; y = a$$

Therefore, according to (9.6.12), we see that

$$H_z = H_0 \cos \sqrt{k_0^2 - k^2}\, y$$

$$E_x = \frac{\omega \mu \sqrt{k_0^2 - k^2}}{i(k^2 - k_0^2)} (-H_0) \sin \sqrt{k_0^2 - k^2}\, y$$

Hence

$$a \sqrt{k_0^2 - k^2} = \pi$$

for the lowest mode. Now

$$k_0^2 = \frac{4\pi^2}{\lambda_0^2} \qquad k^2 = \frac{4\pi^2}{\lambda_g^2}$$

$$\therefore \frac{1}{\lambda_0^2} - \frac{1}{\lambda_g^2} = \frac{1}{4\pi a^2}$$

Cavity resonance is obtained by adding waves along the positive and negative z-direction. Thus

$$H_z = H_z^+ + H_z^-$$

$$= H_0 \cos y\sqrt{k_0^2 - k^2}\,(2i \sin kz)\, e^{-i\omega t}$$

Boundary conditions require E_x to be zero at z = L .

$$\therefore kL = m\pi$$

$$\frac{1}{\lambda_g} = \frac{m}{2L}$$

$$\frac{1}{\lambda_0^2} = \frac{m^2}{4L^2} + \frac{1}{4a^2}$$

7. Electron Nuclear Interaction

The so-called contact electron-nuclear interaction is given by

$$A\, \underline{I} \cdot \underline{S} \tag{7.1}$$

where

$$A = -\frac{8\pi}{3} g_e g_n \beta \beta_n |\psi(0)|^2 \tag{7.2}$$

we shall give a classical derivation of this expression.

For this, we consider the nucleus to be located at the center of a spherically symmetric distribution of electron magnetic matter. Our task then is to calculate the magnetic field due to such a distribution. Suppose then that the electron distribution is such as to give a magnetic moment

density $\underline{M}(r)$, which is a function of the radial distance r only. Furthermore, we shall take the z-axis along the direction of magnetization. Then

$$\underline{M}(r) = M(r)\,\hat{\underline{k}} \tag{7.3}$$

where $\hat{\underline{k}}$ is a unit vector. The equivalent amperian current density $\underline{J}'$ is given by

$$\underline{J}' = \underline{\nabla} \times \underline{M} = \underline{\nabla} \times (M\,\hat{\underline{k}}) = (\underline{\nabla} M) \times \hat{\underline{k}} \tag{7.4}$$

from

$$\nabla \times (u\,\underline{V}) = \underline{\nabla} u \times \underline{V} + u\,\underline{\nabla} \times \underline{V} \tag{7.5}$$

Now, according to Ampere's law, or sometimes called the Biot-Savart's law, the contribution to the magnetic field due to a current element is given by

$$d\underline{H} = \frac{I\,d\underline{s} \times \underline{r}}{|\underline{r}|^3} \tag{7.6}$$

where $\underline{r}$ is a vector pointing from the current element to the point at which the magnetic field is to be evaluated. Generalized to a volume distribution of current, the above expression can be written in the form

$$\underline{H} = \int \frac{\underline{J} \times \underline{r}}{|\underline{r}|^3}\, d\tau \tag{7.7}$$

For our problem, the point of observation is the origin, so that (7.7) can be written

$$\underline{M} = -\int \frac{\underline{J} \times \underline{r}}{|\underline{r}|^3}\, d\tau \tag{7.8}$$

where $\underline{r}$ is now the position vector to the current element.

Now

$$J = \rho \underline{v} = \rho \underline{\omega} \times \underline{r} \tag{7.9}$$

where ω is the angular velocity of the rotating charge. Then

$$\begin{aligned} \underline{H} &= \int \frac{\rho(\underline{\omega} \times \underline{r}) \times \underline{r}}{|\underline{r}|^3} \, d\tau \\ &= -\int \frac{\rho[\underline{r} \cdot \underline{\omega}\, \underline{r} - \omega r^2]}{|r|^3} r^2 \sin\theta \, d\theta \, d\phi \, dr \\ &= -\underline{\omega} \int \rho r (3\cos^2\theta - 1) \sin\theta \, d\theta \, d\phi \, dr \end{aligned} \tag{7.10}$$

$$\therefore \underline{H} = \frac{8\pi}{3} \int \underline{\omega} \rho r \, dr \tag{7.11}$$

But (7.4) and (7.9) we find that

$$\rho \underline{\omega} r = -\frac{d\underline{M}}{dr}$$

$$\therefore \underline{H} = -\frac{8\pi}{3} \int \frac{d\underline{M}}{dr} \, dr$$

$$= -\frac{8\pi}{3} \left[\underline{M}(\infty) - \underline{M}(0) \right] \tag{7.12}$$

So: $$\underline{H} = \frac{8\pi}{3}\underline{M}(0) \tag{7.13}$$

If a nucleus of magnetic moment $\underline{\mu}$ is located in this field, then the energy is

$$E = -\frac{8\pi}{3}\underline{\mu}\cdot\underline{M}(0) \tag{7.14}$$

Now $$\underline{M}(0) = -g_e\beta\underline{S}\,|\psi(0)|^2 \tag{7.15}$$

and $$\underline{\mu} = g_n\beta_n\underline{I} \tag{7.16}$$

$$\therefore\ E = \frac{8\pi}{3}g_e g_n \beta\beta_n |\psi(0)|^2 \underline{I}\cdot\underline{S} \tag{7.17}$$

8. Donor Electron Spin Resonance

A. Single Donor Center

The ESR of donor electrons was first observed by Fletcher et. al.[1] in a sample containing 10^{16} atoms per cm^3, at 4.2°K. The spectrum consists of two lines, separated by 42 gauss, due to the interaction with the nuclear spin I - 1/2 of P^{31} (100%). In samples containing As (I = 3/2), 4 lines separated by 73 gauss were observed.

The most conclusive proof that the spectra are due to donors is provided by antimony-doped silicon. The nuclear

parameters of antimony are tabulated below:

Isotope	Abundance	Spin	Magnetic Moment	gn
Sb^{121}	57.2%	5/2	3.3418	1.3368
Sb^{123}	42.75%	7/2	2.533	.724

Thus the spectrum consists of a set of 2(5/2) + 1 = 6 lines and another set of 2(7/2) + 1 = 8 lines. Since the line separations are proportional to gn, the ratio of the separations in the two sets will be

$$\frac{gn(Sb^{121})}{gn(Sb^{123})} = 1.84$$

The observed separations, 69 and 38 gauss, respectively, give the ratio as 69/38 = 1.82 in good agreement with the prediction.

A donor atom has one more electron in the outer shell than the silicon atom. This extra electron is loosely bound to the donor nucleus so that at normal temperatures, it is free to move about the crystal giving rise to the n-type conductivity. However, as the temperature lowered, the thermal energy of the electron will decrease, so that at sufficiently low temperature, say 4.2°K, the electron will be bound to the donor ion thus forming a center that is reminiscent of a hydrogen atom. There is, however, a difference. For free atoms, the electron charge is confined within a radius of the order of A°. In materials such as Si, for which the dielectric constant is about 13, the electron wave function will be spread out over several atomic

distances. The charge distribution is perhaps as given in the following figure. This figure suggests then that the hyperfine structure of the donor in Si will be appreciably smaller than that of free atom. Also we can expect to observe the interaction of the electron with the nuclear spins of neighboring silicon atoms.

The energy level of the extra electron is found to be in the energy gap just below the conduction band. Since this electron has spin S = $\frac{1}{2}$, the level is doubly degenerate (Ms = $\pm$ 1/2) and will be split in the magnetic field. The spin resonance signal arises from the transition between these levels.

We shall calculate the splitting of the energy levels and show that the line separations are given by the hyperfine structure constant A.

The Hamiltonian for this spin system can be written as

$$\mathcal{H} = g\beta \underline{H} \cdot \underline{S} + A \underline{I} \cdot \underline{S}$$

With the magnetic field H in the z direction, the energy of a particular level specified by M, m is given by

$$E(M,m) = \langle M,m|\mathcal{H}|M,m\rangle$$

$$= g\beta HM + AMm$$

The selection rule for the transitions is

$$\Delta M = \pm 1 \qquad \Delta m = 0$$

hence

$$h\nu = E(M,m) - E(M-1,m)$$
$$= g\beta H + Am$$

for a particular value of m. Or, with fixed microwave frequency ν, the transition will occur at the magnetic field equal to

$$H_m = \frac{1}{g\beta}\left[h\nu - Am\right]$$

The adjacent lines will occur at H equal to

$$H_{m\pm1} = \frac{1}{g\beta}\left[h\nu - A(m\pm1)\right]$$

Thus the separation between the two lines is

$$\Delta H = |H_m - H_{m\pm1}| = \frac{A}{g\beta} = A \text{ (in gauss)}$$

B. Donor Pairs

A close examination of the donor resonance spectrum shows that in addition to the main lines, there exists weaker lines halfway between the main lines. According to the Slichter[2], these weak lines can be attributed to pairs, triples, of donor atoms. His argument is as follows:

The spin Hamiltonian for the interacting pairs of donors can be written in the form,

$$\mathcal{H} = g\beta(\underline{S}_1 + \underline{S}_2)\cdot\underline{H} + J\,\underline{S}_1\cdot\underline{S}_2 + A(I_1 S_1 + I_2 S_2)$$

where the subscripts 1 and 2 refer to the two donors. If $J >> A$ that is, if the electron spins are strongly coupled, as they would be for close pairs, the electron spins form a resultant

$\underline{S}$ given by

$$\underline{S} = \underline{S}_1 + \underline{S}_2 = S_1 + S_2 , S_1 + S_2 - 1, \cdots, |S_1 - S_2|$$

In the case $S_1 = S_2 = 1/2$ we have

$S = 1$ triplet

and

$S = 0$ singlet

The singlet state does not split in the magnetic field and gives no resonance transition. The wave functions for the component of the triplet state can be expressed in terms of the spin functions α and β as follows

$$M = 1 , \quad |+1\rangle = \alpha_1 \alpha_2$$

$$M = 0 , \quad |0\rangle = \frac{1}{\sqrt{2}} [\alpha_1 \beta_2 + \beta_1 \alpha_2]$$

$$M = -1 , \quad |-1\rangle = \beta_1 \beta_2$$

Since $$\underline{S}_1 \cdot \underline{S}_2 = \frac{1}{2} [S^2 - S_1^2 - S_2^2]$$

is a constant within the multiplet of the same S, the term $J \underline{S}_1 \cdot \underline{S}_2$ does not contribute to the energy differences between the levels and can be dropped in the following discussion. Then, the energies are

$$M=1\ ,\quad E(1,m_1,m_2)=g\beta H+\tfrac{1}{2}A(m_1+m_2)$$

$$M=0\ ,\quad E(0,m_1,m_2)=0$$

$$M=-1\ ,\quad E(-1,m_1,m_2)=-g\beta H-\tfrac{1}{2}A(m_1+m_2)$$

or in general,

$$E(M,m_1,m_2)=g\beta HM+\frac{1}{2}AM(m_1+m_2)$$

The energy levels for the case $I_1 = I_2 = 1/2$ are shown below.

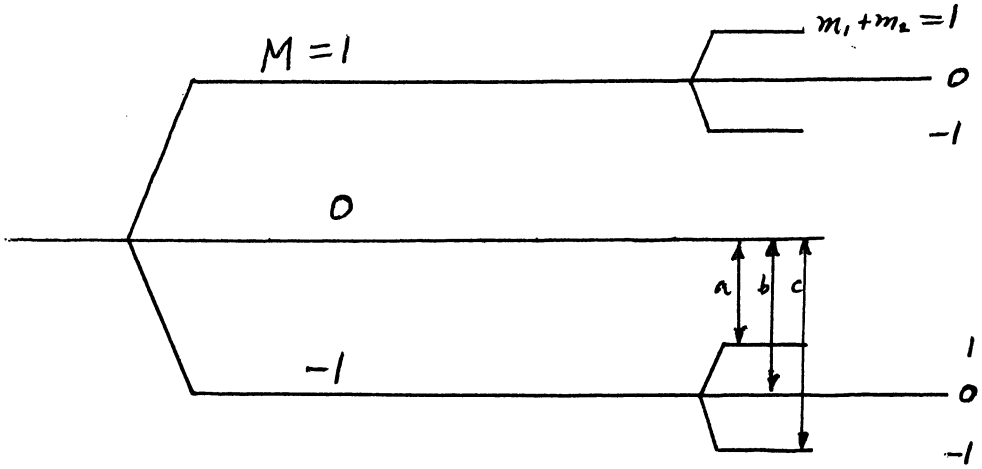

The level with $m_1 + m_2 = 0$ is drawn twice long showing that the statistical weight of this level is twice those of the other levels, stemming from the fact that $m_1 + m_2 = 0$ is obtained for $m_1 = +1/2$, $m_2 = -1/2$, and $m_1 = -\frac{1}{2}$, $m_2 = \frac{1}{2}$

The transitions a, b, c, occur respectively at the magnetic fields

$$H_a = \frac{1}{g\beta}\left(h\nu + \frac{1}{2}A\right)$$

$$H_b = \frac{1}{g\beta}\left(h\nu\right)$$

$$H_c = \frac{1}{g\beta}\left(h\nu - \frac{1}{2}A\right)$$

The line b is twice as intense as line a and c. The spacing between a and c is A (in gauss), thus these two lines coincide with those of the single donor center.

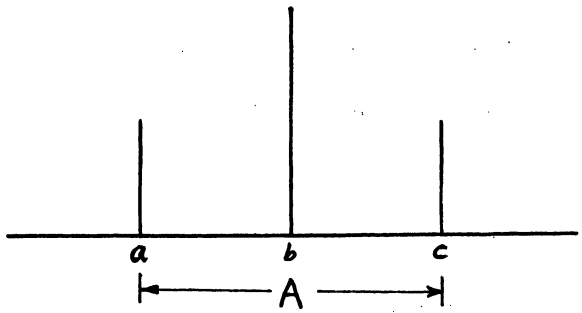

In the same way, one can show that for a pair of donors with I = 3/2, there will 4I + 1 = 7 lines with relative intensities 1:2:3:4:3:2 = 1. The four lines with relative intensities 1 and 3 coincide and are masked by the four lines of the single donor.

These predictions are confirmed experimentally by Feher, Flitcher and Gere[3].

REFERENCES (for 8)

1. R. C. Fletcher, et. al., Phys. Rev. 94, 1392; 95, 844 (1954).

2. C. P. Slichter, Phys. Rev. 99, 479 (1955).

3. G. Feher et. al., Phys. Rev. 100, 1784 (1955).

9. Paramagnetic Resonance Centers in Irradiated Silicon

A. General Feature

Irradiation by nuclear radiation of silicon leads under certain circumstances to the formation of paramagnetic centers. The centers produced by electron irradiation were first reported by Bemski[1] and Watkins and Corbett[2], those produced by fast neutron irradiation were discussed by Nisenoff and Farr[3].

In case of electron irradiation, 9.5 1 Mev electrons from Van de Graff accelerator were used. The radiation dose was $10^{15} \sim 10^{17}$ electrons/cm^2.

The graphite reactor at Oak Ridge and the CP-5 reactor at Argonne were used in the neutron irradiation. The fast neutron flux was $10^{17} \sim 10^{19}$ nvt.

With the increase in the radiation dose, the donor electron decreases and finally disappears. At the same time, new lines appear and increase in the intensities. The spectra are different for different temperatures of the irradiation and different ways by which the silicon crystals are grown (pulled from melt in the presence of air or vacuum floating zone method). Most of the centers can be annealed at high temperatures. ($\sim$ 200°C).

In the following, we shall discuss in detail, the so-called A center* which is produced in N type pulled silicon by electron irradiation.

B. A Center

A Summary of the experimental results:

---

*Also called Si-B1 center in recent literature

(1) Observed in 0.1 - 1 pulled N type silicon by electron bombardment.

(2) Not observed in vacuum floating zone silicon. This suggests that the center involves the oxygen impurity atoms.

(3) Low temperature (90°K) irradiation gives signal one order of magnitude weaker than room temperature irradiation. This implies that the defect is not a primary defect from the irradiation but is created by the thermal motion of the primary defects.

(4) The signal grows linearly as the donor resonance decreases, until the latter has disappeared. At this point it begins to decrease at approximately 1/20 the initial rate of rise. This implies that the centers trap electrons which are originally bound at the donor levels. The decrease of the signal at high irradiation dose is believed to be due to the production of deeper lying acceptor levels.

(5) The intensities of the hyperfine structure lines indicate that the trapped electron interacts with two silicon nucleus equivalently.

(6) The spectrum is angular dependent. Based upon the above results, Watkins, et. al. suggested a model for A center as a silicon vacancy trapped with an oxygen atom. The two of the four broken bonds of the silicons next to the vacancy form bonds with the

oxygen by supplying one electron each. The other two broken bonds pull together to form a weak bond. An electron trapped in the antibonding orbital of this bond is responsible for the paramagnetic resonance. (See the Figure below).

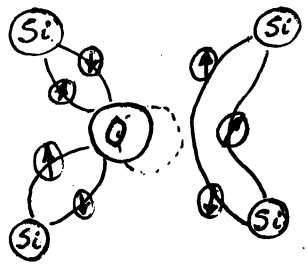

To determine the angular dependence of the spectrum to be expected from such a model, we calculate the g values of the center with the magnetic field in different directions.

The spin Hamiltonian for the center can be written as

$$\mathcal{H} = \beta \underline{H} \cdot \underline{\underline{g}} \cdot \underline{S} + \sum_n I_n \cdot \underline{\underline{A}}_n \cdot \underline{S}$$

In general, $\underline{\underline{g}}$ and $\underline{\underline{An}}$ are tensors of rank two. Usually the first term is much larger than the second, so, let us consider only the first term now.

In a coordinate system in which the g tensor is diagonal, we have

$$\mathcal{H} = \beta \underline{H} \cdot \underline{\underline{g}} \cdot \underline{S}$$

$$= \beta \left[H_x g_x S_x + H_y g_y S_y + H_z g_z S_z \right]$$

In a system with S = 1/2.

The splitting of the degenerate levels M = ± 1/2 by this Hamiltonian can be calculated by the secular equation

$$\begin{vmatrix} \langle \tfrac{1}{2}|\mathcal{H}|\tfrac{1}{2}\rangle - E & \langle \tfrac{1}{2}|\mathcal{H}|-\tfrac{1}{2}\rangle \\ \langle -\tfrac{1}{2}|\mathcal{H}|\tfrac{1}{2}\rangle & \langle -\tfrac{1}{2}|\mathcal{H}|-\tfrac{1}{2}\rangle - E \end{vmatrix} = 0$$

which reads, in this case,

$$\begin{vmatrix} \tfrac{1}{2}\beta H_z g_z - \Delta E & \tfrac{1}{2}\beta (H_x g_x - i H_y g_y) \\ \tfrac{1}{2}\beta (H_x g_x + i H_y g_y) & -\tfrac{1}{2}\beta H_z g_z - \Delta E \end{vmatrix}$$

The solutions are

$$\Delta E_{\pm} = \pm \tfrac{1}{2}\beta \sqrt{H_x^2 g_x^2 + H_y^2 g_y^2 + H_z^2 g_z^2}$$

$$= \pm \tfrac{1}{2}\beta H \sqrt{g_x^2 \cos^2\alpha + g_y^2 \cos^2\beta + g_z^2 \cos^2\gamma}$$

where $\cos\alpha$, $\cos\beta$, and $\cos\gamma$ are the direction cosines of the magnetic field along the three principal axes of the g tensor. If we denote the shift in energy ΔE by

$$\Delta E_{\pm} = \pm \tfrac{1}{2} g \beta H$$

Then

$$g = \sqrt{g_x^2 \cos^2\alpha + g_y^2 \cos^2\beta + g_z^2 \cos^2\gamma}$$

The coordinate system in which g tensor is diagonal can be found by considering the symmetry of the center. As is shown in the figure below, there is a two-fold rotation axis along the intersection of the plane containing Si-O-Si triangle and the other diagonal plane containing the rest of silicon atoms. This axis is taken as the z axis. The x axis is taken in the plane of Si-O-Si triangle and perpendicular to the z axis. The y axis is then in the other diagonal plane. The two diagonal planes are the planes of reflection symmetry.

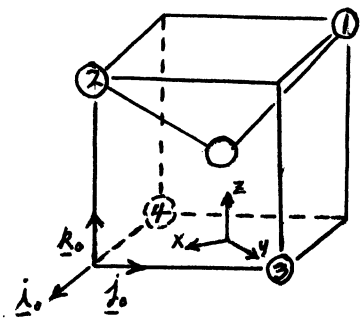

Now we must note that there are six different orientations for the plane Si-O-Si. If we denote a particular orientation by the two numbers assigned to the silicon atoms which bond to the oxygen, then the six orientations are 12, 13, 14, 23, 24, and 34.

The direction cosines of the principal axes of g tensor with respect to the crystal axes, $\underline{i}_o$, $\underline{j}_o$ and $\underline{k}_o$, (see the above figure) are:

(12)

	$\underline{i}_0$	$\underline{j}_0$	$\underline{k}_0$
$\underline{i}$	$\frac{1}{\sqrt{2}}$	$-\frac{1}{\sqrt{2}}$	0
$\underline{j}$	$\frac{1}{\sqrt{2}}$	$\frac{1}{\sqrt{2}}$	0
$\underline{k}$	0	0	1

(23)

	$\underline{i}_0$	$\underline{j}_0$	$\underline{k}_0$
$\underline{i}$	0	$\frac{1}{\sqrt{2}}$	$-\frac{1}{\sqrt{2}}$
$\underline{j}$	0	$\frac{1}{\sqrt{2}}$	$\frac{1}{\sqrt{2}}$
$\underline{k}$	1	0	0

(13)

	$\underline{i}_0$	$\underline{j}_0$	$\underline{k}_0$
$\underline{i}$	$\frac{1}{\sqrt{2}}$	0	$-\frac{1}{\sqrt{2}}$
$\underline{j}$	$-\frac{1}{\sqrt{2}}$	0	$-\frac{1}{\sqrt{2}}$
$\underline{k}$	0	1	0

(24)

	$\underline{i}_0$	$\underline{j}_0$	$\underline{k}_0$
$\underline{i}$	$\frac{1}{\sqrt{2}}$	0	$\frac{1}{\sqrt{2}}$
$\underline{j}$	$\frac{1}{\sqrt{2}}$	0	$-\frac{1}{\sqrt{2}}$
$\underline{k}$	0	1	0

(14)

	$\underline{i}_0$	$\underline{j}_0$	$\underline{k}_0$
$\underline{i}$	0	$\frac{1}{\sqrt{2}}$	$\frac{1}{\sqrt{2}}$
$\underline{j}$	0	$-\frac{1}{\sqrt{2}}$	$\frac{1}{\sqrt{2}}$
$\underline{k}$	1	0	0

(25)

	$\underline{i}_0$	$\underline{j}_0$	$\underline{k}_0$
$\underline{i}$	$\frac{1}{\sqrt{2}}$	$\frac{1}{\sqrt{2}}$	0
$\underline{j}$	$-\frac{1}{\sqrt{2}}$	$\frac{1}{\sqrt{2}}$	0
$\underline{k}$	0	0	1

The components of the magnetic field are

$H \sin\theta \cos\phi$; $H \sin\theta \sin\phi$, and $H \cos\theta$

where θ and ϕ are the polar angles with respect to ($\underline{i}_0$, $\underline{j}_0$, $\underline{k}_0$). Thus with the magnetic field in a general direction, we expect to see six resonance lines corresponding to the six different g values of the six different orientations. But with H in some, special directions, the number of the lines is reduced. For example, if H is in the (110) plane, i.e.

$\phi = -45°$,

$$\underline{H} = H\left(\frac{1}{\sqrt{2}}\sin\theta, -\frac{1}{\sqrt{2}}\sin\theta, \cos\theta\right)$$

the direction cosines $\cos\alpha$, $\cos\beta$, and $\cos\gamma$ for the orientation (12) are

$$\cos\alpha = \sin\theta \; ; \; \cos\beta = 0 \; ; \; \cos\gamma = \cos\theta$$

Hence,

$$g_{12} = \sqrt{g_x^2 \sin^2\theta + g_z^2 \cos^2\theta}$$

Similarly, we have

$$g_{13} = g_{14} = \left[g_x^2\left(\frac{1}{2}\sin\theta - \frac{1}{\sqrt{2}}\cos\theta\right)^2 + g_y^2\left(-\frac{1}{2}\sin\theta - \frac{1}{\sqrt{2}}\cos\theta\right)^2 + g_z^2\left(\frac{1}{\sqrt{2}}\sin\theta\right)^2\right]^{1/2}$$

$$g_{23} = g_{24} = \left[g_x^2\left(-\frac{1}{2}\sin\theta - \frac{1}{\sqrt{2}}\cos\theta\right)^2 + g_y^2\left(-\frac{1}{2}\sin\theta + \frac{1}{\sqrt{2}}\cos\theta\right)^2 + g_z^2\left(\frac{1}{\sqrt{2}}\sin\theta\right)^2\right]^{1/2}$$

$$g_{34} = \sqrt{g_y^2 \sin^2\theta + g_z^2 \cos^2\theta}$$

Thus, with H in a general direction in (110) plane, (13) and (14) are equivalent, and so are (23) and (24). The equivalent centers have the same g values and resonate at the same magnetic field. Hence the number of lines reduces to four, with relative intensities 1:2:2:1.

With H in [001] direction, i.e. $\theta = 0$, we can show that

$$g_{12} = g_{34} = g_z$$

$$g_{13} = g_{14} = g_{23} = g_{24} = \frac{1}{\sqrt{2}}\left(g_x^2 + g_y^2\right)^{1/2}$$

Hence we expect two lines with intensity ratio 1:2, the less intense line gives the value of g_z.

With H in [1$\bar{1}$0] direction, i.e. $\theta = 90°$, we have

$$g_{12} = g_x$$

$$g_{34} = g_y$$

$$g_{13} = g_{14} = g_{23} = g_{24} = \left[\frac{1}{4}\left(g_x^2 + g_y^2\right) + \frac{1}{2}g_z^2\right]^{1/2}$$

The number of lines is four with relative intensities 1:1:4. The weaker lines give the value of g_x and g_y. The measured values are:

g_x = 2.0096		2.0098	
g_y = 2.0019	(Bemski)	2.0025	(Watkins, et al.)
g_z = 2.0029		2.0031	

Now, let us come back to the second term of the spin Hamiltonian - the hyperfine structure term.

$$\mathcal{H}_{HF} = \sum_n \underline{I}_n \cdot \underline{\underline{A}}_n \cdot \underline{S}$$

According to the model, the electron interacts with two of the four Si nuclei equally and strongly. Let's call these two nuclei 1 and 2, i.e.

$$A_1 = A_2 \gg A_3 = A_4$$

Thus if we retain only the largest terms in the summation,

$$\mathcal{H}_{HF} = A\left(\underline{I}_1 + \underline{I}_2\right)\cdot\underline{S}$$

where I_1 and I_2, the nuclear spins of Si-1 and Si-2, are

0 for Si^{28}, (95.3% abundance)

1/2 for Si^{29}, (4.7% abundance)

The energy shift by $\mathcal{H}_{HF}$ is

$$\langle M, m_1+m_2 \mid \mathcal{H}_{HF} \mid M, m_1+m_2 \rangle = A M (m_1 + m_2)$$

where $m_1 + m_2$ can take the values $\pm$ 1, $\pm$ 1/2 and 0, with the relative probabilities:

m_1+m_2	Probability
$\pm$ 1	$(.047)^2 = 5.52 \times 10^{-4} \sim .055$
$\pm$ 1/2	$2(.953)(.047)1/2 = 448 \times 10^{-4} \sim 4.5$
0	$(.953)^2 + (.047) = 9093 \times 10^{-4} \sim 91$

The energy level diagram and the expected spectrum with relative intensities are shown below

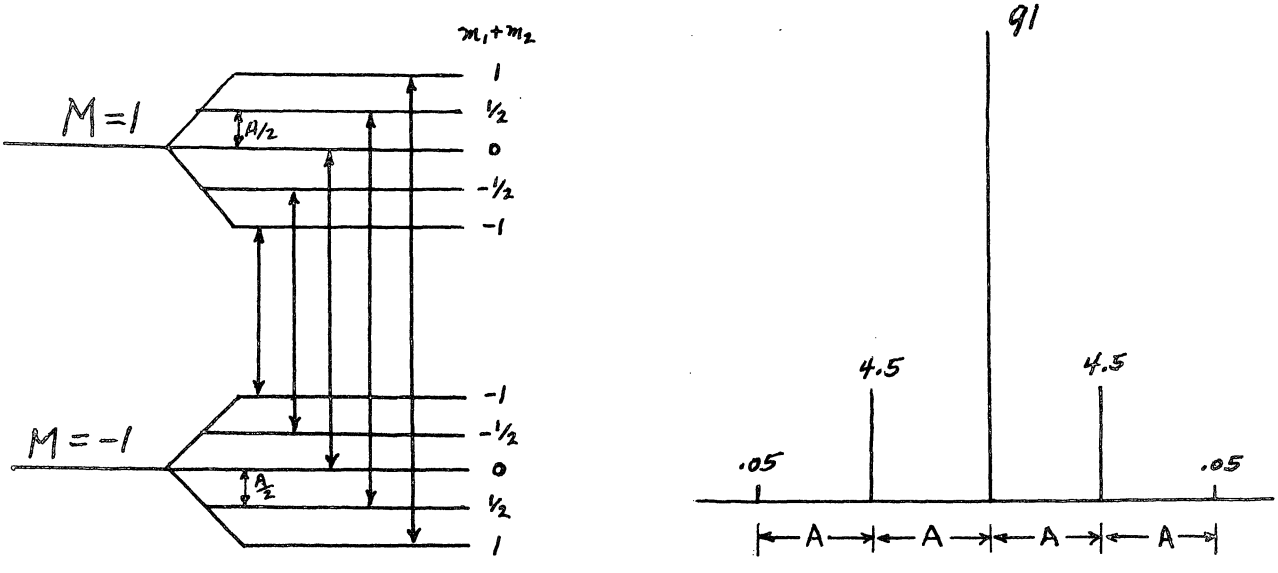

This hyperfine structure with the relative intensities agree with the experimental results, confirming the model of Watkins and Corbett.

Many other paramagnetic centers in irradiated Si have been reported. Among these, the most studied are:

(1) E-center, observed in electron irradiated N type vacuum floating zone silicon[4].

(2) J- and C-centers, are the positively and negatively charged states, respectively, of a divacancy[5]. J-center is observed in P type silicon and C-center is observed in high resistivity material.

REFERENCE (9)

1. G. Bemski, J. Appl. Phys. 30, 1195 (1959).

2. G. D. Watkins and J. W. Corbett, Phys. Rev. 121, 1001, (1961); J. Appl. Phys. 30, 1198 (1959).

3. M. Nisenoff, and H. Y. Fan, Phys. Rev. 128, 1605 (1962).

4. G. D. Watkins and J. W. Corbett, Phys. Rev. 134, A1359 (1964).

5. J. W. Corbett and G. D. Watkins: Phys. Rev. Letters, 7, 314, (1961), Phys. Rev. (to be published).

10. Infrared Absorption and Oxygen Content

Investigations on the role of oxygen on the infrared absorption of silicon have been carried out by W. Kaiser, P. H. Keck, and C. F. Lange, Phys. Rev. 101, 1264 (February 15, 1956); H. J. Hrostowski and R. H. Kaiser, Phys. Rev. 107, 966 (August 15, 1957), and others. Some of the crucial experiments are as follows:

(1) Silicon was crystallized by the floating zone technique which requires no quartz crucible. Absorption measurements showed that the g absorption was greatly reduced.

(2) The absorption increased greatly when melted for 20 minutes in oxygen at 1 mm of Hg pressure.

(3) Water enriched in O^{18} (12%) was introduced during the process of preparing samples by the zone-floating process. New absorption bands developed, which could be assigned to the Si-O bond stretching vibration. At 4.2°K, absorption bands were observed at 1135.5 cm^{-1} and at 1084.6 cm^{-1}. The ratio of the two bands is 1.047. The vibration frequency ratio obtained by assuming that the bands are due to the V_3 bond stretching vibrations of the $Si-O^{16}-Si$ and $Si-O^{18}-Si$ pseudomolecule was found to be 1.04. From these, it was concluded that the oxygen with two silicon atoms form a complex resembling a water molecule.

The purpose of the following discussion is to give the theory for the molecular vibrations of the bent triatomic molecule, such as H_2O molecule and the Si_2O complex.

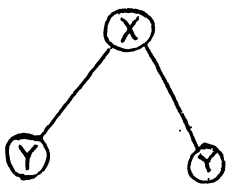

Consider then the molecule xy_2, we shall assume the constituent atoms of the molecule are vibrating about their equilibrium positions with a small amplitude. The contributions of these vibrations to the potential energy of the molecule can be obtained by making a Taylor expansion of the potential function about the equilibrium positions. Then the leading terms aside from a constant, will that are quadratic functions of the displacement. For our problem, since there are three atoms, potential energy increase will depend upon 9 coordinates. Of these 6 can be eliminated because 6 relations can be written down for the non-rotating molecule not having any net transition. Thus there will be only three vibrational modes. Our first task is to determine the nature of these modes.

Suppose then the center of mass motion and the rotations have been eliminated. The the Hamiltonian can be written in the form

$$\mathcal{H} = \frac{1}{2} \sum_{i=1}^{3} M_i \dot{Q}_i^2 + \frac{1}{2} \sum_{i,j=1}^{3} V_{ij} Q_i Q_j \qquad (10.1)$$

According to a well-known theorem (see, for example, Margenan and Murphy, The Mathematics of Physics and Chemistry), by

taking a linear combination of the Q's , say

$$\xi_\alpha = \sum N_{\alpha i} Q_i \qquad (10.2)$$

called the normal coordinates, by means of which (10.1) can be put into the form

$$\mathcal{H} = \frac{1}{2} \sum_{\alpha=1}^{3} \left(\dot{\xi}_\alpha^2 + \omega_\alpha^2 \xi_\alpha^2 \right) \qquad (10.3)$$

Now the above is the Hamiltonian for a molecular system in which the two atoms are indistinguishable. That is, any operation which leaves the particles unchanged or switches the two atoms should have no effect upon the Hamiltonian. In other words the Hamiltonian must be invariant under the group of such operations. This group, for the XY_2 bent molecule, is designated often by C_{2v} . If the plane of the molecule on equilibrium is taken to be the xz-plane, then the operations of this group are E the identity;

$C_2(z)$, the 180° rotation about the z-axis;

$\sigma(x,z)$, the reflection in the xz-plane; and

$\sigma(yz)$, the reflection in the yz-plane.

The character table for this group is as follows:

	E	$C_2(z)$	$\sigma(x,z)$	$\sigma(y,z)$	
A_1	1	1	1	1	T_z
A_2	1	1	-1	-1	R_z
B_1	1	-1	1	-1	T_x, R_y
B_2	1	-1	-1	1	T_y, R_x

This table then shows that if any of the symmetry operations are carried out on the q_α's , such normal coordinates for the molecule will remain unchanged or at most change sign.

To determine the normal modes of vibration, consider then the transformation T that gives the normal coordinates, the translations, and the rotations. Also to shorten the writing we shall put

$$X_1 , X_2 , X_3 , Y_1 = X_4 , Y_2 = X_5 , \cdots , Z_3 = X_9$$

and

$$q_4 = X_1 + X_2 + X_3 \qquad q_5 = Y_1 + Y_2 + Y_3 \qquad q_6 = Z_1 + Z_2 + Z_3$$

$$\begin{aligned} q_7 &= \omega_Y (Z_1 + Z_2 + Z_3) - \omega_Z (Y_1 + Y_2 + Y_3) \\ q_8 &= \omega_Z (X_1 + X_2 + X_3) - \omega_X (Z_1 + Z_2 + Z_3) \\ q_9 &= \omega_X (Y_1 + Y_2 + Y_3) - \omega_Y (X_1 + X_2 + X_3) \end{aligned} \tag{10.4}$$

Then we can write the matrix equation

$$q = T X \tag{10.5}$$

Consider next the symmetry operation S of the group C_{2v} on x and q .

$$X' = SX = M_S' X \tag{10.6}$$

$$q' = Sq = M_S'' q \tag{10.7}$$

where M_S' and M_S'' are the matrices generated when the

symmetry operation S is applied to the column vectors X and g respectively. It is clear that the two matrices in general will be different, but according to (10.5) the two are related by

$$M_S'' = T\, M_S'\, T^{-1} \tag{10.8}$$

so that

$$T_n\, M_S'' = T_n\, M_S' \tag{10.9}$$

Now the group character table gives the traces of the matrices representing the symmetry operation. Consequently the normal vibration modes, each being associated with an irreducible representation of the group, can be readily obtained by examining the traces of the matrices M_S' . Clearly our problem would have been an impossible one if we had to depend upon the matrices which cannot be determined until the problem has been solved. The matrices M_S', on the other hand, can be easily constructed.

To obtain the normal modes, or what is the same thing as the irreducible representation, we need to compute the traces of the matrices representing E, C_2 , $\sigma(xz)$, and $\sigma(yz)$. The trace of the $M(E)$ is 9. For the trace, or the character we shall use the symbol χ. Thus

$$\text{for} \quad M(E) \quad ; \quad \chi(E) = 9$$

Consider next the operation C_2 . For this clearly

x	⟶	-x	1	⟶	1
y	⟶	-y	2	⟶	3
z	⟶	z	3	⟶	2

where 2 and 3 designate the two y atoms. Then

$x_1 \longrightarrow -x_1$	$x_2 \longrightarrow -x_3$	$x_3 \longrightarrow -x_2$
$y_1 \longrightarrow -y_1$	$y_2 \longrightarrow -y_3$	$y_3 \longrightarrow -y_2$
$z_1 \longrightarrow z_1$	$z_2 \longrightarrow z_3$	$z_3 \longrightarrow z_2$

so that $\chi(C_2) = -1$

For $\sigma(xz)$

x	⟶	x	1	⟶	1
y	⟶	-y	2	⟶	2
z	⟶	z	3	⟶	3

$$\therefore \chi(\sigma(x,z)) = +3$$

and for $\sigma(yz)$

x	⟶	-y	1	⟶	1
y	⟶	y	2	⟶	3
z	⟶	z	3	⟶	2

$$\therefore \chi(\sigma(y,z)) = +1$$

Comparison of the set of numbers

	E	C_2	$\sigma(z,x)$	$\sigma(z,y)$
χ	9	-1	3	-1

with the group character table shows that this set can be obtained by

$$\chi = 3A_1 + A_2 + 3B_1 + 2B_2 \tag{10.10}$$

But the translations x, y, and z transform as B_1, B_2, and A_1, and the rotations R_x, R_y, R_z as B_2, B_1, and A_2. Consequently the vibrations transform as

$$2A_1 + B_1 \tag{10.11}$$

Having ascertained the symmetry of the modes, we next need to introduce the coordinates. For this we shall introduce the so-called "symmetry coordinates". The two coordinates of symmetry A_1 and one coordinate of symmetry B_1 can be constructed as follows:

S_1:

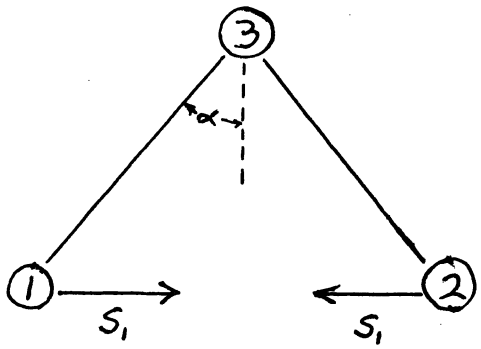

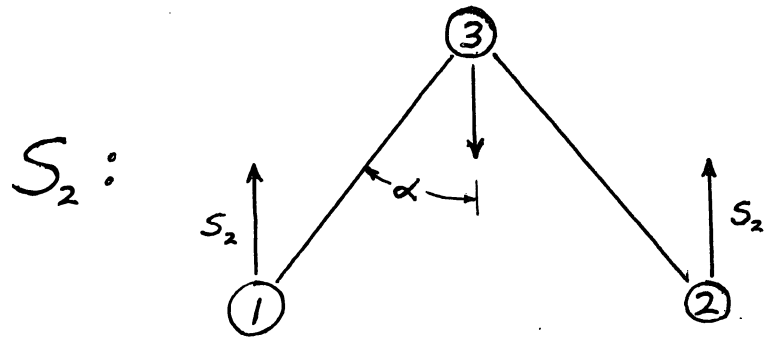

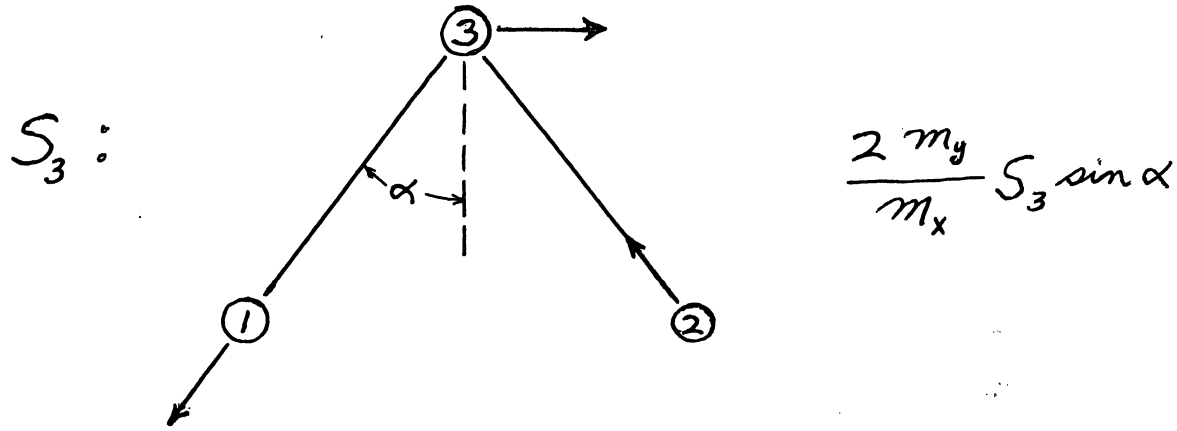

It is to be noted that these coordinates are constructed by giving a displacement to one particle, and the displacements of the remaining particles determined that there is no motion of the center of mass and no rotation of the molecule as a whole. The particles 1 and 2 have masses m_Y and particle 3 has the mass m_X . By inspection it is clear that S_1 and S_2 have the symmetry of A_1 and S_3 has the symmetry of B_1. Using these coordinates the potential and the kinetic energies can be written in the form

$$2V = C_{11} S_1^2 + 2 C_{12} S_1 S_2 + C_{22} S_2^2 + C_{33} S_3^2 \tag{10.12}$$

and

$$2T = d_{11} \dot{S}_1^2 + 2 d_{12} \dot{S}_1 \dot{S}_2 + d_{22} \dot{S}_2^2 + d_{33} \dot{S}_3^2 \tag{10.13}$$

These lead to the secular determinant

$$\begin{vmatrix} C_{11} - \lambda d_{11} & C_{12} - \lambda d_{12} & 0 \\ C_{21} - \lambda d_{21} & C_{22} - \lambda d_{22} & 0 \\ 0 & 0 & C_{33} - \lambda d_{33} \end{vmatrix} = 0 \tag{10.14}$$

so that

$$C_{33} - \lambda d_{33} = 0$$

and

$$\lambda_3 = 4\pi^2 \nu_3^2 = \frac{C_{33}}{d_{33}} \tag{10.15}$$

From the geometry of the symmetry coordinates, it is clear that

$$\begin{aligned} X_1 &= S_1 - S_3 \sin\alpha & Y_1 &= S_2 - S_3 \cos\alpha \\ X_2 &= -S_1 - S_3 \sin\alpha & Y_2 &= S_2 + S_3 \cos\alpha \\ X_3 &= \frac{2 m_Y}{m_X} S_3 \sin\alpha & Y_3 &= -\frac{2 m_Y}{m_X} S_2 \end{aligned} \tag{10.16}$$

Then

$$2T = m_Y\left(\dot{X}_1^2 + \dot{Y}_1^2 + \dot{X}_2^2 + \dot{Y}_2^2\right) + m_X\left(\dot{X}_3^2 + \dot{Y}_3^2\right)$$

$$= m_Y\left(2\dot{S}_1^2 + 2\dot{S}_2^2 + 2\dot{S}_3^2\right)$$

$$+ m_X\left(\dot{S}_3^2\,\frac{4m_Y^2}{m_X^2}\sin^2\alpha + \frac{4m_Y^2}{m_X^2}\,\dot{S}_2^2\right) \qquad (10.17)$$

Comparing (10.13) and (10.17) we obtain

$$d_{11} = 2m_Y$$

$$d_{22} = 2\left(1 + \frac{2m_Y}{m_X}\right)m_Y \equiv 2\rho\, m_Y$$

$$d_{33} = 2\left(1 + \frac{2m_Y}{m_X}\sin^2\alpha\right)m_Y \equiv 2m_Y r \qquad (10.18)$$

$$d_{12} = d_{13} = d_{23} = 0$$

The symmetry coordinates can be expressed in terms of the change in the bond lengths from the equilibrium values, i.e.

$$V = \frac{1}{2}\sum a_{ij}\,Q_i\,Q_j \qquad (10.19)$$

where

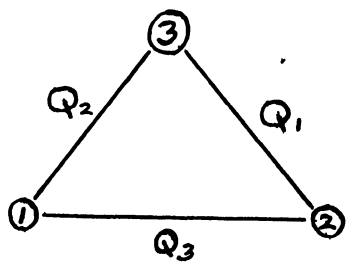

where Q_1, Q_2, and Q_3 are the changes in the bond lengths opposite particles, 1, 2, and 3. If we consider

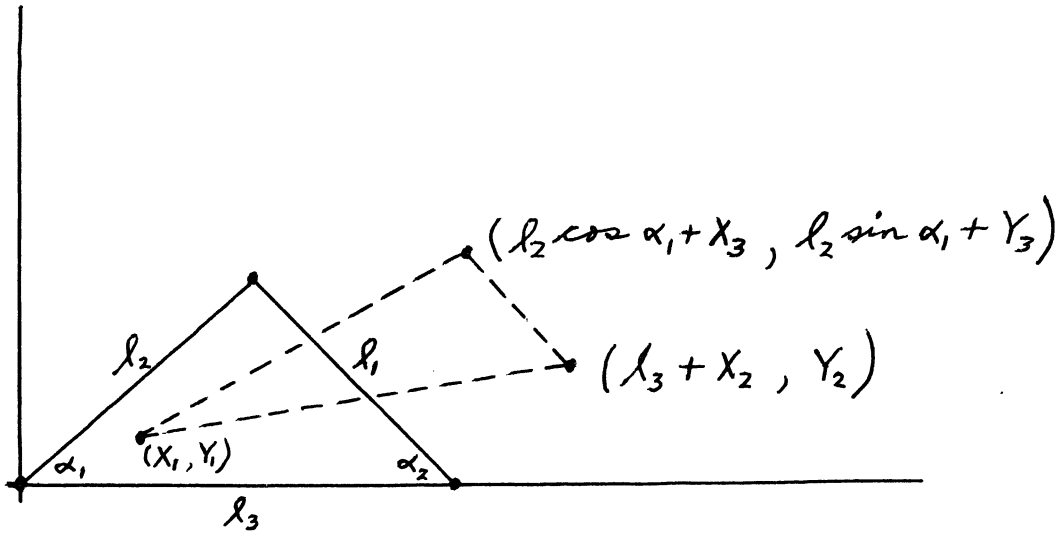

then

$$Q_1 = (X_2 - X_3)\cos\alpha_2 + (Y_3 - Y_2)\sin\alpha_2$$

$$Q_2 = (X_3 - X_1)\cos\alpha_1 + (Y_3 - Y_1)\sin\alpha_1 \qquad (10.20)$$

$$Q_3 = X_2 - X_1$$

Also from the symmetry coordinates, we find that

$$Q_1 = -\sin\alpha\, S_1 - p\cos\alpha\, S_2 - r\, S_3$$

$$Q_2 = -\sin\alpha\, S_1 - p\cos\alpha\, S_3 + r\, S_3 \qquad (10.21)$$

$$Q_3 = -2\, S_1$$

From (10.12), (10.19), and (10.21) we find that

$$C_{33} = 2r^2(a_{11} - a_{12})$$

$$\therefore \lambda_3 = 4\pi^2\nu_3^2 = \frac{2r^2(a_{11} - a_{12})}{2 m_Y r} \qquad (10.22)$$

$$= \left(\frac{1}{m_Y} + \frac{2}{m_X}\sin^2\alpha\right)(a_{11} - a_{12}) \qquad (10.23)$$

Assuming that the angle for Si_2O^{16} and Si_2O^{18} are equal, we find then for the ratio of the bond-stretching vibration frequencies

$$\frac{\nu_3^2(O^{16})}{\nu_3^2(O^{18})} = \frac{m(O^{18})}{m(O^{16})} \frac{16 + 2(28)\sin^2\alpha}{18 + 56\sin^2\alpha}$$

Taking

$$Si - O = 1.6\ \text{Å}$$

$$Si - Si = 2.34\ \text{Å}$$

we find that

$$2\alpha = 110^\circ$$

so that the calculated frequency is 1.04. This is to be compared with the measured value of 1.07.

CHAPTER X

SIMPLIFIED TRANSPORT THEORY IN SOLIDS

I. Introduction

The purpose of this discussion is to provide physical and the theoretical background for the Pem effect and to point out its relation to several other closely related effects.

The objective is to make a systematic investigation of the factors that contribute to the sensitivity of the PEM detector to infrared radiation for the purpose of determining the ultimate capacilities of such detectors. Theory shows that the PEM signal depends upon (a) surface recombination velocity, (b) carrier mobilities, and (c) bulk lifetime.

II. PEM Effect

This can be called the photodiffusion current Hall effect and is one of the transverse galvanomagnetic effects. As shown by the accompanying sketch, Fig. 1, the photons impinging upon the crystal are absorbed at or near the surface. Each

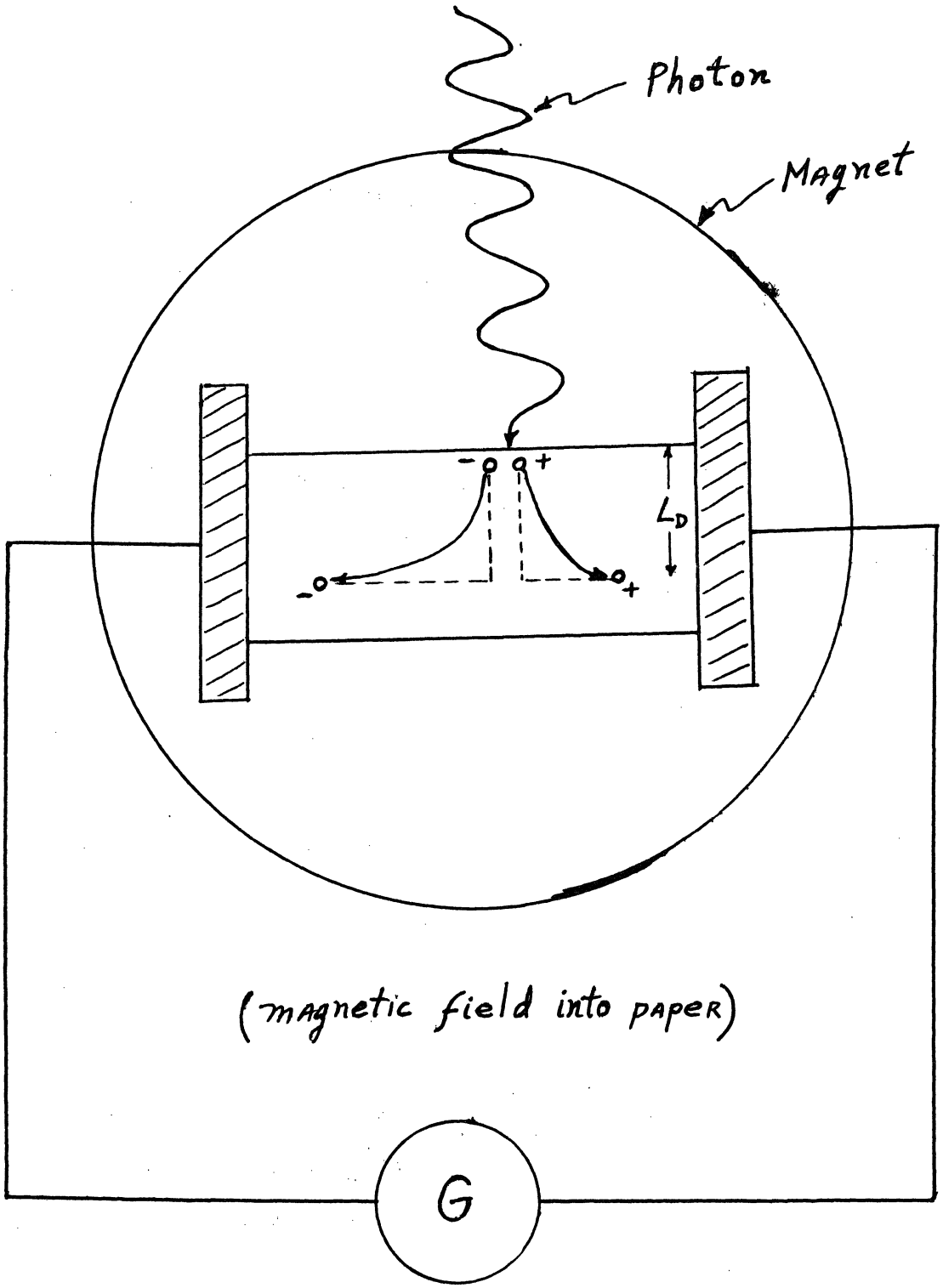

Fig. 1

Schematic Representation of the PEM Effect

photon thus absorbed creates an electron-hole pair. The excess concentration of electrons and holes near the illuminated surface gives rise to a diffusion current of each carrier type toward the opposite, unilluminated surface. If the crystal is located in a magnetic field normal to the diffusion current, the electrons and holes will be deflected in opposite directions, as shown in the sketch. The path of the electron is indicated as being longer because of its greater mobility. If the current is measured with a low-resistance device, the signal is called the short-circuit current; if by a high-resistance device, the open circuit voltage.

By the following physical arguments we can obtain an estimate of the PEM signal to be expected. If the magnetic field were not present, the electrons and holes would on the average travel a distance equal to the diffusion length, L_D, away from the illuminated surface before recombining. However, in a magnetic field the charge carriers will be deflected laterally, the deflections being given by the product of the diffusion length and tangents of the respective Hall angles. The charges induced at the electrodes will then be

$$\frac{e}{l}\left(\mu_n + \mu_p\right) B L_D \qquad (1.1)$$

where the symbols have the following meaning:

e = electron charge

l = crystal length, distance between electrodes

μ_n , μ_p = electron and hole mobilities

B = magnetic field

If the photon intensity is Q and A the illuminated area, and further if the quantum efficiency is assumed to be unity with no surface recombination before diffusion, we obtain

$$\text{PEM signal} = \frac{QAe}{l}(\mu_n + \mu_p) B L_D \tag{1.2}$$

$$= \frac{QAe}{l}(\mu_n + \mu_p) B \sqrt{D_a \tau} \tag{1.3}$$

since

$$L_D = \sqrt{D_a \tau} \tag{1.4}$$

where τ and D_a are the bulk lifetime and the ambipolar (effective) diffusion coefficient respectively. If the values

$Q \sim 10^{18}$ photons/m^2 sec.

$\mu_n \sim 1 m^2$/volt sec.

$L_D \sim 50 \times 10^{-6}$ m

$B \sim 1$ weber/m^2

width $\sim 10^{-3}$ m

are substituted into Eq. (1.2) we obtain for the estimated signal

PEM signal $\sim$ 0.005 microamp.

III. Transport Equations

A rigorous derivation of the basic relations can be obtained from the basic algebraic and differential relations. The carrier transport equations are given by

$$\vec{j}^{\,p} = -eD_p \nabla p + ep\mu_p \vec{E} + \mu_p \vec{j}^{\,p} \times \vec{B} \tag{2.1}$$

for the holes and

$$\vec{j}^{\,n} = eD_n \nabla n + en\mu_n \vec{E} - \mu_n \vec{j}^{\,n} \times \vec{B} \tag{2.2}$$

for the electrons. The terms on the right hand side of the equations are the diffusion, drift, and Hall current terms respectively. For definiteness consider a magnetic field along the z-axis, the optical radiation along the x-axis, and the y-axis the direction along which a signal is developed (see Fig. 2). The above equations then become

$$j_x^p = -eD_p \frac{\partial p}{\partial x} + ep\mu_p E_x + \mu_p B j_y^p \tag{2.3}$$

$$j_y^p = ep\mu_p E_y - \mu_p B j_x^p \tag{2.4}$$

$$j_x^n = eD_n \frac{\partial n}{\partial x} + en\mu_n E_x - \mu_n B j_y^n \tag{2.5}$$

$$j_y^n = en\mu_n E_y + \mu_n B j_x^n \tag{2.6}$$

The symbols in the above equations have the following meaning:

j_x^p, j_y^p = x- and y- components of current density carried by holes, j^p

j_x^n, j_y^n = x- and y- components of current density carried by electrons, j^n

p, n = hole and electron densities

μ_p, μ_n = hole and electron mobilities

D_p, D_n = hole and electron diffusion coefficients,

E_x, E_y = components of electric field

B = magnitude of magnetic field.

The mobility μ and the diffusion coefficient D are related to each other by

$$\mu = \frac{e}{kT} D \tag{2.7}$$

where e, k, and T are the elementary charge, Boltzmann's constant, and the absolute temperature, respectively. The effect of optical illumination is summarized by

$$-\frac{1}{e}\frac{\partial}{\partial x} j_x^n = \frac{1}{e}\frac{\partial}{\partial x} j_x^p = \alpha Q \exp(-\alpha x) - \frac{\Delta p}{\tau} \tag{2.8}$$

The first term on the right represents the rate of creation of holes by the absorbed photons. The letters α and Q represent the absorption coefficient and photon intensity respectively. The second term gives hole annihilation, arising from the recombination of electrons and holes. Furthermore, since

$$\nabla \cdot \vec{j} = \nabla \cdot (\vec{j}^n + \vec{j}^p) = 0 \tag{2.9}$$

we must have

$$j_x^p = -j_x^n \tag{2.10}$$

under steady state conditions. Also

$$\Delta p \equiv p - p_o = n - n_o \equiv \Delta n \; ; \; \frac{\partial n}{\partial x} = \frac{\partial p}{\partial x} \tag{2.11}$$

and

$$s e \Delta p = - j_x^p \; ; \; \text{for } x = 0 \tag{2.12}$$

where s is the surface recombination velocity.

By a straightforward algebraic manipulation, we can obtain from Eqs. (2.3), (2.4), (2.5), (2.6), and (2.10).

$$E_x = - \frac{D_n' - D_p'}{n\mu_n' + p\mu_p'} \frac{\partial p}{\partial x} + \frac{n\mu_n\mu_n' - p\mu_p\mu_p'}{n\mu_n' + p\mu_p'} B E_y \tag{2.13}$$

$$j_y = j_y^n + j_y^p = e(\mu_n + \mu_p) B D_a' \frac{\partial p}{\partial x} + e\left[n\mu_n + p\mu_p - \frac{np\mu_n'\mu_p'(\mu_n + \mu_p)^2}{n\mu_n' + p\mu_p'} B^2 \right] E_y \tag{2.14}$$

$$j_x^p = - j_x^n = - e D_a' \frac{\partial p}{\partial x} + \frac{enp\mu_n'\mu_p'(\mu_n + \mu_p)}{n\mu_n' + p\mu_p'} B E_y \tag{2.15}$$

The primed quantities can be called the "magneto-mobilities" and "magneto-diffusion coefficients", and are defined by

$$D_n' \equiv \frac{D_n}{1 + \mu_n^2 B^2} \; ; \; \mu_p' \equiv \frac{\mu_p}{1 + \mu_p^2 B^2} \; ; \; \text{etc} \tag{2.16}$$

The quantity D_a' defined as

$$D_a' \equiv \frac{n + p}{\frac{n}{D_p'} + \frac{p}{D_n'}} \tag{2.17}$$

can be called the "magneto-ambipolar diffusion coefficient", and reduces to the usual expression for the ambipolar diffusion coefficient when B = 0. The physical significance of D_a' can be

seen immediately from Eq. (2.15): for

$$E_y = 0 \quad ; \quad j_x^{\,p} = -j_x^{\,n} = -eD_a' \frac{\partial p}{\partial x}$$

showing that D_a' is the effective diffusion coefficient of electrons and holes in a magnetic field.

IV. Transport Phenomena

We note that Eqs. (2.13), (2.14), and (2.15) contain the independent physical variables $\frac{\partial p}{\partial x}$, which results from optical illumination: E_y, which results from application of bias voltage; and B, which results by application of external magnetic field. By putting one of the three variables equal to zero, we can obtain the relations for four related transport phenomena: (a) Hall effect and magnetoresistivity when $\frac{\partial p}{\partial x} = 0$, which applies if there is no optical illumination; (b) photoconductivity when the magnetic field B is zero; and (c) PEM effect when the bias electric field $E_y = 0$. The individual cases will not be discussed.

A. Magnetoresistivity (no optical illumination).

Figure 3 indicates schematically how the effect of the magnetic field is studied. The quantity that is measured is

$$R(B) = V/I$$
$$\sigma(B) = j_y/E_y \qquad (3.1)$$

where $\sigma(B)$ is the conductivity of the material in the magnetic field. The theoretical expression for the magnetoresistivity is obtained directly from Eq. (2.14). Putting

$\frac{\partial \rho}{\partial x} = 0$, we obtain

$$\sigma(B) \equiv \frac{j_y}{E_y} = e\,\frac{(n\mu_n+p\mu_p)^2+\mu_n^2\mu_p^2(n-p)^2B^2}{n\mu_n+p\mu_p+\mu_n\mu_p(n\mu_p+p\mu_n)B^2} \qquad (3.2)$$

in agreement with Wilson's result[1]. If the sample is intrinsic, i.e., $n=p$:

$$\sigma(B) = \frac{en(\mu_n+\mu_p)}{1+\mu_n\mu_p B^2} = \frac{\sigma(0)}{1+\mu_n\mu_p B^2} \qquad (3.3)$$

Then

$$\frac{\sigma(0)-\sigma(B)}{\sigma(B)} = \mu_n\mu_p B^2 = \frac{\rho(B)-\rho(0)}{\rho(0)} \qquad (3.4)$$

where resistivity $\rho \equiv 1/\sigma$, showing that the relative resistivity increase should be linear with the square of the magnetic field.

B. Hall Effect

This differs from the magnetoresistivity only in that a signal is measured transverse to the bias electric field. (See Fig. 4). The Hall coefficient R is defined by

$$R \equiv \frac{E_x}{Bj_y} = \frac{E_x}{B\sigma(B)E_y} \qquad (3.5)$$

where E_x is the transverse electric field, or the Hall field. The ratio E_x/E_y can be obtained from Eq. (2.13) after putting $\partial\rho/\partial x = 0$. Using also Eq. (3.2), we obtain

$$R = \frac{p\mu_p^2 - n\mu_n^2 + \mu_n^2\mu_p^2(p-n)B^2}{e\left[(n\mu_n+p\mu_p)^2+\mu_n^2\mu_p^2(p-n)^2B^2\right]} \qquad (3.6)$$

---

(1) A. H. Wilson, The Theory of Metals, Cambridge University Press, 2nd Edition, 1953, p. 216.

in agreement with Wilson's result quoted on p. 213. For an intrinsic sample,

$$R_{intrinsic} = \frac{1}{en}\frac{\mu_p - \mu_n}{\mu_p + \mu_n} \tag{3.7}$$

Thus for an intrinsic sample, the Hall coefficient should be independent of the magnetic field.

C. Photoconductivity

The schematic for the study of this effect is shown in Figure 5. Putting B = 0 in Eq. (2.15), (2.14), and repeating (2.8), we obtain

$$j_x^p = -eD_a\frac{\partial \rho}{\partial x} \tag{3.8}$$

$$j_y = e(n\mu_n + p\mu_p)E_y \tag{3.9}$$

$$\frac{1}{e}\frac{\partial}{\partial x}j_x^p = \alpha Q \exp(-\alpha x) - \frac{\Delta\rho}{\tau} \tag{3.10}$$

If n_o and p_o are the electron and hole concentrations when the crystal is not illuminated, the photocurrent density is given by

$$\begin{aligned} j_{pc} &= j_{light} - j_{dark} \\ &= e(n\mu_n + p\mu_p)E_y - e(n_o\mu_n + p_o\mu_p)E_y \\ &= e(\mu_n + \mu_p)\Delta p\, E_y \end{aligned} \tag{3.11}$$

The photocurrent can then be obtained by integrating the above expression over the sample cross-section. The excess hole concentration Δp is obtained from Eqs. (3.8) and (3.10),

which give

$$-D_a \frac{\partial^2}{\partial x^2} \Delta p = -\frac{\Delta p}{\tau} + \alpha Q \exp(-\alpha x) \tag{3.12}$$

so that

$$\Delta p = A \exp(-\beta x) - \frac{\alpha Q}{D_a \alpha^2 - 1/\tau} \exp(-\alpha x) \tag{3.13}$$

where

$$\beta^2 \equiv \frac{1}{D_a \tau}$$

Because β has the dimension of reciprocal length, we can introduce the quantity diffusion length given by

$$L_D \equiv 1/\beta = \sqrt{D_a \tau} \tag{3.14}$$

The constant of integration A is determined by the boundary condition stated in Eq. (2.12), giving

$$A = \frac{1}{s + \beta D_a} \frac{D_a \alpha^2 + s\alpha}{D_a \alpha^2 - 1/\tau} Q \tag{3.15}$$

so that

$$\Delta p = \frac{Q}{D_a \alpha^2 - 1/\tau} \left[\frac{D_a \alpha^2 + s\alpha}{s + \beta D_a} \exp(-\beta x) - \alpha \exp(-\alpha x) \right] \tag{3.16}$$

If W is the sample width and x_o the thickness, the photocurrent is given by

$$I_{pc} = W \int_0^{x_o} (j_y^p + j_y^n)\, dx = e W E_y (\mu_n + \mu_p) \int_0^{x_o} \Delta p \, dx$$

$$= e W E_y (\mu_n + \mu_p) \frac{Q}{D_a \alpha^2 - 1/\tau} \frac{s(\alpha - \beta) + D_a(\alpha^2 - \beta^2)}{\beta(s + \beta D_a)} \tag{3.17}$$

where we assume that $x_o >> \alpha, \beta$. If in addition

$D_a \alpha^2 >> 1/\tau, \alpha s$; and if further $\alpha >> \beta$:

$$I_{pc} = e W E_y (\mu_n + \mu_p) \frac{Q}{\beta(s + \beta D_a)} \tag{3.18}$$

$$= e W E_y (\mu_n + \mu_p) \frac{\tau Q}{1 + \frac{s\tau}{L_D}} \tag{3.19}$$

Thus we note that for small surface recombination velocity the photocurrent is directly proportional to the bulk lifetime.

D. Short-Circuit PEM Current

The PEM effect can in principle be observed by an arrangement such as shown in Fig. 6. For this case there is no bias voltage, i.e., $E_y = 0$, so that Eqs. (2.14), (2.15), and (2.8) give

$$j_{PEM}^{sc} = j_y = j_y^n + j_y^p = e(\mu_n + \mu_p) B D_a' \frac{\partial \rho}{\partial x} \tag{3.20}$$

$$j_x^p = -j_x^n = -e D_a' \frac{\partial \rho}{\partial x} \tag{3.21}$$

$$\frac{1}{e} \frac{\partial}{\partial x} j_x^p = \alpha Q \exp(-\alpha x) - \frac{\Delta \rho}{\tau} \tag{3.22}$$

Eliminating j_x^p from Eqs. (3.21) and (3.22) and solving the resulting differential equation we find

$$\Delta \rho = \frac{\alpha Q}{\alpha^2 D_a' - 1/\tau} \left[\frac{\alpha D_a' - s}{s + \beta' D_a'} \exp(-\beta' x) - \exp(-\alpha x) \right] \tag{3.23}$$

where $\beta' \equiv \frac{1}{\sqrt{D_a' \tau}}$

Consequently the short-circuit current is given by

$$I_{PEM}^{sc} = W\int_0^{x_0} (j_y^n + j_y^p)\, dx$$

$$= -WBe(\mu_n + \mu_p) D_a' \int_0^{x_0} \frac{\partial \Delta p}{\partial x}\, dx$$

$$= eWB(\mu_n + \mu_p) D_a' \frac{Q}{S + \beta' D_a'} \qquad (3.24)$$

The bulk lifetime can be obtained by taking the ratio of Eqs. (3.18) and (3.24). Thus

$$\frac{I_{pc}}{E_y} \Big/ \left(\frac{I_{PEM}^{sc}}{B}\right)_{B \to 0} = \frac{1}{\beta D_a} = \sqrt{\frac{\tau}{D_a}} \qquad (3.25)$$

so that

$$\tau = D_a \left[\frac{I_{pc}}{E_y} \Big/ \left(\frac{I_{PEM}^{sc}}{B}\right)_{B \to 0} \right]^2 \qquad (3.26)$$

E. <u>PEM Detector Equivalent Circuit and Open Circuit Voltage</u>.

From Eqs. (2.14), (3.2), and (3.20) we obtain

$$j_y = j_{PEM}^{sc} + \sigma(B)\, E_y \qquad (3.27)$$

If the PEM detector is connected across R_{load}, as shown in Fig. 7, voltage V is developed such that

$$E_y = -\frac{V}{\ell} \qquad (3.28)$$

where ℓ is the distance between the electrodes. Consequently

$$j_{PEM}^{sc} = \frac{\sigma(B)}{\ell} V + j_y \qquad (3.29)$$

or after integration

$$I_{PEM}^{sc} = \frac{V}{r(B)} + I_{load} \tag{3.20}$$

The first term on the right is the shunting current through the crystal and the second term the current through the load. The corresponding equivalent circuit is shown in Fig. 8. It is to be noted that the shunting resistance is magnetic-field dependent. From Eq. (3.30) we also obtain

$$I_{PEM}^{sc} = \frac{V}{r(B)} + \frac{V}{R} \tag{3.31}$$

so that

$$V = \frac{R\, r(B)}{R + r(B)}\, I_{PEM}^{sc} \tag{3.32}$$

If $R >> r(B)$, we obtain

$$V_{PEM}^{oc} = V = r(B)\, I_{PEM}^{sc} \tag{3.33}$$

The above is a summary of the theoretical developments that we have carried out. In addition, the effects of surface recombination and of angular dependence of magnetoresistivity have been investigated in greater detail. These, however, will be reported in the appropriate memoranda.

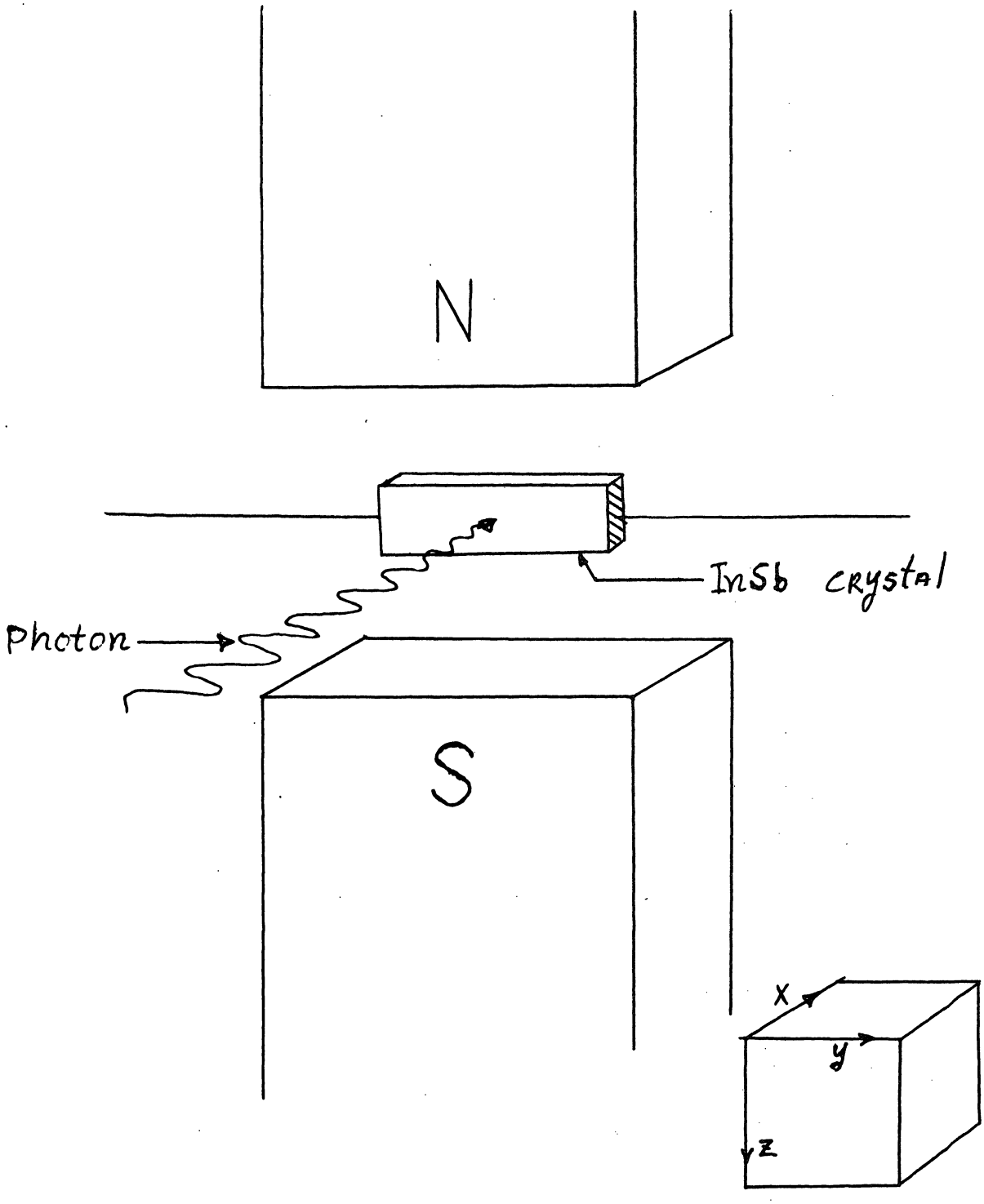

FIG. 2

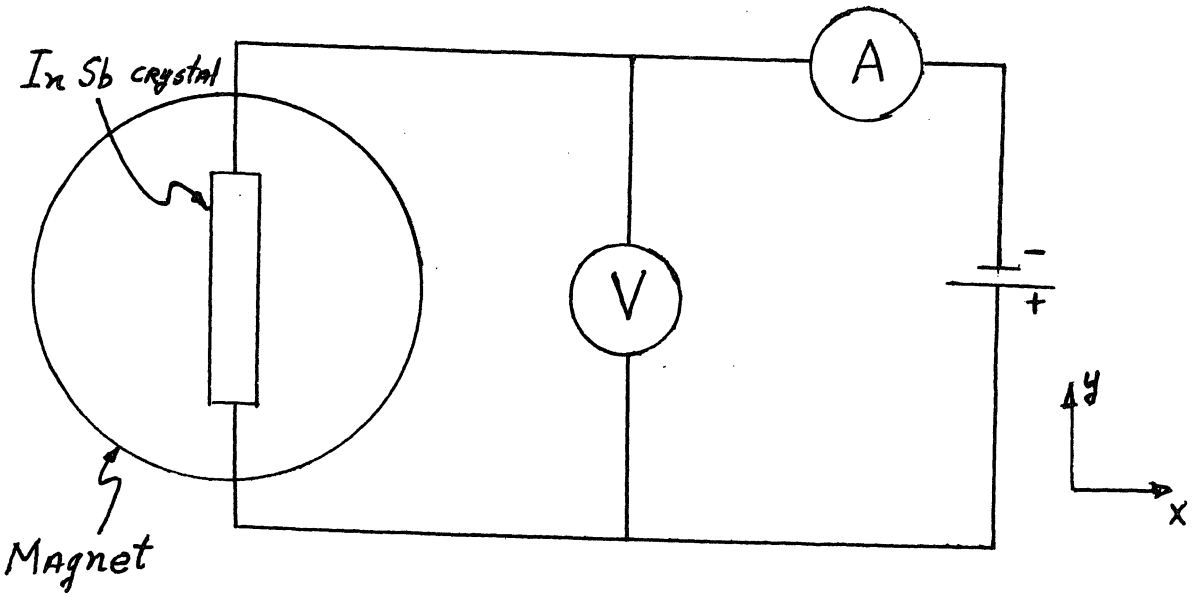

Fig. 3 : Magnetoresistivity

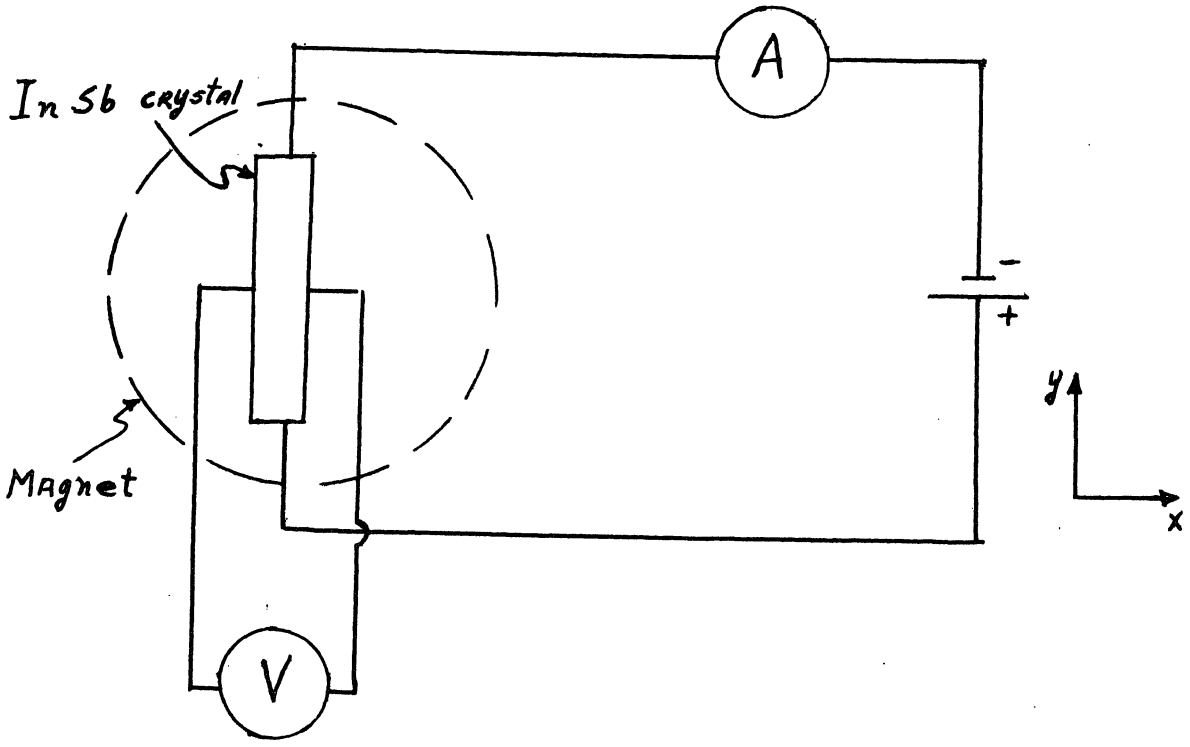

Fig. 4 : Hall Effect

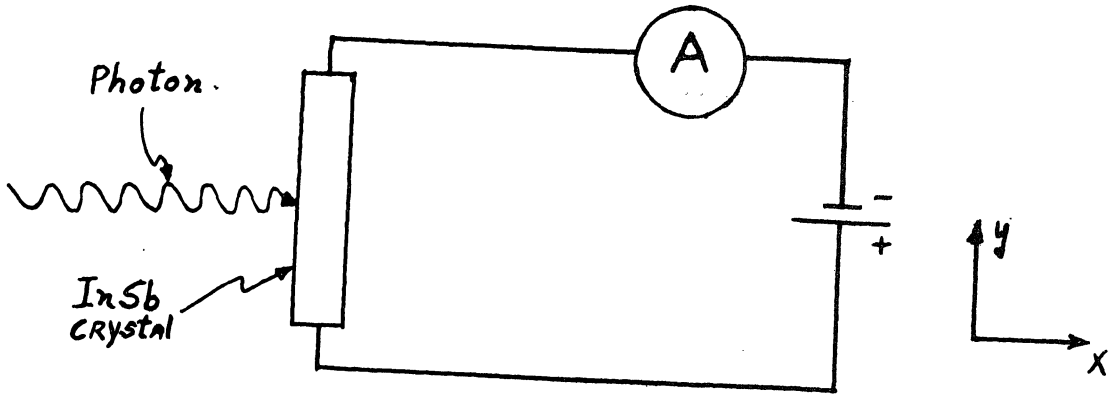

Fig. 5 : Photoconductivity

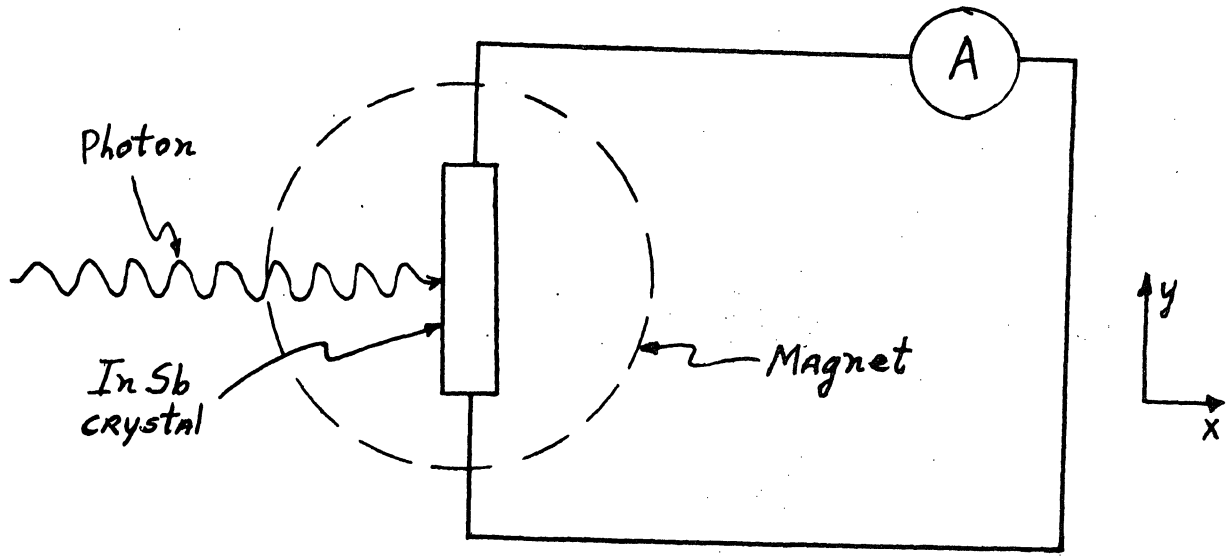

Fig. 6 : Short-Circuit PEM

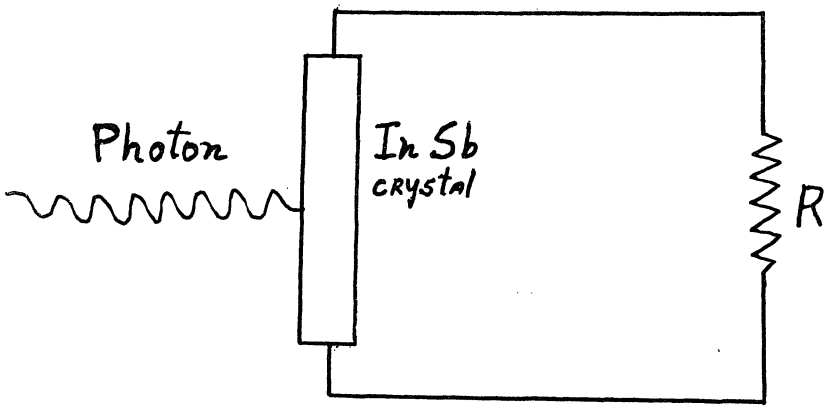

Fig. 7

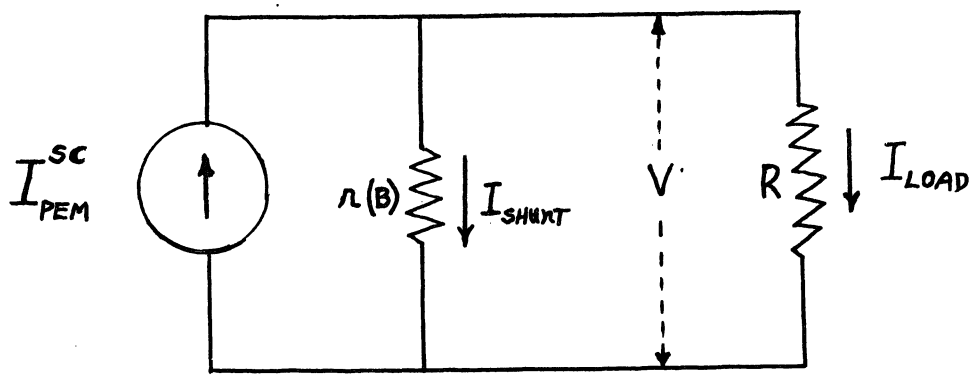

Fig. 8

CHAPTER XX

PLASMA EFFECTS IN SOLIDS

Chihiro Kikuchi

CHAPTER XX

PLASMA EFFECTS IN SOLIDS

So far in our discussion of ionization effects produced by the passage of charged particles, we have used the Rutherford-Niels Bokr approach in which it is assumed that the individual electrons and nuclei act indeptendently and randomly, the excitation of a particle is completely independent of the others, and therefore the total effect is obtained by adding up the energy transferred to the particles (electrons). This, of course, is usual approach and detailed discussions can be found in such texts as Evans.

Although this approach may be adequate in gases, in which atoms are typically about 10 A apart, in solids and in liquids the atoms are about 1 A apart so that several atoms can interact simultaneously with the passing charged particle. Consequently, for condensed materials, we need somehow to take the mutual interaction of the particles (electrons) in the medium into account.

Consequently, we shall approach the problem for the standpoint of classical physics.

The importance of collective, or plasma, effects were noted as early as 1938 by Swann, and the first attempt at a systematic treatment was given by E. Fermi (Phys. Rev. 57, 485 (1940)). This point of view has been developed by such workers as A. Bohr, H. A. Kramers, Pines and others. Excellent summaries can be found in the papers by D. Pines, Electron Interaction in Metals (Solid State Physics, vol. 1) and J. D. Jackson, Classical Electrodynamics, Chapter XIII, Collisions Between Charged Particles, Energy Loss, and Scattering.

It seems that different groups working in seemingly unrelated areas of solid state physics were led to the concept of solid state plasma effects. Possibly the earliest one is the discovery of discrete energy losses--about 20 ev--of electrons in the Kev range in going thin foils of aluminum. The effect was reported by Ruthemann in 1948, and the interpretation in terms of plasmons was given by Pines in 1952. Fermi's formulation apparently was stimulated by the observation that the energy loss by relativistic particles is not as large as predicted by Bohr's theory and the discovery the coherent electromagnetic radiation by Cerenkov in 1937. And possibly one of the latest developments is the discovery of pinch effects in InSb by Glicksman and Steels (Phys. Rev. Letters 2, 461 (1959)), followed by the dramatic thermal pinches in InSb by Ancker-Johnson and Drummond (Phys. Rev. 131, 1961 (1 September 1963)).

20.1 A Review

To get a better appreciation for the order of magnitude of ionization effects, we shall very briefly review energy transfer by the momentum method and also the associated ionization effects.

a. Energy Transfer. Consider

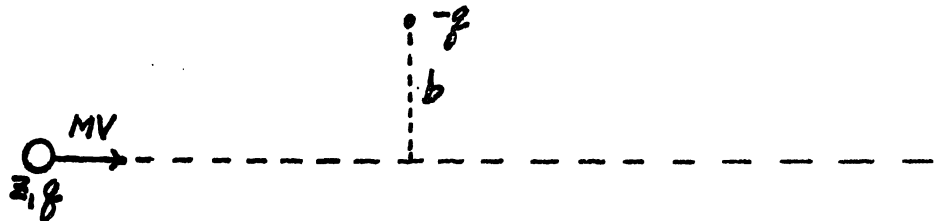

A charged particle going by an electron of charge -q. According to the momentum method, the momentum gained is

$$\Delta p = \int_{-\infty}^{\infty} F_{\perp}\, dt = \frac{2 Z_1 q^2}{bV}$$

so that the energy transferred is

$$Q = \frac{(\Delta p)^2}{2m} = \frac{2 Z_1^2 e^4}{m V^2} \frac{1}{b^2}$$

$$= \frac{M}{m} \frac{Z_1^2 e^4}{E} \frac{1}{b^2}$$

Now

$$\frac{e^2}{2a_0} = 13.5 \text{ ev} \quad (\text{Hydrogen ionization energy})$$

$$a_0 = 0.53 \text{ A}, \quad a_0 = \frac{\hbar^2}{m e^2}$$

so that

$$Q = \frac{4M}{m} \left(\frac{e^2}{2a_0}\right)^2 \frac{1}{(b/a_0)^2}$$

$$= \frac{1.4 A Z_1^2}{E(\text{Mev})} \frac{1}{(b/a_0)^2}$$

For an alpha particle, $Z_1 = 2$, $A = 4$.

Then if E = 1 Mev, we find that

$$Q \cong (22) \frac{1}{(b/a_0)^2}$$

so that for $b \sim a_0 = 0.5$A, the transferred energy is about 30 ev.

Consequently, a reasonable physical picture is

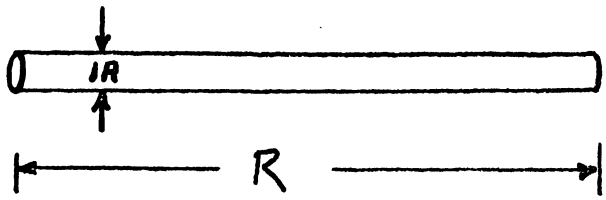

where R is the range of the alpha particle.

For a fission fragment A = 100, Z_1 = 20, E = 100 Mev, so that

$$Q \cong 900 \frac{1}{(b/a_0)^2}$$

so that $b/a_o \sim 5$, for Q = 30 ev. This means that a fission fragment will sweep out an excitation cylinder of the order of 5A in diameter.

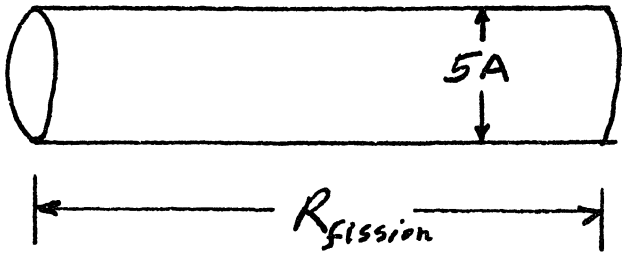

b. Specific Ionization

The number of electrons in cylinder of unit length and radius b and thickness db is given by

$$dn = n_0 Z_2 \, 2\pi b \, db$$

so that

$$\frac{dE}{ds} = 2\pi n_0 Z_2 \int_{b_{min}}^{b_{max}} Q \, b \, db$$

$$= \frac{4\pi n_0 Z_2 Z_1^2 e^4}{m V^2} \ln \frac{b_{max}}{b_{min}}$$

We need to discuss the values of the impact parameters. We shall do this later on. For the moment we need to note that

$$\frac{dE}{ds} = \frac{4\pi n_0 Z_2 Z_1^2 e^4}{m V^2} \ln \frac{2mV^2}{I}$$

We shall apply this to alpha particles and to fission fragments.

First consider alpha particles in air. Then

$$\frac{2mV^2}{I} = \frac{4m}{MI} E = \frac{4}{2000 A I} E$$

For air I $\sim$100 ev (Evans, p. 583, I = 86 ev). Also A = 4, and for E = 1 Mev, we find that

$$\frac{2mV^2}{I} = \frac{4}{2000(4)100} \times 10^6 = 5$$

$$\ln \frac{2mV^2}{I} = 1.6$$

From the coefficient in front, we have

$$\frac{dE}{ds} = \frac{2\pi M}{m} \frac{n_0 Z_2 Z_1^2 e^4}{E} \ln \frac{4m}{M} \frac{E}{I}$$

$$= \frac{2\pi M}{m} \frac{n_0 Z_2 Z_1^2}{E} \left(\frac{e^2}{2a_0}\right)^2 (4a_0^2) \ln \frac{4m}{M} \frac{E}{I}$$

$$= 3.7 \times 10^5 \text{ ev/cm} \cong 10^4 \text{ ion pairs/cm}$$

For Po^{214} alpha's, E = 7.68 Mev, Range = 6.95 cm and at the peak specific ionization about 7 x 10^4 ion pairs/cm are formed. At about 3 cm from the end of the range, this quantity is about 2.7 x 10^4 ion pairs/cm.

Consider next a fission fragment.

$$\frac{4m}{M} \frac{E}{I} = \frac{4}{2000(140)} \frac{10^8}{10^2} = 10$$

$$\therefore \ln \frac{2mV^2}{I} \sim 2.3$$

Also

$$\frac{\left(\frac{dE}{ds}\right)_f}{\left(\frac{dE}{ds}\right)_\alpha} \cong \frac{M_f}{M_\alpha} \left(\frac{Z_f}{Z_\alpha}\right)^2 \frac{E_\alpha}{E_f}$$

$$= \left(\frac{140}{4}\right)\left(\frac{20}{2}\right)^2 \frac{1}{10^2} \sim 40$$

20.2 Maximum Impact Parameter

The expression for specific ionization involves the b_{MAX}, or the maximum impact parameter. We shall first make a qualitative estimate, then attempt a more quantitative analysis.

Consider then an electron bound to an atom at distance b from the direction of motion of charged particle.

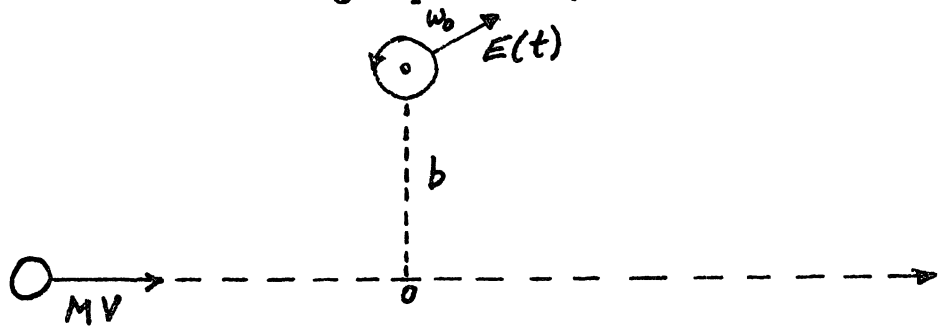

As the charged particle goes by, a rotating E-field is generated at the position of the electron. The E-field will be rotating with different angular velocities, being greatest at point O. Furthermore, we can expect the Fourier components making the largest contribution to the energy transfer to be those near ω_0, because then the E-field will be moving <u>with</u> the electron. Consequently, for energy transfer to occur

$$0 \leq \omega_0 \leq \frac{V}{b}$$

Therefore, we can take for the maximum impact imparameter

$$b_{MAX} = \frac{V}{\omega_0}$$

Consider then a 2 Mev alpha particle

$$V = \sqrt{\frac{2E_0}{M}} = \sqrt{\frac{2E_0c^2}{Mc^2}}$$

$$= c\sqrt{\frac{2E_0}{931A}} \sim 10^9 \text{ cm/sec}$$

$$\omega_0 \cong \frac{E}{\hbar} \sim \frac{10^{-11-7}}{10^{-27}} \sim 10^{16}$$

$$\therefore b_{MAX} \cong \frac{10^9}{10^{16}} \sim 10^{-7}\ cm = 10\ A$$

This value is considerably larger than the radius of the excitation cylinder, computed earlier. The energy transfer associated with this impact parameter is

$$Q = \frac{1.4\, A\, Z_1^2}{E\,(MeV)} \frac{1}{b^2} \cong 0.03\ eV.$$

We analyze the problem more carefully. First we want to show that the energy transferred to a harmonically bound electron is

$$Q = \frac{\pi e^2}{m} |E(\omega_0)|^2$$

To prove this, we shall make use of the Fourier transforms

$$\underline{\Lambda}(t) = \frac{1}{\sqrt{2\pi}} \int_{-\infty}^{\infty} \underline{\Lambda}(\omega) e^{-i\omega t} d\omega$$

$$\underline{\Lambda}(-\omega) = \underline{\Lambda}^*(\omega)$$

and similarly for the E-field. For the energy transferred to a moving charge, we have

$$\frac{dQ}{dt} = \int E' \cdot J'\, dz'$$

This can be shown easily as follows. We have

$$dW = \underline{F} \cdot d\underline{s} = \underline{F} \cdot \underline{v}\, dt$$

If

$$\underline{F} = \rho \underline{E}$$

then

$$\frac{dW}{dt} = F \cdot v = \rho E \cdot v$$

is the rate of doing work on the charges in a unit volume, so that

$$\frac{dW}{dt}\,d\tau = (d\tau\,\rho)\,E\cdot v$$

and for

$$\rho(r') = -q\,\delta(\underline{r}' - \underline{r}(t))$$

we have for the work done on the electron

$$\frac{dQ}{dt} = -q\int E(r')\cdot v(r')\,\delta(r'-r(t))\,d\tau'$$

$$= -q\,E(r)\cdot v(r)$$

Therefore

$$Q = -q\int_{-\infty}^{\infty} E(r)\cdot v(r)\,dt$$

The electron velocity is obtained from the equation of motion

$$\ddot{r} + \Gamma\dot{r} + \omega_0^2 r = -\frac{q}{m}E(t)$$

Upon making a Fourier analysis, we find that the Fourier components at frequency w are related by

$$\underline{r}(\omega) = -\frac{q}{m}\,\frac{E(\omega)}{\omega_0^2 - i\omega\Gamma - \omega^2}$$

so that

$$\underline{v}(\omega) = -i\omega\,\underline{r}(\omega)$$

Then

$$Q = \frac{q^2}{m}\int_{-\infty}^{\infty}\frac{-i\omega\,|E(\omega)|^2}{\omega_0^2 - i\omega\Gamma - \omega^2}\,d\omega$$

Now $|E(\omega)|^2$ can be shown to be a slowly changing function, in comparison to

$$\frac{-i\omega}{\omega_0^2 - i\omega\Gamma - \omega^2}$$

Consequently, using the mean value theorem for the integral of product of function, we obtain

$$Q = \frac{e^2}{m} |E(\omega_0)|^2 \int_{-\infty}^{\infty} \frac{-i\omega}{\omega_0^2 - i\omega\Gamma - \omega^2} \, d\omega$$

The integral can be evaluated by contour integration. The poles are at $\omega = \pm \frac{1}{2}\sqrt{4\omega_0^2 - \Gamma^2} - \frac{i\Gamma}{2}$

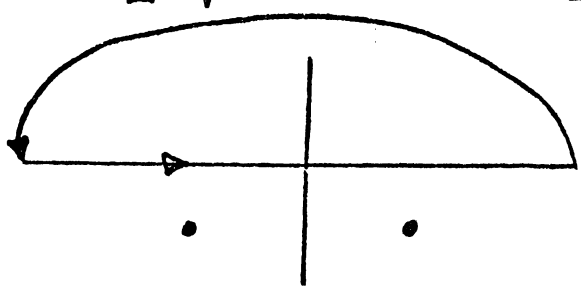

Integrating over the upperhalf of the complex w plane, we have

$$\int_{-\infty}^{\infty} + \int_{\text{C}} = 2\pi i \,(\Sigma \text{ Residues})$$

$$= 0$$

For the circle at infinity, the integrand becomes

$$\frac{-i\omega\, d\omega}{-\omega^2} = \frac{i\, d\omega}{\omega} = -d\theta$$

so that

$$\int_{-\infty}^{\infty} (\quad) \, d\omega = \int_{0}^{\pi} d\theta = \pi$$

20.3 Evaluation of Fourier Component

We next need to evaluate

$$|\underline{E}(\omega_0)|^2 = |E_\perp(\omega_0)|^2 + |E_{11}(\omega_0)|^2$$

For this note that the E-field at the electron is given by

$$E(t) = \frac{z_1 e}{r^2}$$

and

$$E_\perp(t) = \frac{z_1 e\, b}{r^3}$$

and

$$E_{11}(t) = -\frac{z_1 e\, x}{r^3}$$

so that the Fourier component is given by

$$E_\perp(\omega) = \frac{1}{\sqrt{2\pi}} \int_{-\infty}^{\infty} E_\perp(t)\, e^{-i\omega t}\, dt$$

$$= \frac{z_1 e}{bV} \left(\frac{2}{\pi}\right)^{1/2} \left[\frac{\omega b}{V} K_1\left(\frac{\omega b}{V}\right)\right]$$

and

$$E_{11}(\omega) = -\frac{i z_1 e}{bV} \left(\frac{2}{\pi}\right)^{1/2} \left[\frac{\omega b}{V} K_0\left(\frac{\omega b}{V}\right)\right]$$

Putting

$$\xi \equiv \frac{\omega_0 b}{V}$$

we find that the energy transferred is given by

$$Q = \underbrace{\frac{2 z_1^2 e^4}{m V^2} \frac{1}{b^2}}_{\text{Old}} \underbrace{\left[\xi^2 K_1^2(\xi) + \xi^2 K_0^2(\xi)\right]}_{\text{Multiplication factor}}$$

where the coefficient in front of the square bracket is the quantity obtained before. The quantity in the square bracket is appreciably in the range $\xi < 1$, but thereafter it rapidly falls to zero. From the expansions

$$K_0(x) = -\left[\ln\frac{x}{2} + 0.5772\right] = -\ln\frac{x}{1.123}\Bigg\} \quad x \ll 1$$

$$K_1(x) = 1/x$$

$$K_2(x) = \sqrt{\frac{\pi}{2x}}\, e^{-x} \qquad x \gg 1$$

We find that

$$\left[\xi^2 K_1^2(\xi) + \xi^2 K_0^2(\xi)\right] = \begin{cases} 1 & \xi \ll 1 \\ \pi\xi e^{-2\xi} & \xi \gg 1 \end{cases}$$

20.4 Specific Ionization

This obtained from

$$\frac{dE}{ds} = 2\pi n_0 Z_2 \int_{b_{min}}^{b_{max}} Q\, b\, db$$

$$= \frac{4\pi n_0 Z_1^2 Z_2 e^4}{m V^2} \int_{b_{min}}^{b_{max}} \frac{1}{b}\left[\xi^2 K_1^2(\xi) + \xi^2 K_0^2(\xi)\right] db$$

$$= \frac{4\pi n_0 Z_1^2 Z_2 e^4}{m V^2} \int_{\xi_{min}}^{\xi_{max}} \left[\xi K_1^2(\xi) + \xi K_0^2(\xi)\right] d\xi$$

$$\xi_{min} = \frac{\omega_0 b_{min}}{V}$$

Since the quantity in the square bracket decreases exponentially for large values of ξ_{max} (say ≥ 1), the upper limit can be extended to infinity. Upon carrying out the integration, we find that

$$\frac{dE}{ds} = \frac{4\pi n_0 Z_1^2 Z_2 q^4}{m V^2}\left[\xi_{min} K_1(\xi_{min}) K_0(\xi_{min}) - \frac{v^2}{2c^2}\left(K_1^2(\xi_{min}) - K_0^2(\xi_{min})\right)\right]$$

In general $\xi_{min} < 1$, so that the above becomes

$$\frac{dE}{ds} = \frac{4\pi n_0 Z_1^2 Z_2 q^4}{m V^2}\left[\ln B_c - \frac{v^2}{2c^2}\right]$$

where

$$B_c \equiv \frac{1.123\, V}{\omega_0\, b_{min}}$$

20.5 Minimum Impact Parameter

The only remaining undefined quantity is b_{min} . We shall see that care is needed in evaluating this quantity.

Classically, the minimum impact parameter is defined by

$$Q_{MAX} = \frac{2 Z_1^2 q^4}{m V^2}\,\frac{1}{b_{min}^2}$$

The maximum energy transfer occurs for head-on collision. For this case, it can be easily shown that

$$Q_{MAX} = \frac{4mM}{(M+m)^2} E \cong \frac{4m}{M} E \qquad M >> m$$

$$= 2mV^2$$

$$\therefore\ b_{min} = \frac{Z_1 q^2}{m V^2}$$

Consider for example, an alpha particle of energy 1 Mev. According to an early estimate, the velocity is about 10^9 cm/sec. Then

$$b_{min} = \frac{(2)(4.8\times10^{-10})^2}{10^{-27}(10^{18})} \cong 5\times10^{-10}\ cm$$

On the other hand, quantum theory demands that

$$x\,p = \hbar$$

so that

$$x \cong \frac{10^{-27}}{(10^{-27})(10^{9})} \sim 10^{-9}\ \text{cm}$$

Consequently, there is indication that even for energies of about 1 Mev, the minimum impact parameter is smaller than the limit set by quantum mechanics. IN any case, the larger of the two values need to be chosen.

20.6 Some Relativistic Kinematics

To apply the ideas that have been developed to electrons, an important correction has to be made because in the bulk of the cases the electron energies are large in comparison to the rest energy. For example, for the fission product

$$I^{136} \longrightarrow Xe^{136} \qquad T_{1/2} = 36\ \text{s}.$$

the β^-'s have energies of about 2.7, 4.2, 5.6, 7.0 Mev. In the

$$Rb^{90} \longrightarrow Sn^{90}$$

decay, the beta-energies are about 6.8, 5.8, and 2.2 Mev. These values are appreciably larger than the rest energy mc^2 = 0.51 Mev.

It is clear then that relativistic effects have to be taken into account. We shall consider first a simple case - experimentally important - and then go on to the complex case of electron-electron collision.

a. Consider first an electron hitting a heavy particle. The energy-momentum relation is

$$E = \sqrt{c^2p^2 + m^2c^4}$$

so that the correct energy balance equation is

$$\sqrt{c^2p^2+m^2c^4} + Mc^2 = \sqrt{c^2p'^2+m^2c^4} + \sqrt{c^2P^2+M^2c^4}$$

where p and p^1 are the initial and final linear momentum of the electron, and P is the momentum imparted to the heavy particle. The momentum balance gives

$$p = p' + P$$

Intuitively, we expect

$$p \sim -p'$$

so that

$$P \cong 2p$$

Then

$$Q = \frac{1}{2M}(4p^2) = \frac{2}{Mc^2}(E^2 - m^2c^4)$$

$$= \frac{2}{Mc^2}\left[(T+mc^2)^2 - m^2c^4\right]$$

$$= \frac{2T(T+2mc^2)}{Mc^2}$$

Consider a 1 Mev electron hitting a proton. Then

$$Q = \frac{2(2)}{931} \cong \frac{4}{1000} \sim 4\ Kev$$

To verify the intuitive solution, return to the energy equation which gives

$$E + Mc^2 - \sqrt{c^2P^2+M^2c^4} = \sqrt{c^2(p-P)^2+m^2c^4}$$

Squaring and cancelling, we obtain

$$Mc^2 + \frac{c^2pP}{E+Mc^2} = \sqrt{c^2P^2+M^2c^4}$$

$$\therefore \frac{c^2 p P}{E + Mc^2} = Mc^2 \left[\sqrt{1 + \frac{P^2}{M^2 c^2}} - 1 \right]$$

$$= Mc^2 \frac{1}{2} \left(\frac{P^2}{M^2 c^2} \right) = \frac{P^2}{2M}$$

$$\therefore P = \frac{2 p c^2 M}{E + Mc^2} \cong 2p$$

if $Mc^2 >> E$

20.7 Modification of Previous Calculations

If the calculations on energy transfer are to be applied to energetic electrons, the previous analysis has to be modified by taking relativistic effects into account. For example, instead of

$$E_\perp(\omega) = \frac{Z_1 q b}{\sqrt{2\pi}} \int_{-\infty}^{\infty} \frac{e^{i\omega t} dt}{\left[b^2 + V^2 t^2 \right]^{3/2}}$$

given earlier, we should use

$$E_\perp(\omega) = \frac{Z_1 q b \gamma}{\sqrt{2\pi}} \int_{-\infty}^{\infty} \frac{e^{i\omega t} dt}{\left[b^2 + \gamma^2 V^2 t^2 \right]^{3/2}}$$

where

$$\gamma \equiv \frac{1}{\sqrt{1 - \beta^2}} \qquad \beta \equiv \frac{V}{c}$$

Proof of this is given in Jackson, P. 381. This modification results in

$$Q = \frac{2 Z_1^2 q^4}{m V^2} \frac{1}{b^2} \left[\xi^2 K_1^2(\xi) + \frac{1}{\gamma^2} \xi^2 K_0^2(\xi) \right]$$

where

$$\xi \equiv \frac{\omega_0 b}{\gamma V}$$

As before, the maximum impact parameter is then given by

$$b_{max} = \frac{\gamma V}{\omega_0}$$

For energetic electrons, the relativistic factor γ becomes very

large, giving correspondingly larger value for the impact parameter. These relativistic effects then add to the already over-estimated contribution of distant atoms to the energy transfer processes.

20.8 Fermi's Plasma Theory

The word plasma is underlined because Fermi did not use this term. To take the collective effects - the mutual interaction of the electrons - into account, be used classical electrodynamics, in which the dielectric constant takes the effects of the medium into account.

The Maxwell equations, in Gaussian units, are

$$\nabla \cdot D = 4\pi\rho \qquad \nabla \cdot B = 0$$

$$\nabla \times H = \frac{4\pi}{c} J + \frac{1}{c}\frac{\partial D}{\partial t} \qquad \nabla \times E + \frac{1}{c}\frac{\partial B}{\partial t} = 0$$

and

$$D = \epsilon E = E + 4\pi P$$

From the above equations, putting $\mu = \mu_0 = 1$, we obtain

$$-\nabla^2 \Phi + \frac{\epsilon}{c^2}\ddot{\Phi} = \frac{4\pi}{\epsilon}\rho$$

$$-\nabla^2 A + \frac{\epsilon}{c^2}\ddot{A} = \frac{4\pi}{c} J$$

if

$$\nabla \cdot A + \frac{\epsilon}{c}\dot{\Phi} = 0$$

for

$$H = \nabla \times A$$

$$E = -\frac{1}{c}\dot{A} - \nabla\Phi$$

The quantities Φ and A are the scalar and vector potential respectively, or in the language of relativity, the components of a 4-vector.

The source of the electromagnetic field is a charged particle moving with velocity $\underline{V}$. Hence, we shall put

$$\rho(\underline{r},t) = z_1 q\, \underline{\delta}(\underline{r} - \underline{V}t)$$

We need to note that the above is a 3-dimensional deta function, i.e.,

$$\underline{\delta}(\underline{r} - \underline{V}t) \equiv \delta(x - V_x t)\,\delta(y - V_y t)\,\delta(z - V_z t)$$

Related to this is the current density which is given by

$$\underline{J}(r,t) = \underline{V}\,\rho(\underline{r},t)$$

To carry through the analysis, a 4-dimensional Fourier analysis is made. Thus, let

$$F(\underline{r},t) = \frac{1}{(\sqrt{2\pi})^4}\int d^3\underline{k}\int d\omega\, F(\underline{k},\omega)\, e^{i\underline{k}\cdot\underline{r} - i\omega t}$$

so that

$$F(\underline{k},\omega) = \frac{1}{(\sqrt{2\pi})^4}\iint d\tau\, dt\, F(\underline{r},t)\, e^{-i\underline{k}\cdot\underline{r} + i\omega t}$$

Thus, for the Fourier component of the charge density, we obtain

$$\rho(\underline{k},\omega) = \frac{1}{(2\pi)^2}\iint d\tau\, dt\, z_1 q\, \underline{\delta}(\underline{r} - \underline{V}t)\, e^{-i\underline{k}\cdot\underline{r} + i\omega t}$$

$$= \frac{z_1 q}{(2\pi)^2}\int e^{-i(\underline{k}\cdot\underline{V} - \omega)t}\, dt$$

$$= \frac{z_1 q}{2\pi}\,\delta(\omega - \underline{k}\cdot\underline{V})$$

and

$$J(\underline{k},\omega) = \underline{V}\,\rho(\underline{k},\omega)$$

Therefore, we obtain

$$\left[k^2 - \frac{\epsilon\omega^2}{c^2}\right]\Phi(\underline{k},\omega) = \frac{2 z_1 q}{\epsilon}\,\delta(\omega - \underline{k}\cdot\underline{V})$$

or
$$\Phi(\underline{k},\omega) = \frac{2 Z_1 e}{\epsilon} \frac{\delta(\omega - \underline{k}\cdot\underline{V})}{k^2 - \frac{\epsilon\omega^2}{c^2}}$$

Similarly
$$\left[k^2 - \frac{\epsilon\omega^2}{c^2}\right]\underline{A}(\underline{k},\omega) = \frac{2 Z_1 e}{c}\underline{V}\,\delta(\omega - \underline{k}\cdot\underline{V})$$

so that
$$\underline{A}(\underline{k},\omega) = \frac{\epsilon \underline{V}}{c}\Phi(\underline{k},\omega)$$

Therefore
$$\underline{E}(\underline{k},\omega) = i\left[\frac{\omega\epsilon}{c^2}\underline{V} - \underline{k}\right]\Phi(\underline{k},\omega)$$

$$\underline{B}(\underline{k},\omega) = \frac{i\epsilon}{c}\underline{k}\times\underline{V}\,\Phi(\underline{k},\omega)$$

To calculate the energy transfer, we need the Fourier transform of the E-field. That is,

$$\underline{E}(\omega) = \frac{1}{\sqrt{2\pi}}\int_{-\infty}^{\infty}\underline{E}(\underline{r},t)e^{i\omega t}\,dt$$

$$= \frac{1}{\sqrt{2\pi}}\int_{-\infty}^{\infty}e^{i\omega t}dt\,\frac{1}{(2\pi)^2}\iint\underline{E}(\underline{k},\omega)e^{i\underline{k}\cdot\underline{r} - i\omega' t}\,d\underline{k}\,d\omega'$$

$$= \frac{1}{(2\pi)^{3/2}}\int E(\underline{k},\omega)e^{i\underline{k}\cdot\underline{r}}\,d\underline{k}$$

To simplify the analysis, assume the particle to be moving along the Z-axis and consider the field at point $(b, 0, 0)$. The above expression then becomes

$$\underline{E}(\omega) = \frac{1}{(2\pi)^{3/2}}\int\underline{E}(\underline{k},\omega)e^{ik_1 b}\,d\underline{k}$$

so that the Z-component of the E-field is

$$E_3(\omega) = \frac{2i Z_1 e}{\epsilon(2\pi)^{3/2}}\int d\underline{k}\,e^{ik_1 b\left(\frac{\omega\epsilon V}{c^2} - k_3\right)}\frac{\delta(\omega - V k_3)}{k^2 - \frac{\omega^2}{c^2}\epsilon}$$

Since

$$\int f(k_3)\,\delta(\omega - Vk_3)\,dk_3 = \frac{1}{V} f\left(\frac{\omega}{V}\right)$$

we obtain

$$E_3(\omega) = \frac{2iz_1 q}{(2\pi)^{3/2}\epsilon V}\left(\frac{\omega\epsilon V}{c^2} - \frac{\omega}{V}\right)\iint \frac{e^{ik_1 b}\,dk_2\,dk_1}{k_1^2 + k_2^2 + \frac{\omega^2}{V^2} - \frac{\omega^2}{c^2}\epsilon}$$

$$= -\frac{2iz_1 q\omega}{(2\pi)^{3/2} V^2}\left(\frac{1}{\epsilon} - \beta^2\right)\iint \frac{e^{ik_1 b}\,dk_2\,dk_1}{k_1^2 + k_2^2 + \lambda^2}$$

where

$$\lambda^2 \equiv \frac{\omega^2}{V^2} - \frac{\omega^2}{c^2}\epsilon$$

Integrate next with respect to k_2. The poles for the function

$$\frac{1}{k_2^2 + k_1^2 + \lambda^2}$$

are at

$$\pm i\sqrt{k_1^2 + \lambda^2}$$

Consequently, integrating over a path in the upper half of the complex w plane, we find

$$\int_{-\infty}^{\infty} \frac{dk_2}{k_2^2 + k_1^2 + \lambda^2} = 2\pi i\left(\frac{1}{2i\sqrt{k_1^2 + \lambda^2}}\right) = \frac{\pi}{\sqrt{k_1^2 + \lambda^2}}$$

The integration with respect to k_1 gives a Bessel function. The final result then is

$$E_3(\omega) = -\frac{iz_1 q\omega}{V^2}\left(\frac{2}{\pi}\right)^{1/2}\left(\frac{1}{\epsilon} - \beta^2\right) K_0(\lambda b)$$

Similarly, it can be shown that

$$E_1(\omega) = \frac{z_1 q}{V}\left(\frac{2}{\pi}\right)^{1/2}\frac{\lambda}{\epsilon} K_1(\lambda b)$$

$$B_2(\omega) = \epsilon\beta E_1(\omega)$$

20.9 Energy Transfer and Specific Ionization

The transferred energy is given by, as given earlier,

$$Q = 2 q z_2 \, Re \int_0^\infty [-i\omega \underline{\Delta}(\omega) \cdot E^*(\omega)] \, d\omega$$

We wish to relate the displacement amplitude to the dielectric constant. The relation is

$$\epsilon E = D = E + 4\pi P$$

and

$$P = n_0 q \underline{\Delta}$$

so that

$$q \underline{\Delta} = \frac{1}{4\pi n_0} (\epsilon - 1)$$

Therefore

$$Q = \frac{1}{2\pi n_0} Re \int_0^\infty -i\omega (\epsilon - 1) |E(\omega)|^2 \, d\omega$$

$$= \frac{1}{2\pi n_0} Re \int_0^\infty -i\omega \epsilon |E(\omega)|^2 \, d\omega$$

The energy loss to atoms outside of the cylinder of radius a is

$$\frac{dE}{ds} = 2\pi n_0 \int_a^\infty Q \, b \, db$$

Upon carrying out the indicated integrations, we obtain

$$\left(\frac{dE}{ds}\right)_{b>a} = \frac{2}{\pi} \left(\frac{z_1^2 q^2}{V^2}\right) Re \int_0^\infty i\omega \lambda^* a \, K_1(\lambda^* a) K_0(\lambda a) \left[\frac{1}{\epsilon} - \beta^2\right] d\omega$$

a. Plasmon Excitation

In the extreme relativistic limit

$$|\lambda a| << 1 \quad , \quad \beta \cong 1$$

so that the above expression becomes

$$\left(\frac{dE}{ds}\right) \cong \frac{2}{\pi} \frac{(z_1 q)^2}{c^2} Re \int_0^\infty i\omega \left(\frac{1}{\epsilon} - 1\right) \left[\ln \frac{1.123 c}{\omega a} - \frac{1}{2} \ln (1 - \epsilon)\right] d\omega$$

$$\left(\frac{dE}{ds}\right) \cong \frac{(Z_1 q)^2 \omega_p^2}{c^2} \ln \frac{1.123\, c}{a\, \omega_p}$$

where $$\omega_p^2 = \frac{4\pi n_0 Z_2 q^2}{m}$$

The corresponding relativistic expression without the density effect is $$\left(\frac{dE}{ds}\right) = \frac{(Z_1 q)^2}{c^2} \omega_p^2 \left[\ln \frac{1.123\, \gamma c}{a\, \omega_0} - \tfrac{1}{2}\right]$$

We see that the density effect produces a simplification in that the asymptotic energy loss no longer depends on the details of atomic structure through ω_0.

b. Cherenkov Radiation

Next consider whether any energy escapes to infinity. Let then "a" become very large. Then

$$\lim_{a\to\infty}\left(\frac{dE}{ds}\right)_{b>a} = \frac{(Z_1 q)^2}{V^2} \mathrm{Re} \int_0^\infty i\omega \left(\frac{1}{\epsilon} - \beta^2\right)\left(\frac{\lambda^*}{\lambda}\right)^{1/2} e^{-(\lambda+\lambda^*)}\, d\omega$$

If λ has a real part, the exponential factor causes the energy loss to go rapidly to zero at large distances. Since

$$\lambda^2 = \frac{\omega^2}{V^2}\left(1 - \beta^2 \epsilon\right)$$

we note that λ will always have a real part if the medium is absorbent because ϵ has a positive imaginary part. But if ϵ is real λ can be pure imaginary if

$$\beta^2 > 1/\epsilon$$

or

$$\frac{V}{c} > \frac{1}{\sqrt{\epsilon}}$$

Thus $$V > \frac{c}{\sqrt{\epsilon}} = v_p$$

where v_p is the phase velocity of electromagnetic radiation in the medium. This is the condition under which Cherenkov radiation is emitted.

20.9 Further Comments

We present here an alternative derivation of

$$\left(\frac{dE}{dz}\right)_{b>a} = \frac{2}{\pi}\left(\frac{z_1 e}{V}\right)^2 Re \int_0^\infty i\omega \lambda^* a\, K_1(\lambda^* a) K_0(\lambda a)\left(\frac{1}{\epsilon} - \beta^2\right) d\omega$$

This can be done by noting that the electromagnetic energy radiated through a cylinder of radius "a" is just the energy lost per unit time by the incident particle.

From the Poynting vector

$$S = \frac{c}{4\pi} \underline{E} \times \underline{H}$$

which gives the rate of energy flow per unit area, we find that the rate of energy flow is given by

$$-\frac{c}{4\pi} V \int_{-\infty}^{\infty} 2\pi a\, B_2(t) E_3(t)\, dt$$

Also $$\frac{d\mathcal{E}}{dt} = \frac{d\mathcal{E}}{dz}\frac{dz}{dt} = V \frac{d\mathcal{E}}{dz}$$

so that

$$\frac{d\mathcal{E}}{dz} = -\frac{ac}{2} \int_{-\infty}^{\infty} E_3(t)\, B_2(t)\, dt$$

$$\frac{dE}{dz} = -\frac{ac}{2}\int_{-\infty}^{\infty} E_3(\omega)\, B_2^*(\omega)\, d\omega$$

The last result is obtained by using the Fourier transforms of $E_3(t)$ and $B_2(t)$ and noting that

$$\underline{E}(\underline{r},t) = \frac{1}{(2\pi)^2}\int d^3k \int d\omega\, \underline{E}(\underline{k},\omega)\, e^{i\underline{k}\cdot\underline{r} - \omega t}$$

$$= \frac{1}{\sqrt{2\pi}}\int \underline{E}(\omega,\underline{r})\, e^{-i\omega t}\, d\omega$$

Therefore

$$\int_{-\infty}^{\infty} E_3(t)\, B_2(t)\, dt = \frac{1}{2\pi}\int_{-\infty}^{\infty} dt \int E_3(\omega,r)\, e^{-i\omega t}\, d\omega \int B_2(\omega',r)\, e^{-i\omega' t}\, d\omega'$$

$$= \int E_3(\omega,r)\, B_2(-\omega,r)\, d\omega$$

$$\left(\frac{dE}{dz}\right)_{b>a} = -ac\, Re \int_0^{\infty} E_3(\omega,a)\, B_2^*(\omega,a)\, d\omega$$

But

$$E_3(\omega,a) = -\frac{i z_1 \beta \omega}{V^2}\left(\frac{2}{\pi}\right)^{1/2}\left(\frac{1}{\epsilon} - \beta^2\right) K_0(\lambda a)$$

$$B_2(\omega,a) = \epsilon\beta E_1(\omega,a) = \epsilon\beta \frac{z_1 \beta}{V}\left(\frac{2}{\pi}\right)^{1/2}\frac{\lambda}{\epsilon} K_1(\lambda a)$$

$$= \frac{z_1 \beta}{V}\left(\frac{2}{\pi}\right)^{1/2}\lambda\beta K_1(\lambda a)$$

$$\therefore \left(\frac{dE}{dz}\right)_{b>} = \frac{2}{\pi}\left(\frac{z_1\beta}{V}\right)^2 Re \int_0^{\infty} i\omega\lambda^* a\, K_1(\lambda^* a)\, K_0(\lambda a)\left(\frac{1}{\epsilon} - \beta^2\right) d\omega$$

In the extreme relativisitic limit

$$\beta \cong 1 \quad \text{and} \quad |\lambda a| \sim \frac{\omega a}{c} << 1$$

For small values of the argument for the modified Bessel functions, we have

$$K_0(x) = \ln \frac{1.123}{x}$$

$$K_1(x) = \frac{1}{x}$$

so that

$$\left(\frac{dE}{dz}\right)_{b>a} = \left(\frac{2}{\pi}\right)\left(\frac{Z_1 q}{V}\right)^2 Re \int_0^\infty i\omega \left(\frac{1}{\epsilon} - 1\right) \ln \frac{1.123}{\lambda a} \, d\omega$$

We shall return to the task of evaluating the integral later. For now, we need to note that the above integral reduces to

$$\left(\frac{dE}{dz}\right)_{b>a} = \frac{(Z_1 q)^2}{c^2} \omega_p^2 \ln \frac{1.123 c}{a \omega_p}$$

where w_p is the electron plasma frequency

$$\omega_p^2 \equiv \frac{4\pi n_0 Z_2 q^2}{m}$$

The corresponding relativistic effect without the density effect is

$$\left(\frac{dE}{dz}\right)_{b>a} = \frac{(Z_1 q)^2}{c^2} \omega_p^2 \left[\ln \frac{1.123 \gamma c}{a \langle \omega \rangle} - \frac{1}{2}\right]$$

so that the overestimated energy loss is

$$\Delta\left(\frac{dE}{dz}\right)_{b>a} = \frac{(Z_1 q)^2}{c^2} \omega_p^2 \left[\ln \frac{\gamma \omega_p}{\langle \omega \rangle} - \frac{1}{2}\right]$$

20.10 Evaluation of Integrals

We wish now to evaluate

$$\mathrm{Re}\int_0^\infty i\omega\left(\frac{1}{\epsilon}-1\right)\ln\frac{1.123}{\lambda a}\,d\omega$$

where

$$\lambda^2 \equiv \frac{\omega^2}{V^2}(1-\epsilon)$$

For the dielectric constant we shall at first assume

$$\epsilon(\omega) = 1 + \frac{4\pi n_0 Z_2 e^2}{m}\frac{1}{\omega_0^2-\omega^2-i\omega\Gamma}$$

$$= 1 + \frac{\omega_p^2}{\omega_0^2-\omega^2-i\omega\Gamma}$$

The second term is small in comparison to unity, so that

$$\frac{1}{\epsilon}-1 \cong \frac{\omega_p^2}{\omega^2+i\omega\Gamma-\omega_0^2}$$

We then have

$$\mathrm{Re}\int_0^\infty i\omega\left(\frac{1}{\epsilon}-1\right)\ln\frac{1.123}{\lambda a}\,d\omega$$

$$= \mathrm{Re}\int_0^\infty i\omega\frac{\omega_p^2}{\omega^2+i\omega\Gamma-\omega_0^2}\ln\frac{1.123c}{a}\,d\omega$$

$$-\mathrm{Re}\int_0^\infty \frac{i\omega\omega_p^2}{\omega^2+i\omega\Gamma-\omega_0^2}\ln\omega\,d\omega$$

$$-\mathrm{Re}\int_0^\infty \frac{i\omega\omega_p^2}{\omega^2+i\omega\Gamma-\omega_0^2}\ln\sqrt{\frac{\omega_p^2}{\omega^2+i\omega\Gamma-\omega_0^2}}\,d\omega$$

$$= \mathrm{Re}\int_0^\infty \frac{i\omega\omega_p^2}{\omega^2+i\omega\Gamma-\omega_0^2}\ln\frac{1.123c}{a\omega_p}\,d\omega$$

$$-\frac{1}{2}\mathrm{Re}\int_0^\infty \frac{i\omega\omega_p^2}{\omega^2+i\omega\Gamma-\omega_0^2}\ln\frac{\omega^2}{\omega^2+i\omega\Gamma-\omega_0^2}\,d\omega$$

Consider first $$\oint \frac{i\omega\, d\omega}{\omega^2 + i\omega\Gamma - \omega_0^2}$$

around a contour in the first quadrant. Then

$$\oint \frac{i\omega\, d\omega}{\omega^2 + i\omega\Gamma - \omega_0^2} = \int_0^R \frac{i\omega\, d\omega}{\omega^2 + i\omega\Gamma - \omega_0^2}$$

$$+ \int_1^{\pi/2} \frac{-R^2 e^{2i\theta}\, d\theta}{R^2 e^{2i\theta} + iRe^{i\theta}\Gamma - \omega_0^2}$$

$$+ \int_R^0 \frac{i(i\omega)\, d(i\omega)}{-\omega^2 - \omega\Gamma - \omega_0^2} = 0$$

$$\therefore \operatorname{Re} \int_0^R \frac{i\omega\, d\omega}{\omega^2 + i\omega\Gamma - \omega_0^2} = \int_0^{\pi/2} d\theta = \pi/2$$

Also,

$$\oint \frac{i\omega}{\omega^2 + i\omega\Gamma - \omega_0^2} \ln \frac{\omega^2}{\omega^2 + i\omega\Gamma - \omega_0^2}\, d\omega$$

$$= \int_0^\infty \frac{i\omega}{\omega^2 + i\omega\Gamma - \omega_0^2} \ln \frac{\omega^2}{\omega^2 + i\omega\Gamma - \omega_0^2}\, d\omega$$

$$+ \int_\infty^0 \frac{i(i\omega)}{-\omega^2 - \omega\Gamma - \omega_0^2} \ln \frac{-\omega^2}{-\omega^2 - \omega\Gamma - \omega_0^2}\, d(i\omega) = 0$$

$$\therefore \; Re \int_0^\infty \frac{i\omega}{\omega^2 + i\omega\Gamma - \omega_0^2} \ln \frac{\omega^2}{\omega^2 + i\omega\Gamma - \omega_0^2} \, d\omega = 0$$

The expression for the dielectric constant, strictly speaking, applies to gases. Landan and Lifschitz show, however, that the result is true in general.

Cherenkov Radiation

Consider $a \to \infty$ to see whether any energy escapes to infinity. Using the asymptotic form

$$K_\nu(x) = \sqrt{\frac{\pi}{2x}} \, e^{-x}$$

we find that

$$\lim_{a \to \infty} \left(\frac{dE}{dz} \right)_{b \to \infty} = \frac{(ze)^2}{c^2} Re \int_0^\infty i\omega \left(\frac{1}{\epsilon} - \beta^2 \right) \left(\frac{\lambda^*}{\lambda} \right)^{1/2} e^{-(\lambda + \lambda^*)a} \, d\omega$$

If λ has a real part, the energy loss will go rapidly to zero at large distances. This occurs if the medium is absorbent. If, however, ϵ is real (non-absorbent) then λ will be pure imaginary if

$$\beta^2 > 1/\epsilon$$

or

$$V > \frac{c}{n} = v_p$$

where v_p is the phase velocity of light in the medium. Then

$$\lim_{a \to \infty} \left(\frac{dE}{dz}\right)_{b>a} = \frac{(ze)^2}{c^2} \int \omega \left(1 - \frac{1}{\beta^2 \epsilon}\right) d\omega$$

This is the Cherenkov radiation.